F. Pacheco Torgal · Cinzia Buratti
Siva Kalaiselvam · Claes-Göran Granqvist
Volodymyr Ivanov *Editors*

Nano and Biotech Based Materials for Energy Building Efficiency

Springer

Nano and Biotech Based Materials for Energy Building Efficiency

F. Pacheco Torgal · Cinzia Buratti
Siva Kalaiselvam · Claes-Göran Granqvist
Volodymyr Ivanov
Editors

Nano and Biotech Based Materials for Energy Building Efficiency

Springer

Editors
F. Pacheco Torgal
University of Minho
Guimaraães
Portugal

Cinzia Buratti
Department of Engineering
University of Perugia
Perugia
Italy

Siva Kalaiselvam
Department of Applied Science
Anna University
Chennai
India

Claes-Göran Granqvist
Uppsala University
Uppsala
Sweden

Volodymyr Ivanov
School of Civil and Environmental Engineering
Nanyang Technological University
Singapore
Singapore

ISBN 978-3-319-27503-1 ISBN 978-3-319-27505-5 (eBook)
DOI 10.1007/978-3-319-27505-5

Library of Congress Control Number: 2015958850

Printed on acid-free paper

This Springer imprint is published by SpringerNature
The registered company is Springer International Publishing AG Switzerland

Foreword

No one doubts the need to reduce energy consumption in buildings but at the same time ensuring they are healthy for their occupiers. The passive features such as mass, orientation, building form are well-known natural means of controlling the internal thermal conditions. But materials and the ways they are chosen and arranged are vital for low-energy building design. Innovation however can enable materials whether new or traditional ones to perform more effectively in respect of energy consumption and this is the essence of this book. Today, we see on the one hand architects using simple materials such as straw bales, hemp, rammed earth, wood and bamboo but on the other hand others are exploring ways of using materials like titanium, digital embedded structures and nature-inspired biomimetic materials. As insulation improves, operational energy decreases and this means embodied energy is playing an increasing important role in the energy equation too.

This book in 17 chapters reveals the current state of knowledge about nano-materials and their use in buildings ranging from glazing, vacuum insulation to PCM composites. More recent applications of organic photovoltaics, photo-bioreactors, bioplastics and foams make this book an exciting read whilst also providing copious references to current research and applications for those wanting to pursue future possibilities.

Recent buildings such as the Cybertecture Egg office building in Mumbai by James Law with Ove Arup; the Bio-Intelligent Quotient (BIQ) building in Hamburg by Arup and Splitterwerk and the Edge Building by Deloitte with OVG in Amsterdam are all affecting our thinking about architecture and building in terms of materials, sensing systems and use of innovative technology.

The Cybertecture Egg has an intelligent glass façade with variable fritting, shading and tinting, but furthermore it introduces the concept of cybertecture which uses intangible materials of technology, multimedia, intelligence and interactivity. Nanomaterials are part of this story. The façade is not just a climatic moderator but also becomes a communication channel by embedding sensors into materials, and this sees the emergence of interactive facades not just with the climate but also with people. The Edge building has many sensors monitoring the building performance

as well as—like in the Mumbai building—the health of the users (the data of which are protected). The BIQ building has a facade which has bioreactors built in, and algae is grown in them which is harvested for bio fuel whilst also shading the building, and two chapters in this book describe about research in this area.

Nanomaterials can strengthen steel and concrete, make surfaces self-cleaning, make materials fire resistant, detect structural fissures, improve efficiency of solar panels and improve the insulating properties of materials. One example is titanium dioxide particle coatings that when exposed to ultraviolet light can generate reactive molecules which prevent bacterial films forming on surfaces. Various chapters in the book show how nanomaterials improve the insulation of construction with thermal insulation values some 40 times better than traditional fibreglass materials.

There is a need for this book to guide practitioners and researchers through the maze of development taking place in nanomaterials. The distinguished editors have gathered an international team of authors working at the forefront of knowledge in this field and readers will find their knowledge much enriched by what they describe. The chapters also indicate an exciting pathway into the future.

Derek Clements-Croome
Professor Emeritus in Architectural Engineering
University of Reading

Contents

Chapter 1
Introduction to Nano- and Biotech-Based Materials for Energy Building Efficiency

F. Pacheco Torgal

Abstract This chapter starts with an overview of the unsustainable energy consumption which is due to fast population growth and related greenhouse gas emissions. The case of energy efficiency building is introduced. A short analysis of the ambitious European nearly zero-energy building (NZEB) target is presented. Shortcomings of current materials concerning energy building efficiency are reviewed. Examples of promising nano- and biotech-based materials for energy building efficiency are briefly covered. A book outline is presented.

1.1 The Paramount Challenge of Sustainable Energy Consumption

The rise in energy consumption is directly related to the increase in world population (Fig. 1.1). Since each day there are now about 200,000 new inhabitants on planet Earth (WHO 2014), this means that the increase in electricity demand will continue (King et al. 2015). It is also expected that the annual electricity consumption per capita (Fig. 1.2) in low- and middle-income countries will rise as a consequence of future higher income and related higher comfort standards (World Bank 2014). This means increased pressure in electricity demand. It is then no surprise to see that the world net electrical consumption will increase from 20.1 trillion kWh in 2010 to 25.5 trillion kWh by 2020 and 35.2 trillion kWh by 2035 (WEO 2013). Unfortunately, only 21 % of world electricity generation was from renewable energy in 2011 with a projection for nearly 25 % in 2040 (WEO 2013). Also, recent studies (Hadian and Madani 2015) using a stochastic multi-criteria analysis framework to estimate the relative aggregate footprint scores of energy sources under three different sustainability criteria (carbon, water and land footprint) and cost of energy production showed that some of the renewable

F. Pacheco Torgal (✉)
C-TAC Research Centre, University of Minho, Guimarães, Portugal
e-mail: torgal@civil.uminho.pt

F. Pacheco Torgal et al. (eds.), *Nano and Biotech Based Materials for Energy Building Efficiency*, DOI 10.1007/978-3-319-27505-5_1

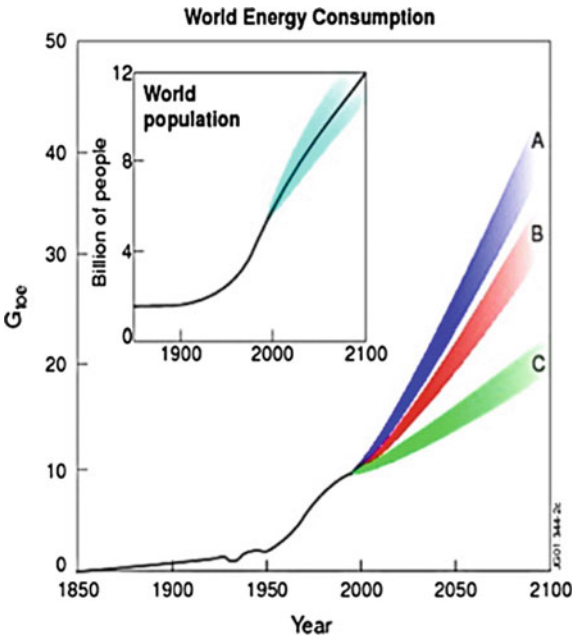

Fig. 1.1 World energy consumption in the past 150 years (Amouroux et al. 2014)

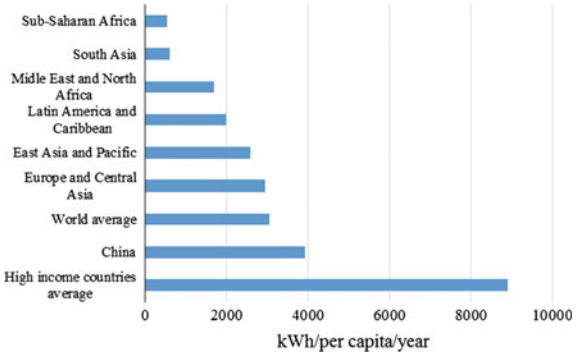

Fig. 1.2 Annual electricity consumption per capita

energy sources (hydropower and solar PV) are not as "green" as perceived based on the current state of the energy production methods/technologies. And some renewable energy sources such as biofuel and ethanol are even worse than the fossil fuels such as natural gas.

As a consequence in the next decades, the majority of electric energy will continue to be generated from the combustion of fossil fuels such as coal, oil and gas releasing not only carbon dioxide but also methane and nitrous oxide. It is worth remember that China is largest energy consumer in the world (10.3 billion tonnes of CO_2, 29 % of world emissions) (JCR 2014) and that Chinese coal plants

are responsible for 80 % of electricity generation (Shealy and Dorian 2009), meaning that its electric production will continue to be associated with high CO_2 emissions. However, it is also important to recognize that China has just a 7.4 tonnes per capita CO_2 emissions level, while Australia, USA and Brazil (the top 3 per capita emitters) are responsible for 16.9, 16.6 and 16.6 tonnes pf CO_2 per capita, respectively (JCR 2014). As the source of two-thirds of global greenhouse gas emissions, the energy sector is therefore pivotal in determining whether or not climate change goals are achieved. Climate change is one of the most important problems faced by the Human being, which is associated with the rise in the sea level, ocean acidification, heavy rain, heat waves and extreme atmospheric events, environment deterioration and wildlife extinction, health problems and infrastructure damage (Williams et al. 2012; IPCC 2014). Tackling climate change will therefore require strong efforts aimed at curbing greenhouse gas emissions from the energy sector. Energy efficiency is very important for this context because efficiency improvements show the greatest potential of any single strategy to abate global GHG emissions from the energy sector (IEA 2013).

1.2 Energy Efficiency Building

The building sector is responsible for high energy consumption, and its global demand is expected to grow in the next decades. Between 2010 and 2050, the global heating and cooling needs are expected to increase by 79 % in residential buildings and 84 % in commercial buildings (Ürge-Vorsatz et al. 2015).

Energy efficiency measures are therefore crucial to reduce GHG emissions of the building sector. Recent estimates (Ürge-Vorsatz and Novikov 2008; UNFCCC 2013) state that energy efficiency concerning buildings' heating and cooling needs could allow a reduction between 2 and 3.2 $GtCO_2e$ per year in 2020. Other estimates mentioned a potential reduction of around 5.4–6.7 $GtCO_2e$ per year in 2030 (UNEP 2013). In order to achieve such reductions, the implementation of building codes associated with the high energy performance must be seen as a top priority. In the last decade, several high energy performance building concepts have been proposed, from low-energy building through passive building and zero-energy building to positive energy building and even autonomous building (Thiers and Peuportier 2012). For the Building Technologies Programme of the US Department of Energy (DOE), the strategic goal is to achieve *marketable zero energy homes in 2020 and commercial zero energy buildings in 2025*. However, commercial definitions maybe tainted by biased view, allowing for energy-inefficient buildings to achieve the status of zero energy thanks to oversized PV systems (Sartori 2012). Rules and definitions for near zero-energy buildings or even zero-energy buildings are still subject to the discussion at the international level (Dall'O et al. 2013). Some authors (Adhkari 2012) use ZEB as "net zero-energy buildings" and NZEB as "nearly zero-energy buildings". "Net" refers to a balance between energy taken from and supplied back to the energy grids over a period of time. Therefore,

Net ZEB refers to the buildings with a zero balance, and the NZEB concept applies to buildings with a negative balance.

The European Energy Performance of Buildings Directive 2002/91/EC (EPBD) has been recast in the form of the 2010/31/EU by the European Parliament on 19 May 2010. One of the new aspects of the EPBD is the introduction of the concept of nearly zero-energy building (NZEB). Of all the new aspects set out by the new directive, the NZEB target is the one that European countries have more difficulty to enforce Member states. The article 9 of the European Directive establishes that, by the 31 December 2020, all new constructions have to be NZEBs; for new public buildings, the deadline is even sooner—the end of 2018. Unfortunately, the status of the EPBD implementation in EU countries is disappointing because so far only a minority of countries have transpose the EPBD into their national laws (Antinucci 2014).

Be there as it may, new buildings have limited impacts on overall energy reduction as they represent just a tiny fraction of the existent building stock (Xing et al. 2011). Also, it is estimated that in Europe, only 1 % of the continent's building stock in any given year is newly built. Existing buildings constitute, therefore, the greatest opportunity for energy efficiency improvements. Besides, new homes use four to eight times more resources than an equivalent refurbishment (Power 2008), which constitutes an extra and sustainable argument in favour of building refurbishment. Building energy efficiency refurbishment is also crucial to address an important social problem, energy poverty. This problem affects between 1.3 billion and 2.6 billion people from underdeveloped regions of the world. Between 50 and 125 million people in Europe alone suffer from energy poverty (Atanasiou et al. 2014). This has important health consequences for children and older people leading to an increase in medical costs. Infants, living in energy-poor homes, are associated with a 30 % greater risk of admission to hospital. Indoor cold is also highly correlated with premature mortality. Between 30 and 50 % of excess winter mortality is attributed specifically to energy-inefficient housing conditions. Besides, direct financial help to low-income households or the use of energy subsidies can only address this problem in a partial manner without solving it in a long term, while the funding of building energy efficiency refurbishment works is also able to generate value-added and economic growth (Atanasiou et al. 2014).

Its important to mention that EPBD recast does not cover existent buildings; however, the Energy Efficiency Directive (2012/27/EU) approved by the European Parliament on 25 October 2012 that each Member states had have to transpose into national laws until 5 June 2014 addresses the energy efficiency refurbishment of existent buildings (Articles 4 and 5). According to Article 4, Member states will have to define *establish a long-term strategy for mobilising investment in the renovation of the national stock of residential and commercial buildings, both public and private*. As to Article 5 content it requires that *each Member state shall ensure that, as from 1 January 2014, 3 % of the total floor area of heated and/or cooled buildings…is renovated each year to meet at least the minimum energy performance requirements*. Also according to the Article 4 of the EED, the first version of the building renovation strategy was to be published by 30 April 2014. However, the report published in November 2014 revealed that only 10 renovation

strategy plans were submitted (BPIE 2014). Of those only the strategies of four (Czech Republic, Romania, Spain and UK) were considered acceptable because they met the basic requirements set by Article 4. The strategies of France, Germany and Brussels capital region needed to be corrected and resubmitted. The strategies of three countries (Austria, Denmark and the Netherlands) were rejected because they do not fulfil the basic requirements of Article 4. In January 2015, an addendum was published (BPIE 2015), showing that only the renovation strategy of Austria remain rejected although his compliance level increased from 28 to 40 % and also that the overall compliance level increased from 58 to 63 %. This means that much more effort must be put in the building energy efficiency refurbishment agenda. The scientific community has some responsibilities in this situation because a recent study on energy-efficient renovation peer-reviewed articles (Friege et al. 2014) concluded that the literature "lacks a deep understanding of the uncertainties surrounding economic aspects and non-economic factors driving renovation decisions of homeowners". Of course, this gap does not help the building renovation decisions nor political decisions that could boost the investments on this field. Pikas et al. (2015) recently found that in all 17 jobs per 1 million euro of investment in building renovation had been generated per year. These authors also found that 32 % tax revenue would be excepted from renovation-related activities, meaning that an official 32 % governmental investment would be economically neutral. This study confirms the predictions of Oliver Rapf, executive director, BPIE when he said that …*renovation of buildings to high energy performance standards could be one of the most cost effective investments a nation can make, given the benefits in terms of job creation, quality of life, economic stimulus, climate change mitigation and energy security that such investments deliver* (Pikas 2015).

1.3 Shortcomings of Current Materials and Promising Nano- and Biotech-Based Investigations Concerning Energy Building Efficiency

New building envelope materials and technologies are needed to increase energy efficiency and energy savings at much lower cost than is possible today (IEA 2013), and some of the technologies needed for the retrofitting of the EU's building stock are already available in the market. However, their diffusion varies across Member states due to a lack of market actors' awareness about the savings potential of the best available technologies (JCR 2015).

Probably, the most-known limitation of current materials concerning energy building efficiency has to do with the "low" performance of current thermal insulators. The urgent need to reduce building energy consumption led to a steady increase in the thickness of thermal insulation materials over the years. In some countries of northern Europe, the insulation thickness has almost doubled (Fig. 1.3). This limitation has important economic and technical consequences. Such high thickness means less available internal space in existent buildings as well as an

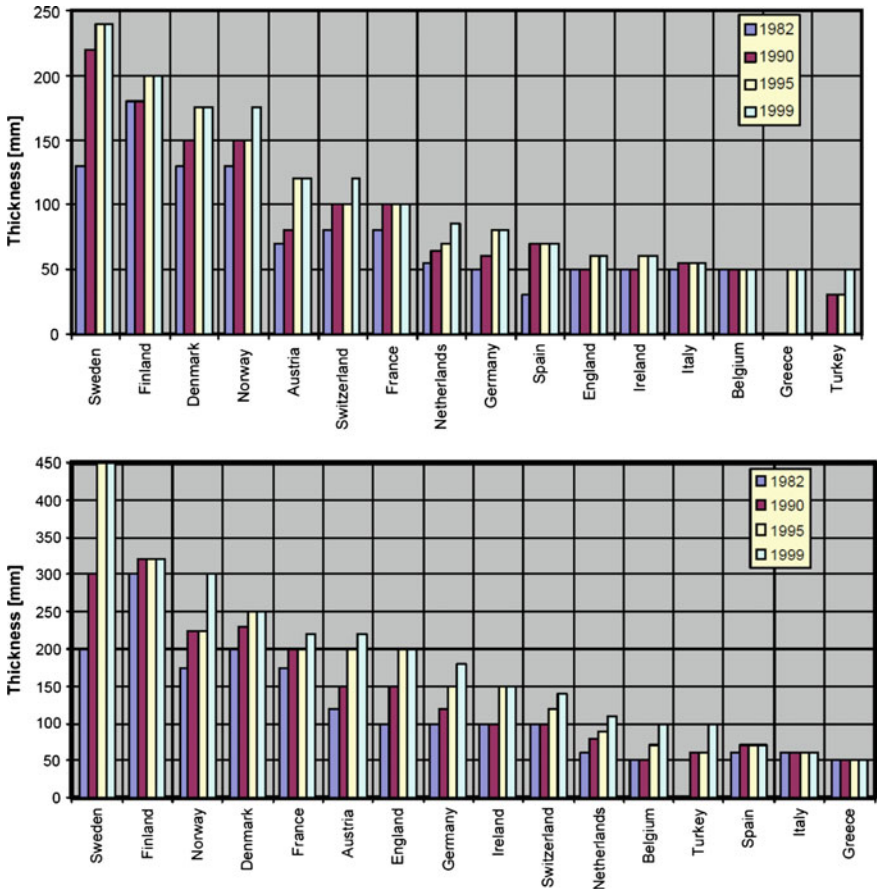

Fig. 1.3 Evolution of thermal insulation thicknesses in several European countries: above in walls and below in roofs (Papadopoulos 2005)

increase in insulation costs. The development of high-performance thermal insulator materials (with low thickness) has thus become a technical and scientific challenge that justified and still justifies new investigations.

Another important issue concerning current building materials and energy efficiency has to do with the fact that there is a limit beyond which no further reductions on energy consumption can be achieved within the EPBD framework. In that context, the use of building materials with lower embodied energy becomes a priority area. The energy embodied in construction and building materials (embodied energy) covers the energy consumed during its service life. There are, however, different approaches to this definition, namely the energy consumed from the extraction of raw materials to the factory gate (cradle to gate), from extraction to site works (cradle to site) or from extraction to the demolition and disposal (cradle to grave). Berge (2009) considers embodied energy as only the energy needed to

bring the material or product to the factory gate (first case), and the transport energy and the energy related to the work execution as being both included in the construction phase of the building. According to this author, the embodied energy represents 85–95 % of the material total energy (the remaining 5–15 % being related to the construction, maintenance and demolition of the building). As to the third case, the embodied energy includes all energy consumption phases from the production at the cradle. As to the transport energy, it depends on the mode of transport: sea, air, road or rail. In recent decades, the operational energy in buildings (lighting, heating, cooling, etc.) was accepted as being the major contributor, while the embodied energy was found to represent only a small fraction (10–15 %). Consequently, much effort has been made towards the reduction of operational energy by increasing the energy efficiency of buildings. However, as operational energy is reduced, the percentage of the embodied energy in the total energy consumption of the buildings becomes increasingly prevalent. Some authors (Sandrolini and Franzoni 2010) recognized that energy savings by means of more efficient thermal insulation (as well as increasing renewable energy use) is an insufficient approach further suggesting the inclusion of embodied energy as an important parameter for sustainable construction.

Szalay (2007) even suggested that the EPBD recast could include requirements of embodied energy. Unfortunately that was not the case. Instead, the European strategy decided to addresses the overall environmental impact of construction and building materials (energy consumption included) in the new Construction Products Regulation—CPR (Directive (EU) 305/2011) which is in effect since 1 July 2013 replacing the Directive 89/106/EEC, already amended by Directive 1993/68/EEC, known as the Construction Products Directive (CPD).

Pacheco-Torgal et al. (2013a, b) studied a 97 apartment-type building, concerning both the embodied energy as well as the operational energy. The results show that the embodied energy in reinforced concrete (concrete plus steel) represents 70 % of the total; therefore, high energy reductions can only occur by lowering the energy in this material. The operational energy was found to signify an average of 187.2 MJ/m^2/yr and the embodied energy accounting for approx. 2372 MJ/m^2 and representing just 25.3 % of the former. If the buildings were in the AA + energy class, this would mean that the embodied energy could be as much as 400 % of the operational energy for a service life of 50 years. A recent review by Cabeza et al. (2013) highlights the research efforts to develop new materials with less embodied energy, which are crucial to the energy building efficiency agenda.

Also important although not directly related to building energy efficiency is the fact that most thermal insulation materials are associated with negative environmental impacts in terms of toxicity. Polystyrene, for example, contains antioxidant additives and ignition retardants; additionally, its production involves the generation of benzene and chlorofluorocarbons. Polyethylene is obtained from the polymerization of ethylene, containing 0.5 % of additives such as phenol-based antioxidants, UV stabilizers and dyes, including aluminium, magnesium hydroxide and chloroparaffin as ignition retardants. Polypropylene is obtained from the polymerization of propylene with additives similar to those used in polyethylene.

Polyurethane is obtained from isocyanates, which are widely known for their tragic association with the Bhopal disaster (Pacheco-Torgal et al. 2012). This substance is highly toxic (Marczynski et al. 1992; Baur et al. 1994), and there are multiple records of serious health problems in workers using polyurethane (Littorin et al. 1994; Skarping et al. 1996). Chester et al. (2005) even reported the death of a worker due to the simple application of polyurethane. The production of polyurethane also involves the production of toxic substances such as phenol and chlorofluorocarbons. Also important is the fact that several thermal insulation materials release toxic fumes when subjected to fire. Liang and Ho (2007) studied the toxicity during fires of several insulation materials and concluded that polyethylene and polyurethane foams should not be used unless covered by incombustible materials. Dourodiani et al. (2012) mentioned that the fumes produced from burning of the expanded polystyrene used in the ceilings caused the death of several workers. Those authors also mentioned that even when the toxic fumes exposition is not high enough to lead to human deads, it can be responsible for other serious health problems such as chromosome damage, cancer and even birth defects. This issue is very important because the information on the toxicity of building materials is a crucial aspect under the new CPR. While the CPD only considered a very limited range of dangerous substances, e.g. formaldehyde and pentachlorophenol, the CPR links this subject to the Regulation (EC) No 1907/2006 (Registration, Evaluation, Authorisation and Restriction of Chemicals—REACH Regulation). The introduction of the CPR states that *the specific need for information on the content of hazardous substances in construction products should be further investigated*. Besides, the Article 67 mentions that *By 25 April 2014, the Commission shall assess the specific need for information on the content of hazardous substances in construction products and consider the possible extension of the information obligation provided for in Article 6(5) to other substances*. Regarding energy building efficiency, high-performance, non-toxic thermal insulators, as well as low embodied energy building materials, are therefore needed.

Although the 1959 speech of Fenyman at the American Physical Society at Caltech is considered the beginning of the nanotechnology era, only in the 1980s has this area start an exponential growth (Glanzel et al. 2003). In the last decades, nanotechnology was became a hot area crossing different scientific areas from electronics to life sciences, and still only in the last years have the nanotech investigations for the construction industry began to have enough expression justified by the published works on that particular field (Smith and Granqvist 2010; Pacheco-Torgal and Jalali 2011; Hanus and Harris 2013; Pacheco-Torgal et al. 2013a).

A 2012 Scopus search of journal papers containing the terms “nanotechnology” and “eco-efficient construction” (Pacheco-Torgal et al. 2013a) revealed only five published papers and all in the field of cement materials. The same search carried out three years later shows twenty-six papers, eight of which are directly related to the energy building efficiency materials. This shows that a research shift from cement nanotech to nanotech energy efficiency materials has occurred in the last years.

Nanoporous aerogel is a perfect example of a high-performance thermal insulator but also of the time lag between nanotech scientific discoveries and the deployment of related commercial products. It was invented in the 1930s (Kistler 1931; Kistler and Caldwell 1932) and further developed in the 1950s by NASA. Aerogel is composed of air above 90 %, and silica nanoparticles have the lowest thermal conductivity of any solid of around 0.01 W/mK (around 13 mW/mK for commercial products).

Since the majority of energy losses in a building occur through windows, the use of aerogel as low thermal conductivity windows or skylights (Schultz et al. 2005; Jelle et al. 2012) with a U-values lower than 0.3 W/m^2 K (Buratti and Moretti 2012, 2013a, b) is especially important for energy building efficiency (Cotana et al. 2014; Ihara et al. 2015). However, since the cost of an aerogel window could be six times higher than a conventional window (Cuce 2014a), this constitutes a challenge that needs to be overcome. Aerogel is non-flammable, not carcinogenic (Buratti and Moretti 2012), has minimal health hazards (Aspen 2015) and does not release toxic fumes during fire, and it thus has a high potential to overcome some of the shortcomings of current thermal insulators being the subject of three chapters of this book. However, a recent study (Cuce et al. 2014a, b) showed that aerogel thermal insulation is not cost-effective for countries with warm climates. Even so it is worth mention that those authors assumed a high aerogel cost (600 €/m^3) and did not count on the economic value of space savings, which is an important advantage of aerogel over current thermal insulators. Since cost efficiency is a crucial aspect in order that aerogel (and other nanotech-based materials) can be widely use by the construction industry, this means that more investigations are needed that could give a more accurate picture of the real cost gap between aerogel and current thermal insulators.

Other important field relates to the development of cool materials incorporating new advanced nanomaterials (Santamouris et al. 2011; Jelle et al. 2015). Cool materials have high solar reflectance allowing for the reduction of energy cooling needs in summer. These materials are specially important for building energy efficiency because as a consequence of climate change, building coolings needs are expected to increase in the coming years (Crawley 2008). Depending on the climate zone, cooling loads are likely to increase by 50 to over 90 % until the end of the century (Roetzel and Tsangrassoulis 2012). According to the IEA (2013), energy consumption for cooling is expected to increase sharply by 2050—by almost 150 % globally and by 300 to 600 % in developing countries. The Cool-Coverings FP7 project (Escribano et al. 2013) which aims at the development of a novel and cost-effective range of nanotech improved coatings to substantially improve near-infrared reflective properties.

Also crucial for energy-efficient buildings is switchable glazing technology-based materials that refer to ‘materials and devices that make it possible to construct glazings whose throughput of visible light and solar energy can be switched to different levels depending on the application of a low DC voltage (electrochromics) or on the temperature (thermochromics) or even by using hydrogen (gasochromics). Electrochromic windows have shown a 54 % energy reduction in electrochromic windows when compared to standard single-glazed windows for a 25 years life cycle

(Papaefthimiou et al. 2006). Other authors (Yoshimura et al. 2009) studied gasochromic windows reporting a 34 % reduction on cooling needs when compared to standard double-glazed windows. Tavares et al. (2015) reported savings of about 14 % in the annual energy needs resulting by single glass replacement with double electrochromic glass controlled by solar radiation. According to these authors for this energy savings, the maximum permissible additional cost per m^2 of EC glass to a simple recover period of 10 years is 33.44 €. Several commercial solutions are already available on the market (SAGE Electrochromics—USA, Econtrol Glas, Saint Gobain Sekurit and Gesimat—Germany, amongst others) with a service life of 30 years and capable of 100,000 switching cycles. The most challenging point of smart windows at the moment is their higher cost compared to the other glazing technologies (Cuce and Riffat 2015). Hee et al. (2015) stated that due to the higher costs of dynamic glazing, it is more suitable to be installed in the building which needed high performance in terms of daylighting and energy saving such as commercial buildings. However, it is expected that in the next years, a higher performance and lower cost switchable glazing windows will be available.

Jelle (2011) predicted that the nano-insulation materials (NIMs), the dynamic insulation materials (DIMs) and the load-bearing insulation materials NanoCon could become promising nanotech-based thermal insulators. However, four years after his statement, no major advances were made concerning those materials not even regarding the wide use by the construction industry of nanotech-based insulator materials. The reason for that may lie on the fact that the construction industry has a risk-averse nature having a recalcitrant approach to new technology adoption (Arora et al. 2014). Fortunately, recent forecasts show that the European market for building energy-efficient products (and services) alone will grow from €41.4 billion in 2014 to €80.8 billion in 2023 (NR 2014), meaning that investigations on high-performance thermal insulators will have an important market to explore justifying its funding.

Much like nanotechnology, biotechnology constitutes another hot scientific field that has grown exponentially in the last decades. Having the potential to develop more sustainable solutions, it also has a huge commercial potential (Meyer 2011). Biotechnology is one of the six key enabling technologies (KETs) that will be funded under the EU Framework Programme Horizon 2020 (Pacheco-Torgal 2014). Investigations on cellulose nanocrystals (cellulose elements having at least one dimension in the 1–100 nm range) constitute an important and recent field with the potential to enable the development of promising eco-efficient high-performance materials (Charreau et al. 2013). Concerning the contribution of biotech advances for energy building efficiency, a new generation of bioaerogels was developed in the past decade from various polysaccharides such as cellulose, cellulose esters, marine polysaccharides, pectin and starch (Demilecamps et al. 2015). Cellulose being the most abundant polymer on Earth, renewable, biodegradable, carbon neutral, having the potential to be processed at industrial-scale quantities and at low cost could become a green source to future aerogel thermal insulators.

Bioplastics are also another recent biotech output that could have future impact on low embodied energy building material, thus contributing for energy building

efficiency. There is not a unique definition on bioplastics, but the one set by the Business–NGO Working Group for safer chemicals and sustainable materials (Alvarez-Chavez et al. 2012) seems to be a very accurate one: "as plastics in which 100 % of the carbon is derived from renewable agricultural and forestry resources such as corn starch, soybean protein and cellulose". Although these current biomaterials have a high cost, the recent investigations (Xu and Yang 2012) show that the production of bioplastics from biowastes could enhance the cost efficiency.

Several books have already been written addressing nanotech-based materials for the construction industry. Still recent investigations (Arora et al. 2014) show that the construction industry practitioners display moderate levels of awareness regarding that issue. Besides, most of them have a narrow focus on the energy building efficiency issue. Also, biotech-based materials for energy building efficiency is a book desert area. Therefore, this book intents to provide a contribution (even small as it is) for the energy building efficiency agenda by gathering important contributions of world experts on nano- and biotech-based materials. This publication will help future standardization efforts regarding these innovative materials. It will also help the building industry stakeholders to be aware of the state-of-the-art energy building efficiency-related materials which is a crucial step to speed up their commercialization and its effective use in deep retrofitting actions.

1.4 Book Outline

Chapter 2 deals with the aerogel-based plasters. A short overview on market trends of thermal insulation plasters is presented. Plaster composition, physics, thermal, acoustic, and hygrothermal properties are discussed. In situ applications of aerogel plasters are analysed, and the potential of the investigated materials is highlighted.

Highly energy-efficient silica aerogel windows are the subject of Chap. 3. The characteristics of the raw material (monolithic and translucent granular) are illustrated. The chapter includes general information about the production process, the main chemical and physical properties, and a market overview. Thermal, visual and acoustic performances of silica aerogel windows are highlighted. A numerical analysis review confirms the contribution of these windows for energy building efficiency.

Chapter 4 contains the state of the art about thermochromic glazings. These high-performance glazings have temperature-dependent properties being able to control the quantity of solar heat and light entering a building by changing its optical properties, thus reducing energy consumption. A review on different chromogenic materials (photochromic, thermocromic and electrochromic) is introduced. A special attention is dedicated to vanadium oxide (VO_2)-based thermochromic glazings including fabrication and performance. A review on energy modelling of buildings with thermochromics glazings is presented.

The use of an optically transparent, thermal energy adsorbing glass is the subject of Chap. 5. A review on vasculature networks is included. The importance of

biomorphic responsive glass for energy building efficiency is highlighted. Investigations on glass with embedded microvascular networks are reviewed as promising research field for future development of photosynthetic composite glass.

Chapter 6 provides an overview of the requirements for product development of adaptive nanobased materials and technologies. The role of building simulation in the development of innovative adaptive materials and technologies is discussed. State-of-the-art advanced methodologies and the characteristics of the tools to support the product development for building-integrated adaptive materials and technologies are presented. A case study concerning the evaluation of the performance of future-generation adaptive glazing and adaptive insulation is also presented.

Chapter 7 addresses the use of nanotech-based vacuum insulation panels (VIPs) for building applications. It includes VIP concepts, the state of the art on VIP products as well as some case studies. Future research pathways for VIP technologies are also included.

The use of nanomaterial-based phase-change materials (nanoPCMs) for thermal energy storage is the subject of Chap. 8. It reviews PCM, nanomaterial and nanoPCM composites. The enhancement of the thermal energy storage capabilities of NanoPCM composites and its role on achieving improved energy efficiency in buildings is highlighted.

Chapter 9 addresses the case of nanotech-based cool materials and its contribution in reducing energy building cooling needs. Recent nanoscale developments are addressed, and the main applications of cool materials are discussed including cool roofs, cool walls, cool shading devices and cool paving materials. The durability performance of cool materials is also covered.

Chapter 10 covers the performance of semi-transparent photovoltaic (STPV) facades. A methodology that quantifies the building energy demand reduction provided by STPV constructive solutions is presented, and the design parameters of STPV solution are analysed.

Chapter 11 reviews the use of organic photovoltaics for building energy efficiency. The functioning principles of hybrid and organic (HOPV) devices that include dye-sensitized solar cells (DSCs) and polymeric cells are described. A description of the actual studies carried on HOPV and energy efficiency in buildings is included. Some showcases that involve the use of HOPV integrated into buildings are also included.

Investigations on biobased polyurethane foam for thermal insulation materials are the subject of Chap. 12. A review on the insulating properties of polyurethane foam is included. Raw materials, synthesis and properties of bio-polyurethane foams are covered.

Chapter 13 is related to the development of biorefinery-derived bioplastics as promising low embodied energy building materials. While current materials based on petrochemical-based plastics produce hazardous non-biodegradable wastes when buildings are demolished. Materials made from the renewable organic sources are biodegradable and can be left in soil or composted after the building demolition. Bioplastics also have the potential to lead to the rise of new building materials with low embodied energy, thus contributing to energy building efficiency.

Chapter 14 addresses the bio-inspired lightweight structural materials as low embodied energy-based materials. Several examples were reviewed including water lily leaves, bird's bones and trunk trees.

Chapter 15 is related to nanocellulose aerogels as promising thermal insulation materials and covers cellulose aerogel produced from bacterial cellulose and from paper pulp, and even aerogel prepared from paper wastes. It includes fabrication methods, mechanical and thermal properties.

Chapter 16 covers photobioreactor-based energy sources. The characteristics of the different industrial-scale photobioreactors are reviewed. A discussion on cost limitations are included.

Several case studies on the architectural integration of photobioreactors in building façades constitute the subject of Chap. 17.

References

Adhikari R, Aste N, Del Pero C, Manfren M (2012) Net zero energy buildings: expense or investment? Energy Procedia 14:1331–1336

Álvarez-Chavez C, Edwards S, Moure-Eraso R, Geiser K (2012) Sustainability of bio-based plastics: general comparative analysis and recommendations for improvement. J Cleaner Prod 23:47–56

Amouroux J, Siffert P, Massue JP, Cavadias S, Trujillo B, Hashimoto K, Rutberg P, Dresvin S, Wang X(2014) Carbon dioxide: A new material for energy storage. Progress in Natural Science: Materials International24:295–304

Antinucci M (2014) Key implementation decisions. Stakeholders' meeting. Concerted action, energy performance directive, Brussels

Arora S, Foley R, Youtie J, Shapira P, Wiek A (2014) Drivers of technology adoption—the case of nanomaterials in building construction. Technol Forecast Soc Change 87:232–244

Aspen (2015) http://www.aerogel.com/. Accessed 11 Oct 2015

Aspen Aerogels. http://www.aerogel.com/ehs.html

Atanasiu B, Knotonasiou E, Mariottini F (2014) Alleviating fuel poverty in the EU. Investing in home renovation. A sustainable and inclusive solution. Buildings Performance Institute Europe (BPIE)

Baur X, Marek W, Ammon J (1994) Respiratory and other hazards of isocyanates. Int Arch Ocup Environ Health 66:141–152

Berge B (2009) The ecology of building materials, 2nd edn. Architectural Press, Elsevier Science. ISBN 978-1-85617-537-1

BPIE (2014) Renovation strategies of selected EU countries. A status report on compliance with article 4 of the energy efficiency directive. Buildings Performance Institute Europe (BPIE), Nov 2014

BPIE (2015) Addendum to the renovation strategies of selected EU countries. A status report on compliance with article 4 of the energy efficiency directive. Buildings Performance Institute Europe (BPIE), Jan 2015

Buratti C, Moretti E (2012) Glazing systems with silica aerogel for energy savings in buildings. Appl Energy 98:396–403

Buratti C, Moretti E (2013a) Chapter 10-Silica nanogel for energy-efficient windows. In: Pacheco-Torgal F, Diamanti MV, Nazari A, Granqvist CG (eds) Nanotechnology in eco-efficient construction: materials, processes and applications. Woodhead Publishing Limited, Cambridge. http://dx.doi.org/10.1533/9780857098832.2.207, ISBN 9780857095442

Buratti C, Moretti E (2013b) Chapter 20-Nanogel windows. In: Pacheco Torgal F, Mistretta M, Kaklauskas A, Granqvist CG, Cabeza LF (eds) Nearly zero energy building refurbishment. A multidisciplinary approach. Springer, London. http://dx.doi.org/10.1007/978-1-4471-5523-2_20, ISBN 978-1-4471-5522-5

Cabeza LF, Barreneche C, Miró L, Morera J, Bartolí E, Fernández A (2013) Low carbon and low embodied energy materials in buildings: a review. Renew Sustain Energy Rev 23:536–542

Charreau H, Foresti ML, Vazquez A (2013) Nanocellulose patents trends: a comprehensive review on patents on cellulose nanocrystals, microfibrillated and bacterial cellulose. Recent Patents Nanotechnol 7(1):56–80

Chester D, Hanna E, Pickelman B, Rosenman K (2005) Asthma death after spaying polyurethane truck bedliner. Am J Indust M 48:78–84

Cotana F, Pisello A, Moretti E, Buratti C (2014) Multipurpose characterization of glazing systems with silica aerogel: in-field experimental analysis of thermal-energy, lighting and acoustic performance. Build Environ 81:92–102

Crawley DB (2008) Estimating the impacts of climate change and urbanization on building performance. J Build Perform Simul 1:91–115

Cuce E, Riffat S (2015) A state-of-the-art review on innovative glazing technologies. Renew Sustain Energy Rev 41:695–714

Cuce E, Cuce P, Wood C, Riffat S (2014a) Optimizing insulation thickness and analysing environmental impacts of aerogel-based thermal superinsulation in buildings. Energy Build 77:28–39

Cuce E, Cuce PM, Wood CJ, Riffat SB (2014b) Toward aerogel based thermal superinsulation in buildings: a comprehensive review. Renew Sustain Energy Rev 34:273–299

Dall'O' G, Bruni E, Sarto L (2013) An Italian pilot project for zero energy buildings: towards a quality-driven approach. Renew Energy 50:840–846

Demilecamps A, Beauger C, Hildenbrand C, Rigacci A, Budtova T (2015) Cellulose–silica aerogels. Carbohydr Polym 122:293–300

Directive (EU) 305/2011—Construction products regulation. Official Journal of the European Union, European Parliament, Brussels

Directive 2012/27/EU of the European Parliament and of the Council of 25 October 2012 on energy efficiency

Doroudiani S, Doroudiani B, Doroudiani Z (2012) Materials that release toxic fumes during fire. In: Pacheco Torgal F, Jalali S, Fucic A (eds) Toxicity of building materials. WoodHead Publishing, Cambridge, pp 241–282

Escribano MAB, Keraben Grupo SA (2013) Development of a novel and cost-effective range of nanotech improved coatings to substantially improve NIR (near infrared reflective) properties of the building envelope, FP7 Project http://cordis.europa.eu/project/rcn/94644_en.html

European Union. Directive 2010/31/EU of the European Parliament and of the Council of May 19th, 2010 on the energy performance of buildings (recast). Official Journal of the European Union, 18 June 2010

Friege J, Chappin E (2014) Modelling decisions on energy-efficient renovations: a review. Renew Sustain Energy Rev 39:196–208

Glanzel W, Meyer M, du Plessis M, Thijs B, Magerman T, Schlemmer B, Debackere K, Veugelers R (2003) Nanotechnology: analysis of an emerging domain of scientific and technological endeavour. Steunpunt O&O Statistoeken, Leuven

Hadian S, Madani K (2015) A system of systems approach to energy sustainability assessment: Are all renewables really green? Ecol Ind 52:194–206

Hanus MJ, Harris AT (2013) Nanotechnology innovations for the construction industry. Progress Mater Sci 58(7):1056–1102

Hee W, Alghoul M, Bakhtyar B, Elayeb O, Shameri M, Alrubaih M, Sopian K (2015) The role of window glazing on daylighting and energy saving in buildings. Renew Sustain Energy Rev 42:323–343

IEA (2013) Technology roadmap: energy efficient building envelopes. International Energy Agency, Paris

Ihara T, Gao T, Grynning S, Jelle BP, Gustavsen A (2015) Aerogel granulate glazing facades and their application potential from an energy saving perspective. Applied Energy 42:179–191

IPCC (2014) Summary for policymakers. In: Field CB, Barros VR, Dokken DJ, Mach KJ, Mastrandrea MD, Bilir TE, Chatterjee M, Ebi KL, Estrada YO, Genova RC, Girma B, Kissel ES, Levy AN, MacCracken S, Mastrandrea PR, White LL (eds) Climate change 2014: impacts, adaptation, and vulnerability. Part A: global and sectoral aspects. Contribution of working group II to the fifth assessment report of the intergovernmental panel on climate change. Cambridge University Press, Cambridge, pp 1–32

JCR (2014) Trends in global CO_2 emissions. Report http://edgar.jrc.ec.europa.eu/news_docs/pbl-2014-trends-in-global-co2-emissions-2014-report-93171.pdf

JCR (2015) Energy renovation: the trump card for the new start for Europe. Joint Research Centre, Institute for Energy and Transport Luxembourg

Jelle BP (2011) Traditional, state-of-the-art and future thermal building insulation materials and solutions–Properties, requirements and possibilities. Energ Buildings 43(10):2549–2563

Jelle BP, Hynd A, Gustavsen A, Arasteh D, Goudey H, Hart R (2012) Fenestration of today and tomorrow: a state-of-the-art review and future research opportunities. Sol Energy Mater Sol Cells 96:1–28

Jelle BP, Kalnæs S, Gao T (2015) Low-emissivity materials for building applications: a state-of-the-art review and future research perspectives. Energy Build 96:329–356

King D, Browne J, Layard R, O'Donnell G, Rees M, Stern N, Turner A (2015) A global Apollo programme to combat climate change

Kistler S (1931) Coherent expanded aerogels and jellies. Nature 127(1931):741–751

Kistler S, Caldwell A (1932) Thermal conductivity of silica aerogel. Ind Eng Chem 26(6):658–662

Liang H, Ho M (2007) Toxicity characteristics of commercially manufactured insulation materials for building applications in Taiwan. Constr Build Mater 21:1254–1261

Littorin M, Truedsson L, Welinder H (1994) Acute respiratory disorder, rhino conjunctivitis and fever associated with the pyrolysis of polyurethane derived from diphenylmethane diisocyanate. Scand J Work Environ Health 20:216–222

Marczynski B, Czuppom A, Hoffarth H, Marek W, Baur X (1992) DNA damage in human white blood cells after inhalation exposure to 4, 4'-methylenediphenyl diisocyanate (MDI)-case report. Toxicol Lett 60:131–138

Meyer HP (2011) Sustainability and biotechnology. Org Process Res Dev 15(1):180–188

NR (2014) Energy efficient buildings: Europe. navigant research. http://www.navigantresearch.com/research/energy-efficient-buildings-europe

Pacheco-Torgal F (2014) Eco-efficient construction and building materials research under the EU Framework Programme Horizon 2020. Constr Build Mater 51:151–162

Pacheco-Torgal F, Jalali S (2011) Nanotechnology: advantages and drawbacks in the field of construction and building materials. Constr Build Mater 25(2):582–590

Pacheco-Torgal F, Fucic A, Jalali S (2012) Toxicity of building materials. Woodhead Publishing Limited Abington Hall, Cambridge

Pacheco-Torgal F, Faria J, Jalali S (2013a) Embodied energy versus operational energy. Showing the shortcomings of the energy performance building directive (EPBD). Mater Sci Forum 730–732:587–591

Pacheco-Torgal F, Diamanti MV, Nazari A, Granqvist CG (2013b) Nanotechnology in eco-efficient construction. Woodhead Cambridge, UK

Papadopoulos A (2005) State of the art in thermal insulation materials and aims for future developments. Energy Build 37:77–86

Papaefthimiou S, Syrrakou E, Yianoulis P (2006) Energy performance assessment of an electrochromic window. Thin Solid Films 502:257–264

Pikas E, Kurnitski J, Liias R, Thalfeldt M (2015) Quantification of economic benefits of renovation of apartment buildings as a basis for cost optimal 2030 energy efficiency strategies. Energy Build 86:151–160

Power A (2008) Does demolition or refurbishment of old and inefficient homes help to increase our environmental, social and economic viability? Energy Policy 36:4487–4501

Roetzel A, Tsangrassoulis A (2012) Impact of climate change on comfort and energy performance in offices. Build Environ 57:349–361
Sandrolini F, Franzoni E (2010) Embodied energy of building materials: a new parameter for sustainable architectural design. Int J Heat Technol 27:163–167
Santamouris M, Synnefa A, Karlessi T (2011) Using advanced cool materials in the urban built environment to mitigate heat islands and improve thermal comfort conditions. Sol Energy 85:3085–3102
Sartori I, Napolitano A, Voss K (2012) Net zero energy buildings: a consistent definition framework. Energy Build 48:220–232
Schultz J, Jensen K, Kristiansen F (2005) Super insulating aerogel glazing. Sol Energy Mater Sol Cells 89:275–285
Shealy M, Dorian J (2009) Growing Chinese coal use: dramatic resource and environmental implications. Energy Policy 38:2116–2122
Skarping G, Dalene M, Svensson B, Littorin M, Akesson B, Welinder H, Skerfving S (1996) Biomarkers of exposure, antibodies, and respiratory symptoms in workers heating polyurethane glue. Occup Environ Med 53:180–187
Smith GB, Granqvist CGS (2010) Green nanotechnology: solutions for sustainability and energy in the built environment. CRC Press, Taylor & Francis Group, London
Szalay A (2007) What is missing from the concept of the new European building directive? Build Environ 42:1761–1769
Tavares P, Gaspar A, Martins A, Frontini F (2015) Electrochromic windows impact on energy performance of buildings in Mediterranean climates: a case study. In: Pacheco-Torgal F, Labrincha JA, Cabeza LF, Granqvist CG (eds) Eco-efficient materials for mitigating building cooling needs: design, properties and applications. Woodhead, Cambridge, pp 499–524
Thiers S, Peuportier B (2012) Energy and environmental assessment of two high energy performance residential buildings. Build Environ 51:276–284
UNEP (2013) The emissions gap report 2013. United Nations Environment Programme (UNEP), Nairobi
UNFCCC (2013) Compilation of information on mitigation benefits of actions, initiatives and options to enhance mitigation ambition. UNFCCC document FCCC/TP/2013/4. United Nations Office at Geneva, Geneva
Ürge-Vorsatz D, Novikova A (2008) Potentials and costs of carbon dioxide mitigation in the world's buildings. Energy Policy 36(2):642–661
Ürge-Vorsatz D, Cabeza L, Serrano S, Barreneche C, Petrichenko K (2015) Heating and cooling energy trends and drivers in buildings. Renew Sustain Energy Rev 41:85–98
WEO/IEA (2013) World energy outlook 2013 executive summary. International Energy Agency, Paris
WHO (2014) Urban population growth. Global health observatory
Williams J, De Benedictis A, Ghanadan R, Mahone R, Moore J, Morrow W, Price S, Torn M (2012) The technology path to deep greenhouse gas emissions cuts by 2050: the pivotal role of electricity. Science 335(6064):53–59, 6 Jan 2012
World Bank (2014) World development indicators: electric power consumption per capita in 2011. http://wdi.worldbank.org/table/5.11
Xing Y, Hewitt N, Griffiths P (2011) Zero carbon buildings refurbishment—a hierarchical pathway. Renew Sustain Energy Rev 15:3229–3236
Xu H, Yang Y (2012) Bioplastics from waste materials and low-value byproducts. ACS Symp Ser 1114:113–140
Yoshimura K, Yamada Y, Bao S, Tajima K, Okada M (2009) Preparation and characterization of gasochromic switchable-mirror window with practical size. Sol Energy Mater Sol Cells 93:2138–2142.

Chapter 2
Aerogel Plasters for Building Energy Efficiency

C. Buratti, E. Moretti and E. Belloni

Abstract Nowadays in many countries, the building sector is the largest energy consumer and one of the best ways to reduce energy demand of buildings is the reduction in heat losses through the envelope. In this scenario, insulating materials with aerogels have growing interest and new applications such as insulating aerogel-based renderings are in development. This chapter deals with the analysis of superinsulating applications for building envelope such as aerogel-incorporated concrete- and aerogel-based renders. After an overall analysis of the market trend for these innovative systems, the rendering compositions, the physics, thermal, acoustic, and hygrothermal properties of aerogel-based renders are discussed. In situ applications of the new developed render are analyzed and the potential of the investigated materials is highlighted, by considering experimental measurements in Sect. 2.4. Finally, a comparison with traditional solutions and the future trends are considered.

2.1 Introduction

Thermal insulation in buildings contributes to reduce the size of the heating and cooling systems and the annual energy consumptions. In particular, in Italy, at least 90 % of buildings were constructed before 1991, the year of the Frame Law on Energy Saving, and they are not in compliance with the current regulations for the

C. Buratti (✉) · E. Moretti · E. Belloni
Department of Engineering, University of Perugia, via G. Duranti 63, 06125 Perugia, Italy
e-mail: cinzia.buratti@unipg.it

E. Moretti
e-mail: elisa.moretti@unipg.it

E. Belloni
e-mail: belloni.unipg@ciriaf.it

F. Pacheco Torgal et al. (eds.), *Nano and Biotech Based Materials for Energy Building Efficiency*, DOI 10.1007/978-3-319-27505-5_2

most part (the most recent norms date from 2006). Therefore, all these buildings would need refurbishment in order to be compliant with normative targets.

The application of innovative solutions can be therefore a useful tool not only for new constructions, but also for the refurbishment of existing buildings, in order to reduce the heat losses of the envelope. Many transparent insulating systems have been proposed and their optical, thermal, and acoustic properties have been investigated at the University of Perugia since 2003, with both experimental campaigns and simulation codes (Buratti and Moretti 2013, 2014; Tabares-Velasco et al. 2012; Kalnæs and Jelle 2015; Buratti et al. 2012, 2016; Moretti et al. 2014; Cotana et al. 2014): Silica aerogel, in particular, is a highly porous nanostructured and light material, and it represents an innovative alternative to traditional solutions because of the high thermal performance (low thermal conductivity 0.014 W/m K) and low density (about 3 kg/m^3). Nevertheless, the costs of the material are high for cost-sensitive building industry and this is a limit for a wide spread of the material in the market. Research aims to improve the insulation performance and to decrease the aerogel production costs. The optical transparency property allows its use for insulating window facades and window panes, but this is only one of the possible applications in the building sector. Aerogel blankets/panels have been developed to as insulation panels for building walls and grounds (Aspen Aerogels 2012). Moreover, the increasing of the thermal performance of wood and steel with local aerogel insulation has been studied by means of experimental tests (Ibrahim et al. 2014b): R-value of wood-framed walls is improved by 9 % and the one of steel-framed walls by 29 %. Recently, other types of silica-aerogel-based materials used in buildings are the aerogel-incorporated mortars/plasters and aerogel-based concretes (Gao et al. 2014; Kim et al. 2013).

In this chapter, some examples of opaque aerogel-based materials are presented with a particular attention on new insulating rendering based on silica aerogel. After a general overview of these materials, the performance assessment of aerogel-based renders are analyzed. Finally, in situ applications of this new material for building refurbishment are described.

2.2 Aerogel-Incorporated Concrete and Plasters: A General Overview

In this section, the attention will be focused on superinsulating coatings such as render and concrete. These kinds of application are important when the thermal buildings insulation would be improved with a small thickness increase of the walls. Generally, lightweight concrete has many important applications in modern buildings, thanks to its strength/weight ratio and heat and sound insulation characteristics higher than the ones of traditional solutions (Kiliç et al. 2003). Lightweight aggregates such as pumice, diatomite, volcanic cinders, and perlite can be added in the mixture in place of normal aggregates (i.e., sand and rocks), but an

intelligent selection of them is necessary in order to avoid possible interactions with the binder phase. The advantage of these concretes is the better thermal insulation properties when compared to conventional solutions, due to the large amount of air void in the matrix. Aerogel is a perfect aggregate for lightweight and thermal insulating concrete, thanks to its extremely low density (3–100 kg/m^3 depending on the porosity), its low thermal conductivity (0.003–0.02 W/m K), and its good fire and acoustic resistances. Nevertheless, the application of this innovative material in thermal insulating concrete has not been widely spread because of the still high manufacture cost of aerogel. Moreover, a limited number of studies are available for aerogel-based thermal insulating renders, due to the high cost. Nevertheless, innovative solutions for thermal insulating plasters based on the materials with pore size in nanometer range, such as aerogel, could reach good thermal performance with a small thickness (Barbero et al. 2014).

2.2.1 Literature Review

Ratke (2008) presented a new application of aerogel-incorporated concrete with interesting fire and sound resistance, and Kim et al. (2013) reported the insulation performance of aerogel cement prepared with aerogel powder and cement paste. Different percentages of aerogel with respect to the mixture mass were considered, ranging from 0.5 to 2 wt%. Also 20 % of pozzolan, composed by SiO_2 and Al_2O_3, was substituted for cement in order to prevent detrimental expansion of the samples. Results are reported in Table 2.1: The thermal conductivity of aerogel cement with an aerogel mass fraction of 2.0 wt% decreased of about 75 %; considering the aerogel cement with 2 % of aerogel and 20 % of pozzolan, the reduction is about 72 %.

Recently, insulating coatings based on silica aerogels have been developed. In particular, a lightweight aerogel-incorporated concrete (AIC) was prepared by replacing the normal aggregate of concrete with silica aerogel particles (Gao et al. 2014). AIC samples were prepared by adding cement, sand, silica fume, water, superplasticizer, and aerogel particles. The cement used has a density of about 3140 kg/m^3; hydrophobic aerogel granules with a density of 100 kg/m^3 was added (the percentages in volume vary in 0–60 % range) together with distilled water (the water–binder (w/b) ratio was set to 0.4). The thermal conductivity of AIC samples

Table 2.1 Percentages of decrease in thermal conductivity of aerogel cement (adapted from Kim et al. 2013)

	Aerogel cement				Aerogel cement and pozzolan			
Aerogel content (wt%)	0	0.5	1	2	0	0.5	1	2
Thermal conductivity (W/m K)	0.51	0.38	0.27	0.13	0.56	0.45	0.33	0.10
Percentage of decrease	–	26	47	75	–	9	29	72

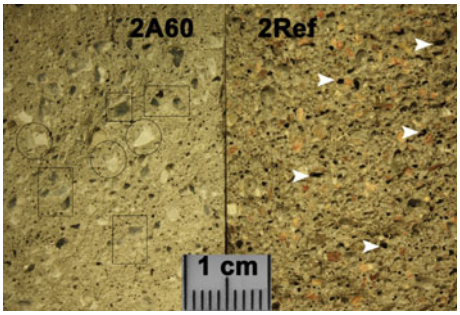

Fig. 2.1 Optical imagines of AIC samples (2A60) compared to the plain concrete sample (2Ref) (Gao et al. 2014)

was analyzed by using a Hot-disk Thermal Constants Analyzer (model TPS 2500S) and a disk-type Kapton Sensor 5465, which acts both as heat source and temperature record. Figure 2.1 shows the imagine of a AIC sample with 60 % of aerogel in volume (2A60) compared to a reference concrete sample: The cement paste in the AIC samples has less air voids than those of the reference sample because the aerogel particles affect the air entrainment by gas diffusion due to the porous nature and the large surface area of aerogel particles.

Moreover, the absorbed CO_2 in aerogel particles would react with $Ca(OH)_2$ from the binder phase to form $CaCO_3$ during the curing process, which changes also the microstructure (see the area marked with circles). Generally, the aerogel content increasing corresponds to a density decreasing: Considering a percentage of aerogel in volume equal to 60 %, the density is about 1000 kg/m^3, compared to 1980 kg/m^3 of the reference plain concrete sample (reduction of about 50 %). Also in this case, the thermal conductivity of AIC decreases [the same behavior is as shown in Kim et al. (2013)]: The reference plain concrete has a thermal conductivity of about 1.86 W/m K, whereas the AIC sample with the aerogel content of 60 vol.% shows a thermal conductivity of only 0.26 W/m K (decreasing of about 86 %) (Fig. 2.2). Also the compressive strength was measured and a value of about 8.3 MPa was obtained considering an aerogel content of 60 %, while the compressive strength of the reference concrete is about 55 MPa, showing a decrease of about 85 %. At an aerogel content of 40 vol.% where a minimum compressive strength of 20 MPa was maintained, the AIC samples registered a thermal conductivity of 0.8 W/m K, rendering this system unfitting for specific insulating purposes (Gao et al. 2014).

Also Serina et al. (2015) shows an experimental investigation of aerogel-incorporated mortar (AIM) with up to 80 vol.% aerogel, prepared by using a reduced ultrahigh-performance concrete (UHPC) mixture. Mechanical strength properties of cured AIM samples were measured according to DIN EN 196-1 standard, while the thermal conductivity was measured with the same Hot-disk Thermal Constants Analyzer of the type TPS 2500S. Both flexural and compressive strength decreased with aerogel loading: When only 20 vol. % aerogel was presented, a difference of 42 % (from 120 to 70 MPa) in compressive strength was

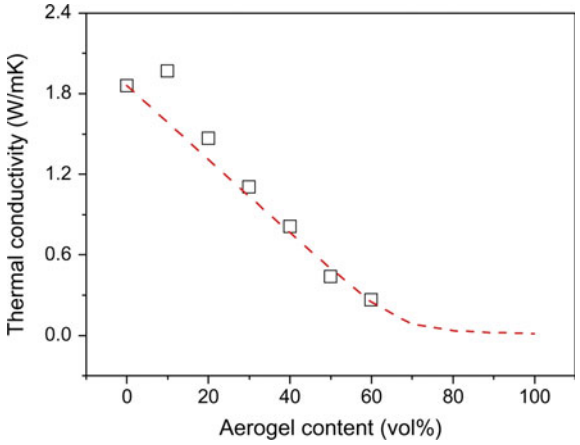

Fig. 2.2 Thermal conductivity of AIC versus aerogel content variations (Gao et al. 2014)

observed. The AIM sample with 50 vol.% aerogel content has a thermal conductivity of about 0.55 W/m K and a compressive strength of 20 MPa; it decreases by almost 4–6 MPa, while only a 20 % reduction in thermal conductivity is obtained, when aerogel content increases to 70 vol.%. By an aerogel loading of 80 %, the compressive strengths were very low (about 4 MPa).

Finally, Fickler et al. (2015) developed a high-performance aerogel concrete by embedding silica aerogel granules in high-strength cement matrix: In this work, a new aerogel-based construction material with extraordinary heat-insulating and load-carrying properties was examined. Various mixtures were examined in terms of their compressive strength and thermal conductivity: Considering 70 % in volume of silica aerogel, the bulk density and the compressive strength decreased in comparison with conventional concrete. The compressive strength could be increased by reducing the percentage of aerogel granules to a minimum of 60 % of volume. The thermal conductivity was determined with the transient hot bridge (THB) measurement principle: Good heat-insulating properties were observed, values variable in the range 0.16–0.37 W/m K were measured, considering a compressive strength variable between 6 and 23 MPa.

A new kind of insulating plasters based on silica aerogel granules has been developed (Stahl et al. 2012); it consists of hydrophobized granular silica aerogel (60–90 vol.%) and contains a purely mineral- and cement-free binder and some additives which enhance the workability of the rendering. It can be applied to walls both manually or by plastering machines. The thermal conductivity has been measured by a special hot plate device (sample dimensions 65 mm × 65 mm and 12–13 mm in thickness). The samples were made manually and dried in a climatic chamber (23 °C, 50 % r.H.) for 28 days. Measurements were carried out for at least 20 samples. Also water vapor transmission resistance was determined by the dry cup method, according to the European standard EN 12086. Conventional insulation renders were also tested in order to compare the results with traditional solutions. For all the plasters, the thermal conductivity increases when samples were

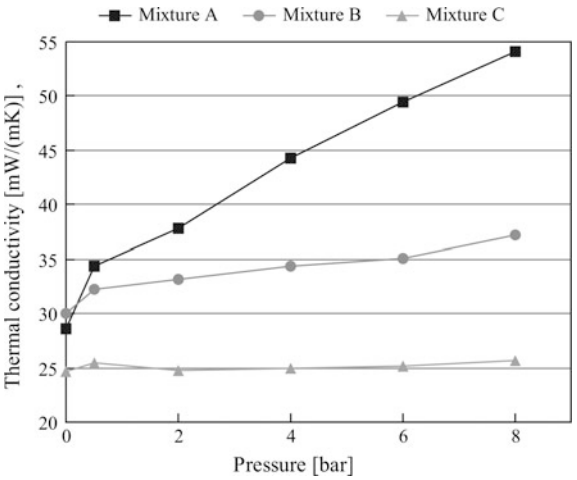

Fig. 2.3 Thermal conductivity of different rendering mixtures as functions of the pressure in the steel pressure vessel (Stahl et al. 2012)

produced by the plastering machine compared to manually produced ones: it was due to the higher water inserting into the render by using plastering machines. The measured thermal conductivity of the aerogel render is 0.025 W/m K and the density is 200 kg/m^3: the λ value is very low in comparison with traditional coatings (0.065–0.103 W/m K). This thermal conductivity generally increases when production pressures increase (Fig. 2.3—Mixture A, with cement binders) because liquid water enters the nanopores of the aerogel granule due to the high pressure, it remains trapped and will take a very long time to dry. The dependence from pressure can be reduced avoiding cement binders in the mixture (see mixture B and C, without cement binders with two different procedures).

Achard et al. (2011) (WIPO Patent WO/083174) developed another innovative insulating rendering based on silica aerogel. It consists of water, a mineral and/or organic hydraulic binder, insulating filler comprising a powder or granules of hydrophobic silica aerogel, and other filler and additives (option). The rendering has been developed mainly for exterior wall surface applications. The coating thermophysical characteristics are presented in Table 2.2. The measured thermal conductivity is only 0.0268 W/m K, very low in comparison with traditional renders (0.2–0.05 W/m K). Unfortunately, the production costs are still high in comparison with other traditional insulation materials and it will be illustrated below (Huang 2012). Moreover, the mechanical properties are still not sufficient enough and reinforcing mesh should be added.

Table 2.2 Thermophysical properties of new aerogel insulating coatings (adapted from Ibrahim et al. 2014c)

Thermal conductivity (W/m K)	0.0268
Specific heat (J/kg K)	990
Density (kg/m^3)	156 (dry)
Vapor diffusion resistance factor (−)	4.25
Water absorption coefficient (kg/m^2 s$^{1/2}$)	0.184

2.2.2 Market Survey

Innovative solutions for thermal insulating plasters could make a significant contribution to energy savings. Aerogel-based renders have high thermal resistances, and high thermal performance can be reached by applying them also in small thicknesses. But new plaster solutions have to respond to specific economical and technical features, in order to be spread in the market. An overall analysis of the thermal insulating plasters in European market was carried out by Barbero et al. (2014). Different characteristics were evaluated for each plaster: the volume mass powder, the dry bulk density of the hardened mortar, the thermal conductivity, and the costs. Currently, the nanomaterials and all the products made with them are more expensive than other commercial solutions.

A market survey was carried out considering all the European countries and in particular the western ones that represent the colder part of the Europe. Technical, chemical, and physical data and the price information of these plasters were directly supplied by each producer and manufacturer. The names of the manufacturers and the commercial products were not published for privacy reasons. The examined plasters were divided into two families: cement-based insulating plasters and natural hydraulic lime-based plasters. The incidence of the cost was evaluated considering both the cost per square meter of each plaster necessary to obtain the same final thermal resistance R_x equal to 1 m^2 K/W and the cost per functional unit (the reference unit is the money required to make 10 mm of thickness). Table 2.3 shows the prices of the analyzed plasters: the average cost of the cement-based products with the same thermal performance is €43/sqm, while the average cost of the natural hydraulic lime-based plasters is €82/sqm. In comparison with these plasters, it is possible to consider the aerogel-based plaster developed and studied by Buratti et al. (2014): the costs of the natural lime plaster with 80 % of granular aerogel is expected to be about 8 €/sqm, considering a thickness of 1 mm of the coat. In this case, the commercial solution of the Agosti Nanotherm aerogel-including render was considered (λ = 0.045 W/m K and 80–90 % in volume of aerogel granules): Higher percentage of aerogel in the mixture can be added to obtain a final render with a thermal conductivity less than 0.02 W/m K. In this context, the large-scale production of aerogel-based plasters can improve the spread of new render solutions, by modifying the final costs of the product and the production system.

In the European market, an aerogel-incorporated render solution is Fixit 222 (Fixit, Fixit 222 Aerogel Hochleistungsdämmputz, 2015), by EMPA (Filate 2014, EMPA 2015). This is another very good product with a density of hardened mortar of 220 kg/m^3 and a thermal conductivity of only 0.028 W/m K. The product has very good performances, and it can be applied in the same way of standard renders (about 2 kg/m^2 for a thickness of 10 mm are necessary). The cost of this material is about 80–90 €/m^2 considering a thickness of 10 mm of the coat (8 €/m^2 for s = 1 mm). It can be compared with conventional plasters shown in Table 2.3: the cost is higher than the ones of traditional plasters, but the thermal conductivity of Fixit 222 is very low in comparison with the others. However, these aerogel-based

Table 2.3 Pricing table of conventional plasters (adapted from Barbero et al. 2014 and Röfix, Fixit Group 2014)

Product	Type	Thermal conductivity (W/m K)	Price [€/sqm R_x for s = 10 mm]	Thickness R_x (mm/sqm)	Price [€/sqm R_x]
1	Cement-based plaster	0.055	3.590	55	19.75
2	Cement-based plaster	0.090	5.437	90	48.94
3	Cement-based plaster	0.074	3.700	74	27.38
4	Cement-based plaster	0.056	4.440	56	24.64
5	Cement-based plaster	0.090	5.200	90	46.80
6	Cement-based plaster	0.062	3.520	62	21.82
7	Cement-based plaster	0.075	4.587	75	34.40
8	Cement-based plaster	0.111	10.840	111	120.32
9	Lime-based plaster	0.200	11.500	200	230.00
10	Lime-based plaster	0.075	8.550	75	64.13
11	Lime-based plaster	0.060	4.800	60	28.80
12	Lime-based plaster	0.091	5.840	91	53.14
13	Lime-based plaster	0.066	11.080	66	73.13
14	Lime-based plaster	0.088	5.360	88	47.17
15	*Aerogel-based plaster Fixit 222*	*0.028*	*80.000*	*28*	*224.00*

solutions are applied as finished paintings and their application thicknesses are very low (about 3–5 mm).

For further information, it can be useful to analyze the influence of the aerogel costs on the optimum thickness of the coating. Figure 2.4 shows the optimum coating thickness for different aerogel costs (from 600 to 2000 €/m^3): As the cost increases the optimum, thickness value decreases (Ibrahim et al. 2015). The higher initial costs due to the application of the coating make difficult their recovery by means of energy savings.

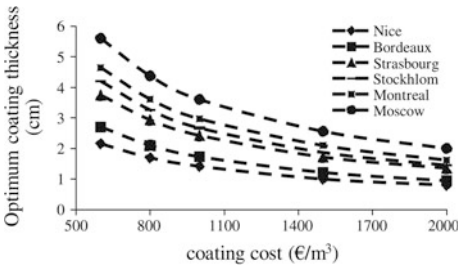

Fig. 2.4 Effect of the aerogel cost on the optimum thickness (Ibrahim et al. 2015)

2.3 Performance Assessment of Aerogel-Based Renders

In this section, the performance assessment of aerogel-incorporated renders is examined considering different points of view. Firstly, different experiences of aerogel-based render manufacturing techniques and their in situ applications will be described. As shown below, the most important characteristics of the innovative renders are the thermal insulation, the acoustic performance, and the hygrothermal properties. The innovative renders have a thermal conductivity very low with respect to traditional solutions (reduction up to 90–96 %) and a better acoustic absorption coefficient when compared to the same plaster without aerogel. Considering the hygrothermal properties, it will be shown that the new renders are able to efficiently reduce the moisture formation.

2.3.1 Rendering Mixing and Setup

Insulation plasters can be applied to external and internal walls. Thanks to its mineral basis, the new plaster is very similar to the original historical building materials, and it is ideal for use on old buildings, on internal as well as external surfaces, offering a noninvasive method for renovating historic buildings and for saving energy without altering their aspect.

The production and in situ setup of the aerogel-based renders are very important. The manufacturing step and the installation of the aerogel-incorporated plaster are described in Buratti et al. (2014). The aerogel in the renders has nanometer-sized pores and consists of 90–98 % of air.

The coating was manufactured by manually mixing natural lime with granular aerogel in different percentages, allowing the absorption of air in the mix. In this way, the density of the plaster decreases of about 90 %. Different kinds of calcium hydroxide were considered, and different percentages of aerogel were mixed in the first mixing phases. Firstly, only a 50 % of aerogel in volume was considered (the thermal conductivity varied in 0.08–0.06 W/m K range). The good properties of the natural lime maturing are important in order to obtain a good quality of the final

Fig. 2.5 Various steps of the mixing: (**a**) original components; (**b**) mixing phase; (**c**) final composition of the plaster (Buratti et al. 2014)

composition. Water was added slowly, in order to obtain a uniform mixture with all aerogel particles having uniform coating of cement floating. The preparation of the product is made by mixing the two components in a bucket: This phase should be slow, accurate, in order to avoid the pulverizing of the granules. The original size of the aerogel granules is usually about 3–4 mm and they are irregular in shape: after the mixing phase, the granules are partially broken, but they are not completely pulverized. In the final mix, the particle dimensions are included in the 0.1–2 mm range. Aerogel granule dimensions have not to be very small because the plaster becomes hydrophobic and its binder properties decrease, even if the thermal conductivity is the same.

Figure 2.5 shows the mixing steps of the different components of the plaster (granular aerogel, calcium hydroxide, and water). The new coating has also the advantage to be simultaneously water repellent and permeable to water vapor. It is much more breathable than conventional plasters, and its surface does not become wet. The hydrophobic nature of aerogel is important because the aerogel particles incorporated into renders avoid the water absorption that could change the volumetric composition of the final mix and the thermal performance.

The direct spray in situ application of the new plaster on to brickwork is represented in Fig. 2.6. The installation is very easy also in complex wall geometries. Moreover, it is possible to eliminate gaps where moisture could form, reducing condensation inside walls that can cause mold.

Also Achard et al. (2011) describe the composition of an innovative insulating coating based on silica aerogel: It consists of water, a mineral hydraulic binder, insulating filler and, in particular, a powder of silica aerogel in granules, and other possible additives and structuralizing fillers. The render is made of aerogel granules used in place of sand and inert, that are usually inserted in conventional coatings. Aerogel granules are industrially manufactured in a specialized plant; then, the mortar/render is prepared industrially as a dry mixing of all the mentioned components; the mix is then stored in bags and transported to the site for use. Finally, the product is mixed with water in order to obtain a viscosity suitable for the application on-site, for example, by spraying on the wall surface.

Fig. 2.6 In situ application of the aerogel-based plaster (courtesy of Agosti Fabrizio, Agosti Nanotherm s.r.l., Naturalcalk-Tillica 2015)

2.3.2 *Thermal Properties*

Thermal conductivities were evaluated in some research works (Stahl et al. 2012; Achard et al. 2011) already described in Sect. 2.2.1. In these cases, aerogel-based renders with thermal conductivities of 0.025 and 0.027 W/m K were performed.

Stahl et al. measured a thermal conductivity of 0.025 W/m K at a density of about 200 kg/m^3. The sample was produced by means of a plastering machine to real-use condition, and a number of commercially available insulating renders was also realized in order to compare the results. All the thermal conductivity measurements were carried out by a guarded hot plate apparatus. The comparison is shown in Table 2.4.

Achard et al. measured the thermal conductivity by means of guarded hot plate and heat flow meter, according to the EN ISO standard 12667. The heat is measured

Table 2.4 Thermal conductivity of insulation renderings in comparison (adapted from Stahl et al. 2012)

	Thermal conductivity (W/m K)	Insulating additives	Density [kg/m^3]
Render 1	0.103	Perlite, cork	432
Render 2	0.099	Mineral	478
Render 3	0.067	Expand polystyrene (EPS)	297
Render 4	0.072	Expand polystyrene (EPS)	318
Render 5	0.072	Expand polystyrene (EPS)	250
Aerogel render	0.025	Aerogel	200

Table 2.5 Thermal measurement results for the examined samples (Buratti et al. 2014)

Specimens	Description	Percentage of granular aerogel in volume (%)	Density ρ (kg/m^3)	Thermal conductivity λ (W/m K)
T0	Natural plaster without aerogel	–	2200	0.50
T1	Natural plaster with granular aerogel	80–90	300–275	0.050–0.045
T2	Natural plaster with granular aerogel	91–95	136–126	0.021–0.019
T3	Natural plaster with granular aerogel	96–99	125–115	0.016–0.014

by means of differential scanning calorimeter (DSC) according to NF EN 1159-3 standard. The density is measured in compliance to the NF EN 1602 standard, and the vapor diffusion resistance factor is measured according the NF EN ISO 12572 standard by means of the cup method. The thermal conductivity obtained is only 0.027 W/m K (with a density of about 156 kg/m^3), better than the ones measured for traditional insulating materials (0.034–0.050 W/m K is obtained, for example, for mineral wool, glass wool, and foam glass), and it can be very useful in order to limit heat losses through thermal bridges both in new and existing buildings.

Considering the thermal characterization of the material, also the research activities of Buratti et al. (2014) are reported. Four kinds of insulating aerogel-based plasters were tested by means of a heat flow meter apparatus and the thermal conductivity of the specimens was calculated in compliance with EN ISO 12667 standard. Natural lime plasters with granular aerogel in different percentages were tested.

Table 2.5 shows the properties of the samples (density, percentage of granular aerogel in the mix) and the thermal conductivity measured. The density of the plaster decreases when aerogel is added in the mix and also the thermal conductivity decreases by about 90–97 %, due to the highly porous light aerogel nature. In fact, granular silica aerogel has a density of about 50–200 kg/m^3 and a thermal conductivity variable in the 0.013–0.018 W/m K range. Nevertheless, for aerogel types T2 and T3, the mechanical resistance of the plasters decreases a little bit because of the high porosity of the aerogel added in the final mix. A good solution that can be launched on the market also characterized by good mechanical resistance properties is the innovative plaster type T1, with an 80 % aerogel (0.050 W/m K). Finally, the compressive strength of this innovative plaster is only 0.36 MPa, very low considering the values obtained for standard mortars (2–12 MPa).

2.3.3 Acoustic Performance

Sound absorption properties of aerogel-based renders were investigated by Buratti et al. (2014). The tests were carried out by means Kundt's tube in order to estimate the acoustic absorption coefficient of the material.

The normal incidence absorption coefficient was measured by means of two-microphone impedance tube (Brüel & Kjær, Nærum, Denmark, model 4206) using the transfer function method and cylindrical samples with diameters of 29 and 100 mm (combined frequency from 50 to 6400 Hz), according to ISO 10534-2 standard (ISO 10534-2 1998 and UNI 10351 1994). Plasters of natural lime with a percentage of granular aerogel of about 80 % was applied to a plasterboard support (thickness 12.5 mm); a preliminary test was carried out considering the only plasterboard support (type A0), in order to establish a reference value for the comparison.

Two kinds of plaster were tested (the thickness of the only plaster is 10 and 30 mm, respectively); in both the samples, a final coat of 2 mm was applied, for a total thickness of 24.5 mm (type A1) and 44.5 mm (type A2), respectively; three specimens were tested for each type and an average trend was analyzed. Figure 2.7 shows the average normal incidence absorption coefficient trends for the samples (large tube measurements); the absorption coefficient of A0 is lower than the others (smaller than 0.05 in 100–1600 Hz range). By increasing thickness, the greatest shift is toward lower frequencies; two picks of the absorption coefficient are observed: for A1 at frequencies 700–800 Hz, for A2 at 400–500 Hz.

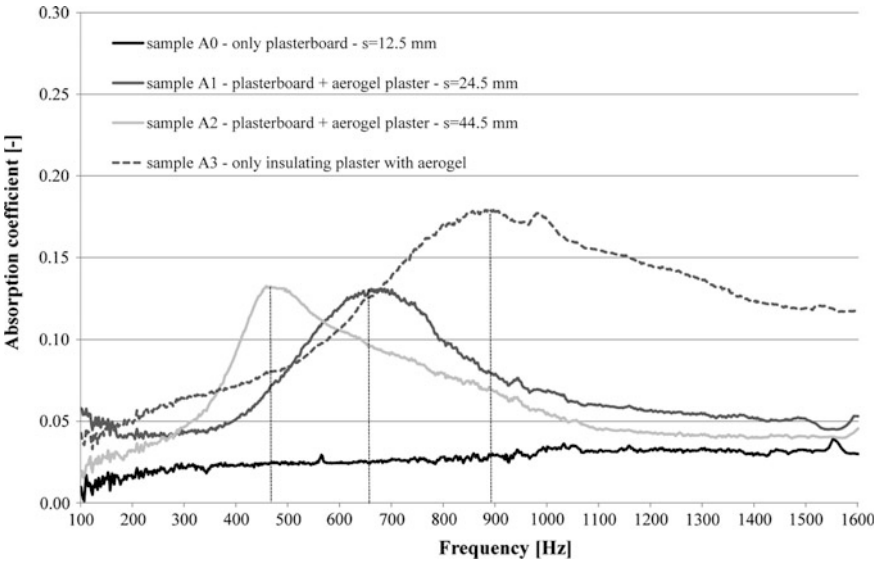

Fig. 2.7 Absorption coefficient at normal incidence (large tube measurements, 100–1600 Hz): comparison with insulating plaster (without final coat) (Buratti et al. 2014)

The acoustic properties of the only insulation plaster with aerogel were measured by removing the final coat layer of the specimens. The absorption coefficient trend of A3 was higher than the others: The final coat of the sample makes the acoustic behavior worse (Fig. 2.7).

It can be observed that the absorption coefficient strongly depends on the final coat, so the aerogel-based plaster layer moderately influences the final value; in any case, the normal incidence absorption coefficient values of the aerogel-incorporated plasters are not very high at all (always small than 0.2). Finally, the evaluation of the noise abatement properties of the render was not considered till now, but this property is not so incisive because of the small thickness of the aerogel-based render applied to a wall.

2.3.4 Hygrothermal Performance

The hydric performance is very important in building envelope design. Moistures problem can cause wood decay, mold growth, poor indoor air quality, corrosion of metals, damage to materials, and loss of structural strength. For these reasons, the installation of external or internal water vapor barriers is often required.

In order to examine the hygrothermal behavior of a patented insulating render based on silica aerogel, a numerical model was developed and an experimental campaign was carried out by Ibrahim et al. (2014c). The aim of the work was the analysis of the hygrothermal performance of walls with new renderings and the comparison with different thermal insulation configurations. The hygrothermal behavior was modeled by using the software WUFI: The numerical model was validated by means of an experimental setup on a test cell having the aerogel-based renders on its south wall. The experimental test unit was built in 1984 (Krauss 1985) at PERSEE in University of Nice Sophia Antipolis, in the southeast of France. It is composed of three cells (current test cell, adjacent cell, and acquisition cell): the test cell (total volume 30 m^3) has two external walls (southeast exposure) and two internal walls (partitions with the other cells). No windows are present in order to avoid the effect of the solar gains. The south wall was considered as test wall. The original stratigraphy of the walls is as follows: concrete (external layer, s = 0.25 m), glass wool (s = 0.16 m), and plaster (internal side, s = 0.013 m). A layer of aerogel-based render was applied at the exterior surface of this wall (s = 0.04 m). The hygrothermal sensor was positioned between the concrete and the external aerogel-based plaster. The experimental campaign was carried out during the two weeks in summer: The validation of the model was carried out considering the measured and simulated temperatures and relative humidity at the interface between the concrete and the aerogel-based coating.

After the model validation, different simulations were examined considering the city of Grenoble (semi-continental French climate, with cold winter and warm summer and abundant rain). It is one of the warmer cities of French in summer (more than 35 °C); in winter, the temperatures are generally very low and the daily

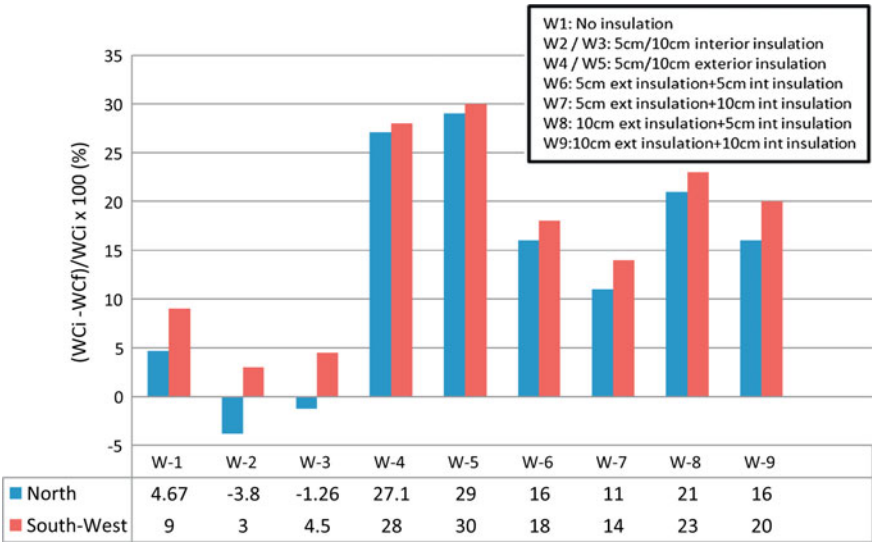

Fig. 2.8 Dryness rate (*DR*) for different walls (Ibrahim et al. 2014c)

Table 2.6 Wall assembly insulation configurations (adapted from Ibrahim et al. 2014c)

Case	Layer 1	Layer 2	Layer 3	Layer 4
W-1	Concrete 20 cm	Plaster	–	–
W-2	Concrete 20 cm	Polystyrene 5 cm	Plaster	–
W-3	Concrete 20 cm	Polystyrene 10 cm	Plaster	–
W-4	*Aerogel render 5 cm*	*Concrete 20 cm*	*Plaster*	–
W-5	*Aerogel render 10 cm*	*Concrete 20 cm*	*Plaster*	–
W-6	Aerogel render 5 cm	Concrete 20 cm	Polystyrene 5 cm	Plaster
W-7	Aerogel render 5 cm	Concrete 20 cm	Polystyrene 10 cm	Plaster
W-8	Aerogel render 10 cm	Concrete 20 cm	Polystyrene 5 cm	Plaster
W-9	Aerogel render 10 cm	Concrete 20 cm	Polystyrene 10 cm	Plaster

temperature range is high. The simulation results can be compared in terms of dryness percentage (DR) over a period of 4 years (it is the difference between the initial water content and the final one at the end of the simulation period, and it represents the drying power of the wall, see Fig. 2.8). Different insulated walls were considered (Table 2.6).

The best behavior in terms of drying potential of the wall assembly is obtained for walls types W-4 and W-5 [aerogel rendering layer with a thickness of 5 and 10 cm, respectively, and concrete (20 cm)]: DR is about 23 %. Moreover, the dryness rate for exterior insulation is the highest of all configurations. The external application of aerogel-based plaster improves the dryness rate also for walls with an internal insulation layer (W-6, W-7, W-8, and W-9): The effect is better when the

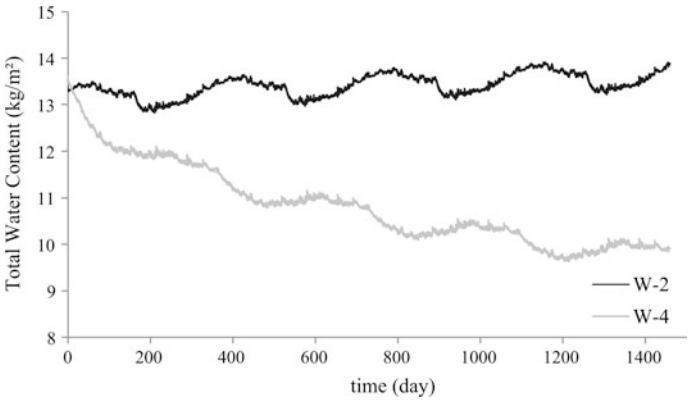

Fig. 2.9 Evolution of the total water content over 4 years for W-2 and W-4 (Ibrahim et al. 2014c)

internal insulation polystyrene has lower thicknesses (5 cm) (W-6 and W-8). Adding the aerogel-based render on the exterior surface of the walls reduces significantly the moisture risks. Figure 2.9 shows the assembly water content over time for a north orientation for two cases: 5-cm polystyrene interior insulation (W-2) and 5-cm aerogel-based rendering exterior insulation (W-4). The drying capacity of the wall decreases considering an interior insulation layer, and the moisture content increases: A vapor barrier is usually added in interior insulating wall. In W-4, the water content decreases and this effect is higher in southwest orientation, thanks to the solar radiation. A heat loss reduction up to 70 % could be achieved thanks to the aerogel-based rendering application and the mold can be easily eliminated.

2.4 Applications in Building Refurbishment

In order to evaluate the real effectiveness of the innovative insulating renders, it is important to examine their in situ applications by experimental monitoring tests. The building's outside envelope interacts with the external environment: External air temperature and solar radiation influence the outside surface temperatures of roofs and walls, and the heat flux through the envelope is affected by fluctuations during the day period. In this context, it is important to carry out deepen researches dealing with optimizing layers configuration in exterior walls. Considering old buildings, it can be useful to analyze their thermal behavior before and after refurbishment actions, such as using aerogel-incorporated renders.

In this section, some examples of in situ applications and a benefit analysis of the new renders are analyzed, considering also a comparison with traditional solutions.

2.4.1 In Situ Applications

The in situ performance of the proposed solutions in different kinds of existent buildings was analyzed considering the refurbishment by using the new plasters (Buratti et al. 2014). Table 2.7 shows the decreasing of the thermal transmittance of different walls, due to the aerogel-based plasters (λ = 0.05 W/m K, 80 % of aerogel). As shown the innovative coating is very effective, above all for a stone wall with a thickness of about 60 cm (type 1) (U value equal to 2.14 W/m^2 K). Applying 5 mm of aerogel-based plaster, the thermal transmittance of the wall becomes 1.73 W/m^2 K (reduction of about 20 %).

Table 2.7 Thermal transmittance values of different types of wall before and after the insulating plastes application (Buratti et al. 2014)

		Before refurbishment		After refurbishment		
Wall type	Description	Total thickness (m)	U value (W/m^2 K)	U value W/m^2 K)	Total thickness (m)	U reduction (%)
1	Stone wall (s = 600 mm), internal and external lime plastered (s = 15 mm)	0.63	2.14	1.73	0.635	19
2	Brick wall (s = 300 mm), internal and external lime plastered (s = 15 mm)	0.33	1.61	1.37	0.335	15
3	Cavity wall (s = 250 mm) (air brick wall 120 mm + 50 mm air gap + air brick wall 80 mm), internal and external lime plastered (s = 15 mm)	0.28	1.10	0.98	0.285	11
4	Cavity wall (s = 250 mm) (air brick wall 120 mm + 50 mm polystyrene + air brick wall 80 mm), internal and external lime plastered (s = 15 mm)	0.28	0.50	0.47	0.285	6

The study of thermal performances can be carried out also by means of simulation model analysis (Cotana et al. 2013). A study of the thermal performance of exterior walls covered with an aerogel-based insulating coating is illustrated by Ibrahim et al. (2014a). A numerical model was developed in order to evaluate the effectiveness of the coating in terms of energy performance and thermal comfort. The reference experimental campaign was described in Sect. 2.3.4: The aerogel-based coating is applied on the exterior surface of the south wall of a test cell.

This experiment was carried out to validate a numerical model using the implicit finite difference scheme (one-dimensional heat conduction equation) under real weather conditions. The energy loads with and without 5 cm of the aerogel-based coating were analyzed considering different construction periods and different climates. Two house models in the period 1968–1974 were considered: the first one (1) with simple-glazed windows and no thermal insulation in the roof and the second one (2) with double-glazed windows and a 6 cm insulation layer in the roof. In the period after 1990, the first type of house (1) has an exterior wall with a 10-cm internal insulation layer and the second kind (2) has no thermal insulation. It can be observed that in old houses (<1974), the percentage of energy reductions are between 40 and 53 % (Mediterranean climate) and 33–40 % in semi-continental climate (Fig. 2.10). Obviously, in new houses the application of the ABC is not very effective and the annual load decreasing is not very high. In any case, the coating application is more interesting and efficient for old uninsulated buildings where a small thickness can reduce a lot the energy load.

In terms of thermal comfort, the number of hours where heating is not needed was analyzed for different coating thicknesses for an old house. It was observed

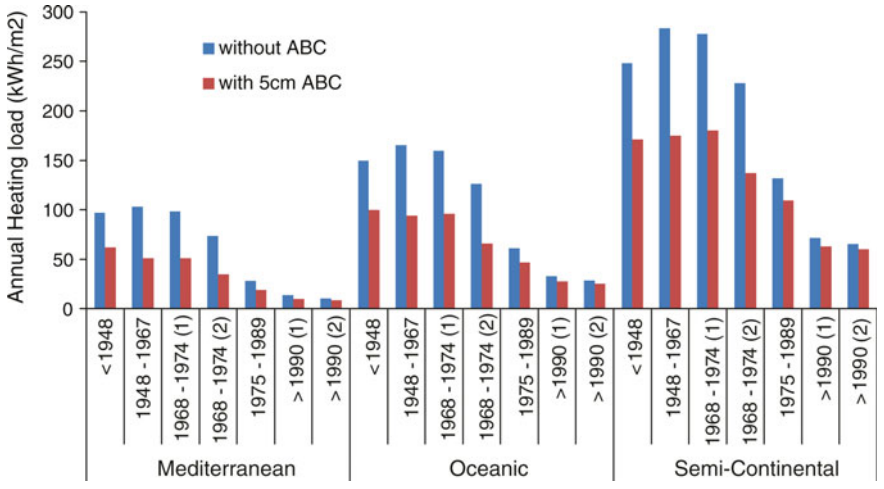

Fig. 2.10 Annual heating loads for different climates and different construction periods (Ibrahim et al. 2015)

that, by increasing the ABC thickness from 0 to 15 cm, the percentage of occupied time where hating is not necessary increases by 10, 6 and 3 %, respectively, for the Mediterranean, Oceanic, and semi-continental climates (Ibrahim et al. 2014a, 2015).

Another study concerning the examination of the long-term behavior of aerogel plaster surfaces (Ghazi Wakili et al. 2015) is described. In situ measurements of temperature, humidity, and heat flux within different layers of a wall were examined. F222 plaster is an aerogel-containing render, easily adaptable to structured façades and a promising solution for improving the thermal behavior of historic buildings. It was applied to the historical building of the Vienna University of Technology with different finishing layers, and a series of temperature and moisture sensors were applied and monitored for 5 months. Four different wall partitions were considered (F1-F4): aerogel plaster F222 was applied (40 mm thick, $\lambda = 0.029$ W/m K) and then covered by the four final finishes (see Table 2.8).

The theoretical value of the thermal transmittance of the walls before the aerogel-based render application is 1.12 W/m^2 K (F0); the U reduction is about 60 % considering the one-dimensional steady-state calculation of U after the refurbishment (0.44 W/m^2 K).

The heat flux through the wall and the internal and external surface temperatures were used in order to find the evolution of the conductance before and after the retrofit. The average method of ISO standard 9869 was used. The thermal transmittance before the refurbishment varies in the 0.97–1.04 W/m^2 K range considering the four kinds of walls (F1-F4); the final values after the refurbishment vary in the 0.58–0.78 W/m^2 K range. The differences depend on the external final finish applied to the walls: Wall type F4 has a humidity value on the external side lower than the other three types, because it has a water-repelling final finish containing silicon resin paint. A similar behavior can be observed for F2 (application of a silicate-paint final finish). For these types of walls, the thermal transmittance is lower (about 0.58–0.60 W/m^2 K).

Table 2.8 Wall type configurations (adapted from Ghazi Wakili et al. 2015)

Case	Layer 1 (15 mm)	Layer 2 (250 mm)	Layer 3 (20 mm)	Layer 4 (40 mm)	Layer 5 (1 mm)
F0	Internal plaster	Hollow bricks	External plaster	–	–
F1	Internal plaster	Hollow bricks	External plaster	F222	External finish R380 + PE819
F2	Internal plaster	Hollow bricks	External plaster	F222	External finish R750 + PE225
F3	Internal plaster	Hollow bricks	External plaster	F222	External finish R380 + PE819S
F4	Internal plaster	Hollow bricks	External plaster	F222	External finish R380 + PE419

Finally, another aspect of the retrofit procedures is the internal comfort condition improvement. In the present paper, Ghazi Wakili et al. (2015) measured the internal air temperatures and the inside surface temperatures: Before the refurbishment, a difference of about 4 °C was observed, reduced to less than 1–2 °C in the post-retrofit conditions.

2.4.2 *Comparison with Traditional Solutions and Benefits Analysis*

In order to evaluate the potential of aerogel-based plasters, a comparison with traditional solutions was carried out by Buratti et al. (2014). In Table 2.9, the thermal conductivities of different types of commercial plasters are compared with the innovative aerogel-based plasters. Traditional plaster values vary in 0.29–0.70 W/m K depending on the type and on the density of the coat.

The thermal benefit of the plaster application in building refurbishment was observed also by means of in situ infrared thermography analysis (Buratti et al. 2014). A three-story apartment was photographed, and a thickness of about 5 mm of aerogel-based plaster ($\lambda = 0.05$ W/m K) was applied on the internal walls of then third floor. On the first and on the second floor, the internal plaster was not applied. The investigated building was built in the 1960s in the north of Italy. The northern façade was considered in order to avoid the influence of the direct solar radiation and the infrared thermography was carried out in autumn (external emissivity

Table 2.9 Comparison with traditional solutions: thermal conductivity values (in Italic innovative plasters, Buratti et al. 2014)

Plasters	Density ρ (kg/m^3)	Thermal conductivity λ (W/m K)
Coating/mortar with different sizes of aggregate	600	0.29
Coating/mortar with different sizes of aggregate	1000	0.47
Coating/mortar with different sizes of aggregate	1200	0.58
Lime-based plaster	1400	0.70
Gypsum-based plaster	1200	0.35
T0-Natural plasters without aerogel	*2200*	*0.50*
T1-Natural plasters with aerogel (80–90 %)	*275–300*	*0.045–0.050*
T2-Natural plasters with aerogel (91–95 %)	*126–136*	*0.019–0.021*
T3-Natural plasters with aerogel (96–99 %)	*115–125*	*0.014–0.016*

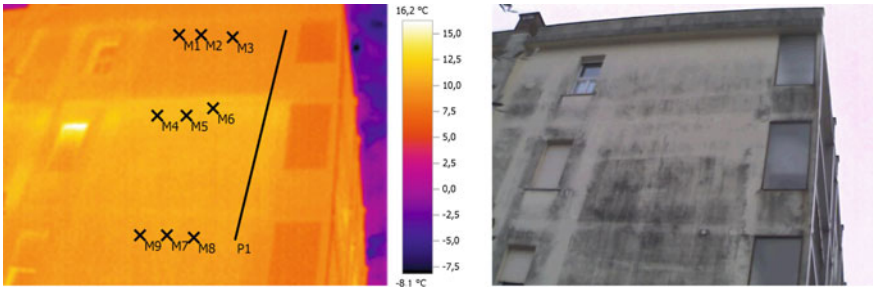

Fig. 2.11 View of the investigated building and corresponding infrared imagine (Buratti et al. 2014)

Table 2.10 Temperature values measured by means of the thermographic camera (Buratti et al. 2014)

Points	Emissivity (–)	Temperatures (°C)
M1	0.93	9.1
M2	0.93	9.2
M3	0.93	9.1
M4	0.93	11.5
M5	0.93	11.4
M6	0.93	11.7
M7	0.93	10.4
M8	0.93	10.4
M9	0.93	10.4

considered equal to 0.93). Figure 2.11 shows a thermogram of this building: it can be observed that the temperature values in M1, M2, and M3 are about 9 °C (third floor), whereas the values are 10.5–11.5 °C in M4–M9 (first and second floor): The decreasing of about 2 °C is due to the aerogel-based plaster application (Table 2.10).

2.4.3 Future Trends and Barriers

New aerogel-based plasters are the focus of the HIPIN Project (HIPIN, 2015, from European Union's Seventh Framework Program). This project aims to test new formulations of aerogel in order to obtain a good mechanical strength and thermal conductivity, other characteristics being equal. Moreover, it aims to develop three nanostructured systems, in which aerogel should be incorporated (paint layers, plasters, and sandwich panels), in order to improve thermal efficiency in existing buildings and new constructions. As regards the incorporation of aerogel into paints, a replacement of a portion of the lime with hydrophobic and hydrophilic aerogel is considered. Three stages are considered for the aerogel plaster preparation: dry

mixing, mixing with water, and pumping in application stage. Generally, the thermal plaster layer has to be covered with a final render of about 2–5 mm, but in future a single aerogel-based plaster insulating layer as final finish of the wall will be developed according to this project. Finally, the developed high-performance aerogel would be included into panels to decrease the thickness of the insulating blanket: the ideal thickness is the lowest possible, but a good common solution could be 3 cm. This insulating layer should allow water transpiration and should be affordable considering the costs: Specific matrix materials with good mechanical and thermal properties should be selected for aerogel binding.

Until now, aerogel has been considered too much expensive and mechanical fragile for the diffusion in the construction sector. Furthermore, many technical changes recently enabled aerogel plasters to have higher mechanical resistance to be manufactured at lower costs. The thermal and mechanical properties of these new materials allow high efficient retrofit also in buildings in which the insulation with conventional solutions is difficult; so they can be considered very impacting in the construction sector also considering their complete integration in the building.

References

Achard P, Rigacci A, Echantillac T, Bellet A, Aulagnier M, Daubresse A (2011) Enduit isolant à base de xerogel de silice. WIPO Patent WO/083174

Aspen Aerogels (2012) Case study: aerogel interior wall insulation reduces U-Values by 44 %, lowers energy use and carbon emissions. Retrieved from: http://www.aerogel.com/markets/Case_Study_Interior_Wall_web.pdf. Accessed June 2015

Barbero S, Dutto M, Ferrua C, Pereno A (2014) Analysis on existent thermal insulating plasters towards innovative applications: evaluation methodology for a real cost-performance comparison. Energy Build 77:40–47

Buratti C, Moretti E (2013) Chapter 10—silica nanogel for energy-efficient windows. In: Torgal FP, Diamanti MV, Nazari A, Granqvist CG (eds) Nanotechnology in eco-efficient construction. Woodhead Publishing Limited, Cambridge, pp 207–235. ISBN:9780857095442, doi:10.1533/9780857098832.2.207

Buratti C, Moretti E (2014) Chapter 20—nanogel windows. In: Torgal FP, Mistretta M, Kaklauskas A, Granqvist CG, Cabeza LF (eds) Nearly zero energy building refurbishment: a multidisciplinary approach. Springer-Verlag London Ltd. doi:10.1007/978-1-4471-5523-2_20

Buratti C, Moretti E, Belloni E (2012) The influence of glazing systems on energy performance of non-residential buildings. In: Proceedings of the 25th international conference on efficiency, cost, optimization and simulation of energy conversion systems and processes, ECOS 2012, 26–29 June 2012. Perugia, Italy, pp 281–294, 206-1–206-14

Buratti C, Moretti E, Belloni E, Agosti F (2014) Development of innovative aerogel based plasters: preliminary thermal and acoustic performance evaluation. Sustainability 6:5839–5852. doi:10.3390/su6095839

Buratti C, Moretti E, Belloni E (2016) Nanogel windows for energy building efficiency. In: Pacheco Torgal F, Buratti C, Kalaiselvam S, Granqvist C-G, Ivanov V (eds) Nano and biotech based materials for energy building efficiency. Springer International Publishing 2016. ISBN: 978-3-319-27503-1

Cotana F, Buratti C, Moretti E, Belloni E (2013) Unsteady simulation of energy performance and thermal comfort in non-residential buildings. Build Environ 59:482–491

Cotana F, Pisello AL, Moretti E, Buratti C (2014) Multipurpose characterization of glazing systems with silica aerogel: in-field experimental analysis of thermal-energy, lighting and acoustic performance. Build Environ 81:92–102. doi:10.1016/j.buildenv.2014.06.014

EMPA material science and technology (2015) http://www.empa.ch//. Accessed 18 June 2015

Fickler S, Milow B, Ratke L, Schnellenbach-Held M, Welsch T (2015) Development of high performance aerogel concrete. In: 6th international building physics conference, IBPC 2015, Turin, 14–17 June 2015

Filate SS (2014) Investigation of an energy refurbishment concept for office building using Nanogel®Aerogel insulation plaster and replaced windows by building simulation. Master Programme in Energy Technology, Uppsala Universitet, Oct 2014

Fixit, Fixit 222 Aerogel Hochleistungsdämmputz (2015) Available at: http://www.fixit.ch/Home/Produkte/Restaurierungs-und-Sanierungsprodukte/Aerogel-Hochleistungsdaemmputz/Fixit-222-Aerogel-Hochleistungsdaemmputz/(language)/ger-DE-9. Accessed 20 June 2015

Gao T, Jelle BP, Gustavsen A, Jacobsen S (2014) Aerogel-incorporated concrete: an experimental study. Constr Build Mater 52:130–136

Ghazi Wakili K, Stahl Th, Heiduk E, Schuss M, Vonbank R, Pont U, Sustr C, Wolosiuk D, Mahdavi A (2015) High performance aerogel containing plaster for historic buildings with structured façades. In: 6th international building physics conference, IBPC 2015, Turin, 14–17 June 2015

HIPIN (2015) High performance insulation based on nanostructure encapsulation of air. Available at: http://www.hipin.eu. Accessed 27 June 2015

Huang L (2012) Feasibility study of using silica aerogel as insulation for buildings. Master of Science thesis, KTH School of Industrial Engineering and Management, Stockholm, Sweden

Ibrahim M, Biwole PH, Achard P, Wurtz E (2014a) Aerogel-based coating for energy-efficient building envelopes. In: 9th international energy forum on advanced building skins, Bressanone, Italy, Oct 2014. Proceedings of energy forum on advanced building skins, pp 753–774 <hal-01112594>

Ibrahim M, Biwole PH, Achard P, Wurtz E (2014b) A study on the thermal performance of exterior walls covered with a recently patented silica-aerogel-based insulating coating. Build Environ 81:112–122

Ibrahim M, Wurtz E, Biwole PH, Achard P, Sallee H (2014c) Hygrothermal performance of exterior walls covered with aerogel-based insulating rendering. Energy Build 84:241–251

Ibrahim M, Biwole PH, Achard P, Wurtz E (2015) Aerogel-based materials for improving the building envelope's thermal behavior: a brief review with a focus on a new aerogel-based rendering. In: Sharma A, Kar SK (eds) Energy sustainability through green energy. Green Energy and Technology, Springer India 2015. doi:10.1007/978-81-322-2337-5_7

ISO 10534-2 (1998) Acoustics-determination of sound absorption coefficient and impedance in impedance tubes-part 2: transfer-function method. ISO, Geneva, Switzerland

Kalnæs SE, Jelle BP (2015) Phase change materials and products for building applications: a state-of-the-art review and future research opportunities. Energy Build 94:150–176

Kiliç A, Atiş CD, Yaşar E, Özcan F (2003) High-strength lightweight concrete made with scoria aggregate containing mineral admixtures. Cem Concr Res 33:1595–1599

Kim S, Seo J, Cha J, Kim S (2013) Chemical retreating for gel-typed aerogel and insulation performance of cement containing aerogel. Constr Build Mater 40:501–505

Krauss G (1985) Etude experimentale des transferts de chaleur entre un batiment et son environment: conception, realization, instrumentation d'une cellue test. PhD thesis, University P. & M. Curie, Paris

Moretti E, Zinzi M, Belloni E (2014) Polycarbonate panels for buildings: experimental investigation of thermal and optical performance. Energy Build 70:23–35. doi:10.1016/j.enbuild.2013.11.045

Naturalcalk-Tillica (2015) Available at: http://www.naturalcalk.com/. Accessed 29 June 2015

Ratke L (2008) Herstellung und Eigenschaften eines neuen Leichtbetons: Aerogelbeton. Beton- und Stahlbetonbau 103:236–243

Röfix, Fixit Group (2015) Available at: http://www.roefix.it/Prodotti/Risanamento-Restauro-Bioedilizia/Bioedilizia/FIXIT-222-Aerogel-Intonaco-altamente-isolante-Intonaco-termoisolante-nel-sistema-ROeFIX-Aerogel. Accessed 29 June 2015

Serina Ng, Jelle BP, Sandberg LIC, Gao T, Wallevik OH (2015) Experimental investigations of aerogel-incorporated ultra-high performance concrete. Constr Build Mater 77:307–316

Stahl Th, Brunner S, Zimmermann M, Ghazi Wakili K (2012) Thermo-hygric properties of a newly developed aerogel based insulation rendering for both exterior and interior applications. Energy Build 44:114–117

Tabares-Velasco PC, Christensen C, Bianchi M (2012) Verification and validation of EnergyPlus phase change material model for opaque wall assemblies. Build Environ 54:186–196

UNI 10351 (1994) Materiali da costruzione. Conduttività termica e permeabilità al vapore; Ente Nazionale Italianodi Unificazione (UNI): Milan, Italy, 1994 (In Italian)

Chapter 3
Nanogel Windows for Energy Building Efficiency

Cinzia Buratti, Elisa Moretti and Elisa Belloni

Abstract The chapter deals with the potential of highly energy-efficient windows with silica aerogel for energy saving in buildings. Aerogel is a low-density nanostructured porous material with very low thermal conductivity (about 0.018 W/m K for translucent granular aerogel at room temperature) and excellent acoustic insulation. It is ideal for energy saving in buildings, also due to its good optical transparency. The characteristics of the raw material (silica aerogel for windows: monolithic and translucent granular) are illustrated with general information about the production process, the main chemical and physical properties, and a market overview; then, nanogel windows are discussed and thermal, visual, and acoustic performance are highlighted. A useful worldwide market overview about the commercial products and the main manufactures is also included. Finally, a state-of-the-art review of nanogel windows in building applications is discussed: the potential of the investigated solutions is described by both experimental results and simulation models of the aerogel windows performance, referring to different case studies. Future research, market trends, and costs are also discussed.

3.1 Introduction

The existing building stock was constructed before 1970, especially in Europe and in the USA: the majority of buildings have high energy consumptions, because of obsolete HVAC systems and inadequate insulation of the envelope; moreover, the indoor comfort conditions of the occupants need to be improved. In Italy and in

C. Buratti (✉) · E. Moretti · E. Belloni
Department of Engineering, University of Perugia, via G. Duranti 63, 06125 Perugia, Italy
e-mail: cinzia.buratti@unipg.it

E. Moretti
e-mail: elisa.moretti@unipg.it

E. Belloni
e-mail: belloni.unipg@ciriaf.it

F. Pacheco Torgal et al. (eds.), *Nano and Biotech Based Materials for Energy Building Efficiency*, DOI 10.1007/978-3-319-27505-5_3

Germany, a great part of building heritage dates before the first energy regulations: in Germany, about 87 % of residential buildings were built before 1977, and in Italy, at least 90 % of buildings before 1991 (BPIE 2011; Pérez-Lombard 2008). Furthermore, current targets of the European Union deal with a 20 % reduction in greenhouse gas (GHG) emissions, 20 % of energy savings compared to projections, and a share of 20 % of renewable energies by 2020 (European Community 2009). Energy efficiency and refurbishment in buildings have been becoming the key words due to the buildings' contribution to the global energy consumption (reaching a value of about 40 % in developed countries) (European Community 2010).

Transparent elements have an important role in buildings in terms of energy demand, thermal comfort, and daylighting: most of the total energy losses (up to 60 %) can depend on the windows (Jelle et al. 2012), especially in highly glazed buildings, because the transparent systems have thermal performance lower than the opaque walls and are influenced by radiation (AbuBakr Bahaj et al. 2008; Buratti et al. 2012c; Buratti et al. 2013).

In order to encourage refurbishment of existing buildings towards nearly zero-energy buildings, innovative materials and solutions should be considered: in this context, the building and construction industry recently started advancing conventional building materials or components by using a variety of nanomaterials. The application of nanotechnology can significantly enhance the performance of building materials, e.g. in terms of strength and durability, and can add useful properties, such as self-cleaning façades, smart windows, and superinsulation materials (Zhu et al. 2004; Ivanov et al. 2010; Kaushik and Sumathy 2003). Aerogel is one of the most promising nanomaterials for use in highly energy-efficient buildings and windows (Jelle et al. 2012; Koebel et al. 2012; Yang 2013; Zhao et al. 2015; Neugebauer et al. 2014; Buratti and Moretti 2013b): it is a highly porous nanostructured material, with a very low thermal conductivity (down to 0.010 W/m K in vacuum conditions), and good optical transparency (light transmittance). Nowadays, aerogels are spreading in the market of building insulation. In the last years, research focussed on more and more low thermal transmittance values, less than 0.3–0.5 W/(m^2 K). In this context, vacuum glazings (VGs) and aerogel windows are considered as the best solutions; nevertheless, VGs have technical limits and at the same time very high costs: a functional vacuum insulation panel (VIP) with *U*-values of 0.1 W/m^2 K is not available due to the problem of keeping the glazing gastight. In the last years, many daylighting systems with translucent granular aerogels in interspace, such as polycarbonate panels, structural panels for continuous façades, and insulated glasses, are spreading in the market, especially in the Northern Europe and in the USA. Nevertheless, advanced glazing systems with aerogel in monolithic form in the interspace are not yet used in mass production (Baetens et al. 2011; Rigacci et al. 2004).

This chapter discusses the state-of-the-art development of silica aerogel and issues to apply this advanced nanostructured porous material in energy-efficient windows.

3.2 Silica Aerogels for Windows: State of the Art

3.2.1 Introduction and History

Aerogels were discovered by Kistler eighty years ago, and they are often described as 'frozen smoke' because of their appearance (Aegerter et al. 2011). The material is a dried gel with nanometer-scale pores (the pore size is typically in the 5–100 nm range), obtained by means of a very complex synthesis. It is a cross-linked internal structure of silicon dioxide (SiO_2) chains and a large number of very small air-filled pores: the porosity is higher than 90 %, and it can reach 99 % (Riffat and Qiu 2012; Cuce et al. 2014a); therefore, the density is in the 50–200 kg/m^3 range. The result is an extremely light solid material, with extraordinary physical, thermal (it has the lowest thermal conductivity among solid materials, down to 0.010 W/m K), optical, and acoustic properties, depending on both the silica source and the preparation process.

The investigated material attracted the attention of researchers in various areas of science and technology, and several fields of aerogels application could be found in the literature (Akimov 2003; Baetens et al. 2011; Aegerter et al. 2011; Pierre and Pajonk 2002; Pajonk 2003): microelectronics; electrical engineering; acoustics; oil and gas pipelines insulation; and finally space exploration. Aerogel is used as a thermal insulation material in US spacecrafts.

3.2.2 Synthesis

Several products have been developed using different raw materials, the most common of which is silica. Inorganic silica-based aerogels (which are used in building applications) are obtained from a gel by replacing the pore liquids with air and maintaining the network structure.

The production process of silica aerogel consists of three general steps, which are summarized as follows (Pierre and Pajonk 2002; Dorcheh and Abbasi 2008):

- *gel preparation*: in the sol-gel process, the precursors (such as tetramethoxysilane (TMOS, $Si(OCH_3)_4$ and tetraethoxysilane (TEOS, $Si(OC_2H_5)_4$)) are dispersed in a liquid, where the solid nanoparticles form a solid three-dimensional network through the liquid. Acidic or basic catalysts are usually added in the process. A simplified reaction for silica aerogel synthesis is as follows:

$$Si(OCH_3)_4 + 2H_2O \leftrightarrow SiO_2 + 4CH_3OH \tag{3.1}$$

- *gel ageing*: the gels are usually aged before drying, in order to increase the stiffness and strength and to mechanically reinforce the tenuous solid skeleton after the sol-gel process;

- *gel drying*: it is the most critical step of the process, because the solid framework of the sol-gel should be isolated from liquid, and the structure can collapse or be fractured, due to the capillary pressure. Two different methods are usually carried out: ambient pressure drying (APD) and supercritical drying (SCD), where the capillary tension can be avoided by removing the liquid above the critical temperature and pressure. For building applications, monolithic aerogels are manufactured with a low-temperature supercritical drying (LTSCD) process. The APD process was nevertheless studied in order to lower the production costs, and it is today the most promising technique. As final remark, during the synthesis, the drying phase is the most energy consumption step and could have a great impact on the environmental features of aerogels (Dowson et al. 2012a).

A more detailed analysis of the synthesis process and of the recent developments could be found in the literature (Dorcheh and Abbasi 2008; Aegerter et al. 2011; Gurav et al. 2010; Koebel et al. 2012; Błaszczyńsk et al. 2013; Buratti and Moretti 2013b).

3.2.3 Physical, Mechanical, and Thermal Properties

The physical, mechanical, and thermal properties of silica aerogels strongly depend on the production process, such as the process methodology and the substances used (catalyst, solvent, and silica precursors) (Tajiri and Igarashi 1998; Anderson et al. 2009; Pajonk 2003). Therefore, the physical, mechanical, and thermal characteristics can vary in a wide range, especially depending on the considered form (Parmenter and Milstein 1998).

In the building insulation material sector, silica aerogels were developed in two main forms (Fig. 3.1).

- *translucent granular*, consisting in translucent granules (grain size in the 0.5–4 mm range typically), used in the interspace of advanced glazing windows or skylights;

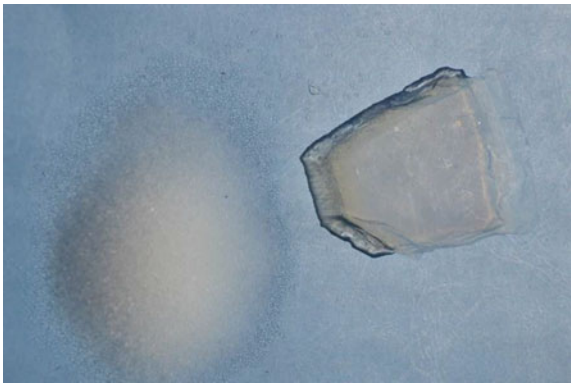

Fig. 3.1 Silica aerogels: granular (*left*) and monolithic pane (*right*)

- *transparent monolithic panels*, used for superinsulating windows (also in vacuum conditions). Nevertheless, cracks could occur during manufacturing large pieces of monolithic silica aerogels, and therefore, glazing systems with aerogel panes are only used in research.

Moreover, *opaque silica aerogel-based materials* appeared on the market. Flexible blankets are available in order to reduce the envelope thermal bridges; the blankets are obtained by adding fibres in the gel before the drying process (Cabot Corporation, Boston, MA, USA; Aspen Aerogels Inc., Northborough, MA, USA). The thermal conductivity is about 0.013 W/m K, but the cost is about 10 times higher than a conventional material with similar performance.

Finally, in the last few years, aerogels are investigated as additives for high thermal performance coatings or construction materials, such as aerogel-based plasters and concrete (Buratti et al. 2014, 2016; Ng et al. 2015).

Researchers focussed their attention on silica aerogels especially because of their excellent thermal properties: the thermal conductivity is the lowest among solid materials, and it varies in the 0.004 W/m K (evacuated monolithic silica aerogel)—0.018 W/m K (granular silica aerogel) range, at room temperature (Koebel et al. 2012). The low thermal conductivity depends on the low density and the pores size: conductive and convective heat transfer in gas is limited by the small pores, while conduction in the solid network is limited by the low density, which offers a reduced number of pathways (Baetens et al. 2011; He and Xie 2015; Bouquerela et al. 2012).

Because of their structure, aerogels are less stiff and strong than the open-cell foams or solids: the tensile strength is negligible, and the compressive strength and the elastic modulus are very low. Their fragility, due to the low density and the solid distribution, is the main limitation (together with cost) that has prevented aerogels from becoming more widely used.

The contact with water must be avoided for monolithic aerogels: in commercial applications, aerogel may be used in vacuum conditions, with evident advantages in terms of thermal insulation.

Finally, when considering safety, the material is not carcinogenic, non-flammable, and non-reactive (Baetens et al. 2011).

The main physical properties are summarized in Table 3.1 (Riffat and Qiu 2012; Buratti and Moretti 2013b; Baetens et al. 2011).

3.2.4 Market Overview

The first commercial aerogels were produced by Monsanto Chemical Corporation (USA) after 1940, following the Kistler's procedure. Then, the production was stopped between the 1960s and restarted in the last two decades: nowadays, it is located in USA, Europe (Sweden, Germany), China, and Japan.

Table 3.1 Physical properties of silica aerogels for building applications

Properties	Values range
Pore diameter	5–100 nm (about 20 nm in general)
Porosity	85–99.8 % (>90 % in general)
Density	50–200 kg/m^3 (about 100 kg/m^3 in building applications)
Typologies	• Opaque (blankets, opaque granules, or powder as additive for coatings or concrete) • Translucent granules • Transparent monolithic panels
Thermal conductivity	0.008–0.020 W/m K (depending on type, temperature, pressure, and production process); typical values: • Blankets: 0.013 W/m K • Granular: 0.018 W/m K at room temperature • Monolithic: 0.010 W/m K (vacuum conditions at room temperature)
Sound speed	40 m/s (monolithic)—300 m/s (granular)
Surface chemistry	• Granular: fully hydroscopic • Monolithic: contact with water must be avoided
Mechanical	Negligible tensile strength, compressive strength, and very low elastic modulus
Safety	Not carcinogenic, non-flammable, and non-reactive

Most granular translucent aerogels are manufactured by Cabot Corporation (Boston, USA), which developed an innovative manufacturing process and allowed a production on large scale since 2003 in a plant in Frankfurt, Germany; it can produce about 10,000 tonnes per year (Werner and Brand 2010; Aegerter et al. 2011). Two commercial products are available on the market (Table 3.2): LUMIRA® aerogel (formerly Nanogel® aerogel), designed to optimize light transmission in architectural daylighting applications, and ENOVA® aerogel, engineered for chemical applications as additive (such as insulation coatings).

The most well-known manufacturer of monolithic aerogels is Airglass AB (Sweden); other laboratories or companies currently involved in developing

Table 3.2 Properties of granular silica aerogels manufactured by Cabot Corporation

Name	Particle size	Thermal conductivity	Density (kg/m^3)	Application	Price
Enova®	2 µm–1.2 mm	0.012 W/m K (at 25 °C)	125–150	Additive for coatings	35–55$/l
Lumira®	0.7–4 mm	0.018 W/m K (at 12.5 °C, bulk			

density = 85 kg/m^3)
0.023 W/m K (at 12.5 °C, bulk density = 65 kg/m^3)120–150Translucent windows20–25$/lAdapted from Cabot Corporation

monolithic panels are as follows: Japan Fine Ceramics Center, Aerogel Technologies, Gyroscope, Guangdong Alison Aerogel, and Surnano Aerogel Inc. (Berardi 2015). Recently, also Aspen Aerogels seems engaged in the development of reinforced and highly translucent monolithic aerogel for 'aerogel window' applications, but the technology is currently under study due to the difficulty to produce monoliths of high optical quality.

3.3 Performance Assessment of Aerogel Glazing Systems

3.3.1 Literature Review

Silica aerogels, monolithic and granular translucent ones, can be used in order to obtain high-insulated nanogel windows, thanks to excellent thermal insulation properties and good light transmission.

Transparent monolithic panes were developed 20–30 years ago in Sweden by Airglass AB; nevertheless, advanced glazing systems with monolithic aerogel have still not penetrated the market and only some prototypes were manufactured for research purposes. Nowadays, this technology is still under evaluation due to the difficulty to produce large monoliths with high optical quality. For these reasons, the building applications focus on glazing systems with granular aerogels.

Duer and Svendsen (1998) presented the main results of a research project founded by the European Commission, aiming to evaluate the benefits and penalties of monolithic aerogel glazings. In this study, the authors discussed a prototype of 450 × 450 mm^2 size, made under vacuum conditions, and the aerogel pane was inserted between two glasses with low-iron covers and antireflection coating. They reported the main measurements of thermal and optical properties of prototypical evacuated aerogel double-glazed units. Then, Schultz and Jensen (2008) evaluated the thermal-energy performance of evacuated aerogel glazings, with particular attention to the evacuation and assembling process (Fig. 3.2a). Additionally, Jensen et al. (2004) studied the heat loss coefficient and the solar transmittance of several prototypes of aerogel sheets developed during the HILIT European project. Nevertheless, the optical quality had a disturbance in the view through, because of a significant diffusion of the light. Some problems have yet to be solved: the production process is too difficult to allow large aerogel panes without defects, cracks, inhomogeneities, and too expensive. In particular, producing large monolithic aerogel panes is a great challenge, due to the fragility of large monolithic sheets, and the maximum size of a crack-free panel is 0.6 m × 0.6 m. In this view, Berardi (2015) recently presented the development of a monolithic aerogel double-glazed unit for a retrofitting project in an educational building located in a cold climate. The study focused on the energy and daylighting analysis with different aerogel configurations, considering typical New England windows, which consisted of 25 individual glass panels, each with dimensions of 0.4 m × 0.3 m.

Fig. 3.2 Example of aerogel glazings: **a** evacuated prototype with monolithic aerogel (Schultz and Jensen 2008); **b** prototype of a PMMA system with granular aerogel installed on ZAE building in Würzburg (Reim et al. 2005)

Important developments of the research about granular aerogels for energy efficiency applications in buildings were illustrated by Reim et al. (2005). In this work, the authors measured the heat transfer coefficients and the solar energy transmittance of granular silica aerogel glazings. The set-up of systems with granular aerogel was also carried out in Reim et al. (2002) who proposed to include aerogel granules in sandwich structures, i.e. between PMMA panels (Fig. 3.2b). Buratti and Moretti (2012a) carried out an in-lab campaign on aluminium frame window prototype with silica granular aerogel in glazing interspace, showing good acoustic properties and excellent thermal performance. The same authors (Buratti and Moretti 2011b, 2012b) assembled several glazing samples with aerogel in interspace (monolithic and granular aerogel, different thicknesses, and kind of glass layers) in order to evaluate thermal and optical performance of the proposed solutions. The impact of particle size in insulating glazing units with silica aerogel granules was also investigated by Gao et al. (2014), considering both thermal and optical performance. Additionally, Ihara et al. (2015a) investigated the influence of convection on thermal performance of granular-filled double glazing systems.

Interesting applications of silica aerogels are in evacuated solar collectors, for their capability to reduce the thickness of conventional flat-plate collectors and to decrease the heat loss by about 40 % (Dowson et al. 2012b). Moreover, the application of silica aerogel in passive Trombe walls for the retrofitting of the existing buildings in UK was investigated by Dowson et al. (2014), demonstrating that small areas of Trombe wall with aerogel can provide a useful energy contribution, without creating a significant overheating risk.

Therefore, the development of glazing systems with aerogel is still at the research stage; in the meantime, many daylighting systems with translucent

granular aerogel in interspace are available on the market (Rigacci et al. 2004), as reported in Sect. 3.3.5. The main findings (in terms of thermal, visual, and acoustic performance) of the above-mentioned studies are discussed in the following paragraphs.

3.3.2 *Thermal Performance*

Thermal performance of monolithic aerogel windows was experimentally evaluated only on few prototypes developed in European research projects, showing excellent properties with moderate thickness (Schultz et al. 2005). Aerogel glazing prototypes were made under vacuum conditions including transparent insulating silica aerogel tiles (thickness about 15 ± 1 mm, 55 × 55 cm^2); a rim seal assured a barrier against atmospheric air and water vapour, and low thermal bridge effects were obtained. The centre *U*-value, measured by means of a hot-plate apparatus, was below 0.7 W/m^2 K, with an estimated thermal conductivity of 0.010 W/m K for the aerogel pane. Moreover, the solar transmittance is high for windows with monolithic aerogels: the measured value for the monolithic window prototype (15 mm aerogel) was higher than 75 % (Jensen et al. 2004), and the *U*-value was equal to the best triple-layered gas-filled glazing units ($U < 0.6$ W/m^2 K).

Thermal properties of granular aerogel glazing systems are significantly affected by aerogel thickness and particle size (Gao et al. 2014a), as shown in Fig. 3.3. In general, small aerogel granules (i.e. Aerogel-AS, blue line in the Fig. 3.2) have a lower thermal conductivity than that of the large ones (i.e. Aerogel-AB, red line). Moreover, a significant reduction in *U*-value was observed by incorporating the aerogel granules into the cavity of double glazings. WIN-AB and WIN-AS in Fig. 3.3 showed 58 and 63 % reduction, respectively, in heat losses when compared to a conventional double glazing unit with the same interspace thickness (14 mm), but with air instead of aerogel granules.

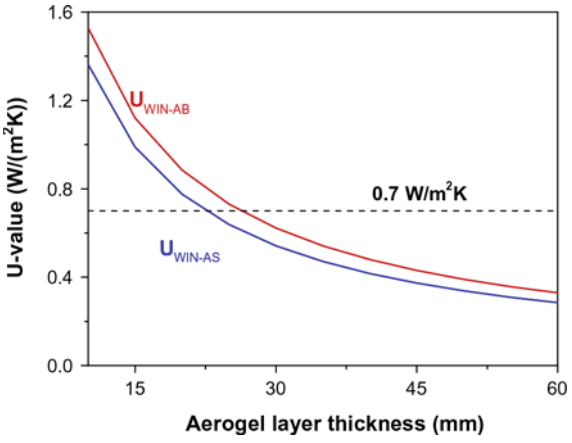

Fig. 3.3 Influence of thickness and particle size (Aerogel-AS: small granules, *blue line*; Aerogel-AB: large granules, *red line*) of aerogel on thermal performance (Gao et al. 2014a)

In order to give an idea about the expected thermal performance, Buratti and Moretti (2012) reported that a glazing consisting of 14-mm-thick layer of aerogel granules (size 0.5–3 mm) and two glass panes had a *U*-value of about 1 W/(m^2 K). When the aerogel thickness increases up to 60 mm, a *U*-value of 0.3 W/(m^2 K) could be achieved (Gao et al. 2014a; Ihara et al. 2015a).

Compared to conventional glazings, granular aerogel systems have also significant benefits when they are used as roofs solutions: *U*-values are not dependent on the tilted angle to vertical plane, such as in the gas-filled glazings (air, argon, or krypton) which have a worse behaviour when used as roofs instead of vertical panels (Fig. 3.4). In general, the centre-of-glass *U*-value increases when a window is tilted from the vertical to the horizontal position, whereas the aerogel granulate windows showed the opposite results, as confirmed experimentally by Ihara et al. (2015), suggesting that the thermal performance of aerogel granulate glazing systems is not affected by convection in the cavity.

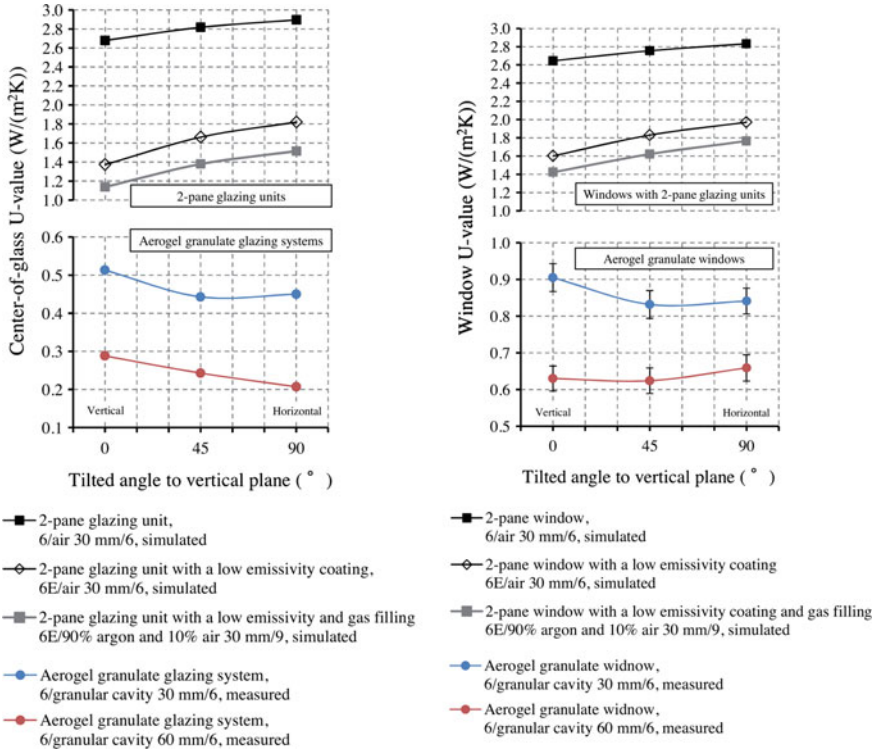

Fig. 3.4 Impact of the convention and tilted angle on thermal performance of granular aerogel glazings: centre-of-glass *U*-value (*left*) and window *U*-value (*right*) (Ihara et al. 2015a)

3.3.3 Visual Performance

The optical properties of silica aerogels are very interesting for building applications, and they are widely investigated in the literature.

The light transmittance of a 10 mm thickness of monolithic aerogels is high and similar to the one of a 6-mm-thickness clear float glass (considering an aerogel pane); its solar transmittance is also high and equal to 0.88. Nevertheless, the quality of the vision through the material is poor and optical images could be hazily deformed (Fig. 3.5). When transmitted through the material, the radiation is scattered, according to the Rayleigh theory, causing reddening of the transmitted light and the bluish appearance of the reflected light (Duer and Svendsen 1998; Baetens et al. 2011; Jensen and Schultz 2004; Reim et al. 2004, 2005; Buratti and Moretti 2011a, b, 2012a, b, Fu et al. 2015). In general, optical properties of aerogel monoliths are strongly influenced by the production process (Tajiri et al. 1998), and the transparency has been improved in the last years.

Granular aerogels light transmission is about 80 % (10 mm thickness, Cabot), lower than the one of the monolithic samples with the same thickness. It decreases by 20 % for each 10 mm thickness increasing. Optical properties, such as thermal transmittance, are significantly affected by the particle size of the aerogel granules (Gao et al. 2014). A 38 % reduction in light transmittance was observed with large aerogel granules in the interspace (particle size 3–5 mm) when compared to a

Fig. 3.5 Aerogel effect on the vision by comparing the double glazed unit with and without the monolithic aerogel panel (Berardi 2015)

Fig. 3.6 Effect of granular aerogel on the vision through a window (Huang and Niu 2015a)

conventional double glazing, while the reduction is 81 % with small aerogel granules (particle size < 0.5 mm). It is known that small particles usually scatter light more efficiently than the large ones do, increasing the reduction in visible light transmittance.

The vision through granular aerogel window is in general limited (Fig. 3.6); nevertheless, it could be preferred in some situations, because the light gets very deep in the room, reducing significantly glare problems in façade or skylight, due to the high diffuse component of the transmitted light. When conventional double glazing has a very low diffuse transmittance, aerogel windows are indeed highly diffusing, as shown in the literature (Buratti and Moretti 2011a, b; Gao et al. 2014). Granular systems with small granules have a total transmittance almost identical to their diffuse transmittance (Gao et al. 2014).

Finally, the quality of the transmitted light through the glazing can be evaluated by the general colour rendering index R_a, as defined in CIE (1964). Experimental results from Buratti and Moretti (2012a) showed a very good quality for glazing systems with aerogel in interspace ($R_a > 90$). It is lower than the one of windows with air in interspace ($R_a = 98$ with float glasses), but it is equal to 93 for float glasses and granular aerogel (14 mm) and to 92 with monolithic aerogel. With a low-e glasses and granular aerogel, R_a downs from 94 to 90–91.

3.3.4 Acoustic Performance

The acoustic properties of silica aerogels are also very interesting.

Figure 3.7 shows the sound absorption coefficient of several systems for 20 mm thickness. The sound absorption properties of aerogel granules (Lumira) are significant, especially at low frequencies; the behaviour can be modified by changing both the mechanical properties of the material as well as the particle size

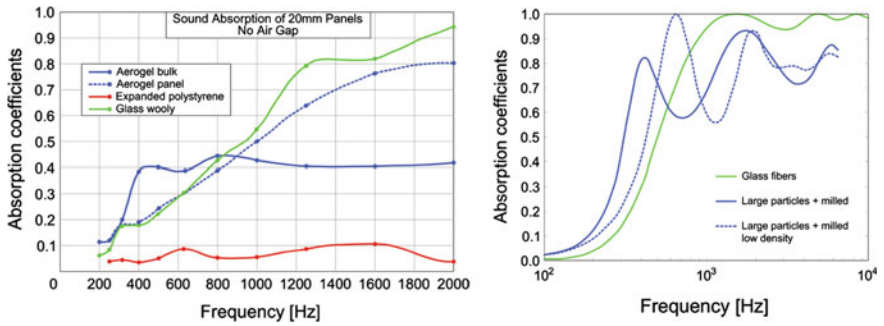

Fig. 3.7 Sound absorption coefficient of granular aerogel: comparison with other systems, 20 mm thickness (*left*), and influence of particle size distribution (*right*) (Adapted from Lumira® Consortium 2015)

distribution: adding low-density milled particles, the maximum absorption shifted to higher frequencies (Lumira® Consortium 2015).

The efficiency of granular silica aerogels as sound insulators is also shown in the literature (Forest et al. 1998, 2001), while the acoustic performance in windows is discussed in Buratti and Moretti (2012a) and Cotana et al. (2014). When used in interspace of glazing systems, granular aerogel can improve the sound insulation of the building envelope, due to the increase in the sound reduction index (R, EN 140), which affects the noise transmitted through the windows. The presence of granular aerogel (15 mm thickness between two float glasses, each one 4 mm thickness) increases the sound reduction index values in all the frequency range (100–500 Hz), especially in the central one (500–2000 Hz), with respect to the same glazing with air in interspace. In a prototype of aluminium frame window with two mobile shutters, the weighted sound insulation index R_w (EN ISO 717-1, 2007) increases 3 dB (from 34 to 37 dB) with a conventional double glazing with granular aerogel in interspace instead of air, confirming very interesting acoustic insulation properties of silica aerogels (Buratti and Moretti 2012a). The results of in-lab studies were also confirmed by in-field investigation, considering the performance of a façade of a prototype building, by comparing windows with and without aerogel (Cotana et al. 2014). The façade weighted sound insulation index was measured: due to aerogel, it was increased by 3 dB, i.e. from 28 to 31 dB. In order to further improve the acoustic performance of the window, the authors recommended integrating granular aerogel into laminated glasses with special acoustic polyvinyl butyral (PVB) layer.

3.3.5 Market Overview

The granular translucent aerogel (manufactured by Cabot) is supplied to various partners in the USA and Europe, which developed and commercialized different

Fig. 3.8 Example of the application of Lumira® aerogel in polycarbonate sheets (Gymnasium at BBS Mainz, outside and inside view of the building. Courtesy of Roda—EMB, Germany)

aerogel daylighting systems for buildings. The most popular commercial systems are multiwall polycarbonate panels for skylights, roofs and walls (Fig. 3.8), structural panels for continuous façades, insulated glass units, U-channel glass (self-supporting systems of glass channels with an extruded metal perimeter frame), and finally tensile structures and roofing (Moretti et al. 2014).

A wide range of properties for granular translucent aerogels daylighting systems can be found on the manufacturers' technical data, depending on the retaining structure (glasses, low-e glasses, PMMA, polycarbonate) and on the thickness of granular aerogel (see Table 3.3): for thickness higher than 50 mm, the *U*-value can be lower than 0.5 W/m^2 K.

3.4 Building Applications of Nanogel Windows

3.4.1 Introduction

Aerogel windows were found to have an important role in improving both thermal performance and daylight in fenestration industry, because of very low conductivity, high acoustic insulation and light transmission, and low weight. A wide number of applications of daylighting systems with granular aerogels could be found in schools, commercial and industrial buildings, airports, etc., especially in USA and in Europe (Lumira® Aerogel Consortium 2015). An example of a recent application as wall system in a multifunctional building (consisting of a home, an office, a workspace, and a retail environment) is shown in Fig. 3.9. Technical Glass Products' Pilkington Profilit™ channel glass systems, insulated with Lumira® aerogel-filled multiwall polycarbonate panels (thickness of 16 mm), were used to

Table 3.3 Daylighting systems with translucent granular aerogels

Type	Manufacturer	Product/reference	Thickness (mm)	Thermal and optical performance		
				U^a	t_v^b	SHGC[c]
Insulated glass units 	Advanced Glazings Ltd, Canada	SOLERA® Glazing System + Lumira® aerogel insulation http://www.advancedglazings.com/product-overview/what-is-lumira-aerogel/	25.4	1.14	10–45	0.10–0.42
			44.45	0.61	9–40	0.09–0.37
			76.2	0.31	7–32	0.07–0.30
	Okalux GmbH, Germany	OKAGEL: translucent façade elements (4-mm low-iron outer pane, 6-mm laminated low-iron glass inner pane, 0.76 PVB foil) filled with Lumira http://www.okalux.com	30	0.6	<59	<0.61
			60	0.3	<45	<0.54
U-channel glass 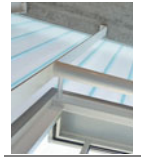	Technical Glass Products, USA	Translucent linear channel glass systems Pilkington Profilit™ filled with Lumira™ aerogel polycarbonate panels (16 and 25 mm) http://www.tgpamerica.com/structural-glass/pilkington-profilit/	16	1.19	50	0.42
			25	1.07	38	0.31
Structural polycarbonate systems and skylights 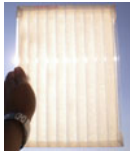	AmeriLux International, WI (USA)	Multiwall polycarbonate systems (Lexan) with Lumira® (10–40 mm thickness) http://www.ameriluxinternational.com/lumira.php	10 (2 wall)	1.87	64	0.64
			16 (3 wall)	1.47	52	0.57
			25 (3 wall)	0.91	49	0.54
			40 (3 wall)	0.57	28	0.42
	Duo-Gard Industries Inc., MI (USA)	Clear cellular polycarbonate with Lumira® aerogel (10–40 mm thickness) http://www.duo-gard.com/wp-content/uploads/2012/09/Lumira.pdf	10	1.47	72	0.81
			16	0.96	62	0.71
			20	0.62	59	0.70
			25	0.51	40	0.53

(continued)

Table 3.3 (continued)

Type	Manufacturer	Product/reference	Thickness (mm)	Thermal and optical performance		
				U^a	t_v^b	SHGC[c]
	KalWall, Manchester, NH, USA	Kalwall polycarbonate systems + Lumira aerogel http://www.structura-uk.com/kalwall/documents/KalwallLumira.pdf	70	0.28	12–20	0.12–0.22
	Roda, Germany	Daylight solutions in polycarbonate sheets with granular Lumira™ aerogel (thickness = 10–40 mm) http://www.roda.de/products/daylight-technology/lumira-aerogel/info/	10	1.93	65	–
			16	1.31	57	–
			25	0.89	32	–
			40	0.54	20	–
	Wasco Skylights, USA	Wasco skylights polycarbonate systems with Lumira® aerogel http://www.wascoskylights.com/	16	1.25	48	0.57
Tensile structures 	Birdair, USA	*Tensotherm™*—triple-layer tensile structure: I—PTFE fibre glass membrane (exterior). II—Translucent blanket with Nanogel® aerogel III—PTFE glass fibre acoustic or vapour barrier http://www.birdair.com/	8	1.16	4.3	5.3
			16	0.76	3	3.4
			24	0.56	2.2	2.3

Data are declared by the manufacturer. The values are just an indication because different test methods could be used

[a] U: thermal transmittance (W/m^2 K)

[b] t_v: light or visible transmittance (%)

[c] SHGC: solar heat gain coefficient (–)

Fig. 3.9 Example of the application of aerogel in polycarbonate sheets in a multifunctional building in Seattle, Washington's Freemont District, Building 115 © William Wright Photography. Image courtesy of Technical Glass Products

diffuse natural light and to provide thermal and acoustic insulation. Granular aerogel is also successfully integrated in skylight systems (Fig. 3.10).

The key results from the literature review about building application of nanogel windows and their benefits are discussed in the following paragraphs, highlighting the recent developments.

3.4.2 In Situ Performance of Granular Aerogel Windows

The potential of high-performance translucent granular aerogel systems in buildings is discussed in the literature by means of building energy simulation tools or calculations, whereas the experimental investigation in buildings is limited to few cases: an experimental investigation was carried out by Dowson et al. (2011) on a prototype polycarbonate panel filled with granular aerogel for a building retrofitting in UK. Thermal-energy, acoustic, and lighting performance of innovative glazing systems with granular aerogel in interspace was evaluated through in-field experiments in two dedicated prototype buildings located at the University of Perugia, in central Italy (Cotana et al. 2014).

Fig. 3.10 Application of aerogel in skylight systems (16 mm clear polycarbonate with Lumira Aerogel): Lafarge Cement Reception hall, UK (Courtesy of Roda—EMB, Germany)

In order to retrofit an office building in London, two prototypes, consisting of a clear twin-wall polycarbonate sheet filled with granular aerogel in interspace (6 and 10 mm aerogel thickness, respectively), were inserted in a test window (simple glass), sealed around the edges. A 15-mm air gap was created between the panels and the existing glazing (Dowson et al. 2011). In situ *U*-values of the prototypes and the control panel were estimated by measuring external and internal temperatures. Light transmission was also measured by means of lux sensors in the centre of each panel. Results of in situ monitoring campaign (from 20 February 2010 to 1 March 2010) showed an excellent behaviour of the investigated solutions. The heat flux reduction was about 73 % for 6-mm aerogel panel and of approximately 80 % for the 10-mm aerogel panel; at same time, the reduction in light transmission was acceptable: light transmission values through the 6-mm aerogel panel, 10-mm aerogel panel, and the control simple glass were 58, 51, and 73 %, respectively.

Silica aerogel glazing system [double glazing with 15 mm aerogel in interspace, grain size in the 0.07–4 mm range: measured thermal transmittance equal to 1 W/(m^2 K)] was integrated into a wood frame window and installed on the south façade in full-scale experimental building prototypes (Cotana et al. 2014, Fig. 3.11a).

The results of a continuous thermal-energy monitoring (winter 2013) showed the aerogel capability to keep the indoor thermal conditions more constant, in moderate

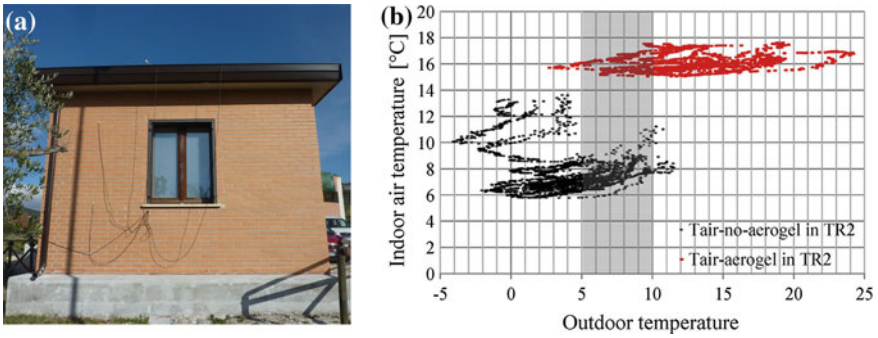

Fig. 3.11 View of the silica granular aerogel window prototype installed on the test room (**a**); effect of the aerogel on the indoor temperature decreasing after heating system switching off (**b**) (Cotana et al. 2014)

climate conditions (Perugia, Central Italy). Indoor temperature decreases less than 3 °C, even several days after the heating system switching off (free-floating regime), whereas the conventional glazing system immediately tended to lower indoor air temperature up to the outdoor temperature values (Fig. 3.11b), by registering a strong decrease (about 6 °C during the first day). In thermal control regime (heating system is turned on), a decrease in energy consumption for heating up to 50 % was observed when the outdoor air temperature is not severe, e.g. during milder winter days with outdoor air temperature around 10 °C, while this difference was negligible at lower outdoor temperatures, less than 5 °C. Analysis of internal glass surface temperatures showed that the effect of aerogel consisted in lowering the maximum thermal peaks during the day and in keeping the internal surface temperature warmer during the night. The comparison between the lighting conditions of the scenario with aerogel with respect to the scenario with no aerogel showed that the aerogel was able to lower the daily average illuminance level by about 36–47 % during cloudy days, while its effect was lower in sunny weather conditions (less than 10 %). Finally, acoustic analyses results confirmed good performance of aerogel (increasing of acoustic insulation level of the façade previous) (see Sect. 3.3.4).

3.4.3 Numerical Analysis

The energy benefits of aerogel glazings have been investigated numerically since 2002 (Reim et al. 2002). In the German climate, during the heating period (15 September to 15 April), translucent aerogel glazings (16-mm-thick double-skin sheet filled with granular silica aerogel, two low emissivity coated glasses and gas filling, U-value = 0.4 W/m^2 K, solar factor: g = 0.3) mounted into a north-oriented façade showed the lowest thermal losses when compared to a triple glazing window

(U-value = 0.8 W/m^2 K, g = 0.6) and to an opaque insulation (U-value = 0.2 W/m^2 K).

The influence of monolithic aerogel windows on the heating energy consumption was also evaluated through simulations for a typical single-family house in Denmark (Schultz and Jensen 2008). An aerogel glazing with 20-mm aerogel thickness, resulting in a centre U-value of 0.5 W/m^2 K and a g-value equal to 0.75, was considered, and the results were compared to a triple-layered argon-filled glazing with two low-e coatings (U = 0.6 W/m^2 K and g = 0.46). The annual energy saving with aerogel glazing was approximately 1200 kWh/year, corresponding to 19 % of the energy for triple glazing (space heating demand equal to 5040 kWh/year for aerogel, 6220 for triple glazing). In a low-energy house (space heating demand < 15 kWh/m^2/year), the energy savings was approximately 700 kWh/year, corresponding to 34 % of annual space heating demand (about 2070 kWh/year). Nevertheless, in southern climates, the increase in cooling needs, due to the higher solar factor, diminishes the advantage of aerogel glazing, and in some cases, higher global energy consumption during the year could be obtained (Buratti and Moretti 2013).

Recently, Wang et al. (2014) performed a feasibility analysis of five types of glazings (3 conventional glazings and two granular aerogel systems) in five climate zones of China (Harbin, Beijing, Shanghai, Guangzhou, and Kunming) by means of eQuest code. Results showed that aerogel glazing systems lead to the lowest total heating and cooling loads in the four cities and close to the lowest total heating and cooling loads in Kunming (temperate climate). The energy saving of the aerogel glazing system compared with the clear glass was 20 % in Harbin and 11 and 9 % in Beijing and Shanghai, respectively. Therefore, the aerogel glazing system could be feasible for the building energy consumption reduction in all the considered zones in China, especially in severe cold region.

Buratti and Moretti (2013a) investigated the influence of glazing system on energy performance of a multifunctional building, consisting of one basement and two floors with ten zones each floor, in six different cities around the world (Rome, London, Moscow, Helsinki, Ottawa, and Beijing). Seven different glazings were considered: conventional glazings (single, double glazing system; low-e double glazing and low-e triple glazing) and innovative systems with silica aerogel granular and monolithic in interspace (Fig. 3.12). Glazings with monolithic aerogel in interspace result as the most efficient systems for cold climates: in Ottawa, the annual energy demand decreases of about 22–27 % when compared to the standard glazings (Fig. 3.12a). Nevertheless, due to the high solar factor (g), the energy demand for cooling increases for monolithic aerogel windows, especially in temperate climates (Fig. 3.12b). The energy demand for cooling is minimum for the granular aerogel glazing system with 40 mm thickness, due to the low solar factor (i.e. 0.25): the cooling energy saved is 25 % (7 kWh/m^2/year) for Beijing and 38 % for Ottawa (about 5 kWh/m^2/year) with respect to the standard double glazing. In general, granular aerogel glazing systems could be therefore considered the best solutions in terms of annual energy demand reduction, especially in cold climates,

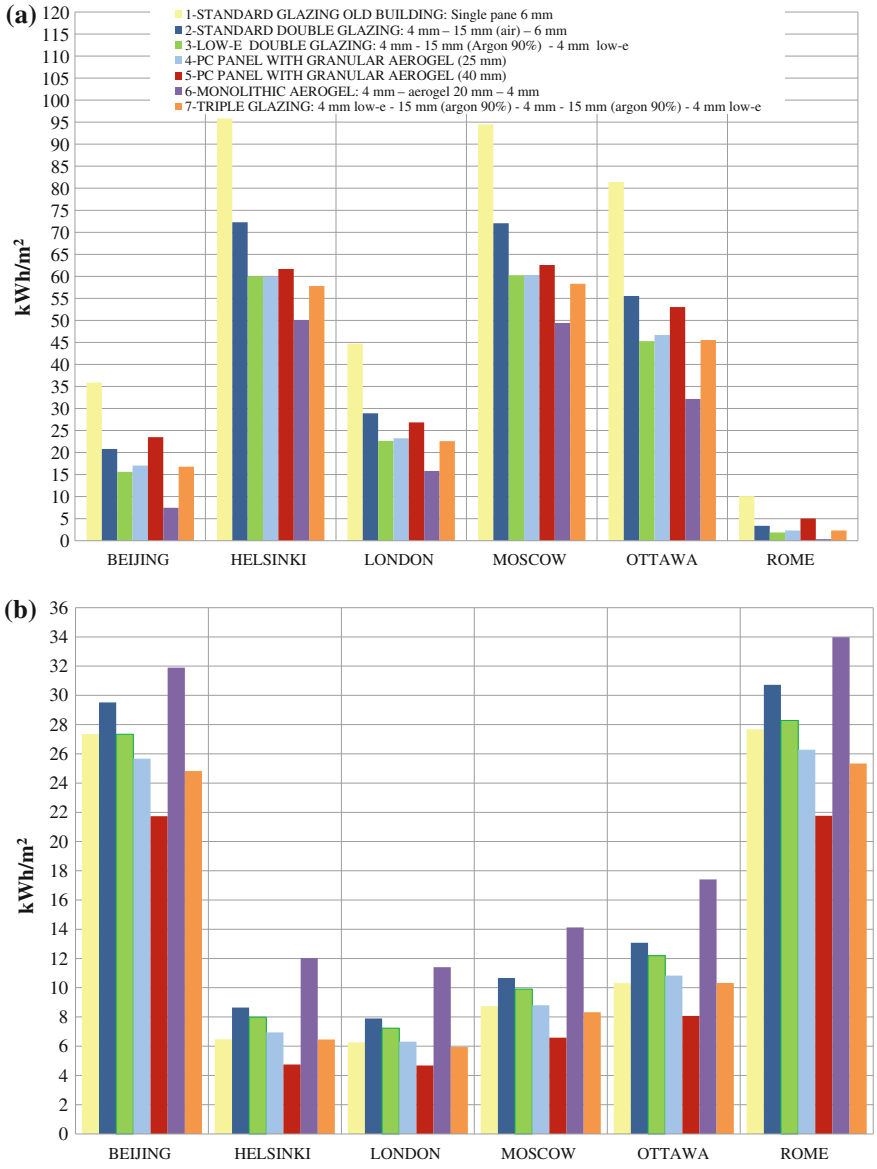

Fig. 3.12 Annual energy demand for heating (**a**) and cooling (**b**) for the six cities and for seven different kinds of glazing (Adapted from Buratti and Moretti 2013a)

resulting in a reduction in the 10–20 % of range with respect to standard double glazing system.

Huang and Niu (2015a) evaluated the influence of the investigated glazing system on the energy performance of HVAC systems in humid subtropical

cooling-dominant climates (Hong Kong). An EnergyPlus yearly based simulation was carried out for a typical commercial building, and the aerogel glazing performance was compared with a conventional glazing one. With respect to the reference case, aerogel glazing systems can reduce the total annual space cooling load (from April to October) by around 4 %, while the reduction could be around 60 % only considering the heat gain from the envelope. The annual cooling load reduction was almost the same the one achieved by the application of a shading-type low-e glazing, which indicates that silica aerogel glazings could be a suitable solution also in cooling-dominated climates. The same authors (Huang and Niu 2015b) also evaluated the energy performance taking into account different control strategies (indoor temperature control, operative temperature control, and occupant's PMV control), and they investigated the influence of aerogel glazing systems on visual performance for the same case study. The illumination level and distribution on the working plane (0.8 m height) and the human sensitivity towards the glazing surface (which is translucent due to aerogel) were investigated using radiance, considering two configurations. In the first case (case C), the conventional glazing was completely replaced with the silica aerogel glazing. In the second solution, the upper part and the lower part of the window were replaced by the silica aerogel glazing, while conventional single clear glazing was considered for the middle part in order to allow the view of the outdoor environment (case B, Fig. 3.13a).

Due to aerogel, the illumination level diminished, especially next to the window; however, the overall illumination level within the office was still satisfactory, also in the case C (Fig. 3.13b). Furthermore, the bright zone near the window area was significantly weakened, and the area of glare was reduced, improving visual comfort conditions (Fig. 3.13c). Results showed that the combination of conventional glazing and silica aerogel glazing could be a suitable solution, also according to Berardi (2015), which investigated monolithic aerogel-glazed windows for a retrofitting project of an educational building in Central Massachusetts. Four configurations with the different rates of aerogel replacements were considered (40, 60, 80, and 100 %, Fig. 3.14a), and the energy demand was evaluated: the heating energy consumption decreased linearly with increasing the aerogel proportion in the windows, whereas the cooling energy consumption kept almost stable with percentages of aerogel above 60 % (Fig. 3.14b). Nevertheless, the daylight analysis performed with DIVA indicated that the 60, 80, and 100 % aerogel windows could have a poorer effect over the daylight availability. Furthermore, the window with 40 % aerogel panels could improve the Useful Daylight Index (UDI, as percentage of time in which the daylight illuminance level is sufficient and useful for occupant) when compared to conventional solutions. Consequently, a 40 % aerogel window could be a good compromise, because it reduces the energy consumption simultaneously improving the daylight availability.

As final remark, from an energy saving perspective, the literature review showed that aerogel granulate glazing systems have the potential to become a solution in not only cold climates, but also in hot and warm ones. In a study by Ihara et al. (2015b),

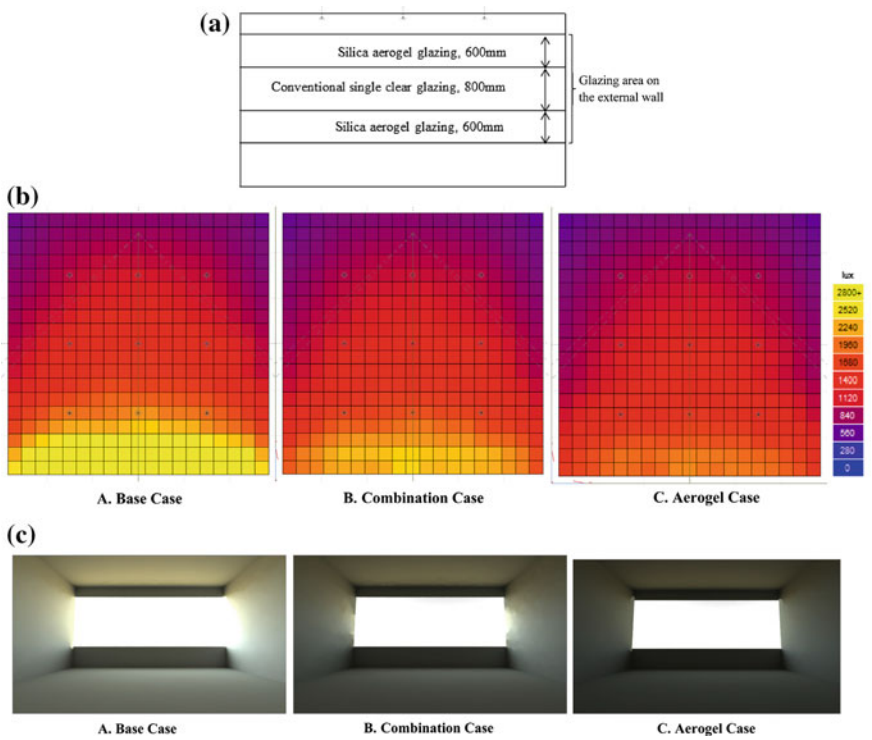

Fig. 3.13 Visual performance of aerogel windows: the second considered aerogel glazing (*B*: combination case) (**a**) impact on indoor illumination level in a south facing office at 12 am, 17 July (**b**) and on human sensitivity towards window (**c**) (Huang and Niu 2015b)

the energy performance of aerogel granulate glazing systems was evaluated by considering an office facade consisting of a translucent aerogel granulate glazing system at spandrels in three different cities (Oslo, Tokyo, and Singapore). The simulation results indicate that aerogel glazing facade can achieve a lower energy demand than a conventional solution (double glazing façade), also in cooling-dominated climates, such as Tokyo (warm) and Singapore (hot). The benefit is achieved by using aerogel glazing systems at spandrels, without any shading system. Triple glazing systems further reduce energy demand, even in hot and warm climates, whereas aerogel glazing systems are not effective when compared to triple glazing systems in such climates. However, the combination of aerogel glazing systems at spandrels and triple glazing systems at the visible part in a facade was indicated as the best solution in terms of energy performance.

Finally, a comparison of different facades performance, also including aerogels at spandrels, was performed taking into account energy (numerical evaluation by simulations), daylighting availability, construction efficiency, and durability

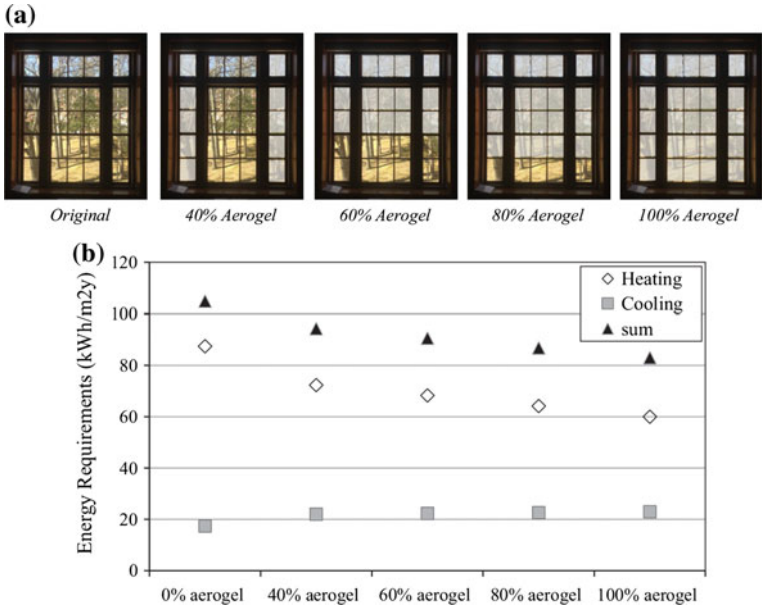

Fig. 3.14 The investigated window configurations with different percentages of aerogel inclusion (**a**); heating and cooling energy requirements for different window systems (**b**) (Berardi 2015)

Facade		Concrete facade	Aerogel granulate glazing facade		Multipane glazing facade	
		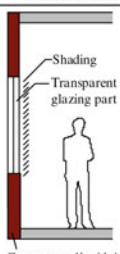 Concrete wall with insulaiton (Insulation thickness depends on location.)	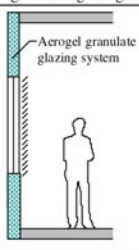 Aerogel granular type		Double glazing systems	Triple glazing systems
			Coarse	fine		
Energy	Cold regions	5	1	3	2	4
	Warm/hot regions	5	1	4	2	3
Daylight amount		1	3	2	5	4
Construction efficiency		1	3-5			2
Durability		5	3-4		1-2	

Better 5 > 4 > 3 > 2 > 1

Fig. 3.15 Comparison of different facades performance according to Ihara et al. (2015b)

(comparison based on conjecture). Aerogel facade could allow better energy performance than a double glazing façade and could achieve similar energy performance as a concrete façade, increasing simultaneously the daylight amount (Fig. 3.15).

The discussed findings suggest the investigation of new architecture techniques in order to include granular aerogel in the facades.

3.5 Economic Assessment and Future Trends

Based on the presented results, daylighting insulating systems with translucent or transparent silica aerogel seem to have the highest potential in fenestration market together with VIPs: the *U*-values can amount to 0.1 W/m^2 K, depending on thickness and technology. Nevertheless, VIP panels have problem of keeping the glazing gas-tight and very high costs. Moreover, aerogel windows have further advantages, such as acoustic insulation and lightness, and they can be easily used as roof solutions, especially in industrial buildings.

The investigated solutions are suitable in building refurbishment and could contribute to reduce the energy consumption in existing buildings, without substantially reducing the light transmission. As shown in the literature review, glazings with monolithic aerogel in interspace are the most efficient systems for very cold climates, because they have a very low thermal transmittance and a high total solar energy transmittance, even if the energy demand for cooling could increase, especially in temperate climates. Nevertheless, before considering a real spreading in the market, the research should take into account two main issues: improve the optical performance, i.e. the phenomenon of light scattering, that reduces optical quality of vision through the material, should be limited, and make progress in the production process, in order to manufacture large sheets of monolithic aerogels avoiding crack.

Therefore, in general, granular aerogel glazing systems could be considered the best solutions in the short and medium term, and they have the potential to become a solution not only in cold, but also in warm climates.

Since windows should last 20–50 years, the durability of nanogel windows should be properly addressed. Gao et al. (2014a) highlighted that aerogel granules may loss, partly or totally, the surface hydrophobicity during their service life, especially considering small-sized aerogel granules, if prepared from the large granules via grinding. Therefore, future studies should focus on the ageing effect of aerogel granules, due to moisture and solar radiation. Furthermore, a problem concerning the stability of granular aerogel windows was observed. Being a particle aggregation system, the volume of the aerogel granules tends to shrink along with time to reach the highest possible packing density, causing an air gap inside the glazing system, which becomes a thermal bridge and decreases the thermal insulation performance (Gao et al. 2014a).

Even though aerogel windows had a lot of extraordinary properties, they need to be more cost effective in order to compete with the conventional solutions. A reference market price for a cubic metre of granular silica aerogel is on the order of 3500 US$ (the price depends on the grain size and on the quantity), but it could drop below the 1500 US$ by the year 2020, due to the expected spreading in the

market. It means that a 15-mm thickness interspace filled with granular aerogels could have now a cost of about 50 US$/m^2 that could become 22.5 US$/m^2 in 2020. However, the cost of an aerogel window could be up to six times than a conventional window (Cuce et al. 2014b), and it is the main barrier to overcome in the near future for a wide-scale use.

Finally, the research on silica aerogel for windows recently touched upon the possibility of achieving high-performance glass materials using silica aerogels (Gao et al. 2014b). Glass materials were successfully prepared by sintering monolithic silica aerogel precursors at high temperatures, achieving lightweight (density in the 1.60–1.79 g/cm^3 range) and insulating glass materials. The thermal conductivity is about 0.17–0.18 W/m K compared to about 1 W/m K for a float glass, together with high transparency (the light transmittance is 91–96 % at 500 nm). During the densification process at high temperatures, the mechanical strength of aerogel glass materials was also enhanced (up to three orders of magnitude when compared to silica aerogel), but probably it is still not sufficient for the application in glazing systems. Due to the obtained structural and functional features, innovative aerogel glass materials are very attractive for future window glazing applications, even if further studies are still necessary to improve the material performance, to investigate the manufacturing process at large scale, and to assess the economic feasibility.

References

AbuBakr Bahaj S, James PAB, Jentsch MF (2008) Potential of emerging glazing technologies for highly glazed buildings in hot arid climates. Energy Build 5:720–731

Aegerter MA, Leventis N, Koebel MM (2011) Aerogels handbook. Springer, Berlin

Akimov YK (2003) Fields of application of aerogels (review). Instrum Exp Tech 3:287–299

Anderson AM, Wattley CW, Carroll MK (2009) Silica aerogels prepared via rapid supercritical extraction: effect of process variables on aerogel properties. J Non-Cryst Solids 2:101–108

Baetens R, Jelle BP, Gustavsen A (2011) Aerogel insulation for building applications: a state-of-the-art review. Energy Build 43:761–769

Berardi U (2015) The development of a monolithic aerogel glazed window for an energy retrofitting project. Appl Energy 154:603–615

Błaszczyński T, Ślosarczyk A, Morawski M (2013) Synthesis of silica aerogel by supercritical drying method. In: 11th international conference on modern building materials, structures and techniques, MBMST 2013. Procedia Engineering vol 57, pp 200–206

Bouquerela M, Duforestel T, Baillis D, Rusaouen G (2012) Heat transfer modeling in vacuum insulation panels containing nanoporous silicas—a review. Energy Build 54:320–336

BPIE (Building Performance Institute Europe) (2011) Europe's buildings under the microscope. Available at http://www.bpie.eu/eu_buildings_under_microscope.html. Last access on 2 July 2015

Buratti C, Moretti E (2011a) Transparent insulating materials for buildings energy savings: experimental results and performance evaluation. In: Proceedings of third international conference on applied energy. Perugia, Italy

Buratti C, Moretti E (2011b) Lighting and energetic characteristics of transparent insulating materials: experimental data and calculation. Indoor Built Environ 20(4):400–411

Buratti C, Moretti E (2012a) Experimental performance evaluation of aerogel glazing systems. Appl Energy 97:430—437. doi:http://dx.doi.org/10.1016/j.apenergy.2011.12.055

Buratti C, Moretti E (2012b) Glazing systems with silica aerogel for energy savings in buildings. Appl Energy 98:396–403. doi:http://dx.doi.org/10.1016/j.apenergy.2012.03.062

Buratti C, Moretti E (2013a) Chapter 20—nanogel windows. In: Torgal FP, Mistretta M, Kaklauskas A, Granqvist CG, Cabeza LF (eds) Nearly zero energy building refurbishment: a multidisciplinary approach. Springer, London, pp 555–582. doi:10.1007/978-1-4471-5523-2_20. ISBN: 978-1-4471-5522-5

Buratti C, Moretti E (2013b) Chapter 10—silica nanogel for energy-efficient windows. In: Torgal FP, Diamanti MV, Nazari A, Granqvist CG (eds) Nanotechnology in eco-efficient construction. Woodhead Publishing Limited, Cambridge, pp 207–235. doi:10.1533/9780857098832.2.207. ISBN 9780857095442

Buratti C, Moretti E, Belloni E (2012c) The influence of glazing systems on energy performance of non-residential buildings. In: Proceedings of the 25th international conference on efficiency, cost, optimization and simulation of energy conversion systems and processes, ECOS 2012, 26–29 June 2012, Perugia, Italy, pp 281–294

Buratti C, Moretti E, Belloni E, Cotana F (2013) Unsteady simulation of energy performance and thermal comfort in non-residential buildings. Build Environ 59:482–491

Buratti C, Moretti E, Belloni E, Agosti F (2014) Development of innovative aerogel based plasters: preliminary thermal and acoustic performance evaluation. Sustainability 6(9):5839–5852. doi:10.3390/su6095839

Buratti C, Moretti E, Belloni E (2016) Aerogel plasters for building energy efficiency. In: Torgal FP, Buratti C, Kalaiselvam S, Granqvist CG, Ivanov V (eds) Nano and biotech based materials for energy building efficiency. Springer International Publishing. ISBN: 978-3-319-27503-1

Cabot Corporation (2015) http://www.cabotcorp.com/solutions/products-plus/aerogel. Last access on 15 Sept 2015

Cotana F, Pisello AL, Moretti E, Buratti C (2014) Multipurpose characterization of glazing systems with silica aerogel: in-field experimental analysis of thermal-energy, lighting and acoustic performance. Build Environ 81:92–102. doi:10.1016/j.buildenv.2014.06.014

Cuce E, Cuce PM, Wood CJ, Riffat SB (2014a) Optimizing insulation thickness and analysing environmental impacts of aerogel-based thermal superinsulation in buildings. Energy Build 77:28–39

Cuce E, Cuce PM, Wood CJ, Riffat SB (2014b) Toward aerogel based thermal superinsulation in buildings: a comprehensive review. Renew Sustain Energy Rev 34:273–299

Dorcheh AS, Abbasi H (2008) Silica aerogel; synthesis, properties and characterization. J Mater Process Technol 199:10–26

Dowson M, Harrison D, Craig S, Gill Z (2011) Improving the thermal performance of single-glazed windows using translucent granular aerogel. Int J Sustain Eng 4(3):266–280

Dowson M, Grogan M, Birks T, Harrison D, Craig S (2012a) Streamlined life cycle assessment of transparent silica aerogel made by supercritical drying. Appl Energy 97:396–404

Dowson M, Pegg I, Harrison D, Dehouche Z (2012b) Predicted and in situ performance of a solar air collector incorporating a translucent granular aerogel cover. Energy Build 49:173–187

Dowson M, Harrison D, Dehouche Z (2014) Trombe walls with nanoporous aerogel insulation applied to UK housing refurbishment. Int J Smart Nano Mater 5:283–303

Duer K, Svendsen S (1998) Monolithic silica aerogel in superinsulating glazings. Sol Energy 63:259–267

European Community (2009) Directive 2009/28/EC of the European Parliament and of the Council of 23 April 2009 on the promotion of the use of energy from renewable sources and amending and subsequently repealing Directives 2001/77/EC and 2003/30/EC. Off J Eur Union L140:16–62

European Community (2010) Directive 2010/31/EU of the European Parliament and of the Council of 19 May 2010 on the energy performance of buildings (recast). Off J Eur Union L153:13–35

Forest L, Gibiat V, Woignier T (1998) Biots theory of acoustic propagation in porous media applied to aerogels and alcogels. J Non-Cryst Solids 225:287–292

Forest L, Gibiat V, Hooley A (2001) Impedance matching and acoustic absorption in granular layers of silica aerogels. J Non-Cryst Solids 285:230–235
Fu T, Tang J, Chen K, Zhang F (2015) Visible, near-infrared and infrared optical properties of silica aerogels. Infrared Phys Technol. doi:http://dx.doi.org/10.1016/j.infrared.2015.03.004
Gao T, Jelle BP, Ihara T, Gustavsen A (2014a) Insulating glazing units with silica aerogel granules: the impact of particle size. Appl Energy 128:27–34
Gao T, Jelle BP, Ihara T, Gustavsen A (2014b) Lightweight and thermally insulating aerogel glass materials. Appl Phys 117:799–808
Gurav JL, Jung IK, Park HH, Kangand ES, Nadargi DY (2010) Silica aerogels: synthesis and applications. J Nanomater 409310. doi:http://dx.doi.org/10.1155/2010/409310
He YL, Xie T (2015) Advances of thermal conductivity models of nanoscale silica aerogel insulation material. Appl Therm Eng 81:28–50
Huang Y, Niu J (2015a) Application of super-insulating translucent silica aerogel glazing system on commercial building envelope of humid subtropical climates: Impact on space cooling load. Energy 83:316–325
Huang Y, Niu J (2015b) Energy and visual performance of the silica aerogel glazing system in commercial buildings of Hong Kong. Constr Build Mater 94:57–72
Ihara T, Grynning S, Gao T, Gustavsen A, Jelle BP (2015a) Impact of convection on thermal performance of aerogel granulate glazing systems. Energy Build 88:165–173
Ihara T, Gao T, Grynning S, Jelle BP, Gustavsen A (2015b) Aerogel granulate glazing facades and their application potential from an energy saving perspective. Appl Energy 142:179–191
Ihara T, Jelle BP, Gao T, Gustavsen A (2015c) Aerogel granule aging driven by moisture and solar radiation. Energy Build 103:238–248. doi:10.1016/j.enbuild.2015.06.017
Ivanov GR, Tomova R, Djambova ST, Nadoliiski M, Dimova–Malinovska D (2010) Functionalized aerogels—new nanomaterials for energy-efficient building. Preliminary AFM, nanoindentation and EIS studies. J Phys: Conf Series 253. doi:10.1088/1742-6596/253/1/012077
Jelle BP, Hynd A, Gustavsen A, Arasteh D, Goudey H, Hart R (2012) Fenestration of today and tomorrow: a state-of-the-art review and future research opportunities. Sol Energy Mater Sol Cells 96:1–28
Jensen KI, Schultz JM, Kristiansen FH (2004) Development of windows based on highly insulating aerogel glazings. J Non-Cryst Solids 350:351–357
Kaushika ND, Sumathy K(2003) Solar transparent insulation materials: a review. Renew Sustain Energy Rev 7:317–351
Koebel M, Rigacci A, Achard P (2012) Aerogel-based thermal superinsulation: an overview. J Sol-Gel Sci Technol 63:315–339. doi:10.1007/s10971-012-2792-9
Lumira® Aerogel Consortium (2015) http://www.lumiradaylighting.com/. Last access on 24 June 2015
Moretti E, Zinzi M, Belloni E (2014) Polycarbonate panels for buildings: experimental investigation of thermal and optical performance. Energy Build 70:23–35. doi:10.1016/j.enbuild.2013.11.045
Neugebauera A, Chenb K, Tangc A, Allgeierd A, Glicksmana LR, Gibsonc LJ (2014) Thermal conductivity and characterization of compacted, granular silica aerogel. Energy Build 79:47–57
Ng S, Jelle BP, Sandberg LIC, Gao T, Wallevik OH (2015) Experimental investigations of aerogel-incorporated ultra-high performance concrete. Constr Build Mater 77(4):307–316
Pajonk GM (2003) Some applications of silica aerogels. Colloid Polym Sci 281:637–651
Parmenter KE, Milstein F (1998) Mechanical properties of silica aerogels. J Non-Cryst Solids 223 (3):179–189
Pérez-Lombard L, Ortiz J, Pout C (2008) A review on buildings energy consumption information. Energy Build 40:394–398
Pierre AC, Pajonk GM (2002) Chemistry of aerogels and their applications. Chem Rev 102:4243–4265

Reim M, Beck A, Körner W, Petricevic R, Glora M, Weth M, Schliermann T, Schmidt CH, Pötter FJ, Fricke J (2002) Highly insulating aerogel glazing for solar energy usage. Solar Energy 1:21–29

Reim M, Reichenauer G, Körner W, Manara J, Arduini-Schuster M, Korder S, Beck A, Fricke J (2004) Silica-aerogel granulate—structural, optical and thermal properties. J Non-Cryst Solids 350:358–363

Reim M, Korner W, Manara J, Korder S, Arduini-Schuster M, Ebert HP, Fricke J (2005) Silica aerogel granulate material for thermal insulation and daylighting. Sol Energy 2:131–139

Riffat SB, Qiu G (2012) A review of state-of-the-art aerogel applications in buildings. Int J Low-Carbon Technol Adv Access

Rigacci A, Einarsrud M, Nilsen E, Pirard R, Ehrburger-Dolled F, Chevalier B (2004) Improvement of the silica aerogel strengthening process for scaling-up monolithic tile production. J Non-Cryst Solids 350:196–201

Schultz JM, Jensen KI (2008) Evacuated aerogel glazings. Vacuum 82:723–729

Schultz JM, Jensen KI, Kristiansen FH (2005) Super insulating aerogel glazing. Sol Energy Mater Sol Cells 89:275–285

Tajiri K, Igarashi K (1998) The effect of the preparation conditions on the optical properties of transparent silica aerogels. Sol Energy Mater Sol Cells 4:189–195

Wang H, Wu H, Ding Y, Feng J, Wang S (2014) Feasibility and optimization of aerogel glazing system for building energy efficiency in different climates. Int J Low-Carbon Technol 1–8

Werner M, Brand L (2010) Focus report 2010—aerogels, general sector reports, chemistry and materials, observatory NANO. Available at http://www.observatorynano.eu/project/filesystem/files/WP2_ChemistryMaterials_FocusReport_Aerogels_29_04_2010.pdf. Accessed 22 Jan 2013

Yan Z (2013) A review of aerogels and their application as a multi-functional building material. Appl Mech Mater 253–255:564–567

Zhao Y, Tang GH, Du M (2015) Numerical study of radiative properties of nanoporous silica aerogel. Int J Ther Sci 89:110–120

Zhu W, Bartos PJM, Porro A (2004) Application of nanotechnology in construction. Summary of a state-of-the-art report. Mater Struct 37:649–658

Chapter 4
Thermochromics for Energy-Efficient Buildings: Thin Surface Coatings and Nanoparticle Composites

Yu-Xia Ji, Mats Boman, Gunnar A. Niklasson and Claes-Göran Granqvist

Abstract This chapter outlines the state of the art of the thermochromic glazings that are able to provide energy efficiency by letting in more solar energy at a low temperature than at a high temperature, thereby leading to diminished need for space cooling. Thermochromic technology employs VO_2-based materials as thin coatings or nanoparticle composites. For coatings, suitable switching between conditions with high and low solar energy throughput at low and high temperature, respectively, can be achieved by replacing some of the vanadium atoms by tungsten, and luminous transmittance can be enhanced by the addition of some magnesium. Antireflection (AR) coatings can give further improvements. By going to nanoparticle composites with VO_2 dispersed in a transparent host, it is possible to combine high luminous transmittance with large modulation of solar energy transmittance. This modulation ensues from plasmonic absorption in metallic-like VO_2 nanoparticles. Thermochromic glazings are not yet (2015) available as products, but the rapid development during recent years has led to performance limits that appear very interesting for practical applications. Energy modeling of buildings with thermochromic glazings points at very substantial savings. A further development may be to integrate thermochromic nanoparticles in laminated electrochromic devices.

4.1 Introduction

Thermochromic glazings are characterized by their temperature-dependent properties and are able to transmit more solar energy at low temperature than at high temperature. The property change should be related to the building's "balance

Y.-X. Ji · G.A. Niklasson · C.-G. Granqvist (✉)
Department of Engineering Sciences, The Ångström Laboratory,
P.O. Box 534, SE-75121 Uppsala, Sweden
e-mail: claes-goran.granqvist@angstrom.uu.se

M. Boman
Department of Chemistry, The Ångström Laboratory,
Uppsala University, P.O Box 538, SE-75121 Uppsala, Sweden

F. Pacheco Torgal et al. (eds.), *Nano and Biotech Based Materials for Energy Building Efficiency*, DOI 10.1007/978-3-319-27505-5_4

temperature" separating cooling-dominated from heating-dominated conditions. Thermochromic glazings are not a new subject, and early work by Lee and Jorgenson (1986), Jorgensen and Lee (1986) and Babulanam et al. (1986, 1987) dates back about thirty years. The topic met with initial enthusiasm (Jorgenson and Lee 1990), but the interest faded when it was realized that the temperature-dependent modulation that actually could be accomplished was too small to be of much practical value and also occurred at an inadequate temperature range. Material development during the 2000s has changed the situation, however, and thermochromic glazings—i.e., windows as well as glass facades—are back in the limelight. The topic has been surveyed recently by Granqvist (2014a, 2015a, b), but the development progresses at a sufficient pace that a new and more detailed examination is justified. It is given in the present chapter.

Why is thermochromics of interest for energy-efficient buildings? The heating, cooling, lighting, and ventilation of buildings account for 30–40 % of the world's primary energy, as reported by the United Nations Development Program (UNEP 2007), and the fraction tends to increase at least in the most developed countries. Thus, the buildings shares of the primary energy use in the USA were 34, 36, 38, and 41 % in 1980, 1990, 2000, and 2010, respectively, according to the Department of Energy (US DOE 2012). Glazings are generally considered weak links in buildings' energy systems and usually let in or out too much energy, which then has to be compensated by heating and cooling. Thermal insulation of the glazings can diminish the heat transfer to ~ 1 $\mathrm{Wm^{-2}\,K^{-1}}$ or less if multiple panes are used and if the glass has a layer of a transparent reflector for thermal infrared radiation in the 3–50 μm wavelength range, and excessive solar energy inflow can be prevented if the glass is reflecting near-infrared solar radiation at 0.7–3 μm (Smith and Granqvist 2010; Granqvist 2015a, b). These types of glazings make use of coatings—referred to as low-emittance coatings and solar-control coatings, respectively—that have been developed for decades and now have properties close to those allowed by the laws of nature applied to known materials (Granqvist 2007, 2015b). The main problem with these coatings is that they have *static* properties, whereas nature provides a *dynamic* ambience for the buildings which is sometimes undesirably warm or too cold so that energy-demanding cooling and heating of buildings cannot be avoided, even if the energy for cooling and heating is lowered as a consequence of the static coatings referred to above. Therefore, the glazings must have adjustable properties and be able to respond to varying environmental conditions, which take us to the class of materials known as *chromogenic* (Granqvist 1990; Lampert and Granqvist 1990; Smith and Granqvist 2010).

There are several types of chromogenic materials, which are able to respond to different external stimuli:

- *photochromic* materials darken under ultraviolet solar irradiation and bleach in the absence of such radiation and are well known especially in sunglasses,
- *thermochromic* materials have different optical transmittance depending on their temperature and will be discussed with regard to buildings-related applications in this chapter,

- *electrochromic* materials can be integrated into multilayer devices and are able to alter their transmittance by the insertion/extraction of charge or by the application of a voltage (Granqvist 1995, 2012, 2013a, b, 2014b), and
- *gasochromic* materials change their transmittance when exposed to reducing/oxidizing gas.

Electrochromic glazings are already on the market and are used on a small scale by early adopters (Granqvist 2012, 2014b; Pittaluga 2015). Thermochromic glazings are not yet as advanced, but their development is rapid and—in the author's opinion—applications may soon be possible either by use of thermochromic thin films or nanoparticles as such or through a combination with electrochromics. Photochromic and gasochromic fenestrations seem to be more remote.

Some basic facts about visible light (luminous radiation), solar irradiation, and thermal radiation should be well understood and are needed for assessing the energy efficiency of glazings. The necessary information is found in Fig. 4.1. We first consider *thermal radiation*, which is obtained by multiplying a blackbody curve for the temperature τ in case—as shown in panel (a)—by an empirical emittance that is less than unity; this radiation is confined to $\lambda > 2$ μm, where λ denotes wavelength, for temperatures of practical interest. The *solar radiation* onto the atmosphere corresponds approximately to the blackbody curve for the sun's surface temperature (5505 °C), and the irradiation at ground level is obtained by multiplying with the atmospheric absorption. Figure 4.1b shows this radiation for typical clear weather and shows that the radiation lies at $0.3 < \lambda < 2$ μm, which indicates that there is almost no overlap between the wavelength intervals for solar and thermal radiation, i.e., a material can have entirely different properties for these two wavelength ranges. Only part of the solar radiation is *visible light*, and Fig. 4.1b shows that the

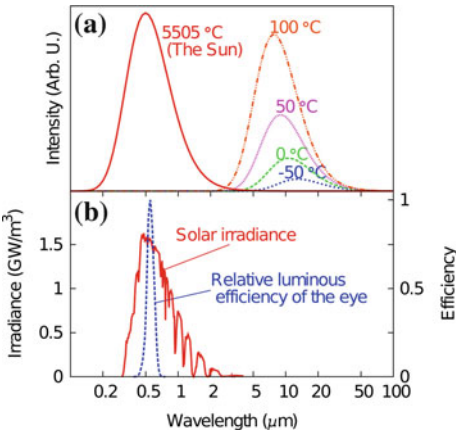

Fig. 4.1 *Upper panel* illustrates blackbody spectra for five temperatures, one of which approximates the sun's surface temperature. *Lower panel* shows a typical solar irradiance spectrum for clear weather conditions and at sea level, and the sensitivity of the light-adapted human eye

eye's sensitivity can be represented by a bell-shaped curve in the range $0.4 < \lambda < 0.7$ μm with a peak at $\lambda = 0.55$ μm. In terms of solar energy, about 50 % falls in the infrared ($\lambda > 0.7$ μm), whereas about 5 % falls in the ultraviolet ($\lambda < 0.4$ μm).

Quantitative data on the temperature-dependent luminous (lum) and solar (sol) transmittance for thermochromic materials, denoted $T_{\mathrm{lum}}(\tau)$ and $T_{\mathrm{sol}}(\tau)$, can be obtained from

$$T_{\mathrm{lum,sol}}(\tau) = \int \mathrm{d}\lambda\ \varphi_{\mathrm{lum,sol}}(\lambda) T(\lambda, \tau) / \int \mathrm{d}\lambda\ \varphi_{\mathrm{lum,sol}}(\lambda), \tag{4.1}$$

where $T(\lambda, \tau)$ is spectral transmittance, φ_{lum} is the sensitivity of the light-adapted human eye (Wyszecki and Stiles 2000), and φ_{sol} is the solar irradiance when the sun is at 37° above the horizon (at "air mass 1.5," implying that the path-length through the atmosphere is 50 % longer than for vertically incident radiation) (ASTM 2008). For the subsequent analysis, we need quantitative data on solar energy modulation ΔT_{sol}, which is defined by

$$\Delta T_{\mathrm{sol}} \equiv T_{\mathrm{sol}}(\tau < \tau_c) - T_{\mathrm{sol}}(\tau > \tau_c). \tag{4.2}$$

This chapter is organized as follows: Sect. 4.2 introduces VO_2 and argues that it is the thermochromic material of choice for practical glazing applications. Section 4.3 then treats the manufacturing of thin films and nanoparticles of this material, mainly from a thermodynamics point of view. In Sect. 4.4, we discuss how VO_2 can be modified by doping, nanostructuring, and overcoating in order to be of practical interest for thermochromic glazings; results from recent energy modeling of buildings are included too. Finally, Sect. 4.5 gives conclusions and outlook.

4.2 Vanadium Dioxide: The Thermochromic Material of Choice

There are a large number of thermochromic materials, both inorganic and organic. The number of options for glazings is quite limited, however. First, we exclude the many organics (Seeboth and Lötzsch 2014) which most probably are too sensitive to ultraviolet irradiation to permit long-term applications. Secondly, we contemplate that the surface areas needed to be covered with thermochromic materials, either as thin films or nanoparticle composites, are huge and this limits the choice of materials to sufficiently "simple" ones that can be manufactured on the relevant scale. In order to appreciate this scale, it should be realized that flat-glass production—mostly by the float process and for glazing applications—is forecast to reach 9.2×10^9 square meters per year in 2016 (Freedonia 2013).

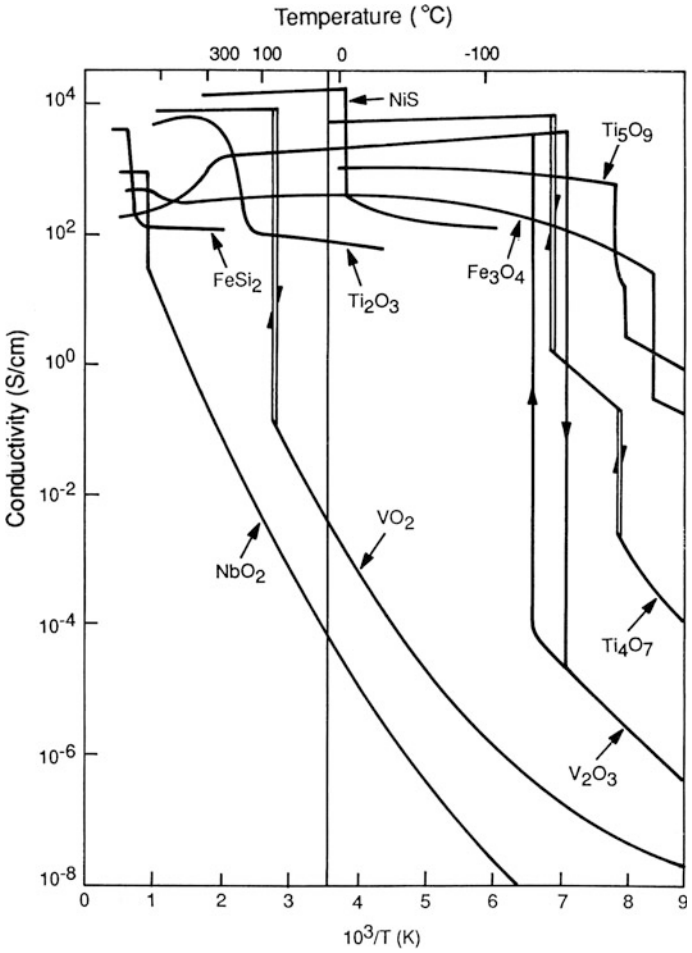

Fig. 4.2 Electrical conductivity versus reciprocal temperature (*lower horizontal axis*) and temperature (*upper horizontal axis*) for several metal-based compounds. The *vertical line* indicates room temperature. From Jorgensen and Lee (1986)

Figure 4.2 shows data on a selection of some remaining options, specifically on temperature-dependent electrical conductivity for oxides and other materials (Jorgenson and Lee 1986). Abrupt changes take place at well-defined values of a "critical" temperature τ_c and signal structural changes. Vanadium dioxide, VO_2, is particularly interesting since $\tau_c \approx 68$ °C, i.e., in the vicinity of room temperature, as discovered more than 50 years ago by Morin (1959). Therefore, this material stands out as the most viable candidate for thermochromic glazings and, in fact, almost all investigations for this application have VO_2 as a starting point. The switching at τ_c

occurs between a *low-temperature semiconducting phase* with small infrared absorption (and hence high infrared transmittance as a thin film) and monoclinic crystal structure and a *high-temperature metal-like phase* with large infrared reflectance and rutile-type crystal structure. The physical nature of the transition at τ_c is of lingering scientific interest and has kept materials physicists busy for decades.

Figure 4.3 summarizes the most salient optical properties of VO_2-based materials. Left-hand panels report spectral transmittance (upper) and reflectance (lower) for 50-nm-thick VO_2 coatings on glass in the wavelength range pertinent to solar radiation, and it is seen that $T(\lambda, \tau)$ is much larger in the semiconducting state than in the metallic state—i.e., below and above τ_c, respectively—when $\lambda > 1$ μm. The difference in the spectral transmittance between low and high temperature gets larger for increasing wavelength. Obviously, this kind of variation in $T(\lambda, \tau)$ is the desired one, at least in principle, and a glazing with a thermochromic VO_2-based coating lets in more energy at low temperature than at high temperature, as has been found experimentally many times (Saeli et al. 2010a, b; Gao et al. 2012; Hoffman et al. 2014; Li et al. 2014; Warwick and Binions 2014). Figure 4.3 also shows that the corresponding reflectance curve increases monotonically toward long wavelengths for the metallic-like state, which is as expected. Right-hand panels in Fig. 4.3 refer to nanoparticles of VO_2 and will be discussed later.

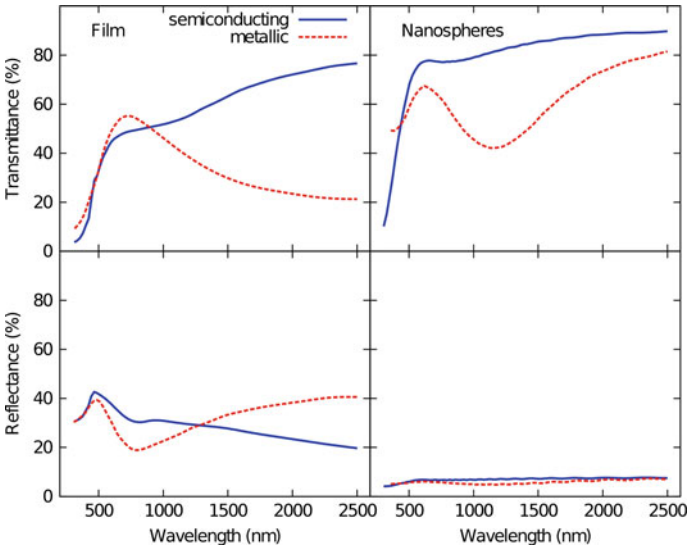

Fig. 4.3 Spectral transmittance (*upper panels*) and reflectance (*lower panels*) for a 50-nm-thick coating of VO_2 (*left-hand panels*) and for a layer consisting of a dilute dispersion of VO_2 nanospheres, having an equivalent VO_2 thickness of 50 nm, in a medium characteristic of transparent glass and polymer

4.3 On the Fabrication of VO_2 Coatings and Nanoparticles

4.3.1 Reaction Routes

Techniques for practical fabrication of VO_2 coatings and nanoparticles are of obvious interest and are in a state of rapid development. We first observe that vanadium has high affinity for oxygen and can form compounds with the metal in several different oxidation states, specifically +5, +4, +3, and +2 (Anderson and Khan 1970; Mukherjee and Wach 1983). It is therefore not surprising that the vanadium–oxygen phase diagram, illustrated in Fig. 4.4, is complicated and contains nearly twenty different phases, often with only small variations in composition (Smith 1989; Wriedt 1989; Kang 2012; Bahlawane and Lenoble 2014). The difficulties in the synthesis of VO_2 are associated with the coexistence of these diverse oxide forms and also with various polymorphs (Gulbransen and Andrew 1950; Andersson 1956). Therefore, it is usually hard to obtain phase-pure VO_2, which is formed only in a very narrow range of oxygen partial pressure.

Elemental solid (s) vanadium reacts with oxygen gas (g) in a simple and direct way and produces vanadium dioxide according to the overall reaction

$$\mathrm{V(s) + O_2(g) \rightarrow VO_2(s)}, \tag{4.3}$$

and various physical vapor deposition techniques—such as thermal evaporation (Marvel et al. 2013), pulsed laser deposition (Jian et al. 2013), and sputtering (Li et al. 2013a; Ji et al. 2014a, b)—have been employed to synthesize VO_2 coatings by deposition in an atmosphere with controlled oxygen partial pressure and at high temperature, typically being $\sim$450 °C although lower temperatures are possible for special sputtering techniques (Fortier et al. 2014; Aijaz et al. 2015). However, such process control is challenging, and vanadium oxidizes rapidly at high temperature and goes progressively from tetragonal VO_2 to V_6O_{13} and V_3O_7, until it ultimately reaches thermally stable orthorhombic V_2O_5 in accordance with the phase diagram in Fig. 4.4 (we return to this point in Sect. 4.4.4 below).

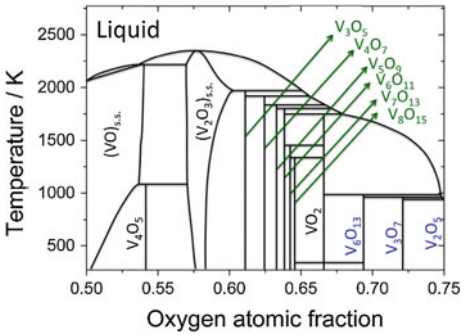

Fig. 4.4 Phase diagram for the VO–$VO_{2.5}$ system. From Kang (2012)

For more convenient thin film manufacturing, it may be advantageous to use a mild oxidation agent as an alternative to oxidation according to reaction (4.3), and below we discuss the usefulness of SO_2, following a recent study by Ji et al. (2016). The benefit of the sulfur-based route stems from the fact that sulfur can have multiple oxidation states and displays both oxidizing and reducing ability as has been known for a long time (Lepsoe 1940; Ivanov and Balzhinimaev 1987). For example, it has been demonstrated that the reduction of sulfur dioxide by reactive transition metals will form elemental sulfur and metal oxide (Liu et al. 1994). The oxidation of vanadium by SO_2 can be captured by the overall reaction

$$\mathrm{V(s) + SO_2(g) \rightarrow VO_2(s) + S(g).} \tag{4.4}$$

If SO_2 is completely decomposed, the products from the reaction would be VO_2 and S, and the sulfur can be vaporized and removed at high enough temperature.

4.3.2 Thermodynamic Analysis of Reaction Products

The characteristic features of reactions (4.3) and (4.4) for making VO_2 films can be assessed from a thermodynamic analysis, which gives some basic understanding of the reaction and ascertains that the desired reaction will happen. In general, the change in free energy for the reaction—i.e., the Gibbs free energy ΔG_r—determines the reaction direction, and a negative value of ΔG_r indicates that it is thermodynamically favorable for the reaction to proceed to its products side, whereas a positive ΔG_r means that the reaction will not take place. If more than one reaction is thermodynamically possible, the one with the most negative ΔG_r should take place since it leads to the most stable reaction products. For a closed reaction system, equilibrium compositions under given conditions of pressure P, temperature τ, and input concentration of reactants can be determined by the use of thermodynamic methods under constraints of mass conservation. Starting with the given reactants and given P and τ, this analysis identifies possible gaseous and condensed chemical species and calculates possible reaction products without kinetic considerations.

Specifically, we simulated how VO_2 would be formed from metallic vanadium in gaseous O_2 and SO_2 environments. Ideally, one mole of V reacts with one mole of O_2 or SO_2 according to reactions (4.3) or (4.4), respectively, but in practice it is very hard to balance the mole ratio exactly, and the simulations therefore used an excess of the gases, viz., two mole of O_2 or SO_2. Figure 4.5 refers to the V–SO_2 system and shows an example of stable reaction products at four SO_2 pressures in the $0.001 < P_{SO_2} < 1$ atm range and for $100 \leq \tau \leq 700$ °C. It is predicted that VO_2 is obtained in the lower temperature range and that V_2O_3 is created at higher temperatures. Liquid sulfur is also formed as a condensed phase on the VO_2, and this

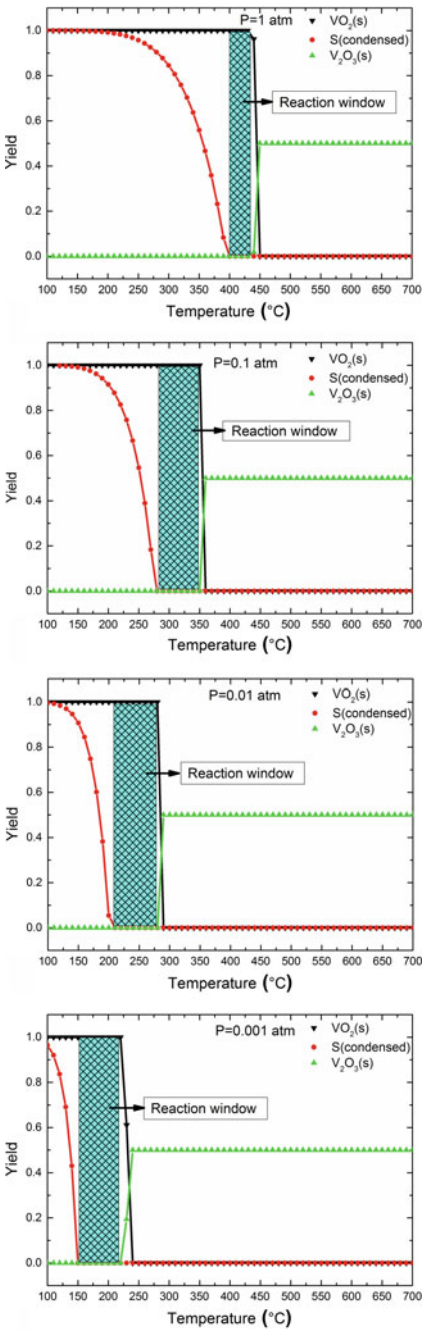

Fig. 4.5 Calculated yields for the formation of stable compounds in equilibrium at the shown pressures P and temperatures when the input reactants are one mole of V and two mole of SO_2. The products are in solid (s) and condensed form. Hatched regions indicate reaction windows for VO_2 film deposition

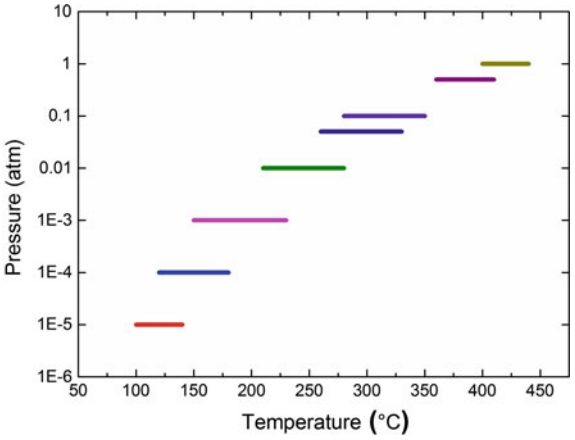

Fig. 4.6 Calculated reaction window versus pressure when the input reactants are one mole of V and two mole of SO_2

sulfur can be vaporized at sufficiently high temperature. Consequently, there is a thermodynamically calculated reaction window for VO_2 film growth at 400–440 °C for $P_{SO_2} = 1$ atm, and this window drops monotonically upon decreasing pressure until it reaches 150–230 °C for $P_{SO_2} = 0.001$ atm. The connection between reaction window and P_{SO_2} is further illustrated in Fig. 4.6, which makes it clear that the width of the reaction window is increased from ~40 to ~80 °C when P_{SO_2} drops from 1 to 0.001 atm., and the width is then decreased as P_{SO_2} is further diminished to 10^{-5} atm.

Figure 4.7 provides more detailed comparisons of the formation conditions for VO_2 in the V–SO_2 system and the V–O_2 system and reports the yield of formation of VO_2 at $100 \le \tau \le 700$ °C and $10^{-7} \le P \le 10$ atm. of SO_2 (upper panel) and O_2 (lower panel). For the V–O_2 system, the lower panel in Fig. 4.7 illustrates the well-known fact that VO_2 deposition requires high temperature and low pressure of O_2. However, the properties of the V–SO_2 system are very different, as shown in the upper panel in Fig. 4.7 which indicates that VO_2 is formed in a lower temperature ranges from 100 to 500 °C and at a wide range of pressures from 10^{-7} to 1 atm. Clearly, the VO_2 formation reaction with SO_2 proceeds at rather low temperature and does not require high vacuum. As a final note, it should be stressed that thermodynamic calculations only give the direction of the reaction and indicate whether a phase can be formed or not, but the equilibrium composition might take an unacceptably long time to reach.

4.3.3 Comments on Nanoparticle Preparation

VO_2-based nanoparticles can be prepared by a variety of techniques, and references to this work can be found in recent papers (Li et al. 2010, 2013a). The nanoparticles can be more or less rounded as well as rod- and wire-like structure. Figure 4.8

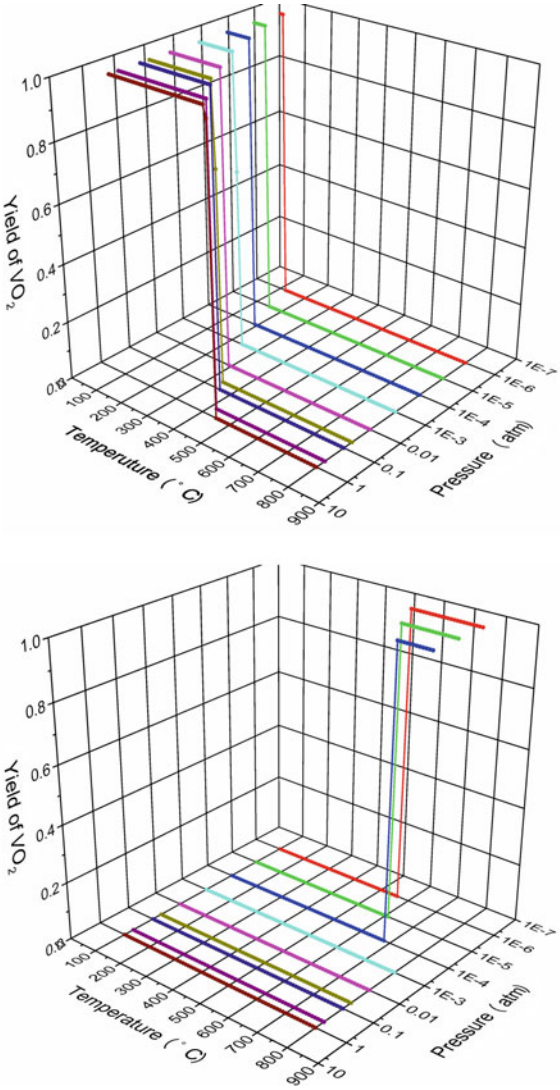

Fig. 4.7 Calculated yields for the formation of VO_2 by oxidation of metallic vanadium versus temperature and pressure for gaseous SO_2 (*upper panel*) and O_2 (*lower panel*)

shows nanorods made by Li et al. (2013a) via sputter deposition onto glass plates heated to ~460 °C in the presence of O_2 and Ar. The oxygen fraction, given by

$$\Gamma = \phi_{O_2}/\left(\phi_{Ar} + \phi_{O_2}\right), \tag{4.5}$$

where ϕ denotes flow rate, is a particularly significant parameter.

The substrate material is also very important for the particle growth, as elaborated recently for the case of sputtering by Montero et al. (2015). Figure 4.9 refers to VO_2 sputter deposited at ~450 °C onto bare glass and glass precoated with electrically

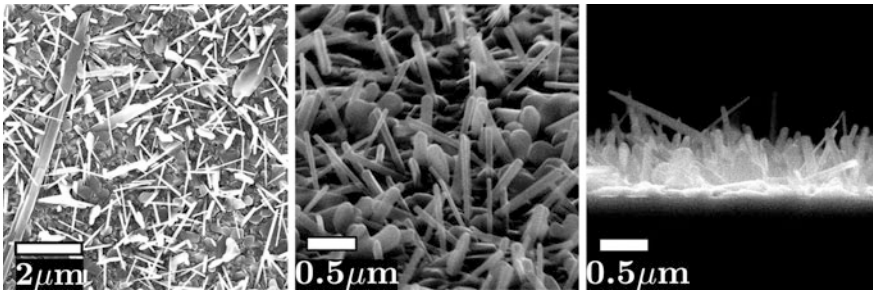

Fig. 4.8 Scanning electron micrographs of a VO_2 layer deposited onto heated glass and having an (equivalent) thickness of 102 nm. *Left-hand*, *middle*, and *right-hand* images refer to a top view, imaging at 70° between electron beam and sample normal, and a cross-sectional view, respectively. The magnifications differ among the images. From Li et al. (2013a)

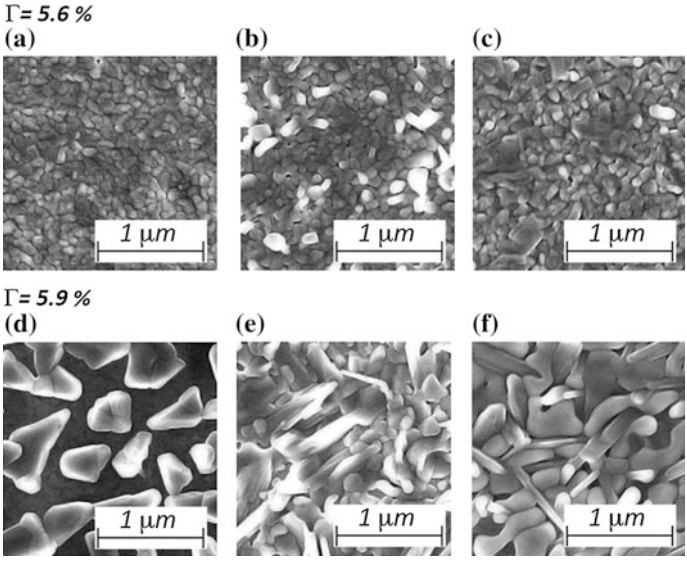

Fig. 4.9 Scanning electron micrographs of VO_2 layers with an (equivalent) thickness of 60 nm deposited onto heated substrates of ITO/glass, SnO_2/glass, and bare glass at the shown values of Γ. From Montero et al. (2015). **a** VO_2/ITO/glass. **b** VO_2/SnO_2/glass. **c** VO_2/glass. **d** VO_2/ITO/glass. **e** VO_2/SnO_2/glass. **f** VO_2/glass

conducting In_2O_3:Sn (i.e., indium–tin oxide, known as ITO) or non-conducting SnO_2. It is evident that ITO tends to give a layer of well-defined nanoparticles if the value of Γ is chosen adequately. Process control must be stringent, and deposits with different nanostructures are obtained when Γ is 5.6 and 5.9 %.

The sublayer of ITO on the glass substrate is important also because it widens the process window for making coatings with good thermochromism. This feature is illustrated in Fig. 4.10, which shows that the transmittance modulation at

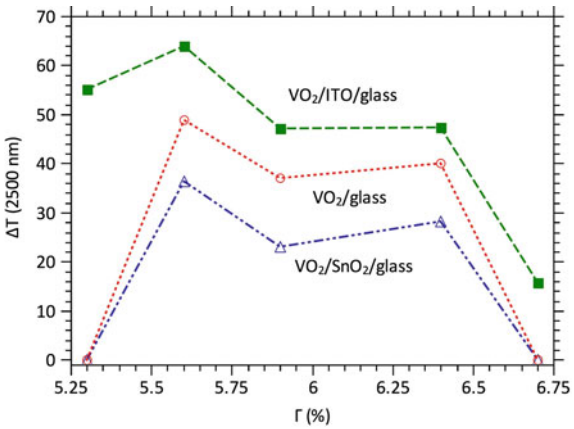

Fig. 4.10 Modulation of the optical transmittance at $\lambda = 2500$ nm, denoted ΔT (2500 nm), versus oxygen content Γ for sputter-deposited VO_2. The data refer to coatings with approximately the same thickness backed by the indicated substrates. From Montero et al. (2015)

$\lambda = 2500$ nm is strong for a much broader range of Γ when VO_2 is deposited onto ITO than when the substrate is SnO_2 or bare glass.

4.4 Toward Practically Useful VO_2-Based Coatings for Glazings

Do the data on $T(\lambda, \tau)$ in the left-hand panels of Fig. 4.3 really show that VO_2-based coatings can be used for energy-efficient fenestration? The honest answer is "no," but the properties of VO_2 are sufficiently close to the desired ones that it is meaningful to try to modify this material as considered next (Li et al. 2012). Specifically, the following items require careful attention for VO_2-based coatings and are discussed below:

- the transition between semiconducting and metallic properties takes place at ~68 °C, which obviously is too high for practical buildings;
- the luminous transmittance is no more than ~40 %, which is too low for most glazings; of course, the transmittance would be larger for a VO_2 coating thickness below 50 nm, but such a coating would also have an undesirably low magnitude of the solar energy modulation;
- the transmittance modulation is large only at wavelengths where the solar irradiation is rather weak, as apparent from Fig. 4.1, which limits the solar energy modulation to no more than ~10 %, which is too small to be of much interest for a practical glazing; and
- vanadium dioxide is not a thermodynamically stable material but further oxidation would tend to transform it to non-thermochromic V_2O_5, as discussed above.

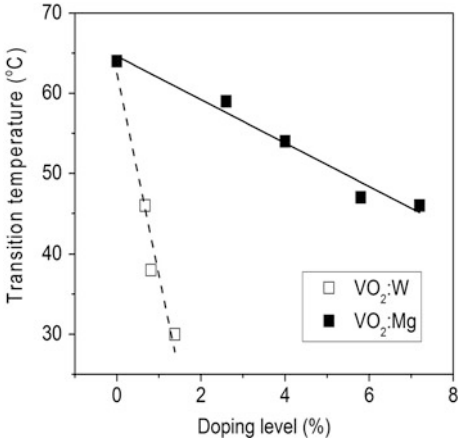

Fig. 4.11 Temperature for the transition between semiconducting and metallic states in thermochromic VO_2 coatings doped with W or Mg. From Mlyuka et al. (2009a)

4.4.1 *Having τ_c at Room Temperature*

It has been known since the early 1970s that the addition of tungsten, as well as some other elements, to bulk VO_2 leads to a depression of τ_c (Goodenough 1971), and the same effect exists in thin films (Greenberg 1983). Figure 4.11, reproduced from Mlyuka et al. (2009a), shows that ~ 2 % of *W* puts τ_c at about room temperature.

4.4.2 *Increasing T_{lum}*

Figure 4.3 shows that strong optical absorption sets in at $\lambda < 500$ nm, which is connected with the optical band gap in VO_2 being undesirably small. A partial solution was found some years ago by Mlyuka et al. (2009a), who discovered that Mg incorporation led to a wider band gap, and subsequently it was reported that Zn had a similar effect (Jiang et al. 2014). Figure 4.12 shows the spectral transmittance for 50-nm-thick coatings of Mg-doped and pure VO_2 at $\tau < \tau_c$ and $\tau > \tau_c$ and indicates that the dopant shifts the region of high transmittance toward shorter wavelengths but also diminishes the magnitude of the solar energy modulation. The shift of the optical absorption is indeed due to band gap widening, as demonstrated both experimentally (Li et al. 2013b) and computationally (Hu et al. 2012) in recent work. It can be seen from Fig. 4.11 that τ_c drops as the Mg content is increased, although not as rapidly as for *W* doping. Figure 4.13 shows that T_{lum} is enhanced from 39 to 51 % when the Mg content is enlarged from zero to 7.2 %. Increased values of T_{lum} can also be achieved by replacing some oxygen in VO_2 by fluorine (Khan and Granqvist 1989; Burkhardt et al. 2002; Kiri et al. 2011).

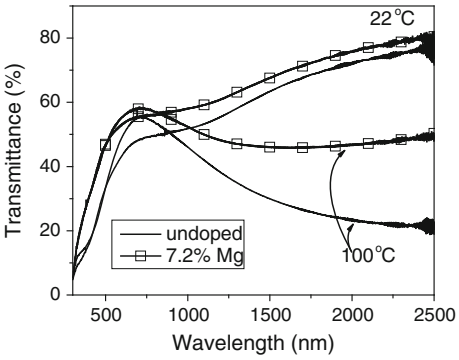

Fig. 4.12 Spectral transmittance for 50-nm-thick films of undoped and Mg-doped VO_2 coatings in semiconducting (τ = 22 °C) and metallic (τ = 100 °C) states. From Mlyuka et al. (2009a)

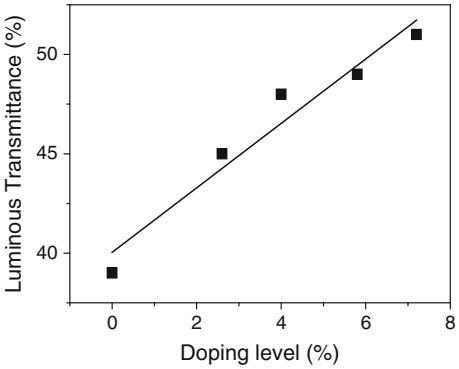

Fig. 4.13 Luminous transmittance versus Mg content in 50-nm-thick VO_2-based coatings as recorded at τ = 22 °C. The line was drawn for convenience. From Mlyuka et al. (2009a)

4.4.3 Boosting T_{sol}

The limited modulation of the solar transmittance between the semiconducting and metallic states in VO_2 coatings has probably been the greatest obstacle for the development of practically useful thermochromic glazings. A clear step toward the realization of such glazings was taken in recent work by Li et al. (2010, 2011) who found by computation that a layer comprising VO_2 *nanoparticles*—instead of a continuous VO_2 coating as studied in earlier work—could lead to a strong boost in ΔT_{sol}. Further calculations have demonstrated that the particle size should not exceed $\sim$20 nm in order to avoid optical scattering known as "haze" (Laaksonen et al. 2014). Such "nanothermochromism," using a term coined by Li et al. (2010), was introduced in the right-hand panels in Fig. 4.3, which show spectral transmittance and reflectance for a 5-μm-thick layer of a transparent medium, with

refractive index representative of typical glass and polymers, containing 1 vol.% of well-dispersed non-scattering VO_2 nanospheres. This selection of parameters yields an equivalent VO_2 thickness of 50 nm so that the data for the nanospheres and the continuous coating can be compared in a straight-forward manner.

It is evident that there are qualitative differences between data for the nanoparticle composites and the coatings:

- the nanosphere-containing material is much more transparent than the corresponding coating;
- the metallic nanoparticles show a pronounced transmittance minimum in the $0.7 < \lambda < 1.5$ μm wavelength range, which significantly limits the solar transmittance that is intense at these wavelengths, while the visible optical properties are hardly affected at all; and
- the nanospheres absorb rather than reflect.

The conspicuous transmittance minimum—i.e., absorption maximum—in the infrared is caused by plasmon resonance among the free electrons in VO_2 and is centered at $\lambda \sim 1.2$ μm. This feature is almost ideally located for absorbing infrared solar radiation without affecting the luminous optical properties (cf. Fig. 4.1). The plasmonic character of the near-infrared absorption seems to have been first discussed by Lopez et al. (2002).

4.4.4 Avoiding Further Oxidation of VO_2

Coatings and nanoparticle composites based on thermochromic VO_2 that are intended for glazings must be durable enough to last for many years without losing their performance more than marginally. This requirement needs careful consideration since vanadium pentoxide (V_2O_5)—not VO_2—is the thermodynamically stable oxide as seen from the phase diagram in Fig. 4.4.

Figure 4.14 shows recent data on 80-nm-thick VO_2 coatings heat treated in dry air at 300 °C for one hour from work by Ji et al. (2014a). The as-deposited coating displays the expected thermochromic behavior in its spectral transmittance (cf. Figs. 4.3 and 4.12), but the heat-treated coating has a completely different spectral response which indicates that it has been transformed to non-thermochromic V_2O_5 (Talledo and Granqvist 1995; Lykissa et al. 2014). This conversion is expected to be much slower at temperatures of relevance for most practical applications, but the data in Fig. 4.14 nevertheless indicate that VO_2-based materials should be protected against further oxidation.

Figure 4.15 shows spectral transmittance for similar VO_2 coatings with top coats consisting of 10 and 30 nm of sputter-deposited aluminum oxide and heat treated at 300 °C for durations in the interval $1 < t_h < 30$ h (Ji et al. 2014a). Clearly the top coat gives excellent protection, and only the thinnest Al_2O_3 layer and the largest value of t_h led to a minor deterioration of the thermochromic performance. Al nitride layers gave similar protection of an underlying VO_2 coating (Ji et al. 2014b).

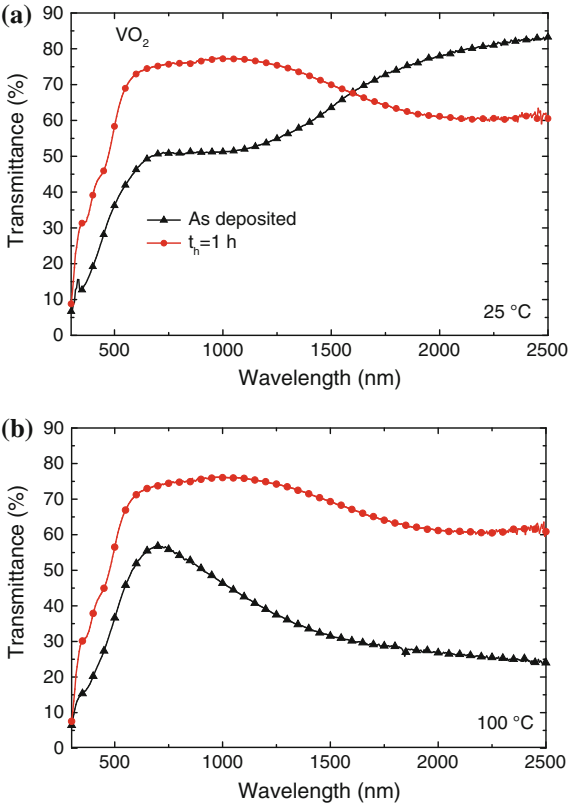

Fig. 4.14 Spectral transmittance for an 80-nm-thick VO_2 coating in as-deposited state and after heating at 300 °C for one hour. Data were recorded for coatings in **a** semiconducting (τ = 25 °C) and **b** metallic (τ = 100 °C) states. From Ji et al. (2014a)

Multilayer coatings can be produced by numerous deposition techniques, and nanoparticles with core–shell structures and VO_2 centers surrounded by SiO_2 or TiO_2 have been prepared several times (Li et al. 2013c, d, 2014). Hence, the data in Fig. 4.15 strongly indicate that long-term applications of VO_2-based materials are possible. Top coats similar to those discussed above were effective also under humid conditions (Ji et al. 2014a).

4.4.5 *Approximate Performance Limits for Thermochromic Glazings*

The discussion above shows that various combinations of T_{lum} and ΔT_{sol} can be achieved in VO_2-based materials and Fig. 4.16, reproduced from Li et al. (2014), surveys today's (2015) state of the art for $T_{lum}(\tau < \tau_c)$ and ΔT_{sol}. It should be noted that T_{lum} is almost the same at $\tau < \tau_c$ and $\tau > \tau_c$.

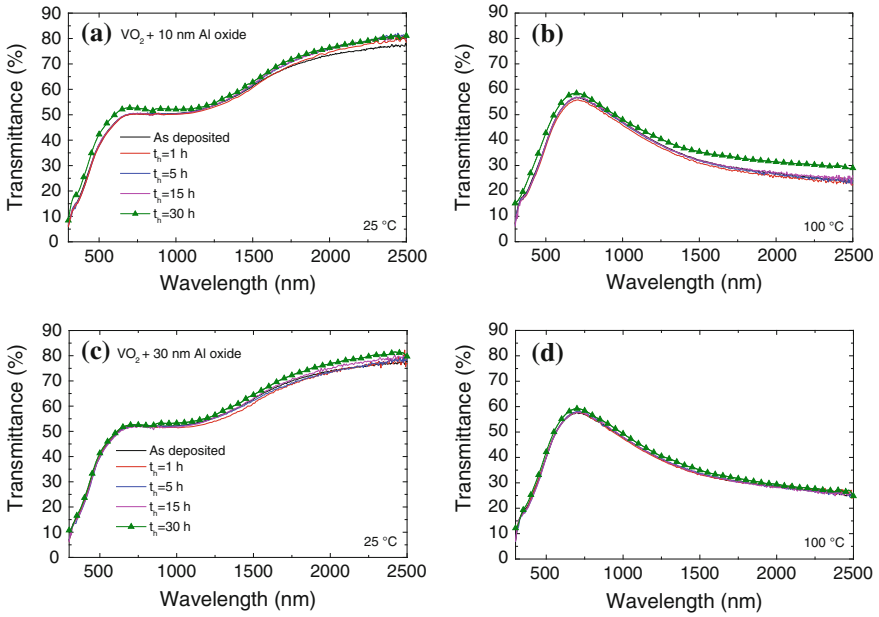

Fig. 4.15 Spectral transmittance for 80-nm-thick VO_2 coatings, covered with 10 nm (panels **a** and **b**) and 30 nm (panels **c** and **d**) of Al_2O_3, in as-deposited state and after heating at 300 °C for the shown durations t_h. Data were recorded for coatings in semiconducting (τ = 25 °C) and metallic (τ = 100 °C) states. From Ji et al. (2014a)

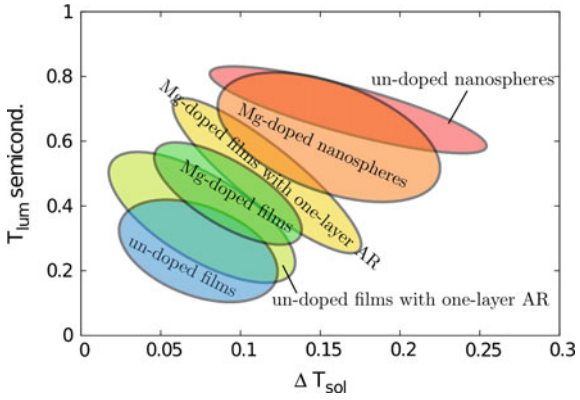

Fig. 4.16 Schematic rendition of performance limits for various VO_2-based materials (thin films and nanospheres) with regard to thermochromic glazings. From Li et al. (2014)

Clearly, pure VO_2 coatings give the lowest values of $T_{lum}(\tau < \tau_c)$ and ΔT_{sol}, but the optical data can be enhanced by AR layers. In particular, good properties were reached with multilayers of TiO_2 and VO_2 (Mlyuka et al. 2009b; Chen et al. 2011). "Bio-inspired" cone-shaped surfaces constitute another possibility to increase T_{lum} (Taylor et al. 2013). Mg-containing VO_2 coatings have superior properties, which can be further boosted by AR layers. However, superior performance is achieved by

VO_2 nanoparticles which, for example, can give $T_{lum}(\tau < \tau_c) \approx 60$ % together with $\Delta T_{sol} > 20$ %. Perhaps surprisingly, Mg-containing nanoparticles do not give better performance than nanoparticles of pure VO_2, the reason being that Mg addition yields diminishing solar modulation, as apparent in Fig. 4.12, to an extent that is not balanced by the enlarged short-wavelength transmittance.

4.4.6 *Energy Modeling of Buildings with Thermochromic Glazings*

Several computer simulations, aimed at assessing the energy savings that are possible with thermochromic glazings in buildings, have been reported recently (Saeli et al. 2010a, b; Ye et al. 2012, 2013, 2014; Long and Ye 2014; Warwick and Binions 2014; Warwick et al. 2014, 2015). All of these simulations are based on highly simplifying assumptions and do not account for the recent advances that form the main basis of Fig. 4.16. Nevertheless, the outcomes of the simulations are interesting, and most studies show that thermochromic glazings offer significant advantages over glazings with static coatings or tinting.

Detailed simulations were reported by Saeli et al. (2010a) who used standard software to model the energy consumption in air-conditioned rooms, $6 \times 5 \times 3$ m^3 in size, with restrictions on the illumination level and with internal heat load due to occupancy. The environment was taken to represent Cairo (Egypt); Palermo, Rome, and Milan (Italy); London (UK); Helsinki (Finland); and Moscow (Russia). The building had a south-facing window covering either a quarter of the wall or the entire wall; the window was double-glazed with a 12-mm-wide air cavity. Four types of thermochromic coatings on glass were considered: a VO_2 film (Th1), such a film with inclusion of some gold nanoparticles in order to affect the color (Th2), a VO_2 film with a growth-directing surfactant (Th3), and a film with both gold nanoparticles and surfactant (Th4). In addition, the calculations encompassed glass with a sputter-deposited silver-based "solar-control" film which transmitted most of the visible light but reflected near-infrared solar radiation ("Suncool Brilliant", SB) and a blue body-tinted glass ("Arctic Blue," AB). Simulations with plain float glass (denoted C) served as a baseline. Th1–Th4 were specified with regard to $T(\lambda)$ and $R(\lambda)$ at $\tau < \tau_c$ and $\tau > \tau_c$; these data were qualitatively similar though differing in details. Other aspects of the calculations are given in the original paper (Saeli et al. 2010a) and in references cited therein; some of the results are also presented elsewhere (Saeli et al. 2010b; Warwick and Binions 2014).

Figure 4.17 reports data on total annual energy consumption—accounting for heating, cooling, and artificial lighting—and its improvement for a glazed south-facing wall equipped with the various types of coated or tinted glass and for different geographical locations. It is evident that all of the coatings, as well as the tinting, offer advantages, which are most prominent for the thermochromic coatings. The maximum improvement for a thermochromic coating is ~40 % (Th3, Rome), which can be compared with the best property for a static glazing which is 32 %

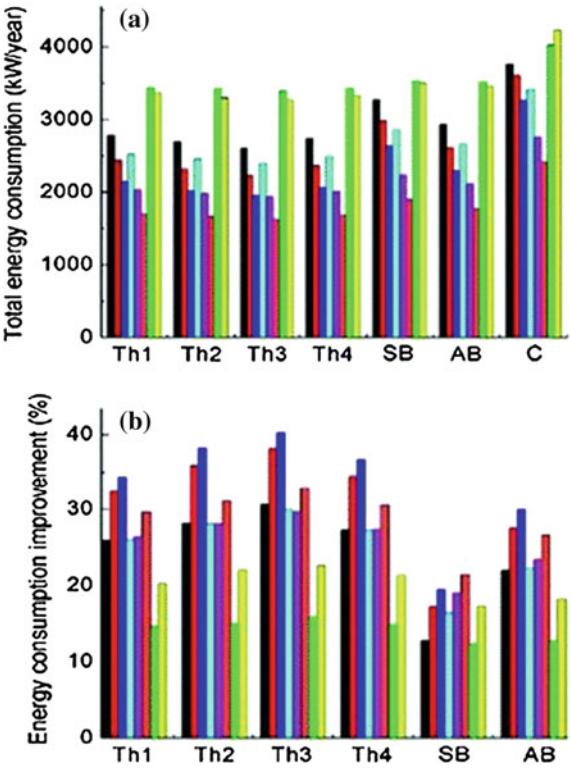

Fig. 4.17 Total annual energy consumption (**a**) and percent improvement compared to a clear glazing (**b**) for a number of thermochromic (Th), solar-control-coated (SB), and body-tinted (AB) glazings, as discussed in the main text. Color coding: *black* (Cairo), *red* (Palermo), *dark blue* (Rome), *light blue* (Milan), *violet* (Paris), *orange* (London), *green* (Moscow), and *yellow* (Helsinki). From Saeli et al. (2010a)

(AB, also Rome). Even better data seem to be possible by optimizing τ_c and the abruptness of the thermochromic transition (Warwick et al. 2014, 2015). We caution again that the calculations are based on a large number of assumptions and are only indicative.

Other model calculations have considered an idealized case wherein the thermochromic coating is taken to be wavelength-independent in the $0.7 < \lambda < 2.5$ μm wavelength range, with a much higher transmittance level at $\tau < \tau_c$ than at $\tau > \tau_c$ (Saeli et al. 2010a; Hoffmann et al. 2014). In particular, Hoffmann et al. (2014) found from extensive modeling that the annual energy savings could be as large as 14 and 17 % for Chicago and Houston, respectively, compared with the case for a glazing with a static solar-control coating for the assumptions underlying their calculations.

We note that a modeling study by Ye et al. (2012), considering Chinese conditions, was unable to document any obvious advantage of a thermochromic VO_2 coating. However, this work compares results to those of an idealized glazing system and not to a standard case, and subsequent work by the same authors did report that glazings with VO_2 coatings performed better than ordinary glazings (Ye et al. 2013).

4.5 Conclusion and Outlook

This chapter presented an overview over progress on thermochromic glazings for energy-efficient buildings. This technology employs VO_2-based materials as thin coatings or nanoparticle composites. For coatings, the switching between states

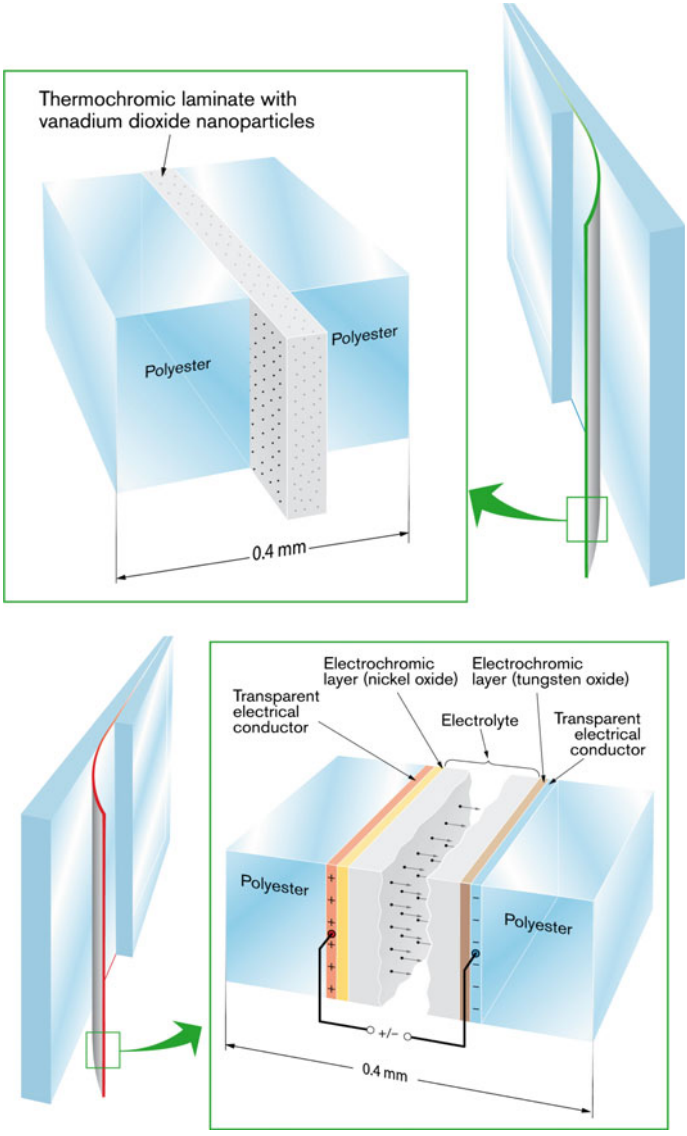

Fig. 4.18 Thermochromic (*upper panel*) and electrochromic (*lower panel*) foil-based devices used for glass lamination

with high and low solar energy throughput at low and high temperature, respectively, can be achieved by replacing some of the vanadium atoms by tungsten, and luminous transmittance can be enhanced by an addition of magnesium. AR layers can give further improvements. By going to nanoparticle composites with VO_2 dispersed in a transparent host, it is possible to combine high luminous transmittance with a large modulation of solar energy transmittance. This modulation ensues from plasmonic absorption in metal-like VO_2 nanoparticles.

Concerning practical implementation in thermochromic glazings, VO_2-based thin films can be applied in insulated glass units in principally the same way as in today's technology which usually employs metal-based coatings with static properties (Smith and Granqvist 2010). Alternatively, VO_2 coatings can be transferred to flexible polymer foils (Kim et al. 2013). Thermochromic nanoparticles—perhaps with protective shells surrounding VO_2 cores—might be dispersed in polymers and used for lamination purposes, as sketched in the upper panel of Fig. 4.18. A further development may be to use this thermochromic laminate as an electrolyte in electrochromic devices which modulate their transmittance of visible light and solar energy when electrical charge is shuttled between thin films based on tungsten oxide and nickel oxide, as illustrated schematically in the lower panel of Fig. 4.18.

Acknowledgments Helpful comments on the text were obtained from Professor Ludvik Martinu. Financial support was obtained from the European Research Council under the European Community's Seventh Framework Program (FP7/2007–2013)/ERC Grant Agreement No. 267234 (GRINDOOR).

References

Aijaz A, Ji Y-X, Montero J, Niklasson GA, Granqvist CG (2015) Low-temperature synthesis of thermochromic vanadium dioxide thin films by reactive high power impulse magnetron sputtering (to be published)

Anderson JS, Khan AS (1970) Phase equilibria in the vanadium–oxygen system. J Less-Common Metals 22:209–218

Andersson G (1956) Studies on vanadium oxides II. The crystal structure of vanadium dioxide. Acta Chem Scand 10:623–628

ASTM G173-03 (2008) Standard tables of reference solar spectral irradiances: direct normal and hemispherical on a 37° tilted surface. In: Annual book of ASTM standards, vol 14(04). American society for testing and materials, Philadelphia, PA, USA

Babulanam SM, Eriksson TS, Niklasson GA, Granqvist CG (1986) Thermochromic VO_2 films for energy-efficient windows. Proc Soc Photo-Opt Instrum Eng 692:8–18

Babulanam SM, Eriksson TS, Niklasson GA, Granqvist CG (1987) Thermochromic VO_2 films for energy-efficient windows. Sol Energy Mater 16:347–363

Bahlawane N, Lenoble D (2014) Vanadium oxide compounds: structure, properties, and growth from the gas phase. Chem Vap Deposition 20:299–311

Burkhardt W, Christmann T, Franke S, Kriegseis W, Meister D, Meyer BK, Niessner W, Schalch D, Scharmann A (2002) Tungsten and fluorine co-doping of VO_2 films. Thin Solid Films 402:226–231

Chen Z, Gao Y, Kang L, Du J, Zhang Z, Luo H, Miao H (2011) VO_2-based double-layered films for smart windows: optical design, all-solution preparation and improved properties. Sol Energy Mater Sol Cells 95:2677–2684

Fortier J-P, Baloukas B, Zabeida O, Klemberg-Sapieha JE, Martinu L (2014) Thermochromic VO_2 thin films deposited by HiPIMS. Sol Energy Mater Sol Cells 125:291–296

Freedonia (2013) World flat glass to 2016: industry market research, market share, market size, sales, demand forecast, market leaders, company profiles, industry trends. The Freedonia Group, Cleveland, OH, USA

Gao Y, Luo H, Zhang Z, Kang L, Chen Z, Du J, Kanehira M, Cao C (2012) Nanoceramic VO_2 thermochromic smart glass: a review on progress in solution processing. Nano Energy 1:221–246

Goodenough JB (1971) The two components of the crystallographic transition in VO_2. J Solid State Chem 3:490–500

Granqvist CG (1990) Chromogenic materials for transmittance control of large-area windows. Crit Rev Solid State Mater Sci 16:291–308

Granqvist CG (1995) Handbook of inorganic electrochromic materials. Elsevier, Amsterdam

Granqvist CG (2007) Transparent conductors as solar energy materials: a panoramic review. Sol Energy Mater Sol Cells 91:1529–1598

Granqvist CG (2012) Oxide electrochromics: an introduction to devices and materials. Sol Energy Mater Sol Cells 99:1–13

Granqvist CG (2013a) Switchable glazing technology for eco-efficient construction. In: Pacheco-Torgal F, Diamanti MV, Nazari A, Granqvist CG (eds) Nanotechnology in eco-efficient construction. Woodhead, Cambridge, pp 236–269

Granqvist CG (2013b) Switchable glazing technology: electrochromic fenestration for eco-efficient buildings. In: Pacheco-Torgal F, Mistretta M, Kaklauskas A, Granqvist CG, Cabeza LF (eds) Nearly zero energy building refurbishment. Springer, London, pp 583–613

Granqvist CG (2014a) Oxide-based chromogenic coatings and devices for energy efficient fenestration: brief survey and update on thermochromics and electrochromics. J Vac Sci Technol B 32:060801/1–060801/13

Granqvist CG (2014b) Electrochromics for smart windows: oxide-based thin films and devices. Thin Solid Films 564:1–38

Granqvist CG (2015a) Fenestration for reducing building cooling needs: an introduction to spectral selectivity, thermochromics, and electrochromics. In: Pacheco-Torgal F, Labrincha JA, Cabeza LF, Granqvist CG (eds) Eco-efficient materials for mitigating building cooling needs: design, properties and applications. Woodhead, Cambridge, pp 441–471

Granqvist CG (2015b) Applications of transparent conductors to solar energy and energy efficiency. In: Ginley D, Hosono H, Paine DC (eds) Handbook of transparent conductors, 2nd edn. Springer Science+Business Media, New York (to be published)

Greenberg CB (1983) Undoped and doped VO_2 films grown from $VO(OC_3H_7)_3$. Thin Solid Films 110:73–82

Gulbransen EA, Andrew KF (1950) The kinetics of the reactions of vanadium with oxygen and nitrogen. J Electrochem Soc 97:396–404

Hoffmann S, Lee ES, Clavero C (2014). Examination of the technical potential of near-infrared switching thermochromics windows for commercial building applications. Sol Energy Mater Sol Cells 123:65–80

Hu S, Li S-Y, Ahuja R, Granqvist CG, Hermansson K, Niklasson GA, Granqvist CG (2012) Optical properties of Mg-doped VO_2: absorption measurements and hybrid functional calculations. Appl Phys Lett 101:201902/1–201902/4

Ivanov II, Balzhinimaev BS (1987) New data on kinetics and reaction-mechanism for SO_2 oxidation over vanadium catalysts. React Kinet Catal Lett 35:413–424

Ji Y-X, Li S-Y, Niklasson GA, Granqvist CG (2014a) Durability of thermochromic VO_2 thin films under heating and humidity: effect of Al oxide top coatings. Thin Solid Films 562:568–573

Ji Y-X, Niklasson GA, Granqvist CG (2014b) Durability of VO_2-based thin films at elevated temperature: towards thermochromic fenestration. J Phys: Conf Proc 559:012005/1–012005/5

Ji Y-X, Niklasson GA, Granqvist CG, Boman M (2016) Thermochromic VO_2 films by thermal oxidation of vanadium in SO_2. Sol Energy Mater Sol Cells 144:713–716

Jian J, Chen A, Zhang W, Wang H (2013) Sharp metal-to-insulator transition of VO_2 thin films on glass substrates. J Appl Phys 114:244301/1–244301/6

Jiang M, Bao S, Cao X, Li Y, Li S, Zhou H, Luo H, Jin P (2014) Improved luminous transmittance and diminished yellow color in VO_2 energy efficient smart thin films by Zn doping. Ceram Int 40:6331–6334

Jorgenson GV, Lee JC (1986) Doped vanadium oxide for optical switching films. Sol Energy Mater 14:205–214

Jorgenson GV, Lee JC (1990) Thermochromic materials and devices: inorganic systems. In: Lampert CM, Granqvist CG (eds) Large-area chromogenics: materials and devices for transmittance control. SPIE Optical Engineering Press, Bellingham, pp 142–159

Kang Y-B (2012) Critical evaluation and thermodynamic optimization of the VO–$VO_{2.5}$ system. J Eur Ceram Soc 32:3187–3198

Khan KA, Granqvist CG (1989) Thermochromic sputter-deposited vanadium oxyfluoride coatings with low luminous absorptance. Appl Phys Lett 55:4–6

Kim K, Kim Y, Kim KS, Jeong HY, Jang A-R, Han SH, Yoon DH, Suh KS, Shin HS, Kim TY, Yang WS (2013) Flexible thermochromic window based on hybridized VO_2/graphene. ACS Nano 7:5769–5776

Kiri P, Warwick MEA, Ridley I, Binions R (2011) Fluorine doped vanadium dioxide thin films for smart windows. Thin Solid Films 520:1363–1366

Laaksonen K, Li S-Y, Puisto SR, Rostedt NKJ, Ala-Nissila T, Granqvist CG, Nieminen RM, Niklasson GA (2014) Nanoparticles of TiO_2 and VO_2 in dielectric media: conditions for low optical scattering, and comparison between effective medium and four-flux theories. Sol Energy Mater Sol Cells 130:132–137

Lampert CM, Granqvist CG (eds) (1990) Large-area chromogenics: materials and devices for transmittance control, SPIE institutes for advanced optical technologies, vol 4. SPIE Optical Engineering Press, Bellingham

Lee JC, Jorgenson GV, Lin RJ (1986) Thermochromic materials research for optical switching. Proc Soc Photo-Opt Instrum Eng 692:2–7

Lepsoe R (1940) Chemistry of sulfur dioxide reduction: kinetics. Ind Eng Chem 32:910–918

Li S-Y, Niklasson GA, Granqvist CG (2010) Nanothermochromics: calculations for VO_2 nanoparticles in dielectric hosts show much improved luminous transmittance and solar energy transmittance modulation. J Appl Phys 108:063525/1–063525/8

Li S-Y, Niklasson GA, Granqvist CG (2011) Nanothermochromics with VO_2-based core–shell structures: calculated luminous and solar properties. J Appl Phys 109:113515/1–113515/5

Li S-Y, Niklasson GA, Granqvist CG (2012) Thermochromic fenestration with VO_2-based materials: three challenges and how they can be met. Thin Solid Films 520:3823–3828

Li S-Y, Namura K, Suzuki M, Niklasson GA, Granqvist CG (2013a) Thermochromic VO_2 nanorods made by sputter deposition: growth conditions and optical modeling. J Appl Phys 114:033516/1–033516/11

Li S-Y, Mlyuka NR, Primetzhofer D, Hallén A, Possnert G, Niklasson GA, Granqvist CG (2013b) Bandgap widening in thermochromic Mg-doped VO_2 thin films: quantitative data based on optical absorption. Appl Phys Lett 103:161907/1–161907/4

Li S, Li Y, Jiang M, Ji S, Luo H, Gao Y, Jin P (2013c) Preparation and characterization of self-supporting thermochromic films composed of VO_2(M)@SiO_2 nanofibers. ACS Appl Mater Interfaces 5:6453–6457

Li Y, Ji S, Gao Y, Luo H, Jin P (2013d) Modification of Mott phase transition characteristics in VO_2@TiO_2 core/shell nanostructures by misfit-strained heteroepitaxy. ACS Appl Mater Interfaces 5:6603–6614

Li S-Y, Niklasson GA, Granqvist CG (2014) Thermochromic undoped and Mg-doped VO_2 thin films and nanoparticles: optical properties and performance limits for energy efficient windows. J Appl Phys 115:053513/1–05351310

Liu W, Sarofim AF, Flytzani-Stephanopoulos M (1994) Reduction of sulfur-dioxide by carbon-monoxide to elemental sulfur over composite oxide catalysts. Appl Catal B: Environ 4:167–186

Long L, Ye H (2014) Discussion of the performance improvement of thermochromics smart glazing applied in passive building. Sol Energy 107:236–244

Lopez R, Haynes TE, Boatner LA, Feldman LC, Haglund Jr RF (2002) Temperature-controlled surface plasmon resonance in VO_2 nanorods. Opt Lett 27:1327–1329

Lykissa I, Li S-Y, Ramzan M, Chakraborty S, Ahuya R, Granqvist CG, Niklasson GA (2014) Electronic density-of-states of amorphous vanadium pentoxide films: electrochemical data and density functional theory calculations. J Appl Phys 115:183701/1–183701/5

Marvel RE, Appavoo K, Choi BK, Nag J, Haglund Jr RF (2013) Electron-beam deposition of vanadium dioxide thin films. Appl Phys A 111:975–981

Mlyuka NR, Niklasson GA, Granqvist CG (2009a) Mg doping of thermochromic VO_2 films enhances the optical transmittance and decreases the metal–insulator transition temperature. Appl Phys Lett 95:171909/1–171909/3

Mlyuka NR, Niklasson GA, Granqvist CG (2009b) Thermochromic VO_2-based multilayer films with enhanced luminous transmittance and solar modulation. Phys Status Solidi A 206:2155–2160

Montero J, Ji Y-X, Li S-Y, Niklasson GA, Granqvist CG (2015) Sputter deposition of thermochromic VO_2 films on In_2O_3:Sn, SnO_2 and glass: structure and composition versus oxygen partial pressure. J Vac Sci Technol B 33:031805/1–031804/7

Morin FJ (1959) Oxides which show a metal-to-insulator transition at the Neel temperature. Phys Rev Lett 3:34–36

Mukherjee A, Wach SP (1983) Kinetics of the oxidation on vanadium in the temperature range 350–950 °C. J Less-Common Metals 92:289–300

Pittaluga M (2015) Electrochromic glazing and walls for reducing building cooling needs. In: Pacheco-Torgal F, Labrincha JA, Cabeza LF, Granqvist CG (eds) Eco-efficient materials for mitigating building cooling needs: design, properties and applications. Woodhead, Cambridge, pp 473–497

Saeli M, Piccirillo C, Parkin IP, Binions R, Ridley I (2010a) Energy modelling studies of thermochromic glazing. Energy Buildings 42:1666–1673

Saeli M, Piccirillo C, Parkin IP, Ridley I, Binions R (2010b) Nano-composite thermochromic thin films and their application in energy-efficient glazing. Sol Energy Mater Sol Cells 94:141–151

Seeboth A, Lötzsch D (2014) Thermochromic and thermotropic materials. Pan Stanford, Singapore

Smith JF (ed) (1989) Phase diagrams of binary vanadium alloys, monograph series on alloy phase diagrams. ASM International, Metals Park

Smith GB, Granqvist CG (2010) Green nanotechnology: solutions for energy and sustainability in the built environment. CRC Press, Boca Raton

Talledo A, Granqvist CG (1995) Electrochromic vanadium-pentoxide-based films: structural, electrochemical, and optical properties. J Appl Phys 77:4655–4666

Taylor A, Parkin I, Noor N, Tummeltshammer C, Brown MS, Papakonstantinou I (2013) A bioinspired solution for spectrally selective thermochromic VO_2 coated intelligent glazing. Opt Express 21:A750–A764

UNEP (2007) Buildings and climate change: challenges and opportunities. United Nations Environmental Programme, Paris, France

US DOE (2012) 2011 buildings energy data book. US Department of Energy, Washington, DC, USA

Warwick MEA, Binions R (2014) Advances in thermochromic vanadium dioxide films. J Mater Chem A 2:3275–3292

Warwick MEA, Ridley I, Binions R (2014) The effect of transition gradient in thermochromic glazing systems. Energy Buildings 77:80–90

Warwick MEA, Ridley I, Binions R (2015) The effect of variation in the transition hysteresis width and gradient in thermochromic glazing systems. Sol Energy Mater Sol Cells 140:253–265

Wriedt HA (1989) The O–V (oxygen–vanadium) system. Bull Alloy Phase Diagr 10:271–277
Wyszecki G, Stiles WS (2000) Color science: concepts and methods, quantitative data and formulae, 2nd edn. Wiley, New York
Ye H, Meng X, Xu B (2012) Theoretical discussions of perfect window, ideal near infrared solar spectrum regulating window and current thermochromic window. Energy Buildings 49:164–172
Ye H, Long L, Zhang H, Xu B, Gao Y, Kang L, Chen Z (2013) The demonstration and simulation of the application performance of the vanadium dioxide single glazing. Sol Energy Mater Sol Cells 117:168–173
Ye H, Long L, Zhang H, Gao Y (2014) The energy saving index and the performance evaluation of thermochromics windows in passive buildings. Renewable Energy 66:215–221

Chapter 5
Photosynthetic Glass: As a Responsive Bioenergy System

M.E. Alston

Abstract Can photosynthesis of leaves evolve glass into a photoactive energy system? To create a transculent material that emulates the chemical reaction cycle of leaves by endothermic principles as a metabolic cycle for thermal conductance heat targeting. The evolution of glass envelopes into a photoactive adsorption layer, at an integrated multiscale level, in response to climatic regionalization. Nature's biological systems are living multifunctional mechanical information systems of chemical composition. They have the ability to learn and adapt to changing climatic conditions by self-regulation of solar adsorption, to achieve thermal management. These self-programmable controls of adaptive material performance will progress the surfaces of a skyscraper, from being a mere material entity to a dynamic one. This response to real-time performance change by the hour, season and weather conditions is exothermic management of a glass material as an energy flow cycle. The transformation of glass envelopes into a dynamic energy system that responds to the environment and contributes to the planet's energy needs. This chapter focuses on the use of an optically transparent, thermal energy adsorbing glass composite that is in the conceptual phase. Progression of this has just entered the laboratory testing of the first phototype composite.

Keywords Biosystem · Energy · Adsorption · Conductance · Multifunctional · Cycle

5.1 Introduction

Cities across the globe are responsible for up to 70 % of global carbon emissions and 75 % of global energy consumption. By 2050, it is estimated that 70 % of the world's population will live in cities (Malcolm et al. 2013). Cities and urban areas consume

M.E. Alston (✉)
University of Salford Manchester, Salford, UK
e-mail: M.E.Alston@salford.ac.uk

F. Pacheco Torgal et al. (eds.), *Nano and Biotech Based Materials for Energy Building Efficiency*, DOI 10.1007/978-3-319-27505-5_5

up to 80 % of this generated energy, hence they are at the heart of the problem. However with this concentration of energy into city core areas, this enables measures to contain city energy consumption flows. The level of the energy consumption of a city is dependant upon the building typology and geographical location. The requirement of heating, moving air for cooling, lighting and other device applications increases energy consumption, and this prevents particularly for glass skyscrapers in hot climates where temperature is greater than 40° or higher (Table 5.1).

Table 5.1 Description of Köppen climate symbols and defining criteria

1st	2nd	3rd	Description	Criteria*
A			Tropical	$T_{cold} \geq 18$
	f		• Rainforest	$P_{dry} \geq 60$
	m		• Monsoon	Not (Af) and $P_{dry} \geq 100 - MAP/25$
	w		• Savannah	Not (Af) and $P_{dry} < 100 - MAP/25$
B			Arid	$MAP < 10 \times P_{threshold}$
	W		• Desert	$MAP < 5 \times P_{threshold}$
	S		• Steppe	$MAP \geq 5 \times P_{threshold}$
		h	– Hot	$MAT \geq 18$
		k	– Cold	$MAT < 18$
C			Temperate	$T_{hot} \geq 10$ and $0 < T_{cold} < 18$
	s		• Dry summer	$P_{sdry} < 40$ and $P_{sdry} < P_{wwet}/3$
	w		• Dry winter	$P_{wdry} < P_{swet}/10$
	f		• Without dry season	Not (Cs) or (Cw)
		a	– Hot summer	$T_{hot} \geq 22$
		b	– Warm summer	Not (a) and $T_{mon10} \geq 4$
		c	– Cold summer	Not (a or b) and $1 \leq T_{mon10} < 4$
D			Cold	$T_{hot} \geq 10$ and $T_{cold} \leq 0$
	s		• Dry summer	$P_{sdry} < 40$ and $P_{sdry} < P_{wwet}/3$
	w		• Dry winter	$P_{wdry} < P_{swet}/10$
	f		• Without dry season	Not (Ds) or (Dw)
		a	– Hot summer	$T_{hot} \geq 22$
		b	– Warm summer	Not (a) and $T_{mon10} \geq 4$
		c	– Cold summer	Not (a, b or d)
		d	– Very cold winter	Not (a or b) and $T_{cold} < -38$
E			Polar	$T_{hot} < 10$
	T		• Tundra	$T_{hot} > 0$
	F		• Frost	$T_{hot} \leq 0$

**MAP* mean annual precipitation, *MAT* mean annual temperature, T_{hot} temperature of the hottest month, T_{cold} temperature of the coldest month, T_{mon10} number of months where the temperature is above 10, P_{dry} precipitation of the driest month, P_{sdry} precipitation of the driest month in summer, P_{wdry} precipitation of the driest month in winter, P_{swet} precipitation of the wettest month in summer, P_{wwet} precipitation of the wettest month in winter, $P_{threshold}$ varies according to the following rules (if 70 % of MAP occurs in winter, then $P_{threshold} = 2 \times MAT$; if 70 % of MAP occurs in summer, then $P_{threshold} = 2 \times MAT + 28$, otherwise $P_{threshold} = 2 \times MAT + 14$). Summer (winter) is defined as the warmer (cooler) six-month period of ONDJFM and AMJJAS

Current low zero carbon (LZC) technology themes should lead to energy efficiency, energy effectiveness and energy optimization in reducing primary energy demands. LZC technologies of component assemblies are focused on the building envelope. These component systems represent the main challenge in achieving energy efficiency strategies. The envelope acts as an environmental modifier as it interfaces and transcends between internal comfort conditions and climate. Greater demands have been placed to minimize operational building energy use and to maximize the generation of energy from solar renewable sources that are integrated within the building envelope (These include double facades, hybrid facades and decentralized mechanical services.).

The development of these manufactured systems with possible integrations of solar (thermal, pv) and/or ventilation systems should in principle enable multifunctional facade. Despite this, technological progression of these systems lacks a holistic approach to building energy strategies, as they are unable to sync with changing real-time environmental condition or recognition of climatic regionalization. These technologies are not transformable adaptive systems, as they do not at present give a holistic intelligent surface, i.e. solution approach. This lack of integration of component assembly technologies must evolve at a multiscale design level and this is the new frontier of interdisciplinary thinking (Gutierrez et al. 2013). Hence, building of component assemblies must be revolutionized, conceived and investigated from the inception of material behaviour to the environmental influence. Glass envelope performance strategy is based upon measures in the reduction of heat conduction, to resolve the conflicts between services and fabric provisions (heating systems, fighting cooling systems). These envelope technologies focus upon external thermal insulating systems, such as ventilate facades, double skin glass facades and solar shading.

Solar-adsorbing anti-heat glass is used to block solar radiation to prevent heat built-up. The introduction of nano-silver-coating oxide enables the reflection of solar radiation away from the internal building surfaces to inhibit heat transfer to enable solar transmittance to regulate solar radiation (Paceco-Torgal et al. 2013). However, this current response is a nonreactive static system that cannot comprehend energy consumption of a building typology to climatic zone. In addition, the understanding of the level of economic development in the region has also an influence in shaping the energy usage pattern. Energy demands in buildings bring together a range of complex relationships between the environment, the individuals and their perception of comfort.

This is in contrast to nature that has developed multifunctional biological systems. These systems are reactive materials of multiple-structured functionality that respond to climatic changes to enable proliferation. These materials respond to the influence of ambient temperature, solar radiation gain, exposure to wind and changing microclimatic variation. Nature's use of vascular formation to give adaptive functions can be implanted into glass, to create a composite material for absorptivity management. To progress glass envelopes of a skyscraper, from being a mere material entity to a dynamic energy system by the application of biologically inspired engineering. These are adaptive strategies to influence and change material

composition and behaviour. The research goal was to create photosynthetic responsive glass by thermoregulation and why vasculature and cardiovascular nature can enable bioinspired engineering of glass envelopes.

These desired morphologies to embed within a multifunctional glass material, to enable thermal conductivity regulation and exothermic management can progress glass skyscrapers into reactive, surface intelligent energy system. This composite structure will act as an adaptive cooling mechanism of high emissivity, a multifunctional system. That can regulate thermal conductivity behaviour as a bioengineering approach by the aims of:

1. Glass material absorbency.
2. Glass material autonomy.

5.2 Vasculature Networks

5.2.1 Biovasculature

Ecosystems upon this earth are evolving systems as they learn, defend, communicate and protect themselves by the mechanisms of synergy to environmental influence. Nature uses biochemical mechanisms in a evolutionary perspective encapsulating multi-chemical compounds of action to give adaptable strategies.

This biochemical process used by leaves is called the Krebs cycle. Plants have been practicing and perfecting combinatorial chemistry on an evolutionary timescale (Page 2004). This synthesis of molecular behaviour enables multiple pathways embracing and involving chemical material connectivity as an adaptive influence to climatic patterns. Plants use and embrace chemicals, semiochemicals, to enable communication and pyrrolizidine alkaloid as defensive mechanisms in response to climatic regionalization. Biological materials react and give adaptive strategies in response to external stimuli by environmental condition influence. These organic materials are multifunctional systems as they are mechanically strong and resilient formed by chemical composition. They are information systems that can self-adapt to the changes in ambient conditions by chemical and mechanical signals (Chen et al. 2012). This ability to learn and self-organize material composition by biochemical mechanisms is the process of continued development of materials at an evolutionary perspective. These materials have emerged through hierarchical self-assembly from nanoscale components to determine the composite structure. These living cells are the ultimate intelligent materials to give reactive response to the environment and understanding of geographical location. Plants and trees are transformable structures as they have autonomous self-healing and intelligent surfaces (leaves), and are adaptive to light and colour. The structure of a tree is a direct response to solar orientation; Fig. 5.1, as the shape and distribution of the branches, defines the tree structure. This geometry orientation has developed in response to the maximization of daylight capture.

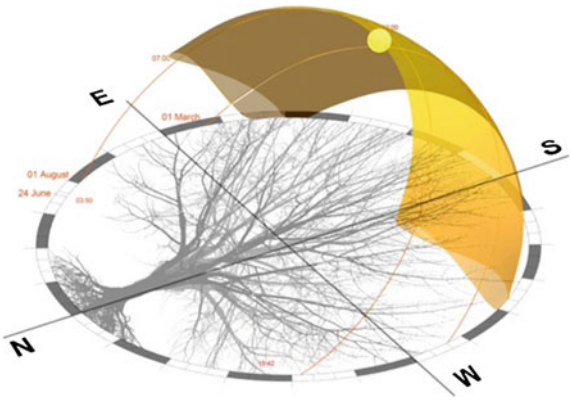

Fig. 5.1 Tree structural geometry in relationship to solar orientation

Light capture (interception of the leaves for photosynthesis processes) of the tree canopy is defined by rule-based geometry, canopy volume, total leaf area density and angular distribution of leaf surfaces (Sinoquet et al. 2005). Beer's law on light interception computations can determine these parameters. This approach to solar orientation and adsorption of light energy by biochemical processes are responsive measures, a dynamic system. However, each leaf and its relationship to geometry solar orientation is for the maximization of daylight capture. Each leaf is an independent photosystem acting as a unit within a whole canopy geometry-structured system. Each leaf has the ability to maintain its functional performance as it has inbuilt mechanisms to do so. This multiscale function of photosynthesis, molecular assembly and damage light stress regeneration by biosynthesized molecules is the response to irradiance adsorption.

Leaves and plants are able to control irradiance adsorption via photosynthetic measures by constant fluidic flows for dehydration and autonomous self-healing surfaces as a photoactive system by biovenation networks.

These networks are focused upon the process of change to give hierarchical material component control. Venation networks enable circulation of ions, water and photoactive molecules (Blonder et al. 2011). Nature uses these embedded microfluidic networks as a means for multifunctional, mechanical measures for transport of photosynthetic fluidics. There are multiple ranges of venation reticulated network patterns that have been created. These formation of venation networks determine leaf network patterns is the response to light capture by climatic influence as a dynamic relationship. Leaf vascular vein tissue is created by auxin. This molecule chemical trigger behaviour enables to self-organize the leaf vein network formations of isotropic auxin flows between cells (Feugier et al. 2005). Auxin flux is a carrier protein that flows between plant cells. This singular carrier protein is pumped between the intercellular spaces between cells, i.e. the plasma membrane. The reaction transport of this protein out of one cell into another cell determines isotropic auxin movement flux strength reaction. The flux strength and rate through cells determines the vascular network patterns. If the flux rate is weak, then the diameter of the network will decrease and fade away in correlation with the

auxin strength that creates a diminishing vein network in response to this. This is the self-generation of leaf venation network formations generated by molecule influence of auxin. The qualitative disposition of the auxin flux has a direct impact on venation leaf geometry patterns. The dynamics of auxin flux strength that creates vein formations is in response to the regulation and carrier flow protein pattern concentrations, which determine microfluidic veneration networks. These network vein patterns are determined by responsive function as a carrier protein regulation for vascular tissue formations. The geometry distribution and branching network patterns of leaf veneration determines fluidic flow for photosynthesis are determined at a molecular multiscale biochemical approach.

5.2.2 Cardiovascular

The human body itself is a complex system of controlled mechanisms in response to changing environmental influence to protect and control the human body by DNA programmable self-awareness, the ultimate intelligent material. These living multifunctional cells are information systems of chemical composition forming hierarchical structures. They have the ability to learn and adapt to changing circumstances and self-regulation of thermal adsorption from nanoscale components.

A definition of the cardiovascular system is that it "comprises the heart and the blood vessels with their contained fluid, the blood. The heart is the central organ of the entire system and consists of a hollow muscle; by its contraction, the blood is pumped to all parts of the body through a complicated series of tubes termed arteries. The arteries undergo enormous ramification in the course throughout the body and end up as minute vessels called arterioles, which in turn open into a close-meshed network of microscopic vessels termed capillaries. After blood has passed through the capillaries, it is collected into a series of larger vessels called veins by which they are returned to the heart. The passage of blood through the heart and blood vessels is termed as circulation of the blood" (Grey 2012). The heart is a double, self-adjusting muscular pump, the two parts of which work in unison. The heart propels the blood through the blood vessels. The right side of the heart receives venous blood and pumps it to the lungs where the blood becomes oxygenated. The left side of the heart receives the oxygenated blood from the lungs and pumps it into the aorta for the distribution to the body (Moore 1985).

The four main functions of the cardiovascular system are given as follows:

- To transport nutrients and oxygen to cells around the body and remove carbon dioxide and waste from cells.
- To protect the body from infection and blood loss.
- To help maintain a constant body temperature—thermoregulation
- To help maintain the fluid balance within the body.

5.2.3 Thermoregulation

Humans have the ability to tolerate great variations in the temperature of their external environment. Humans can survive and indeed live in parts of the world where the temperature may reach as low as −65 °C or as high as 50 °C. In some parts of the world, there are daily temperature changes of as much as 35 °C.

The core temperature range for a healthy adult is between 36 and 38 °C with 37 °C regarded as the average normal temperature. If the core drops below this range, it is called as hypothermia and above this range hyperthermia (Saffrey et al. 2001). As the temperature moves further into hypo- or hyperthermia, it becomes life-threatening. The body works continuously to maintain the temperature in a healthy range. This is thermoregulation and is a classic homeostatic mechanism. Temperature changes within the body are detected by sensory receptors called thermoreceptors, which relay information about the changes to the hypothalamus within the brain stem. The hypothalamus's chief role is homeostasis, which is mediated by the autonomic nervous system (Ashcroft 2001). When a deviation in temperature outside of the core range is detected by the thermoreceptors, the hypothalamus initiates mechanisms to control the temperature.

There are four main adjustments:

- *Sweat glands*. In hyperthermia, the sweat glands are stimulated to secrete sweat onto the surface of the skin. This allows heat to be lost through evaporation and cools the skin.
- *Smooth muscle in arteriole walls*. In hyperthermia, smooth muscle around the arterioles walls relax causing vasodilation, which increases the volume of blood nearer to the skin allowing heat loss through convection. In hypothermia, the smooth muscle contracts around the arteriole walls, reducing blood flow and therefore heat loss.
- *Skeletal muscle*. In hypothermia, skeletal muscles shiver, which are fast small muscular contractions, which produce heat to help warm the blood.
- *Endocrine glands*. In hypothermia, the hypothalamus stimulates the release of hormones, e.g. thyroxin and adrenaline which increases the metabolic rate and therefore heat production.

Humans are exceptional in their ability to cope with extreme conditions (McLaughlin et al. 2007). The ability to adapt is through the mechanism of thermoregulation, which is central to the bodies' ability to survive. Embedded venation networks are applied by nature in response to measures in regulation of material thermal behaviour. This is achieved by thermal management of material composition within the human cardiovascular and plant vascular networks. Conventional glass properties and behaviour is an issue for energy consumption. Current glass technology depends upon [or combination of] solar shading, air cooling [to reduce solar temperature gains] or the deployment of highly reflective nano-oxide-coating materials [to reduce sun light]. As a consequence of using the current technology, buildings consume significant level of energy [over its life cycle] due to the

increased artificial lighting levels to compensate for the loss of natural lighting and the reliance of AC systems to cool the buildings. Learning from nature and applying reactive thermoregulation mechanisms is the progression glass material technology, as a theoretic/conceptual background for the biomorphic photosynthetic glass.

5.3 Biomorphic Responsive Glass

5.3.1 Biotic Thermal Management

To increase the overall performance of a glass envelope to enable pan global aims for zero carbon buildings, a step change is needed. A multiscale-integrated strategy to advance a glass composite material in relationship to adaptive, responsive and self-optimizing performance. An endothermic system focuses on the process of change in relationship to conductivity management of capturing near-infrared radiation (NIR) in a material. Once solar radiation is captured, thermal conductivity can be controlled via absorptivity embedment of active transport networks (fluidic) to influence glass internal and external temperatures. This thermal conductivity management control of glass can be viewed as an energy system.

This energy system is an absorber of thermal flow energy by molecular understanding of heat transfer, to enable thermal transport exchange between glass pane interfaces and a fluidic medium for temperature management. Fluidics within vascular networks capillary channels are the methods employed by nature to regulate and control material conductivity in response to solar radiation. This absorptivity of self-programmable control heat flow management will enable energy generation as a cyclic energy system (Alston 2014). An energy system that responds to change of state by environmental influence. Climatic regionalization creates the process of change by biochemical triggers to create an energy flow chain reaction cycle. This biochemical process is used by leaves and this energy cycle is called the Krebs cycle. This aerobic citric acid cycle uses chemical reaction chains as responsive reactions to generate energy. This metabolic pathway of chemical trigger enables conversion of carbohydrates, fats and proteins into carbon dioxide and water to generate a usable form of energy. Regulating the material glass conductivity in real time by thermal flow transport management as an exothermic action/reaction system to NIR can be considered as a closed-loop energy system. The management of interface heat transfer would need to be supported by a decision-support monitoring, to act and to respond to the fluctuations in material temperature. This thermal exchange and transfer by control of fluidic flow behaviour is a reactive system to external climatic influence, Fig. 5.2.

This energy transfer exchange cycle will be maintained within the photosynthetic responsive glass composite. The primary stage is setting the datum point temperature for a glass composite in relationship to functionality parameters and climatic conditions. Setting primary data set point temperatures that is determining

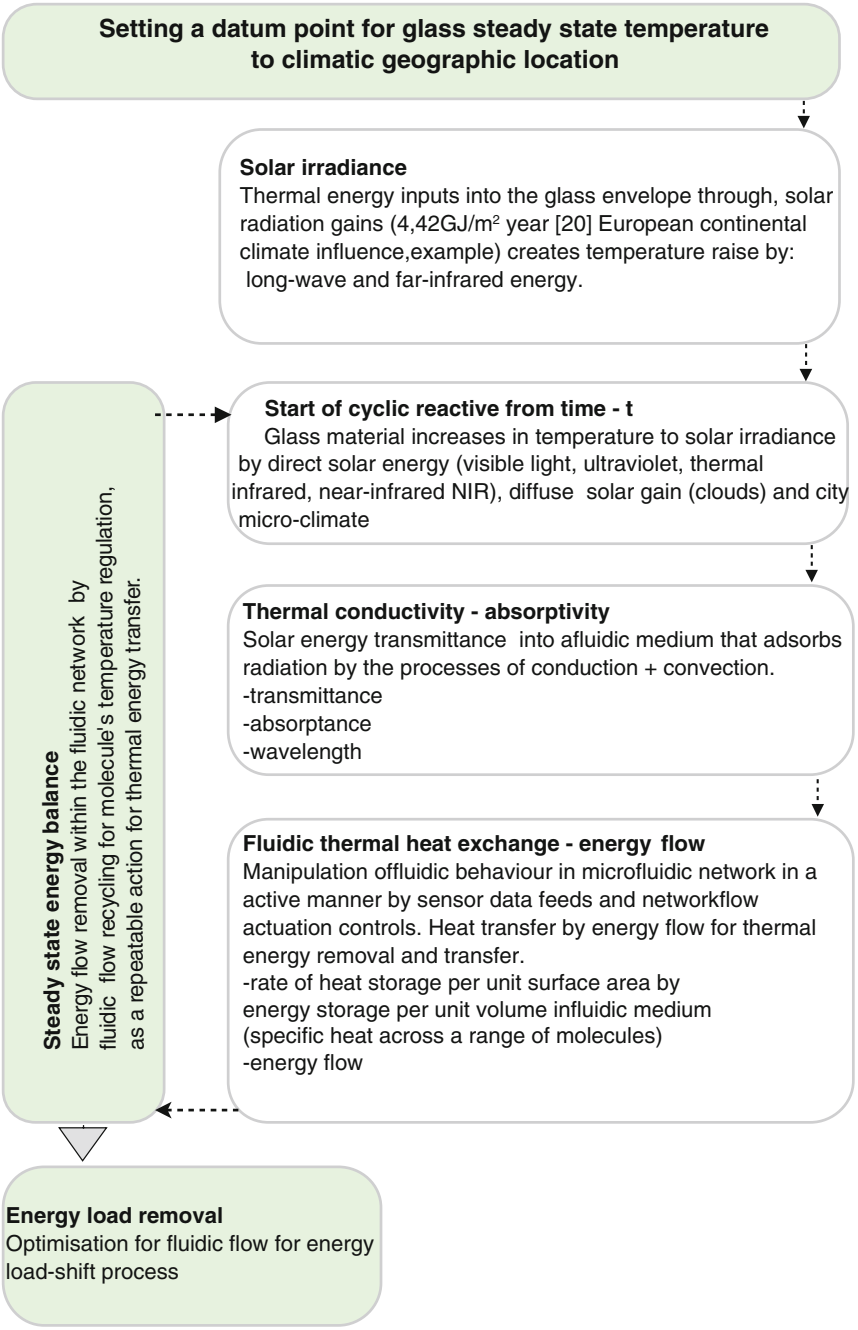

Fig. 5.2 Exothermic energy cycle

by thermal conductance measurement is critical. This establishes reaction sequence response that is required to maintain a steady-state temperature of the glass material to irradiance influence. The energy inputs from solar radiation, microclimate and surrounding building overshadowing will start a sequence of energy exchange reaction. These reactions will be determined by the energy transmission into a fluid to act as a temperature trigger. Channel-embedded networks within the glass composite will contain full volume of fluidic material. This fluid will act as the energy absorber to transfer, and the thermal flow gained energy away from the internal building surfaces. The rate of heat storage per unit area in connection with unit fluidic volume of the liquid will be monitored by sensors. Sensors will act as the programmable decision-support system to enable manipulation of fluidic flows, by actuators, to determine the rate of fluidic flow for energy removal. This reactive response is a direct relationship to datum point temperature setting. This sequence commencement is the starting point of an energy transfer exchange and thermal heat transport cycle for conductivity management/regulation.

The energy unload process is key to enabling fluidic absorbed energy thermal flow removal, as an energy cycle. This energy cycle is focused on energy unload processes of the fluid and this is determined by data set point temperature setting. Once the fluid conductance level is diminished (to a predetermined temperature point), the liquid is then recirculates back into the vascular network. The removal of the adsorbed energy heat transport flow from the fluidic medium, Fig. 5.2 (by thermal stores/electrical generation), enables a thermal extraction cycle. This is a cyclic action of molecule temperature regulation, as a repeated action for thermal energy adsorption. Rates of thermal adsorption are dependant upon the time of day, wind exposure, orientation and city temperature, and heat island effects. This process to adsorb NIR, for stabilization of material temperature, is the response to climatic influence and this is the approach of nature's biosystems.

5.3.2 Climatic Regionalization

Nature's plants, organisms and animals are moulded by their environment. Ecosystems have an understanding of adaptation to the environment at a biodiversity ecological perspective. These interactions of the physical environment (matter) and biological systems for energy conversion are mechanisms of control at a multilevel scale that are nested within climatic regionalization. However, this ecosystem approach is not represented in the human habitation of our building structures or cities in which we live. The relationship of materials and energy for buildings and cities should depend on its typology, technological solutions, employed location and user-specific issues and the most important of which are the following:

1. Building typology in relationship to size, form and placement on site.
2. Climate, user occupant numbers, behaviour/required performance level.

3. Insulation capacity of the envelope and thermal capacity.
4. Efficiency of heating, ventilation, water supply and lighting systems, automation and control systems.

The current aim of the glass envelope's performance is based upon the measures in the reduction of heat transport conductance, to resolve the conflicts between services and envelope (heating systems fighting cooling systems). Photosynthetic glass would give enhanced thermal properties for energy efficiency by applying new concepts of heating and/or cooling sources, interfaced into a glass composite. This new methodology of thermal heat transport management will influence and reduce consumer energy consumption demands. Climate is having greater impacts on energy requirements by the increasing dependence to cool buildings in warm climates and this is indicated in the heating degree days (HDD) Fig. 5.3.

VTT project has evaluated the potentials at a European level to assess climatic effects to measure impacts for inherent measures for building facades. Measuring of the technical solutions of facade behaviour, to climatic conditions, in connection with building typologies was observed. Results indicated in Southern European countries that cooling demand becomes increasingly important for the overall energy consumption of a building due to higher requirements of thermal comfort. The study found that in warm climatic zones the cooling demand can be reduced drastically by a combination of lowering the internal heat loads by greater control of thermal conductivity. This had environmental impacts on the total primary energy demand according to climatic zone and building group typology.

The development of adaptive glass envelops as an optimal energy absorber for different kinds of user energy demands synced to a climatic behaviour model—is one of the new approaches. The energy thermal flow-targeting model Fig. 5.2 will be depended upon climatic classification in order to set primary data functions in terms of fluidic steady-state mechanisms. The understanding of the conductivity facade behaviour of buildings and its implications on energy performance has been researched by VTT (2012) to enable direct linkage to climatic conditions. Climatic classification analysis is critical in order to set behaviour responsive range parameters as a reactive energy system to external climatic temperature influence. The research into climatic methodology has been undertaken by the Koppen system (Peel et al. 2007). The observed data from present and global historical climatology networks have enabled data sets for the classification of climatic conditions Fig. 5.4.

These climatic regionalization data sets enable assessment of climatology for global mapping. This climatic classification can be applied, in setting fluidic temperature as a datum point value. Setting a steady-state temperature is the mechanism that will determine reaction or nonreaction boundaries in relationship to fluidic temperature, in networks within a glass composite. This reaction system is a real-time interrelationship to climate as an energy cyclic flow that has been determined by temperature data sets of climatic classification. If we are setting the steady-state temperature to climatic classification for behavioural response, could the fluidic material itself also relate to climatic regionalization? The fluidic material chemical composition could be created as a designer molecule approach synthesized the

Range of heating degree days [HDD]	Corresponding countries			
	Country	HDD	Population in 2003 [Mio.]	Building stock [Mio. m^2]
Zone 1: South European countries	Malta	564	0.40	11
564 to 2 500 HDD (1 269 HDD)[a]	Cyprus	787	0.72	40
	Portugal	1 302	10.41	337
	Greece	1 698	11.01	351
	Spain	1 856	41.55	1 454
	Italy	2 085	57.32	2 076
	France	2 494	59.64	2 109
Zone 2: Central European countries	Belgium	2 882	10.36	359
2 501 to 4 000 HDD (3 272 HDD)	The Netherlands	2 905	16.19	561
	Ireland	2 916	3.96	125
	Hungary	2 917	10.14	221
	Slovenia	3 044	2.00	45
	Luxembourg	3 216	0.45	21
	Germany	3 244	82.54	3 463
	United Kingdom	3 354	59.33	1 567
	Slovakia	3 440	5.38	82
	Denmark	3 479	5.38	230
	Czech Republic	3 559	10.20	237
	Austria	3 569	8.10	292
	Poland	3 605	38.22	706
Zone 3: North European countries	Lithuania	4 071	3.46	62
4 000 to 5 823 HDD (4 513 HDD)	Latvia	4 243	2.33	45
	Estonia	4 420	1.36	28
	Sweden	5 423	8.94	338
	Finland	5 823	5.21	151

a) Numbers in brackets indicate average weighted HDD
Sources: [EUROSTAT 2005a, GIKAS & KEENAN 2006]

Fig. 5.3 HDD extract, energy efficient façade system (VTT 2012)

material to a particular climatic data set. This is a functional performance response as an energy absorber. The design and selection of a fluidic material, in vascular networks, must be selected in relationship to thermal high energy densities.

5.3.3 Bioenergy System

To progress glass skyscrapers from being a mere material entity to becoming an energy system of adaptive performance is a step change. The evolution of a

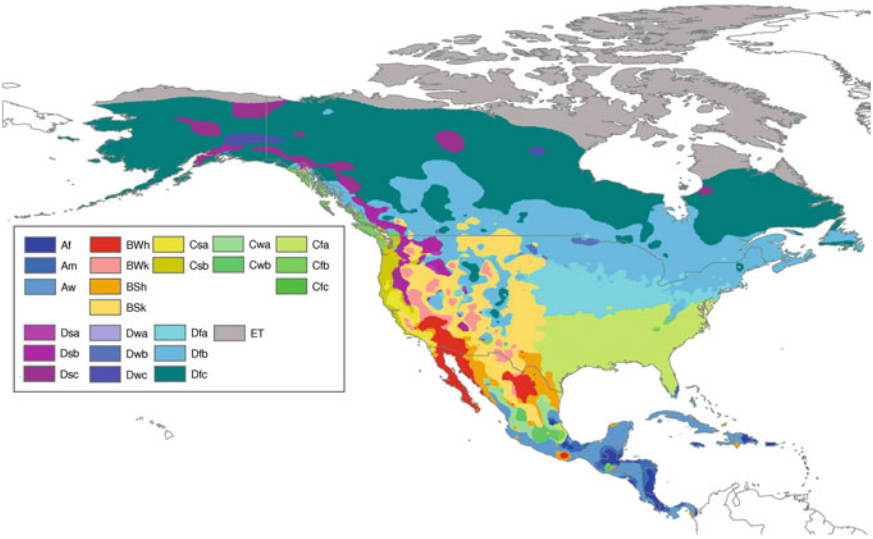

Fig. 5.4 Extract from updated world map of the Koppen-Geiger climate classification (Peel et al. 2007)

dynamic glass surface Fig. 5.5 as an optimized, multilevel intelligent surface of thermal behaviour exchange and conductivity management by fluidics is the new frontier. This bioenergy system is a material matter energy cycle, in relationship to regionalization. This transdisciplinary, multiscale approach has emerged through a higher complexity of reactive, responsive triggers than current glass technologies. This flow of energy reaction triggers are driven by:

- Capture by material absorbance of solar radiation.
- Control to regulate, enabling material autonomy for thermal management of microfluidic absorptivity.

However, building typologies located within cities are components within it and therefore must react and be resilient to environmental surroundings. Localized environmental conditions will influence a step-wise flow in the relationship between energy and matter (Odum and Barrett 2005). These energy input variables are depending upon the orientation of the glass surface, relationship to surrounding buildings, microclimatic conditions, wind flow paths and diffuse solar gain via clouds. A multilevel approach is needed as the performance aims and functional role of current glass envelopes is a static response that does not adjust to environmental change or influence.

The employment of a glass composite material enables optimization to control solar irradiance by thermal behaviour, exchange and management of conductivity by fluidics. To create the energy resilience of a glass envelop to form the surfaces of skyscrapers must evolve into an adaption intelligent layer. That can regulate its own

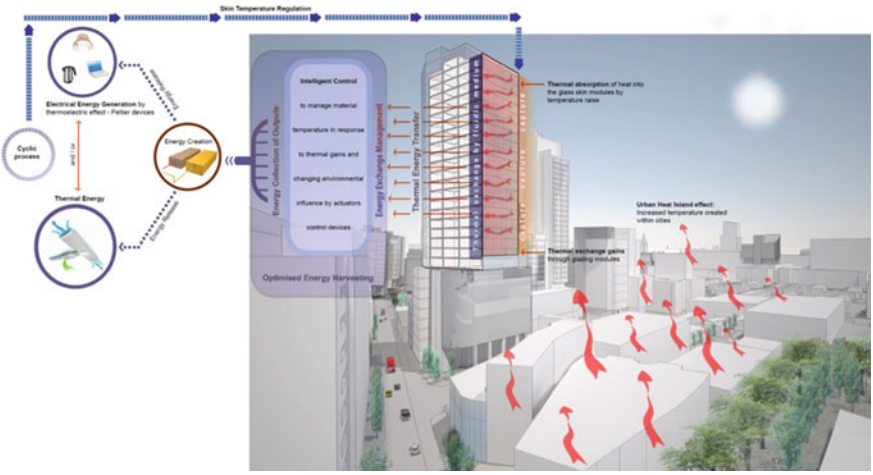

Fig. 5.5 Glass composite exothermic energy cycle

thermal conductivity levels in response to performance change by the hour, season and weather conditions in enabling real-time thermal flow management of conductivity.

5.4 Thermodynamic Adaptive Glass

Research has been undertaken to introduce fluidics into windows. This investigation focused upon using the cavity void between two panes, by infusion of water as conductivity adsorbed of solar radiation. However, this research did not investigate the use of microvascular networks to influence fluidic flow management. The research indicated water flow gave cooling of glass surfaces by naturally flowed upward buoyancy and extraction of water for heating applications (Chow et al. 2011). The use of water enabled higher conductivity for effective window cooling designs in warm climates (Chow et al. 2011). Findings indicated that adsorption of heat energy from solar gain was achieved. Hence, indoor heat absorbency by thermal convection and radiation exchange gave a temperature difference of 10° between the inner glass panes. Water flow in the experiments was set at 200 ml/min with the greater efficiency gained in higher incident of solar radiation for working in efficient conditions (Chow et al. 2013). However, the lack of fluidic flow management within the free-flowing volume resulted in flow turbulence and water movement uncontrolled by gravity.

This created variations in temperature within the water volume between the two glass pane surfaces. The other critical issue was water flow velocity rates; this was considered to have a great impact on the effectiveness to enable reduction for internal cooling load by fluid heat removal. The associated weight of a full volume,

water cavity fill dramatically added to the structural loading of the external wall. Hence for a single window within a wall, this could be contained. However if applied to a skyscraper with dynamic structural forces, wind pressure force directions, air velocity, frequency wind range, temperature differential and gravity, the effectiveness applied to this building typology is reduced. Current glass technologies consider a glass building to be one surface, notwithstanding this one surface is comprised of a number of assembly components, frames, mullions, waterproofing gaskets, and drainage channels for example.

However, could the surfaces of skyscrapers be formed from multiple photoactive layering of autonomous glass surfaces?

We consider this surface as photoactive layers that interconnect, Fig. 5.6, at a multiscale level to create a holistic glass envelop. These are the mechanisms applied by trees, in the creation of a canopy to form the leaf area density of a tree as a multiple laying approach. Each leafs' geometry and functionality is connected to orientation for the maximization of daylight capture.

The creation of photoactive layering enables control influence in dealing with orientation, temperature differentials and gravity effects. These multiple autonomous, horizontal surfaces enable fluidic flow working with gravity feed by a layer-by-layer approach, Fig. 5.6. This photoactive layering gives avoidance of multiple floor, vertical fluid transfer and consequential increased pumping pressures demands. The ramification of this is the creation of autonomous cellular floors zones that will have energy generation from glass photoactive surfaces to respond to energy floor zone demands. An intrinsic link of energy generation to consumer energy demands at a localized level.

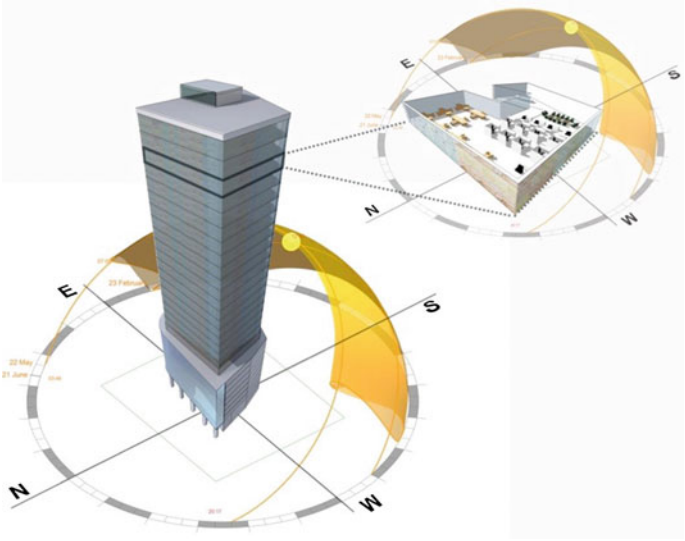

Fig. 5.6 Photoactive layering

5.4.1 Artificial Microvascular Networks

Microfluidic systems give greater control of fluidic behaviour flow and fluidic management. These capillary networks of solar absorbing chemical composition fluid are activity flowing and circulating within this network. Microvascular volume-filled fluidic networks enable heat transport interfaces between two glass panes as an absorber of solar radiation. This application enables active material temperature control by fluidic flow rates and absorptivity of the fluidic material for higher conductivity. The flow of fluids within this microvascular network is achieved by continuous circulation within it, through it and out of it, enabling capture and removal of energy by recirculation, Fig. 5.2, for thermal heat unload processes. These are bioengineering measures applied by nature vascularization systems as photoactive layers. Leaves use microfluidic networks as a photosystem for the circulation of ions, water and photosynthetic for photosynthesis and regenerative functions. This method of using a fluidic material as a means to adsorb inward thermal conduction and solar radiation heat transfer is nature's mechanisms of conductivity regulation. If shortwave irradiance/infrared spectrum NIR (but avoidance visible light) is captured and the energy obtained is removed, this process enables temperature control of the photosynthetic glass composite.

The embedment of a vascular network with a material (domain) inserted between two panes of glass creates a photoactive adsorption layer. The domain materials such as PMMA, PDMS, Epoxy for example are the interface between the two glass panes as a thermal flow bridge. The network geometry embedded within the domain material will be designed and orientated to the maximization of captured energy in connection with solar radiation. Hence, the performance efficiency of the network is intrinsically linked to the network design geometry, Fig. 5.7. This optimization of microvascular networks geometry design can be quantified by thermal flow analysis.

This higher conductivity adsorption of a glass material would be optimization by the vascular network channel geometry. Each channel will have a direct relationship to thermal gain as this will influence the glass pane thermal conductance. Microchannel vascular network density will affect functionality and depend on two key drivers.

- Singular channel (within a network) cross-sectional dimensional size.
- Network geometry channel density embedded within a domain.

A singular channel within a network will vary depending on the exposure to a heat source and fluidic dynamics pressure flow. The embedded microchannel network geometry design will correspond to material conductivity by heat source impact (Olugebefola et al. 2010). This is heat seeking targeting to regulate thermal flow between two glass panes as an adsorption photoactive interface layer.

Microvascular network embedded in polydimethylsiloxane (PDMS) bonded to a single pane of glass has been researched by Hatton. The PDMS material contained within its material domain a series of capillary 100-μm-high channels created a

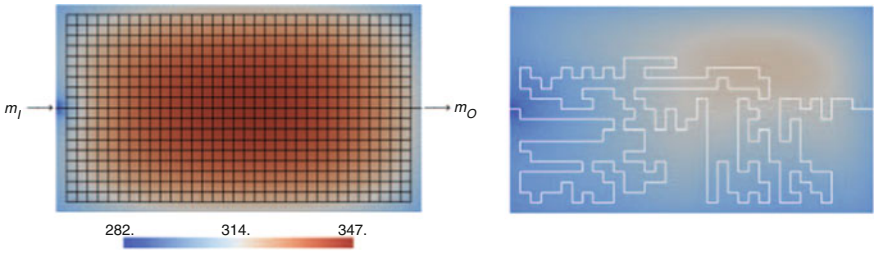

Fig. 5.7 Microvascular network geometry design to uniform heat source (Olugebefola et al. 2010)

diamond network patterns to enable fluidic flow. A uniform heat load of 35–40° was applied and measurements taken. Differing flow rates were assessed (0.2, 2.0, 10 m/L/min) to measure surface conductivity. Fluid chosen for the experiment was water. The objective was to monitor the effectiveness of flow rates and fluid temperature input to measure thermal energy transfer absorptivity of the water (Hatton et al. 2013), Fig. 5.8.

The results concluded the input water temperature and flow rate was significant in order to regulate material temperature via thermal energy transfer. However, the only fluidic input temperature that gave encouraging results required cool water at medium to high flow rates. This research did not undertake or investigation the fluidic material performance or thermal behaviour within the microvascular network. Network vascular geometry and fluidic conductivity will impact on the effectiveness for capturing thermal temperature gains. However, channel design and network geometry to regulate interface heat transfer are inevitably intertwined. The enhancement of thermal properties of the fluidic absorber to increase heat transport by chemicals has advantages. This is a designer molecule approach in enabling nanoscale conductance intensification. Nature uses biochemical composition for

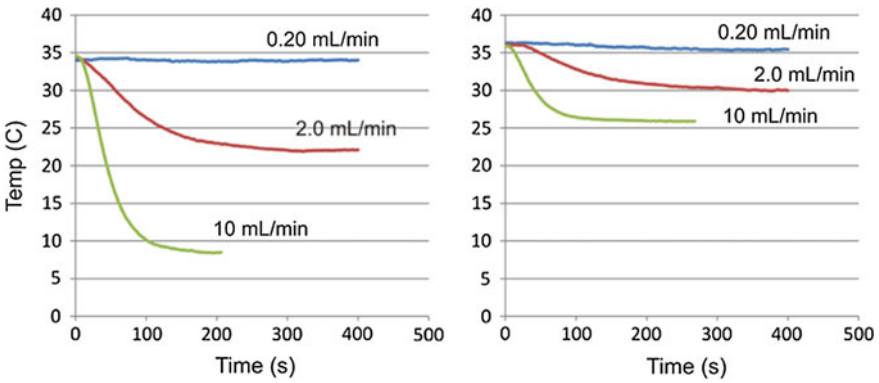

Fig. 5.8 Average temperature line graph between inlet and outlet as a function of time for water input temperature of 0° as indicated on the *left* and room temperature on the *right* (Hatton et al. 2013)

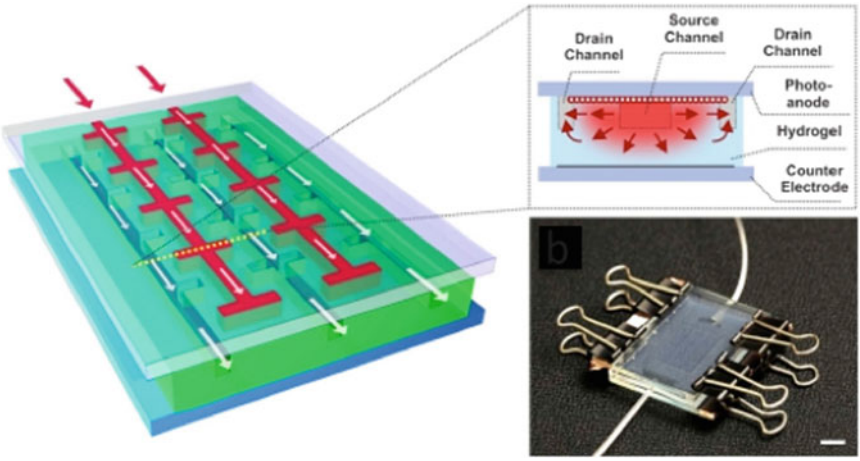

Fig. 5.9 Biomimetic microfluidic infusion network (Hyung-Jun et al. 2013)

regeneration, self-assembly and adaptation. These chemical compounds of action and reaction have been undertaken by Hyung within self-heal photovoltaic.

Vascular networks have been used as regenerative functions for hydrogel photovoltaic devices by photosensitive organic dye infusion, Fig. 5.9, to enable solar cell high functioning performance. This hydrogel solar cell utilizes an embedded microfluidic channels (fabricated by moulding) to enable photosensitive dye molecules to adsorb photons and inject electrons in a conductive band to generate energy (Hyung-Jun et al. 2013). These molecules were distressed by photodegradation due to NIR intensity, and hence, regenerative cycles are needed to maintain energy generation. The vascular network enabled electrolytes inclusion for regenerative chemisorbed dye molecules.

The network contributed to the energy generation performance to give photoregeneration of the hydrogel solar cell system and the impact of photoelectrochemical oxidation by the introduction of chemical dye fluidics. The linkage to the vascular network and the fluidic performance is integrated for the infusion replacement of damaged photosensitive molecules. This same process can be applied to photosynthetic glass to create thermal high-conductivity advancement by continuously circulating a fluid into, through and out of the network to adsorb as a recirculation process. These parameters will achieve steady-state temperature of a glass composite material that is based upon biochemical engineering endothermic principles.

5.4.2 Fluidic Energy Densities

To gain high-thermal properties for heat flow transport is dependent on latent heat release and internal thermal conductivity. Nanofluidics have these inherent

compound properties (Agbossou et al. 2010), Fig. 5.10. This chemical designer molecule approach of thermal conductance, to adsorb energy at the interface between two panes of glass, provides heat seeking targeting as an abiotic absorptivity layer. The thermal properties of this photoactive layer of heat transport are criteria for higher conductivity management of a external glass surface and interior heat absorbency with a microvascular network.

Nanofluidic chemical engineering of heat transport flow enables adsorption of light photons at a nanoscale level of heat exchange management. The pursuit of fluidic thermal high energy densities, as an optimized absorber, would be chemically designed to climatic regionalization. This is a chemical designer approach synthesizing thermal conductance, viscosity, specific heat and diffusivity in avoidance of low energy density fluidics, water. This improved thermal property of convective heat transport coefficients, via nanoparticles (metal oxide, carbon nanotubes for example) for photosynthetic glass to increase absorbency of sensitive heat from air and irradiance. These properties enable nanofluidic advancement of heat transport applications by high-thermal conductance. This is achieved by the following:

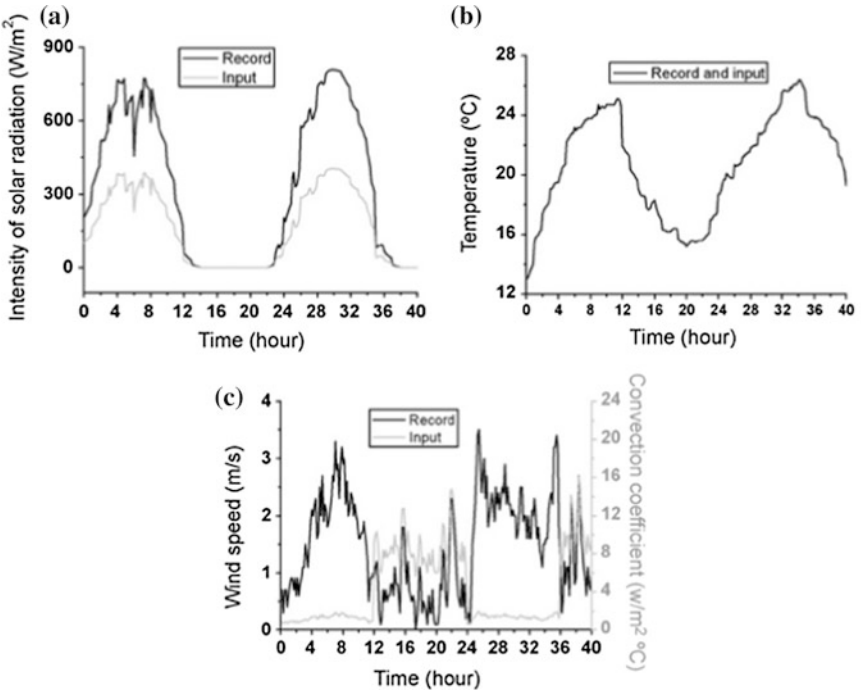

Fig. 5.10 A typical ambient thermal loading: **a** intensity of solar radiation, **b** ambient temperature and **c** wind speed (forced convection generation) (Agbossou et al. 2010)

1. The suspended nanoparticles increase the surface area and the heat capacity of the fluid.
2. The suspended nanoparticles increase the effective (or apparent) thermal conductivity of the fluid.
3. The interaction and collision among particles, fluid and the flow passage surface are intensified as well as the mixing fluctuation and turbulence.
4. The dispersion of nanoparticles fattens the transverse temperature gradient of the fluid.

The resulting compound referred to as nanofluids possesses a substantially, larger thermal conductivity (Shin and Debjyoti Banerjee 2010) compared to the original base fluids enabling greater heat flow transport. Experimental studies conducted have indicated that the effective thermal conductivity increases remarkably under macroscopically stationary conditions. Hence, nanofluids are attractive materials for progressing and improving thermal conductivity of the heat transfer liquid within photosynthetic glass. A starting point to establish a base fluidic material within the vascular network could be as simple as a water/salt hydrate solution and increasing its complexity to a chemical designer molecule approach. Therefore, could a theoretical model of heat flow characteristics be aligned to climatic regionalization and nanofluidic energy densities, by a classification nanoscale thermal measurement system? This chemical designer approach is the evolution of fluidic thermophysical optimization to correlate to climate and microclimatic conditions, as a photoactive abiotic conductance layer.

5.4.3 Abiotic Adaptive Layer

Evaluation of heat flow monitoring and consequent reaction triggers are needed to actively manage nanoscale absorptivity within microvascular networks and thermal conductance effects upon the glass material. The engagement of sensors and actuators controlled by an algorithm management response will enable parameters setting in connection with solar radiation gain. This is achieved by fluidic flow rate control and load shift energy removal from the heat absorber carrier fluid. Hence, nanoscale fluidic monitoring by the evaluation of heat flow within the network and temperature monitoring decay by that of heat loss are strategic functions. This analysis to quantify thermal flow directly relates to, Fig. 5.2, datum temperature point setting. This tracking of thermal flow creates a cyclic nanoscale system for conductivity regulation by energy load–unload processes. This energy load shift tracking of conduction is intrinsic to indoor set point temperatures.

The entire glass surface of a skyscraper could not be treated as one entity, as the vascular network will have a resistance to flow and this would be considerable. Pumping pressures need to be controlled, as energy generation from active conductivity control of glass would be outweighed by the pumping energy demands with in the network. However, the separation of the facade into multiple

photoactive layers, Fig. 5.6, to work with gravity and reduce pumping pressure is the starting point of this control process (Alston 2015) Fig. 5.11.

These photoactive autonomous layers have shared data communication interfaces to enable temperature monitoring of conductivity by fluid for heat seeking targeting. This targeting will enable real-time adjustment to fluidic flow rates, by actuators to manipulate fluidic thermal flow rate as a heat recirculation evaluation cycle. This active management of thermal heat transport flow will feed into tank reservoirs for energy unload process removal. Once the energy is removed from the photosynthetic glass, the fluid recirculates back into the network. This feedback loop completes the closed-loop exothermic cycle. These are learnt and applied reaction responses to changing solar radiation patterns and absorptivity. The energy unload process is created at a localized level, serving the microvascular networks in avoidance of extended distribution feeds. This gives the optimization of pumping energy demands and localized energy load–unload processes. The ability to use tank storage reservoirs enables heat to electricity conversation by semiconducting engineering. The developments of semiconducting nanocomposites to yield high-performance energy conversion (Yuanfeng et al. 2013), Fig. 5.12, have been undertaken. The quantum dots, for the thermopower enhancement of electrical conductivity by energy generation using thermopower, have strong application here. This coupled with thermostorage and gives optimization energy generation

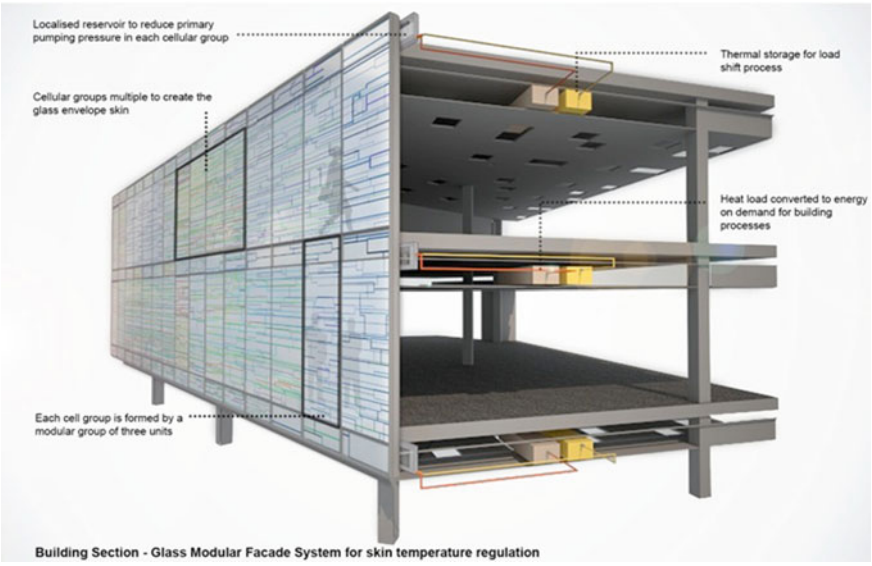

Fig. 5.11 Multiscale-integrated photoactive layers

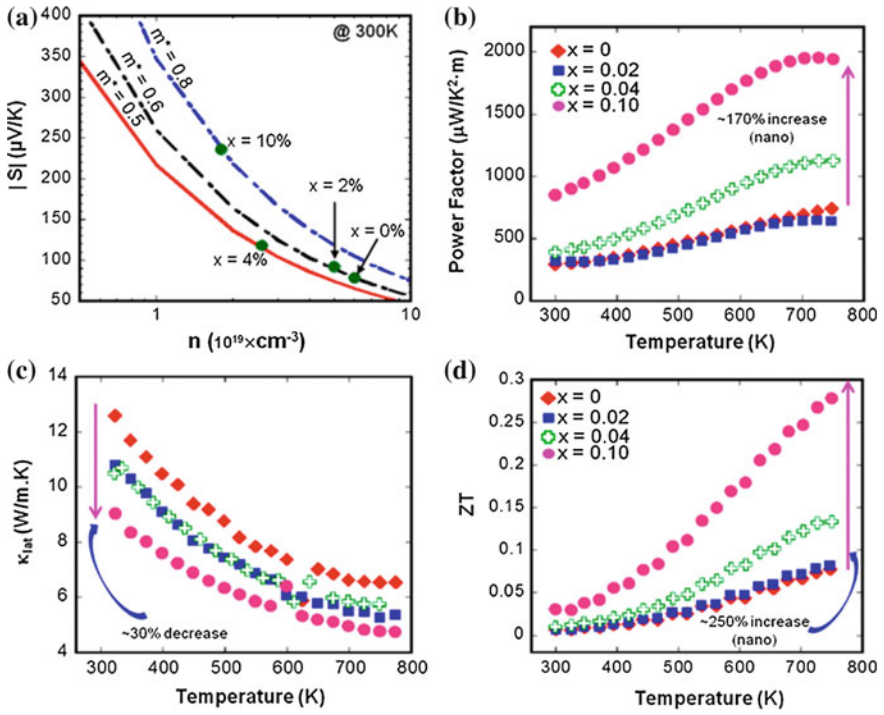

Fig. 5.12 **a** Pisarenko plot showing large enhancements of the thermopower (S) due to simultaneous decrease in carrier concentration and increase in the carrier effective mass (m*) with increasing excess Ni. Temperature-dependent **b** power factor; **c** lattice thermal conductivity; and **d** thermoelectric figure (Yuanfeng et al. 2013)

capacity Fig. 5.6 in meeting consumer energy requirement demands per floor level by creating an automatous energy community to building floor level.

Each photoactive layer is directly related to a particular floor level to enable energy floor level syncing. Each level will have its own energy consumer demands, as skyscrapers have multifunctional typologies. Therefore, the energy generation ratio, for demands for electrical and water heating, would be synced to the consumer activity requirement. These energy demand requirements of differing energy ratios can be demonstrated by Burji Khalifa:

- Armani Hotel: Concourse, Ground, floor levels: 1–8 and 38–39 with Armani Residence 9–16 and 19–37.
- Sky Lobby with swimming pools, library and recreational rooms: floor levels 43, 76 and 123.
- Private residences: floor levels 44–72 and 77–110.

- Corporate Suites: floor levels 111–121, 125–135 and 139–154.
- Restaurant: floor level 122.
- Observatory floor 124.

5.4.4 *Energy Syncing*

The optimization of energy generation will be specific to consumer activity (office, residential, recreational, etc.) giving energy modelling profiling per floor level zone. The development of photosynthetic glass as a multifunctional system, and energy production, distribution and storage technologies, into a glass envelope are new methodologies. The integration of comfort systems for energy management and localized energy generation is the new technological frontier. The breakdown of the glass facades into an autonomous photoactive layer is a new direction than present technological energy solutions—serves all approach. This connects energy demands to a multifunction glass composite as a bioenergy system. System functionality is however intrinsically linked to climatic influence and response. Glass facades must be climatic adaptive, in response to regionalization. The selection, design and application of the fluidic absorber within vascular networks, for thermal high densities optimization, must be synced to meteorology. For the optimization of this multiscale-integrated approach for reduction in primary energy demands, green house gas reduction will enable energy generation and carbon footprinting to sync with differing climates and typology.

The surface temperature of a building has variations due to orientation, localized climatic conditions and relationship to surrounding buildings. This imbalance in the exposure to solar radiation creates relative cooler surface temperatures to the building envelope perimeter.

Therefore, the geometry design of the vascular network will change in its complexity, in relationship to surface temperature fluctuations to building orientation geometry. The determination of these two geometry systems can be obtained by absorptivity calculation modelling (Alston 2015). The NIR input and conductivity output values will enable determination of vascular network geometry in response to building geometry orientation. The absorbency and solar radiation exposure of the fluidic material in Fig. 5.13 would also change in differing building surfaces in response to irradiance. This approach simulates nature's response, where leaf density patterns and leaf surface area, changes in response to solar orientation.

Monitoring the photosynthetic glass temperature fluctuations of thermal conductance at a nanoscale heat transfer level enables dynamic response to city heat island effects. Heat islands create microclimatic conditions that have an impact on regionalization climatic data sets. These variables relate to localized climatic conditions, air temperature, air velocity, relative humidity, user behaviour and indoor

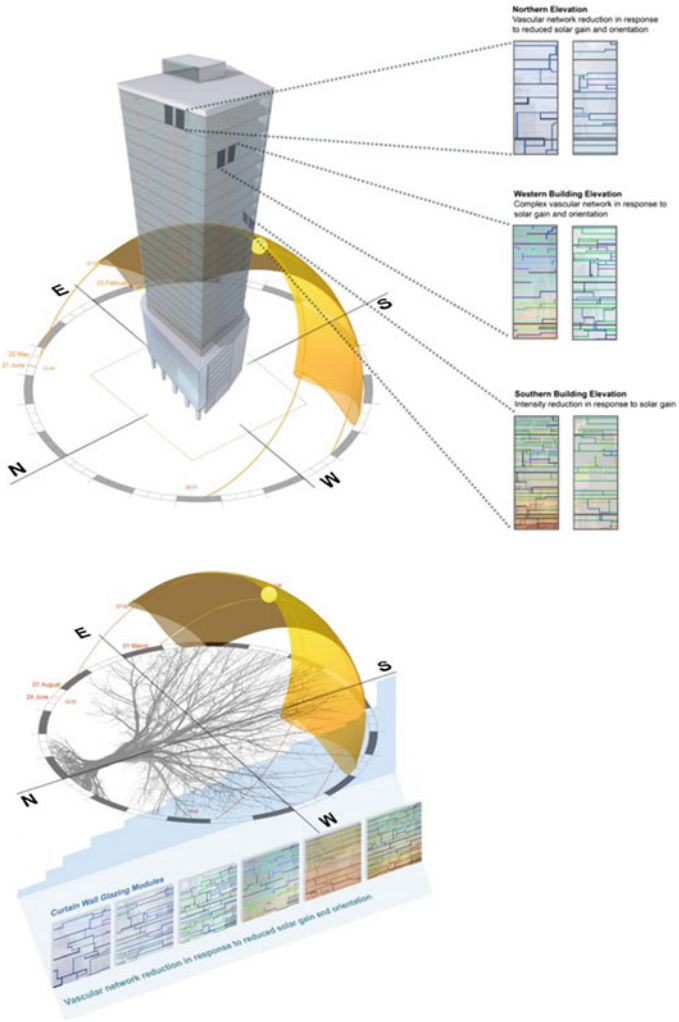

Fig. 5.13 Vascular geometry linked to building surface geometry

heat load. A meteorological behaviour-forecasting module has been investigated. A simulated data performance modelling has been undertaken, via algorithms, to enable real-time climatic tracking. This data relates to ambient temperature, irradiance, occupancy profiling and indoor temperature and this system is called artificial neural networks (ANN) (Argiriou et al. 2004). ANN is an energy management controller to forecast weather parameters to maintain indoor conditions within a determined comfort zone, Fig. 5.14. This meteorological performance module

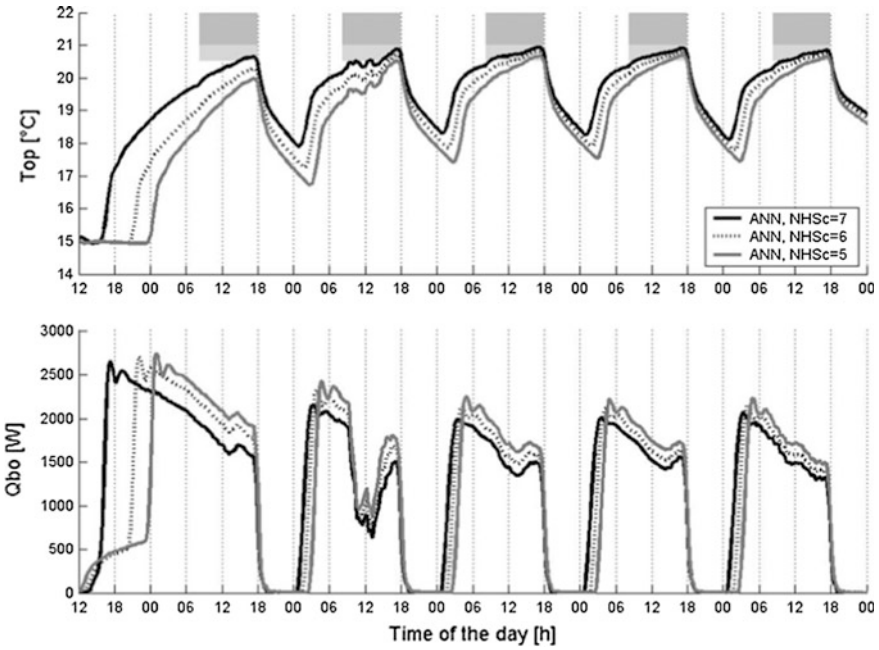

Fig. 5.14 Performance of the ANN controller during the cold week. *Top graph* shows operative temperature; *bottom graph* shows heating power (*grey rectangles* are comfort range)

enables indoor set point temperatures for predicting heating energy demands. However, this could be applied to programmable management for microvascular functionality in warm climates.

The ANN control module can accurately calculate required response, to maintain indoor set point temperature to predict fast variations of irradiance, for example clouds creating shadowing and temperature effect changes on the surfaces of buildings via wind paths. The response of this changing evaluation of endothermic heat flow would create surface-changing patterns of thermal absorptivity.

The surface effects of absorptivity of a fluidic heat transport carrier fluid will create varying action and reaction chemical trigger responses to NIR. If the heat carrier fluid chemical compounds contained photosensitive molecules, this would create changing patterns of colour in response to interface heat transport within the microvascular network. Synthesizing the nanofluid with adsorbing chemical dye pigments fluidics enables chemical colour trigger response to NIR for the creation of a myriad of changing colour patterning. The effects of thermal conductance of interface heat transport will be displayed in colour, by the influence of irradiance, building surface geometry, orientation and city core temperatures, Fig. 5.15.

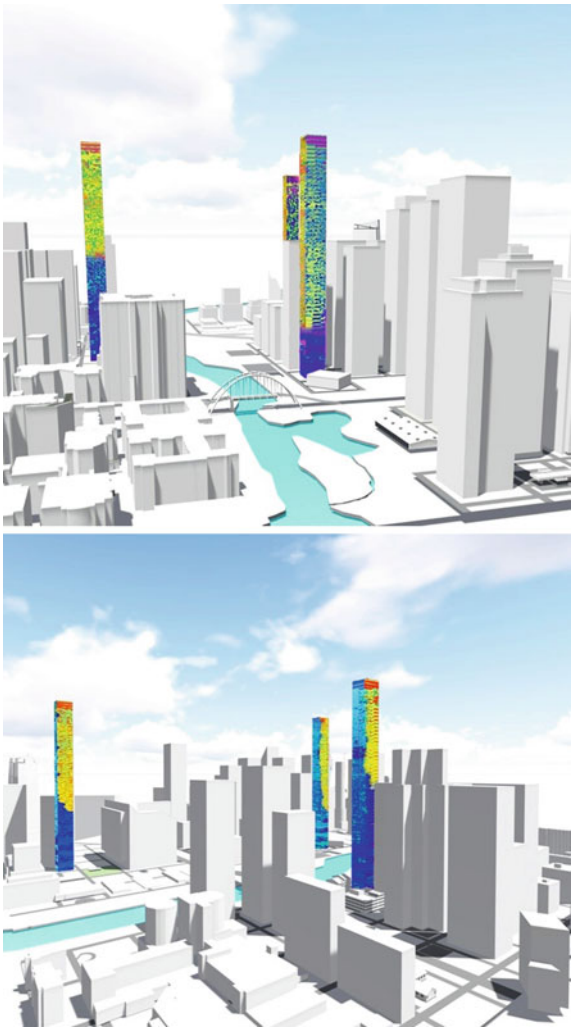

Fig. 5.15 Photosynthetic glass matter/energy Biosystem

5.5 Future: Endothermic Glass

To gain a fundamental understanding of the interrelationship of glass matter and energy for the regulation of thermal conductance to enable heat seeking targeting is nested within climatic regionalization, city core temperatures and building typology. These are biologically applied engineering principles by self-regulation of thermal adsorption from nanoscale components. The fulfilment of photoactive abiotic layers of daylight capture, to control irradiance absorptivity via photosynthetic evaluation measures, will evolve glass surfaces into an intelligent material, is the new frontier. The linkage of vascular network geometry, building orientation

geometry and nanofluidics energy densities for high solar radiation capture and climatic regionalization are focusing upon absorptivity.

These principles of active evaluation of heat flow trigger mechanisms by thermal flow conductance interface regulation will create a optically clear transparent glass composite for autonomous glass photoactive surfaces. These learn and apply reaction response to regulate material conductance by biochemical, multifunctional, nanoscale photoactive engineering will give emergent properties of thermal transport programmable control of collective control.

A metabolic sequence of thermal transfer for indoor comfort conditions will be achieved at a multiscale-integrated exothermic, recirculation cycle. The evolution of an optically transparent facade as an energy system that responds to the environment and contributes to the planets energy needs. To enable reduction in indoor cooling demands by lowering internal ventilation loads by greater control of glass conductance in warm climates. This thermal adsorption cycle uses climatic methodology data sets for programmable reaction boundaries by steady state, set point temperature setting. An energy flow system for real-time reaction by the hour seasons for energy harvesting syncing to consumer demands for multitypology buildings. This conductance of heat flow cycle will enable dehumidification of glass surfaces, an abiotic absorptivity layer of material hierarchical control to create city resilience for the well-being of urban communities. This chapter is presenting and discussing a conceptual construct for new photosynthetic composite glass material. Further research is expected on building and testing of the prototype.

Acknowledgements Dr. Nikolaus Nestle, Research physicist at BASF SE, Ludwigshafen, Germany. Susan Ringham, M.Sc., Grad. dip. Phys. MCSP.

References

Agbossou A, Zhang Q, Sebald G, Guyomar D (2010) Solar micro-energy harvesting based on thermalelectric and latent heat effects. J Sens Actuators A: Phys 163:277–283

Alston ME (2014) Energy adaptive glass matter. J Archit Eng Tech 3:115. doi:10.4172/2168-9717.1000115

Alston ME (2015) Natures building as trees: biologically inspired glass as an energy system. Opt Photonics J 5:136–150. doi:10.4236/opj.2015.54013

Argiriou A, Bellas-Velidis I, Kummert M, Andre P (2004) A neural network controller for hydronic heating systems of solar buildings. Neutral Netw 7:427–440 (Elsevier)

Ashcroft F (2001) Life at the extremes, published by flamingo (an imprint of Harper Collins publishers), London. ISBN 0-06551254

Blonder B, Violle C, Bentley LP, Enquist BJ (2011) Venation networks and the origin of the leaf economics spectrum. Ecol Lett 14:91–100

Chen PY, Joanna MK, Meyers MA (2012) Biological materials: functional adaptations and bioinspired designs. Progress in Mater Sci 57:1492–1704. doi:10.1016/j.pmatsci.2012.03.001

Chow TT, Chunying L (2013) Liquid-filled solar glazing design for buoyant water-flow. Build Environ 60:45–55

Chow TT, Chunying L, Zhang L (2011a) Thermal characteristics of water-flow double-pane window. Int J Therm Sci 50:140–148

Chow TT, Chunying L, Zhang L (2011b) The function of solar absorbing window as water-heating device. Build Environ 46:955–960

Feugier FG, Mochizuki A, Iwasa Y (2005) Self organization of vascular systems in plant leaves: inter-dependent dynamics of auxin flux and carrier proteins. Theor Biol 236:366–375

Gray H (2012) Gray's anatomy. Fifteenth edition, Published by Bounty books (a division of Octopus Publishing Group Ltd), London. ISBN 978-0-753723-89-0

Gutierrez MP, Luke PL (2013) Multiscale design and integration of sustainable building functions. Science 341(6143):247–248

Hatton BD, Wheeldon I, Hancock MJ, Kolle M, Aizenberg Ingber DE (2013) Artificial vasculature for adaptive thermal control of windows. Solar Energy Mater Solar Cells. doi:10.1016/j.solmat.2013.06.027

Hyung-Jun K, Orlin DV (2013) Regenerable photovoltaic devices with a hydrogel-embedded microvascular network. Nat Sci Rep 3:2357. doi:10.1038/srep02357

Malcolm E, Dixon T, May T, Hunt M (2013) City futures: exploring urban retrofit and sustainable transitions. Build Res Inf 41(5):504–516. doi:10.1080/09613218.2013.085063

McLaughlin D, Stamford J, White D (2007) Human physiology, Published by Taylor and Francis, Abingdon. OX14 4RN, ISBN 978-0-415-35546-9

Moore KL (1985) Clinically orientated anatomy. Second edition, Published by Williams and Wilkins, Baltimore. ISBN 0-683-06132-1

Odum EP, Barrett GW (2005) Fundamentals of ecology. Thomson/Cole

Olugebefola SC, Aragon MA, Hansen CJ, Hamilton A, Wu W (2010) Polymer microvascular networks composites. J Compos Mater 44:2587–2603

Paceco-Torgal F, Diamanti MV, Nazari A, Granqvist CG (2013) Nanotechnology in eco-efficient: materials, processes and applications. Woodhead Publishing Series in Civil and Structural Engineering 43

Page SW (2004) Advances in insect chemical ecology. Bull World Health Organ 82:955

Peel MC, Finlayson BL, McMahon TA (2007) Updated world map of the koppen-geiger climate classification. Hydrol Earth Syst Sci Discuss 4:439–473. www.hydrol-earth-syst-sci-discuss.net/4/439/2007/ © Author(s) 2007

Saffrey J, Stewart M (2001) Maintaining the whole: human biology and health book three published by Open University, Milton Keynes. ISBN 0-7492-81545

Shin D, Debjyoti Banerjee D (2010) Enhanced thermal properties of PCM based nanofluid for solar thermal energy storage. In: ASME 2010 4th International Conference on Energy Sustainability

Sinoquet H, Sonohat G, Phattaralerphong J, Godin C (2005) Foliage randomness and light interception in 3D digitised trees: an analysis from multiscale discretisation of the canopy. Plant Cell Environ 28:1158

VTT (2012) Energy efficient façade system for building retrofitting. FP7, ENV

Yuanfeng L, Pranati S, Julien PA, Makongo Xiaoyuan Z, Sung-Joo K, Hang C, Ctirad U, Xiaoqing P, Poudeu PF (2013) Large enhancements of thermopower and carrier mobility in quantum dot engineered bulk semiconductors. J Am Chem Soc 135:7486–7495. doi:10.1021/ja311059m

Chapter 6
Simulation-Based Evaluation of Adaptive Materials for Improved Building Performance

Fabio Favoino

Abstract This chapter presents a method to evaluate the performance and to support product development of adaptive micro- and nanobased material and technologies, integrated into buildings. In the first section, an introduction to adaptive building concepts is provided, followed by an overview of adaptive micro- and nanomaterials for building envelope integration in the second part. The role of building simulation in the development of innovative adaptive materials and technologies is discussed in the third section, together with the limitations and challenges of predicting by means of computation the performance of adaptive materials. The most advanced methodologies and the characteristics of the tools to support product development for building-integrated adaptive materials and technologies are presented in the fourth section. Finally, a case study is described to demonstrate and illustrate some of the potential of those methodologies, consisting in the evaluation of the performance of future generation adaptive glazing.

6.1 Adaptive Building Concepts for Improved Building Performance

The 20-20-20 European policy established new and more stringent CO_2 emission targets. This imposes bigger challenges for the development of new concepts and technologies, capable of reducing the energy demand of buildings, while maintaining acceptable levels of or improving the indoor environmental comfort. In fact, the 2010 EPBD Recast (Energy Performance of Buildings Directive 2010/31/EU) requires that by the end of 2020 (2018 for public buildings), all new constructions should be "nearly zero energy building" (nZEB). The definition of "nearly ZEB" given by the Directive is a building that has "very high energy performance […]

F. Favoino (✉)
Glass and Façade Technology Research Group, Faculty of Engineering, University of Cambridge, Cambridge CB2 1PZ, UK
e-mail: ff279@cam.ac.uk

F. Pacheco Torgal et al. (eds.), *Nano and Biotech Based Materials for Energy Building Efficiency*, DOI 10.1007/978-3-319-27505-5_6

and where […] the nearly zero or very low amount of energy required should to a very significant extent be covered by energy from renewable sources, including renewable energy produced on-site and nearby" (EPBD recast 2010). Although the definition of the nearly (or net) ZEB given by the Directive allows a certain degree of freedom, and a shared understanding of what exactly a nZEB is should be reached, the achievement of this target requires the development of new concepts, technologies and materials that can improve further the energy efficiency in buildings. Among the others, technologies that improve the match between on-site renewable energy production profiles and building load profiles are considered for crucial relevance (Sartori et al. 2012).

The building envelope can play a significant role in the achievement of these ambitious targets, due to its main function of heat and mass transfer interface between the indoor and the outdoor environment. From the perspective of the building envelope, the improvement of the building energy efficiency can be achieved by means of two different design strategies: an "exclusive" and a "selective" approach. In IEA Annex 44—Responsive Building Concepts and Responsive Building Elements (Perino 2007; IEA-ECBCS 2010), the limits of the "exclusive" approach at the energy balance of buildings are pointed out. A limit exists for the energy saving achievable by means of energy-efficient building concepts, which are created by excluding the outdoor environment from the indoor environment, such as very well-insulated and airtight building constructions. This represents a limit not only as far as the energy efficiency is concerned, but also in terms of improved indoor environmental comfort and cost reduction. This can be easily clarified by means of a simple example, which was ad hoc built for the present chapter and which can be replicated by any designer or researcher. In Fig. 6.1a, the results from the evaluation of the total primary energy consumption of a reference building (i.e. office building located in London, with 40 % transparent façade area) are shown. The example building under analysis complies with the national regulations at different points in time, in terms of building envelope characteristics (on the x-axis, the specific total heat transfer coefficient of the

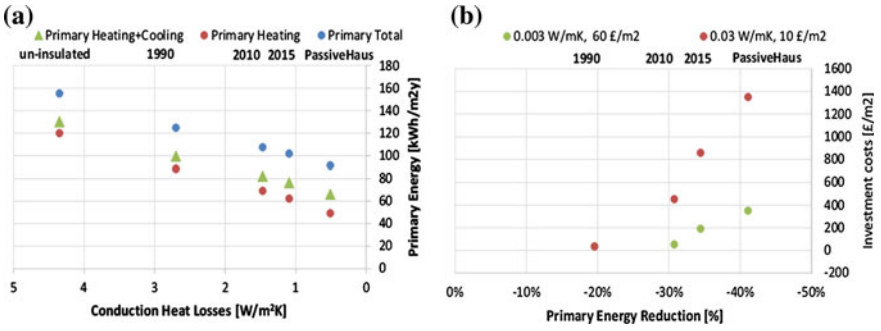

Fig. 6.1 **a** Total primary energy use of office reference building in London, 40 % transparent area, South–North-oriented, compliant to subsequent building regulations; **b** cost of the additional insulation compared to the uninsulated baseline

building envelope is plotted, for a building with a ratio of façade to floor area of 1). In Fig. 6.1b, the cost of the additional insulation compared to the uninsulated case is shown. In the cost model, the following hypotheses are included: the additional cost of the material is 10 £/m^2 for conventional insulation and 60 £/m^2 for the state-of-the-art insulation; the loss in sellable area due to the additional insulation thickness is 5000 £/m^2 (average London price); the energy cost is 0.20 £/kWh with an interest rate of 2 %; and the whole life of the façade is 25 years. From Fig. 6.1a, the following observation can be drawn:

- by reducing the heat transfer through the building envelope to zero, a significant amount of energy is still needed to operate the building;
- while the primary energy use for heating is decreasing linearly, the cooling energy use is increasing, eventually resulting in an increase in total primary energy use, if the total heat exchange through the building envelope is reduced further;
- to offset the building energy use to achieve the nZEB target, a very large amount of renewable energy should still be provided on site, which may result in a solution which is rather than spatially and/or economically feasible.

From Fig. 6.1b, on the other hand, it is immediate to realise that to achieve the same improvement in energy saving performance, higher and higher costs need to be invested. In other words, with the same sum of money, a lower and lower improvement in terms of energy saving could be achieved by increasing the insulation level alone. This is known in economics as "law of diminishing returns" (Shephard and Färe 1974). Therefore, alternative energy-conscious designs yielding a higher improvement in energy efficiency need to be implemented to achieve significant reductions in building energy use, making the nZEB target easier to achieve.

6.1.1 Evolution of Adaptive Façade Concepts

In contrast, in IEA-ECBCS (2010), the potentials of a "selective" approach at building design are highlighted: energy-efficient building concepts can be created by designing the building shape and envelope as a "selective filter" between the outdoor and the indoor environment. In this approach, the building envelope is not considered any more as a "static barrier" towards the outdoor environment, as it was traditional, but it can incorporate the functions of managing and modulating the energy and mass flow between the outdoor and the indoor environment, with the aim of maximising the energy saving and the indoor environmental comfort. This feature can be achieved by means of tempering, storing, shifting, admitting, redirecting and transforming the energy and mass flow through the envelope, together with the function of rejecting them (Fig. 6.2).

The different functions described in Fig. 6.2 can be achieved by making use of adaptive or responsive building elements (RBEs) and systems. The adaptive

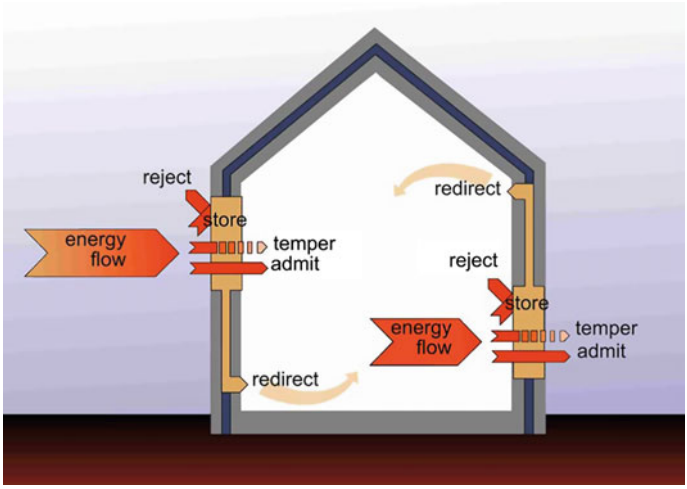

Fig. 6.2 The functions of the building envelope (IEA-ECBCS 2010)

building envelope is only one designation for a concept that has been described in many different ways and sometimes with slightly different meanings. This concept identifies the capability of the building envelope to adapt and tune its physical properties according to changing boundary conditions. Different words have been used as a synonym of adaptive, such as dynamic, responsive, smart, intelligent, multifunctional, advanced, active, polyvalent and switchable, only to cite some of them. In this chapter, only the terms adaptive or responsive will be used to avoid ambiguity, in contrast to the word "static", which identifies a traditional building envelope or façade that exhibits constant physical properties across the range of boundary conditions. Hence, an adaptive building envelope is defined as the element of separation between the indoor and outdoor, which has the ability to repeatedly and reversibly change its functions, features or behaviours over time in response to changing performance requirements and variable boundary conditions, with the aim of improving overall building performance (Loonen et al. 2013). With the word "performance", different concepts can be included, i.e. building energy use, exploitation of available renewable energy sources (e.g. solar energy, wind energy, geothermal energy), improved indoor environmental levels and so on.

Although recently developed as a clear and comprehensive definition, this concept is far from being new. In fact, the first idea of a building envelope which can actively manage the ventilation in order to respond to changing climatic boundary condition and improve the building energy consumption traces back to Le Corbusier, in 1930, with his "Mur Neutralisant": "two membranes with a space of a few centimetres between them [… where…] hot air is pushed if in Moscow, cold air if at Dakar" (Le Corbusier 1930). These two membranes were intended to be made of glass and/or stone. Thus, "Le Mur Neutralisant" can be easily represented as the ancestor of modern double-skin facades. A more recent concept design for an

adaptive wall is presented by Mike Davies in 1981, in his article "A Wall for All Seasons" (Davies 1981). Davies' idea was more evolved than Le Corbusier's one, consisting of a multilayered wall construction of few millimetres thickness, made up of different electrically and chemically active layers able to tune their thermo-physical properties, according to the stimuli coming from the indoor and outdoor environment, accommodating conflicting and changing requirements:

> …A environmental diode, a progressive thermal and spectral switching device, a dynamic interactive multi-capability processor acting as a building skin…trading energy surplus for energy need…adapting itself to provide best possible interior conditions… (Davies 1981, p. 1) (Fig. 6.3)

Since Davies' inspiration, despite the impressive technological innovation in the material science, in sensor and control technologies, as well as in human comfort and behavioural science, it is not yet entirely possible to design building envelopes which are able to behave in the way Davies envisioned. But this concept is still a target to aim at for the future. In fact, nowadays, the stricter environmental regulation for building energy efficiency brings designers back to a situation similar to the one that generated such a vision. The idea of an "environmental diode" was one of the building designers' answer to the increased cost of energy caused by the '70s oil crisis. In fact, there was a growing awareness that indoor environmental comfort could not be achieved, in an energy-efficient way, demanding the whole need for indoor climate control to heating, ventilation and air conditioning (HVAC) systems, but that an energy-conscious design of the building envelope was needed, in order to decrease the energy use of the building, providing at the same time a comfortable indoor environment, in contrast to the uncomfortable indoor conditions and high energy consumptions often created by modernist fully glazed building skins.

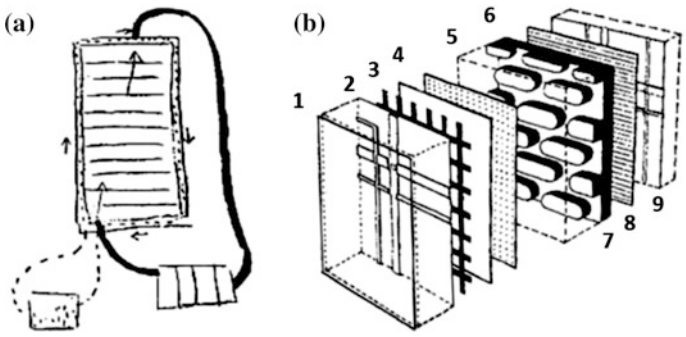

Fig. 6.3 **a** Concept of "Le Mur neutralisant" by Le Corbusier (1930). **b** the "Polyvalent wall" by Davies and Rogers (1981). (*1*: Silica weather skin and deposition substrate; *2*: sensor and control logic layer—external; *3*: photoelectric grid; *4*: thermal sheet radiator/selective absorber; *5*: electroreflective deposition; *6*: micropore gas flow layers; *7*: electroreflective deposition; *8*: sensor and control logic layer—internal; *9*: silica deposition substrate and inner skin)

One of the first steps towards Davies' concept was the introduction of double-skin facade (DSF), which became very popular in the 1990s (Oesterle et al. 2001). These consist of controlling the air-flow pattern and characteristics, and eventually the shading devices, comprised between two construction layers (either both of them transparent, or the more external transparent and the more internal opaque), according to the boundary conditions. Another fundamental step towards the adaptive building envelope concept was achieved, thanks to the new developments in material science applied to the building envelope, by introducing in the building skin new micro- and nanobased materials with adaptive and responsive features (Ritter 2007), as well as energy producing materials, such as photovoltaics. Among these are chromogenic (electro-, thermo- and photochromic) materials, thermoelectric and thermostrictive materials, shape memory alloys (SMAs) and phase change materials (PCMs). The features and characteristics of some of these materials were already extensively discussed in the previous chapters of this book. Nowadays, many examples of building envelopes presenting adaptive and responsive features exist (Loonen et al. 2013). Among these technologies there are Double-Skin Facades or Advanced Integrated Façades (Saelens et al. 2003), switchable glazing (Baetens et al. 2010), movable solar shading (Nielsen et al. 2011), wall-integrated phase change materials (Kuznik et al. 2012), dynamic insulation (Kimber et al. 2014) and multifunctional solar facades (Quesada et al. 2012a, b).

6.2 Adaptive Micro- and Nanomaterials for Building Integration

The unique feature of adaptive building envelopes is the capability to adapt their thermo-optical properties in a reversible way to varying boundary conditions (either external, such as the climate, or internal such as occupants' requirements), in order to respond to changing priorities (i.e. minimising the building energy use, maximising the use of natural light). But many implicit concepts are embedded in this definition, which need to be considered in order to correctly integrate RBEs into buildings. This concept, in fact, includes the definition of the scale of the adaptive mechanisms; the physical properties that are able to change dynamically and their range of variability; the relevant physical domains in which the adaptation takes place and that need to be evaluated; the timescale and the control of the adaptive mechanisms; and the boundary conditions driving the adaptation. Different classifications and reviews of building-integrated adaptive material and concepts were proposed based on all these considerations (Loonen et al. 2015).

The mechanisms that foster adaptation can be distinguished into two scales, depending on the spatial resolution at which the variation of physical properties takes place. We are talking about macroscale if the modulation of system properties is due to a change in the physical arrangement of the façade system and operating mode (i.e. double-skin façades, operable shading devices) or about micro- and nanoscale if this is due to a change in physical properties of a material embedded

into the building envelope due to reversible chemical processes (i.e. electro- and thermochromism, shape memory, phase change). Also a combination of both could be possible. The considerations and the methodologies presented in this chapter apply to both scales. But from now on, this chapter will refer exclusively to the micro- and nanoscale. In this section, an overview of the adaptive materials that can be integrated into buildings at a micro- and nanoscale is provided, based on the specific material properties that can be modulated. These materials can be integrated into building envelope components, either transparent or opaque, to vary their solar properties (transmission, absorption and reflection coefficients) and their heat transfer (thermal conductivity) and/or heat storage (specific thermal capacity) properties. For a full description of the specific material features and performance and integration issues, the reader is directed to the specific chapters in the present book in which the material is treated.

6.2.1 Modulation of Solar Properties

Adaptive glazing technologies are capable of dynamically modulating their thermo-optical properties in response to external stimuli. This is achieved by inserting a functional layer (or more) between two layers of glass, including a so-called chromogenic material, which is the one able to modulate its transmission and/or absorption coefficients (i.e. the amount of solar radiation that is transmitted through and/or absorbed by the material), which are wavelength dependent. The modulation of thermo-optical properties can be either a self-triggered adaptive mechanisms, in which case the technology is said to have a passive or smart adaptive behaviour, or triggered by an external stimulus, whereby the technology is said to be active or intelligent.

Passive technologies include thermochromic TC (Granqvist 2007), thermotropic TT (Nitz and Hartwig 2005; Mueling et al. 2009) and photochromic PC glazing. In these technologies, the modulation of thermo-optical properties is triggered by a change in the internal energy of the adaptive layer. A phase transition or phase separation is induced by this change of internal energy, which in TC and TT layers is revealed by a temperature variation.

Active technologies, such as electrochromic EC, suspended particle device (SPD) and liquid crystal device (LCD), require a change in the electrical potential to trigger a change in thermo-optical properties. The adaptation in EC is achieved by changing the amount of electron density in a metal-based oxide, such as W, Mo, Ir, Ti, V, Ni and Nb oxides, or polymers such as PANI and PEDOT (Granqvist 2007; Jelle 2013). Various technologies exploit the EC feature of these materials in order to achieve an optically controllable window. The molecules of these materials can be found in gaseous state (gasochromic), or in solid state (all-solid-state electrochromics). In all-solid-state EC, an electrical field is applied in order to inject/remove electrons into/from the metal oxide molecules in the solid state, while hydrogen molecules are used instead of voltage to gasochromic EC, which results

in the colouring/bleaching of the material. In photo–electro–chromic (PEC) the layer of EC material is coupled with a photovoltaic material layer for electron injection, so that the EC system can be self-powered. An evolution of PEC is represented by photo–volta–chromic (PVC), which differs from PEC in that the photovoltaic and electrochromic functions can be separated, thereby facilitating their integration with building management systems (Cannavale et al. 2013). The modulation of optical properties in SPD and LCD is triggered by an electrical current inducing an electromagnetic field, to align the suspended particles or the liquid crystals, which are otherwise randomly ordered, thus allowing the light to pass through it. Therefore, LC and SP devices need continuous stable potential difference to maintain a certain state, thus requiring a higher electrical energy demand than EC materials.

More advanced smart glazing is able to modulate only the infrared part of the solar spectrum, without compromising the transparency to the visible radiation, and these could be either thermochromic (Warwick and Binions 2014) or electrochromic glazing (Garcia et al. 2013). Recently, a new transparent material was engineered (Llordes et al. 2013), which shows independent electrochromic features in both the visible and infrared portions of the solar spectrum, so that also the relative proportion of solar spectrum transmitted through the glazing can be modulated.

The performance of adaptive glazing systems can be characterised by their ability to modulate (1) the total solar heat gain coefficient (*g-value*), which is the proportion of total (direct and indirect) solar radiation transmitted through the glazing, and the visible transmission (T_{vis}), which is the proportion of solar visible

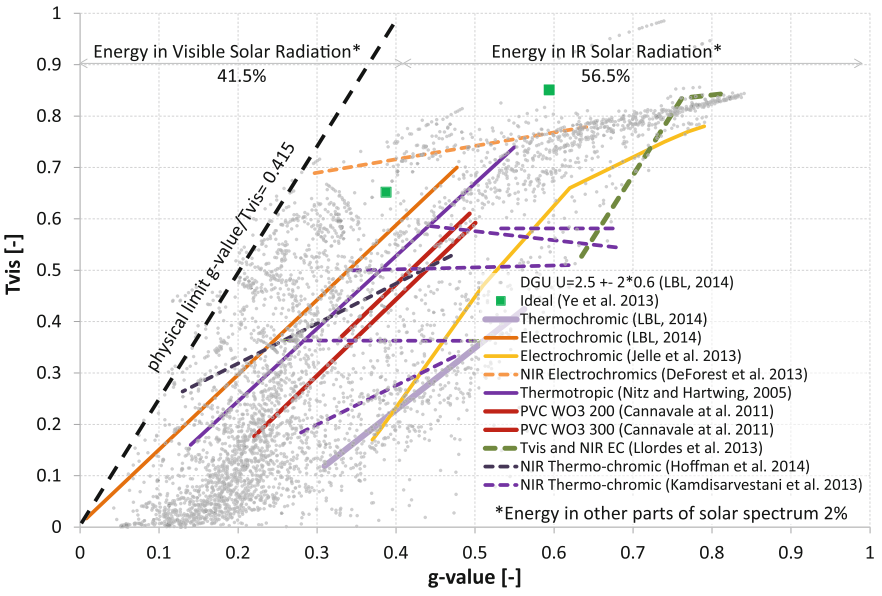

Fig. 6.4 T_{vis} and *g*-value of smart glazing technologies (variable thermo-optical properties along the coloured lines) compared to standard double-glazing units (*grey* data points)

radiation transmitted through the glazing. In Fig. 6.4, the modulation capability of glazing adopting transparent adaptive micro- and nanomaterial is shown in terms of g-value and T_{vis} for different smart glazing technologies, compared to conventional "static" double-glazing unit (DGU). While only a single couple of g-value and T_{vis} value is possible for each DGU configuration, smart glazing technologies adopting transparent adaptive micro- and nanomaterial are able to control the g-value and T_{vis} along the lines in Fig. 6.4.

6.2.2 Modulation of Heat Transfer Properties

Modulation of heat transfer in an opaque component (also referred to as dynamic insulation) is usually achieved controlling the convection of a fluid in a closed cavity, either at a microscale level (in a nanoporous of microencapsulated material), or at a macroscale level. From this classification, double-skin façades are excluded, because the cavity of the system is not sealed to the outdoor and/or indoor environment, and therefore, the insulation level is influenced by the property of the air itself. Earlier dynamic insulation was achieved by integrating a facade with a system based on heat convection through air (Brunsell 1995) or liquid (Buckley 1978). The former involves a cavity that heats up the fresh air before it comes into a room and reuses the heat from exhaust air. This technology, however, requires the building to have a high level of airtightness, and the heat recovery system required would make it less cost-effective (Gan 2000). The latter, so-called bidirectional thermodiode, is capable of transferring heat in one direction and providing insulation in the other. Different design variations of the bidirectional thermodiode have been proposed and tested. The one developed by Varga, Armando and Afonoso (2002) for cooling season achieved switchable apparent conductivity from 0.07 W/mK up to 0.35 W/mK. In Pflug et al. (2015), a dynamic insulation system, which can be also translucent, is developed by means of controlling the convection in a multicavity wall, just by allowing convection between cavities in a multilayered construction. This is achieved in this case by movable panels in the construction element, allowing communication between the cavities. Micro- and nanobased technologies to achieve controllable thermal conductivity adopt different strategies, by means of variation of gas pressure, mean free path of the gas molecules and gas–surface interaction in an insulation panel. In Xenophou (1976), a system is patented to vary the thermal conductivity by controlling the pressure in a wall with a cell structure. Another example is found in Benson et al. (1994), in which a variable thermal transmittance is achieved by changing the pressure of hydrogen gas by means of absorption/desorption process of the gas itself. Berge et al. (2015) developed a system to modulate the thermal conductivity of the air in the nanoporous fumed silica structure of a vacuum insulation panel (VIP) or in an aerogel blanket, by means of controlling the air pressure, while in Kimber et al. (2014), the thermal transmittance of a wall is controlled by controlling the distance between multilayered polymeric membranes.

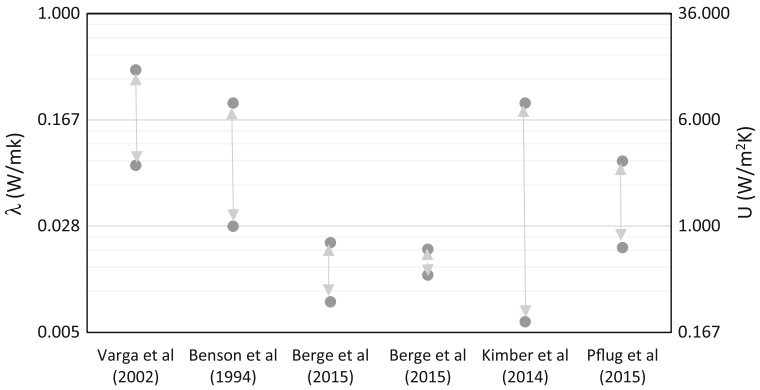

Fig. 6.5 Thermal conductivity (λ) and *U*-value modulation of adaptive insulation materials and technologies (*y*-axis with logarithmic scale). Where only one indicator is found in the literature (i.e. only the *U*-value or only λ), the other one is calculated supposing a 2.5 cm thickness of the insulation layer

The performance of such systems/materials can be compared in terms of modulation capability of the thermal conductivity of the material, or U-value (total heat transfer coefficient) of the construction element. Figure 6.5 compares the different solutions found in the literature.

6.2.3 Modulation of Heat Storage Properties

Phase change materials (PCMs) are materials which are able to vary their specific heat capacity at ambient temperatures. This feature is achieved by storing the energy in the form of latent heat in the material, inducing a phase change (solid to liquid and vice versa); therefore, little temperature variation is measured in the material during the phase change (Cabeza et al. 2011). This allows us to store a higher amount of energy compared to the energy that could be stored in a material experiencing the same temperature variation. The advantage of PCMs is that they can be designed in order to store energy in the form of latent heat at a desired temperature, so that they can be used as a heat regulator in the building envelope or in heat exchanger devices, with the main function of storing the heat when is not needed and releasing it back when necessary. Different materials can be used as PCMs in building applications, such as organic (paraffins, fatty acids, oleochemical carbonates and polyethylene glycols) and inorganic (hydrated salts). They present different durability fire resistance, hysteresis and supercooling issues. A full analysis of these issues is reviewed by Rathod and Banerjee (2013). Different applications of PCMs in buildings can be found in the literature, mainly in opaque components. They can be integrated in building envelope elements (as walls and slabs) as a passive heat storage (Kuznik et al. 2012) or activated on demand

Table 6.1 Phase change materials' thermal properties

Material	Latent heat (kJ/kg)	Phase change temperature (°C)
Paraffins	120–266	−57 to 112
Fatty acid	150–220	30–70
Oleochemical carbonates	144–227	−5.9 to 46.9
Polyethylene glycols	108–166	10–55
Inorganic PCM	126–251	−31 to 116
Water	334	0

(Favoino et al. 2014a, b), integrated in building services systems (Cabeza et al. 2011) or integrated in renewable energy systems (Serale et al. 2015). Some PCMs are transparent in the liquid phase and translucent in the solid one (paraffin waxes); therefore, they can also be used in transparent/translucent facades as well (Goia et al. 2013).

Phase change materials' performance can be described in terms of the amount of energy that they can store in the form of latent heat (without experiencing an increase in temperature) per unit mass and in terms of the temperature at which the heat is stored (phase change temperature). Table 6.1 provides an overview of the properties of different phase change material types that can be used in the building industry.

6.2.4 Challenges for Performance Evaluation of Adaptive Building Envelope Materials

Evaluating the performance of adaptive materials integrated in the building envelope presents more challenges to be addressed than conventional static materials and façades.

The influence of varying one or more of these material properties on the indoor environment can be evaluated in different relevant physical domains: thermal, visual, mass flow (air and/or moisture) and acoustic. The variation of a material physical property can induce (or can be determined by) an influence in each one of these physical domains. Most of the time, the effect on one single physical domain cannot be separated from the others; for example, the change of the amount of solar radiation with an electrochromic material is influencing both the thermal and the visual domain. Hence, the evaluation of the performance has to rely on multiple, interrelated building models, across different physical domains.

An important aspect influencing the performance of such materials is the way they are operated. Ritter (2007) defined as "smart" those materials that show reversibly changeable physical properties in response to some physical (thermal, optical and mechanical) or chemical influence, while Aschehoug, Andresen, Kleiven and Wyckmans (2005) refer to "intelligent" to describe any material or

device that has the ability to adjust to changing boundary conditions due to a subsystem that is able to sense and control the actuate on the material. Even if they are often referred to as "smart" or "intelligent", this does not ensure effective operations, consequently increasing energy efficiency and occupant comfort. In fact, to reach an effective performance, different components of an advanced facade need to adjust to changing boundary conditions synergistically, cooperating together and with other building services. This is a non-trivial task, as conflicts and trade-offs need to be addressed in order to provide energy efficiency and a comfortable environment at the same time.

The boundary conditions that the adaptive building envelope can adapt to can be defined according to the different elements that interact with it (Compagno, 2005). In the building environment, three main levels of interaction can be defined (Fig. 6.6). These are not alternative but different levels that can occur simultaneously:

1. **Climate:** The adaptive building envelope can modulate its thermo-optical properties according to the changes in climatic parameters (i.e. temperature, solar radiation, air velocity). Generally, the interactivity with this domain is the one considered with the highest energy saving potential. Saelens, Roels and Hens (2004) show this concept applied to the operating mode and the evaluation of performance of double-skin facades, while Kasinalis et al. (2013) evaluated the energy saving and improved environmental quality potential of responsive materials integrated into the building envelope adapting their physical properties according to the seasonal climatic variation.
2. **Building services:** The modulation of the thermo-optical properties of the adaptive building envelope cannot disregard the capability of the building services to cope and integrate with this feature. For example, Saelens, Roels and Hens (2008) show that the HVAC system can be integrated with a double-skin

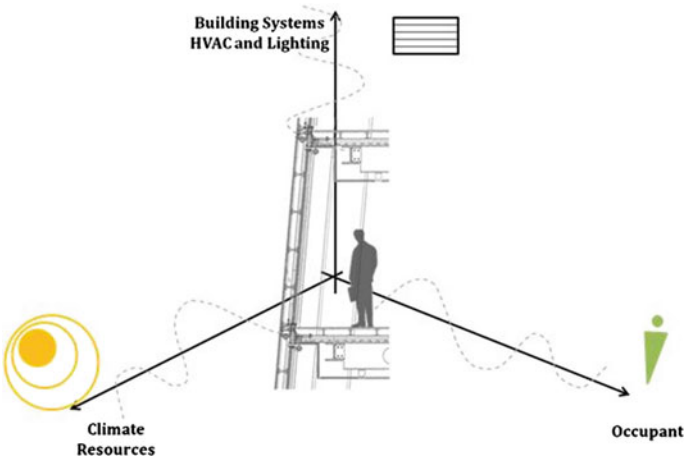

Fig. 6.6 Adaptive building envelope boundary conditions

façade, such that the solar energy harvested in the air or water flowing in the façade cavity can be used in order to reduce the energy consumption of the HVAC itself. On the other hand, Nielsen, Svendsen and Jensen (2011) and Correia da Silva, Leal and Andersen (2012) show the impact on building energy saving of control strategies of adaptive glazing and shading devices integrated with either the HVAC or the lighting system.

3. **Occupant:** The aim of an adaptive building envelope is not only maximising the energy saving but also providing the building occupants with the required level of indoor environmental comfort. Therefore, ensuring that an adaptive façade is correctly designed in order to be controlled by the user, accommodating and learning from occupant preferences, is of central importance. Even though very few experimental studies have addressed the mutual influence between occupant comfort, control and façade adaptation (Bakker et al. 2014), Aschehoug et al. (2005) and Clements-Croome (1997) point out the main issues about integration of intelligent control of adaptive envelopes with the building occupant; Correia Da Silva, Leal and Andersen (2013) quantify that user behaviour can have a significant impact on design parameters and on the performance (building energy use in this case) of different adaptive façade solutions during operations.

When designing and evaluating the performance of adaptive micro- and nano-materials integrated into the building envelope, it is very important to address all these different issues and challenges, which are normally not present, or less important, in the design of façades adopting conventional "static" materials. In particular, the interaction and integration of the façade with these three general types of boundary conditions define the performance of the interior space and the building as a whole. The performance and the requirements for the indoor space can vary from time to time and can sometimes be conflicting; therefore, the façades can assume the role of an active regulator, finding trade-offs and mitigating conflicting requirements, according to how it is operated in regard to the variation of boundary conditions.

6.3 Role of Building Performance Simulation for Product Development

It is intuitively understandable that a higher performance is achievable by using a building skin which integrates materials able to respond to changing environmental conditions and occupants' comfort requirements. But the design and operation of such a complex system is a challenging task.

In the design phase, the comparison of an adaptive solution to another, or to a static one, cannot simply rely on "static" performance metrics such as U-values and g-values, as these are no longer meaningful for building envelopes integrating adaptive components (Goia et al. 2014); in fact, they can be dependent on the boundary conditions. Even though some performance indicators have been

developed, they are specific to the adaptive technology evaluated, i.e. dynamic insulation efficiency ε (Corgnati et al. 2007) and preheating efficiency η (DiMaio and Van Paassen 2001) for double-skin facades, and are enable to compare one specific adaptive technology to another, or to conventional solutions.

Moreover, design and control aspects are strongly interrelated due to the dynamic interactions between the adaptive material, the outdoor environment, the building services, the indoor environment and the building occupant (Loonen et al. 2013). The performance of systems integrating adaptive materials fully depends on the control logic for facade adaptation during operation. In fact, to identify the optimal design characteristics of high-performance adaptive building envelope systems, not only design considerations (i.e. system parameters), but also insights into operation strategies already need to be taken into account in the design phase. This kind of problems, where the performance of design alternatives (upper level) depends on the results of the control strategy (lower level) and vice versa, has been described as bi- or multilevel optimisation problem by Evins (2015), who addressed this kind of problem already for building services and energy systems design.

Using whole building performance simulation (BPS) enables the designer to simulate all the possible configurations of the large number of components included in the facade, with many possible control strategies, given a set of boundary conditions (environment and occupants) across the boundaries of multiple physical domains (thermal, luminous, acoustic, etc.). By doing so, the virtual model of the building created within the software can be used to predict the whole building performance, therefore allowing an absolute and true comparison between different materials (either adaptive or static), systems and controls, by means of overall building performance metrics (i.e. total primary energy, long-term comfort/discomfort indexes as in Carlucci et al. (2015), whole-life value as in Jin and Overend (2013)).

BPS in relation to adaptive materials and systems can be used in a different context (research, product development, design and operation) and for different purposes. According to Clarke and Hensen (2015), BPS can be applied to the design of advanced building concepts (in this case adaptive building envelope materials and systems) in order to (a) inform the decision making to support the design process towards optimal performance regarding occupant comfort and economic and environmental aspects; (b) predict the energy saving potential compared to a baseline design as part of green building certification processes such as LEED and BREEAM[1]; (c) virtual rapid prototyping to evaluate different future-oriented concepts/materials; (d) exploration of high-potential control strategies that can maximise the performance during operation; (e) HVAC system sizing and fine-tuning of the interaction between building envelope and other building

[1]LEED and BREEAM are voluntary assessment methodologies, whose main aim is to assess, rate and certify the fulfilment of multiple building environmental performance criteria for different phases of the building construction process (building design, construction and operation). For more information about these building environmental performance assessment methodologies please refer to Kubba (2012).

services; and (f) virtual testing of the robustness of materials and systems with respect to occupant behaviour and variable weather influences, even if the application of whole BPS in relation to adaptive building envelope is still largely unexplored (Loonen et al. 2014a, b). In fact, inspired by Davies' vision, many new concepts of multifunctional and adaptive facades and materials have been developed, but their adoption in the building industry is restricted by many barriers, one of them being the inadequacy of BPS tools in representing their performance (Favoino et al. 2015a, b).

6.3.1 *Computational Evaluation of Adaptive Materials' Performance to Support Product Development*

In the area of adaptive micro- and nanomaterials and systems, many researchers attempted to respond to the above-listed aims of R&D, building design and operation activities.

Some authors used parametric studies to understand the effect of changing adaptive material design parameters (i.e. speed, range or mechanisms of variation of physical properties), or context (i.e. building parameters, orientation, climate), on building performance indicators (i.e. energy use, indoor environmental quality). Saeli et al. (2010) and Warwick et al. (2013) performed a parametric analysis to understand the effect of varying thermochromic material design parameters, such as switching temperature and modulation range, on the total building energy use. Cannavale et al. (2013) used a simulation model in order to evaluate the improved visual comfort of different photo–volta–chromic design alternatives. DeForest et al. (2013) performed a parametric analysis on context parameters (climatic context) in order to understand the effectiveness of near-infrared electrochromics to reduce building total energy use.

Other authors attempted to evaluate ideal characteristics of adaptive materials or operation of adaptive systems in a certain context, either with a theoretical inductive method, or by applying inverse methodologies proper of operational research. Ye et al. (2012) and Ye et al. (2013) devised and tested optimal adaptive glazing thermo-optical properties for different climatic locations in China, based on the sum of building energy use for heating and cooling. Zeng et al. (2011) elaborated an inverse methodology in order to devise optimal adaptive material properties of an opaque building construction (i.e. thermal conductivity, thermal capacity and melting temperature), based on the minimisation of the energy for heating. Favoino et al. (2014b) attempted at devising ideal adaptive glazing material properties for different contexts (climate and orientations), based on the minimisation of total energy use in an office building.

All these studies and approaches present some constraints to be generally applicable, as they are (i) application-oriented, as based on an energy model restricted to a specific technology, or (ii) based on partial models, as only one aspect

of performance is taken into account (i.e. heating energy use only, daylight comfort only), or (iii) based on model assumptions and simplifications that may invalidate their general results, due to the inability of current BPS tools to provide a general simulation framework to model adaptive building materials.

In fact, current BPS tools present many barriers to a correct and easy evaluation of adaptive building envelope concepts and strategies (Favoino et al. 2015a, b). Among them are (a) the inability of simulating adaptive material properties, apart from some application-oriented cases (modelling capability of a specific adaptive technology/material) included in the user interface of the specific BPS tool; (b) the inability of simulating high-performance operations of dynamic systems; and (c) the limitation in scope of the specific BPS tool that is the availability of models in order to take into account the performance of the adaptive systems in multiple domains (i.e. not only thermal and air-flow but also visual and acoustic).

6.3.2 Simulation Strategies for Computational Evaluation of Adaptive Materials

In order to overcome some of these limitations, different approaches have been used to date by researchers. A first evaluation approach is circumvent the aforementioned limitations by adopting workarounds, in order to simulate varying material properties and advanced operation. In Kasinalis et al. (2014), Favoino et al. (2014b), De Forest et al. (2013), Loonen et al. (2011), Goia and Cascone (2014), and Gonzalez and Fiorito (2015), time frames from separate independent simulation models of different static systems, each one representing a possible state in the adaptive material, are combined in a single representation. Therefore, the results of independent simulations of static solutions are combined to provide the yearly performance of the adaptive system. The way the time frames are composed together can mimic advanced operations, such as a control strategy that minimises the total primary energy consumption of the building for each time frame. This approach has three downsides when applied to shorter adaptive system dynamics (shorter than monthly): (i) it enables to account for delayed thermal response of the system due to storage effect in the thermal mass of the building; (ii) it fails at taking into account previous operation of the building system for each time frame (thermal history); and (iii) it is not able to minimise the energy use of the building as it only considers the current state of the dynamic system but not the effect of future predictions in current operations (receding horizon control,[2] RHC, Mattingley et al. 2011).

[2]RHC is a feedback nonlinear control technique, solving an optimisation problem at each time step to determine the control sequence (sequence of optimal adaptive building envelope properties) by optimising a certain cost function, over a certain time horizon, which includes a certain future time frame that, together with the present time step, the "planning horizon" constitutes the "cost horizon".

A second approach is to develop ad hoc thermal network models, which are validated with experimental measurements. For example, Zanghirella et al. (2011) developed a thermal network model for a double-skin façade in order to test different operation strategies and to evaluate the energy performance of a building adopting such a technology. Zeng et al. (2011) and Zhang et al. (2015) applied a nonlinear optimisation method (sequential quadratic programming) in order to evaluate the ideal characteristics (melting temperature and latent heat storage capacity) of a wall-integrated phase change material. The advantage of this approach is that the user has more flexibility to extend the model and fit model equations to model purposes, i.e. varying thermo-optical properties of the material during simulation runtime and/or integrating explicit optimisation algorithm in order to optimise the operations of building-integrated adaptive materials in a time-efficient way. Although in this case the model can often be limited in scope, that is only a single thermal zone can be simulated, it integrates few validated models and/or physical domains.

Finally, other researchers developed an integrated framework to simulate adaptive building materials and systems by means of the state-of-the-art BPS tools (Loonen et al. 2014a, b; Favoino and Overend 2015). In these simulation strategies, the abovementioned limitation of current whole BPS tool overcomes integrating multiple software, which performs different tasks on different levels: a coordination software/layer, an optimisation software/layer and one or more evaluation software/layers (the whole BPS tools used). The overall architecture and tasks of these simulation strategies are summed up in Fig. 6.7. In the coordination layer, a software is used to manage the simulation time and the thermal history in the evaluation software (updates of building states, such as surface and construction temperatures, according to the previous operations); the exchange of information between different evaluation software (either by managing cosimulation[3] or by creating lookup tables for the different adaptive material states); and the optimisation parameters in the optimisation layer/software (i.e. objective functions, optimisation algorithm parameters). In the optimisation layer, an optimisation algorithm can be used to optimise design and control parameters of the adaptive material/systems, integrated with the operation of other building systems (i.e. HVAC and artificial lighting) or perform sensitivity analysis, according to one or more performance requirements (i.e. minimise the total primary energy use of the building, and/or maximise the occupant thermal comfort, and/or maximise the amount of natural light, and/or minimise the amount of glare). In particular, to optimise the operation of the system together with the design alternatives, for each design option, the optimisation layer generates alternative control options to be evaluated. The evaluation layer is used to evaluate the performance metrics of each single design alternative (with different design and control parameters) generated by

[3]Cosimulation is a simulation strategy in which two or more simulators solve systems of coupled equations, by exchanging data during simulation runtime (Trcka et al. 2009). The cosimulation functionality can be enabled by means of middleware software, such as BCVTB (Wetter 2011a).

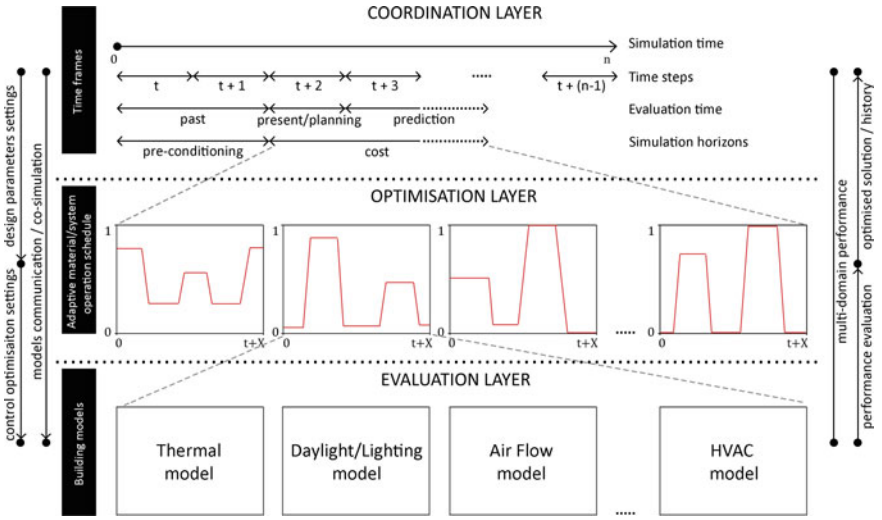

Fig. 6.7 Integrated simulation strategy for design and control optimisation in multiple physical domains for adaptive/material systems

the optimisation layer. Different BPS tool alternatives can be adopted in this framework in the evaluation layer, such as EnergyPlus (Favoino and Overend 2015), TRNSYS and DAYSIM (Loonen et al. 2014a, b). The advantage of these simulation strategies is that they overcome the limitations of current BPS tools at evaluating building-integrated adaptive materials and systems, both design and control aspects can be optimised together, and advanced operations of dynamic system integrated with building service systems can be simulated (i.e. receding horizon control). The main drawbacks of this simulation strategy are the time intensity of the modelling tasks prior to the simulation, the non-user-friendly graphical user interface and the time efficiency of the whole simulation process when many variables have to be optimised.

6.3.3 Simulation-Based Prototyping of Adaptive Materials

The introduction of novel, more accurate and comprehensive simulation strategies opens new perspectives to the use of building simulation in the prediction of direct and indirect benefits of the use of adaptive micro- and nanobased materials in buildings. By direct benefit, it is meant the improved performance of the built environment and its occupants, while indirect benefits can indicate the capability of

adaptive solutions to counterbalance and compensate an eventual loss in performance due to the depletion of other building systems or to changing scenarios.

The potential applications of the integrated simulation strategy, depicted in Fig. 6.7, could be to:

- evaluate and compare the adoption of existing adaptive materials and technologies in energy-conscious building design;
- support the optimisation of the design of existing adaptive materials and technologies for a certain application;
- support the optimisation of the operation of existing adaptive systems integrated with building services control strategies;
- support the product development and the engineering of innovative adaptive materials and systems, driven by the product performance, rather than by the technological development;
- evaluate the viability/performance of new adaptive material concepts;
- evaluate the robustness of adaptive material solutions to changing scenario (i.e. building local external context, climatic context, building internal layout and purpose, change of building component performance during the building life, change in energy supply prices and policies).

Documenting the applicability and the potentials of this simulation-based approach, some studies have been published already. Loonen et al. (2014a, b) performed a parametric study to analyse the effect of design- and rule-based control parameters of a smart glazing technology, combining liquid crystal switchable windows and luminescent solar concentrators, on the total energy use and visual and thermal comfort of office buildings. Khandelwal et al. (2015) analysed the potential energy saving in terms of building total energy use for an office building in different climates, adopting innovative transparent infrared switchable reflectors integrated in the glazing, based on a proposed control strategy. Jin et al. (2015) evaluated the ultimate energy saving potential and thermal comfort improvements of adopting an adaptive insulation system in a specific building and climatic context, by minimising both thermal discomfort and building total energy use. In another study, Favoino and Overend (2015) evaluated the performance (in terms of energy use and thermal and visual comfort) of adopting advanced control for standard electrochromic glazing and of adopting independent switchable visible infrared electrochromic glazing with advanced operation, for a specific case study.

Finally, Favoino et al. (2015a) devised optimal adaptive thermo-optical properties for future smart glazing and evaluated their energy saving potential for different buildings and climatic contexts. This is obtained by applying an inverse methodology in order to solve a multilevel optimisation problem, in a specific simulation strategy framework, as the ones presented above. In the next section, this last case study will be briefly presented, in order to describe and explain the potential of such a simulation-based inverse approach.

6.4 Methodology and Simulation Framework

6.4.1 Methodology for Simulation-Based Support for Adaptive Materials' Product Development

The simulation-based case studies illustrated in the previous section are all based on a similar common methodology that can be separated in clear different steps. Loonen et al. (2014a, b) mapped out the different fundamental stages of this process in order to be applied to support product development of new adaptive materials for building integration. This process (Fig. 6.8) can be expanded to include the following consequential tasks:

1. set the goals and the multiple performance objectives, whom the adaptive material/technology needs to respond to (1 in Fig. 6.8);
2. select performance indicators for the specific set of objectives, used either to compare different design and operation alternatives, or to be optimised by the operation of the adaptive material/system (2 in Fig. 6.8);
3. choose the appropriate modelling and simulation strategy, according to the capability of the software tool to either model the specific adaptive technology or model the advanced adaptive material operations (3 in Fig. 6.8);
4. choose the benchmark case(s), whose performance is compared to the performance of the analysed adaptive technology; this could be another product

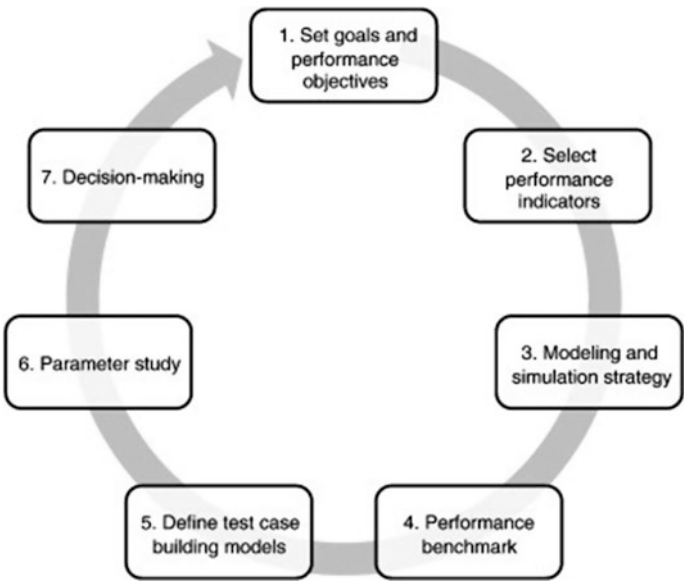

Fig. 6.8 Simulation-based methodology for decision support in R&D of building envelope technologies (Loonen et al. 2014a, b)

and/or the same adaptive material with ideal/optimal properties (whose performance can be evaluated by means of optimal design and optimal control) (4 in Fig. 6.8);
5. define test case building models, to analyse the applicability and performance of the specific solutions in different building scenarios (5 in Fig. 6.8);
6. use sensitivity analysis in order to eliminate insignificant scenario or design alternatives, reducing the search space for the eventual optimisation and parametric analysis;
7. use parametric analysis to analyse the robustness of the design/control alternatives to scenario uncertainties (Hopfe and Hensen 2011), making use of scenario-based optimisation (Matsuko and Borrelli 2012) (6 in Fig. 6.8);
8. define the alternative design and control parameters of the adaptive material and/or system that need to evaluated/optimised;
9. perform the optimisation on the design and/or control parameter chosen;
10. postprocess the results of the optimisation/parametric study, in order to communicate and interpret them better, according to project aims and objectives;
11. communicate effectively the results from the scenario-based optimisation and/or sensitivity analysis to stakeholders; this step is of crucial importance according to many experts in the building optimisation community (Attia 2012);
12. support decision making guiding the development of the most promising technological solution(s) for one or more design scenarios (7 in Fig. 6.8).

6.4.2 *A Software Simulation Framework for Adaptive Materials' Performance Evaluation*

In this section, the architecture of a tool adopting the general simulation strategy presented in Sect. 6.3.2 (Fig. 6.7) is herewith detailed. This tool can be used to support the development of adaptive material and technologies by means of simulation. It integrates (a) an evaluation layer for calculating the cost functions (i.e. energy use and comfort), making use of the building energy simulation software EnergyPlus (NREL 2011; LBNL 2011; Crawley et al. 2001); (b) an optimisation layer for the optimisation of the control of adaptive thermo-optical properties, making use of MATLAB (Matlab 2013) for multiobjective optimisation problems and GenOpt (Wetter 2011b) for single-objective optimisation ones; and (c) a coordination layer designed with MATLAB (Matlab 2013) to manage the time horizons of the simulation strategy and to overcome some simulation issues of the specific BPS tool adopted, related to the evaluation of adaptive technologies.

The evaluation layer based on EnergyPlus is capable of simulating different dynamic materials and technologies, thanks to the use of the embedded energy management system (EMS) (NREL 2013). This is employed for the following tasks: (a) varying the thermo-optical properties of a material or a construction during simulation runtime according to a predetermined control strategy;

(b) computing the variables used for building services integration in the EMS (i.e. illuminance levels and glare); (c) integrating the control of the dynamic building envelope with the artificial lighting system, if needed (Favoino and Overend 2015); and (d) computing the objective functions and the constraints used by the optimisation layer from EnergyPlus outputs (i.e. total primary energy, long-term thermal comfort, daylight autonomy, glare discomfort). The thermal history management (THM) method is adapted from (Corbin et al. 2013) to deal with adaptive building envelope properties, in order to set the initial boundary conditions of the building according to the ending boundary conditions of the previous optimisation. Because explicit state update in EnergyPlus is not possible, with this method, the building is resimulated for a certain period (preconditioning horizon) with the previously optimised control strategy for the adaptive building envelope properties, until the start of the planning horizon before the start of every subsequent optimisation.

The optimisation layer consists of two submodules: a single-objective optimisation and a multiobjective optimisation. The single-objective optimisation submodule is based on GenOpt, and a few different optimisation algorithms are available including generalised pattern search (GPS), particle swarm optimisation (PSO) (Wetter 2011b), genetic algorithms (GAs), and hybrid optimisation algorithms (GA + GPS, PSO + GPS). The multiobjective optimisation module is based on a genetic algorithm script in MATLAB and Non-dominated Sorting Genetic Algorithm (NSGA-II) (Deb et al. 2002), adapted by the authors from (Kanpur Genetic Algorithm Laboratory 2010), to fit the specific optimisation problem.

In the coordination layer, the inputs of the optimisation and the evaluation layers are defined. These inputs include: the building envelope adaptive properties, their modulation ranges and modulation time; the length of the planning, cost and preconditioning horizons; the optimisation algorithm; the seeding strategy for optimisation, where known solutions (i.e. simpler control strategies or previously optimised controls) are introduced in the initial population for the optimisation; the selection criteria for the solution in the Pareto Front of the optimised control sequences (sequences of optimised adaptive properties), if multiobjective optimisation is performed.

The simulation process of the bespoke tool is shown in Fig. 6.9. Continuous arrows indicate the model/input flow, while dashed arrows indicate result/output flow between the layers. In this specific simulation strategy, two simulation loops are performed: an inner one, control optimisation loop, and an outer one, simulation and time management loop. In the inner loop, which is between the optimisation and evaluation layers, the control strategy for the adaptive material/technology is optimised for a certain cost horizon. The outer loop is used to move the cost horizon and the simulation forward in time, resimulating previous optimised control and coordinating the results from different building models. A step forward in the outer loop is not performed until the inner optimisation loop for the specific cost horizon

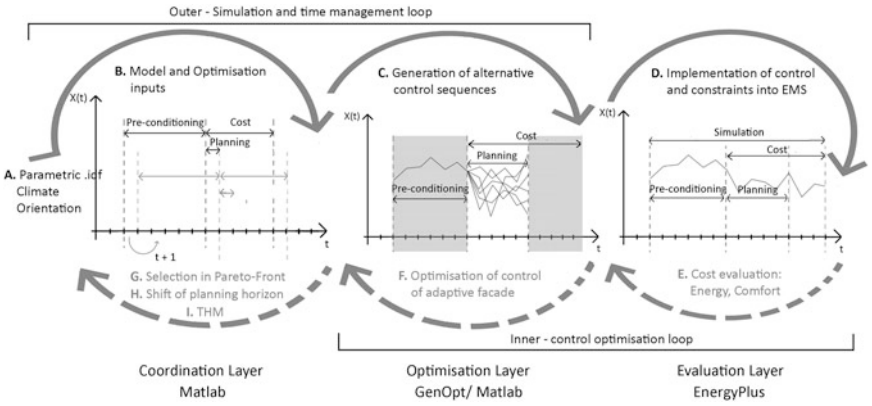

Fig. 6.9 Software framework architecture. The *arrows* represent the flow of inputs/models (*continuous line*) and of outputs/results (*dashed line*)

is not completed. In multiobjective optimisation problems, a Pareto front[4] is generated for each planning horizon, which is a set of solutions which are all Pareto optimal. In order to proceed with the simulation, moving forward in time the planning and cost horizon in the outer loop, a control solution needs to be chosen and adopted from the Pareto front.[5]

The first part of the optimisation workflow (Fig. 6.9), (A) and (B), requires a model to be built and is performed at the beginning of the simulation only, while steps (C) to (I) are iterative and automated, until the end of the simulation period is reached. The tasks performed in the different steps by the different layers are as follows:

(A) a parametric model (EnergyPlus in this case) with variable orientation, climate, material properties and control strategy created;
(B) the coordination layer (MATLAB) is used to set the different parameters of the model and the inputs for the optimisation (including the selection criteria of the solutions in the Pareto front);
(C) the parametric model and the seeds for the optimisation are automatically fed to the optimisation layer (GenOpt or MATLAB), which generates alternative control sequences for the adaptive properties to be evaluated;
(D) each specific control sequence for the adaptive façade system and the constraints of the cost functions are implemented into the model (EMS system of EnergyPlus);

[4]The Pareto front is a set of solutions, and all of them are Pareto optimal, that is, none of the objective functions can be improved in value without degrading some of the other objective values. With no additional preference information, all the solutions in a Pareto front are considered equally good (Miettinen 1999).

[5]For this task, different approaches can be used based on methods for multiobjective decision making (Marler and Arora 2004; Pohekar and Ramachandran 2007).

(E) the cost functions are evaluated by the evaluation layer (EnergyPlus), and the results are returned to the optimisation layer in an iterative way until convergence of the optimisation is reached;
(F) the optimisation layer defines the optimal control strategy (single-objective optimisation problem) or the Pareto front of optimal control strategies (multiobjective optimisation), which is the time sequence of optimal façade properties;
(G) if in the multiobjective optimisation the coordination layer selects one solution from the current Pareto front and generates the seeds for the following optimisation period, according to the optimised control of the future time horizon of the current optimisation;
(H) the optimisation horizon is shifted forward for a period equal to the planning horizon by the coordination layer;
(I) THM is performed by the evaluation layer, i.e. the building is resimulated until the start of the control horizon for the previous optimised period adopting the optimised control sequence found in (F) or (G); steps (C) to (I) are repeated until the optimisation horizon reaches the end of the simulation period and all the results are stored.

6.5 Towards Future Generation Adaptive Material for Smart Glazing

Different researchers applied similar methodologies in order to provide robust results from their analyses/evaluations supporting product development of innovative adaptive materials for building integration. To date, few case studies of simulation-based support for adaptive materials' product development exist, detailed in Sect. 6.3.1. In the present section, the methodology mapped in one study (Loonen et al. 2014a, b) and expanded previously (Sect. 6.4.1) is used to analyse a different case study with different objectives than that used by Loonen et al. 2014a, b. This concerns the evaluation of ideal adaptive thermo-optical properties for glazing applications (Favoino et al. 2015a). These ideal thermo-optical properties are expected to vary with the climatic location, the orientation, the type of building, etc. Therefore, the methodology applied makes use of parametric analysis coupled with optimisation to establish ideal adaptive glazing for specific boundary conditions and identify the salient characteristics of an ideal technology in different scenario to steer the development of the future generation of adaptive glazing. This case study will be illustrated by going through the different part of the methodology outlined in the previous section, to demonstrate that the methodology developed in Loonen et al. (2014a, b) could be generally applicable to different purposes concerning evaluation and product development support for adaptive materials and technologies. The tool detailed in Sect. 6.4.2 is used to develop the case study.

6.5.1 Goals and Objectives

An ideal adaptive material for building envelope application can be defined as that material that minimises the total energy use in the indoor space by means of adapting its thermo-optical properties, in order to modulate overall building envelope design parameters.

Sensitivity analysis is therefore adopted in order to evaluate which are the most significant adaptive building envelope material properties influencing total primary energy use. This was derived from the previous study (Jin and Overend 2013), in which sensitivity analysis was performed on building performance in terms of energy use, indoor environmental quality and whole-life cost of early-stage design parameters (including façade, architectural and building services design parameters). These findings are partly summarised in Fig. 6.10, which shows the ranked influences on the total energy use (heating, cooling and lighting) of an enclosed office building located in Helsinki, London and Rome, of (a) the window-to-wall ratio (WWR); (b) the *U*-value (U_g), *g-value* and visible transmission T_{vis} of the transparent façade; (c) the *U*-value of the opaque façade (U_p); and (d) the infiltration rate (IR). The ranking is obtained from the absolute value of the standardised regression coefficients and Sobol coefficients of the global sensitivity analysis.

From Fig. 6.10, it is evident that the glazing thermo-optical properties, i.e. the U_g, *g-value* and T_{vis}, together with the *WWR*, have the largest influence on the total energy use of office buildings for different climates and orientations. This is also confirmed for indoor environmental quality and whole-life value results. From this, it is pertinent to assume that adaptive transparent building envelopes would have a significant impact on the energy use in buildings.

Therefore, the building envelope parameters, whose modulation will be explored to define ideal adaptive building envelope systems, are the ones pertinent to the transparent part of the building envelope, namely the T_{vis}, *g-value* and *U-value* of the glazing. The following properties and characteristics need to be established in order to identify an ideal adaptive glazing:

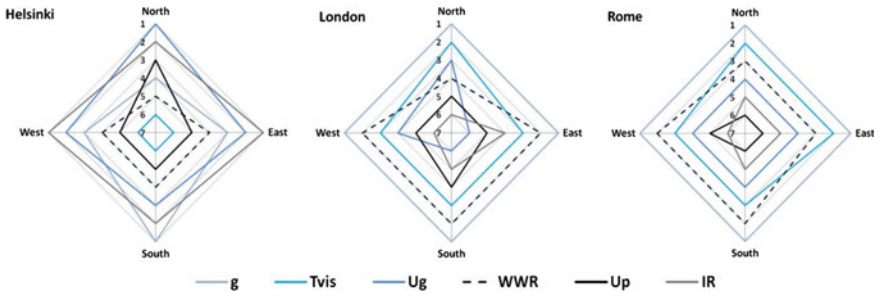

Fig. 6.10 Influence of façade design parameters on total energy use in an office building for different locations and orientations, as published by Favoino et al. (2015a), under CC-BY licence

(a) the most effective modulation range of each thermo-optical property;
(b) the interdependencies between the modulations of different properties;
(c) the most effective timescale of the modulation range (i.e. seasonal, daily);
(d) the best control strategy for the switching of thermo-optical properties.

6.5.2 Performance Indicators

The primary total energy use of the building is chosen as the only indicator in order to measure the performance of the ideal smart glazing technology. The specific primary total energy use, E_p (kWh/m^{2}y), is therefore evaluated as a normalised sum on the building surface of the yearly primary energy use for heating $E_{p,heat,}$ cooling $E_{p,cool}$ and lighting $E_{p,light}$. Other performance indicators could have been used either together or alternatively to the E_p, for example long-term thermal comfort indexes (as in Carlucci et al. 2015), or visual comfort indicators, such as useful daylight illuminance and/or glare discomfort probability (as in Gonzalez and Fiorito 2015), or net energy exchange indicator as profile matching index between energy consumption and on-site energy production by means of renewable energy systems, promoting energy self-consumption.

6.5.3 Simulation Strategy

The aim of this case study is to evaluate objectives a) to c) in 6.5.1, but this is strongly dependent on how the ideal adaptive material is controlled (objective d)). In order to detach the analysis, and therefore the characteristics of the ideal material, from the control problem, an inverse approach is adopted. That is the ideal material is supposed to have an optimal control as far as the performance indicator chosen is, consisting in adopting a control that minimises the E_p. This approach differs from the analysis presented by Loonen et al. (2014a, b), in which 6 different control alternatives were tested. In this last case, the ranking of different design alternatives could be dependent on the control strategy supposed, and therefore, the result may not be considered absolute. To this purpose, the simulation framework detailed in Sect. 6.4.2 was implemented, applying RHC to the control of the ideal adaptive material, and integrated with the other building services.

6.5.4 Choice of the Benchmark

The choice of the benchmark for the ideal adaptive material performance could be an arbitrary decision. The purpose of this case study is to show the potential of

adopting an optimal adaptive solution compared to a conventional static one, as well. For this reason, the benchmark itself could not be a design solution set a priori, but it is the product of the same optimisation process (adopting the same design variables and performance objective of the ideal adaptive solution), with the only difference that the benchmark design alternative presents conventional "static" material properties. For this reason, two benchmarks were adopted, a reference building complying with building regulation (R) and an ideal "static" solution (Y, as the same ideal material properties are maintained throughout the whole period of evaluation consisting of one reference year).

6.5.5 Test Case Buildings

The test case building is a typical office reference room (3 m wide × 5 m deep × 3.5 m high), with a WWR of 40 % on a single façade. The typical office room is flanked by identical offices on its other three sides at the same level and on the level immediately above and below it. The glazing of the façade (40 % of 3 m × 3.5 m) has adaptive thermo-optical properties, and the opaque part of the façade meets the minimum requirements set in the national standards. Indoor comfort is considered as a requirement of the indoor space which is always met by the building services if the adaptive ideal material alone is not able to provide it. This means that indoor temperature has fixed set points for heating and cooling (20 and 26 °C, respectively) with a nocturnal setback (12 and 40 °C, respectively); the primary air ventilation rate is set to 1.4 l/s m^2 when the office is occupied. The threshold of 500 lux is considered for the minimum illumination level (EN ISO 15251:2007) to be maintained by a combination of daylight and a 5-step dimmable artificial lighting system (at desk level, 0.8 m high, 1.5 m far from the façade). Even though a more recent study suggests that lower thresholds, such as 300 lux, could be sufficient to maintain visual comfort by means of daylight and artificial lighting systems (Mardaljevic et al. 2012), but this has not been reflected in standards yet. Schedules and peak loads for the building services, lighting, equipment and occupation are defined according to the UK NCM database (BRE 2010). The lighting power density is set to 12.75 W/m^2, the equipment power density is 13.45 W/m^2, and the occupation density is 0.111 person/m^2. An average seasonal efficiency of the heating plant of 0.85 is considered, and a seasonal energy efficiency ratio of 3.5 is set for the cooling plant.

6.5.6 Sensitivity Analysis

Sensitivity analysis can be used at this stage in order to find the most influential parameters of the building model on the performance indicators, to reduce to the

minimum extent the number of the significant variables in the model, allowing us to reduce the number of cases for the parametric study, as in Loonen et al. (2014a, b).

6.5.7 *Parametric Analysis*

Parametric analysis is used to evaluate the performance of the ideal adaptive material under different scenarios. In fact, the specific thermo-optical properties of the ideal glazing depend on the boundary conditions of the system, which consist of the external boundary conditions. For this reason, a unique case study cannot be considered representative; hence, a series of case studies is investigated. This is also a way to test the robustness of the ideal solution to scenario uncertainties (Hopfe and Hensen 2011), or to investigate what is the impact and effectiveness of an adaptive material solution in a different market context (different countries or types of building). The approach by which a design and/or control alternative is optimised according to different scenarios is also referred to in the literature as scenario-based optimisation (Matusko and Borrelli 2012). The different parameters varied in this specific parametric study are the climate of the building, the orientation and the thermal inertia of the reference room. Therefore, the evaluated case studies are located in three different temperate climates (Helsinki, London and Rome), in the four cardinal orientations. Different reference facades and fuel factors are used in order to account for different national climatic and legislation contexts in Rome, London and Helsinki, according to the EN ISO 13790:2008 (Table 6.2).

In order to assess the sensitivity of the results to the thermal inertia of the building, an office room with lower thermal inertia is also evaluated, and this is referred to LI (low inertia). This office reference room with lower thermal inertia adopts an opaque curtain wall and a composite concrete–steel deck slab construction, resulting in a time constant between 15 and 24 h, compared to the 42–63 h of the insulated brick cavity wall and reinforced concrete slab of the higher inertia alternative. The time constant is used to quantify the thermal inertia of the office reference room. This is calculated numerically by means of measuring the response of the reference room (in terms of indoor air temperature) to a step solicitation in outdoor temperature.[6] The time constant is measured as the time required by the indoor air temperature to decrease its value by 63.2 % of the step temperature solicitation. The thermal capacity (internal and external), the superficial mass and the time lag of the constructions used in the high and low thermal inertia

[6]For this evaluation, no internal loads (occupant, lights and equipment) and no solar loads are considered in the room model.

Table 6.2 Office reference room and reference façade (R) characteristics, as published by Favoino et al. (2015a), under CC-BY licence

Climate	Heating degree days [base] (°C)	U_{wall} (W/m^{2}K)	$U_{glazing}$ (W/m^{2}K)	g-value (–)	T_{vis} (–)	f_{Elec} (–)	$f_{Nat\ Gas}$ (–)
Rome	1415 [20]	0.29	2.00	0.72 (N, S) −0.58 (E, W)	0.76 (N, S) −0.61 (E, W)	2.180	1.000
London	1828 [15.5]	0.27	2.00			1.026	2.580
Helsinki	3902 [18.5]	0.16	1.00			1.700	1.000

Table 6.3 Thermal capacity of the constructions adopted in the office reference room, as published by Favoino et al. (2015a), under CC-BY licence

	Unit	Insulated cavity brick wall	Curtain wall (LI)	Concrete slab	Concrete–steel deck slab (LI)
Internal thermal capacity[a]	kJ/m^{2}K	36.2	21.7	67.8	67.2
External thermal capacity[a]	kJ/m^2 K	106.3	23.2	29.3	29.9
Superficial mass	kg/m^2	412	54	675	315
Time lag	h	11.61	1.63	10.61	6.26

[a]In the case of a horizontal partition, if it is considered as a ceiling, the internal and external thermal capacity needs to be inverted

office are summarised in Table 6.3, and these are calculated according to EN ISO 13786:2008.

6.5.8 *Material/System Design and Control Parameters*

Since RHC control is adopted for the operation of the ideal adaptive material, only design parameters are present. The design parameters are the speed of the adaptive mechanisms, ranging from ideal static (Y) to monthly (M) and daily (D) and the ideal material properties. The ideal properties that can be controlled dynamically are overall performance indicators of the glazing portion, the *U-value* (W/m^2 K), the *g-value* (–) and the T_{vis} (–). For each property, a modulation range is calculated assuming that an ideal adaptive glazing can modulate its thermo-optical properties in a continuous way within the full physically feasible thermo-optical range. These physically feasible ranges are confined by the properties of existing static state-of-the-art double-glazing unit systems. In Table 6.4, the modulation ranges are detailed. Moreover, a physical constraint exists limiting the maximum ratio between T_{vis} and *g-value*.[7]

[7]This theoretical maximum is limited by the ratio of the energy contained in the solar visible spectrum compared to the whole solar spectrum at the sea level, which is approximately 42 %.

Table 6.4 Modulating ranges of glazing thermo-optical properties, as published by Favoino et al. (2015a), under CC-BY licence

	U-value (W/m^2 K)	g-value (–)	T_{vis} (–)
Range (min–max)	0.2–5.14	0.01–0.84	0.01–0.98

6.5.9 Optimisation

The optimisation problem can be formulated as follows:

$$\min \begin{cases} \text{if } Z(X(t)) \leq 0.41 \quad f(X) = E_p = E_{p,heat} + E_{p,cool} + E_{p,ligh} \quad \left[\frac{kWh}{m^2 y}\right] & (6.1) \\ \text{if } Z(X(t)) > 0.41 \quad f(X) = E_{p,heat} + E_{p,cool} + E_{p,ligh} + kZ(X(t))^2 \quad \left[\frac{kWh}{m^2 y}\right] & (6.2) \\ \text{where } Z(X(t)) = \frac{g\text{-value} - 0.42 \cdot T_{vis}}{\sqrt{1 + 0.42^2}} \quad [-] & (6.3) \\ \text{and } X(t) = \left(U\text{-value}(t)\left[\frac{W}{m^2 K}\right], g\text{-value}\,(t)[-], T_{vis}(t)[-]\right) & (6.4) \end{cases}$$

where $X(t)$ is the vector of adaptive glazing properties as defined in Table 6.4, $Z(X)$ is a penalty function introduced to constrain the variable space $X(t)$, representing the distance of the solution from the physical limit (see footnote 5), f(X) is the cost function, $k = 10$ for daily adaptive façade and $k = 10^2$ for the monthly one, and t is the modulation time of the façade thermo-optical properties (monthly, M, and daily, D). The value k is chosen such that the penalty function is one order of magnitude larger than the total primary energy use in the building.

A hybrid algorithm, named particle swarm optimisation (with constriction coefficients) with generalised pattern search Hookes–Jeeves implementation (GPSPSOCCHJ), was used for the optimisation (Wetter 2011a, b). This algorithm was chosen as it offered the best trade-off between computational time and optimality of the results when compared with alternative algorithms. The hybrid optimisation algorithm (GPSPSOCCHJ) achieves this as it couples a global stochastic population-based optimisation algorithm (PSOCC) with a local one (GPSHJ), ensuring that a result close to the global minimum is found with the first algorithm, which is then improved by the local search.

Other optimisation algorithms can be used depending on the number of objectives of the problem and on the nature of the objective function(s), for example in Jin, Favoino and Overend (2015) a Genetic Algorithm was used in order to solve a two-objective optimisation problem.

6.5.10 Postprocessing of Results

For each alternative scenario, a time series of optimal states (thermo-optical properties) is generated, for each modulation time of the adaptive material. Each data and time series has also embedded information regarding its performance, in

terms of total primary energy, primary energy for heating, cooling and lighting saved. This is a large amount of information, whose content and usefulness need to be readable by the stakeholders of the design process. The way this information is postprocessed and communicated depends on the specific design problem, and it relates to the aims and objectives set at the beginning of the process. One of the aim of this study is to understand what are the adaptive glazing material properties with the largest influence, what is the most effective interval of variation of thermo-optical properties and whether there is any relationship between different adaptive properties. This is done by introducing a frequency analysis in order to understand (1) the most frequent intervals/values for each adaptive property and (2) the intervals/values for each thermo-optical property, which make the largest contribution to reducing energy demand with respect to the yearly optimised static material, *Y*. Moreover, this analysis could be useful to establish the frequency distribution of each single adaptive property in its domain of variability, thereby establishing whether technologies with the same ability to modulate a specific thermo-optical property could be effective in different orientations and in different climates and whether discrete values of thermo-optical properties could effectively replace a continuous modulation range.

In order to perform the frequency analysis, two measures are defined:

- the cumulated time frequency ctf of each adaptive property Xi over the yearly period:

$$ctf_{X_i} = \frac{\int_{X_{iO}}^{X_{iO}+\Delta X_i} \frac{1}{t}\Big|_{X_i-\delta<X_i<X_i+\delta}}{\int \mathrm{d}t}(\%) \tag{6.5}$$

that can range from 0 to 100 % and indicates the proportion of time during the year (t) during which a certain property (X_i) lies within a certain interval of values;

- the performance frequency η_Y of each adaptive property X_i compared to the best static solution (Y):

$$\eta_{X_i} = \frac{Ep_{\mathrm{opt}Y} - Ep_{\text{ideal adaptive}}}{Ep_{\mathrm{opt}Y}}\Bigg|_{X_i-\delta<X_i<X_i+\delta}\Bigg|_t (\%) \tag{6.6}$$

that ranges from 0 to 100 % and defines the energy saved by varying each adaptive property X_i in a certain range compared to the static yearly optimised solution over the same period (t).

6.5.11 Communication of Results

The results of the scenario-based optimisations undertaken are presented in three ways: (1) the energy saving potential of the optimal adaptive transparent material with progressively shorter modulation time of adaptive thermo-optical properties (from month to day); (2) the modulation ranges (i.e. the variability of the adaptive properties) required to minimise the total primary energy use; and (3) frequency distribution of each thermo-optical property in its modulation range and the effectiveness along the modulation range in terms of energy saving. Moreover, the relationships between different properties and the common features of the ideal glazing technology that could guide the development of next-generation switchable glazing are discussed.

The results of this study will not be entirely presented and discussed here, for the sake of brevity. In this section, only partial results will be presented, and for the entire results and interpretation and set of data, please refer to Favoino et al. (2015a). A general discussion about results outcomes and interpretation is provided in the next section.

The specific total primary energy use of the office building and the share in the primary energy for heating, cooling and lighting is shown in Fig. 6.10 and in Table 6.5. The analysis is performed for three climates, i.e. Helsinki, London and Rome, and four orientations (North, East, South and West), but only the London results are herewith presented. Four different case studies are considered for each location and orientation: (a) the reference façade *(R)*, which satisfies the minimum requirements in each national context; (b) the yearly optimised glazed façade (*Y*), which minimises the total yearly primary energy use and corresponds to the best possible "static" glazing materials in the domain defined by commercially available products (Fig. 6.5, grey data points); (c) the ideal monthly adaptive glazing materials *(M),* which are able to adapt their thermo-optical properties on a monthly basis; and (d) the ideal daily adaptive ones *(D)*, which are able to adapt the thermo-optical properties on a daily basis.

Both reference *R* and yearly optimised *Y* glazing materials represent state-of-the-art "*static*" solution, and a difference between *R* and *Y* case indicates that in terms of total energy use for the specific building typology and climate, better performing "static" glazing materials than the ones required by national standards could be chosen. Consequently, the *Y* façade is a more appropriate benchmark, as it provides the highest energy saving achievable with the conventional "static" design alternatives. However, energy saving (ES) potential in Fig. 6.10, and in Table 6.5, is expressed with respect to the reference façade R.

The optimal properties (*U-value*, *g-value* and T_{vis}) of the ideal adaptive glazing system in a South-orientated façade in Rome are represented in Fig. 6.11. Different cases are represented in a 3D space including a) Case *D* (small green data points) and their projections on the different planes (*U-value–g-value* small yellow data points*, U-value–*T_{vis} small blue data points and *g-value–*T_{vis} small red data points); (b) Case *M* (white data points with white projections); (c) Case *Y* (large green data

Table 6.5 Energy use and energy saving potential of ideal adaptive glazing material, as published by Favoino et al. (2015a), under CC-BY licence

		Ep tot (kWh/m^{2}y)	Ep heat (kWh/m^{2}y)	Ep cool (kWh/m^{2}y)	Ep light (kWh/m^{2}y)	ES tot (%)	ES heat (%)	ES cool (%)	ES light (%)
R	North	153.61	117.55	2.40	33.66				
	East	150.22	109.61	5.13	35.48				
	South	126.26	81.89	12.93	31.44				
	South —LI	133.63	81.61	20.58	31.44				
	West	152.19	110.16	7.53	34.51				
Y	North	130.19	86.62	6.52	37.05	15	26	−172	−10
	East	128.62	77.79	14.20	36.63	14	29	−177	−3
	South	111.67	64.18	12.10	35.39	12	22	6	−13
	South —LI	113.07	64.38	13.30	35.39	15	21	35	−13
	West	131.69	81.83	14.07	35.79	13	26	−87	−4
M	North	126.80	87.95	1.78	37.07	17	25	26	−10
	East	115.34	75.76	2.65	36.94	23	31	48	−4
	South	98.37	56.58	6.07	35.72	22	31	53	−14
	South —LI	103.78	60.53	7.08	36.17	22	26	66	−15
	West	117.78	77.15	4.36	36.26	23	30	42	−5
D	North	116.17	73.46	0.24	42.47	24	38	90	−26
	East	100.49	61.05	0.43	39.02	33	44	92	−10
	South	85.17	44.93	1.62	38.62	33	45	87	−23
	South —LI	87.45	46.46	1.97	39.02	35	43	90	−24
	West	100.74	63.00	0.78	36.96	34	43	90	−7

Fig. 6.11 Specific total primary energy use for different orientation and reaction time of the ideal adaptive glazing material for the climate of London (*R* = Reference, *Y* = Yearly optimised, *M* = Monthly adaptiveness, *D* = Daily adaptiveness,). Percentages indicate the energy savings compared to the *R* static glazing material. As published by Favoino et al. (2015a), under CC-BY licence

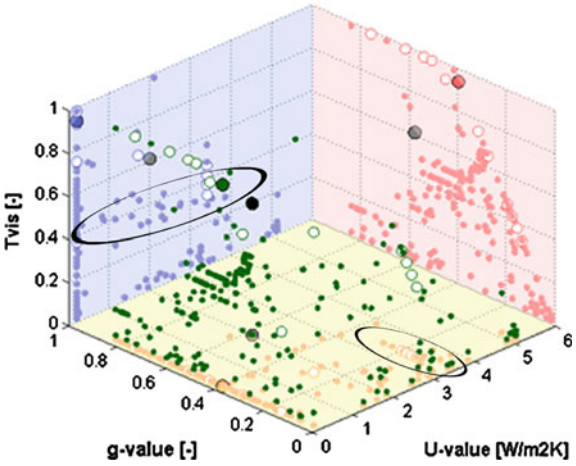

Fig. 6.12 Ideal adaptive glazing material thermo-optical properties (reference: *grey big dot*; yearly: *green big dot*; monthly: *white dots*; min: *green small dots*) and their projections for Rome, South-oriented case. As published by Favoino et al. (2015a), under CC-BY licence

points with large coloured projections); and d) Case *R* (black dot with grey projections). The black circles in Fig. 6.12 represent concentrations of optimal solutions in certain areas, which will be evaluated in the frequency analysis.

The values of the *ctf* and of the η_Y of each adaptive property X_i are shown in Fig. 6.12, for different climates (Helsinki, London and Rome), for the South-oriented façade (darker lines) and for the office room with high and low inertia (LI, with lighter colour lines). The four graphs in the figure present the results for (a) *U-value*, (b) T_{vis}*/g-value*, (c) T_{vis} and (d) *g-value*, respectively. The slope of the *ctf* profiles indicates that the relevant property under analysis has a higher frequency in that corresponding interval, while peaks of η_Y indicate the percentage of energy saved when the corresponding property lies within a certain interval of values, with respect to the best static materials, whose corresponding property values are indicated by dashed vertical lines (Fig 6.13).

6.5.12 *Decision Making: Directions for the Development of Ideal Adaptive Glazing Properties*

After one or more design process loops through the previous stages, a synthesis of the results and eventually a design decision is finally required. In this case, there is not a unique design decision, but a set of directions for transparent adaptive material development.

The results of this case study constitute the upper limit of the performance achievable by a monthly and daily adaptive glazed façade for commercial buildings.

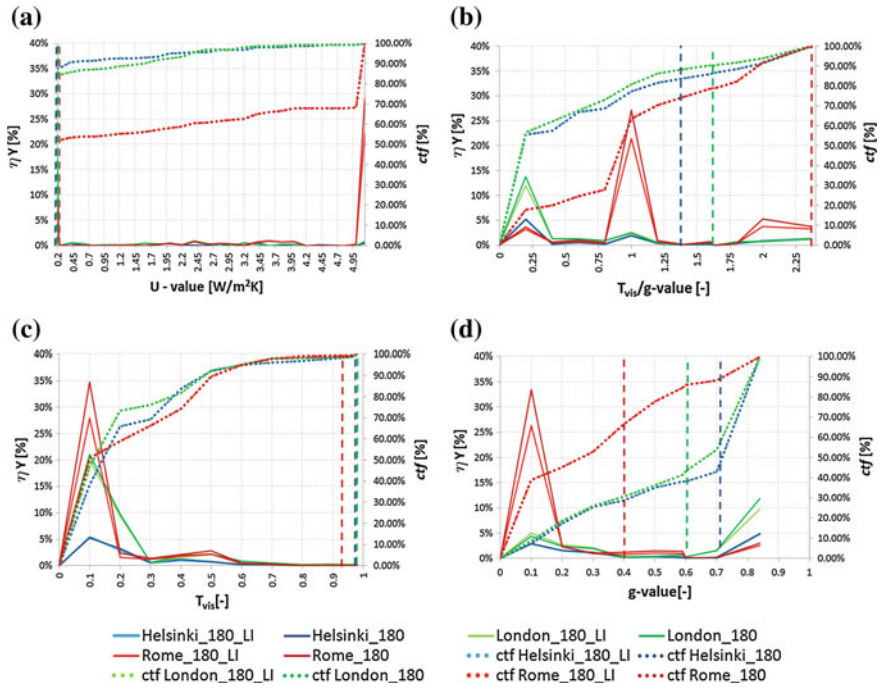

Fig. 6.13 Frequency analysis for South-oriented ideal adaptive glazing material properties: **a** *U*-value, **b** T_{vis}/g-value, **c** T_{vis}, **d** *g*-value. As published by Favoino et al. (2015a), under CC-BY licence

The term ideal or optimal, in fact, stands for an ideal range of variability, whose limits were derived theoretically. The limits are physically achievable, although the appropriate glazing products have yet to be developed. Moreover, a future development should be translating these results, which are in terms of overall glazing system properties, to transparent material physical properties (spectral transmission, absorption and reflection coefficients, and equivalent thermal conductivity of the glazing cavity), although some important considerations regarding physical properties can already be depicted from these results.

Moreover, important observations can be drawn from these results concerning the operational energy saving potential of ideal adaptive glazing materials, the features required to achieve this saving and the most effective modulation ranges of the thermo-optical properties.

It was shown that the energy saving potential is proportional to the modulation speed of the glazed façade (Fig. 6.10 and Table 6.5). The magnitude of the achievable energy savings is sensitive to the climate and orientation of the room/building (Figs. 6.10 and 6.12), but the most effective modulation ranges and values of thermo-optical properties of the optimal adaptive glazing appear to be independent of the climate and the orientation (Fig. 6.12). In particular, it was found

that in colder climates, like London and Helsinki, a significant reduction in operational energy can be achieved by modulating the optical properties on a daily basis when compared to a monthly modulation (Fig. 6.5). Furthermore, modulating the *U-value* of the glazing in these climates yields limited energy savings (Fig. 6.12a). In hotter climates, such as Rome, larger energy savings are achievable, due to the capability of reducing the cooling energy demand by means of seasonal and daily adaptive glazing materials. In particular, a step change in energy saving is achieved when adopting a monthly adaptive glazing in lieu of a static one (Table 6.5). Moreover, adaptive glazing appears to have a high potential in mitigating the effects of future climate scenarios, as they are able to reduce cooling demands, more effectively than heating energy use (Table 6.5). This could become particularly important as in terms of total primary energy reduction, as cooling loads are becoming preponderant also in colder climates, due to the significant increase of insulation levels and airtightness promoted by the building regulations.

From a technological point of view, the desirable features for future generation adaptive glazing in terms of energy saving are as follows: (a) providing the largest possible modulation range in *U-values* particularly for hotter climates (Fig. 6.12a); (b) independently modulating the transmission of the glazing in the visible and the infrared portion of the solar spectrum (Fig. 6.12b); (c) providing a higher luminous efficacy closer to its theoretical limit of 2.41 (Fig. 6.12b); (d) the modulation range of the visible transmission and the total solar transmission do not need to be extended to the entire physically feasible range, but can be limited to an upper bound of 0.5–0.6 (Fig. 6.12c, d); and (e) the ideal thermo-optical states of the adaptive glazing could be reduced to a few discrete states in order to reduce the technological complexity of the solution and of the control strategy (Fig. 6.12), but the effectiveness of this possibility needs further investigation. Moreover, the optimal thermo-optical properties of the adaptive façade calculated with the present method are not affected by the thermal inertia of the building (Fig. 6.12). Even though the effectiveness of an adaptive façade is sensitive to the thermal inertia of the building, this sensitivity reduces with the modulation time of the adaptive façade (Table 6.5).

On this basis, by analysing the data from different climates and orientations, it is possible to develop a single glazing technology, adopting adaptive materials that can accommodate the performance characteristics and the level of adaptiveness of different climates, orientations and buildings. In particular, an independent visible–infrared tunable adaptive material is already under development (Llordes et al. 2013), but the same features of this technology could be eventually achieved by coupling infrared and normal electrochromics, but the feasibility of this solution has never been explored. As far as controlling the *U-value* in a glazing cavity, the approaches of controlling (a) the convection in a close cavity (Pflug et al. 2015), (b) the distance between different polymeric transparent layers in a cavity (Kimber et al. 2014) and (c) the gas pressure in a close cavity (Berge et al. 2015) deserve further investigation.

6.6 Conclusions

Adaptive micro- and nanobased material integrated into buildings and building envelopes could unleash a great potential towards the achievement of nZEB target. In fact their adoption in buildings can reduce their energy use, match the energy demand with energy availability, while maintaining or even improving the level of indoor environmental quality. To date, these potentials remain largely unproved and unexplored. This is partly due to the inability of current methodologies and simulation strategies to cope with (i) the evaluation of new and existing adaptive materials and (ii) the design and control optimisation of these new technologies for building integration.

In this chapter, an introduction to adaptive concepts and technologies was given first, contextualised to the current regulatory and performance context at a building level, followed by an overview on different micro- and nanobased technologies to achieve adaptive behaviour in building materials and building envelope components.

The evaluation of adaptive building technologies presents additional challenges with respect to conventional static building constructions. Among the others are the interconnection between design and control aspects and the mutual influence between building-integrated adaptive materials and boundary conditions, in multiple physical domains. Therefore, the use of building performance simulation can assume an important role to support the evaluation and the product development of existing and new adaptive micro- and nanomaterials, as discussed in Sect. 6.3.

For this purpose, accurate and comprehensive methodologies and simulation strategies are needed, but to date, few case studies have been presented to validate and develop such methodologies and simulation frameworks, which are presented in Sect. 6.4.

In the last sections of this chapter, the methodology for simulation-based support for adaptive materials and technology for building energy efficiency, which was developed by one research group, is explored and detailed by means of a case study developed by different researchers. This is done to reinforce the generality of the methodology and to elucidate it with a different case study. This concerns the characterisation of ideal adaptive material/technology properties for different climatic and building scenarios. It is demonstrated that this method and simulation framework can be used to guide and provide simulation-based support for product development of adaptive materials (micro- and nanobased) and in general for adaptive building technologies.

Acknowledgements This chapter is based on an earlier published paper: Favoino et al. (2015a) "The optimal thermo-optical properties and energy saving potential of adaptive glazing technologies", Applied Energy 156, 1–15. This paper is under CC-BY licence, and it is herewith revised, expanded and updated. The author would like to acknowledge EPSRC to sponsor the open access availability of the aforementioned paper; Eng. Roel Loonen, researcher at the Department of the Built Environment, University of Eindhoven, for providing continuous debate, collaboration and inspiration to this work; Dr. Mauro Overend, senior lecturer at the Department of Engineering, University of Cambridge, for his support and feedback on this work; and Eng. Maite Santiuste Cardano, for the proof reading.

References

Attia S (2012) Optimisation for zero energy building design: interviews with twenty eight international experts, International Energy Agency (IEA) Task 40: towards net zero energy buildings subtask B

Baetens R, Jelle BP, Gustavsen A (2010) Properties, requirements and possibilities of smart windows for dynamic daylight and solar energy control in buildings. Sol Energy Mater Sol Cell 94:87–105

Bakker LG, Hoes-van Oeffelen ECM, Loonen RCGM, Hensen JLM (2014) User satisfaction and interaction with automated dynamic facades: a pilot study. Build Environ 78:44–52

Benson DK, Potter TF, Tracy CE (1994) Design of variable conductance vacuum insulation. In: Proceedings of SAE 1994, Detroit, US

Berge A, Hagentoft C, Wahlgren P, Adl-Zarrabi B (2015) Changing internal pressure to achieve variable thermal conductivity in Thermal Insulation. In: Proceedings of advanced building skins 2015, Graz, Austria

BRE (2010) National calculation methodology database of construction, glazing and activities

Brunsell J (1995) The performance of dynamic insulation in two residential buildings. Air In®ltration Rev 16:4, 7–11

Buckley S (1978) Thermic diode solar panels for space heating. Solar Energy 20:495–503

Cabeza LF, Castell A, Barreneche C, De Gracia A, Fernandez AI (2011) Materials used as PCM in thermal energy storage in buildings: a review. Renew Sustain Energy Rev 15:1675–1695

Cannavale A, Manca M, Malara F, De Marco L, Cingolani R, Gigli G (2011) Highly efficient smart photovoltachromic devices with tailored electrolyte composition. Energy Environ Sci 4:2567. doi:10.1039/c1ee01231b

Cannavale A, Fiorito F, Resta D, Gigli G (2013) Visual comfort assessment of smart photovoltachromic windows. Energy Build 65:137–144. ISSN 0378-7788. http://dx.doi.org/10.1016/j.enbuild.2013.06.019

Carlucci S, Cattarin G, Causone F, Pagliano L (2015) Multi-objective optimization of a nearly zero-energy building based on thermal and visual discomfort minimization using a non-dominated sorting genetic algorithm (NSGA-II). Energy Build 104:378–394, ISSN 0378–7788, http://dx.doi.org/10.1016/j.enbuild.2015.06.064

Clarke JA, Hensen JLM (2015) Integrated building performance simulation: progress, prospects and requirements. Build Env, 1–13. doi:10.1016/j.buildenv.2015.04.002

Clements-Croome TDJ (1997) What do we mean by intelligent buildings? Autom Constr 6:395–400

Corbin CD, Henze GP, May-Ostendorp P (2013) A model predictive control optimization environment for real-time commercial building application, J Build Perform Simul 6 (3):159–174

Corgnati SP, Perino M, Serra V (2007) Experimental assessment of the performance of an active transparent facade during actual operating conditions. Solar Energy 81:993–1013

Correia da Silva P, Leal V, Andersen M (2012) Influence of shading control patterns on the energy assessment of office spaces. Energy Build 50:35–48. ISSN 0378-7788

Correia da Silva P, Leal V, Andersen M (2013) Occupants interaction with electric lighting and shading systems in real single-occupied offices: results from a monitoring campaign. Build Environ 64:152–168. ISSN 0360–1323

Crawley DB, Lawrie LK, Winkelmann FC, Buhl WF, Huang YJ, Pedersen CO et al (2001) EnergyPlus: creating a new-generation building energy simulation program. Energy build, 33(4):319–331

Davies M, Rogers R (1981) A wall for all seasons. RIBA J 88(2):55–57

Deb K, Pratap A, Agarwal S, Meyarivan T (2002) A fast and elitist multiobjective genetic algorithm: NSGA II. IEEE Trans Evol Comput 6:2, 182–197

DeForest N, Shehabi A, Garcia G, Greenblatt J, Masanet E, Lee ES, Selkowitz S, Milliron DJ (2013, March) Regional performance targets for transparent near-infrared switching electrochromic window glazings. Build Environ 61:160–168 (Elsevier Ltd)

DiMaio F, Van Paassen AHC (2001) Modelling the air infiltrations in the second skin façade. In: Proceedings of IAQVEC 2001—the 4th international conference on indoor air quality, ventilation and energy conservation in buildings, Changsha (China), pp 873–880, 2–5 Oct 2001

EN ISO 13786:2008, Thermal performance of building components: dynamic thermal characteristics–calculation methods

EN ISO 13790:2008, Energy performance of buildings—calculation of energy use for space heating and cooling.

EN ISO 15251:2007, Indoor environmental parameters for assessment of energy performance of buildings—addressing indoor air quality, thermal environment, lighting and acoustics

Energy Performance of Buildings Directive Recast 2010/31/EU (2010). http://www.eceee.org/policy-areas/buildings/EPBD_Recast/EPBD_recast_19May2010.pdf

Evins R (2015) Multi-level optimization of building design, energy system sizing and operation. Energy. available online http://dx.doi.org/10.1016/j.energy.2015.07.007, 26 July 2015, ISSN 0360-5442

Favoino F, Overend M (2015) A simulation framework for the evaluation of next generation responsive building envelope technologies. In: Proceedings of 6th international building physics conference 2015, Torino, Italy

Favoino F, Goia F, Perino M, Serra V (2014a) Experimental assessment of the energy performance of an advanced responsive multifunctional façade module. Energy Build 68:647–659, ISSN 0378-7788

Favoino F, Jin Q, Overend M (2014b) Towards an ideal adaptive glazed façade for office buildings. In: Proceedings of 6th international conference on sustainability in energy and buildings 2014, Cardiff, UK, July 2014, Energy Procedia 62, pp 289–298, ISSN 1876-6102

Favoino F, Overend M, Jin Q (2015a) The optimal thermo-optical properties and energy saving potential of adaptive glazing technologies, Appl Energy 156:1–15

Favoino F, Loonen RCGM, Hensen JLM, Overend M (2015b) Modeling and simulation for performance analysis of adaptive building envelope systems. in preparation for J Build Perform Simul

Gan G (2000) Numerical evaluation of thermal comfort in rooms with dynamicinsulation. Build Environ 35: 445-453.

Garcia G, Buonsanti R, Llordes A, Runnerstrom EL, Bergerud A, Milliron DJ (2013) Near-infrared spectrally selective plasmonic electrochromic thin films. Adv Opt Mater 1:215–220

Goia F, Cascone Y (2014) The impact of an ideal dynamic building envelope on the energy performance of low energy office buildings. Energy Procedia 58:185–192

Goia F, Perino M, Serra V (2013) Improving thermal comfort conditions by means of PCM glazing systems. Energy Build 60:442–452

Goia F, Bianco L, Serra V, Perino M (2014) Energy Performance Assessment of Advanced Integrated Façades by Means of Synthetic Metrics. In: Proceedings of the 8th international symposium on heating, ventilation and air conditioning, pp 21–28

González J, Fiorito F (2015) Daylight design of office buildings: optimisation of external solar shadings by using combined simulation methods. Buildings 5(2):560–580. doi:10.3390/buildings5020560

Granqvist CG (2007) Transparent conductors as solar energy materials: a panoramic review. Sol Energy Mater Sol Cell 91:1529–1598

Hoffmann S, Lee ES, Clavero C (2014) Examination of the technical potential of near-infrared switching thermochromic windows for commercial building applications. Sol Energy Mater Sol Cell 123:65–80. doi:10.1016/j.solmat.2013.12.017

Hopfe CJ, Hensen JLM (2011) Uncertainty analysis in building performance simulation for design support. Energy Build 43(10):2798–2805, ISSN 0378-7788. http://dx.doi.org/10.1016/j.enbuild.2011.06.034.

IEA–ECBCS Annex 44 (2010) Integrating environmentally responsive elements in buildings. Design Guide—vol II

Jelle BP (2013) Solar radiation glazing factors for window panes, glass structures and electrochromic windows in buildings—Measurement and calculation. Sol Energy Mater Sol Cell 116:291–323

Jin Q, Overend M (2013) Sensitivity of façade performance to early stage design variables. Energy and Buildings

Jin Q, Favoino F, Overend M (2015) Study in the Potential of opaque Adaptive façade for office building in a temperate climate. In: Proceedings of building simulation 2015, Hyderabad, India, 7–9 Dec 2015

Kamalisarvestani M, Saidur R, Mekhilef S, Javadi FS (2013) Performance, materials and coating technologies of thermochromic thin films on smart windows. Renew Sustain Energy Rev 26:353–364

Kanpur Genetic Algorithm Laboratory (2010) "NSGA_II source code". Available http://www.iitk.ac.in/kangal/. Accessed 08 Dec 2010

Kasinalis C, Loonen RCGM, Cóstola D, Hensen JLM (2014) Framework for assessing the performance potential of seasonally adaptable facades using multi-objective optimization. Energy Build 79:106–113, ISSN 0378-7788. http://dx.doi.org/10.1016/j.enbuild.2014.04.045.

Khandelwal H, Loonen RCGM, Hensen JLM, Debije MG, Schenning APHJ (2015) Electrically switchable polymer stabilised broadband infrared reflectors and their potential as smart windows for energy saving in buildings. Scientific Rep 5:11773

Kimber M, Clark W, Schaefer L (2014) Conceptual analysis and design of a partitioned multifunctional smart insulation. Appl Energy 114:310–319, ISSN 0306-2619. http://dx.doi.org/10.1016/j.apenergy.2013.09.067.

Kubba S (2012) Handbook of green building design and construction: LEED, BREAM and Green Globes. Elsevier, Philadelphia, ISBN: 978-0-12-385128-4

Kuznik F, David D, Johannes K, Roux J, (2012) A review on phase change materials integrated in building walls. Renew Sustain Energy Rev 15(1):379–391

LBNL (2011) IGDB database 37.0 (accessed in August 2014)

Le Corbusier (1930) Precisions sur un etat present de l`architecture et de l`urbanisme. Cres, Paris

Llordes A, Garcia G, Gazquez J, Milliron DJ (2013) Tunable near-infrared and visible-light transmittance in nanocrystal-in-glass composites. Nature 500:323–327

Loonen RCGM, Trčka M, Hensen JLM (2011) Exploring the potential of climate adaptive building shells. In: Proceedings of building simulation 2011, Sydney, Australia, pp 2148–55

Loonen RCGM, Trčka M, Cóstola D, Hensen JLM (2013) Climate adaptive building shells: state-of-the-art and future challenges. Renew Sustain Energy Rev 25:483–493, ISSN 1364-0321

Loonen RCGM, Singaravel S, Trcka M, Cóstola D, Hensen JLM (2014a) Simulation-based support for product development of innovative building envelope components. Autom Constr 45:86–95

Loonen RCGM, Singaravel S, Trčka M, Cóstola D, Hensen JLM (2014b) Simulation-based support for product development of innovative building envelope components. Autom Constr 45:86–95, ISSN 0926-5805. http://dx.doi.org/10.1016/j.autcon.2014.05.008

Loonen RCGM, Rico-Martinez JM, Favoino F, Brzezicki M, Menezo C, La Ferla G, Aelenei L (2015) Design for façade adaptability – Towards a unified and systematic characterization. In: Proceedings of economic forum advanced building skins 2015, Bern, Switzerland

Mardaljevic J, Andersen M, Roy N, Christoffersen J (2012) Day lighting metrics: is there a relation between useful daylight illuminance and daylight glare probability? In: Proceedings of the building simulation and optimization conference (BSO12), Loughborough, UK

Marler RT, Arora JS (2004) Survey of multi-objective optimization methods for engineering. Struct Multidiscip Optim 26(6):369–395

MATLAB Release 2013a (2013) The MathWorks, Inc., Natick, Massachusetts, United States
Mattingley J, Wang Y, Boyd S (2011) Receding horizon control. IEEE Control Syst 31(3):52–65
Matusko J, Borrelli F (2012) Scenario-based approach to stochastic linear predictive control, in Decision and Control (CDC). 2012 IEEE 51st annual conference, pp 5194–5199, 10–13 Dec 2012. doi: 10.1109/CDC.2012.6425849.
Miettinen K (1999) Nonlinear multiobjective optimization. Springer, Berlin, Retrieved Dec 2014, ISBN 978-0-7923-8278-2
Mueling O, Seeboth A, Haeusler T, Ruhmann R, Potechius E, Vetter R (2009) Variable solar control using thermotropic core/shell particles. Sol Energy Mater Sol Cell 93:1510–1517
Nielsen MV, Svendsen S, Jensen LB (2011) Quantifying the potential of automated dynamic solar shading in office buildings through integrated simulations of energy and daylight. Sol Energy 85(5):757–768
Nitz P, Hartwig H (2005) Solar control with thermotropic layers. Sol Energy 79:573–582
NREL (National Renewable Energy Laboratory) (2011) EnergyPlus8.1, California, USA
NREL (National Renewable Energy Laboratory) (2013) Energy plus, application guide for EMS, energy management system user guide
Oesterle E, Lieb RD, Lutz M, Heusler W (2001) Double-skin façades-integrated planning. Prestel, Munich
Perino M (ed), IEA–ECBCS Annex 44 (2007) Integrating environmentally responsive elements in buildings, State of the art review
Pflug T, Kuhn TE, Nörenberg R, Glück A, Nestle N, Maurer C (2015) Closed translucent façade elements with switchable U-value—A novel option for energy management via the facade, Energy Build 86:66–73, ISSN 0378-7788. http://dx.doi.org/10.1016/j.enbuild.2014.09.082.
Pohekar SD, Ramachandran M (2007) Application of multi-criteria decision making to sustainable energy planning—a review. Renew Sustain Energy Rev 8(4):365–381, ISSN 1364-0321. http://dx.doi.org/10.1016/j.rser.2003.12.007
Quesada G, Rousse D, Dutil Y, Badache M, Hallé S (2012a) A comprehensive review of solar facades. Opaque solar facades. Renew Sustain Energy Rev 16(5):2820–2832
Quesada G, Rousse D, Dutil Y, Badache M, Hallé S (2012b) A comprehensive review of solar facades. Transparent and translucent solar facades. Renew Sustain Energy Rev 16 (5):2643–2651
Rathod MK, Banerjee J (2013) Thermal stability of phase change materials used in latent heat energy storage systems: a review. Renew Sustain Energy Rev 18:246–58
Ritter A (2007) Smart materials in architecture, interior architecture and design. Walter de Gruyter, Basel
Saelens D, Carmeliet J, Hens H (2003) Energy performance assessment of multiple skin facades. Int J HVAC&R Res 9(2):167–186
Saelens D, Roels S, Hens H (2004) The inlet temperature as a boundary condition for multiple-skin facade modelling Energy Build 36(8):825–835, ISSN 0378-7788.
Saelens D, Roels S, Hens H (2008) Strategies to improve the energy performance of multiple-skin facades. Build Environ 43:1208–650
Saeli M, Piccirillo C, Parkin IP, Binions R, Ridley I (2010) Energy modelling studies of thermochromic glazing. Energy Build 42(10):1666–1673. doi:10.1016/j.enbuild.2010.04.010
Sartori I, Napolitano A, Voss K (2012) Net zero energy buildings: a consistent definition framework. Energy Build 48:220–232, ISSN 0378-7788.
Serale G, Fabrizio E, Perino M (2015) Design of a low-temperature solar heating system based on a slurry Phase Change Material (PCS). Energy Build
Shephard RW, Färe R (1974) The law of diminishing returns. Lect Notes Econ Math 99:287–318
Trcka M, Hensen JLM, Wetter M (2009) "Co-Simulation of innovative integrated HVAC systems in buildings. J Build Perform Simul 2(3):209–30. doi:10.1080/19401490903051959.
Varga S, Armando CO, Afonoso CF (2002) Characterisation of thermal diode panels for use in the cooling season in buildings. Energy Build 34:227–235
Warwick MEA, Binions R (2014) Advances in thermochromic vanadium dioxide films. J Mater Chem A 2:3275–3292

Warwick M, Ridley I, Binions R (2013) The effect of transition hysteresis width in thermochromic glazing systems. Open J Energy Eff 2:75–88. doi: 10.4236/ojee.2013.22011

Wetter M (2011a) Co-simulation of building energy and control systems with the building controls virtual test bed. J Build Perform Simul 4(3):185–203. doi:10.1080/19401493.2010.518631

Wetter M (2011b) GenOpt generic optimization program user manual, Version 3.1.0, Building Technologies Department, LBNL, USA

Wickmans A, Aschehoug O, Hestnes AG (2005) The intelligent building envelope—concept and qualifications, glass in buildings conference proceedings, Bath, UK

Xenophou T (1976) System of using vacuum for controlling heat transfer in building structures, motor vehicles and the like, US Patent No. 3,968,831

Ye H, Meng X, Xu B (2012) Theoretical discussions of perfect window, ideal near infrared solar spectrum regulating window and current thermochromic window. Energy Build 49:164–172

Ye H, Meng X, Long L, Xu B (2013) The route to a perfect window. Renew Energy 55:448–455

Zanghirella F, Perino M, Serra V (2011) A numerical model to evaluate the thermal behaviour of active transparent façades. Energy Build 43(5):1123–1138

Zeng R, Wang X, Di H, Jiang F, Zhang Y, (2011) New concept and approach for developing energy efficient buildings: ideal specific heat for building thermal mass. Energy Build 43:1081–1090

Zhang Y, Zhang Y, Shi W, Shang R, Cheng R, Wang X (2015). A new approach, based on the inverse problem and variation method, for solving building energy and environment problems: Preliminary study and illustrative examples. Build Environ 91:204–218, ISSN 0360-1323. http://dx.doi.org/10.1016/j.buildenv.2015.02.016

Chapter 7
Nanotech-Based Vacuum Insulation Panels for Building Applications

Bjorn Petter Jell and Simen Edsjo Kalnæs

Abstract Vacuum insulation panel (VIP) represent a state-of-the-art high-performance thermal insulation solution. The pristine non-aged centre-of-panel thermal conductivity value for a VIP can be as low as 0.002–0.004 W/(m K) depending on the core material. Normally, declared average values accounting for thermal bridge effects and ageing during, e.g. 25 years are to be given, typical an effective thermal conductivity value between 0.007 and 0.008 W/(m K) for VIPs with fumed silica cores. VIPs enable highly insulated solutions for building applications, both for the construction of new buildings and for the renovation of existing buildings, and may hence be a measure to reduce the energy usage in buildings without having to employ very thick building envelopes. This study gives a state-of-the-art review of VIP products found available on the market today and explores some of the future research possibilities for these products. The application of nanotechnology is regarded as a promising pathway for achieving and improving both vacuum- and non-vacuum-based high-performance thermal insulation materials. During the last years, VIPs have been utilized with success for building applications in increasing numbers, where one of the main driving forces is the increased focus on, e.g. passive houses, zero energy buildings and zero emission buildings. Thus, VIPs are now in the early market stages as a building product. The implementation of VIPs in various building constructions has lead to an increased interest in the utilization of this product, both in new and refurbished constructions. Even though there is not enough data to conclude the effect over a lifetime of a building yet, the immediate result in decreased energy usage can be seen. However, the challenge of guaranteeing a set of lifetime expectancy, along with high costs, is one among some major reasons why VIPs are met with a certain scepticism in the building industry. Aiming to give better-quality assurance for the users, make further advances in VIP envelope technologies and the development of VIP core materials, along with a further cost reduction, represent crucial aspects for VIPs to become a competing thermal insulation solution for buildings.

B.P. Jell (✉) · S.E. Kalnæs
Department of Civil and Transport Engineering, Norwegian University of Science and Technology, Trondheim, Norway
e-mail: bjorn.peter.jelle@sintef.no

F. Pacheco Torgal et al. (eds.), *Nano and Biotech Based Materials for Energy Building Efficiency*, DOI 10.1007/978-3-319-27505-5_7

7.1 Introduction

The production and usage of energy in the world today relies on a large amount of fossil fuels. However, the continued use of fossil fuels will strain our resources, as well as lead to large amounts of pollution, especially through CO_2 emissions. The heating and cooling of buildings require a considerable amount of energy. A reduction in energy usage for the building sector will have a beneficial effect on CO_2 emissions. In the European Union, buildings represent 40 % of the total energy usage, and the existing building stock represents the single largest potential sector for energy savings (European Union 2012). By the principle of the Kyoto Pyramid, the most cost-effective method of reducing energy usage is to provide better thermally insulated buildings. To obtain the demanded *U*-values with traditional insulation materials, buildings are required to have walls up to 50 cm thickness. This leads to more complex building details and transportation of thicker materials to the building sites (Jelle 2011).

Vacuum insulation panels (VIP) represent one of the most promising building insulation material technologies. Two main types shall be distinguished, i.e. VIPs with fumed (pyrogenic) silica cores and VIPs with glass fibre cores. The VIPs with fumed silica cores have a centre-of-panel insulation performance which normally ranges from 0.004 W/(m K) in pristine condition to typical 0.008 W/(m K) after 25 years of ageing. This is 5–10 times better, depending on ageing, than traditional insulation used in buildings today (Jelle 2011). Therefore, VIPs enable highly insulated constructions for walls, roofs and floors, especially within refurbishing of older buildings where space is often limited. When perforated and thus loss of vacuum, a VIP with fumed silica as core material typically attains a thermal conductivity value of 20 mW/(m K). Normally, declared average values accounting for thermal bridge (edge) effects and ageing during, e.g. 25 years are to be given, typical an effective thermal conductivity value between 0.007 and 0.008 W/(m K) for VIPs with fumed silica cores.

Integrating VIPs successfully into constructions requires careful planning with regard to its durability, the lack of flexibility, thermal bridging and lifetime expectations (Tenpierik 2009). The uncertainties around expected lifetime is a crucial factor for scepticism concerning VIPs. Research is being conducted on determining ways of interpreting in situ measurements and conduct reliable accelerated ageing tests. The need to better understand the mechanisms of ageing and general loss of thermal resistance over time has been mentioned by Baetens et al. (2010a), Brunner and Ghazi Wakili (2014), Schwab et al. (2005a, b, c, e) and Simmler and Brunner (2005), where various forms of accelerated climate ageing tests have been described by Wegger et al. (2011). Quality assurance of VIPs is an important factor to promote the use of VIPs in the building sector (Erb and Brunner 2012). It is important to be able to differentiate between panel damage as a consequence of production errors, and damages caused by ageing and service failures, which hence will help the technology improve further (Brunner et al. 2012a).

The first objective of this work is to present a brief overview and examples of different VIP manufacturers, products and building applications, and to evaluate the effect and durability of these products. Furthermore, it is important to know how VIPs are tested with respect to lifetime performance in building applications. These investigations may help form guidelines for a new testing scheme and point to future research opportunities. This state-of-the-art VIP review builds on already existing VIP reviews, e.g. by Alam et al. (2011), Baetens et al. (2010a), Jelle (2011), Johansson (2012), Tenpierik (2009) and Wang et al. (2007), and is extending these further by collecting and focusing on a comprehensive review with examples of existing VIP manufacturers and products. The second objective of this study is to bridge the gap from state-of-the-art VIPs to discuss and explore future research pathways for VIPs. The work presented herein is based on the earlier study given in a journal article by Kalnæs and Jelle (2014), wherein further details about specific VIP manufacturers and products may be found.

7.2 Vacuum Insulation Panel (VIP) Concepts

7.2.1 General

A VIP consists of a porous core enveloped by an air- and vapour-tight barrier. The core has an open pore structure to allow all the air to be evacuated, and to create a vacuum. The envelope needs to be air and vapour tight for the panel to uphold its thermally insulating properties over time. Figure 7.1 shows a schematic of a VIP. The initial pristine centre-of-panel thermal conductivity of the core is normally around 0.004 W/(m K), however, increasing with elapsed time due to air and moisture diffusion through the barrier envelope and into the core. In general, the thermal transport in a material may be divided as the following:

$$\lambda_{tot} = \lambda_{sol} + \lambda_{gas} + \lambda_{rad} + \lambda_{conv} + \lambda_{coup} \tag{7.1}$$

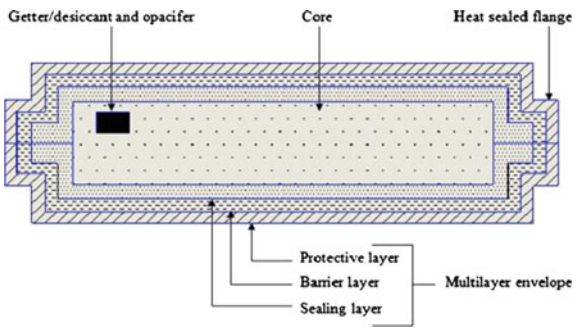

Fig. 7.1 Schematic of a VIP (not drawn to scale) (Alam et al. 2011)

where λ_{tot} is the total thermal conductivity, λ_{sol} is the solid-state thermal conductivity, λ_{gas} is the gas thermal conductivity, λ_{rad} is the radiation thermal conductivity, λ_{conv} is the convection thermal conductivity, and λ_{coup} is the thermal conductivity of coupling effects. Coupling accounts for second-order effects between the various thermal conductivity terms and is relevant for powder and fibre materials. This means that the total centre-of-panel thermal conductivity will be larger than the sum of the four first terms in Eq. (7.1) due to interactions between them. The coupling effect has been described more closely by Heinemann (2008). Another view on the coupling term stems from the interaction between the gas molecules and the solid material in the pore walls. However, this last coupling term is often included as a factor when the gas conductivity is calculated by the Knudsen effect (Jelle 2011). Coupling effects is a complex effect and is considered to be negligible in most theoretical approaches for the thermal performance of VIPs (Heinemann 2008; Wegger et al. 2011). Conventional insulation based on air-filled (larger) pores at atmospheric pressure can never aim to achieve a thermal conductivity lower than stagnant air at around 0.026 W/(m K). A VIP as a high-performance thermal insulation solution by far surpasses this with a much lower value. For non-homogenous materials or components, e.g. for a sandwich solution like a VIP, we may in Eq. (7.1) add a term accounting for the thermal bridge effects due to the VIP envelope.

As VIPs with fumed (pyrogenic) silica core type typically have a thermal conductivity value of about 0.020 W/(m K) when punctured (and about 0.004 W/(m K) in pristine condition at centre-of-panel), which is considerably below the stagnant air value of about 0.026 W/(m K), this demonstrates that the Knudsen effect is into play in VIPs, i.e. indicating air voids with dimensions down into the nano range. Hence, continued development applying nanotechnology may decrease the thermal conductivity even further in VIPs and similar material technologies. In short, the gas thermal conductivity λ_{gas} including gas–solid state interactions taking into account the Knudsen effect may be written in a simplified way as Baetens et al. (2010a), Bouquerel et al. (2012a), Jelle (2011), Jelle et al. (2010), Kaganer (1969):

$$\lambda_{gas} = \frac{\lambda_{gas,0}}{1 + 2\beta\,\mathrm{Kn}} = \frac{\lambda_{gas,0}}{1 + \frac{\sqrt{2}\beta k_B T}{\pi d^2 p \delta}} \tag{7.2}$$

where

$$\mathrm{Kn} = \frac{\sigma_{mean}}{\delta} = \frac{k_B T}{\sqrt{2}\pi d^2 p \delta} \tag{7.3}$$

where λ_{gas} is the gas thermal conductivity in the pores [W/(m K)], $\lambda_{gas,0}$ is the gas thermal conductivity in the pores at standard temperature and pressure (STP) [W/(m K)], β is a coefficient characterizing the molecule-wall collision energy transfer (in) efficiency (between 1.5 and 2.0), k_B is the Boltzmann's constant ($\approx 1.38 \times 10^{-23}$ J/K), T is the temperature (K), d is the gas molecule collision

diameter (m), p is the gas pressure in pores (Pa), δ is the characteristic pore diameter (m), and σ_{mean} is the mean free path of gas molecules (m).

The development of VIPs focuses on two main aspects of the panel, i.e. the core and the envelope. Thus, a more detailed description for these two parts will be given separately in the following.

7.2.2 The Core

7.2.2.1 Cores in General

The purpose of the core material is to provide the insulating and mechanical properties of the VIPs. Hence, there is a large focus on the core material as this is important for a VIP to attain the highest possible thermal resistance. To optimize the conditions of the VIPs, the core needs to fulfil certain requirements. These are described in a comprehensive review by Baetens et al. (2010a):

1. The core material's pore diameter needs to be small. In materials with large pores, the pressure has to be very low to obtain a low thermal conductivity. This is difficult to maintain with methods and materials in use today. By using a nano-porous material, the pressure is not required to be as low, and a low thermal conductivity can be reached with a higher pressure. The relation between effective thermal conductivity of different potential VIP core materials as function of the internal gas pressure is shown in Fig. 7.2.
2. The pore structure needs to be 100 % open so all the gas in the panel can be easily evacuated.
3. The core material needs to withstand compression. The normal range of the initial internal pressure in VIPs is between 0.2 and 3 mbar (about 20 Pa for glass fibre cores and 300 Pa for fumed silica cores). The external pressure on the panel is around 1 atm (101,325 Pa). See also Fig. 7.2.

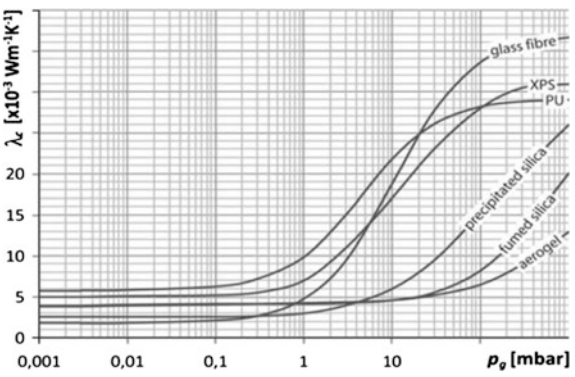

Fig. 7.2 Effective thermal conductivity of different potential VIP core materials as function of internal gas pressure (Tenpierik 2009)

4. The material has to be impermeable to infrared radiation, which will reduce the radiative heat transfer in the panel.

Several different materials are being tested for use as core materials in VIPs, such as fibre-powder composites (Mukhopadhyaya et al. 2009), polycarbonates (Kwon et al. 2011), phenolic foam (Kim et al. 2012) and ultrafine glass fibres (Di et al. 2013). Different core materials have different advantages and drawbacks. Hence, the type of core material needs to be determined for each application. Core materials found in various VIP types will be presented in the following chapters.

7.2.2.2 Fumed Silica

Fumed silica is produced by pyrolysis of $SiCl_4$, which is then vapourized and reacts with oxygen, thus forming SiO_2 which is a fine white powder. This powder is pressed into boards, normally with added fibres for structural stability and opacifiers to reduce infrared radiation (Alam et al. 2014; Caps and Fricke 2000; Caps et al. 2001). Figure 7.3 shows a VIP with fumed silica as a core.

Due to its small pore size, ranging from 30 to 100 nm, and ability to withstand compression, the fumed silica core fulfils all the criteria stated earlier. The normal material properties for fumed silica are a mass density of around 200 kg/m^3 and a thermal conductivity of 0.003–0.006 W/(m K) under a pressure of 20–100 mbar (Wang et al. 2007). However, pure fumed silica is not able to block thermal radiation very well. While the heat transfer through reduced gas conductivity in a vacuum panel is especially low, the contribution from radiation will give a significant relative contribution to the total thermal conductivity. Therefore, it is a common solution to add opacifiers to the fumed silica in order to reach an initial centre-of-panel thermal conductivity as low as around 0.004 W/(m K).

Fumed silica is a very common core material for VIPs in the building sector today. Several advantages of fumed silica make it a good choice for building applications. Silica is non-toxic, incombustible and recyclable, and it does not

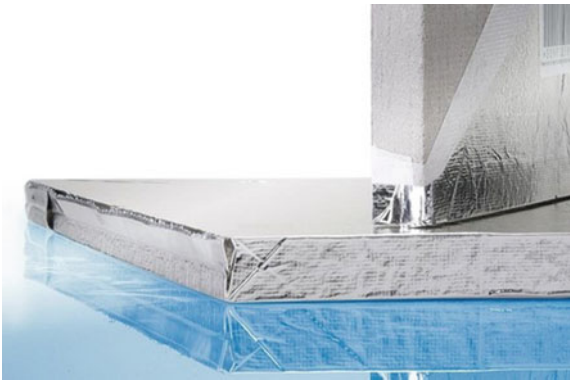

Fig. 7.3 VIP with a fumed silica core (va-Q-tec 2013)

release harmful emissions to the environment. A core of fumed silica works as a desiccant, absorbing water vapour permeating through the envelope. Applying threefold metallized laminates enabling low thermal bridge effects leads to low thermal conductivity values in the internal pressure range 1–100 mbar (Brunner et al. 2006; Ghazi Wakili et al. 2004).

In the case of panel perforation, fumed silica cores will still have a rather low thermal conductivity of around 0.020 W/(m K) at atmospheric pressure. And importantly, note then that the difference between 0.004 W/(m K) (pristine condition) and 0.020 W/(m K) (punctured) of 0.016 W/(m K) is due entirely to the gas thermal conductivity including gas–solid state interactions (see the Knudsen effect) (not taking into account any changes to the solid core due to the loss of vacuum). That is, the combined solid state and radiation thermal conductivity of fumed silica is as low as 0.004 W/(m K) or in principle somewhat lower (as there may still be a very small concentration of air inside a VIP a small part of the 0.004 W/(m K) value is due to gas conduction). Hence, as it is possible to make materials with such a very low solid state and radiation conductivity, there are rather good opportunities to make a high-performance thermal insulation material functioning at atmospheric pressure by lowering the gas thermal conductivity. That is, nanotechnology is a promising tailor-making tool for the development of high-performance thermal insulation materials, including both VIPs and other materials technologies.

7.2.2.3 Aerogels

Aerogels are produced in two steps: first, wet gel formation by acidic condensation or solgel process and second, the wet gel is dried by using supercritical or ambient drying. This produces a nanoporous material with pore sizes around 20 nm and a mass density that can vary from 3 to 350 kg/m^3. When used as a core material for VIPs, aerogels may deliver a low thermal conductivity. At an ambient pressure of 50 mbar, and with an addition of carbon black to suppress the radiative transfer, silica aerogels may reach a low thermal conductivity of 0.004 W/(m K), whereas at ambient pressure the thermal conductivity rises to 0.0135 W/(m K) (Baetens et al. 2011; Jelle et al. 2015e).

Silica aerogel is non-flammable and non-reactive. However, due to its high cost, aerogel-core VIPs are not yet an economically reasonable product for building applications. Nevertheless, aerogel may be used as a heat bridge breaker in buildings and structures where space is restricted. Furthermore, in its translucent or transparent state, aerogel has an added value which may be exploited in several building applications. Aerogel boards and aerogel renders are emerging innovations of the last few years regarding building applications of aerogel. While the building application of aerogels is still rather small, thermal insulation of various technical installations with aerogel sheets are more common. Regarding the above-mentioned high cost, there are interesting activities ongoing worldwide to lower the cost.

7.2.2.4 Polyurethane and Polystyrene Foams

Polyurethane (PUR) and polystyrene (PS) foams are widely used thermal insulation materials by their own. The first VIPs were created with PUR foams as the core material. PUR has the mechanical strength and the open pore structure required for a core material. However, the pore size in PUR and PS is larger than in fumed silica and aerogel. That is, a PUR or PS core requires a lower vacuum to reach the same low thermal conductivity as the fumed silica and aerogel. For a VIP with a PUR or PS core to maintain its designed low thermal conductivity value, the pressure has to stay below 1 mbar (see e.g. Fig. 7.2), over this value the conductivity will rise substantially (Fricke et al. 2008; Yang et al. 2012). This is not feasible with the envelopes of today. PUR and PS foam core VIPs are less expensive to produce, but the short effective lifetime of these panels do not make them as fit for building applications.

7.2.2.5 Glass Fibre

Glass fibre cores have similar issues as PUR foam cores, but with the advantage of lower centre-of-panel thermal conductivity values. Because of the relatively large pore size, ranging from 1 to 12 μm, the gas pressure needs to be very low for the panel to maintain its low thermal conductivity. At a gas pressure of about 0.1 mbar, the centre-of-panel thermal conductivity can be as low as 0.0015 W/(m K). Because of its high thermal stability, Araki et al. (2009) have investigated the use of glass fibre core VIPs for high-temperature applications. The core material itself is relatively inexpensive, but Di et al. (2013) concluded that the lifetime expectancy for a glass fibre core VIP is about 15 years. This is the commonly requested lifetime for refrigerators, but far too low for glass fibre VIP cores to be considered as a choice for building applications. As of today, it is still mostly used for shipping containers, freezers, etc. Using ultrafine glass fibre core VIPs for building applications has recently been mentioned in an article by Boafo et al. (2013). However, so far no monitoring tests have been found with these VIP types.

7.2.2.6 Desiccants, Getters and Opacifiers

A major and crucial drawback of VIPs is the thermal conductivity increase as time passes. The low conductive heat transfer of VIPs is highly dependent on a low gas pressure inside the panel. Vapour and gases that permeate through the envelope therefore contribute to a lower effectiveness of VIPs. To counteract this and to increase the expected service lifetime of VIPs, desiccants and getters are often added to the core, especially for VIPs with longer requested durability like for refrigerators and buildings. These are components or chemicals that adsorb residual or permeating gases (getters) or water vapour (desiccants). They will maintain a steady thermal conductivity inside the core until their capacity is reached.

Desiccants are made of highly hydroscopic materials and work by entrapping moisture. Getters are highly porous structures with large surfaces. They work by attracting and bonding with permeating gases to maintain a low pressure inside the panel. Some core materials have properties that fulfil the functions of desiccants and getters themselves, so they are not always necessary to add. Even though these materials slightly increase the solid-state thermal conductivity and increase the costs of a panel, they are important to add (Thorsell 2012). Opacifiers are added to the core of the panel to reduce the heat loss through thermal (infrared) radiation. With added opacifiers, the radiative thermal conductivity can be decreased to a value below 0.001 W/(m K) (Bouquerel et al. 2012a). Fumed (pyrogenic) silica does act as a desiccant and has good thermal performance at an internal pressure level, where no getters may be needed.

7.2.3 The Envelope

7.2.3.1 Envelopes in General

The main purpose of the envelope is to provide an air- and vapour-tight enclosure for the core material, i.e. to maintain a vacuum in the VIP core. Furthermore, it is important that the envelope does not introduce a too large thermal bridge effect. As the thermal performance of VIPs is highly dependent on the conservation of the vacuum inside, any gases or water vapour that permeates through the barrier will diminish the effectiveness of VIPs. This makes a VIP a fragile thermal insulation material compared with conventional insulation (Wegger et al. 2011). Permeation through the envelope is also affected by the outer environment. Changes in temperature and relative humidity will affect the permeation rate (Simmler and Brunner 2005).

Depending on the choice of envelope, thermal bridging around a VIP and the VIP dimensions are also significant factors to consider. The core material has great insulating properties; however, thermal bridging from the envelope material and the gaps between two adjacent VIPs will increase the panel equivalent thermal conductivity for an area covered with VIPs. An increase in panel dimensions will lead to a decrease in the thermal bridging effect. Hence, one should aim to use the largest panel dimensions possible (Ghazi Wakili et al. 2005). Further studies on the thermal bridging effect of VIPs in both single and double layers have been conducted by Ghazi Wakili et al. (2004, 2011). Note that with larger panel dimensions, larger areas and volumes of the building envelope will have a reduced thermal resistance when some of the VIPs are punctured.

The envelope is often divided into the sealing layer, the barrier layer and a protective layer as seen in Fig. 7.4. These layers are described by Alam et al. (2011) and Brunner et al. (2006). The inner layer is the sealing layer. This layer seals the core material in the envelope, and traditionally consists of low- or high-density polyethylene (PE). The laminate surfaces are heat-sealed by two hot bars under

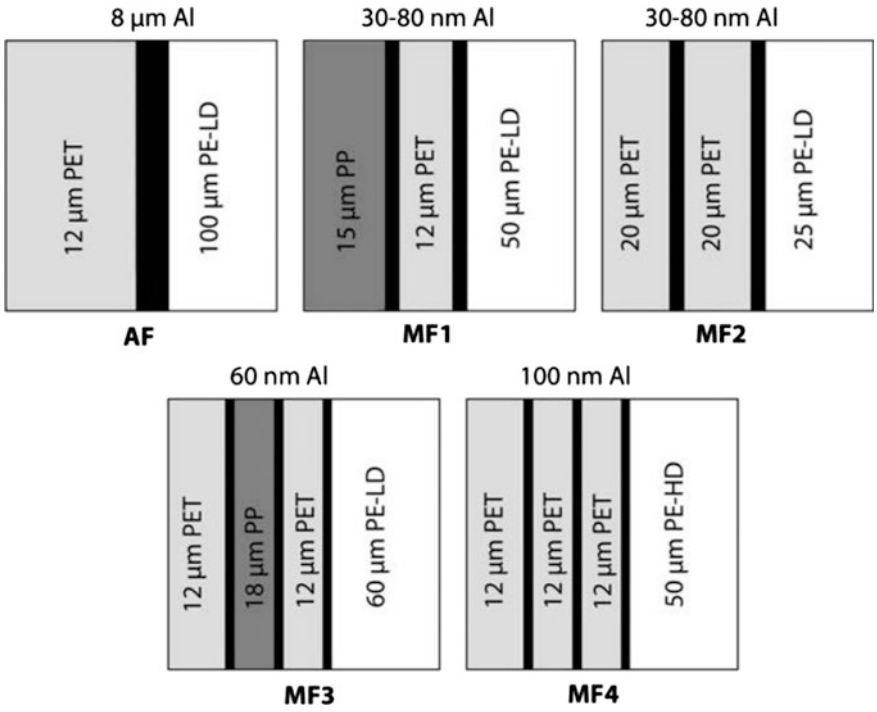

Fig. 7.4 Illustration of an aluminium foil laminate (AF) and metallized polymer film MF [Wegger et al. (2011) based on Simmler et al. (2005), see also Brunner et al. (2006) and Simmler and Brunner (2005)]

pressure to bond together. The middle layer is the barrier layer in the case of the aluminium foil laminate (AF) type (Fig. 7.4). Furthermore, metallized polymer film multilayer laminates (MF) are in common usage, where the metallized coating is typically deposited on a polyethylene terephthalate (PET) film (Fig. 7.4). The purpose of the barrier layer is to prevent water vapour and air transmission through the envelope and into the VIP core. An outer protective layer may be added, e.g. for improving the fire resistance properties, and may consist of glass fibre fabric or transparent lacquer. Environmental and handling stresses may damage the panel, so sometimes an additional protective layer aims to make the panel more robust, e.g. applying expanded polystyrene (EPS), extruded polystyrene (XPS) or rubber granule layers or hard polymeric plates. The material chosen for the envelope should also be able to withstand general handling through transportation and installation without tearing. The common PET layer also works as a substrate for the barrier layer due to its superior flatness for the metallization process (coating).

The sealed edges in a panel may often be a weak point in maintaining the vacuum, especially for cores with high vacuum demands such as the glass fibre ones. The sealing is a complex process which is important to develop a further

understanding in order to maximize the lifetime of VIPs. Important factors in the heat sealing process are mentioned by Marouani (2012).

7.2.3.2 Metal Foil Laminate

The solution with a metal foil laminate, most commonly aluminium foil laminate (AF), consists of a central aluminium foil (with a thickness of 5–10 μm) as a barrier layer, laminated between an outer PET protective layer for better scratch resistance and an inner PE sealing layer (see Fig. 7.4). The complete aluminium foil laminate (AF) is also often called just aluminium foil (AF).

Aluminium laminate as a barrier layer lowers the permeation through the envelope, increasing the lifetime of a panel. However, the thickness of the metal laminate contributes to a higher thermal bridging effect as the thermal conductivity for aluminium is 210 W/(m K), compared to the core at around 0.004 W/(m K), and the polymer layers at 0.25–0.30 W/(m K). For a high-performance insulation material, this thermal bridge effect will have severe effects on the equivalent thermal resistance of VIPs (Bouquerel et al. 2012b; Brunner et al. 2006; Ghazi Wakili et al. 2004). Another envelope type based on stainless steel is also advocated by some.

7.2.3.3 Metallized Polymer Film Multilayer Laminate

The metallized polymer film MF solution consists of up to three barrier layers of metal-coated PET films and an inner sealing layer of PE. The coating is performed with aluminium with a thickness of 20–100 nm (see Fig. 7.4) by a process called vacuum web coating. For applications requiring shorter durability than for building applications, also laminates with two barriers are on the market.

The MF solution is, as of today, the common solution for VIPs intended for building applications. The multiple aluminium layers give the envelope a better protection from permeation compared with a single layer and thus with a reduced total thickness, while the polymers reduce the thermal bridging effect. The MF consists of two to three barrier layers, though triple-layered MF is common among VIPs for building applications as of today. However, the reduced total metal thickness for MFs compared to AFs leads to a considerably faster moisture and air permeation through the VIP envelope and into the core for VIPs with MF envelopes, as determined by Schwab et al. (2005a, b, c, d, e), Simmler and Brunner (2005) and Simmler et al. (2005) for VIP cores of mainly fumed silica. Hence, during several years the centre-of-panel thermal conductivity will increase much faster in VIPs with MF envelopes than with AF envelopes. For thermal conductivity versus time up to 100 years for various VIP dimensions and envelopes, refer to the studies by Baetens et al. (2010a) and Wegger et al. (2011), see Fig. 7.5 (various VIP envelopes). Furthermore, see also the studies by Schwab et al. (2005a) and Simmler and Brunner (2005).

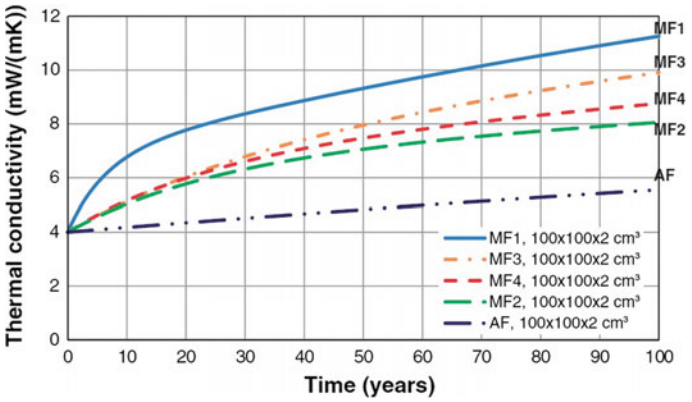

Fig. 7.5 Thermal conductivity versus time for different VIP envelope solutions (Wegger et al. 2011). Note that an air transmission rate per panel area (ATR_A) for *MF2* was not resolvable due to tested on limited panel size; hence, the thermal performance of VIPs with *MF2* is expected to be slightly overestimated in the given graphical plot above and would probably be between the *MF1* and the *MF3* plots

7.3 State-of-the-Art Vacuum Insulation Panel Products

7.3.1 VIP Products

VIPs are most commonly used for refrigerators, freezers, and shipping boxes and containers for temperature sensitive materials. However, for the last decade the most interesting aspect of VIPs has been their growing introduction to the building sector. In the following, a short explanation of the use of VIPs in appliances will be given. Thereafter, the use of VIPs in constructions up until today will be looked upon. Both laboratory experiments and in situ measurements will be treated. As it would be too extensive to show all the possible buildings that have been tested with VIPs till now within this study, only a handful of selected examples will be given. Through these examples, the use of VIPs, experiences learned during construction and monitoring after completion will be explored.

Tables 7.1, 7.2 and 7.3 show examples of different VIP products available on the market today. The tables have been divided into VIPs for appliances (Table 7.1) and VIPs specified as possible to use in buildings (Tables 7.2 and 7.3). The VIPs for building applications have been further divided into VIPs that are delivered as unprotected panels (Table 7.2) and VIPs that are delivered with various protective coverings (Table 7.3). These tables give a short overview of the different products. Further information and details about the manufacturers and the products are given in the study by Kalnæs and Jelle (2014). For more VIP manufacturers, see, e.g. the members of the Vacuum Insulation Panel Association (VIPA 2015).

In a worldwide context, the core materials for VIPs that are intended for appliances mostly consist of materials with larger pores or aerogel powders, while

Table 7.1 Literature data for examples of manufacturers of VIPs for appliances

Manufacturer	Product	λ^{e} [W/(m K)]	Initial gas pressure	Core	Envelope
Jinko	VIP	0.001–0.006[a]			
Rparts	VIP				
Va-Q-tec	va-Q-pur	0.007–0.009[a]	<1 mbar	PUR foam	Al foil
	va-Q-mic	0.0028–0.0035[a]	<1 mbar	Micro-fleece	
Foamcore INC	Therm-max	R-40 per inch[a]		Aerogel	MF
Nanopore	VIP	0.004		Silica, titania and/or carbon	MF
Guangdong	VIP				
Xiamen Goot	VIP	0.004[a]	<0.1 Pa	Fibre glass	
American Aerogel	Aerocore VIP	0.0019–0.0042[a]		Organic aerogel	MF
Fujian Supertech	VIP	0.0025[a]			
Porextherm	Vacupor NT			Fumed silica, opacifiers	MF
	Vacupor MS			Fumed silica, opacifiers	MF
Microtherm	VIP			Fumed silica, opacifiers	MF
Unifrax	Exelfrax 200	0.00375		Fumed silica, opacifiers	Laminated PE film

See the study by Kalnæs and Jelle (2014) for further information
[a]No specific information given
[b]Aged value allowing for edge effect
[c]Initial value
[d]Rated value
[e]Aged thermal conductivity values and lifetimes are not given for most of the VIP products, although these are very crucial properties for the VIPs

in Europe the VIP production is to the authors' insight clearly dominated by cores of fumed (pyrogenic) silica and similar fine powder cores. As explained earlier, aerogel is still too expensive to be a reasonable choice for most building applications, but its excellent thermal properties at a higher pressure give aerogel a higher expected lifetime. Aerogel as a term describes a class of materials with monoliths, particles/granulates and even finer ones as powders. The distinction between powder aerogel and precipitated silica from their properties may get smaller and more unclear, e.g. if the applied powder should be named as an aerogel. Core materials with larger pore sizes such as glass fibres are expected to lose the low thermal conductivity earlier than materials with a smaller pore size due to permeation through the envelope. However, these materials with larger pore sizes are also less expensive. More detailed information about the manufacturers and products can be found in the study by Kalnæs and Jelle (2014).

Table 7.2 Literature data for examples of manufacturers of VIPs for building applications

Manufacturer	Product	λ^e [W/(m K)]	Initial gas pressure	Core	Envelope
va-Q-tec	va-Q-vip	0.005[a]	<5 mbar	Fumed silica	High gas barrier film
	va-Q-plus	0.0035[a]	<5 mbar	80 % fumed silica, opacifiers, organic fibres	
	va-Q-plus A	0.0035[a]	<5 mbar		
Panasonic USA	U-Vacua	R-60 per inch[a]			
Neofas AG	Vakutherm	0.0045[c]–0.008[b]		Pyrogenic silica	MF
Qingdao	Creek VIP	0.0035[a]	<0.001 Pa	Fibre glass	
ThermoCor	VIP				
Caralon Global	CG Max-Thermic	0.0038[a]	<1 mbar	Inert alkaline earth silicate glass wool	Al_2O_3
LG Hausys	VIP	0.004[a]		Glass fibre board	Al laminated film
Porextherm	Vacupor NT-B2-S	0.005[c]	<5 mbar	Fumed silica, opacifiers and fibre filaments	MF
	Vacuspeed	0.0043[c]	<5 mbar	Fumed silica, opacifiers	MF
	Vacupor NT		<5 mbar		
Dow Corning	VIP	0.00369[c]		Fumed silica	MF
Microtherm	Slimvac	0.0042[c]	<5 mbar	Filament reinforced silica and opacifier	MF
Vaku-isotherm	Standard	0.005[c]		Fumed silica, opacifiers and cellulose fibres	MF
	VakuVIP B2	0.005[c]		Fumed silica, opacifiers and cellulose fibres	MF
Variotec	QASA	0.007[a]	<7 mbar	Pyrogenic silica, opacifiers	
Suzhou VIP	VIP	0.008[a]		Glass fibre	
Kingspan	OPTIM-R	0.007[b]			
Nanopore insulation	VIP				

See the study by Kalnæs and Jelle (2014) for further information

[a]No specific information given

[b]Aged value allowing for edge effect

[c]Initial value

[d]Rated value

[e]Aged thermal conductivity values and lifetimes are not given for most of the VIP products, although these are very crucial properties for the VIPs

Table 7.3 Literature data for examples of manufacturers of VIPs with added protective coverings, i.e. sandwich VIPs, for building applications

Manufacturer	Product	λ^e [W/(m K)]	Initial gas pressure	Core	Envelope
va-Q-tec	va-Q-vip B	0.0043[c]	<5 mbar	Fumed silica	Foil and glass fibre
	va-Q-plus B	0.0035[c]	<5 mbar	80 % fumed silica, opacifiers, organic fibres	Foil and glass fibre
Porextherm	Vacupor XPS-B2-S	0.005[c]	<5 mbar	Fumed silica, opacifiers and fibre filaments	MF + XPS
	Vacupor RP-B2-S	0.005[c]	<5 mbar	Fumed silica, opacifiers and fibre filaments	MF + rubber granulate
	Vacupor PS-B2-S	0.005[c]	<5 mbar	Fumed silica, opacifiers and fibre filaments	MF + PS sheet
	Vacupor TS-B2-S	0.005[c]	<5 mbar	Fumed silica, opacifiers and fibre filaments	MF + sound absorbing plastic board
Vaku-isotherm	Gum-1	0.005[c]		Fumed silica, opacifiers and cellulose fibres	MF + rubber granulate
	SP-1	0.005[c]		Fumed silica, opacifiers and cellulose fibres	MF + PS
	SP-2/E	0.005[c]		Fumed silica, opacifiers and cellulose fibres	MF + PS plates and sides covered with EPS
	Protekt-1	0.005[c]		Fumed silica, opacifiers and cellulose fibres	MF + fleece
	Bauplatte	0.005[c]		Fumed silica, opacifiers and cellulose fibres	MF + plastic plates and sides covered with EPS
	Sandwich Paneel 1	0.005[c]		Fumed silica, opacifiers and cellulose fibres	MF + glass plates and sides covered with EPS
	Sandwich Paneel 2	0.005[c]		Fumed silica, opacifiers and cellulose fibres	MF + glass/Al and sides covered with EPS
	Sandwich Paneel 3	0.005[c]		Fumed silica, opacifiers and cellulose fibres	MF + Al/Al and sides covered with EPS

(continued)

Table 7.3 (continued)

Manufacturer	Product	λ^e [W/(m K)]	Initial gas pressure	Core	Envelope
Variotec	QASA	0.007[a]	<7 mbar	Pyrogenic silica, opacifiers	

See the study by Kalnæs and Jelle (2014) for further information
[a]No specific information given
[b]Aged value allowing for edge effect
[c]Initial value
[d]Rated value
[e]Aged thermal conductivity values and lifetimes are not given for most of the VIP products, although these are very crucial properties for the VIPs

Table 7.2 shows examples of manufacturers of VIPs with products that can be applied for building constructions. The general choice for core material among these VIPs is dominantly fumed silica. One important factor which is lacking for almost all producers is an expected lifetime of the VIP. As mentioned earlier, the difficulty in predicting a useful lifetime for VIPs is one of the main reasons VIPs are still struggling to become a renowned choice for thermal building insulation. Some manufacturers do however mention a theoretical rise in gas pressure per year. This value is in the range of 0.5–4 mbar/year. Note that VIPs applied for building constructions may also be used for other purposes. More information about the manufacturers of VIPs intended for buildings and their products can be found in the study by Kalnæs and Jelle (2014).

Table 7.3 shows examples of manufacturers who produce VIPs with added protective coverings for building applications. The benefits of such sandwich panels are explained in more detail later. More information about the manufacturers of sandwich VIPs and their products can be found in the study by Kalnæs and Jelle (2014).

From the products found on the market, it is clear that fumed silica is the current choice for building applications, while various core materials are used for all other applications. Product-related requirements that separate VIPs intended for buildings from other VIPs have been discussed by Tenpierik et al. (2007). These are requirements concerning structural stability, fire protection, hygiene, health and environment, application safety and fitness for use, acoustic performance, thermal performance and service life. VIPs for building applications put more requirements on the core material. As seen in Fig. 7.2, fumed silica cores can maintain a stable thermal conductivity up to about 10 mbar and has a centre-of-panel thermal conductivity of about 0.008 W/(m K) at 100 mbar. This gives VIPs with silica cores a higher expected lifetime. Further advantages of fumed silica for building applications have been discussed earlier in this review. Even though the cost of fumed silica is higher than glass fibre or PUR foam, it is necessary to fulfil the requirements for building applications.

VIPs have been used with success in applications for some years. Glass fibre and PUR foam may give the same initial thermal conductivity as silica core VIPs, but the expected lifetime is lower and various other requirements are not so strict for VIP cores of glass fibre or PUR foam. Glass fibre or PUR foam cores are also less

expensive to produce, making these VIP cores a better choice whenever they are possible to use. In this study, it is found that producers of building intended VIPs from Europe offer a large variety of different covering solutions for their products, which is well intended for use in buildings as they make the products more robust. However, the VIP coverings may also represent some drawbacks. For example, covering a VIP with EPS makes it more difficult to detect loss of vacuum, and furthermore, the EPS has a higher thermal conductivity than the VIP area and thickness (volume) it replaces (Jelle 2011).

Overall, there are very few producers who state an expected lifetime and a guarantee for their panels. Some manufacturers state a lifetime service which is only valid for specific conditions and therefore not possible to compare with conditions in use. Many of the thermal conductivities are given without stating anything else. For the customers of this product, an aged value or an intended design value is important. However, as this study will discuss later, these values rely on many factors concerning the environment in which the product is applied. Therefore, many manufacturers state that the values are only for guidance, and that each case has to be considered specifically.

7.3.2 VIPs in Appliances

VIPs have shown good results in domestic appliances and for logistic purposes. Recently, researches on VIPs that can withstand higher temperatures have also been performed. These VIPs have been introduced to insulate hot-water equipment and other high-temperature applications (Araki et al. 2009; Berge and Adl-Zarrabi 2014). For most typical appliances such as refrigeration, thermal packaging, the normal lifetime expectancy for these panels are seldom required to exceed 15 years. This makes it possible to use glass fibre or PUR cores for these VIPs. Requirements are not so strict for general applications as broken panels rarely lead to anything else than replacing a broken ware.

7.3.3 VIPs in the Building Sector

7.3.3.1 VIPs in Monitoring Projects

VIPs show great promise as a thermal insulation material solution for today and the near future. However, there are several drawbacks that have to be addressed when considering VIPs for building applications. A VIP requires a low pressure inside. If the panel is perforated or broken in any way which leads to a loss of this vacuum, the thermal conductivity will increase to about 0.020 W/(m K) for VIPs containing fumed silica. Cutting and adapting the panel on-site is not possible. Insulating a building with VIPs therefore requires detailed planning from an early stage and a

layout plan of how and where the panels shall be put into place. Practice also shows that the most common cause of damage to the panels occurs before and during installation (Kunic 2012). Extra precautionary matters need to be taken with the handling of VIPs as they are a fragile construction material. Damaged panels do not only decrease the thermal resistance of the building, but depending on how the VIPs are implemented there is also a risk of condensation and possibly mould growth (Parekh and Mattock 2011).

In Germany, there have been a lot of test projects with constructions implementing VIPs, both refurbished and new constructions. Some were built as early as 2001 and have been monitored on a regular basis since. Bayerisches Zentrum für Angewandte Energieforschung (ZAE Bayern) in collaboration with various VIP producers have many interesting projects which show how the implementation of VIPs into buildings has proceeded. ZAE Bayern conducted a research project called VIP-Prove, where the aim was to see how VIPs behaved under practical conditions. To choose these projects, ZAE Bayern had certain criteria the buildings had to fulfil, giving them a score up to 85 points, where the higher the score was the more suitable a construction was for monitoring.

The first criterion (Heinemann and Kastner 2010) depended on how suited the construction elements were for a thermographic scanning. When conducting a thermographic scan of the building element, the VIPs should not be covered with heavy building elements or air-filled spaces that would disrupt the measurements and give unclear results to whether the panels are functioning as planned or not. Figure 7.6 shows a thermographic scan which shows a presumably broken panel

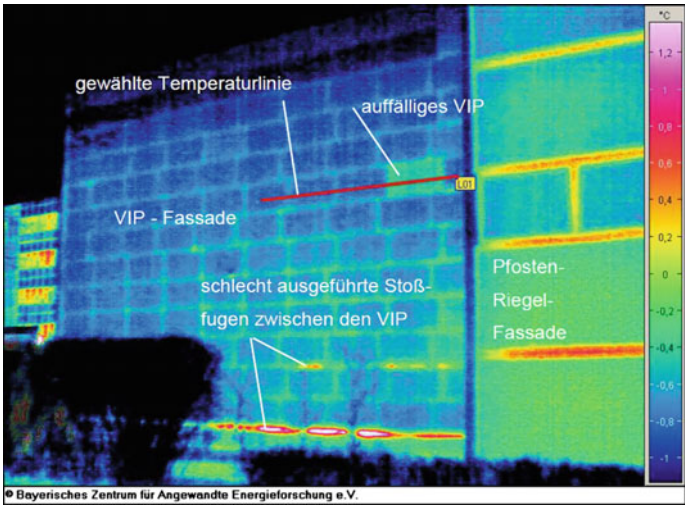

Fig. 7.6 Thermography of a VIP facade from the outside. Due to the very high-temperature resolution of the thermography even the week pronounced regular effect of thermal bridging at the joints may be seen. The *green square* denoted as "auffälliges VIP" (conspicuous VIP) shows a VIP presumably no longer evacuated, whereas the *red* and *white lines* indicate poorly executed joints (Heinemann and Kastner 2010)

and the thermal bridges between the panels, where it is also seen that several of the joints between the panels have been poorly executed. The second criterion was how many different areas the VIPs could be applied to. More areas which could be applied with VIPs were to prefer, as this would give more and comparable results within the same building. The third criterion was the age of the panel. Preferably, VIPs that had been implemented before 2005 should be monitored. The longer the panels had been in the building, the more interesting it was to study if and how their properties had changed. The fourth criterion was the possibility to conduct other measurements to show the results of the thermal performance of the panels. These results could be used in comparison with the thermography measurements.

For the VIP-Prove project, a total of 29 objects with an area of 8206 m^2 installed with VIPs were assessed. Out of these, 19 objects with an area 3224 m^2 installed with VIPs were found to be suitable for investigation by thermographic scanning. These 19 objects were also further investigated by determining the heat transfer coefficient and the internal pressure of the VIPs. The results showed that 12.8 % of the VIPs in these 19 objects were classified as faulty. However, three buildings were particularly faulty and stood out in the statistical evaluation. By removing these three buildings, the per cent of broken panels fell to 4.9 %. This might mean that these three projects have failed to handle the panels properly, that they have been installed wrongly or that a production error has affected many of the panels (EnOB 2013). Some of these monitoring projects will be mentioned in the following chapters about new and refurbished constructions.

7.3.3.2 Lifetime Predictions

The useful lifetime can be explained as the time until the centre-of-panel thermal conductivity reaches a critical (high) level. Usually this point is at around 0.008 W/(m K), meaning that when *U*-values are being calculated this should be the design value (Simmler and Brunner 2005). The VIPs will still function when this value is reached, but the thermal conductivity will continue to increase, thus also increasing the *U*-value and heat loss.

For VIPs meant for building applications, the lifetime is one of the most important and crucial properties. Buildings should be dimensioned with a lifetime of up to at least 50 years in mind, preferably up to 100 years. Today, most VIPs using a MF3 laminate can be said to have a lifetime of over 25 years under specific conditions (Baetens et al. 2010a; Heinemann and Kastner 2010; Simmler and Brunner 2005). The uncertainties surrounding the exact lifetime of VIPs when they are in use are still major factors for scepticism. Predicting the useful lifetime of VIPs has therefore been an aim of many studies. Accelerated climate ageing and comparative ageing of in situ panels and panels kept in laboratories have been conducted. The focus here is on permeating gases and water vapour through the envelope, as this increases the thermal conductivity. VIPs for building purposes should never have an increase of more than 2 mbar/year (Schwab et al. 2005a). For

a panel with fumed silica, an increase of 2 mbar/year would equal a lifetime of almost 50 years.

A laboratory ageing test of 20 VIPs performed by The National Research Council-Institute for Research in Construction (NRC-IRC) in Canada over seven years showed that the average loss of *R*-value was about 2 % per year. In a test-hut wall of the NRC construction, 18-month field exposure was performed with 5 different VIP products, 15 specimens from different manufacturers showed 5 % ageing in 4 out of 5 products, and 2 out of 15 specimens failed. Therefore, they concluded that VIPs show promising long-term performance for service life of 25–50 years (NRC 2012).

Wegger et al. (2011) mentioned that there are no standardized ways of performing accelerated ageing tests for VIPs. To get a prediction of a VIP's effective lifetime within a shorter time frame, such tests will be necessary to define. Several factors such as pressure, temperature, ultraviolet and infrared radiation, moisture, water exposure and freezing/thawing were tested, along with various climate cycling tests. The results showed that the change in performance was relatively low compared to the initial thermal performance. However, two of the panels which were tested showed signs of failure from other factors than the accelerated ageing testing. This shows that VIPs are still a fragile material when exposed to high moisture and temperature, or that they may have defects from the manufacturing process.

7.3.3.3 Economics

Modern-day passive houses built with traditional thermal insulation require a wall thickness of 35 cm or more, meaning that a large part of the building volume is filled up by insulation. By building with VIPs, the required thickness can be reduced, thus increasing the value of a building through increased living space. VIPs are still far more expensive than conventional insulation; however, studies have been made to show that the increased living space achieved by decreasing the wall thickness may still make VIP a more economically favourable choice. Studies that mention the cost benefit of the increased living space have been conducted by Alam et al. (2011) and Jelle (2011). Alam et al. (2011) also show that the payback time for VIPs is drastically reduced if the benefit of the increased usable area is included. This is based on that each square metre gained will lead to increased market value, which naturally is highly dependent on the value per square metre in the given area. For frame constructions, there is also a possibility to reduce the use of materials where the size of the cavity traditionally has been increased to fit the thickness of conventional thermal insulation beyond what has been required for structural strength, i.e. by applying VIPs instead. This will lead to a reduction in use of materials and also reduce the transportation of materials to the building site. The economical impact of this has so far not been discussed in detail.

7.3.3.4 Acoustic Performance

Enabling thinner layers of thermal insulation is a clear benefit when constructing with VIPs. However, from a building physical point of view, thermal insulation is not the only factor to consider. The impact on acoustic performance must also be taken into account (Lenz et al. 2005). Baetens et al. (2010a) mentioned that the acoustical properties and knowledge of VIPs could be divided into three groups when used for building insulation purposes: (i) A single VIP, (ii) VIPs built into sandwich elements and (iii) insulated massive walls with built-in VIPs. Maysenhölder (2008) studied the three different groups. For a single VIP, it was found that it has a critical frequency in the range of speech and traffic noise ($\sim$1 kHz), which reduces the sound reduction in this range. It was also found that perforating a VIP would reduce the sound reduction. However, he concluded that it would be more beneficial to study the acoustical properties in layered systems with internal VIPs, rather than single VIPs by themselves. Various sizes and core materials will also affect how a VIP performs acoustically. Further information concerning acoustical properties of VIPs may be found in the work by Tenpierik (2009). The focus forward for acoustic studies should be on VIPs in such practical applications, i.e. layered systems. To the authors' knowledge, there is a limited literature on the acoustical properties of VIPs available. Forward, field measurements on VIP systems should be conducted to obtain more results on how VIPs perform acoustically. Thus, even though the thermal properties of VIPs represent the major driving forces, it is also important to address the other building physical properties such as the acoustical properties.

7.3.4 VIP Sandwich Elements

For building projects completed so far, it is evident that most of the damaged panels have been damaged during transport or while they are being installed at the building site. In order to protect VIPs, both under construction and during usage, encasing the panels with other materials, may be a good solution. Such sandwich elements will reduce the risk of damaging the panels unintentionally. Some of the solutions also completely envelope the sides of the panels with EPS (Nussbaumer et al. 2006). This is a favourable solution for adapting the panels on-site as the EPS can be cut to fit the panels in the construction without perforating the VIPs. However, note that the EPS (or other) covering makes it more difficult to discover loss of vacuum. Besides, EPS has a higher thermal conductivity than the VIP area and thickness (i.e. volume) it replaces (Jelle 2011).

Some manufacturers already produce finished sandwich elements of different kinds, with protective layers such as granulated rubber, glass fibre boards, aluminium or glass plates and PS plates. Different sandwich solutions are given in Table 7.3. Another solution, where it is possible, is to prefabricate building elements with integrated VIPs. This is by some referred to as a structural vacuum panel

(SVP) as demonstrated in Fig. 7.7. Producing SVPs can be performed under controlled conditions where the risk of damaging panels can be reduced. The VIPs inside the finished elements will also be a lot less likely to be damaged during transport.

A prefabricated building from Scotland has been built using SVPs, showing that it is possible to attain a low *U*-value. This building was built with 125-mm-thick SVPs with a 25-mm VIP at its core. The overall *U*-value for the wall ended up at 0.10 W/(m^2K) for a thickness of 234 mm (Kevothermal 2012). However, prefabrication of buildings and various building elements are entirely different issues which will have to be addressed for each individual project and the desires of the end users.

Fig. 7.7 Illustration of a structural vacuum panel (SVP) (Kevothermal 2012)

7.3.5 Constructing with VIPs

VIPs may be applied to many different areas of a construction. This chapter will shortly describe some of the most common areas which are suited for VIP applications and discuss some important considerations when they are applied to these areas. More detailed information on different areas where VIPs can be implemented and more detailed descriptions on building details have been made by Johansson (2012).

7.3.5.1 Facades and Walls

For facades, it is possible to either thermally insulate the exterior or the interior part of the wall. For frame constructions, there is a third possibility to insulate inside the cavity as well.

Internal facade insulation with VIPs may be an excellent choice for retrofitting as long as the moisture issues are well addressed utilizing building physics expertise. The thin layers of VIPs required, compared to conventional insulation, will enable lower *U*-values after retrofitting without the same loss of indoor space. This is especially interesting for listed buildings where the outside design is not allowed to be altered. However, careful planning concerning low exterior surface temperatures, increased number of freezing/thawing cycles and the risk of condensation has to be made to avoid damages and mould forming. See, e.g. the hygrothermal numerical simulations and laboratory investigations concerning interior insulation retrofit of a historical brick wall using VIPs by Johansson et al. (2014).

Insulating the outer facades is beneficial for the reduction of thermal bridging and can be made easy by using adhesives to stick the VIPs to the facade.

In wall constructions, VIPs will not only give positive results in reduced energy usage, but also be quite visible through slimmer wall constructions. As mentioned earlier, this will work towards making VIPs more economically favourable with respect to increased indoor living space.

7.3.5.2 Glazing Structures

For glazing structures, the transition between glass areas and opaque areas may be made more architecturally appealing by insulating with VIPs. The high thermal resistance enables slim facades and smoother transitions (see, e.g. Fig. 7.8). In some areas, VIPs were integrated into the glazed parts between enamelled glass panes (Pool 2009).

Fig. 7.8 Residential and office building in Munich, photograph by Sascha Kletzsch (BINE Informationsdienst 2013)

7.3.5.3 Doors

Due to a restricted thickness, doors are a part of a construction which is hard to insulate properly with traditional insulation, and hence, the doors become a source for heat to leave the building. By inserting a VIP into a door, it is possible to increase the thermal resistance of doors and thus reduce the total heat loss from the building. Nussbaumer et al. (2005) showed that a wooden door system with an implemented VIP reduced the energy usage for the doors by 25 %.

7.3.5.4 Roofs

VIPs for roofing purposes have been tested for both flat roofs and sloped roofs. VIPs have shown to be especially good for roofs under terrace floors, where conventional insulation often makes it hard to get the entrance in line with the outer floor because of the requirements for insulating properly over the room below. Here, the VIPs enable a thinner insulation layer making it possible to insulate within the requirements and at the same time enabling an entrance in line with the outside floor.

Brunner and Simmler (2008) have monitored VIPs in a flat roof construction over a three-year period. Assuming that the initial thermal conductivity was 0.0045 W/(m K) and the practical service life ended when the thermal conductivity exceeded 0.008 W/(m K), the panels used had an expected lifetime of about 25 years.

7.3.5.5 Floors

Gaining space through insulating with VIPs in the floor is not highly economically beneficial. Nevertheless, for rooms with large temperature difference demands such as cold storage rooms, the use of VIPs may be a good choice for reducing energy demands. Furthermore, in heated floors VIPs may increase the efficiency of the floor heating system. VIPs may also represent a good choice when there are different space or thickness restrictions, e.g. restricted floor to ceiling height. Finally, transitions between floors and outdoor areas can be made stepless by insulating with VIPs.

Refurbishing poorly insulated floors may also be accomplished with VIPs. An example from UK showed that insulating over an existing concrete floor slab could reduce the *U*-value from 0.78 to 0.15 W/(m^2 K) by using 20-mm VIPs. The new floor had a minimal increase in thickness (Kevothermal 2011).

7.3.6 New Construction Examples

Selected examples of new constructions with VIPs will be shown here. These examples will be given to illustrate how VIPs may be implemented in new buildings. General considerations and experiences that were learned from these examples will be given as well. Building details will not be discussed in detail as these vary from each individual project. As VIPs are still considered as a new material solution in the construction sector, there are still a lot of uncertainties about how they actually perform when implemented in a building, and how to plan the construction phase with VIPs. Different forms of buildings affect the way VIPs have to be applied to the constructions. In Nordic countries, the most common way to build houses is by building with a lightweight timber frame construction. However, central European countries such as Germany and Switzerland, where most of the studies on VIPs have been conducted, rely more on massive structures such as brick and concrete for housing purposes.

7.3.6.1 Munich

The first building over two storeys to be entirely insulated with VIPs was a residential and office building in Munich (Figs. 7.8 and 7.9). Here the goal was to show the economical benefits of achieving a slimmer facade by applying VIPs. With a total area of 1350 m^2, the building's heating requirement is just 22 kWh/(m^2year). This project was also a part of the earlier discussed ZAE Bayern's VIP-Prove project. Under an inspection in 2009, 450 m^2 out of a total of 750 m^2 of VIPs were monitored with thermographic scans. None of these showed any signs of damage (BINE Informationsdienst 2013). The project showed that a big hurdle for VIPs, in addition to the uncertainties considering lifetime, is the lack of certified building systems. Getting the required certifications took several months and added extra

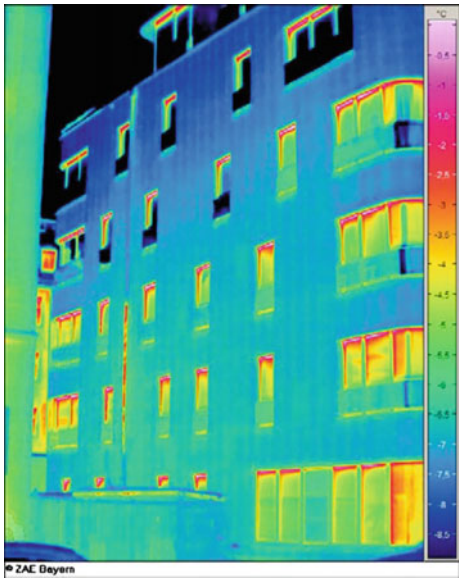

Fig. 7.9 Thermographic scan of the VIP project from Munich (Pool 2009). Thermography photograph taken as part of the research project VIP-Prove (copyright ZAE Bayern)

costs to the project. Planners took on a lot of extra risk and work to make this happen (Pool 2009).

7.3.6.2 Freiburg

In Fig. 7.10, the Sun Ship from Freiburg completed in 2006 is shown. The supporting structure is made from reinforced concrete and the facade is constructed from a wooden post-beam construction. A total of 1198 m^2 of VIPs are fit into place within the facade. Energy-efficient design, along with the VIPs and installation of photovoltaic solar cell modules, has made the Sun Ship the first commercial plus-energy building. The building has won several awards for its energy-efficient profile (SolarArchitektur 2013). That is, VIPs may be implemented and acknowledged in the aim for a more energy-efficient architecture.

7.3.6.3 Leipzig

A single family house was built in Leipzig in 2006 using a total of 265 m^2 of VIPs (Fig. 7.11). The VIPs were implemented in the outer part of the wall construction. The building was raised with a steel skeleton. The goal was to build a light construction that was energy efficient, ecologically flexible and of materials that were recyclable.

Fig. 7.10 The Sun Ship building in Freiburg, photograph by Rolf Disch SolarArchitecture (VIP-Bau 2013)

Fig. 7.11 Single-family house in Leipzig, photograph by Frank Hülsmeier (VIP-Bau 2013)

7.3.6.4 Laboratory Examples with Timber Frame Constructions

Hot-box measurements on a timber frame construction with 40-mm-thick VIPs demonstrated that it was possible to reach a *U*-value of 0.10 W/(m^{2}K) with a wall thickness of ∼20 cm. However, it was clear that building with VIPs requires more effort in the planning phase because of the lack of adaptability (Haavi et al. 2012). Hot-box experiments with VIPs in a timber frame construction were also conducted by Grynning et al. (2011), including single and double layers, tape and stacking/overlapping effects. Retrofitting of timber frame walls with VIPs between two climate rooms and subsequent investigations of the condensation risks was studied by Sveipe et al. (2011) and Jelle et al. (2013a). Furthermore, accelerated climate ageing of VIPs in a timber frame construction was carried out by Wegger et al. (2011).

7.3.7 *Retrofitting Examples*

VIPs hold great possibilities within the refurbishing of existing constructions. High-performance thermal insulations such as VIPs may be applied even where space is limited and help to reduce the heat loss from the buildings considerably, i.e. reducing the total energy usage. In constructions where it is difficult to modify the thickness of the building, implementation of high-performance insulation is an efficient option to achieve a greater energy efficiency through insulation. The efficient use of space also opens up for possibilities of renovating listed buildings, which are not allowed to be renovated at the expense of changing the building design. Investigations comparing single and double (non-staggered and staggered joints) layered VIPs of the same thickness are carried out by Brunner et al. (2012b) and Grynning et al. (2011), which are interesting for both new constructions and retrofitting cases.

ZAE Bayern has also conducted monitoring projects on retrofitted buildings. From the VIP-Prove project of ZAE Bayern, the highest score for a refurbished construction was achieved from a project in Berlin. For this project, a total area of 96 m^2 of wall was built with VIPs.

7.3.7.1 Laboratory Example with a Historical Brick Wall Construction

Hygrothermal numerical simulations and laboratory investigations for interior thermal insulation retrofit of a historical brick wall using VIPs were carried out by Johansson et al. (2014). The laboratory experiments were conducted in a large-scale vertical building envelope climate simulator as depicted in Fig. 7.12. The studies showed that adding interior VIPs could reduce the energy use substantially in brick buildings, and that various moisture considerations should be taken.

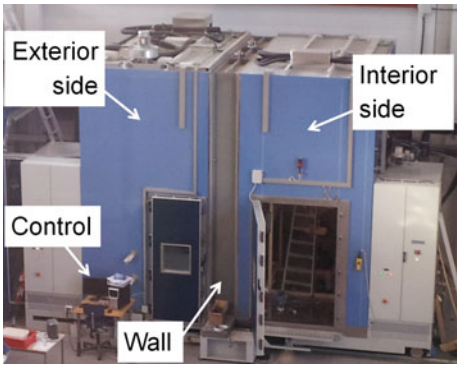

Fig. 7.12 Applying a large-scale vertical building envelope climate simulator for laboratory investigations for interior thermal insulation retrofit of a historical brick wall using VIPs (Johansson et al. 2014)

7.3.7.2 Laboratory Example with a Timber Frame Construction

An investigation of retrofitting with VIPs in a timber frame construction has been conducted by Sveipe et al. (2011) and Jelle et al. (2013a). The study looked at the potential to retrofit old Norwegian buildings with VIPs, hence lowering the energy usage to that of a passive house. A test module as depicted in Fig. 7.13 was built between two climate rooms to test how the VIP constructions performed with respect to moisture transport and risk of condensation, both when applied on the inside and outside of the wall. Insulating the outside of the wall will enable the reduction of thermal bridges, which is one reason this is normally the preferred solution when applying conventional vapour open systems. However, when using vapour-tight VIPs retrofitted at the exterior side, there may be a risk of condensation on the inner side of the VIPs. With 100-mm mineral wool retrofitted with 30-mm-thick VIPs, the wall achieved an U-value of 0.143 W/(m^2 K) for VIPs in pristine condition. When ageing of the panels were considered [panels reaching a thermal conductivity of 0.008 W/(m K)], the wall had an U-value of 0.181 W/(m^2 K). These results did not account for the small thermal bridging of the vertical VIP joints.

7.3.7.3 Practical Example from Canada

At the 10th international vacuum insulation symposium (IVIS-X) in Canada in 2011, a few construction retrofit examples from Canada were presented. One of these was the retrofitting of an institutional building in Yukon. The interest for a new and high-performing insulation material with high insulation values per units of thickness and weight is increasing. Determining the VIP qualities in the harsh

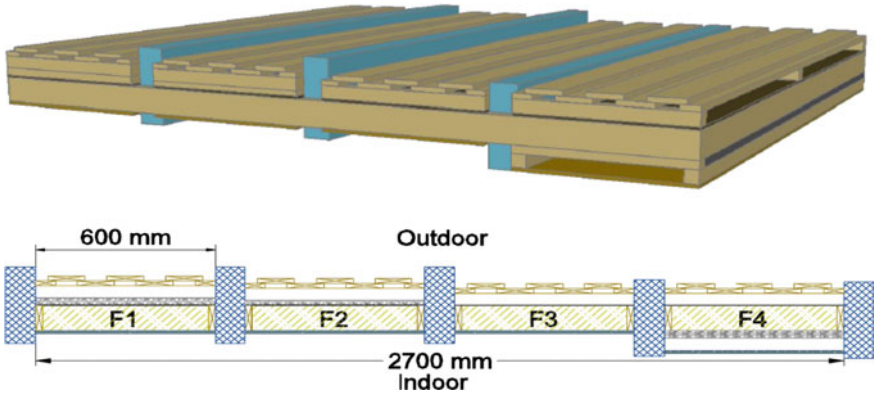

Fig. 7.13 Retrofitting with VIPs in a timber frame construction depicting a 3D view as seen from the bottom of the test module (*top*) and a horizontal cross section of the test module (*bottom*) (Sveipe et al. 2011; Jelle et al. 2013a)

Fig. 7.14 Installation of VIPs with adhesives (MacLean et al. 2011)

environment of northern Canada was of interest. Initially, one exterior facade was insulated using VIPs. As costs were high, contractors were hesitant to insulate an entire building with this new technology. By testing one section of the building first, the results might lead to increased trust and willingness to conduct more projects with VIPs.

The evaluation of the construction experience after the project was positive. Local interest around VIPs was said to increase. The low weight and small thickness made the installation easy, and as a result, the labour was completed under budget. The VIPs were easily installed with adhesives, i.e. they were stuck directly on the wall as shown in Fig. 7.14. However, the project is still being monitored further so there are no conclusive results of the VIP performance yet, even though the initial indications are positive. An important point that was highlighted was the need to train all staff on how to install and handle VIPs. The panels are still expensive and difficult to replace. At the end of a workday, the VIPs should always be covered by some form of protective layers. The areas where the VIPs are to be installed must always be investigated for elements that may harm the envelope through mechanical rubbing (MacLean et al. 2011).

7.4 Future Research Pathways

7.4.1 Other State-of-the-Art Insulation Materials

VIPs show great promise as a thermal insulation material solution for today and the near future. However, it is not the only thermal insulation material solution under development. Other interesting materials and technologies that may compete with VIPs in the future will be mentioned in the following chapters. Furthermore, some of these may also be used as a core material in the future VIPs.

7.4.1.1 Aerogels

Aerogels are dried gels with a very high porosity, high specific surface area, low apparent density and a low refraction index. The pore volume of aerogel may vary from 85 to 99.8 %. This gives the material a bulk density as low as 3 kg/m^3, making it the lightest solid-state material known. For building applications, the density is in the range of 70–150 kg/m^3. At ambient pressure, the thermal conductivity may be as low as 0.0135 W/(m K), which can be reduced down to 0.004 W/(m K) at a pressure of 50 mbar (Baetens et al. 2011; Jelle et al. 2015e; Smith et al. 1998). Aerogels at ambient pressure have thermal conductivity values 2–3 times lower than conventional insulation, and unlike VIPs, the aerogels can be cut and adjusted at the building site. However, aerogels have a very low tensile strength, making the aerogel materials very fragile. The optical properties of aerogels are quite remarkable. It is possible to produce aerogels which are opaque, translucent or transparent (Fig. 7.15), thus enabling a wide range of applications such as in windows, facades and roofs which will allow solar radiation and daylight to pass through (Baetens et al. 2011; Jelle et al. 2012a, 2015e). For further information on aerogels, see e.g. the studies by Aegerter et al. (2011), Cuce et al. (2014), Koebel et al. (2012), Lee et al. (1995a, b), Levy and Zayat (2015) and Wong et al. (2014).

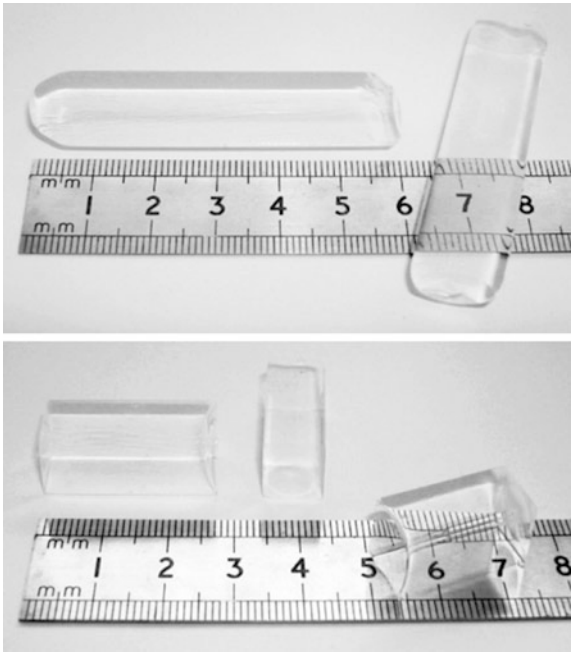

Fig. 7.15 Transparent aerogel samples made by high-temperature supercritical drying (HTSCD) (*top*) and low-temperature supercritical drying (LTSCD) (*bottom*) (Dowson et al. 2012)

7.4.1.2 Gas-Filled Panels (GFP)

Gas-filled panels (GFP) consist of a gas between reflective layers sealed within a low-emissivity barrier envelope. The reflective layer inside a GFP is called a baffle. Figure 7.16 shows the cross section of a normal GFP. The gas inside the core can either be air or be other heavier gases that further reduce the thermal conductivity. Theoretical values of 0.020 W/(m K) and 0.012 W/(m K) for argon- and krypton-filled panels, respectively, have been found. However, prototype GFPs have given a thermal conductivity of 0.040 W/(m K) for panels filled with argon in practical use in a building construction. As a technology with the same fragility and lack of flexibility as VIPs, but still showing a higher thermal conductivity, the future of GFPs is questionable (Baetens et al. 2010c).

7.4.1.3 Nanoinsulation Materials (NIM)

Nanoinsulation materials (NIM) can be described as materials that are basically homogenous and which achieve high-performance thermal insulating qualities mainly due to their open or closed nanoporous structure. By reducing the pore size until the maximum pore size in the material is lower than the mean free path of air, the gaseous thermal conductivity can be substantially reduced. From the conceptual ideas of NIMs (Baetens et al. 2010a; Jelle 2011; Jelle et al. 2009, 2010), the first experimental steps have been carried out in order to actually make NIMs in the laboratory (Gao et al. 2012, 2013, 2014a; Gao and Jelle 2015; Jelle et al. 2011, 2014a, 2015c; Sandberg et al. 2013). One main focus for trying to make NIMs today is manufacturing of hollow silica nanospheres (HSNS) (Fig. 7.17), where powder samples of these spheres have measured thermal conductivity values typically in the range of 0.020–0.090 W/(m K), though some uncertainties in the Hot

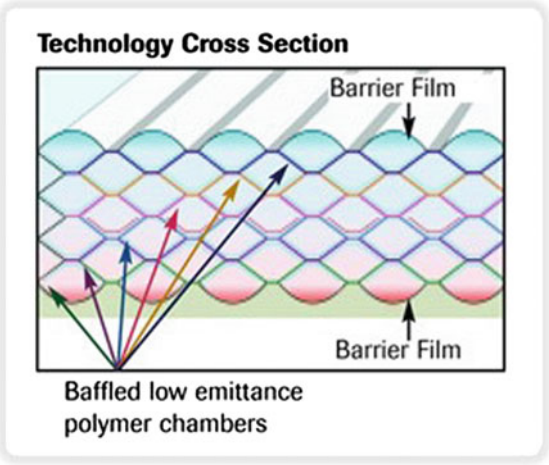

Fig. 7.16 Technology cross section of a GFP (Fi-Foil company 2013)

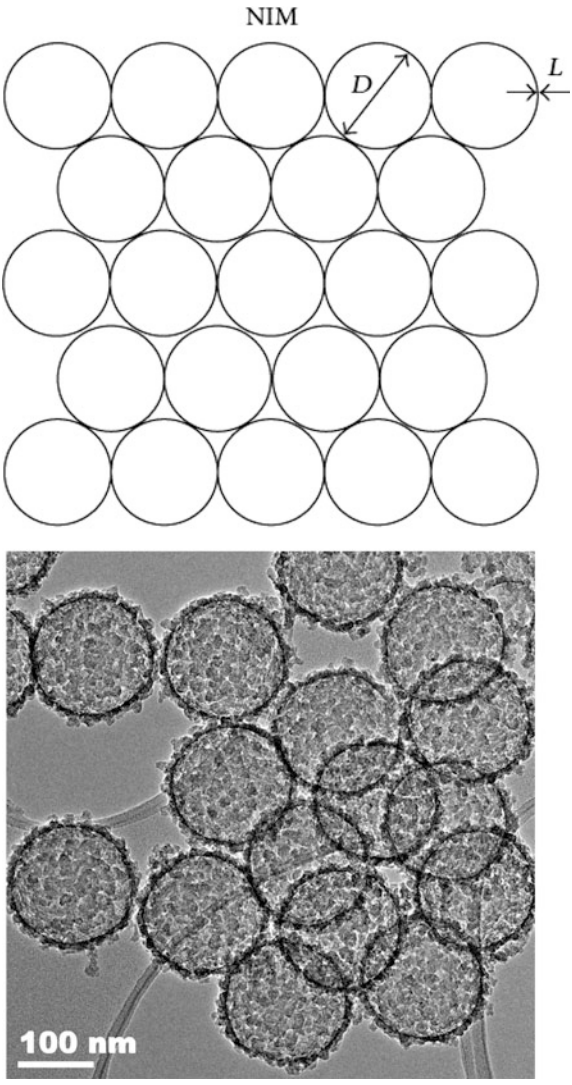

Fig. 7.17 Conceptual model of a NIM based on hollow nanospheres (*left*) and a transmission electron microscope (TEM) image of actual hollow silica nanospheres (*right*) (Sandberg et al. 2013)

Disk apparatus measurement method have to be further clarified (Grandcolas et al. 2013; Jelle et al. 2013b). Production and measurements on the thermal insulation ability of HSNS are further described by Liao et al. (2011) and Sandberg et al. (2013).

The above-described NIM research is mainly focused on various attempts to tailor-make HSNS by manufacturing and applying different sacrificial templates, synthesis procedures, parameter variations, and inner diameters and shell thicknesses of the nanospheres. A crucial issue will be how to assemble the HSNS together into a practical bulk material. Furthermore, it should be noted that the

future NIM may not necessarily be based on HSNS, nevertheless the investigations on the HSNS represent a possible stepping-stone towards the ultimate goal of achieving thermal superinsulation materials (SIM). Safety and health aspects are also important in this regard. No one wants any similar cases as the well-known asbestos case. Fabrication of NIM according to membrane foaming and gas release methods should definitely not be forgotten as they may still represent a possible way of achieving SIM and NIM, also directly as a bulk material without the need of, e.g. piecing nanospheres together. Finally, it should be emphasized that also methods and materials not included within this summary, even hitherto unknown methods and materials, may hold the solution for the future SIM and NIM.

7.4.2 Possible Future Research on Current VIP Technologies

7.4.2.1 Various Requirements

As addressing the future possibilities of VIPs, the problem areas of today should be considered. Thermal insulation materials intended for building applications have to fulfil several requirements, e.g. as suggested by Jelle (2011) and Jelle et al. (2009, 2010). It is proposed that the initial thermal conductivity should be 0.004 W/(m K) or below, whereas it should not exceed 0.005 W/(m K) after 100 years. Perforation should not affect the thermal performance of the material, and it should be robust when considering climate stresses such as freezing/thawing cycles and ageing. The thermal insulation material should be adjustable on the building site, and furthermore, it should have a low negative environmental impact. In addition, the insulation material should be cost-competitive in comparison with other products.

For VIPs of today, a lot of the suggested requirements are not met. The path forward can either focus on improving the current technologies or explore new technologies based on similar principles as those that have been used while working with VIPs. In the following, some of the work and reflections about the future of VIPs will be discussed.

As mentioned earlier, the two main components that lead to and maintain the low thermal conductivity of VIPs are the core and the envelope. However, they are not directly depending on each other. That is, improving one of the two individually will contribute positively to a better VIP. Thus, research being conducted on improving the core and envelope can be explored separately.

7.4.2.2 The Core

There are several factors with the current core technology that can be addressed to make VIPs more attractive, i.e.:

1. Developing core materials that better resist permeating gases and water vapour. Introducing getters and desiccants to the core is not a permanent solution to gases permeating through the envelope. They will eventually reach their capacity for adsorbing water vapour and gases and the core material will begin to lose its thermal resistance properties. New core materials with smaller pores, a stronger structure and generally better resistance, may increase the expected lifetime of a VIP.
2. Producing core materials that can achieve a lower solid and radiative conductivity. Further reduction of the thermal conductivity may be achieved through reducing the heat loss from conduction in the solid material and the radiative heat transfer through the voids in a VIP. However, as noted earlier, the solid-state conductivity and radiation conductivity are already very low, i.e. a combined total value of 0.004 W/(m K) or lower.
3. Reducing the production costs of the current core materials or seek new materials that can be produced at less costs. For VIPs manufactured for the building sector, the core materials are mainly nanoporous materials. As of today, the production costs for these materials are still very high. Exploring new methods to produce the core materials can therefore make VIPs more cost-competitive.
4. Developing core materials that are better at maintaining a vacuum, and less vulnerable towards perforation and cutting [e.g. vacuum insulation materials (VIM)], and ultimately core materials that have low thermal conductivities at atmospheric pressure (e.g. NIM) (Baetens et al. 2010a; Jelle 2011; Jelle et al. 2009, 2010). That is, such core material developments are moving beyond the very concept of *vacuum* insulation *panels*, i.e. not requiring vacuum or (enveloped) panels.

Hence, the utilization of various nanotechnologies is seen in one of the major promising development areas for VIP core improvement.

The National Research Council-Institute for Research in Construction (NRC-IRC) (Canada) has noted the costs of VIPs to be one of the major factors that is stopping the wide use of VIPs in the construction sector. To meet this challenge, they have started ongoing research to find less expensive core materials. By using a vacuum-guarded hot plate (VGHP), different open porous insulating materials can be tested at different pressure levels. None of the materials tested so far has been commercialized, but work is still ongoing (Mukhopadhyaya et al. 2008).

7.4.2.3 The Envelope

The envelope is the weak point of VIPs as of today. Permeation through the envelope leads to an increase in thermal conductivity, heat bridging contributes to a higher thermal conductivity, and the envelope is fragile and can easily be perforated. These are some of the major issues that need to be further improved. One aim is to develop an envelope without the aluminium layers. The aluminium in today's

laminates leads to an increase in thermal bridging. However, they are necessary to reduce the permeability through the envelope as polymers do not have the same resistance against permeation. Thus, if a polymer material with a much larger permeation resistance could be introduced, this would work favourably for the reduction of thermal bridging. Reducing the permeation sufficiently would also allow for less expensive materials such as glass fibres and PUR foams to be used as core materials with an extended lifetime. Note the earlier discussion herein concerning the faster increase in VIP thermal conductivity when applying thin-metallized polymer film MF than when applying the thicker aluminium foils (AF).

The production method may also lead to flaws with today's envelopes. Material imperfections and processing errors need to be handled to increase the trust in VIPs. Material imperfections such as pinholes are impossible to notice by just a visual inspection, but may reduce the lifetime of the panel. New methods of assuring the quality should be considered. This will also be beneficial as it will allow monitoring of panels without results being affected by a faulty production process.

There is also the problem with the lack of robustness for the envelope. Steel casings have already been tried for use as envelopes. Stainless steel makes for an almost impermeable envelope with only a few mm thickness. The steel will also represent a robust panel, which is not easily perforated. However, there is the issue of a greatly increased thermal bridging as well as possible corrosion of many stainless steel qualities. A method with serpentine edging to minimize edge loss has been investigated by Thorsell and Källebrink (2005). Figure 7.18 shows an illustration of how serpentine edges work in a two-dimensional view. For a steel casing with 11 serpentines with a depth of 20 mm, the thermal bridging effect was found to be 0.010 W/(m K). The robustness of these serpentine edges may be questioned, however. Furthermore, the actual thermal resistance of the joint between two such VIPs with serpentine edges may also not be as high as desirable.

Further research must also be made on the sealing technique for the envelope. The heat-sealed flange is often considered as a weak point in the modern VIPs. Understanding the processes around the sealing process may help to improve the seals and reduce the permeation through it. There are also investigations going on as to where it is most beneficial to put the seal, i.e. either along the panel edges, or on one of the large area surfaces on the panel.

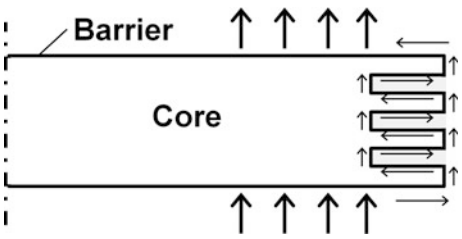

Fig. 7.18 Serpentine edging in VIPs. Redrawn from Thorsell and Källebrink (2005)

7.4.3 Further Reflections

One important factor to consider is the "economies of scale". VIPs have not yet been widely used as a thermal insulation material, and even though there are a variety of manufacturers, the production scale is not comparable to conventional insulation. As VIPs gain confidence as an insulation material, the scale of production will increase and most likely lead to a reduction of production costs for VIPs (Mukhopadhyaya et al. 2011).

As mentioned earlier, there are other insulation materials in development that may end up competing with VIPs in the future. The outlook is interesting for both aerogels and NIM, and further studies are being conducted on these materials. Their ability to be adapted at the building site, lack of inherent thermal bridges and generally higher robustness makes them more suited for building applications. The nature of the construction industry is known to be conservative. Introducing VIPs, that are a fragile and not a very flexible material, will put new demands on contractors and building planners for how to plan, handle and implement the VIPs correctly. Aerogels and NIMs, however, could be implemented much like conventional insulation today, and would make for a much more seamless adaption (Tenpierik 2009). One may also envision applications of VIPs together with other thermal building envelope materials, e.g. phase change materials (PCM) for absorbing and releasing heat (Baetens et al. 2010b; Demirbas 2006; Farid et al. 2004; Hasnain 1998; Kalnæs and Jelle 2015; Khudhair and Farid 2004), or integrated with other building envelope elements such as building integrated photovoltaics (BIPV) for harvesting the solar energy for electricity generation (Jelle et al. 2012b; Jelle and Breivik 2012a, b). To attempt to reach as low emissivity (Jelle et al. 2015a) as possible for use in envelope surfaces or within the pores (inner pore walls) of a core material may represent viable research paths for future solutions. Utilizing state-of-the-art materials technologies as mentioned above together with VIPs represent possible pathways for achieving the energy-efficient and energy-producing buildings of the future. In such energy-efficient buildings, another important technology is smart windows including electrochromic windows for regulating the solar transmittance throughput in windows and other glazing structures (Granqvist 1995, 2005, 2008, 2012; Jelle 1993, 2013a, 2015; Jelle and Hagen 1993, 1998, 1999; Jelle et al. 1993, 1998, 2007; Lampert 1998, 2004; Ribeiro and Mortimer 2015), which may be seen as part of the development of intelligent buildings. Furthermore, to keep these glass surfaces free from dirt, snow and ice, e.g. for smart windows and BIPV, the research on self-cleaning surfaces, superhydrophobicity and icephobicity should also be noted (Eberle et al. 2014; Hejazi et al. 2013; Jelle 2013b; Jung et al. 2011; Midtdal and Jelle 2013; Schutzius et al. 2015; Zhang and Lv 2015).

Various advantages and drawbacks of applying nanotechnology in the construction sector are reviewed by Pacheco-Torgal and Jalali (2011). Certainly, as one in the coming years will experience many new and innovative materials and solutions based on nanotechnology, one also has to address any toxicity issues to

avoid any health and safety hazards. That also goes for the improvement of VIPs and development of new thermal insulation materials and other technologies to be used in the building envelope such as the ones mentioned in the above. Several of these new materials will probably be developed by research groups within the European Commission Horizon 2020 programme, where the utilization of nanotechnology also will play an important role (Pacheco-Torgal 2014).

7.4.4 *Producing Vacuum Insulation with New Technology*

The general idea of VIPs is that the vacuum greatly reduces the gaseous conductivity through a material. However, with the current manufacturing technology, an open porous structure is a requirement for panels to be totally evacuated to a vacuum. A new thought is to create a material with a closed pore structure in combination with vacuum (Fig. 7.19). This would give the same low thermal conductivities as a VIP, but without the need for a sealing envelope. Should a material like this be perforated the result would just be a local thermal bridge, and the material could also be cut and adjusted at the building site. Such a material is referred to as a VIM (Baetens et al. 2010a; Jelle 2011; Jelle et al. 2009, 2010).

However, a problem for this solution would be that gases (air) and water vapour would also permeate through the solid-state pore walls similar to as it would through the envelope of a VIP.

Synthesis of closed porous silica has been studied by Pei et al. (2004). A challenge concerning a closed pore-structured material is that the material can no longer be evacuated. Therefore, a material like this may have to be manufactured under vacuum to create an evacuated closed pore structure or a material blowing itself up from within or pore walls absorbing all of the initial gases in the pores (Jelle et al. 2009, 2010).

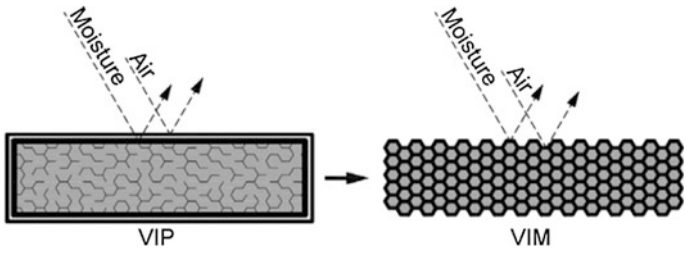

Fig. 7.19 Illustration of a vacuum insulation material (VIM) (Baetens et al. 2010a)

7.4.5 The Path Forward for VIPs in the Construction Sector

As VIPs improve and become a part of the building envelope of tomorrow, it will be necessary to create standards for their use. As of today, the building projects which have been completed have had to be approved individually. Applying for approval for each individual building from local building regulators is time consuming and makes it harder for VIPs to gain access to the building sector at a larger scale. As we have seen however, many of the reference projects have given positive results. New standards should include how to properly handle, store and install VIPs. As mentioned by Brunner (2009), a standard which is in line with the other European product standards EN13162 to EN13171 on how to handle thermal insulation, should be made for VIPs as well. These standards do, among other issues, state initial testing and production control for the materials. Other important factors that need to be described are design guidelines, more clear material specification standards and handling instructions.

Another goal for the building sector may also be to innovate how constructions are being built around VIPs. The thermal conductivity increase in VIPs by a factor of about five times if the panel is punctured is a major weak point. New planning of constructions to make it possible to monitor the VIPs and easily replace broken VIPs might make them more suitable and desired for constructions. For various experimental tests on VIPs for building applications, it is referred to the investigations by Grynning et al. (2011), Haavi et al. (2012), Sveipe et al. (2011), Wegger et al. (2011) and Johansson et al. (2014), whereas for more general information about accelerated climate ageing of building materials, components and structures, including new materials and solutions (e.g. VIPs), it is referred to the studies by Jelle (2012) and Jelle et al. (2012c). Performing a robustness assessment of these materials and components may also be found to be beneficial (Jelle et al. 2014b). Brunner et al. (2014) address in a recent review the continuous challenges and developments for VIPs for building applications.

The manufacturers of VIPs and contractors should also work together to establish a common norm for the use of VIPs in buildings. Enabling standard formats for VIPs would be beneficial for all participants. Allowing VIPs to be stored in the factory after production may enable the manufacturers to notice broken panels before they are shipped out. Broken panels will be easier to reorder from stock and a standardized production process may lead to fewer defect panels. As of today, production problems are still critical for faith in the VIP technology (Zimmermann and Brunner 2011). The need for quality assurance is present in the market. Standardized tests to assure that there are no microscopical damages or relatively large leakages through weak seals should be guaranteed to the customers through a quality label (Erbenich 2009).

It is still difficult to measure the gas pressure inside VIPs. When defect panels are discovered, the only solution is to exchange the panels. Caps et al. (2008) have demonstrated that technology for measuring the gas pressure inside the panels is

available. For the future, the use of measurement technology has to be more common so that the quality of all VIPs can be assured.

In Europe, a Common Understanding of Assessment Procedure (CUAP) and globally an ISO Working Group have been established to deal with testing procedures for VIPs. The definition of clear test methods will help to define when panels are damaged due to faults in production versus bad handling during transport and installation (Brunner et al. 2012a). Noteworthy in this respect is the establishment of the International Energy Agency (IEA) Annex 65 Task "Long-Term Performance of Super-Insulating Materials in Building Components and Systems" (Quenard 2015a, b) and the "Vacuum Insulation Panel Association" (VIPA) (VIPA 2015). Meanwhile, the research on VIPs continues in various studies including theoretical, experimental and field investigations (Baetens 2013; Li et al. 2015; Boafo et al. 2014; Mandilaras et al. 2014; Miesbauer et al. 2014; Mukhopadhyaya et al. 2014; Pons et al. 2014; Sallée et al. 2014; Sprengard and Holm 2014; Voellinger et al. 2014; Yrieix et al. 2014; Fricke et al. 2008; Tenpierik and Cauberg 2010; Alotaibi and Riffat 2014; Jelle et al. 2015d). One may incorporate VIPs in sandwich elements with concrete (Voellinger et al. 2014), and one may also envision to make a new and better thermally insulating concrete material by, e.g. incorporating aerogel granules into the concrete matrix (Gao et al. 2014b; Ng et al. 2015a, b; Jelle et al. 2015b) and aerogel renders (Ghazi Wakili et al. 2014; Ibrahim et al. 2015; Stahl et al. 2012). With all these continued efforts, the future looks bright for improvements and innovations within high-performance thermal insulation materials.

7.5 Conclusions

VIP manufacturers on the market today offer a wide variety of VIP products. VIPs in general applications have already been used on the market for nearly two decades with success. For the construction sector, there are still challenges to overcome. The lack of certified building systems and official approvals from governmental agencies are providing hurdles that will need to be handled. Education and further promotion of VIPs are important in order to accelerate the implementation of VIPs in constructions. Hence, the challenges are placed with the manufacturers, needing to improve the quality assurance of their VIP products, and to be able to give a guarantee the end users can rely on. It is important that data from already finished constructions are gathered and shared, so that the uncertainty of how VIPs perform at practical conditions can be reduced. Removing uncertainties around VIPs, and reducing the costs, represent important factors for a larger commercialization of this product.

VIPs show great promise as a building insulation material for today and in the near future. Many projects have already been completed with VIPs, where many show good initial results. If the technology may be further improved, and the current lifetime can be extended and guaranteed, VIPs will become a more trusted

choice for thermal insulation. However, even if the moisture and air diffusion into the VIP core somehow could be reduced to almost zero (which is far from the situation today), the lack of flexibility and the risk of perforation will always be major drawbacks for the application of VIPs. Other high-performance insulation solutions have been described briefly, where some of these show great promise, combined with the possibilities of increased flexibility and being able to be adapted at the building site. Thus, these may eventually become a favourable choice over VIPs if or when they are able to be commercialized. The application of nanotechnology for achieving and improving these high-performance thermal insulation materials, both for vacuum and non-vacuum based solutions, seems to be a logical and promising pathway to follow.

Acknowledgements This work has been supported by the Research Council of Norway and several partners through *The Research Centre on Zero Emission Buildings* (ZEB). The authors are grateful for the useful comments from and discussions with Samuel Brunner (Empa, Switzerland), Ulrich Heinemann (ZAE Bayern, Germany) and Daniel Quenard (CSTB, France).

References

Aegerter MA, Leventis N, Koebel MM (2011) Aerogels handbook. Springer, Berlin

Alam M, Singh H, Limbachiya MC (2011) Vacuum insulation panels (VIPs) for building construction industry—a review of the contemporary developments and future directions. Appl Energy 88:3592–3602

Alam M, Singh H, Brunner S, Naziris C (2014) Experimental characterisation and evaluation of the thermo-physical properties of expanded perlite—fumed silica composite for effective vacuum insulation panel (VIP) core. Energy Build 69:442–450

Alotaibi SS, Riffat S (2014) Vacuum insulated panels for sustainable buildings: a review of research and applications. Int J Energy Res 38:1–19

Araki K, Kamoto D, Matsuoka S (2009) Optimization about multilayer laminated film and getter device materials of vacuum insulation panel for using at high temperature. J Mater Process Technol 209:271–282

Baetens R (2013) High performance thermal insulation materials for buildings. In: Pacheco-Torgal F, Diamanti MV, Nazari A, Granqvist C-G (eds) Nanotechnology in eco-efficient construction. Woodhead Publishing, Cambridge, pp 188–206

Baetens R, Jelle BP, Thue JV, Tenpierik MJ, Grynning S, Uvsløkk S, Gustavsen A (2010a) Vacuum insulation panels for building applications: a review and beyond. Energy Build 42:147–172

Baetens R, Jelle BP, Gustavsen A (2010b) Phase change materials for building applications: a state-of-the-art review. Energy Build 42:1361–1368

Baetens R, Jelle BP, Gustavsen A, Grynning S (2010c) Gas-filled panels for building applications: a state-of-the-art review. Energy Build 42:1969–1975

Baetens R, Jelle BP, Gustavsen A (2011) Aerogel insulation for building applications: a state-of-the-art review. Energy Build 43:761–769

Berge A, Adl-Zarrabi B (2014) Evaluation of vacuum insulation panels used in hybrid insulation district heating pipes. In: Proceedings of the 14th international symposium on district heating and cooling, Stockholm, Sweden, 7–9 Sept 2014

BINE Informationsdienst (2013) In practice II: new residential and office building. http://www.bine.info/en/publications/themeninfos/publikation/daemmen-durch-vakuum/aus-der-praxis-ii-neubau-wohn-und-geschaeftshaus/. Accessed 31 May 2013. (Originally from Pool Architekten and with photographer Sascha Kletzsch, Germany)

Boafo FE, Chen ZF, Wu WP, Chen Q, Li BB (2013) Ultrafine glass fiber vacuum insulation panel for building insulation. Adv Civ Eng Build Mater

Boafo FE, Chen Z, Li C, Li B, Xu T (2014) Structure of vacuum insulation panel in building system. Energy Build 85:644–653

Bouquerel M, Duforestel T, Baillis D, Rusaouen G (2012a) Heat transfer modeling in vacuum insulation panels containing nanoporous silicas—a review. Energy Build 54:320–336

Bouquerel M, Duforestel T, Baillis D, Rusaouen G (2012b) Mass transfer modeling in gas barrier envelopes for vacuum insulation panels: a review. Energy Build 55:903–920

Brunner S (2009) Quality assurance and declaration of vacuum insulation for building application. In: Paper presentation on 9th international vacuum insulation symposium (IVIS 2009), London, UK, 17–18 Sept 2009

Brunner S, Ghazi Wakili K (2014) Hints for an additional aging factor regarding the thermal performance of vacuum insulation panels with pyrogenic silica core. Vacuum 100:4–6

Brunner S, Simmler H (2008) In situ performance assessment of vacuum insulation panels in a flat roof construction. Vacuum 82:700–707

Brunner S, Gasser P, Simmler H, Ghazi Wakili K (2006) Investigation of multilayered aluminium-coated polymer laminates by focused ion beam (FIB) etching. Surf Coat Technol 200:5908–5914

Brunner S, Stahl T, Ghazi Wakili K (2012a) An example of deteriorated vacuum insulation panels in a building facade. Energy Build 54:278–282

Brunner S, Stahl T, Ghazi Wakili K (2012b) Single and double layered vacuum insulation panels of the same thickness in comparison. In: Proceedings of conference on 3rd building enclosure science and technology (BEST 3—2012), Atlanta, Georgia, USA, 2–4 April 2012

Brunner S, Ghazi Wakili K, Stahl T, Binder B (2014) Vacuum insulation panels for building applications—continuous challenges and developments. Energy Build 85:592–596

Caps R, Fricke J (2000) Thermal conductivity of opacified powder filler materials for vacuum insulation. Int J Thermophys 21:445–452

Caps R, Heinemann U, Ehrmanntraut M, Fricke J (2001) Evacuated insulation panels filled with pyrogenic silica powders: Properties and applications. High Temp High Pressures 33:151–156

Caps R, Beyrichen H, Kraus D, Weismann S (2008) Quality control of vacuum insulation panels: methods of measuring gas pressure. Vacuum 82:691–699

Cuce E, Cuce PM, Wood CJ, Riffat SB (2014) Toward aerogel based thermal superinsulation in buildings: a comprehensive review. Renew Sustain Energy Rev 34:273–299

Demirbas MF (2006) Thermal energy storage and phase change materials: an overview. Energy Sources Part B Econ Plann Policy 1:85–95

Di X, Gao Y, Bao C, Hu Y, Xie Z (2013) Optimization of glass fibre based core materials for vacuum insulation panels with laminated aluminium foils as envelopes. Vacuum 97:55–59

Dowson M, Grogan M, Birks T, Harrison D, Craig S (2012) Streamlined life cycle assessment of transparent silica aerogel made by supercritical drying. Appl Energy 97:396–404

Eberle P, Tiwari MK, Maitra T, Poulikakos D (2014) Rational nanostructuring of surfaces for extraordinary icephobicity. Nanoscale 6:4874–4881

EnOB (2013) Vacuum insulation under the spotlight. http://www.enob.info/en/new-technologies/projects/details/vacuum-insulation-under-the-spotlight/. Accessed on 03 June 2013

Erb M, Brunner S (2012) Vacuum insulation for building applications. Product declaration and design values. Technical report

Erbenich G (2009) How to identify a high quality VIP. In: Proceedings of the 9th international vacuum insulation symposium (IVIS 2009), London, UK, 17–18 Sept 2009

European Union (2012) Directive 2012/27/EU of the European parliament and of the council of 25 October 2012 on the energy efficiency. Official Journal of the European Union, L 315, vol 55, pp 1–57

Farid MM, Khudhair AM, Razack SAK, Al-Hallaj S (2004) A review on phase change energy storage: materials and applications. Energy Convers Manage 45:1597–1615
Fi-Foil Company (2013) http://www.gfpinsulation.com/. Accessed on 08 Jul 2013
Fricke J, Heinemann U, Ebert HP (2008) Vacuum insulation panels—from research to market. Vacuum 82:680–690
Gao T, Jelle BP (2015) Fiber reinforced hollow silica nanospheres for thermal insulation applications. In: Proceedings of the 12th international vacuum insulation symposium (IVIS 2015), Nanjing, China, 19–21 Sept 2015, pp 31–33
Gao T, Sandberg LIC, Jelle BP, Gustavsen A (2012) Nano insulation materials for energy efficient buildings: a case study on hollow silica nanospheres. In: Mendez-Vilas A (ed) Fuelling the future: advances in science and technologies for energy generation, transmission and storage. BrownWalker Press, Boca Raton, pp 535–539
Gao T, Jelle BP, Sandberg LIC, Gustavsen A (2013) Monodisperse hollow silica nanospheres for nano insulation materials: synthesis, characterization, and life cycle sssessment. ACS Appl Mater Interfaces 5:761–767
Gao T, Sandberg LIC, Jelle BP (2014a) Nano insulation materials: synthesis and life cycle assessment. Proc CIRP 15:490–495
Gao T, Jelle BP, Gustavsen A, Jacobsen S (2014b) Aerogel-incorporated concrete: an experimental study. Constr Build Mater 52:130–136
Ghazi Wakili K, Bundi R, Binder B (2004) Effective thermal conductivity of vacuum insulation panels. Build Res Inf 32:293–299
Ghazi Wakili K, Nussbaumer T, Bundi R (2005) Thermal performance of VIP assemblies in building constructions. In: Proceedings of the 7th international vacuum insulation symposium, Dübendorf, Switzerland, 28–29 Sept 2005, pp 131–138
Ghazi Wakili K, Stahl T, Brunner S (2011) Effective thermal conductivity of a staggered double layer of vacuum insulation panels. Energy Build 43:1241–1246
Ghazi Wakili K, Binder B, Zimmermann M, Tanner Ch (2014) Efficiency verification of a combination of high performance and conventional insulation layers in retrofitting a 130-year old building. Energy Build 82:237–242
Grandcolas M, Etienne G, Tilset BG, Gao T, Sandberg LIC, Gustavsen A, Jelle BP (2013) Hollow silica nanospheres as a superinsulating material. In: Proceedings of the 11th international vacuum insulation symposium (IVIS 2013), Dübendorf, Zürich, Switzerland, 19–20 Sept 2013, pp 43–44
Granqvist C-G (1995) Handbook of inorganic electrochromic materials. Elsevier, Amsterdam
Granqvist C-G (2005) Electrochromic devices. J Eur Ceram Soc 25:2907–2912
Granqvist C-G (2008) Oxide electrochromics: why, how, and whither. Sol Energy Mater Sol Cells 92:203–208
Granqvist C-G (2012) Oxide electrochromics: an introduction to devices and materials. Sol Energy Mater Sol Cells 99:1–13
Grynning S, Jelle BP, Uvsløkk S, Gustavsen A, Baetens R, Caps R, Meløysund V (2011) Hot box investigations and theoretical assessments of miscellaneous vacuum insulation panel configurations in building envelopes. J Build Phys 34:297–324
Haavi T, Jelle BP, Gustavsen A (2012) Vacuum insulation panels in wood frame wall constructions with different stud profiles. J Build Phys 36:212–226
Hasnain SM (1998) Review on sustainable thermal energy storage technologies, part I: heat storage materials and techniques. Energy Convers Manage 39:1127–1138
Heinemann U (2008) Influence of water on the total heat transfer in ‘evacuated’ insulations. Int J Thermophys 29:735–749
Heinemann U, Kastner R (2010) VIP-Prove, Vakuumisolationspaneele - Bewährung in der Baupraxis - wissenschaftliche Begleitforschung. ZAE Bayern, Report ZAE 2 - 1210 - 11, 2010
Hejazi V, Sobolev K, Nosonovsky M (2013) From superhydrophobicity to icephobicity: forces and interaction analysis. Sci Rep 3(2194):1–6

Ibrahim M, Biwole PH, Achard P, Wurtz E (2015) Aerogel-based materials for improving the building envelope's thermal behavior: a brief review with a focus on a new aerogel-based rendering. In: Sharma A, Kar SK (eds) Energy sustainability through green energy. Springer, Berlin, pp 163–188

Jelle BP (1993) Electrochemical and spectroscopic studies of electrochromic materials. Ph.D. thesis, 131. Department of Applied Electrochemistry, The Norwegian Institute of Technology, Trondheim, Norway, 1993

Jelle BP (2011) Traditional, state-of-the-art and future thermal building insulation materials and solutions—properties, requirements and possibilities. Energy Build 43:2549–2563

Jelle BP (2012) Accelerated climate ageing of building materials, components and structures in the laboratory. J Mater Sci 47:6475–6496

Jelle BP (2013a) Solar radiation glazing factors for window panes, glass structures and electrochromic windows in buildings—measurement and calculation. Sol Energy Mater Sol Cells 116:291–323

Jelle BP (2013b) The challenge of removing snow downfall on photovoltaic solar cell roofs in order to maximize solar energy efficiency—research opportunities for the future. Energy Build 67:334–351

Jelle BP (2015) Electrochromic smart windows for dynamic daylight and solar energy control in buildings. In: Mortimer RJ, Rosseinsky DR, Monk PMS (eds) Electrochromic materials and devices. Wiley-VCH, London, pp 419–502

Jelle BP, Breivik C (2012a) State-of-the-art building integrated photovoltaics. Energy Proc 20:68–77

Jelle BP, Breivik C (2012b) The path to the building integrated photovoltaics of tomorrow. Energy Proc 20:78–87

Jelle BP, Hagen G (1993) Transmission spectra of an electrochromic window based on polyaniline, prussian blue and tungsten oxide. J Electrochem Soc 140:3560–3564

Jelle BP, Hagen G (1998) Electrochemical multilayer deposition of polyaniline and prussian blue and their application in solid state electrochromic windows. J Appl Electrochem 28:1061–1065

Jelle BP, Hagen G (1999) Correlation between light absorption and electric charge in solid state electrochromic windows. J Appl Electrochem 29:1103–1110

Jelle BP, Hagen G, Hesjevik SM, Ødegård R (1993) Reduction factor for polyaniline films on ITO from cyclic voltammetry and visible absorption spectra. Electrochim Acta 38:1643–1647

Jelle BP, Hagen G, Birketveit Ø (1998) Transmission properties for individual electrochromic layers in solid state devices based on polyaniline, prussian blue and tungsten oxide. J Appl Electrochem 28:483–489

Jelle BP, Gustavsen A, Nilsen T-N, Jacobsen T (2007) Solar material protection factor (SMPF) and solar skin protection factor (SSPF) for window panes and other glass structures in buildings. Sol Energy Mater Sol Cells 91:342–354

Jelle BP, Gustavsen A, Baetens R (2009) Beyond vacuum insulation panels—how may it be achieved? In: Proceedings of the 9th international vacuum insulation symposium (IVIS 2009), London, UK, 17–18 Sept 2009

Jelle BP, Gustavsen A, Baetens R (2010) The path to the high performance thermal building insulation materials and solutions of tomorrow. J Build Phys 34:99–123

Jelle BP, Tilset BG, Jahren S, Gao T, Gustavsen A (2011) Vacuum and nanotechnologies for the thermal insulation materials of beyond tomorrow—from concept to experimental investigations. In: Proceedings of the 10th international vacuum insulation symposium (IVIS 2011), Ottawa, Canada, 15–16 Sept, pp 171–178

Jelle BP, Hynd A, Gustavsen A, Arasteh D, Goudey H, Hart R (2012a) Fenestration of today and tomorrow: a state-of-the-art review and future research opportunities. Sol Energy Mater Sol Cells 96:1–28

Jelle BP, Breivik C, Røkenes HD (2012b) Building integrated photovoltaic products: A state-of-the-art review and future research opportunities. Sol Energy Mater Sol Cells 100:69–96

Jelle BP, Nilsen T-N, Hovde PJ, Gustavsen A (2012c) Accelerated climate aging of building materials and their characterization by Fourier transform infrared radiation analysis. J Build Phys 36:99–112

Jelle BP, Sveipe E, Wegger E, Uvsløkk S, Grynning S, Thue JV, Time B, Gustavsen A (2013a) Moisture robustness during retrofitting of timber frame walls with vacuum insulation panels: Experimental and theoretical studies. In: de Freitas VP, Delgado JMPQ (eds) Hygrothermal behavior, building pathology and durability. Building pathology and rehabilitation, vol 1. Springer, Berlin, pp 183–210

Jelle BP, Gao T, Tilset BG, Sandberg LIC, Grandcolas M, Simon C, Gustavsen A (2013b) Experimental pathways for achieving superinsulation through nano insulation materials. In: Proceedings of the 11th international vacuum insulation symposium (IVIS 2013), Dübendorf, Zürich, Switzerland, 19–20 Sept, pp 99–100

Jelle BP, Gao T, Sandberg LIC, Tilset BG, Grandcolas M, Gustavsen A (2014a) Thermal superinsulation for building applications—from concepts to experimental investigations. Int J Struct Anal Des 1:43–50

Jelle BP, Sveipe E, Wegger E, Gustavsen A, Grynning S, Thue JV, Time B, Lisø KR (2014b) Robustness classification of materials, assemblies and buildings. J Build Phys 37:213–245

Jelle BP, Kalnæs SE, Gao T (2015a) Low-emissivity materials for building applications: a state-of-the-art review and future research perspectives. Energy Build 96:329–356

Jelle BP, Gao T, Sandberg LIC, Ng S, Tilset BG, Grandcolas M, Gustavsen A (2015b) Development of nano insulation materials for building constructions. In: Proceedings of 5th international symposium on nanotechnology in construction (NICOM5), Chicago, Illinois, USA, 24–26 May, pp 429–434

Jelle BP, Gao T, Mofid SA, Ng S, Tilset BG, Grandcolas M (2015c) Hollow silica nanospheres as a stepping-stone toward thermal superinsulation materials. In: Proceedings of the 12th international vacuum insulation symposium (IVIS 2015), Nanjing, China, 19–21 Sept, pp 254–256

Jelle BP, Helgerud SC, Brunner S, Gao T, Rognvik E (2015d) Experimental investigations of vacuum insulation panels in an alkaline environment. In: Proceedings of the 12th international vacuum insulation symposium (IVIS 2015), Nanjing, China, 19–21 Sept, pp 302–306

Jelle BP, Baetens R, Gustavsen A (2015e) Aerogel insulation for building applications. In: Levy D, Zayat M (eds) The sol-gel handbook. Wiley-VCH, London

Johansson P (2012) Vacuum insulation panels in buildings, a literature review. Chalmers University of Technology, Göteborg

Johansson P, Geving S, Hagentoft C-E, Jelle BP, Rognvik E, Kalagasidis AS, Time B (2014) Interior insulation retrofit of a historical brick wall using vacuum insulation panels: hygrothermal numerical simulations and laboratory investigations. Build Environ 79:31–45

Jung S, Dorrestijn M, Raps D, Das A, Megaridis CM, Poulikakos D (2011) Are superhydrophobic surfaces best for icephobicity? Langmuir 27:3059–3066

Kaganer MG (1969) Thermal insulation in cryogenic engineering. IPST Press, Jerusalem (Russian version 1966)

Kalnæs SE, Jelle BP (2014) Vacuum insulation panel products: a state-of-the-art review and future research pathways. Appl Energy 116:355–375

Kalnæs SE, Jelle BP (2015) Phase change materials and products for building applications: a state-of-the-art review and future research opportunities. Energy Build 94:150–176

Kevothermal (2011) Vacuum insulation panels in construction, Case study 001. http://www.nanopore.eu/sites/default/files/case_study001_vips_in_flooring.pdf. Accessed on 21 Oct 2015

Kevothermal (2012) Vacuum insulation panels in construction, Case study 011. http://www.nanopore.eu/sites/default/files/Case%20study011%20Structural%20Vacuum%20Panel.pdf. Accessed 21 Oct 2015

Khudhair AM, Farid MM (2004) A review on energy conservation in building applications with thermal storage by latent heat using phase change materials. Energy Conserv Manage 45:263–275

Kim J, Lee JH, Song TH (2012) Vacuum insulation properties of phenolic foam. Int J Heat Mass Transfer 55:5343–5349

Koebel M, Rigacci A, Achard P (2012) Aerogel-based thermal superinsulation: an overview. J Sol-Gel Sci Technol 63:315–339

Kunic R (2012) Vacuum insulation panels—an assessment of the impact of accelerated ageing on service life. J Mech Eng 58:598–606
Kwon JS, Jung H, Yeo IS, Song TH (2011) Outgassing characteristics of a polycarbonate core material for vacuum insulation panels. Vacuum 85:839–846
Lampert CM (1998) Smart switchable glazing for solar energy and daylight control. Sol Energy Mater Sol Cells 52:207–221
Lampert CM (2004) Chromogenic smart materials. Mater Today 7:28–35
Lee D, Stevens PC, Zeng SQ, Hunt AJ (1995a) Thermal characterization of carbon-opacified silica aerogels. J Non-Cryst Solids 186:285–290
Lee K-H, Kim S-Y, Yoo K-P (1995b) Low-density, hydrophobic aerogels. J Non-Cryst Solids 186:18–22
Lenz K, Leistner Phl, Sedlbauer K, König N (2005) Vakuumisolationspaneele aus hygrothermischer und akusticher sicht. In: VIP-Bau (ed) Proceedings of the 2nd Fachtagung "Erfahrungen aus der Praxis", Wismar, Germany, 16–17 June, E1–E13
Levy D, Zayat M (eds) (2015) The sol-gel handbook. Wiley-VCH, London
Li H, Chen H, Li X, Duan W (2015) Degradation of VIP barrier envelopes exposed to alkaline solution at different temperatures. Energy Build 93:208–216
Liao Y, Wu X, Liu H, Chen Y (2011) Thermal conductivity of powder silica hollow spheres. Thermochim Acta 526:178–184
MacLean D, Korn J, Mukhopadhyaya P (2011) Vacuum insulation panels (VIPs) arrive in northern Canada. In: Proceedings of the 10th international vacuum insulation symposium (IVIS-X), Ottawa, Ontario, Canada, 15–16 Sept 2011, pp 59–67
Mandilaras I, Atsonios I, Zannis G, Founti M (2014) Thermal performance of a building envelope incorporating ETICS with vacuum insulation panels and EPS. Energy Build 85:654–665
Marouani S (2012) Investigation of the resistance welding of multilayer aluminum-coated polymer complexes used as envelopes of vacuum insulation panels. Mater Des 36:546–556
Maysenhölder W (2008) Sound transmission loss of vacuum insulation panels. Fraunhofer Institute for Building Physics, Stuttgart
Midtdal K, Jelle BP (2013) Self-cleaning glazing products: a state-of-the-art review and future research pathways. Sol Energy Mater Sol Cells 109:126–141
Miesbauer O, Kucukpinar E, Kiese S, Carmi Y, Noller K, Langowski H-C (2014) Studies on the barrier performance and adhesion strength of novel barrier films for vacuum insulation panels. Energy Build 85:597–603
Mukhopadhyaya P, Kumaran K, Normandin N, van Reenen D, Lackey J (2008) High-performance vacuum insulation panel: development of alternative core materials. J Cold Reg Eng 22: 103–123
Mukhopadhyaya P, Kumaran K, Normandin N, van Reenen D (2009) Fibre-powder composite as core material for vacuum insulation panels. In: Proceedings of the 9th international vacuum insulation symposium (IVIS-2009), London, UK, 17–18 Sept 2009
Mukhopadhyaya P, Kumaran K, Ping F, Normandin N (2011) Use of vacuum insulation panel in building envelope construction: advantages and challenges. In: 13th Canadian conference on building science and technology, Winnipeg, Manitoba, 10–13 May, pp 1–10
Mukhopadhyaya P, MacLean D, Korn J, van Reenen D, Molleti S (2014) Building application and thermal performance of vacuum insulation panels (VIPs) in Canadian subarctic climate. Energy Build 85:672–680
Ng S, Sandberg LIC, Jelle BP (2015a) Insulating and strength properties of an aerogel-incorporated mortar based on UHPC formulations. Key Eng Mater 629–630:43–48
Ng S, Jelle BP, Sandberg LIC, Gao T, Wallevik ÓH (2015b) Experimental investigations of aerogel-incorporated ultra-high performance concrete. Constr Build Mater 77:307–316
NRC (2012) Long-term performance of vacuum insulation panels (VIP) in the Canadian climate. http://www.nrc-cnrc.gc.ca/ci-ic/article/v17n3-1. Accessed 04 June 2013
Nussbaumer T, Bundi R, Tanner Ch, Muehlebach H (2005) Thermal analysis of a wooden door system with integrated vacuum insulation panels. Energy Build 37:1107–1113

Nussbaumer T, Ghazi Wakili K, Tanner Ch (2006) Experimental and numerical investigation of the thermal performance of a protected vacuum-insulation system applied to a concrete wall. Appl Energy 83:841–855

Pacheco-Torgal F (2014) Eco-efficient construction and building materials research under the EU framework programme Horizon 2020. Constr Build Mater 51:151–162

Pacheco-Torgal F, Jalali S (2011) Nanotechnology: advantages and drawbacks in the field of construction and building materials. Constr Build Mater 25:582–590

Parekh A, Mattock C (2011) Incorporation of vacuum insulation panels in a wood frame net zero energy home. In: Proceedings of the 10th international vacuum insulation symposium (IVIS-X), Ottawa, Ontario, Canada, 15–16 Sept, pp 46–50

Pei L, Kurumada KI, Tanigaki M, Hiro M, Susa K (2004) Closed-porosity mesoporous silica produced by high temperature rapid drying. J Mater Sci 39:663–665

Pons E, Yrieix B, Heymans L, Dubelley F, Planes E (2014) Permeation of water vapor through high performance laminates for VIPs and physical characterization of sorption and diffusion phenomena. Energy Build 85:604–616

Pool M (2009) Insulation of a mixed use building with 7 storeys in Munich with VIP. In: Proceedings of the 9th international vacuum insulation symposium (IVIS 2009), London, UK, 17–18 Sept 2009

Quenard D (2015a) International Energy Agency (IEA) annex 65 task long-term performance of super-insulating materials in building components and systems, http://www.iea-ebc.org/projects/ongoing-projects/ebc-annex-65/. Accessed 28 Jul 2015

Quenard D (2015b) International Energy Agency (IEA) annex 65 task long-term performance of super-insulating materials in building components and systems. http://www.enob.info/fileadmin/media/News/Dateien/EBC_Annex_65_Factsheet_X.pdf. Accessed 28 Jul 2015

Ribeiro AS, Mortimer RJ (2015) Electrochromic polymers. In: Encyclopedia of polymer science and technology. Wiley, London

Sallée H, Quenard D, Valenti E, Galan M (2014) VIP as thermal breaker for internal insulation system. Energy Build 85:631–637

Sandberg LIC, Gao T, Jelle BP, Gustavsen A (2013) Synthesis of hollow silica nanospheres by sacrificial polystyrene templates for thermal insulation applications. Adv Mater Sci Eng 6 (Article ID 483651)

Schutzius TM, Jung S, Maitra T, Eberle P, Antonini C, Stamatopoulos C, Poulikakos D (2015) Physics of icing and rational design of surfaces with extraordinary icephobicity. Langmuir 31:4807–4821

Schwab H, Heinemann U, Beck A, Ebert HP, Fricke J (2005a) Permeation of different gases through foils used as envelopes for vacuum insulation panels. J Thermal Envelope Build Sci 28:293–317

Schwab H, Heinemann U, Beck A, Ebert HP, Fricke J (2005b) Dependence of thermal conductivity on water content in vacuum insulation panels with fumed silica kernels. J Thermal Envelope Build Sci 28:319–326

Schwab H, Heinemann U, Wachtel J, Ebert H-P, Fricke J (2005c) Predictions for the increase in pressure and water content of vacuum insulation panels (VIPs) integrated into building constructions using model calculations. J Thermal Envelope Build Sci 28:327–344

Schwab H, Stark C, Wachtel J, Ebert H-P, Fricke J (2005d) Thermal bridges in vacuum–insulated building facades. J Thermal Envelope Build Sci 28:345–355

Schwab H, Heinemann U, Beck A, Ebert H-P, Fricke J (2005e) Prediction of service life for vacuum insulation panels with fumed silica kernel and foil cover. J Thermal Envelope Build Sci 28:357–374

Simmler H, Brunner S (2005) Vacuum insulation panels for building application: basic properties, aging mechanisms and service life. Energy Build 37:1122–1131

Simmler H, Brunner S, Heinemann U, Schwab H, Kumaran K, Mukhopadhyaya P, Quènard D, Sallèe H, Noller K, Kücküpinar-Niarchos E, Stramm C, Tenpierik M, Cauberg H, Erb M (2005) Vacuum insulation panels. Study on VIP-components and panels for service life

prediction in building applications (subtask A). In: HiPTI—High Performance Thermal Insulation, IEA/ECBCS Annex 39, Sept 2005
Smith DM, Maskara A, Boes U (1998) Aerogel-based thermal insulation. J Non-Cryst Solids 225:254–259
SolarArchitetektur (2013) Die Solarsiedlung in Freiburg. http://www.rolfdisch.de/index.php?p=home&pid=78&L=0&host=2#a285. Accessed 08 June 2013
Sprengard C, Holm AH (2014) Numerical examination of thermal bridging effects at the edges of vacuum-insulation-panels (VIP) in various constructions. Energy Build 85:638–643
Stahl Th, Brunner S, Zimmermann M, Ghazi Wakili K (2012) Thermo-hygric properties of a newly developed aerogel based insulation rendering for both exterior and interior applications. Energy Build 44:114–117
Sveipe E, Jelle BP, Wegger E, Uvsløkk S, Grynning S, Thue JV, Time B, Gustavsen A (2011) Improving thermal insulation of timber frame walls by retrofitting with vacuum insulation panels—experimental and theoretical investigations. J Build Phys 35:168–188
Tenpierik MJ (2009) Vacuum insulation panels applied in building constructions. In: (VIP ABC), PhD thesis, Technische Universiteit Delft
Tenpierik MJ, Cauberg JJM (2010) Encapsulated vacuuminsulation panels: theoretical thermal optimization. Build Res Inf 38:660–669
Tenpierik MJ, Cauberg JJM, Thorsell TI (2007) Integrating vacuum insulation panels in building constructions: an integral perspective. Constr Innovation 7:38–53
Thorsell TI (2012) Advances in thermal insulation—vacuum insulation panels and thermal efficiency to reduce energy usage in buildings. PhD thesis, KTH—The Royal Institute of Technology, 2012
Thorsell TI, Källebrink I (2005) Edge loss minimization in vacuum insulation panels. In: Jóhannesson G (ed) Proceedings of the 7th symposium on building physics in the Nordic countries, Reykjavik, Iceland, 13–15 June 2005, vol 2. The Icelandic Building Research Institute, Reykjavik, pp 945–952
va-Q-tec (2013) http://www.va-q-tec.com/va-q-vip_en.html. Accessed 30 May 2013
VIPA (2015) Vacuum insulation panel association. http://vipa-international.com/. Accessed 28 Jul 2015
VIP-Bau (2013) http://vip-bau.de/d_pages/monitoring/alle_objekte.htm. Accessed 7 June 2013
Voellinger T, Bassi A, Heitel M (2014) Facilitating the incorporation of VIP into precast concrete sandwich panels. Energy Build 85:666–671
Wang X, Walliman N, Ogden R, Kendrick C (2007) VIP and their applications in buildings: a review. Constr Mater 160:145–153
Wegger E, Jelle BP, Sveipe E, Grynning S, Gustavsen A, Baetens R, Thue JV (2011) Aging effects on thermal properties and service life of vacuum insulation panels. J Build Phys 35:128–167
Wong JCH, Kaymak H, Brunner S, Koebel MM (2014) Mechanical properties of monolithic silica aerogels made from polyethoxydisiloxanes. Microporous Mesoporous Mater 183:23–29
Yang CG, Li YJ, Gao X, Xu L (2012) A review of vacuum degradation research and the experimental outgassing research of the core material—PU foam on vacuum insulation panels. Phys Proc 32:239–244
Yrieix B, Morel B, Pons E (2014) VIP service life assessment: Interactions between barrier laminates and core material, and significance of silica core ageing. Energy Build 85:617–630
Zhang P, Lv FY (2015) A review of the recent advances in superhydrophobic surfaces and the emerging energy-related applications. Energy 82:1068–1087
Zimmermann M, Brunner S (2011) VIP market development recommendations based on the SELF experimental building. In: Proceedings of the 10th international vacuum insulation symposium (IVIS-X), Ottawa, Ontario, Canada, 15–16 Sept, pp 122–125

Chapter 8
Nanomaterial-Based PCM Composites for Thermal Energy Storage in Buildings

R. Parameshwaran and Siva Kalaiselvam

Abstract Energy efficiency in buildings is a vital factor to be addressed in every stages of development of building envelopes, since buildings consume almost one-third to one-quarter of energy being produced globally. In the spectrum of techniques available to cater the building cooling and heating load demands, there has been a continuous quest toward latent thermal energy storage (LTES) systems for achieving energy redistribution requirements in buildings. The interesting fact about the LTES systems relies on the phase change materials (PCMs) being used to store and release heat energy depending upon the thermal load demand. A step ahead, the utilization of nanomaterials paves the way for accomplishing enhanced thermal performance of such PCMs on a long run. This chapter is exclusively dedicated to provide better understanding of a variety of nanomaterial-based PCM composites for thermal energy storage and energy efficiency in buildings. This is an ever-growing as well as emerging field of interest to wide scientific and engineering communities globally. The nucleus of this chapter is focused on the enhancement of thermal energy storage capabilities of NanoPCM composites which would contribute for achieving improved energy efficiency in buildings.

R. Parameshwaran (✉)
Department of Mechanical Engineering, Birla Institute of Technology & Science-Pilani, Hyderabad Campus, Hyderabad 500078, India
e-mail: parameshwaranr@hyderabad.bits-pilani.ac.in; parameshviews@gmail.com

S. Kalaiselvam
Department of Applied Science and Technology, Anna University, AC Tech Campus, Chennai 600025, India
e-mail: kalai@annauniv.edu; nanokalai@gmail.com

F. Pacheco Torgal et al. (eds.), *Nano and Biotech Based Materials for Energy Building Efficiency*, DOI 10.1007/978-3-319-27505-5_8

8.1 Introduction

In the quest toward energy conservative design of thermal systems, several methods dedicated to reducing the energy consumption in buildings have gained impetus globally. In recent years, the concept of integrating latent thermal energy storage (LTES) systems for building envelopes has been increasingly attractive.

In recent years, many research studies have been performed globally in order to enhance the latent thermal energy storage mechanisms of phase change materials (PCMs) for various industrial, commercial, residential (domestic) cooling and heating applications (Gracia and Cabeza 2015). These research studies primarily investigated the different heat transfer enhancement techniques for thermal energy storage systems.

Although the LTES system offers better energy storage capability at nearly isothermal conditions, the PCMs packed inside these systems possess certain inherent limitations in heat transfer characteristics which directly affect the overall performance of the LTES system. Because of the very low thermal conductivity observed in the conventional PCMs, the effect of supercooling dominates in many PCMs, while they undergo the phase change processes. Hence, it is of great importance to enhance the thermal properties of PCMs and to ensure better thermal performance during the phase transition as well.

In particular, the modern research works on the LTES systems using PCMs are now especially focusing toward using the advanced technologies for achieving improved energy savings potential in buildings (Jamekhorshid et al. 2014). In this context, scientists and researchers across the world have come out with a better solution in the form of a technology, which is altogether referred to as *nanotechnology*.

Nanotechnology serves as a means to produce engineered materials at nanoscale level (0.1–100 nm) with tunable physicochemical and thermophysical properties (Pacheco-Torgal 2014). The success of nanotechnology has been realized in almost all the fields of engineering and technology, and the application of nanotechnology can be considered to serve as an effective tool to confront the energy challenges in buildings.

8.2 NanoPCM Composites for Thermal Energy Storage in Buildings

8.2.1 Phase Change Materials (PCMs) and Their Properties

The significance of integrating the PCMs or LTES materials in buildings can be experienced through their phase transition characteristics with respect to the thermal load demand persisting in the building enclosure. PCMs are commonly referred to as chemical compounds which remain in either solid or liquid state at atmospheric

conditions, and whose fusion temperature would be in the range of redistributing the thermal load demand in buildings on timely basis.

Typically, the operational mechanism behind all PCMs is their tendency to freeze or melt depending upon the head load being supplied or extracted from them. For instance, a liquid PCM (at atmospheric conditions) if subjected to a temperature lower than its freezing temperature, the PCM would tend to solidify accordingly. Precisely, the phase transformation from liquid to solid state is governed by heat addition, thermophysical properties, etc., of the PCM.

The internal energy change taking place during phase transformation at almost isothermal conditions would give a measure of the latent heat of fusion of the PCM. Similar is the case for melting of the PCM. In practice, a variety of latent heat storage materials are available as shown in Fig. 8.1. Depending upon the type of phase change mechanism and thermophysical properties the LTES materials would exhibit, they can be used to cater the energy redistribution requirements in buildings suitably.

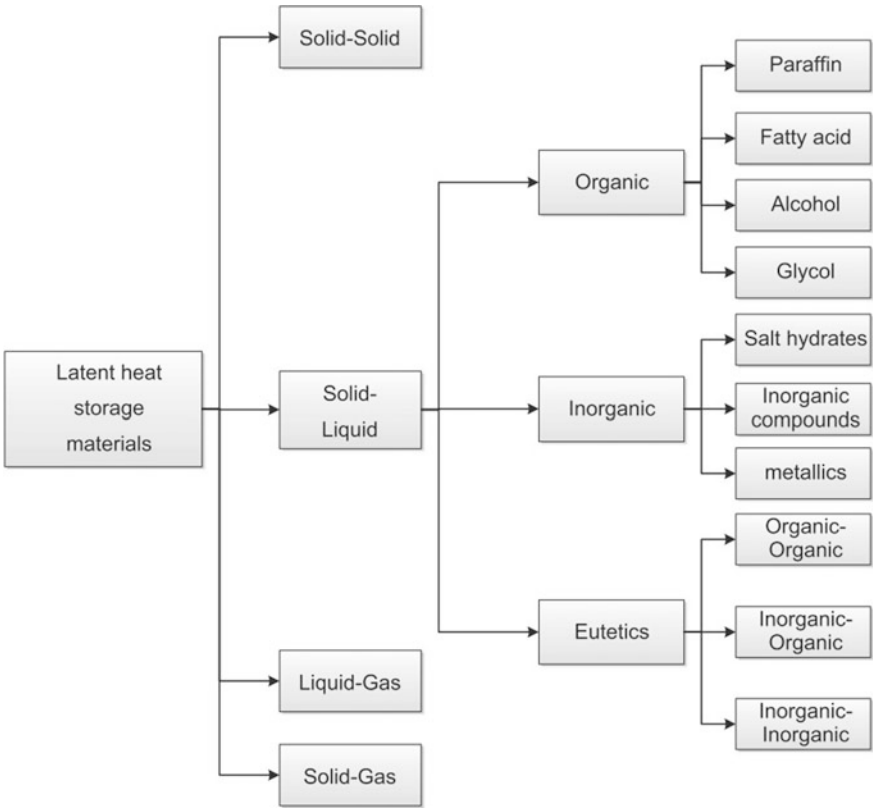

Fig. 8.1 Classification of PCMs (Su et al. 2015)

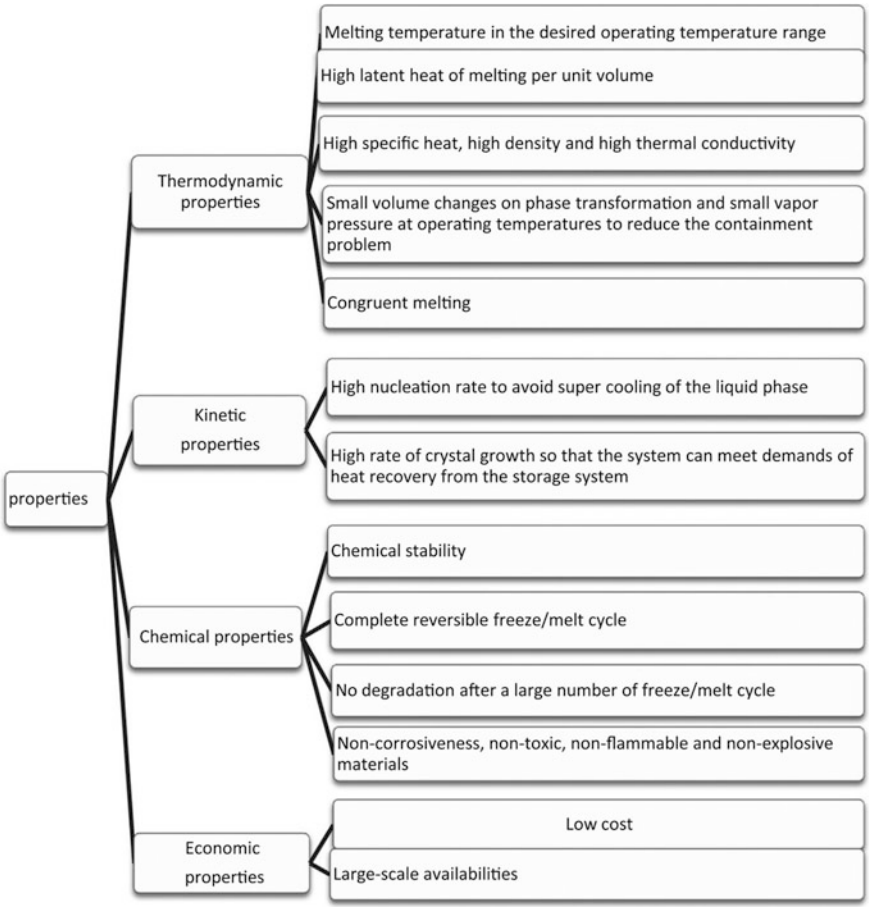

Fig. 8.2 Selection criteria for latent heat storage materials (Zhou et al. 2015)

The properties which are considered most essential for LTES materials are categorized in Fig. 8.2. These properties would basically help the design engineers, architects, or the building developers to select or judge appropriate LTES materials, which are highly suitable for energy-efficient building applications.

In addition to these essential properties, the LTES materials should also satisfy some of the vital performance parameters while incorporated into building components, which are as follows:

- Thermal load demand persisting in building enclosures;
- Type of heat storage (either by passive or by active method);
- Swift phase transition characteristics;
- Integration with cooling and/or heating systems in buildings;
- Energy/cost savings potential on an overall.

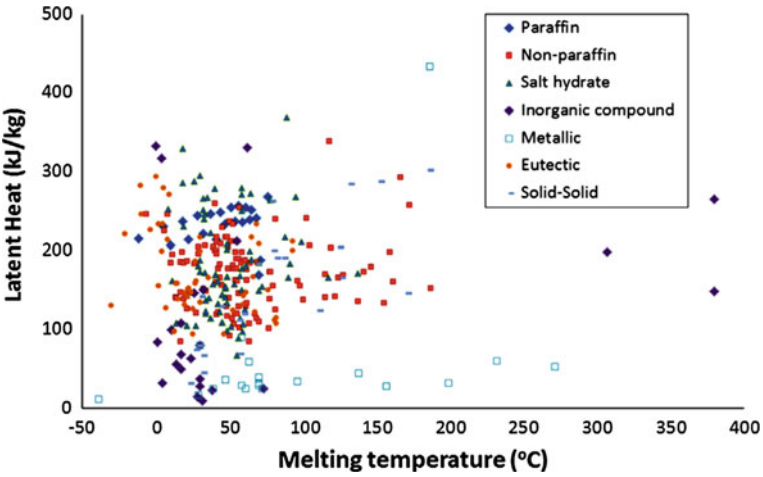

Fig. 8.3 Melting temperature and latent heat distribution for different types of PCMs (Su et al. 2015)

The relationship between the range of melting temperature and latent heat capacity of LTES materials is represented in Fig. 8.3. It is clearly observed that the LTES materials of the category organic, salt hydrate, eutectic, and solid–solid PCMs exhibit relatively lower melting temperatures. On the other hand, the inorganic and metallic PCMs do have higher melting temperature range; however, most of the metallic compounds possess relatively lowest latent heat storage capacity.

Similarly, the relationship between the melting temperature and thermal conductivity (in log scale) reveals that the metallic PCMs do have higher thermal conductivity when compared to the inorganic and organic PCMs, by over 10 W/m K (Log (k) > 1). Also, the thermal conductivity of the inorganic PCMs is higher than the organic PCMs.

The inherent merits and limitations of organic and inorganic salt hydrates and eutectic heat storage materials are summarized in Tables 8.1 and 8.2.

8.2.2 Nanomaterials and Their Characteristics

Owing to the excellent properties of materials found at the nanoscale level, which is significantly different from the one in its bulk state, the integration of nanotechnology in thermal energy storage has been gaining impetus in recent years. However, nanotechnology is considered to have been evolved over many years ago, but due to the technological advancements that are taking place in materials science and engineering, the adaptation of nanoscale analysis from the engineering perspectives is seen equally vital for modern building applications.

Table 8.1 Merits of the LTES materials

Organic (paraffins and non-paraffins)	Inorganic salt hydrates	Eutectics
They are available in a large range of temperature	They possess high volumetric latent heat storage capacity	They exhibit application-specific sharp phase change temperature (melting temperature)
Values of latent heat of enthalpy are high (e.g., fatty acids have much higher latent heat of fusion than the paraffins)	They possess low vapor pressure in the melt state	Exhibit slightly high volumetric thermal storage density than the organic compounds
Supercooling degree or superfusion effect is normally low during freezing process	They are non-corrosive, non-reactive, non-flammable, and not dangerous	They possess low or no segregation. Thermal reliability is good with congruent phase transition characteristics
Relatively low segregation even after several thermal cycles (thermal reliability). High thermal stability, congruent phase transition process	Have good compatibility with the conventional construction materials. Recyclable, cost-effective, and ease of availability	
Show self-nucleation and growth rate properties	Exhibit high latent heat of enthalpy and sharper phase transformation. High thermal conductivity with lower volumetric changes during phase change. Safe to the environment in terms of handling and disposing when compared to the paraffins	

In particular, the application of nanotechnology in materials which would store and release heat energy based on the thermal load demand in buildings is inexorable. The thermophysical and physicochemical property changes occurring at nanoscale level in latent heat storage materials are identified to be functional as well as energy efficient, while they are incorporated into building structures.

Basically, nanomaterials or nanostructures refer to a class of materials whose size normally ranges from 0.1 nm to 100 nm, thereby giving extraordinary performance when they are blended with the base material. The resulting nanocomposite material would then have excellent thermophysical attributes which ultimately enhance the heat energy storage performance of the LTES material. The broad classification of nanostructured materials is presented in Fig. 8.4.

The most commonly preferred routes of producing nanomaterials are as follows: (a) top-down approach and (b) bottom-up approach. As depicted in Fig. 8.5, it can be seen that in a top-down approach, the nanostructured materials can be formed by fragmentation of large coarse bulk materials into smaller size particles in sizes ranging from few nanometers to micrometers. In the case of bottom-up approach,

Table 8.2 Limitations of LTES materials

Organic (paraffins and non-paraffins)	Inorganic salt hydrates	Eutectics
Density, thermal conductivity, and latent heat of fusion are inherently lower	Relatively high supercooling properties	Analysis of eutectics for thermal energy storage applications is limited due to the insufficient and non-availability of the thermophysical property data
Inflammable, less compatible with plastic containments	Low degree of nucleation (requires nucleating additives and thickening constituent materials)	In some cases, fatty acid eutectics evolve pungent odor, making them less suitable for PCM wallboard thermal energy storage applications in indoor environments
Larger volumetric changes are possible during charging and discharging (applicable to some grade of organic compounds). Expensive by nature	Incongruent phase change and dehydration occur during freezing and melting cycles	
	Decomposition associated with phase separation. Compatibility with some building materials is limited. Exhibit corrosion properties when subjected to most metals. Slightly toxic in nature	

the nanostructures of desired shape and size can easily be formed by the self-assembly of atoms or molecules well within the nanoscale level from the bottom range of 0.1 nm up to 100 nm. In general, the production of nanomaterials through the bottom-up approach is much appreciated due to the precision and process efficiency in acquiring the desired morphology of the nanoparticles for real-time applications.

8.2.3 NanoPCM Composites

The term "nanocomposite" usually refers to the materials being blended at nanoscale level or embedding of nanostructured material into the bulk material. The purpose of infusing a nanomaterial into the bulk material (which is usually different from that of the nanomaterial being produced) is to improve certain vital properties related to its operational performance on a long run. In the case of thermal energy storage, the LTES materials which are either organic or inorganic or eutectic compounds do have certain deficiencies in terms of their operational performance. For which, through the doping of specific nanomaterial in them would certainly improve their thermal storage properties significantly. For instance, most of the organic PCMs possess relatively low thermal conductivity. Thus, the incorporation of nanomaterials as heat

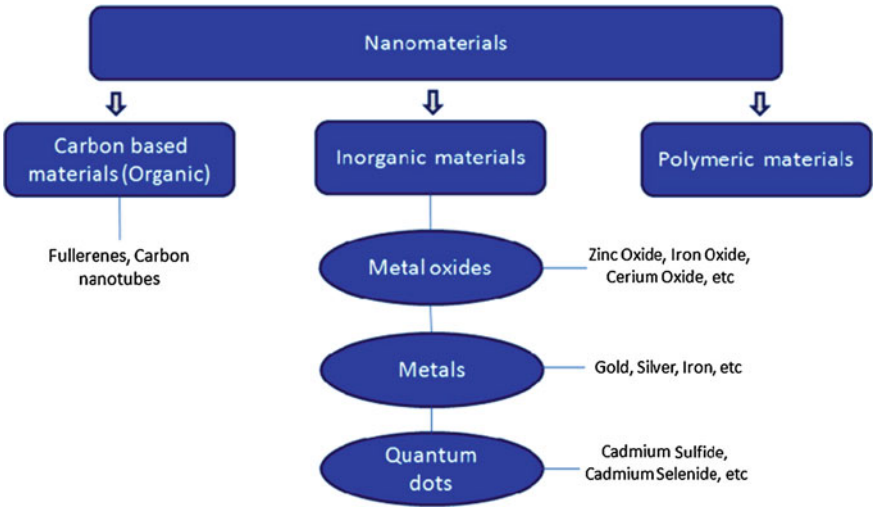

Fig. 8.4 Classification of nanomaterials (Manikam et al. 2011)

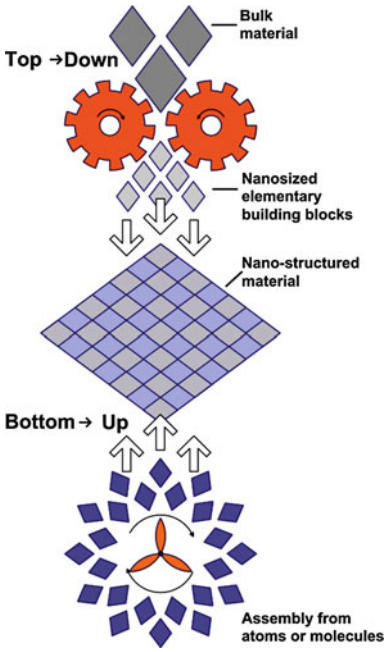

Fig. 8.5 Illustration of the "top-down" and "bottom-up" approaches in nanotechnology (Sobolev and Ferrada-Gutiérrez 2005; Sanchez and Sobolev 2010)

enhancement materials into the bulk organic PCMs can enable them to perform better while undergoing phase transition processes (Fig. 8.6).

In this context, Jeong et al. (2015) performed an experimental study on LTES material containing exfoliated graphite nanoplatelets and showed that by infusing

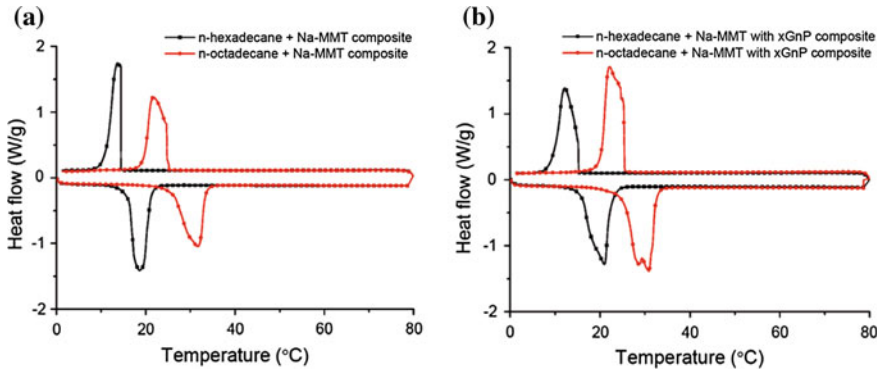

Fig. 8.6 DSC graph of **a** paraffinic PCM-based composite PCM and **b** paraffinic PCM-based composites with xGnP (Jeong et al. 2015)

nanostructures, thermal conductivity of the organic PCMs can be enhanced by several folds. That is, the *n*-octadecane-based nanocomposite PCM yielded 254 % increase of thermal conductivity with respect to the normal *n*-octadecane composite PCM.

Furthermore, the thermal analysis results also confirmed the significance of embedding the graphite nanoplatelets into the paraffinic PCM. That is, more PCM has been filled into the porous structure of the exfoliated graphite nanoplatelets, thereby resulting in the enhanced thermal efficiency and high latent heat capacity which can be considered suitable for building applications.

Sayyar et al. (2014) demonstrated the usefulness of NanoPCM wall for catering the cooling and heating loads in buildings. The analysis on the control wall (without PCM) and the NanoPCM wall clearly indicates that by introducing the graphite interconnected nanosheet-based PCM, the temperature in indoor environment is found to be maintained near to the comfort zone.

The colored regions in the graph depict the differences in the heat fluxes. This signifies the real importance of the NanoPCM utilization in offsetting the cooling load demand, which also contributes for energy savings potential in buildings. Overall, about 79 % of total energy savings have been made possible by these NanoPCM walls, catering for the total reduction in the heating/cooling energy demand ranging from 4191 to 877 J.

In recent years, the incorporation of nanomaterials into PCM for satisfying the cooling requirements in buildings has also been increasingly attractive. As could be observed from the study performed by Sayyar et al. (2014), another interesting research work carried out by Fang et al. (2013) also supports the integration of NanoPCMs in buildings in order to make them energy efficient on a long-term basis.

Fang et al. (2013) reported that the organic PCM (*n*-tetradecane, shortly referred as Tet) which acts as the core material and the polystyrene that serves as the shell material exhibit good thermal energy storage performance for cool storage applications in buildings. The nanoencapsulated PCM being produced in this work

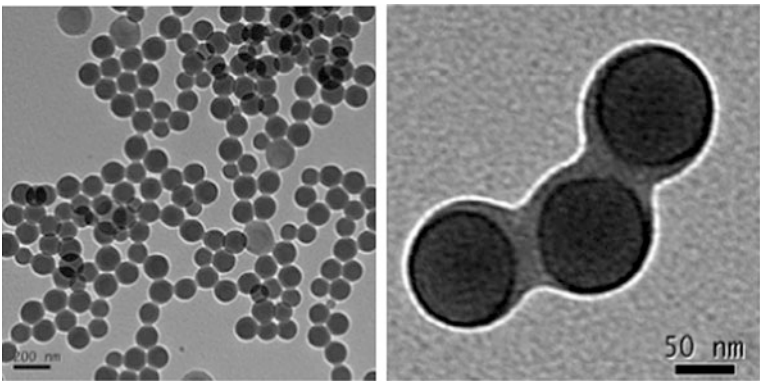

Fig. 8.7 TEM images of Tet/PS nanocapsule (Fang et al. 2013)

(Fig. 8.7) is observed to have better thermal stability (more than 40 thermal cycles) and no delamination and is completely stable.

Moreover, the phase transition characteristics are also equally good with freezing at −3.43 °C, melting at 4.04 °C, and latent heat of enthalpy for freezing and melting to be 91.27 and 98.71 J/g, respectively. The nanocapsules (containing PCM) are suggested to be viable and efficient candidates for heat storage in buildings. Biswas et al. (2014) also demonstrated the usefulness of nano-PCM wallboard, which yielded higher load factors, produced effective thermal management in indoor environment as well as contributed for the reduction in the electrical energy consumption and costs.

Similarly, the development of polymer nanocomposite PCMs is gaining impetus in building applications in recent years, which is due to the improved thermal energy storage properties being exhibited by such NanoPCMs. Here, the nanocapsules are prepared such that the PCM acts as the core material and the shell is formed by a copolymer.

In a recent study performed by Tumirah et al. (2014), the NanoPCM containing *n*-octadecane as the core material and styrene-methyl methacrylate (St/MMA) copolymer shell has been prepared through the miniemulsion in situ polymerization method. Several samples have been prepared for estimating the thermal storage performance of the nanoencapsulated PCMs.

The micrographs shown in Fig. 8.8 clearly indicate that the organic PCM (dark spherical particle) has been encapsulated by the shell copolymer (outer ring). It is revealed that the nanocapsules being tested exhibited increased stability (both thermal and chemical) without compromising on the morphology and the smoothness.

In addition, the nanocapsules are 102 nm in diameter (average measurement value), which signifies that the mass ratio of St/MMA plays an important role in determining the encapsulation efficiency as well as the structural morphology of the as-prepared nanocapsules. Based on the test results, it is pertinent to note that the NanoPCMs exhibited good heat transfer characteristics, latent heat of enthalpy, and

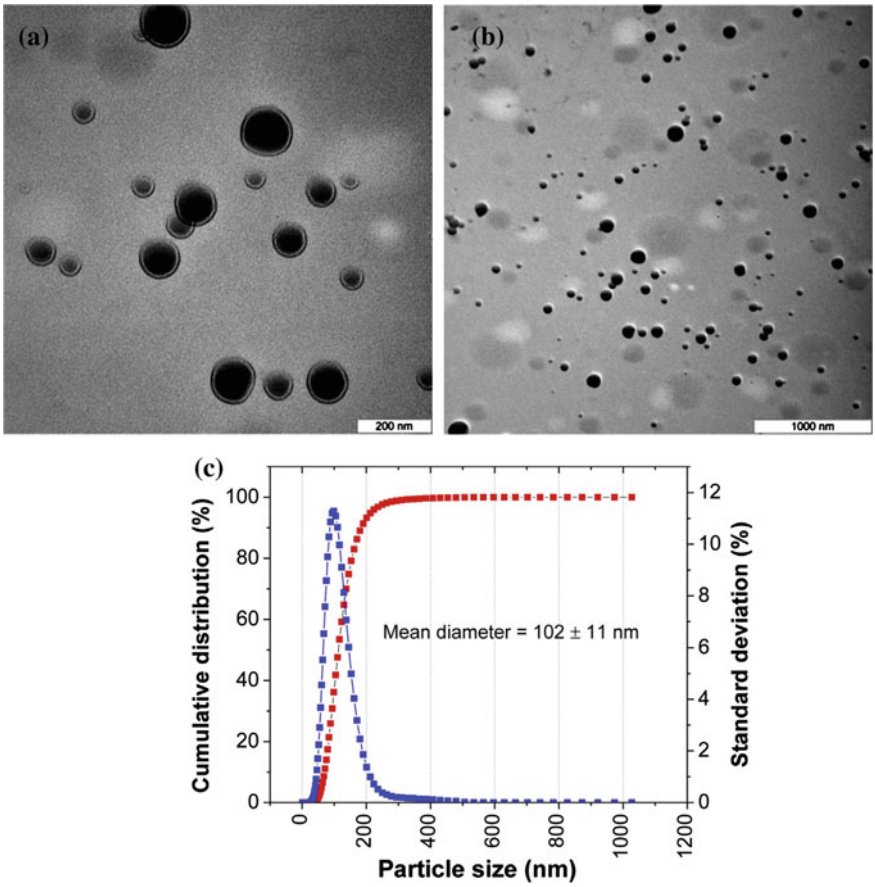

Fig. 8.8 TEM image of the *n*-octadecane/St-MMA nanocapsules of sample A4 at two different TEM setting views: **a** magnification 100 k and **b** magnification 30 k **c** particle size distribution studied using DLS (Tumirah et al. 2014)

phase transition temperature during charging and discharging cycles, provided the thermal conductivity of which actually depends on the encapsulation efficiency of the nanocapsules.

Khadiran et al. (2015a, b) described the thermal energy storage potential of activated carbon-based shape-stabilized *n*-octadecane nanocomposites for building applications. Factually, the porous wall of the activated carbon (AC) acts as a nucleating agent, thereby effectively promoting the phase change processes of the organic PCM. The lesser the PCM concentration, the deeper the penetration of the PCM into the porous matrix of the activated carbon. Thus, the encapsulation efficiency of the nanocomposites is equally good, which is about 42.5 % for PCM loading of 43.4 %.

The adsorption of the PCM into the porous structure of the activated carbon matrix can be easily visualized from the micrographs, which further signifies the

molecular interaction between the two materials. Due to the capillary action as well as the high surface ratio of activated carbon, the organic PCM gets occupied into the filler regions of the activated carbon, resulting in the good thermal stability and latent heat capacity, highly suitable for building applications.

Cao et al. (2015) revealed the vital aspects of nanocomposite PCM for building applications through experimental studies. It can be seen from the micrographs (Fig. 8.9) that fatty acid eutectics have been impregnated into the porous structure of the nanofibrous mats, which in turn yielded mechanical strength, good phase transition properties, and thermal stability for the PCM. The adsorption of the PCM into the porous structure of the nanomats was really good in the sense that even during repeated melting cycles, the PCMs are observed to be well intact (no leakage) with the nanofibrous mats.

The phase change enthalpies and temperatures of the as-prepared nanocomposite PCM are measured to be 120.1–165.4 kJ/kg and 19.8–31.4 °C for PAN mats, and 92.1–128.0 kJ/kg and 18.8–30.7 °C for carbon mats, respectively (Fig. 8.10). It is worth to note that the as-prepared form of stable nanocomposite PCMs exhibited suitable phase change properties for thermal energy storage applications including building energy conservation, temperature regulation in underfloor boards or wallboards, and solar space heating.

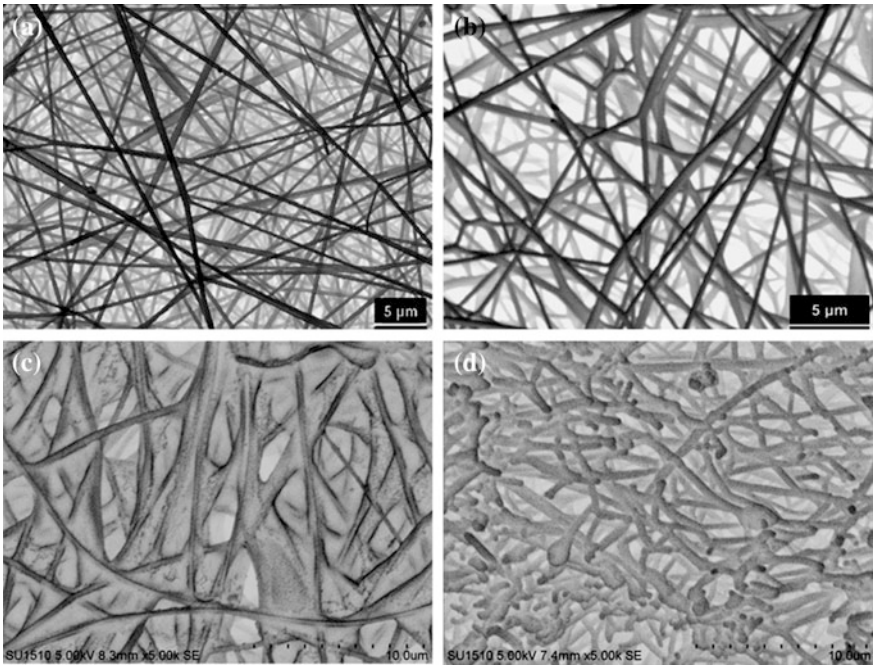

Fig. 8.9 The SEM images of **a** electrospun PAN, **b** carbon nanofibrous mats, **c** CA–PA/PAN, and **d** CA–PA/carbon (Cai et al. 2013; Cao et al. 2015)

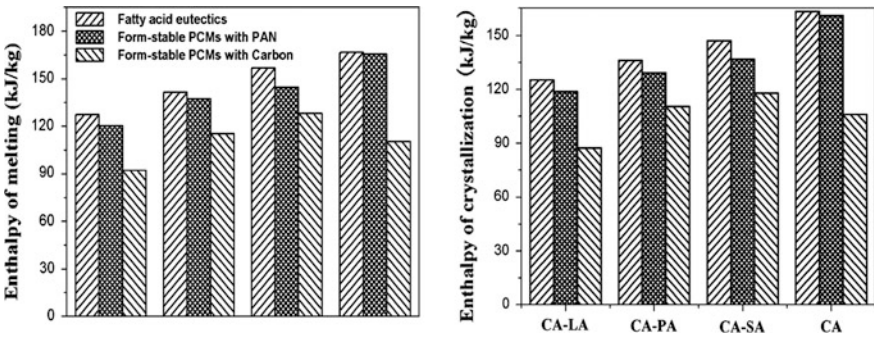

Fig. 8.10 Comparisons on absorption capacities of electrospun PAN and carbon nanofibrous mats on fatty acid eutectics (extracted from DSC measurements) (Cai et al. 2013; Cao et al. 2015)

In a similar way but earlier point in time, Do et al. (2012) developed core/shell composite nanofibers as composite PCM through coaxial electrospinning method. Here, polyethylene glycol (PEG) which is an organic PCM with three different molecular weights has been utilized for testing thermal energy storage capability for building applications. The thermal properties of the NanoPCMs are summarized in Table 8.3. Based on the test results, it is inferred that the thermal characteristics of the NanoPCMs are well maintained, showing good thermal stability.

In order to study the properties of a variety of PCMs, in particular encapsulated organic PCMs (OPCMs), Khadiran et al. (2015a, b) have identified different characterization techniques and suitably presented those which are most commonly used to characterize both pure PCMs and the NanoPCMs as well.

Depending upon the type of PCMs being selected and the nanomaterials to be infused into them, the necessary characterization technique can be used to measure their thermophysical and thermal storage properties. The most essential aspects of encapsulation techniques are to achieve maximum possible thermal storage properties with cost-effectiveness, thereby enabling the PCMs or the NanoPCMs ready for applications with tunable dimensions.

Table 8.3 Thermal properties of PEG and electrospun PEG/PVDF composite nanofibers (Do et al. 2012; Cao et al. 2015)

PEG	Core feed rate (mL/h)	Melting point (°C)	Latent heat (J/g)	Crystallization point (°C)	Latent heat (J/g)	Enthalpy ratio (% PEG)
PEG1000	Pure	41.1	97	24.4	92	–
	0.126	37.8	22	17.0	19	23.0
PEG2000	Pure	55.6	112	27.2	107	–
	0.126	53.5	32	24.2	27	25.0
	0.150	53.7	36	23.9	29	32.0
PEG4000	Pure	64.7	161	31.8	155	–
	0.126	63.1	43	31.4	40	26.8
	0.210	62.8	68	31.6	62	42.5

However, the cost of impregnation or encapsulation of PCMs either with or without heat enhancement materials implies a direct measure on its utilization index into real-time building cooling applications. The economic analysis performed by Kosny et al. (2013) on the aspects of cost-effectiveness for PCM-enhanced building envelopes gave a good insight about the target cost levels at which the PCM could be considered cost-effective. They estimated that for a payback period of 10 years and assuming 30 %-by-weight of the PCM being dispersed in wall insulation, the target cost level for PCMs with latent heat capacity between 120 and 220 kJ/kg to be of $3.30–8.80/kg ($1.50–4.00/lb). On the other hand, from the current context, the cost of the PCM having latent heat capacity of 116 kJ/kg has been projected to be less than or around $4.40–6.60/kg ($2–3/lb), while produced commercially.

In a recent study performed by Biswas and Abhari (2014), a low-cost novel PCM containing naturally occurring fatty acids/glycerides embedded into the high-density polyethylene (HDPE) pellets has been prepared and tested for its thermal energy storage performance in a building fabric component. It is suggested that adding PCM to only the inner section of the exterior wall could yield better thermal performance with cost savings potential, instead of incorporating the PCM to the whole wall cavity.

Figure 8.11 illustrates the overview of type of supporting materials which can be found suitable for encapsulating the OPCMs using different production techniques. A review of properties of nanoencapsulated OPCMs which were prepared using different chemical methods is summarized in Table 8.4.

From the perspective of environmental concerns, scientists and researchers across the world are putting significant efforts in developing the environment-friendly PCMs for building applications. In this regard, Konuklu et al. (2015) developed a series of four nanocapsules which contain *n*-alkanes (C_nH_{2n+2}) including tetradecane, pentadecane, hexadecane, and heptadecane in poly(styrene-co-ethylacrylate) through emulsion copolymerization method.

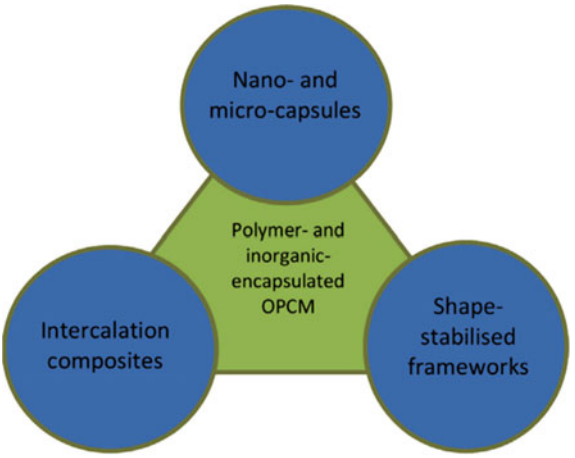

Fig. 8.11 The encapsulation methods and supporting materials that can be used to encapsulate OPCMs (Khadiran et al. 2015a, b)

Table 8.4 Properties of nanoencapsulated OPCMs prepared using different chemical methods (Khadiran et al. 2015a, b)

Chemical method	OPCMs	Shell	Particle size (nm)	Encapsulation efficiency (%)	Temperature of melting (peak) (°C)	Latent heat of melting (J/g)	Reference(s)
Ultrasonic-assisted miniemulsion in situ polymerization	*n*-octadecane	Polystyrene	100–123	–	–	124.4	Fang et al. (2008)
In situ polymerization	*n*-tetradecane	Urea formaldehyde	100	61.8	9.01	134.16	Fang et al. (2009)
In situ polymerization	*n*-octadecane	Resorcinol-modified melamine formaldehyde	20	92	26.91	146.25	Zhang and Wang (2009)
Direct miniemulsion polymerization	*n*-hexadecane	Poly(alkyl methacrylate)	50–140	–	–	–	Black et al. (2010)
Interfacial redox initiation miniemulsion polymerization	*n*-octadecane	Polystyrene and polymethyl methacrylate	<100	95	–	114	Kwon (2010)
Miniemulsion polymerization	Paraffin	Polystyrene	100	48.6	26.2	107.1	Wu et al. (2011)
Miniemulsion polymerization	*n*-dodecanol	Poly(methyl methacrylate)	150	82.2	18.2	98.8	Chen et al. (2012)
Direct miniemulsion method	*n*-octadecane	Poly(ethyl methacrylate), poly (methyl methacrylate)	140 and 119	89.5	32.2 and 31.9	198.5 and 208.7	Zhang et al. (2012a)
Ultrasonic-assisted miniemulsion in situ polymerization	*n*-tetradecane	Poly(styrene)	132	89	4.04	98.71	Fang et al. (2013)
Miniemulsion polymerization	RT80	Styrene-butyl acrylate	52–112	80	80.9	10–20	Fuensanta et al. (2013)

(continued)

Table 8.4 (continued)

Chemical method	OPCMs	Shell	Particle size (nm)	Encapsulation efficiency (%)	Temperature of melting (peak) (°C)	Latent heat of melting (J/g)	Reference(s)
One-step miniemulsion in situ polymerization	*n*-octadecane	Styrene-methyl methacrylate copolymer	60–130	45.1	29.5	107.9	Tumirah et al. (2014)
Ultraviolet photoinitiated emulsion polymerization	Eicosanoic, stearic acid eutectic	Poly(methyl methacrylate)	46	68.8	56.9	126.4	Wang et al. (2014)
Time-saving ultrasonically initiated miniemulsion polymerization	*n*-dotriacontane	Poly(styrene)	168.2	61.23	70.9	174.8	Fang et al. (2014)
Emulsion copolymerization	*n*-octadecane, palmitic acid	Poly(styrene-co-ethyl acrylate)	166, 265	32.12, 47.79	42.39, 64.57	49.03, 97.93	Giro-Paloma et al. (2015)

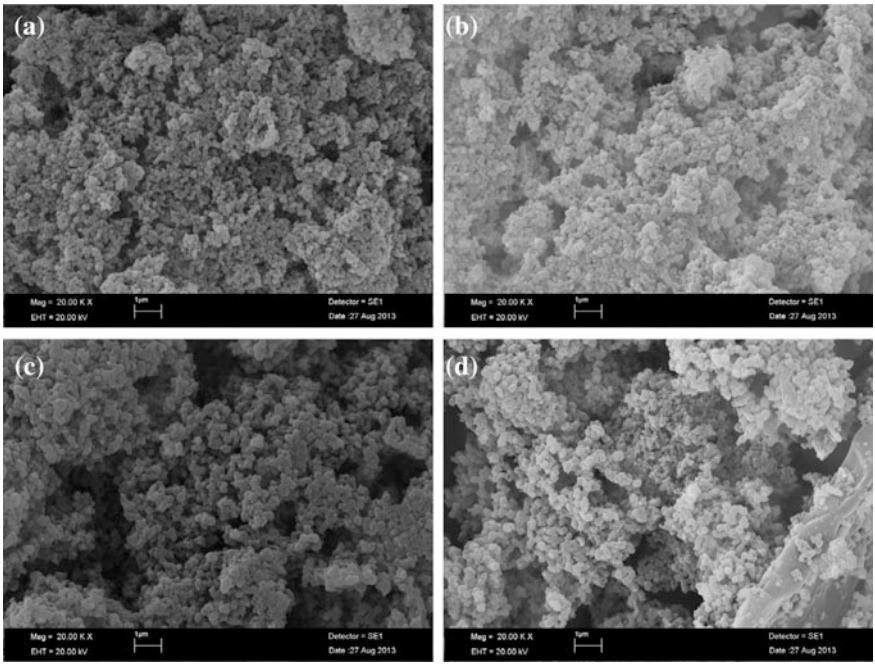

Fig. 8.12 SEM micrographs of NanoT (**a**), NanoP (**b**), NanoH (**c**), and NanoHP (**d**), at 2000 kX and 2000 kV (Konuklu et al. 2015)

The micrograph results (Fig. 8.12) reveal that the nanocapsules are approximately uniform and possess spherical profiles. It is obvious that increasing the proportion of the core material would increase the encapsulation efficiency and the latent heat capacity as well. In short, the maximum encapsulation efficiencies obtained in this study ranged from 69 to 87 %, wherein the best core material–shell polymer ratio has been figured out to be 3:1.

Sari et al. (2015a, b) reported the thermal energy storage potential of PMMA/C-SEM micro/nanocapsules for the latent heat storage applications in buildings. They have synthesized the aforementioned micro/nano-PCM capsules by using the emulsion polymerization technique. Based on the test results, it is realized that the micro/nanoencapsulated PCM possessed good thermal reliability, thermal conductivity, and chemical stability as well. Thus, it is suggested that the micro/nanoencapsulated PCM can be utilized into the building fabric components in order to reduce the temperature swings in indoor environment depending upon the climatic conditions.

Wi et al. (2015) investigated the thermal performances of shape-stabilized PCMs for saving energy in buildings. In this study, two shape-stabilized PCMs have been prepared by impregnating the naturally available coconut oil and palm oil, which serve as the PCMs, into the exfoliated graphite nanoplatelets as supporting material. The morphology of the nanocomposite PCMs is represented in Fig. 8.13.

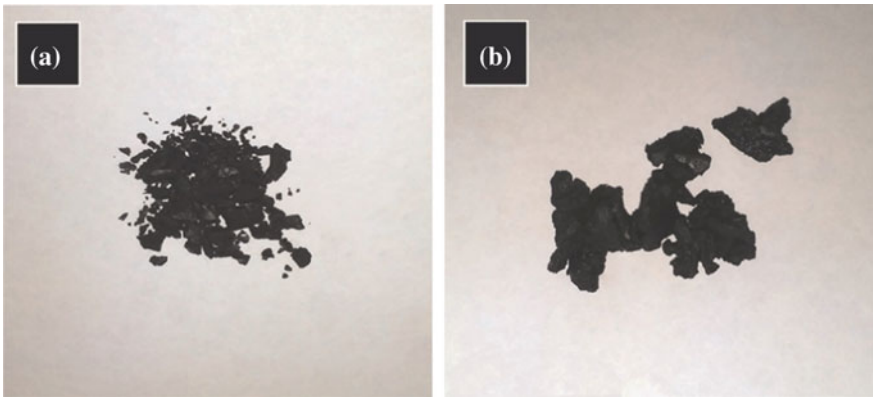

Fig. 8.13 Morphology of **a** coconut oil/xGnP and **b** palm oil/xGnP SSPCMs (Wi et al. 2015)

As expected, the PCMs were completely incorporated into the porous structure of the exfoliated graphite nanoplatelet matrix. Furthermore, the nanocomposite PCMs exhibited good chemical stability and thermal conductivity of them increased over 400 % than at their pure state. In addition, the latent heat storage capacity of the nanocomposite PCMs is nearly 75 % of those at pure state.

Hossain et al. (2015) studied the heat transfer effectiveness of thermally conductive nanoparticles being dispersed into a PCM containing porous medium. It is proposed that the void space inside the porous medium is occupied by a nano-PCM (cyclohexane + CuO nanoparticles). It is observed that for a given porosity of the porous medium, the PCM containing nanoparticles melted swiftly, thus revealing the importance of dispersing nanoparticles into PCM.

8.3 NanoPCM Composites for Energy-Efficient Buildings

8.3.1 Attributes of NanoPCMs' Thermal Energy Storage

In the spectrum of techniques which are available to achieve enhanced energy efficiency in buildings at macroscale level, the nanotechnology, which is associated with the enhancement of material properties at nanoscale level, is finding its application in the enhancement of building energy efficiency. As discussed in the earlier sections, the nanomaterials which are capable of improving the thermal performance of the PCMs are highly preferred in modern building construction as well as for refurbishment in buildings. There are numerous studies being performed to evaluate the thermal performance of PCMs embedded with nanomaterials. The review of few research studies revealing the type of PCMs and nanomaterials being utilized for building applications along with their improved thermophysical properties is reported in Table 8.5, which is self-explanatory.

Table 8.5 Summary of utilized PCM and nanostructured thermal conductivity enhancers (Khodadadi et al. 2013)

Authors (year)	PCM (materials and properties)	Nanostructured materials		
		Materials and properties	Dimension etc.	Fractions of enhancers
Siegel (1977)	Molten salts, k: 0.4–4 W/m K	Stainless steel, iron (Fe), aluminum (Al), and copper (Cu) particles, k: 15, 60, 204, and 386 W/m K	N/A	0–100 vol.%[a]
Seeniraj et al. (2002)	Molten salts, k: 0.4–4 W/m K	Stainless steel and Cu particles, k: 50 and 380 W/m K	N/A	0–100 vol.%
Elgafy and Lafdi (2005)	Paraffin wax, T_m: ~67 °C, k: ~0.24 W/m K, α: 1.61×10^{-7} m^2/s	Carbon nanofibers (CNF), ρ: ~1600 kg/m^3	Outer diameter: ~100 nm, length: ~20 μm	1, 2, 3, and 4 wt%
Khodadadi and Hosseinizadeh (2007)	Water, ρ: 997.1 kg/m^3, C_p: 4179 J/kg K, k: 0.6 W/m K, μ: 8.9×10^{-4} kg/ms, L: ~335,000 J/kg	Cu nanoparticles, ρ: 8954 kg/m^3, C_p: 383 J/kg K, k: 400 W/m K	10 nm	10 and 20 vol.%
Hong et al. (2007a, b)	PAC[b], EG solutions (with 50 vol.% water), T_f: −35.6 °C	Single-walled carbon nanotubes (SWCNT), alumina (Al_2O_3), MgO nanoparticles	N/A	0.05, 0.1, and 0.2 wt%
Zeng et al. (2007)	1-Tetradecanol ($C_{14}H_{30}O$), T_m: ~38 °C, L: ~230,000 J/kg	Silver (Ag) nanoparticles	500 nm	2–94 wt%
Xie et al. (2008)	Deionized (DI) water	Al_2O_3, titanium oxide (TiO_2) nanoparticles	~8 nm (Al_2O_3); ~3.8 nm (TiO_2)	1.54–6.19 wt% (Al_2O_3); 2.616–7.85 wt% (TiO_2)
Weinstein et al. (2008)	Paraffin wax, T_m: 56 °C, C_p: 2100 J/kg K, k: 0.25 W/m K, L: ~234,000 J/kg	Graphite nanofibers (GNF) of three types: ribbon, platelet, and herringbone	Diameter: 4–10 nm, length: ~1 μm	0.25, 0.5, 1, and 5 wt %

(continued)

Table 8.5 (continued)

Authors (year)	PCM (materials and properties)	Nanostructured materials		
		Materials and properties	Dimension etc.	Fractions of enhancers
Zeng et al. (2008)	$C_{14}H_{30}O$ and $C_{14}H_{30}O$/PANI[c], T_m: ~35 °C, L: 221, 250, and 119,140 J/kg	Multiwalled carbon nanotubes (MWCNT)	Outer diameter: 10–30 nm, length: 5–15 μm	0.5, 1, 2.5, and 5 wt%
Shaikh et al. (2008)	Paraffin wax (shell wax 100), L: 156,300 J/kg	SWCNT, MWCNT, and CNF	Diameter: 1, 10, and 100 nm	0.1, 0.4, 0.7, and 1 vol.%
Wang et al. (2008)	Palmitic acid (PA), purity 98 %, T_m: 62.5–64 °C, ρ: 853 kg/m^3, k: 0.24 W/m K, L: 207,800 J/kg	MWCNT, surface-oxidized by a mixed acid with 1:3 of concentrated nitric and sulfuric acids	Diameter: 30 nm, length: 50 μm, specific surface area: 60 m^2/g	0.5, 1, 2, and 5 wt%
Kim and Drzal (2009)	n-docosane, T_m: 53–57 °C, k: 0.26 W/m K, L: 157,300 J/kg	Exfoliated graphite nanoplatelets (xGnP)	Diameter: 15 μm, thickness: <10 nm, surface area: 30 m^2/g	1, 2, 3, 5, and 7 wt%
Zeng et al. (2009)	PA, T_m: 59.48 °C, T_f: 58.78 °C, k: 0.318 W/m K, L: ~201,000 J/kg	Long and short pristine MWCNT; surface-oxidized MWCNT (by two acids)	Outer diameter: 10–30 nm, length: 5–15 μm (long), 1–2 μm (short)	0.099–4.76 wt% (without surfactants) and 0.095–4.5 wt% (with surfactants)
Liu et al. (2009)	Saturated barium chloride ($BaCl_2$) aqueous solution, T_f: −8 °C, pH: 8	TiO_2 nanoparticles	20 nm	0.167, 0.283, 0.565, and 1.13 vol.%
Wu et al. (2009)	Distilled water, k: 0.6008 W/m K	Al_2O_3 nanoparticles	20 nm	0.05, 0.1, and 0.2 wt%
Ho and Gao (2009), Gao (2008)	n-octadecane ($C_{18}H_{38}$), T_m: 26.5 °C, T_f: 25.1 °C, L: ~243,100 J/kg	Al_2O_3 nanoparticles, ρ: 3600 kg/m	33 nm (159.6 and 196.0 nm in suspensions)	5 and 10 wt%

(continued)

Table 8.5 (continued)

Authors (year)	PCM (materials and properties)	Nanostructured materials		
		Materials and properties	Dimension etc.	Fractions of enhancers
Wang et al. (2009)	Paraffin wax, T_m: 53 °C, L: ~165,300 J/kg	MWCNT, treated by ball milling	Diameter: 30 nm, length: 50 μm, specific surface area: 60 m^2/g	0.2, 0.5, 1, and 2 wt%
Zeng et al. (2010)	$C_{14}H_{30}O$, k: 0.32 W/m K, L: ~220,000 J/kg	Ag nanowires	N/A	9.09–62.73 wt%
Wang et al. (2010a, b, c, d)	PA, purity 98 %, T_m: 62.4 °C, ρ: 853 kg/m^3, k: 0.22 W/m K (solid), 0.16 W/m K (liquid), L: 208,000 J/kg	MWCNT, treated by mechanochemical reaction with potassium hydroxide/ball milling	Diameter: 30 nm, length: 50 μm, specific surface area: 60 m^2/g	0.2, 0.5, and 1 wt%
Wang et al. (2010a, b, c, d)	Paraffin wax, T_m: ~48.1 °C, L: 142,200 J/kg	γ-Al_2O_3 nanoparticles ρ: 3900 kg/m^3	20 nm	1, 2, and 5 wt%
Wang et al. (2010a, b), c, d)	PA, purity 98 %, T_m: 62.5–64° C, k: 0.223 W/m K (solid), 0.154 W/m K (liquid)	MWCNT, treated by surface oxidation, mechanochemical reaction, ball milling, and grafting following acid oxidation	Diameter: 30 nm, length: 50 μm, specific surface area: 60 m^2/g	0.2, 0.5, and 1 wt%
Wang et al. (2010a, b), c, d)	Paraffin wax, purity 99.99 %, T_m: 58–60 °C	Cu nanoparticles, purity: 99.9 %	Diameter: 25 nm, specific surface area: 30–50 m^2/g	0.1, 0.5, 1, and 2 wt%
Wu et al. (2010)	Paraffin, T_m: 58–60 °C, k: 0.2699 W/m K (solid), 0.1687 W/m K (liquid), L: 204,000 J/kg	Cu, Al, and C/Cu nanoparticles, purity: 99.9 %	Diameter: 25 nm	0.1 wt% for all the three kinds of nanoparticles, 0.1, 0.5, 1, and 2 wt% for Cu nanoparticles
Mo et al. (2011)	DI water	MWCNT	Diameters: 10–30, 40–60, and 60–100 nm, length: 5–15 μm	0.1 wt%

(continued)

Table 8.5 (continued)

Authors (year)	PCM (materials and properties)	Nanostructured materials		
		Materials and properties	Dimension etc.	Fractions of enhancers
Cui et al. (2011)	Paraffin and soy wax, T_m: 52–54 °C	CNF, MWCNT (purity: 95 %)	Outer diameter: 200 nm (CNF); diameter: 30 nm, length: 50 μm, specific surface area: 60 m^2/g (MWCNT)	1, 2, 5, and 10 wt%
Xiang and Drzal (2011)	*n*-docosane, T_m: 53–57 °C	Exfoliated graphite nanoplatelets (xGnP); xGnP with ball milling treatment	Diameter: 15 μm, thickness: 10 nm, surface area: 20–40 m^2/g, and diameter: 1 μm, surface area: 100–130 m^2/g after ball milling	1, 2, 4, 6, 8, and 10 wt%
Yavari et al. (2011)	1-octadecanol, T_m: ~66 °C, ρ: 812 kg/m^3, k: 0.38 W/m K, L: ~250,000 J/kg	Graphene flakes	N/A	0.2, 0.5, 1, 2, and 4 wt%
Fan and Khodadadi (2012)	Cyclohexane, T_m: 65 1 °C, ρ: 850 kg/m^3 (solid), 779 kg/m^3 (liquid), L: 32,557 J/kg	Copper oxide (CuO) nanoparticles	Diameter: 5–15 nm	1, 2, and 4 wt%
Fan and Khodadadi (2011)	Eicosane, T_m: ~37 °C	Copper oxide (CuO) nanoparticles	Diameter: 5–15 nm	1, 2, 5, and 10 wt%

[a]vol.% and wt% stand for volumetric and mass fractions, respectively
[b]PAC and EG stand for prediluted antifreeze coolant and ethylene glycol, respectively
[c]PANI denotes polyaniline

8.3.2 Role of NanoPCMs for Energy Efficiency in Buildings

Energy efficiency in buildings is intensely coupled with the amount of energy actually required to generate or produce the desired comfort conditions in indoor environment. In other words, energy efficiency refers to the usage of energy at minimum level for performing an associated task.

In terms of thermal energy storage, the basic criterion for a LTES system is to store and release the energy during the cooling or heating load demand situations in buildings. That is, redistribution of energy from on-peak to off-peak periods and vice versa would enable the LTES system to enhance the efficiency of the cooling/heating system in buildings.

It is well known that the PCMs are those materials which are highly preferred to achieve the energy redistribution requirements in building in several ways by means of the LTES system. To add value to the technology, energy efficiency in buildings could further be realized by incorporating nanomaterial-embedded PCMs into building structures.

The incorporation of NanoPCMs in building components may be passive or active depending upon the constructional features of the building envelope. Whatsoever may be the arrangement, the NanoPCMs are capable of addressing the cooling/heating load demand in buildings, which can enhance the operational performance of such systems without sacrificing energy efficiency.

The swift phase transformation processes, high thermal conductivity, thermal stability, chemical stability, durability, and reliability are some of the key functional aspects or decisive factors governing the operational performance of PCMs. To substantiate the role of NanoPCMs for energy efficiency in buildings, Parameshwaran and Kalaiselvam (2013b) investigated the importance of hybrid nanocomposite PCM for cooling applications in buildings.

In this study, the preparation, characterization, and experimentation of the hybrid nanocomposite PCM have been dealt in detail. It is pertinent to note that the hybrid nanocomposite PCM-based LTES system while integrated with the conventional air conditioning system could be able to redistribute the cooling load demand in building. Besides, the improved thermal properties of the hybrid nanocomposite PCM enabled for acquiring on-peak energy conservation potential of 24.8 and 27.3 % in summer and winter conditions, respectively.

In another work performed by Parameshwaran and Kalaiselvam (2014), the silver nanoparticle-embedded organic PCM-based LTES air conditioning system yielded energy savings potential ranging from 36 to 58 %, using different ventilation schemes in summer and winter conditions (Fig. 8.14).

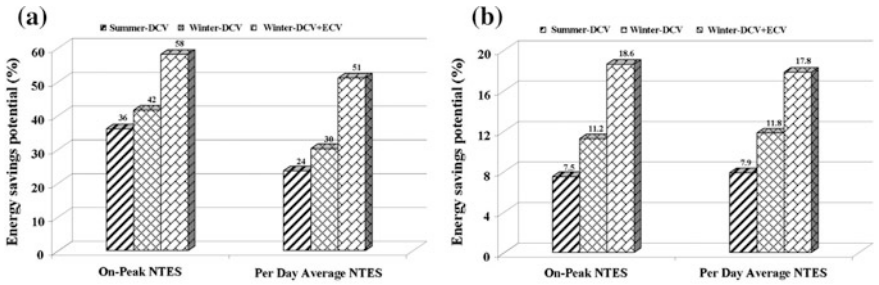

Fig. 8.14 Energy savings potential of proposed A/C system compared with **a** conventional A/C system and **b** basically similar VAV A/C system (Parameshwaran and Kalaiselvam 2014)

8.4 Scope for Future Research

From the perspective of the research studies being carried out in the field of nanotechnology in recent times, there are much more possibilities for innovation to take place especially in the front of enhancement of energy efficiency in buildings. Some of the challenges which are to be confronted to accomplish further scope and development in the NanoPCMs are suggested below:

- Nanomaterials being infused into the PCMs are often prone to non-uniform dispersion leading to segregation and agglomeration or aggregation (Zhang et al. 2012b; Parameshwaran and Kalaiselvam 2013a; Parameshwaran et al. 2014), due to which the thermal storage properties of the PCMs may be altered or get affected.
- Nanostructures prepared in a range of sizes and with different shapes would exhibit different tendencies toward acquiring the desired thermal energy storage capabilities of the PCMs. In some instances, the mass concentration or weight proportion of nanoparticles would significantly influence the thermal performance of PCMs.
- Standardization of thermophysical properties of both PCMs and the nanomaterials is the need of the hour, which if could be framed on global perspective would help to select appropriate NanoPCMs for energy-efficient building applications.
- As discussed in the earlier sections, biobased PCMs doped with nanostructured materials are gaining momentum as potential candidates for energy-efficient building applications. Thus, as per the Richard Feynman's statement—*There's Plenty of Room at the Bottom*, in nanoscale level to pursue interdisciplinary research works toward the enhancement of energy efficiency in buildings using NanoPCMs.

8.5 Conclusion

The utilization potential of a variety of nanomaterial-incorporated PCMs for the enhancement of energy efficiency in buildings is reviewed and discussed. The bottom-up approach is considered to be the most promising method for producing nanomaterials, which is basically due to the tunable properties that can bring in the desired morphology and thermal properties.

In particular, the nanomaterials being utilized as thermal enhancement materials for PCMs enable them to achieve good nucleation kinetics, swift phase change properties, thermal stability, reliability, etc. The improved thermal properties of NanoPCMs are expected due to the creation of densely packed network of thermal interfaces in between the PCM and the nanoparticles in molecular level.

In addition, the mass proportion of the nanoparticles also plays a vital role in determining the desired thermal performance of the PCMs. Increased mass concentration of nanoparticles in pure PCM can enhance thermal conductivity, nucleation kinetics, reduced supercooling, etc. However, the mass concentration ratio of NanoPCM has to be kept at optimum value for experiencing the improvement in thermal properties on a long-term basis.

Based on the review of research studies presented, the role of NanoPCMs has been justified to satisfying the decisive factors, which in turn contributed for acquiring the enhancement of energy efficiency in buildings.

Acknowledgements The authors gratefully acknowledge Birla Institute of Technology and Science, Pilani, for providing financial support to carry out this research work under Research Initiation Grant (BITS/GAU/RIG/54) and UGC Major Research Project (F. No. 42-894/2013 (SR)).

References

Biswas K, Abhari R (2014) Low-cost phase change material as an energy storage medium in building envelopes: experimental and numerical analyses. Energy Convers Manag 88:1020–1031

Biswas K, Lu J, Soroushian P, Shrestha S (2014) Combined experimental and numerical evaluation of a prototype nano-PCM enhanced wallboard. Appl Energy 131:517–529

Black JK, Tracy LE, Roche CP, Henry PJ, Pesavento JB, Adalsteinsson T (2010) Phase transition of hexadecane in poly(alkyl methacrylate) core–shell microcapsules. J Phys Chem B 114:4130–4137

Cai YB, Zong X, Zhang JJ, Hu YY, Wei QF, He GF (2013) Electrospun nanofibrous mats absorbed with fatty acid eutectics as an innovative type of form-stable phase change materials for storage and retrieval of thermal energy. Solar Energy Mater Solar Cells 109:160–168

Cao L, Su D, Tang Y, Fang G, Tang F (2015) Properties evaluation and applications of thermal energy storage materials in buildings. Renew Sustain Energy Rev 48:500–522

Chen Z-H, Yu F, Zeng X-R, Zhang Z-G (2012) Preparation characterization and thermal properties of nanocapsules containing phase change material n-dodecanol by miniemulsion polymerization with polymerizable emulsifier. Appl Energy 91:7–12

Cui Y, Liu C, Hu S, Yu X (2011) The experimental exploration of carbon nanofiber and carbon nanotube additives on thermal behavior of phase change materials. Solar Energy Mater Solar Cells 95:1208–1212

de Gracia Alvaro, Cabeza LF (2015) Phase change materials and thermal energy storage for buildings. Energy Build 103:414–419

Do CV, Nguyen TTT, Park JS (2012) Fabrication of polyethylene glycol/polyvinylidene fluoride core/shell nanofibers via melt electrospinning and their characteristics. Solar Energy Mater Solar Cells 104:131–139

Elgafy A, Lafdi K (2005) Effect of carbon nanofiber additives on thermal behavior of phase change materials. Carbon 43:3067–3074

Fan L, Khodadadi JM (2011) Temperature-dependent thermal conductivity of eicosane-based phase change materials with copper oxide nanoparticles. In: International symposium on thermal and materials nanoscience and nanotechnology, Antalya, Turkey, 8 p

Fan L, Khodadadi JM (2012) An experimental investigation of enhanced thermal conductivity and expedited unidirectional freezing of cyclohexane-based nanoparticle suspensions utilized as nano-enhanced phase change materials (NePCM). Int J Thermal Sci 62:120–126

Fang Y, Kuang S, Gao X, Zhang Z (2008) Preparation and characterization of novel nanoencapsulated phase change materials. Energy Convers Manage 49:3704–3707

Fang G, Li H, Yang F, Liu X, Wu S (2009) Preparation and characterization of nanoencapsulated n-tetradecane as phase change material for thermal energy storage. Chem Eng J 153:217–221

Fang Y, Yu H, Wan W, Gao X, Zhang Z (2013) Preparation and thermal performance of polystyrene/n-tetradecane composite nanoencapsulated cold energy storage phase change materials. Energy Convers Manage 76:430–436

Fang Y, Liu X, Liang X, Liu H, Gao X, Zhang Z (2014) Ultrasonic synthesis and characterization of polystyrene/n-dotriacontane composite nanoencapsulated phase change material for thermal energy storage. Appl Energy 132:551–556

Fuensanta M, Paiphansiri U, Romero-Sanchez MD, Guillem C, Lopez-Buendia AM, Landfester K (2013) Thermal properties of a novel nanoencapsulated phase change material for thermal energy storage. Thermochim Acta 565:95–101

Gao JY (2008) An experimental study on melting heat transfer behavior of a phasechange-material containing Al2O3 nanoparticles in a vertical rectangular enclosure. MS thesis, National Cheng Kung University, Taiwan 86 p. Aavailable online at http://ethesys.lib.ncku.edu.tw/ETD-db/ETD-search/view_etd?URN=etd-0825108-153106

Giro-Paloma J, Konuklu Y, Fernandez AI (2015) Preparation and exhaustive characterization of paraffin or palmitic acid microcapsules as novel phase change material. Sol Energy 112:300–309

Ho CJ, Gao JY (2009) Preparation and thermophysical properties of nanoparticle-inparaffin emulsion as phase change material. Int Commun Heat Mass Transfer 36:467–470

Hong H, Wensel J, Peterson S, Roy W (2007a) Efficiently lowering the freezing point in heat transfer coolants using carbon nanotubes. J Thermophys Heat Transfer 21:446–448

Hong H, Zheng Y, Roy W (2007b) Nanomaterials for efficiently lowering the freezing point of anti-freeze coolants. J Nanosci Nanotechnol 7:1–5

Hossain R, Mahmud S, Dutta A, Pop I (2015) Energy storage system based on nanoparticle-enhanced phase change material inside porous medium. Int J Thermal Sci 91:49–58

Jamekhorshid A, Sadrameli SM, Farid M (2014) A review of microencapsulation methods of phase change materials (PCMs) as a thermal energy storage (TES) medium. Renew Sustain Energy Rev 31:531–542

Jeong S-G, Chang SJ, Seunghwan W, Sumin K (2015) Energy efficient thermal storage montmorillonite with phase change material containing exfoliated graphite nanoplatelets. Solar Energy Mater Solar Cells 139:65–70

Khadiran T, Hussein MZ, Zainal Z, Rusli R (2015a) Encapsulation techniques for organic phase change materials as thermal energy storage medium: a review. Solar Energy Mater Solar Cells 143:78–98

Khadiran T, Hussein M Z, Zainal Z, Rusli R (2015b) Shape-stabilised n-octadecane/activated carbon nanocomposite phase change material for thermal energy storage. J Taiwan Inst Chem Eng (in press)

Khodadadi JM, Hosseinizadeh SF (2007) Nanoparticle-enhanced phase change materials (NEPCM) with great potential for improved thermal energy storage. Int J Heat Mass Transfer 34:534–543

Khodadadi JM, Fan L, Babaei H (2013) Thermal conductivity enhancement of nanostructure-based colloidal suspensions utilized as phase change materials for thermal energy storage: a review. Renew Sustain Energy Rev 24:418–444

Kim S, Drzal LT (2009) High latent heat storage and high thermal conductive phase change materials using exfoliated graphite nanoplatelets. Solar Energy Mater Solar Cells 93:136–142

Konuklu Y, Halime OP, Unal M (2015) Nanoencapsulation of n-alkanes with poly (styrene-co-ethylacrylate) shells for thermal energy storage. Appl Energy 150:335–340

Kosny J, Shukla N, Fallahi A (2013) Cost analysis of simple phase change material-enhanced building envelopes in southern U.S. climates, report for U.S. Department of Energy, Fraunhofer CSE, http://cse.fraunhofer.org/Portals/55819/docs/ba_pcm_enhanced_building_envelopes.pdf

Kwon HJ (2010) Preparation of n-octadecane nanocapsules by using interfacial redox initiation in miniemulsion polymerization. Macromol Res 18(9):923–926

Liu Y-D, Zhou Y-G, Tong M-W, Zhou X-S (2009) Experimental study of thermal conductivity and phase change performance of nanofluids PCMs. Microfluid Nanofluid 7:579–584

Manikam VR, Cheong KY, Razak KA (2011) Chemical reduction methods for synthesizing Ag and Al nanoparticles and their respective nanoalloys. Mater Sci Eng, B 176:187–203

Mo S, Chen Y, Yang J, Luo X (2011) Experimental study on solidification behavior of carbon nanotube nanofluid. Adv Mater Res 171–172:333–336

Pacheco-Torgal F (2014) Eco-efficient construction and building materials research under the EU Framework Programme Horizon 2020. Construct Build Mater 51:151–162

Parameshwaran R, Kalaiselvam S (2013a) Effect of aggregation on thermal conductivity and heat transfer in hybrid nanocomposite phase change colloidal suspensions. Appl Phys Lett 103:193113

Parameshwaran R, Kalaiselvam S (2013b) Energy efficient hybrid nanocomposite-based cool thermal storage air conditioning system for sustainable buildings. Energy 59:194–214

Parameshwaran R, Kalaiselvam S (2014) Energy conservative air conditioning system using silver nano-based PCM thermal storage for modern buildings. Energy Build 69:202–212

Parameshwaran R, Deepak K, Saravanan R, Kalaiselvam S (2014) Preparation, thermal and rheological properties of hybrid nanocomposite phase change material for thermal energy storage. Appl Energy 115:320–330

Sanchez F, Sobolev K (2010) Nanotechnology in concrete—a review. Constr Build Mater 24:2060–2071

Sari A, Alkan C, Özcan AN (2015a) Synthesis and characterization of micro/nano capsules of PMMA/capric-stearic acid eutectic mixture for low temperature-thermal energy storage in buildings. Energy Build 90:106–113

Sari A, Alkan C, Döğüşcü DK, Kızıl Ç (2015b) Micro/nano encapsulated n-tetracosane and n-octadecane eutectic mixture with polystyrene shell for low-temperature latent heat thermal energy storage applications. Sol Energy 115:195–203

Sayyar M, Weerasiri RR, Soroushian P, Lu J (2014) Experimental and numerical study of shape-stable phase-change nanocomposite toward energy-efficient building constructions. Energy Build 75:249–255

Seeniraj RV, Velraj R, Narasimhan NL (2002) Heat transfer enhancement study of a LHTS unit containing dispersed high conductivity particles. J SolEnergy Eng 124:243–249

Shaikh S, Lafdi K, Hallinan K (2008) Carbon nanoadditives to enhance latent energy storage of phase change materials. J Appl Phys 103(094302):6

Siegel R (1977) Solidification of low conductivity material containing dispersed high conductivity particles. Int J Heat Mass Transf 20:1087–1089

Sobolev K, Ferrada-Gutiérrez M (2005) How nanotechnology can change the concrete world: part 1. Am Ceram Soc Bull 84:14–17

Su W, Darkwa J, Georgios K (2015) Review of solid–liquid phase change materials and their encapsulation technologies. Renew Sustain Energy Rev 48:373–391

Tumirah K, Hussein MZ, Zulkarnain Z, Rafeadah R (2014) Nano-encapsulated organic phase change material based on copolymer nanocomposite for thermal energy storage. Energy 66:881–890

Wang J, Xie H, Xin Z (2008) Thermal properties of heat storage composites containing multiwalled carbon nanotubes. J Appl Phys 104(113537):5

Wang J, Xie H, Xin Z (2009) Thermal properties of paraffin based composites containing multi-walled carbon nanotubes. Thermochim Acta 488:39–42

Wang J, Xie H, Li Y, Xin Z (2010a) PW based phase change nanocomposites containing γ-Al2O3. J Therm Anal Calorim 102:709–713

Wang J, Xie H, Xin Z, Li Y (2010b) Increasing the thermal conductivity of palmitic acid by the addition of carbon nanotubes. Carbon 48:3979–3986

Wang J, Xie H, Xin Z, Li Y, Chen L (2010c) Enhancing thermal conductivity of palmitic acid based phase change materials with carbon nanotubes as fillers. Sol Energy 84:339–344

Wang N, Yang S, Zhu D, Ju X (2010d) Preparation and heat transfer behavior of paraffin based composites containing nano-copper particles. In: Proceedings of the seventh international conference on multiphase flow, Tampa, FL, 4 p

Wang Y, Zhang Y, Xia T, Zhao W, Yang W H (2014) Effects of fabricated technology on particle size distribution and thermal properties of stearic-eicosanoic acid/polymethylmethacrylate nanocapsules. Solar Energy Mater Solar Cells 120B:481–490

Weinstein RD, Kopec TC, Fleischer AS, D′Addio E, Bessel CA (2008) The experimental exploration of embedding phase change materials with graphite nanofibers for the thermal management of electronics. J Heat Transfer 130(042405):8

Wi S, Seo J, Jeong S-G, Chang SJ, Kang Y, Kim S (2015) Thermal properties of shapestabilized phase change materials using fatty acid ester and exfoliated graphite nanoplatelets for saving energy in buildings. Sol Energy Mater Sol Cells 143:168–173

Wu S, Zhu D, Li X, Li H, Lei J (2009) Thermal energy storage behavior of Al_2O_3–H_2O nanofluids. Thermochim Acta 483:73–77

Wu S, Zhu D, Zhang X, Huang J (2010) Preparation and melting/freezing characteristics of Cu/paraffin nanofluid as phase-change material (PCM). Energy Fuels 24:1894–1898

Wu W, Bostanci H, Chow LC, Ding SJ, Hong Y, Su M, Kizito JP, Gschwender L, Snyder CE (2011) Jet impingement and spray cooling using slurry of nanoencapsulated phase change materials. Int J Heat Mass Transf 54:2715–2723

Xiang J, Drzal LT (2011) Investigation of exfoliated graphite nanoplatelets (xGnP) in improving thermal conductivity of paraffin wax-based phase change material. Sol Energy Mater Sol Cells 95:1811–1818

Xie H, Wan J, Chen L (2008) Effects on the phase transformation temperature of nanofluids by the nanoparticles. J Mater Sci Technol 25:742–744

Yavari F, Raeisi Fard H, Pashayi K, Rafiee MA, Zamiri A, Yu Z (2011) Enhanced thermal conductivity in a nanostructured phase change composite due to low concentration graphene additives. J Phys Chem C 115:8753–8758

Zeng JL, Sun LX, Xu F, Tan ZC, Zhang ZH, Zhang J (2007) Study of a PCM based energy storage system containing Ag nanoparticles. J Therm Anal Calorim 87:369–373

Zeng JL, Liu YY, Cao ZX, Zhang J, Zhang ZH, Sun XL (2008) Thermal conductivityenhancement of MWNTS on the PANI/tetradecanol form-stable PCM. J Therm Anal Calorim 91:443–446

Zeng JL, Cao Z, Yang DW, Xu F, Sun LX, Zhang XF (2009) Effects of MWNTS on phase change enthalpy and thermal conductivity of a solid-liquid organic PCM. J Therm Anal Calorim 95:507–512

Zeng JL, Cao Z, Yang DW, Sun LX, Zhang L (2010) Thermal conductivity enhancement of Ag nanowires on an organic phase change material. J Therm Anal Calorim 101:385–389

Zhang H, Wang X (2009) Fabrication and performances of microencapsulated phase change materials on n-octadecane core and resorcinol-modified melamine-formaldehyde shell. Colloids Surf A 332:129–138

Zhang GH, Bon SAF, Zhao CY (2012a) Synthesis characterization and thermal properties of novel nanoencapsulated phase change materials for thermal energy storage. Sol Energy 86:1149–1154

Zhang S, Wu J-Y, Tse C-T, Niu J (2012b) Effective dispersion of multi-wall carbon nano-tubes in hexadecane through physiochemical modification and decrease of supercooling. Sol Energy Mater Sol Cells 96:124–130

Zhou Z, Zhang Zuo J, Huang K, Zhang L (2015) Phase change materials for solar thermal energy storage in residential buildings in cold climate. Renew Sustain Energy Rev 48:692–703

Chapter 9
Nanotech-Based Cool Materials for Building Energy Efficiency

Anna Laura Pisello, Riccardo Paolini, Maria Vittoria Diamanti, Elena Fortunati, Veronica Lucia Castaldo and Luigi Torre

Abstract Cool materials represent an interesting and acknowledged solution able to produce a threefold benefit: the reduction of cooling energy needs in buildings, the mitigation of the urban heat island phenomenon, the counterbalance of global warming trend at larger scale. In fact, they are environmentally friendly and relatively cost-effective materials characterized by high solar reflectance and infrared thermal emittance properties. Therefore, they are helpful to mitigate the urban microclimate by decreasing air and surface temperature when applied over building envelopes, i.e., roofs and walls, and urban paving surfaces. This chapter will discuss about the key research contributions to the development and testing of such cool materials' effectiveness with a specific focus on the material engineering and characterization. More in details, the recent nanoscale developments will be addressed and the main applications of cool materials will be discussed in order to provide quantitative and quantitative assessment of the effectiveness of such technology for building energy efficiency.

A.L. Pisello (✉)
CIRIAF, Dipartimento di Ingegneria, University of Perugia,
Via Duranti 67, 06125 Perugia, Italy
e-mail: anna.pisello@unipg.it

R. Paolini · V.L. Castaldo
Dipartimento ABC, Politecnico di Milano, Milan, Italy

M.V. Diamanti
Dipartimento di Chimica, Materiali ed Ingegneria Chimica
"G. Natta" - Politecnico di Milano, Milan, Italy

E. Fortunati · L. Torre
Dipartimento di Ingegneria Civile ed Ambientale, University of Perugia, Perugia, Italy

F. Pacheco Torgal et al. (eds.), *Nano and Biotech Based Materials for Energy Building Efficiency*, DOI 10.1007/978-3-319-27505-5_9

9.1 Introduction

The solar radiation is commonly associated with light; however, light is only the visible portion of it, while the solar radiation transmitted through the Earth's atmosphere provides measurable power in the spectral range between 280 and 2800 nm, which is the measurement range of common pyranometers.

To analyze the relative weight of the different portions of the solar spectrum, the solar spectral irradiance distribution can be modeled with the parametrization implemented in the model SMARTS 2.9.5 (Gueymard 2001, 2005). Considering, for instance, the global solar spectral irradiance on the horizontal plane for air mass equal to one computed with a spectral resolution of 5 nm (as in Levinson et al. 2010), namely at the equator at solar noon, the solar power between 280 and 2800 nm, is equal to 1090 W m^{-2}. With the visible range defined between 380 and 780 nm (ISO 2003), the solar power in this portion is approximately 55 % of the total power in the whole solar spectrum, while in the ultraviolet (UV) and near-infrared (NIR) ranges, there are, respectively, the 5 and 40 % of the solar power.

However, in the range 380–400 nm plus 700–780 nm the average human eye perceives less than 0.5 % of what is perceived in the whole 380–780 nm range. Therefore, considering the visible range between 400 and 700 nm (Lienhard 2010), the visible portion is only 45 % of the solar power, while the NIR accounts for approximately the 48 %.

Vernacular architectures in Mediterranean and other hot climates rely on white finishes to reduce summer overheating of buildings (Steen et al. 2003), but this is not the sole option. In fact, a material can be considered cool if it offers high solar reflectance (ρ_S) and high thermal emittance (ε) (Levinson et al. 2005a). Therefore, a "cool" material is able to moderate urban microclimates by decreasing air and surface temperature when applied over building envelopes, and urban paving surfaces, since it can effectively reflect the incident solar radiation given its high solar reflectance and thermal emittance (Gentle and Smith 2015; Kolokotsa et al. 2013).

The solar reflectance, also referred to as albedo, is the ratio of hemispherically reflected radiation over the incident radiation, integrated over the solar wavelength range. It is measured on a scale of 0–1 (or 0–100 %). The thermal emittance is the measure of the capability of a surface to release the absorbed heat. It represents the potential of a surface to radiate energy compared with a black body at the same temperature, and it is measured on a scale from 0 to 1 (or 0–100 %). The Solar Reflectance Index (SRI) is an additional indicator for cool materials which combines both ρ_S and ε. It quantifies how hot a flat surface would get relative to a reference black (ρ_S = 5 %, ε = 90 %) and a standard white surface (ρ_S = 80 %, ε = 90 %) (ASTM 2011; LBNL 2015). However, not only white surfaces may be cool, but also colored surfaces. Some colored materials display higher near-infrared reflectance than conventional colored materials, with the same visible reflectance and aspect (Synnefa et al. 2006a, b, 2007). This is possible by replacing standard pigments with alternative ones weakly absorbing and strongly backscattering in the near-infrared portion of the solar spectrum (Levinson et al. 2007b), as conventional

pigments tend to absorb in the NIR. The cool alternatives developed with this approach would then have the same color, but higher ρ_S than the standard coating or material. Often, carbon black is used since it is a strong UV absorber, with an absorption coefficient which decreases exponentially with wavelength (Lindberg et al. 1993). Cool colors are also useful to preserve the urban landscape and the cultural heritage, when conservation interventions are needed, with their original aesthetics (Pisello 2015a).

Non-white NIR-reflective coatings for clay roofing tiles that offer a solar absorptance reduction ranging between 0.15 and 0.37 can reduce the roof surface temperature by 5–14 K, namely by approximately 35.5 K per kW m^{-2} of incoming solar radiation, and ceiling heat flux by 13–21 % for typical constructions (Levinson et al. 2007a). The largest improvement is shown for black tiles, which exhibit ρ_S equal to 0.04 in their standard version, while equal to 0.41 for their cool alternative. A comparable performance was found for a variety of architectural cool colored coatings (Synnefa et al. 2007).

In this panorama, innovative and nanostructured coatings for optimizing building energy efficiency for cooling currently represent an interesting research development (Gobakis et al. 2015; Georgakis et al. 2014). The need to investigate about new materials and technologies for reducing cooling energy uses of buildings (Karlessi and Santamouris 2015; Pisello et al. 2015a) and to save natural resources represent the two main motivations discussed in this chapter, where the recent research contributions about new cool and nanostructured materials are addressed.

More in details, this preliminary section will concern the main background and motivation of the huge research effort around this issue (Santamouris et al. 2015; Santamouris 2015). Then, Sect. 9.2 will deal with the analysis of existing materials already in the market or existing in nature. Section 9.3 will investigate the main techniques implemented to develop and apply cool materials in different case studies. Section 9.4 will concern the main cool materials and their experimental demonstrative applications all around the world, where also their quantitative effect will be considered for reducing building cooling needs. Section 9.5 will deal with the innovative recent contributions about nanostructured materials for thermal barrier applications. Section 9.6 will discuss about the durability of passive cooling performance of such materials over time. Finally, Sect. 9.7 will mention key research developments and future potentialities around this research issue.

9.1.1 Motivation

The motivation to study thin films and nanostructured "cool" material solutions is directly imputable to the fast and massive increase in the urban density and population and the relative modification of urban microclimate and mesoclimate conditions, mainly related to the Urban Heat Island (UHI) effect (Santamouris et al. 2015; Santamouris and Kolokotsa 2015). The large potential of cool materials to

mitigate UHIs is given by the fact that currently, in the urban fabric, most materials exhibit low ρ_S, especially asphalt (Kotthaus et al. 2014).

A United Nation study (United Nations 2011) showed how the increase in urban population is estimated to be around 40 % by 2050, consisting of households moving from rural to urban areas, exacerbating environmental quality issues in urban areas already affected by UHIs. In this view, two of the main research efforts are focused on the (i) development of materials that could effectively counteract the UHI effect for their passive cooling potential and on the (ii) development of eco-efficient techniques and technologies aimed at reducing the demand of the world's resources. Both these research and technology transfer issues are dealt with in this chapter, where the most recent investigations about cool materials and technologies are assessed, by paying dedicated attention to nanobased solutions currently under development (Chen et al. 2014; Revel et al. 2013). Cool materials are those materials that are characterized by high ρ_S and high ε, with the twofold purpose to reflect solar radiation and to reradiate the previously absorbed heat. The main benefit of the application of cool materials over buildings' envelope and urban paving exposed to the solar radiation is threefold, since cool materials demonstrated to produce non-negligible effect at several scales (Akbari and Matthews 2012, Hernández-Pérez et al. 2014). Firstly, cool materials are able to reduce building cooling needs and to improve indoor thermal comfort conditions in free-floating thermal zones located in proximity to the roof, e.g., attics (Carnielo and Zinzi 2013). Secondly, high-albedo surfaces can maximize the amount of solar radiation that is reflected upwards, namely outside the urban environment, therefore without contributing to the UHI exacerbation (Ferrari et al. 2015; Rossi et al. 2014). Thirdly, by applying the same thermal energy balance approach, high-albedo (cool) surfaces are also able to reduce global overheating and they could be considered a countermeasure to global warming countermeasure. In fact, their contribution could be calculated in terms of CO_{2eq} offset contribution (Cotana et al. 2014; Bonamente et al. 2013).

Despite these acknowledged benefits, cool materials are still relatively scarcely used in real-world applications, mainly due to lack of widespread awareness and lack of dedicated local regulations encouraging the implementation of these solutions. In fact, most of the regulations, in Europe at least, aimed at optimizing energy efficiency in buildings are still focused on the heating demand reduction.

9.2 White and Non-white Cool Materials

Several materials that are naturally cool have been used for building finishing and roofing since centuries, even though their optical–radiative response in the NIR has been quantitatively characterized only during the last century. Among those, white and non-white non-engineered cool materials are rutile, calcite, iron oxides, and chromium oxides.

9.2.1 White Pigments

Rutile and calcite are two simple examples of white minerals offering high ρ_S (Fig. 9.1). Rutile, the most common polymorph of titanium dioxide, is commonly used as a white pigment, as it is widely available and therefore cheap. With an average particle size of 200 nm in commercial products, it is a strong UV absorber, while its reflectance is highest at 420 nm, and then monotonically decreasing. More than 5 million tons of TiO_2 are used annually worldwide as opacifier or white pigment (Smithers Apex 2009). It is often referred to as the perfect white thanks to its excellent coverage capability and opacity, which have led to its introduction as substitute for toxic lead oxide pigments since early twentieth century. Also the anatase form of TiO_2 provides high reflectance.

Calcite exhibits high reflectance in the whole Vis–NIR range. This constituent provides high opacity and filling effect: for this reason, it is often used as smaller-particle-size extender in paints and varnishes containing rutile, to reduce TiO_2 flocculation, improve its dispersion and therefore decrease the required amount of white pigment (Stieg 1989). Yet, calcite is stable in neutral to alkaline environments, but it easily dissolves in acid water (Morse 1983; Morse and Arvidson 2002)—this is the origin of dripstone caves, formed by the slow dissolution of calcareous rocks during ages. As a consequence, it may leach out in case of repeated acid rains, such as precipitations in polluted urban environments (Thornbush and Viles 2007).

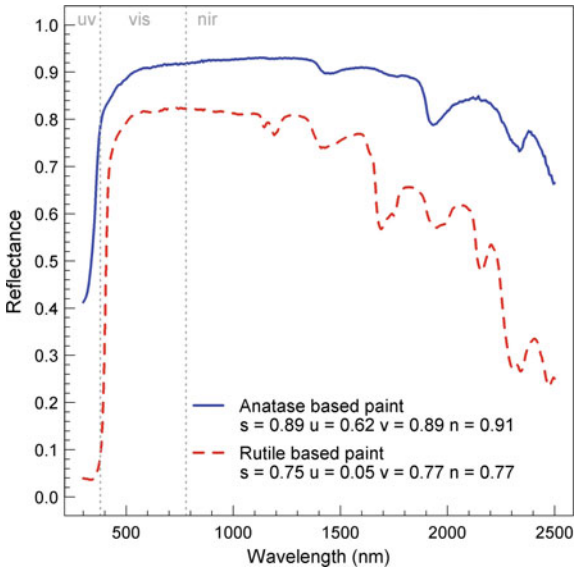

Fig. 9.1 Solar spectral total (diffuse + specular) reflectance of an anatase-based paint and of a rutile-based paint measured with a Perkin Elmer Lambda 950 spectrometer. The provided broadband values are the solar (*s*), ultraviolet (*u*), visible (*v*), near infrared (*n*) reflectances

9.2.2 Other Pigments

An extensive survey of common pigments used for architectural coatings was offered by Levinson et al. (2005b), who measured the solar spectral optical properties for 87 single-pigment films, having thickness between 10 and 37 μm. The same authors also developed a model, based on the Kubelka–Munk theory (Kubelka 1948), to compute the solar spectral reflectance of a non-opaque coating over a generic background of known spectral reflectance.

Iron oxide-based pigments span from brown to red, to yellow hues, depending on the chemistry of the oxides and hydroxides involved. Fe_2O_3 and Fe_3O_4 provide a cool version of brown and red pigments, being hematite Fe_2O_3 mostly used in red hues, magnetite Fe_3O_4 alone as gray pigment and a combination of the two—or the sole hematite—to produce brown (sienna and umber hues). Yellow hues can be obtained by using goethite, FeOOH (Diamanti et al. 2013). As a consequence, among non-white materials commonly used in buildings, terracotta is a good reflector in the NIR as it contains iron oxides, although it shows low reflectance in the visible range (Fig. 9.2).

Other heavy metals can also give rise to oxides and complex minerals that can be included in cool pigments. Concerning chromium, it is possible to list chrome titanate yellow, a standard component in high-durability systems but with moderate chroma (Ryan 2013), and modified chromium oxide green (Cr_2O_3). While chromium oxide green is the most stable green pigment known, its modified version allows an increase in NIR reflectance by almost 40 %. Other heavy metal pigments with high NIR reflectance include cadmium sulfides and sulfoselenides—yellow and orange hues,

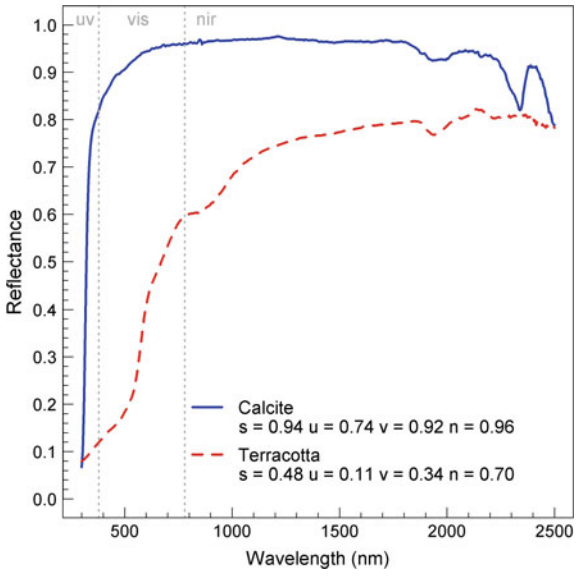

Fig. 9.2 Solar spectral reflectance of a calcite powder and a terracotta sample. The calcite powder was measured with a quartz laboratory glass over an opaque layer of the mineral

respectively—and nickel titanate: the latter is again a yellow hue, with slightly lower cool characteristics compared with chrome titanate (Levinson et al. 2005b).

Cool colored materials often have a slightly higher thermal emittance—usually by approximately 0.02–0.03—than the conventional option, as the high reflectance in the near infrared does not immediately drop once in the far-infrared range. However, this slight decrease in the long-wave radiative cooling potential does not yield to huge differences in surface temperature. For instance, an adiabatic flat roof with ρ_S equal to 0.80 would have a surface temperature of 44.6 °C with ε equal to 0.9 and of 45.3 °C with ε equal to 0.8, computed in the conditions defined by (ASTM 2011).

9.3 Simple Options Available to Develop Cool Materials

In the previous section, a review of available information concerning highly reflective materials was provided, but to develop a cool surface attention shall be paid also to other factors, such as the stratification and the surface roughness.

A basic option is the application of a cool topcoat weakly absorbing in the NIR onto a NIR-reflective basecoat (Brady and Wake 1992). This may be achieved by means of a one-coat system whether the substrate is already NIR-reflective, or with a two-coat system, if the substrate is weakly backscattering in the NIR (Levinson et al. 2007b). Even though the optical response in the visible range is the same, the absorption and backscattering of the substrate in the NIR influences the NIR reflectance, and thus ρ_S, of a NIR transmitting coating (Fig. 9.3).

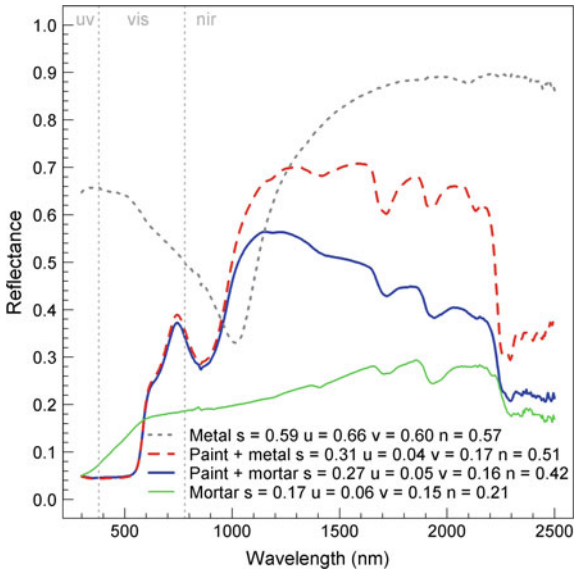

Fig. 9.3 Solar spectral reflectance of a red paint over a mortar substrate, or over a metal substrate (zinc on steel)

In addition to the combined response of the coating system and of the substrate, also the surface roughness strongly influences the overall optical–radiative response. In fact, many surfaces are rough, and the solar and the spectral reflectances differ from those of a smooth surface of the same material. This is because, between the cavities, multiple reflections, and scattering occur. Moreover, the total area of a rough surface is higher than the nominal area (e.g., for a surface made of hemispheres, the total area is twice the nominal one; in other cases even more); thus, the reflectance of a rough surface is much lower than that of a smooth surface. Furthermore, masking and shadowing between the facets may lead to large variability in reflectance, depending on the radiation incidence angle. However, the impact of roughness is maximum for intermediate reflectances, and tending to zero as the reflectance of the flat material tending to 0 or 1 (Berdahl et al. 2008a).

Moreover, the directional response of a rough surface is somewhere in between that of a Lambertian (i.e., purely diffusive) and that of a specular (i.e., mirror-like) material (Lienhard 2010). Therefore, to increase ρ_S of surface, its roughness shall be reduced. An example is the case of the finish coats for External Thermal Insulation Composite Systems with rendering (ETICS, in North America referred to as EIFS). In the recent years, architects were demanding for dark-colored façades made with finished reinforced mortar on exterior insulation. However, these building envelope components are very sensitive to thermal shocks and dilatation–contraction cycles induced by thermal stress (Amaro et al. 2013). Consequently, conventional black coatings may yield to early failures of ETICS, and reducing the surface roughness, for instance with a paint onto the finish coat, may further increase the solar reflectance (Fig. 9.4).

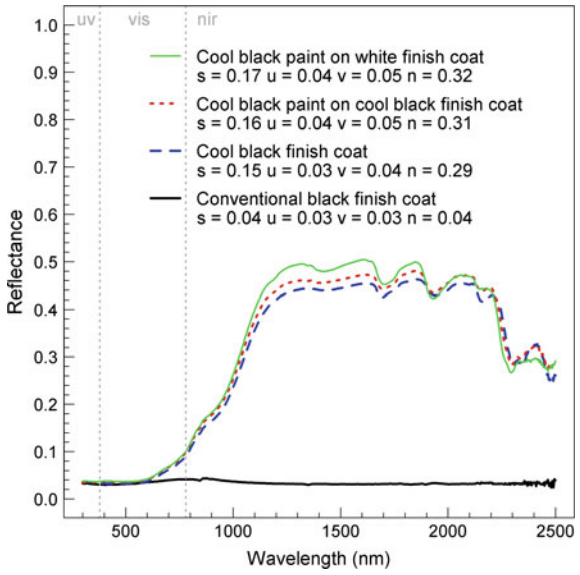

Fig. 9.4 Solar spectral reflectance of finish coats (those used for ETICS/EIFS): a conventional black finish coat, a cool black finish, a cool black paint over a cool black finish, and a cool black paint on a white finish coat

What discussed concerns the solar range, but a surface, to be considered cool, shall also exhibit high thermal emittance, namely it shall be able to dissipate heat by means of radiative cooling in the infrared range of the electromagnetic spectrum (4–80 μm). Most materials present a thermal emittance of the magnitude of 0.9, with the exception of polished metals, that usually have low thermal emittance, in the range of 0.05–0.20. However, also metal slates may be cool if a coating thick enough is applied onto the metal substrate, so that the thermal emittance of the roof surface is that of the coating and not that of the metal panel (Levinson et al. 2011a, b). Thus, it is possible to achieve a thermal emittance approaching 0.90 also for metal roofing or façade elements.

9.4 Applications and Impact of Cool Materials

Among all the strategies proposed for improving building energy efficiency of buildings and the indoor/outdoor thermal comfort (Santamouris 2014a, b; Coutts et al. 2013), "cool" solutions represent one of the most suitable and convenient strategies to mitigate UHIs (Pacheco-Tordal et al. 2011; Akbari and Matthews 2012; Synnefa et al. 2008a, b; Akbari et al. 2009). In fact, they are environmentally friendly, relatively cost-effective, and can easily be applied over existing buildings and urban surfaces. These materials can mitigate urban heat islands by decreasing air and surface temperature when applied over building envelopes, i.e., roofs and walls, and urban paving surfaces. In this scenario, the following paragraphs concern a brief review of the main "cool" solutions developed over the last decade to counteract the urban heat island effect.

9.4.1 Cool Roofs

The building envelope optical and radiative properties are crucial in determining the thermal energy performance of a building, especially during the summer season, when solar gains though both façades and roofs strongly affect the energy demand (Zinzi et al. 2012; Hosseini et al. 2015).

In this panorama, cool roofs represent a suitable passive system to improve building indoor thermal comfort conditions, reduce heat loads for air-conditioning, decrease the energy consumption, and CO_2 released into the atmosphere at urban scale. Cool roofs are indeed demonstrated to reduce surface temperatures up to 37.8 °C and peak summer cooling energy demand up to 15 % (Energy Star 2015; Chung et al. 2015) (Fig. 9.5).

Arumugam et al. (2015), for instance, studied the thermal energy benefits deriving from the surface treatment and thermal property modification of several roof combinations in five climate zones in India.

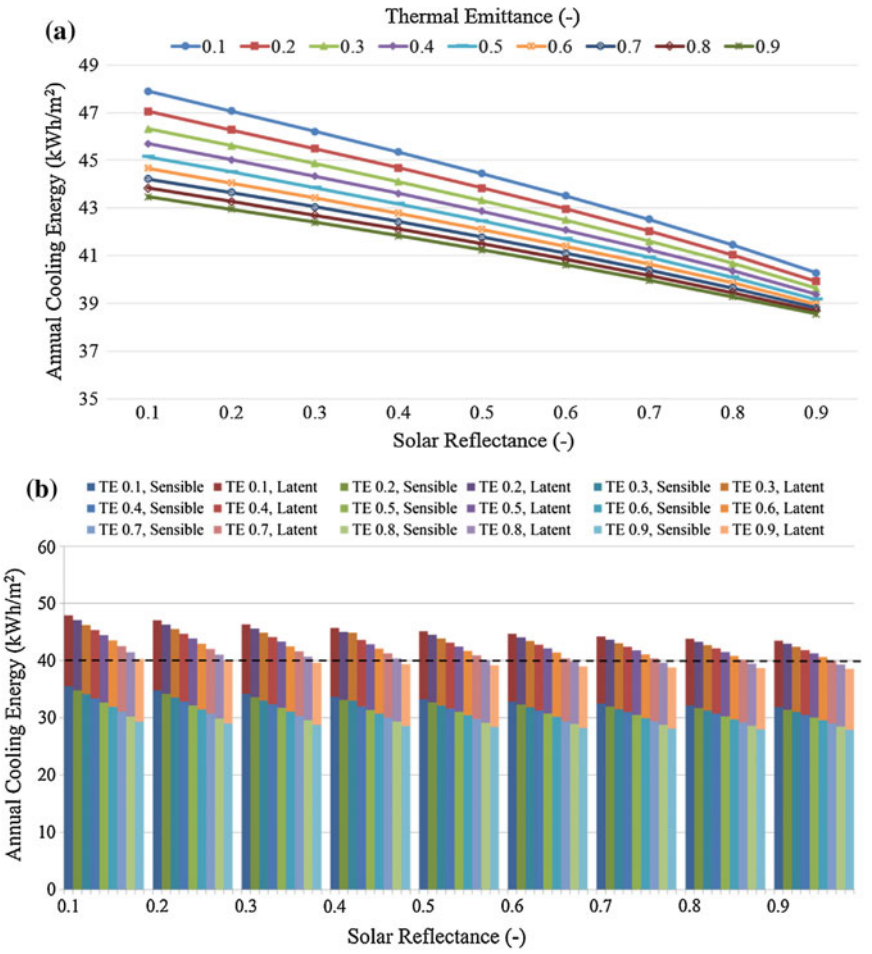

Fig. 9.5 Annual cooling energy of an existing detached house in Seoul, Korea (Chung et al. 2015). **a** Total cooling energy, **b** sensible and latent cooling energy

Akbari et al. (2005) demonstrated that a cool roof may reduce the peak surface temperature by 33–42 °C of commercial buildings in California, with 50 % monitored daily average cooling energy savings, just increasing the albedo from 0.21 to 0.80. They also documented cooling savings after the retrofit with cool roofs for buildings in California, Florida, Georgia, Nevada, and Texas.

Cheng et al. (2005) experimented with test cells a maximum air temperature discrepancy of about 12 °C between the black and the white cell, for lightweight construction in a hot and humid climate. Nevertheless, the potency of cool roofs to decrease the building energy uses and peak power demand has been demonstrated also in cold climates. In fact, Hosseini and Akbari (2015) demonstrated that cool roofs can reduce the peak electric demand of the retail buildings up to 1.9 and 5.4 W/m^2 in Toronto and Montreal, respectively (Fig. 9.6).

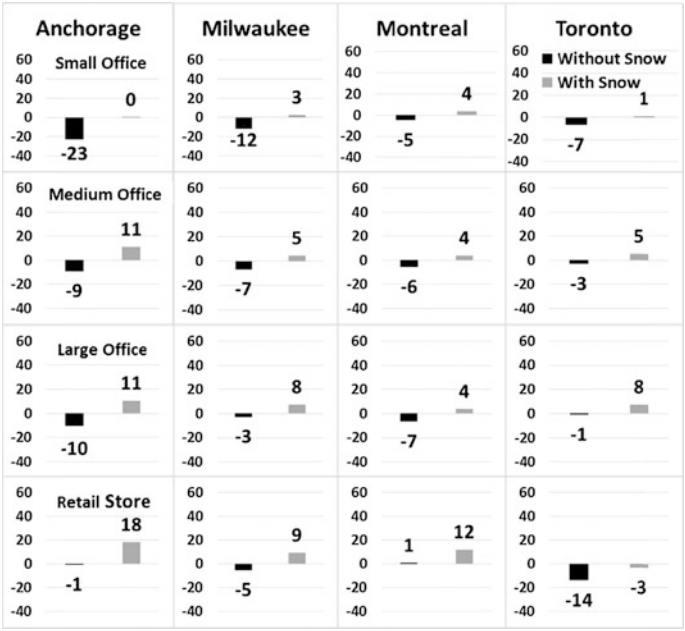

Fig. 9.6 Annual savings ($/100 m^2) of cool roofs with and without the effect of snow for the new buildings with all-electric HVAC systems (Hosseini and Akbari 2015)

Both white and light-colored roofs can be listed as cool roofing systems and represent a suitable alternative to metal roofing solutions usually characterized by high ε but low ρ_S (Synnefa et al. 2006a, b).

Cool roof products can be distinguished in cool coatings, single-ply roofing systems, tiles, asphalt shingles, light-colored roofs, modified bitumen roofs, and metal roofs. Furthermore, cool roofs can be classified as (i) low-slope or flat roofs and (ii) steep-slope roofs. While different types of coatings and membranes are usually applied over low-sloped or flat roofs, the most commonly roofing materials applied over the second category of roofs, i.e., steep-slope roofs, are represented by ceramic or natural stone tiles, shingles, and metal systems.

Cool coatings usually applied over low-sloped and flat roofs are mainly represented by (i) elastomeric and cementitious coatings and (ii) water-based or solvent-based coatings. Additionally, they can be white, aluminum-based, and cool colored coatings depending on their ρ_S and ε. White coatings are mainly composed by acrylic polymers and a white pigment to enhance their ρ_S, usually the rutile form of titanium dioxide or zinc oxide. These coatings are usually characterized by ρ_S ranging between 70 and 85 %. A 19.3 % energy saving due to the application of an innovative white polyurethane-based coating on a typical commercial building in central Italy was found compared to a more traditional dark-colored bitumen membrane (Pisello et al. 2014, 2015a) (Fig. 9.7).

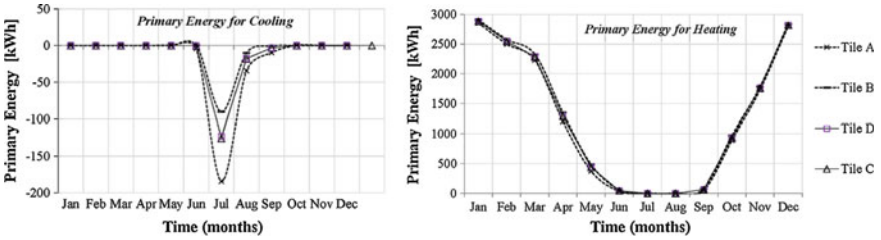

Fig. 9.7 Comparison between four roof scenarios in terms of primary energy requirement. *Tile A* represents the natural uncoated clay tile; *Tile B* is coated with titanium dioxide engobe and with a pigmented white opaque stabilized potassium silicate-based binder and mineral pigments; *Tile C* is obtained from *Tile A*, with the same engobe of *Tile B*, but with different pigmented topcoat mixture; *Tile D* is obtained from *Tile A*, with the previously mentioned engobe and a thin layer of topcoat, where the binder is a self-made sodium silicate-based binder in water (Pisello et al. 2015a)

Aluminum-based coatings are usually composed by an asphalt-type resin containing "leafing" aluminum flakes. Therefore, the upper layer is an aluminum layer, which protects the asphalt from the sun's ultraviolet rays. The aluminum flakes enhance ρ_S up to more than 50 % (LBNL 2015; Synnefa et al. 2006a, b). A recent research evaluated the potential energy saving deriving from thermochromics and phase change materials (PCM)-doped infrared reflective coatings (Karlessi and Santamouris 2013). Comparative tests proved that PCM-doped infrared reflective coatings present lower surface temperatures than cool and common coatings of the same color.

With reference to steeped-slope roofs, terracotta ceramic tiles, light-colored concrete, and clay tiles represent one of the main cool roofing solutions. Such roofing systems are detected to have reflectance values between a minimum of 2 % (ceramic and gray concrete tiles) and a maximum of 75 % (white-colored tiles). In this panorama, innovative cool clay tiles characterized by ε equal to 89 % and ρ_S equal to 77 % were developed by Pisello and Cotana (2014). The continuous monitoring of the thermal energy performance of such original solution when applied over the roof of a typical Italian residential building showed a decrease in the summer peak indoor overheating of 4–7 °C (Fig. 9.8). The same authors

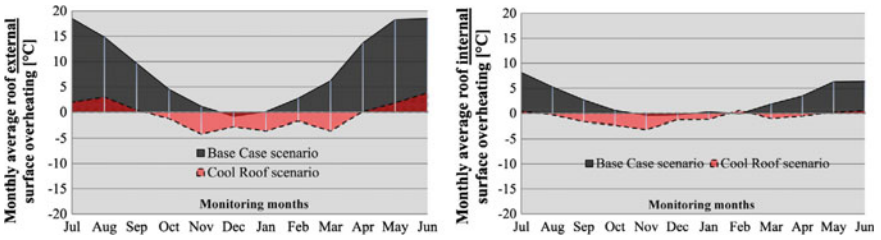

Fig. 9.8 Monthly average overheating values of external–internal surface of the roof (Pisello and Cotana 2014)

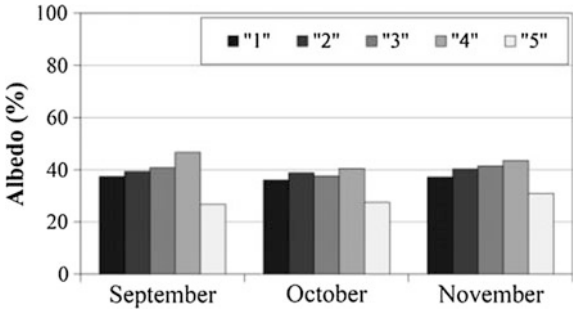

Fig. 9.9 Monthly average in-field albedo of the five gravel samples, from the greatest grain size ("*1*") to the smallest grain size ("*4*") (Castaldo et al. 2015)

proposed a new cool clay tile with similar visual appearance of traditional tiles suitable for application in historical areas (Pisello et al. 2013, Pisello 2015a). The newly developed tile reaches up to solar reflectance values of 87 %.

Another typical cool, natural, low-cost, and low-impact solution for steeped-slope roofs application is represented by shingles and aggregates. Levinson et al. (2014) proposed and validated three new methods for measuring roofing aggregates albedo with irregular surfaces, by testing 17 different specimens. Additionally, Castaldo et al. (2015) demonstrated that albedo of natural gravels have albedos that decrease with increasing grain size (Fig. 9.9).

Finally, metal roof systems are usually produced starting from galvanized steel or aluminum. Metal roofing can be classified into (i) corrugated, (ii) standing-seam, and (iii) with a 3D-profile. A preapplied coating is needed in order to avoid corrosion and improve the durability. There are several shapes available for metal roof elements, such as sheets, trims, and ridge material. White painted metal roof can reach an average ρ_S of 70 % and ε up to 90 %.

9.4.2 Cool Walls

The use of cool solutions for the vertical building envelope, i.e., building walls, appears to be slightly less investigated if compared to cool roofing systems. This is motivated by the fact that the incident solar radiation on a vertical surface is less than that on a horizontal or almost horizontal surface, i.e., roof; therefore, the impact on building thermal energy performance is slightly reduced. Yet, the thermal benefits deriving from a cool façade are worthy being studied, as the use of cool materials on building façades can lead up to 50 % reduction of heat flux through the building envelope (Revel et al. 2014a) (Fig. 9.10).

Therefore, highly reflective paints have a huge potential in terms of passive cooling, as they can significantly reduce solar heat gains, improve thermal comfort,

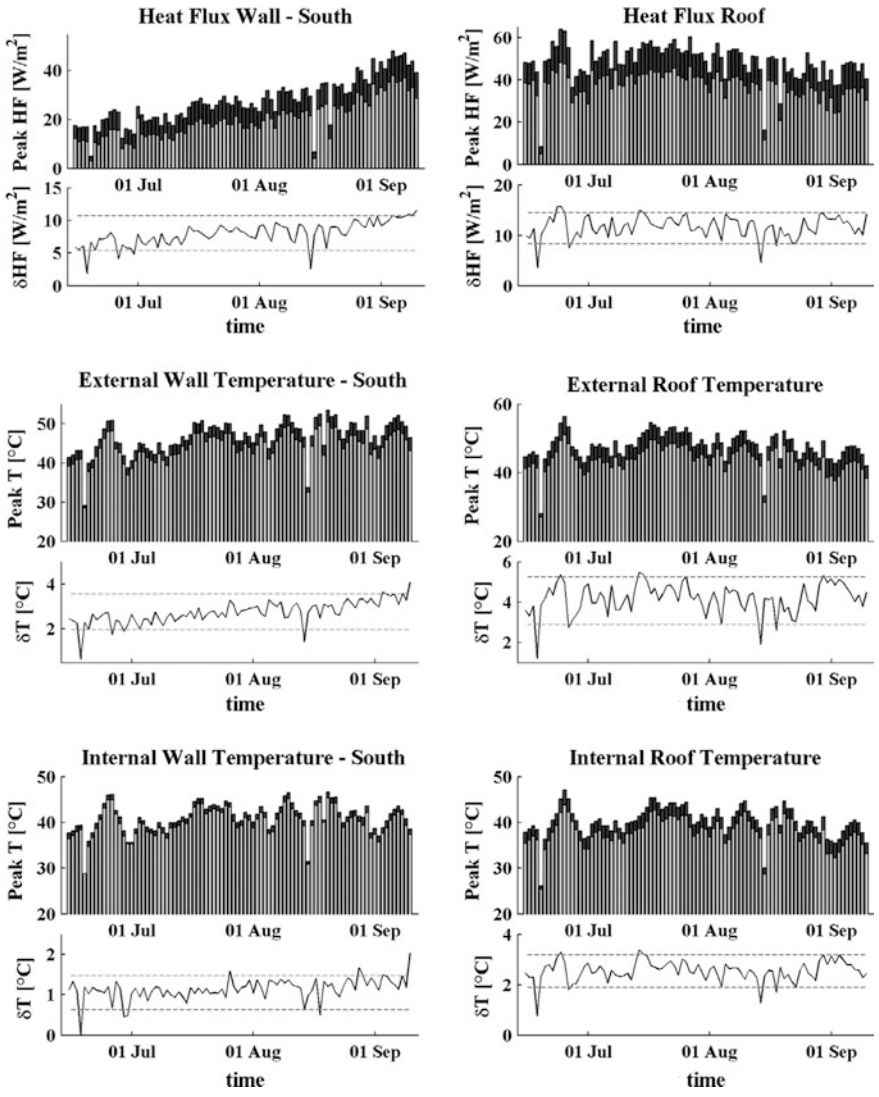

Fig. 9.10 Comparison of peak heat flux and wall temperature measured on mock-ups covered with standard (*black*) and cool (*light gray*) coatings. The left column refers to thermal parameters measured on the south walls of mock-ups #1 and #2 covered with standard and cool façade tiles. The right column reports the same parameters measured on the roof of mock-ups #3 and #4 for standard and cool membranes. Each histogram is shown together with a plot of the peak difference (*solid line*) and the 5 % and 95 % percentile (*dashed line*) (Revel et al., 2014a)

and building energy efficiency during summer. Moreover, for tall and very tall buildings the incident solar radiation on walls may be the largest fraction of the total amount of the solar radiation incident on the building envelope.

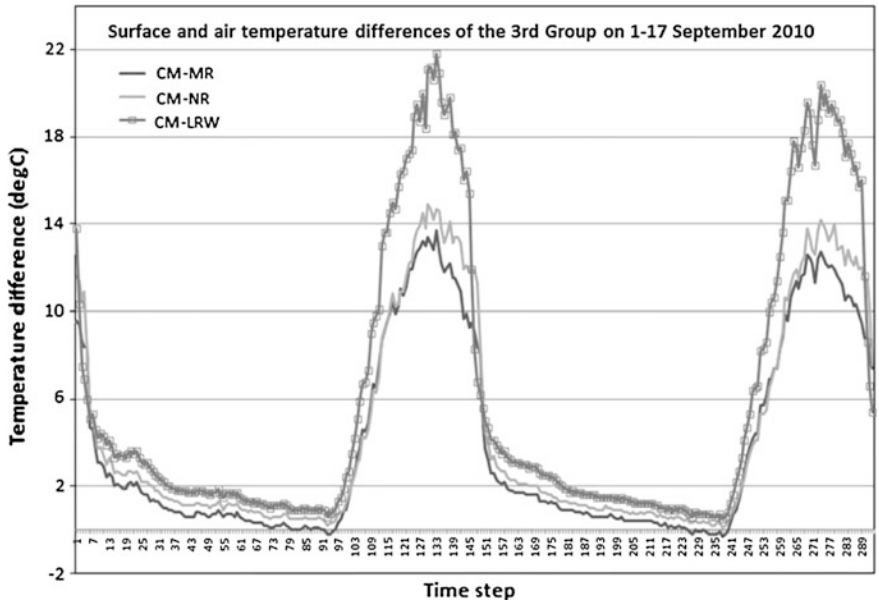

Fig. 9.11 Surface temperature measurements of mineral-based samples estimated by infrared thermography (Kolokotsa et al. 2012)

Commercially available cool materials for walls include mainly reflective coatings, ceramic tiles, and acrylic paints. The passive cooling capabilities of such cool materials suitable for both roof and façades applications have been widely investigated over the past few years. Surface temperature differences up to 11 °C between a conventional and a white reflective paint were detected with in-field measurements performed on a prototype building (Luís et al. 2015). Additionally, the suitability of mineral-based coatings as passive solar technique contributing to buildings' energy efficiency was investigated by Kolokotsa et al. (2012) (Fig. 9.11).

This analysis confirms how cool painting applied on buildings' façade has a non-negligible role in reducing summer heat gains. Pisello et al. (2015b) assessed the role of a cool façade with respect to a cool roof by performing a sensitivity analysis. It was demonstrated that, even if the contribution of the cool roof is decisive for the enhancement of the indoor thermal comfort conditions in terms of operative temperature, the role of the cool façade painting is not negligible in terms of building wall surface temperature reduction (i.e., 25 %).

Synnefa et al. (2006a, b) performed a comparative analysis on 14 different reflective coatings to investigate their capability to lower both the exterior surface temperatures of buildings and ambient air temperatures by means of sensors and infrared thermography. A reduction of 4 and 2 °C of the surface temperature of a white concrete tile was detected under hot summer conditions and during the night, respectively.

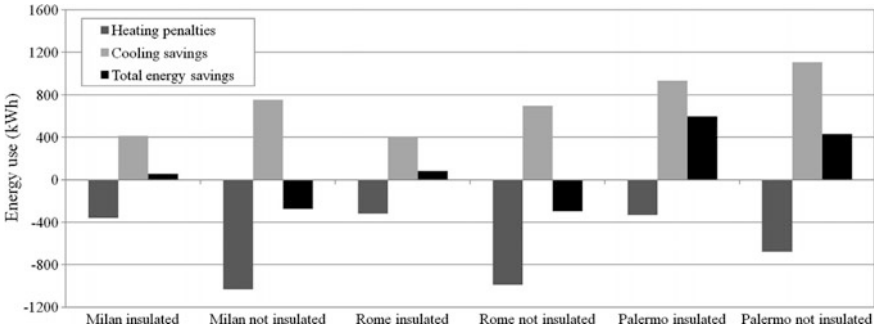

Fig. 9.12 Heating penalties (*red histogram*), cooling savings (blue histogram), total energy penalties/savings (*green histogram*) achieved implementing the cool facade technology (Zinzi et al. 2015)

A cool pigmented paint for masonry walls was characterized by Zinzi (2015), who computed that the cool façade provided 5 % global energy savings a typical Italian residential building (Fig. 9.12). Additionally, 6 and 1.6 °C reductions of the peak external surface temperatures and indoor operative temperature, respectively, were also computed with dynamic simulations.

Dias et al. (2014) modeled the energy uses of a residential building with cool (ρ_S = 92 %) and standard paint (ρ_S = 50 %) and reported a 2 °C indoor temperature reduction for the ground floor during peak summer conditions.

Innovative cool colored ceramic tiles and acrylic paints for façades have been developed and tested at laboratory scale by Revel et al. (2014b). An increase up to 40 % of the solar reflectance was achieved in the near-infrared range while maintaining the dark color and high absorbance in the visible. The thermal impact of different cool façade coatings characterized by 42 and 62 % was investigated and compared by Shen et al. (2011) to a standard coating with solar reflectance of 32 %. The results showed a reduction up to 20 and 4.7 °C of the exterior and interior surface temperatures with respect to the same wall assembly with a standard coating.

A cool façade can generate a positive thermal energy effect also at urban scale, as it is able to reduce for instance the heat accumulated inside urban canyons. The use of cool coatings applied on pavements and walls inside a urban canyon can indeed decrease up to 8 and 3 °C the ground surface temperature and walls' surface temperature, respectively (Georgakis et al. 2014) (Fig. 9.13).

Moreover, the comparison between temperatures of a street canyon with brown cool selective paint façades and with a standard brown coating performed in France by (Doya et al. 2012) showed that the cool selective facade paint led to a 1.5 and 2.5 °C reduction of peak surface temperatures and indoor air temperature, respectively.

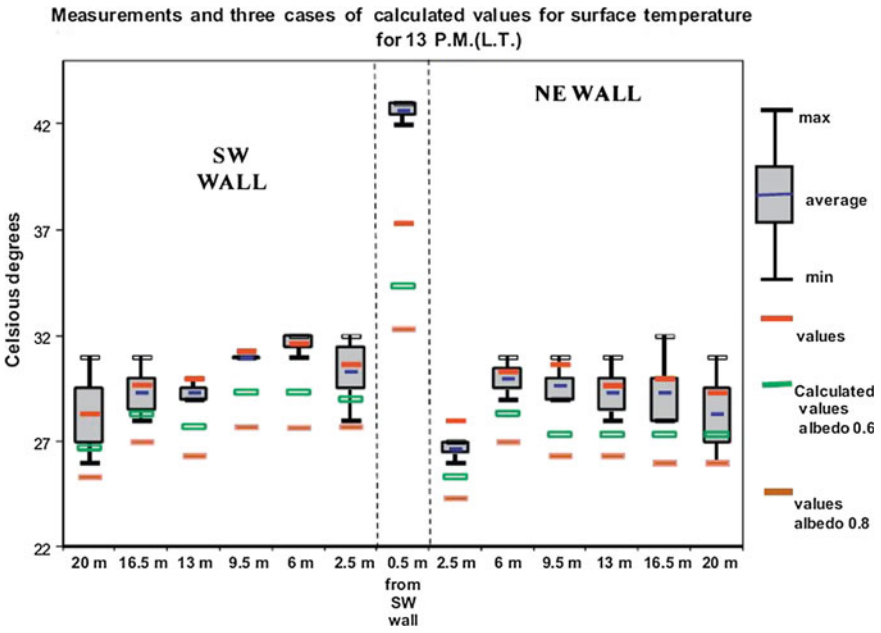

Fig. 9.13 Surface temperature measurements and calculated values for different coatings, at 13:00 L.T. (Georgakis et al. 2014)

9.4.3 Cool Shading Devices

While cool roofing and paving solutions have been largely studied by means of both experimental and numerical approaches (Synnefa et al. 2012; Santamouris et al. 2012), the role of high-albedo façades still needs to be deeply evaluated. In particular, the effect of cool shading systems on building thermal energy performance was detected to be non-negligible. In fact, solar shading devices have an important impact on the temperature trends of the adjacent layers, on yearly energy consumptions, on indoor thermal comfort, as well as on the level of the natural light depending on their geometry, optical–thermal properties, and permeability. Therefore, a proper shading system must be selected not just to control solar heat gains through the building envelope. In fact, the management, the visual comfort, and the acoustic performance must be taken into account too.

An accurate description and evaluation of the main typologies of solar control systems in different climatic locations (Berlin, Milan, Florence, and Athens) is provided by Carletti et al. (2014) (Fig. 9.14).

The thermal behavior of the shadings was also assessed by means of the dynamic simulation tool EnergyPlus. It was demonstrated that the use of shading devices as passive control systems leads to improved thermal sensation during summer and reduced thermal loads for air-conditioning. In this respect, Pisello (2015b) evaluated the thermal energy performance of cool louvers of shutters compared to dark-colored

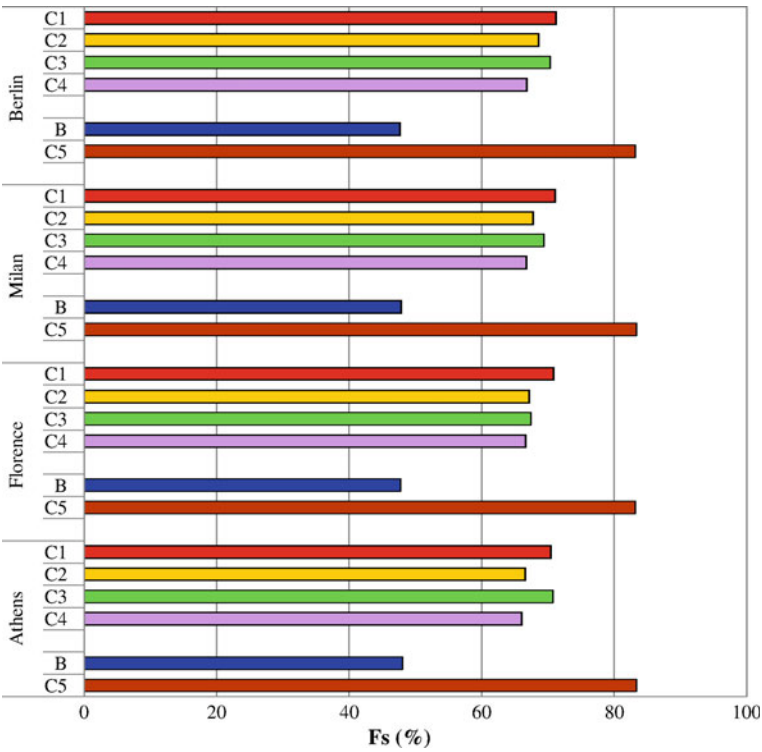

Fig. 9.14 Reduction factor of summer solar gains Fs for different shading systems selected for the four locations, relatively to south orientation (Carletti et al. 2014)

traditional shading systems. An increase of 75 % of the solar reflectance in the cool shutters lead to a decrease up to 2 °C of the indoor air temperature in free-floating conditions. A corresponding energy saving of 25 % was found. Additionally, Zinzi et al. (2012) studied the effect of cool coatings applied over window shading systems demonstrating how this solution could produce up to 7.1 % net cooling energy saving in summer, by reducing the solar gain entering the window.

Stazi et al. (2014) performed an experimental and analytical comparative study of sliding perforated panels, ventilated double-glazed window, aluminum horizontal louvers, aluminum persiana, and traditional wooden persiana to evaluate the performance of the different shadings in a Mediterranean climate in terms of thermal comfort, day lighting, and environmental impact. It was demonstrated that the wooden solution may provide a good compromise and that the aluminum louver screen is suitable as it allows to set different shading configurations given the movable slats.

The effect of highly reflective systems is significant also in reducing the energy consumption for artificial lighting. Hashemi (2014), for instance, carefully analyzed the effect of internal reflective louvers for office buildings with a focus on the role of

such shading systems on daylighting. The results showed how the system could reduce by 60 % the need for artificial lighting.

9.4.4 Cool Paving Materials

Paved surfaces, such as roads, squares, play a significant role in determining urban heat island effect, given their contribution to the overheating of the air close to the surface by storing heat during the day and releasing it at night. Standard paving materials can reach surface temperatures up to 48–67 °C, due to the typically very low solar reflectance of these materials (Santamouris 2014a, b; Santamouris et al. 2007; Doulos et al. 2001; Synnefa et al. 2008a, b). For instance, the common black asphalt concrete has solar reflectance equal to 0.04–0.06. It is demonstrated that by increasing pavements' solar reflectance by only 25 % a reduction of 10 °C of the surface temperature can be achieved. Increasing the albedo of a paved surface generates the reduction of convection of heat to air by consequently lowering the ambient air temperature. This phenomenon leads to reduced building energy consumption and urban smog generation rate. Therefore, high-albedo urban pavements represent a good and cost-effective solution to fight urban heat island phenomenon, as they generate less absorption of incident solar radiation by decreasing greenhouse gas concentrations both at local and global scale (Akbari et al., 2009). Furthermore, lower pavement surface temperatures positively affect the durability of paving materials.

To make a street pavement "cool," it is possible to (i) increase its solar reflectance, (ii) increase its permeability, and (iii) create a composite structure, which emits less heat at night (EPA 2015). Ongoing research mainly focuses on white paints for paving systems, infrared-colored paints, the same infrared-colored paints to cover aggregates, and also peculiar color-changing paints (Santamouris 2013). Therefore, the main cool pavement technologies are represented by (i) light-colored aggregates; (ii) permeable pavement, i.e., shingle and gravels; and (ii) solar-reflective finishing. Of course, the optimal solution depends on the specific configuration and local climate conditions of the location, which influences the thermal performance of cool materials when applied over urban paving surfaces (Chen et al. 2009). Compared to cool roofs, cool coatings for paving materials do not respond only to the necessity of presenting high solar reflectance and thermal emittance, but have to comply also with the characteristics of a pavement coating. Therefore, they must include a reflective inorganic finishing, non-organic fillers, and antiskid aggregates. The inorganic fillers influence the color and the roughness of the pavement surface. Nevertheless, cool pavements are demonstrated to be as effective as cool roof materials in mitigating urban heat island by reducing urban surfaces' albedo. It was estimated that the use of cool paving materials to cover 4500 m^2 of reflective pavements in an urban park in the greater Athens area leads to a reduction of 1.9 and 12 K of the peak ambient temperature and surface temperature, respectively, during a typical summer day (Santamouris et al. 2012) (Fig. 9.15).

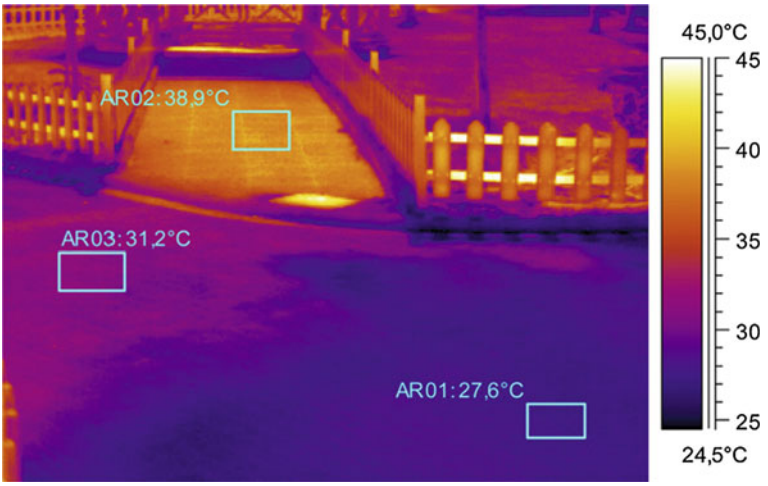

Fig. 9.15 Surface temperature of the cool shaded (*AR01*), the conventional non-shaded (*AR02*), and the cool non-shaded pavement (*AR03*) (Santamouris et al. 2012)

Among the main organic polymers suitable for being used as cool coatings for pavements, it is possible to identify epoxy resins and acrylic polymers, which contribute to the chemical and mechanical stability of the material. The inorganic polymeric fillers are used to increase the solar reflectance of the material. In the case of cool paving materials, mostly NIR-reflective pigments are used in order to avoid glare issues to walking or driving people. Synnefa et al. (2011) found out a 12 °C decrease in the pavement surface temperature by comparing a traditional dark-colored asphalt with cool colored coated asphalts. Furthermore, a 17 to 5 °C decrease of the pavement surface temperature was reported by Wan et al. (2012), by comparing an innovative cool coating with high NIR reflectance, i.e., 81 % with the traditional asphalt and cement, respectively.

The most diffuse aggregates for paving applications are represented by porcelain and silica sand, which do not have a very high solar reflectance but can be effective in reducing surface temperatures when integrated into concrete cement. Levinson and Akbari (2002) provide detailed data about albedo of several Portland cement concrete pavements, by characterizing 32 different composition mixes.

An increase of albedo from to 37 to 91 % was achieved by repaving a courtyard in Michigan (USA) with a white-colored aggregate, yielding to a mean radiant air temperature decrease of about 1.3 °C (Taleghani et al. 2014). In the same scenario, innovative gravels for pavement applications were proposed by Pisello et al. (2014, 2015a) as an original natural, low-cost, low-impact, and highly reflective material suitable for paving applications (Fig. 9.16).

It was demonstrated that the gravels albedo increases with the decrease of the gravels grain size. Also, Berdhal et al. (2008a) evaluated the solar reflectance of innovative cool asphalt roofing shingles covered with pigmented mineral roofing

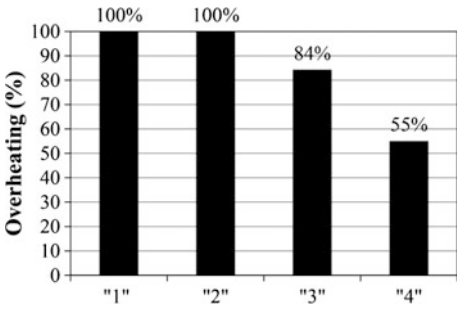

Fig. 9.16 Maximum surface temperature difference between gravels with different grain sizes and the same natural origin, calculated in the monthly average day. Gravel "*1*" presents the greatest grain size and gravel "*4*" has the smallest grain size (Castaldo et al. 2015)

granules. The use of reflective base grains coupled with reflective coatings increased the solar reflectance.

9.5 Nanostructured Materials as Thermal Barrier Coatings for Thermal Energy Storage

As previously mentioned, the development of new sustainable cities with widespread application of cool surfaces has been proposed as a countermeasure against UHIs (Synnefa et al. 2007). Considerable interest has been dedicated to roofing materials and, in this context, basic nanostructured materials and composites or nanocomposites, characterized by different specific properties have been recently considered (Comite et al. 2015). For instance, adding additives like nanoparticles, nanofluids, pigments, or adopting a nanocomposite approach, not only improves the appearance of the coatings, but also helps to improve many properties of the coatings such as UV resistance, corrosion resistance, and mechanical properties like resistance to scratch and abrasion. To achieve the highest possible thermal insulation resistance, in fact, new insulation materials and other solutions have been and are being developed, in addition to using the current traditional insulation materials. A brief overview on the most recent nanostructured materials used as potential thermal barrier coatings for thermal energy storage will be the focus of this section. In this context, many materials are available which often fall under the following types:

- Organic materials,
- Inorganic materials,
- Metallic or metallized reflective membranes.

According to Guo et al.'s study, the heat-reflective insulation coating could reduce the exterior wall surface temperature effectively, and the maximum temperature change is about 8–10 °C (Guo et al. 2012). Jose et al. found that new type of

pigments, Y_2BaCuO_5 and lanthanum–strontium copper silicates, not only possess high chemical and thermal stability, but also have high near-infrared reflectance (61 % at 1100 nm) (Jose et al. 2014). As previously mentioned (Sect. 9.2), conventional inorganic pigments are mainly composed of metal oxides, such as chromium green, cobalt blue, cadmium stannate, lead chromate, cadmium yellow, and chrome titanate yellow. Yet, most of them are detrimental to human health and external environment and therefore are strictly controlled by government legislation and regulations in many countries (Zhao et al. 2015). A large number of rare-earth-based NIR-reflective pigments are proposed as alternatives to traditional transition metal oxides pigments because of their low toxicity. In this context, Zhao et al., recently reported about the synthesis of NIR reflecting inorganic nanopigments $Y_{6-x}Nd_xMoO_{12}$ (x ranges from 0 to 1.0) via sol–gel, investigating also the crystalline temperature, the chromaticity, near-infrared reflective properties, and thermal and chemical stability of the novel proposed (Zhao et al. 2015). The authors proved that the novel environment-friendly near-infrared reflective nanopigments with particle size less than 100 nm exhibited a reflectance exceeding 97 % within the spectral range 1000–1500 nm. The pigments were also thermally and chemically stable, thus making them excellent candidates for use as cool pigments. Moreover, Wang and Mingfeng 2014) recently reported about the possibility to use a coprecipitation method to prepare Fe^{3+} doped with $KZn_{1-x}(Fe)_xPO_4$ considering the influences of the doping content on the structure, color, and near-infrared reflective properties of the material. They proved that $KZn_{1-x}(Fe)_xPO_4$ pigments can be well served as "cool colorant." The results showed, in fact, that after doping with Fe^{3+}, the crystal structure of $KZnPO_4$ did not change. Furthermore, while the color of the sample deepened with the increasing concentration of Fe^{3+}, the band gap decreased from 2.00 eV to 1.95 eV, and the near-infrared reflectance was reduced from 74.7 to 67.1 %. Finally, for the aluminum sheet coated with $KZn_{0.9}(Fe)_{0.1}PO_4$ pigment, with coating thickness of 312 μm, the near-infrared reflectance could reach 46.7 %, higher than the reflectance of conventional pigments of similar color (32.1 %) (Wang and Mingfeng 2014). Always in this context, a reflective heat insulation coating was prepared using a geopolymer, which mainly consisted of sodium silicate solutions and metakaolin, by Zhang and coworkers (Zhang et al. 2015). The authors proposed a new, environmentally friendly inorganic coating with many capabilities, such as good water retention, simple spraying, compacted paint, high durability, dirt resistance, high reflectivity, and remarkable heat insulation. The results indicate a titanium dioxide content of approximately 12 and 6 % hollow glass microspheres provided a coating with a reflectance exceeding 90 % and thermal insulation performance (internal and external surface temperature difference) of up to 24 °C.

Furthermore, in recent years, pigments of different colors with cool properties have been commercialized. The color features of pigment materials (one or more) depend on their visible absorption, on their size (which varies scattering properties), and on their composition (Thongkanluang et al. 2010). To tune the color of a material, pigments with different chemical compositions are used. Demarchis et al. (2015) used two different synthesis methodologies to produce red cubic and spherical hematite cool pigments of different particle size. Cubic and spherical

particles with larger particle sizes were obtained through a gel–sol method using chloride and nitrilotriacetate ions as shape controllers, and changing the starting temperature to control the final particle size. Smaller spherical particles were synthesized more rapidly following a catalytic phase transformation method in which the size control is obtained by varying the reagent concentration. The authors proved that the cool properties differ depending on the particle size and shape (Demarchis et al. 2015).

In the last 20 years, waterborne coatings have also gained increasing importance due to strict environmental regulations on the emission of volatile organic compounds from solvent-borne coatings. To maintain constant product quality and to develop new products, structural characterization and measurement of barrier properties of these new coatings has become crucial. Waterborne coatings usually contain different additives and an appropriate choice among various alternatives of these additives brings a challenge to both manufacturers and researchers.

The great chemical stability of Al_2O_3 at elevated temperatures makes it a particularly attractive material for wear-resistant coatings. Furthermore, the relatively small thermal conductivity of Al_2O_3 at high temperatures will provide more effective thermal protection for the substrate (Comite et al. 2015). Recently, Comite et al. reported about the effect of the addition of high surface area Al_2O_3 as pigment on the performance of waterborne coatings, in particularly regarding the barrier properties and the thermal resistance. Compared to conventional layers, the new buildings' coatings developed by Comite et al. are environmentally preferable, non-solvent based, and energy efficient. The authors proved that the introduction of γ-alumina microparticles, with peculiar high surface area, in waterborne paint formulation, allows to obtain interesting textural layer and due to both the high surface area of particles and the presence of interstitial cavities in the thin film, the product seems to be very interesting as insulation material (Comite et al. 2015). Furthermore, Chieruzzi et al., proved the effect of silica (SiO_2), alumina (Al_2O_3), titania (TiO_2), and a mix of silica–alumina (SiO_2–Al_2O_3) nanoparticles in different nanofluids with phase change behavior. The formulations were developed by mixing a molten salt-based fluid (selected as phase change material) with the different selected nanoparticles using the direct-synthesis method. The authors proved that the proposed nanofluids can be used in concentrating solar plants with a reduction of storage material if an improvement in the specific heat is achieved. In particular, the research demonstrated that the addition of silica–alumina nanoparticles has a significant potential for enhancing the thermal storage characteristics of the $NaNO_3$–KNO_3 binary salt (Chieruzzi et al. 2013), while SEM images clearly suggested a higher interaction between the SiO_2–Al_2O_3 nanoparticles and the salt especially with 1.0 wt% of nanoparticles. Always in this context, the nanoenhanced PCMs (NePCMs) were recently proposed by Khodadadi and Hosseinizadeh (2007), for improving thermal energy storage by increasing heat conductivity. It was noteworthy that nanoparticles had been formerly utilized, to develop advanced heat transfer fluids, i.e., nanofluids (Gao et al. 2009). Recently, Parameshwaran et al. studied new organic ester PCMs embedded with the silver–titania hybrid nanocomposite (HyNPCM) with mass proportions ranging from 0.1 to 1.5 %

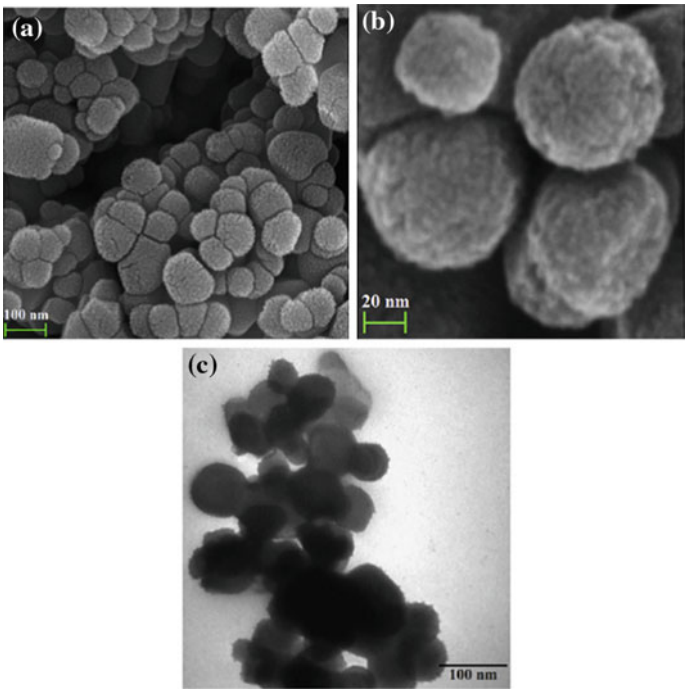

Fig. 9.17 FESEM images (**a** and **b**) of Ag–TiO_2 HyNC, and TEM image (**c**) of Ag–TiO_2 HyNC dispersed in the organic ester PCM (Parameshwaran et al. 2014)

(Parameshwaran et al. 2014). Spherical nanocomposite particles of size ranging between 60 and 98 nm, which essentially comprised of the silver nanoparticles adsorbed over the surface of chain-like-structured titania nanoparticles dispersed in PCM, were considered in this work (Fig. 9.17).

The HyNPCM embedded with the surface-functionalized hybrid nanocomposite exhibited improved thermal conductivity from 0.286 to 0.538 W m^{-1} K^{-1}, congruent phase change temperature (6.8 °C), high latent heat capacity (90.81 kJ kg^{-1}), substantial reduction in the supercooling degree (1.82 °C), thermal stability (191 °C), and chemical stability, as compared to the pure PCM. Experimental results reveal that, the freezing and the melting times of the HyNPCM were reduced by 23.9 and 8.5 % respectively, when compared to the pure PCM. The authors demonstrated that the improved thermal properties and the heat storage potential of the HyNPCM has facilitated them to be considered as a viable candidate for the cool thermal energy storage applications in buildings without sacrificing the energy efficiency (Parameshwaran et al. 2014).

9.6 Performance Over Time of Cool Materials

Although efforts are being made to improve the optical–radiative properties of cool materials, any assessment on pristine samples is not sufficient, as aging, namely the complex of weathering, soiling, and biological growth may strongly affect the performance over time of such materials (Sleiman et al. 2011; Kültür and Türkeri 2012).

When exposed to the outdoor environment, materials with high initial ρ_S (e.g., greater than 0.6) tend to lose reflectance with time, while materials with low initial ρ_S (e.g., less than 0.3) tend to experience an increase with aging. Materials that exhibit intermediate values, instead, are almost unchanged (Sleiman et al. 2011). The thermal emittance of metal increases with time (e.g., from 0.2 to approximately 0.4), while that of nonmetallic surfaces in most cases is slightly altered (Cool Roof Rating Council 2015).

The main aging actions induced by environmental agents that contribute to the alteration of the optical–radiative response can be identified as follows (Wypych 1995; Berdahl et al. 2002, 2008b, 2012):

- Mechanical stress induced by sunlight and temperature variations, as well as by wind, repeated in cycles of dilatation–contraction or thermal shocks due to sudden variations (Daniotti et al. 2013, 2014);
- Photodegradation of polymers and other organic materials;
- Moisture (including rain, hail, snow, frost, and dew);
- Atmospheric gases and pollutants;
- Soiling (Ichinose et al. 2009);
- Biological growth (Shirakawa et al. 2014).

In fact, heat fluctuation can accelerate chemical reactions, moisture can cause damage to materials by both physical and chemical processes, air pollutants can cause chemical reactions with atmospheric oxygen, and water vapor can provoke the formation of oxides and hydroxides on materials resulting in a decrease of their solar reflectance. Additionally, the growth of fungi on materials due to moisture or the deposition of organic substances can also alter the optical properties of materials. Rain represents the only external agent which could contribute to the cleaning of surfaces from dust deposition by restoring solar reflectance and infrared emittance values of cool materials. However, rain can lead also to the deposition of atmospheric pollutants or soil on cool surfaces.

In particular, for roofing materials with initial ρ_S greater than 0.80, weathering and soiling might yield to a mean absolute loss of about 0.16 (average maximum of 0.24) after three years of natural exposure at low or moderately polluted non-urban or suburban sites (Sleiman et al. 2011). In the polluted metropolitan areas of Rome and Milano, roofing membranes with initial ρ_S equal to 0.80 get, respectively, to 0.63 and 0.56 after two years of natural exposure (Paolini et al. 2014b).

If for highly reflective roofing membranes relevant variations occur already during the first months, for façade materials, given the vertical exposure, the first

months mainly provide information about color change, with modest losses of ρ_S (Diamanti et al. 2013). However, even though it takes several years for the solar reflectance of high-albedo façades to get to a steady value, already after 1.5 years, weathering and soiling may induce a loss of approximately 0.15 with an initial ρ_S of 0.73 (Paolini et al. 2014a).

Cleaning procedures to restore the initial reflectance were studied in the literature, but these were found ineffective for porous materials (Ferrari et al. 2014), or effective only introducing bleaching for white PVC membranes (Levinson et al. 2005c).

For these reasons, several options appear as promising to retain as much as possible the initial solar reflectance and solar emittance. These include as follows:

- Self-cleaning anatase added photocatalytic materials (Ganesh et al. 2011; Graziani et al. 2013, 2014; Diamanti and Pedeferri 2013);
- Fluoropolymers such as PVDF (Berdahl et al. 2008b) and ETFE (Mainini et al. 2014);
- NIR-reflective materials. In fact, the absorption coefficient has an exponential trend decreasing with increasing wavelength (Lindberg et al. 1993; Kirchstetter and Novakov 2007), and also the effects of UV aging are evident mainly at short wavelengths. Therefore, between two materials with the same solar reflectance, one reflecting more in the visible, and another one more in the near-infrared, the latter is less subject to reflectance losses with time (Paolini et al. 2014b);
- Smooth finishing and tilt. Very smooth materials (such as glass or ceramic) when installed steep sloped show losses in reflectance in coincidence with specific events of soil deposition (e.g., airborne sand), but are more easily rain-washed almost recovering the initial reflectance. When exposed low sloped, instead, they do not exhibit a very different behavior from that of rougher materials (Paolini et al. 2014b);
- The absence of plasticizers that may reach the surface, or decoupling of the surface from those substances. Plasticizers that migrate to the surface are believed to be one of the major reasons that yield to the loss in solar reflectance of roofing membranes, as they become sticky and favor the adhesion of particulate matter to the surface (Miller et al. 2004);
- Construction details. As the performance of a cool material in use conditions is that of the whole building, one of the most relevant aspects is the care paid to design the building envelope so as to avoid ponding water (especially on flat roofs), obstruction of drains, and in general accumulation of dirt and leaves.

Some standards and methods were already been detected to experimentally determine the degradation level of materials based mainly on the continuous monitoring of the properties after the exposition of the materials to the outdoor environment (ASTM 2003; Jacques 2000).

As natural exposure programs take several years to provide an answer, an accelerated weathering and soiling protocol was developed to reproduce the impact of three years natural exposure in the USA of roofing materials (Sleiman et al. 2014; ASTM 2015), and its application was later extended to European urban areas

and to façade materials (Paolini et al. 2014a). These may foster the development of new cool material with enhanced performance over time. However, the full complex of agents inducing changes in solar reflectance of porous materials appears to need further investigation, and other relevant mechanisms such as biological growth and freeze–thaw shall be introduced in such accelerated protocols.

9.7 Future Trends

The Achilles' heel of the "cool" strategies described in the previous sections is durability. In fact, the thermal–optical and radiative properties of cool materials, i.e., solar reflectance and infrared emittance, as previously mentioned, change over time due to the action of external agents and to the exposure to ambient and weather conditions (Synnefa et al. 2006a, b). For this reason, future trends of the research in the field of cool materials to fight urban heat island are mainly focused on the analysis of how the thermal energy performance of such solutions can be deteriorated over time. More specific research effort is still required on the side of durability assessment and natural and accelerated protocols.

Another important future development of the international research about cool materials is represented by the development of technologies for the use of nanomaterials for improving the passive cooling potential (Escribano and Keraben Grupo 2010–2013). In fact, the use of nanotechnology for integration in cool materials is still scarcely diffused. However, it has a great potential in the development of eco-efficient construction technologies, especially in the form of films and nanostructured coatings (Pacheco-Tordal et al. 2013). For instance, the potential of PCMs as latent heat storage materials when integrated in building envelopes has already been proved (Ferrer et al. 2015; De Gracia and Cabeza 2015). Therefore, the performance of such materials as cool products when included into cool roofing, façade, and paving systems must now be investigated in terms of both energy savings and indoor–outdoor microclimate enhancement. Additionally, future trends are detected toward the development of innovative and cost-effective technologies for the production of PCM-doped reflective coatings.

9.8 Conclusions

This chapter has provided a wide panorama around building physics and material science point of view for looking at innovative materials for building energy efficiency characterized by high passive cooling capability. In particular, the threefold benefit of cool surfaces has been presented and several applications at material and building scale were dealt with. Finally, the performance during the course of the time was discussed, and key recent and promising applications of nanoscience and

nanoengineering in this field were presented by showing the great potential of nanotech-based cool materials for building energy efficiency.

A literature review has been carried out, with the main objective to make the reader aware of specific applications and new trends in the field of high-albedo passive cooling and protective strategies in constructions.

References

Akbari H, Damon Matthews H (2012) Global cooling updates: reflective roofs and pavements. Energy Build 55:2–6

Akbari H, Levinson R, Rainer L (2005) Monitoring the energy-use effects of cool roofs on California commercial buildings. Energy Build 37(10):1007–1016

Akbari H, Menon S, Rosenfeld A (2009) Global cooling: increasing world-wide urban albedos to offset CO_2. Clim Change 94:275–286

Amaro B, Saraiva D, de Brito J, Flores-Colen I (2013) Inspection and diagnosis system of ETICS on walls. Constr Build Mater 47:1257–1267. doi:10.1016/j.conbuildmat.2013.06.024

Arumugam RS, Garg V, Vinayaka Rama V, Bhatia A (2015) Optimizing roof insulation for roofs with high albedo coating and radiant barriers in India. J Build Eng 2:52–58

ASTM D1669 (2003), standard practice for preparation of test panels for accelerated and outdoor weathering of bituminous coatings. American Society of Testing and Materials, West Conshohocken, PA, USA

ASTM E1980–11 (2011) Standard practice for calculating solar reflectance index of horizontal and low-sloped opaque surfaces

ASTM (2015) ASTM D 7897. Standard practice for laboratory soiling and weathering of roofing materials to simulate effects of natural exposure on solar reflectance and thermal emittance

ASTM G7-97 (1997) Standard practice for atmospheric environmental exposure testing of nonmetallic materials, American Society of Testing and Materials, West Conshohocken, PA, USA

Berdahl P, Akbari H, Rose LS (2002) Aging of reflective roofs: soot deposition. Appl Opt 41:2355–2360

Berdahl P, Akbari H, Jacobs J, Klink F (2008a) Surface roughness effects on the solar reflectance of cool asphalt shingles. Sol Energy Mater Sol Cells 92:482–489. doi:10.1016/j.solmat.2007.10.011

Berdahl P, Akbari H, Levinson R, Miller W (2008b) Weathering of roofing materials—an overview. Constr Build Mater 22:423–433. doi:10.1016/j.conbuildmat.2006.10.015

Berdahl P, Akbari H, Levinson R, Jacobs J, Klink F, Everman R (2012) Three-year weathering tests on asphalt shingles: Solar reflectance. Sol Energy Mater Sol Cells 99:277–281

Bonamente E, Rossi F, Coccia V, Pisello AL, Nicolini A, Castellani B., Cotana, F., Filipponi, M., Morini, E., Santamouris, M (2013) An energy-balanced analytic model for urban heat canyons: comparison with experimental data. Adv Build Energy Res 7(2):222–234.

Brady RF, Wake LV (1992) Principles and formulations for organic coatings with tailored infrared properties. Prog Org Coatings 20:1–25. doi:10.1016/0033-0655(92)85001-C

Carletti C, Sciurpi F, Pierangioli L (2014) The energy upgrading of existing buildings: window and shading device typologies for energy efficiency refurbishment. Sustainability 6:5354–5377. doi:10.3390/su6085354

Carnielo E, Zinzi M (2013) Optical and thermal characterisation of cool asphalts to mitigate urban temperatures and building cooling demand. Build Environ 60:56–65

Castaldo VL, Coccia V, Cotana F, Pignatta G, Pisello AL, Rossi F (2015) Thermal energy analysis of natural "cool" stone aggregates as passive cooling and global warming mitigation technique. Urban Clim J (in press)

Chen MZ, Wei W, Wu SP (2009) On cold material of pavement and high temperature performance of asphalt concrete. Mater Sci Forum 620:379–382
Chen C, Wang Y, Pan G, Wang Q (2014) Gel-sol synthesis of surface-treated TiO_2 nanoparticles and incorporation with waterborne acrylic resin systems for clear UV protective coatings J Coat Technol Res 11(5):785–791
Cheng V, Ng E, Givoni B (2005) Effect of envelope color and thermal mass on indoor temperatures in hot humid climate. Sol Energy 78–4:528–534
Chieruzzi M, Cerritelli GF, Miliozzi A, Kenny JM (2013) Effect of nanoparticles on heat capacity of nanofluids based on molten salts as PCM for thermal energy storage. Nanoscale Res Lett 8:448
Chung MH, Park JC, Ko MJ (2015) Effect of the solar radiative properties of existing building roof materials on the energy use in humid continental climates. Energy Build 102:172–180
Comite A, Cozza ES, Di Tanna G, Mandolfino C, Milella F, Vicini S (2015) Thermal barrier coatings based on alumina microparticles. Prog Org Coat 78:124–132
Cool Roof Rating Council (2015) CRRC rated products directory. http://coolroofs.org/products/results. Accessed 9 July 2015
Cotana F, Rossi F, Filipponi M, Coccia V, Pisello AL, Bonamente E, Petrozzi A, Cavalaglio G (2014) Albedo control as an effective strategy to tackle Global Warming: a case study. Appl Energy 130:641–647
Coutts A, Daly E, Beringer J, Tapper NJ (2013) Assessing pratical measures to reduce urban heat: green and cool roofs. Build Environ 70:266–276
Daniotti B, Cecconi FR, Paolini R, et al (2014) Multi-Physics Modelling for Durability Evaluation of ETICS. In: Quattrone M, John VM (eds) XIII International conference on durability of building materials and components, São Paulo, Brazil, pp 514–521
Daniotti B, Paolini R, Cecconi FR (2013) Durability of building materials and components. Springer, Berlin
De Gracia A, Cabeza LF (2015) Phase change materials and thermal energy storage for buildings Energy Build (in press)
Demarchis L, Sordello F, Minella M, Minero C (2015) Tailored properties of hematite particles with different size and shape. Dyes Pigm 115:204–210
Diamanti MV, Del Curto B, Ormellese M, Pedeferri MP (2013) Photocatalytic and self-cleaning activity of colored mortars containing TiO_2. Constr Build Mater 46:167–174. doi:10.1016/j.conbuildmat.2013.04.038
Diamanti MV, Pedeferri MP (2013) Concrete, mortar and plaster using titanium dioxide nanoparticles: applications in pollution control, self-cleaning and photosterilisation. In: Pachego-Torgal F, Diamanti MV, Nazari A, Goran-Granqvist C (eds) Nanotechnology in eco-efficient construction. Woodhead Publishing Ltd., Cambridge
Dias D, Machado J, Leal V, Mendes A (2014) Impact of using cool paints on energy demand and thermal comfort of a residential building. Appl Therm Eng 65:273–281. doi:10.1016/j.applthermaleng.2013.12.056
Doulos L, Santamouris M, Livada I (2001) Passive cooling of outdoor urban spaces. The role of materials. Solar Energy 77:231–249
Doya M, Bozonnet E, Allard F (2012) Experimental measurement of cool façades' performance in a dense urban environment. Energy Build 55:42–50
Energy Star (2015) http://www.energystar.gov/index.cfm?fuseaction=find_a_product.showProductGroup&pgw_code = RO
EPA (2015) Pavements draft report 2015. http://www.epa.gov/hiri/resources/pdf/CoolPavementReport_Former%20Guide_complete.pdf
Escribano MAB and Keraben Grupo SA 2010–2013, Development of a novel and cost-effective range of nanotech improved coatings to substantially improve NIR (Near Infrared Reflective) properties of the building envelope, CORDIS Project founded by FP7-CP
Ferrari C, Gholizadeh Touchaei A, Sleiman M et al (2014) Effect of aging processes on solar reflectivity of clay roof tiles. Adv Build Energy Res 1–13. doi:10.1080/17512549.2014.890535

Ferrari C, Muscio, A., Siligardi, C., Manfredini, T (2015) Design of a cool color glaze for solar reflective tile application. Ceram Int (in press)
Ferrer G, Solé A, Barreneche C, Martorell I, Cabeza LF (2015) Review on the methodology used in thermal stability characterization of phase change materials. Renew Sustain Energy Rev 50:665–685
Gao RTZJW, Ohtani H, Zhu ZS, Chen G (2009) Experimental investigation of heat conduction mechanisms in nanofluids. Clue on clustering. Nano Lett 9(12):4128–4132
Ganesh VA, Raut HK, Nair AS, Ramakrishna S (2011) A review on self-cleaning coatings. J Mater Chem 21:16304. doi:10.1039/c1jm12523k
Gentle AR, Smith GB (2015) A subambient open roof surface under the mid-summer sun. Adv Sci. doi:10.1002/advs.201500119
Georgakis C, Zoras S, Santamouris M (2014) Studying the effect of "cool" coatings in street urban canyons and its potential as a heat island mitigation technique. Sustain Cities Soc 13:20–31
Gobakis K, Kolokotsa D, Maravelaki-Kalaitzaki N, Perdikatsis V, Santamouris M (2015) Development and analysis of advanced inorganic coatings for buildings and urban structures. Energy Build 89:196–205
Graziani L, Quagliarini E, Bondioli F, D'Orazio M (2014) Durability of self-cleaning TiO_2 coatings on fired clay brick façades: effects of UV exposure and wet & dry cycles. Build Environ 71:193–203. doi:10.1016/j.buildenv.2013.10.005
Graziani L, Quagliarini E, Osimani A et al (2013) Evaluation of inhibitory effect of TiO_2 nanocoatings against microalgal growth on clay brick façades under weak UV exposure conditions. Build Environ 64:38–45. doi:10.1016/j.buildenv.2013.03.003
Gueymard CA (2001) Parameterized transmittance model for direct beam and circumsolar spectral irradiance. Sol Energy 71:325–346. doi:10.1016/S0038-092X(01)00054-8
Gueymard CA (2005) Interdisciplinary applications of a versatile spectral solar irradiance model: a review. Energy 30:1551–1576. doi:10.1016/j.energy.2004.04.032
Guo W, Qiao X, Huang Y, Fang M, Han X (2012) Study on energy saving effect ofheat-reflective insulation coating on envelopes in the hot summer and coldwinter zone. Energy Build 50:196–203
Hashemi A (2014) Daylighting and solar shading performances of an innovative automated reflective louvre system. Energy Build 82:607–620
Hernández-Pérez I, Álvarez G, Xamán J, Zavala-Guillén I, Arce J, Simá E (2014) Thermal performance of reflective materials applied to exterior building components—a review. Energy Build 80:81–105
Hosseini M, Akbari H (2015) Effect of cool roofs on commercial buildings energy use in cold climates Energy Build (in press)
Ichinose M, Inoue T, Sakamoto Y (2009) Long-term performance of high-reflectivity exterior panels. Build Environ 44:1601–1608. doi:10.1016/j.buildenv.2008.10.003
ISO (2003) ISO 9050—glass in building—determination of light transmittance, solar direct transmittance, total solar energy transmittance, ultraviolet transmittance and related glazing factors.
Jacques L (2000) Accelerated and outdoor/natural exposure testing of coatings. Prog Polym Sci 25:1337–1362
Jose S, Prakash A, Laha S, Natarajan S, Reddy ML (2014) Green colored nano-pigments derived from Y2BaCuO5: NIR reflective coatings. Dyes Pigments 107:118–126
Karlessi T, Santamouris M (2013) Research on thermochromic and PCM doped infrared reflective coatings. Adv Develop Cool Mater Built Environ 83–103
Karlessi T, Santamouris M (2015) Improving the performance of thermochromic coatings with the use of UV and optical filters tested under accelerated aging conditions. Int J Low-Carbon Technol 10(1):45–61
Khodadadi JM, Hosseinizadeh SF (2007) Nanoparticle-enhanced phase change materials (NEPCM) with great potential for improved thermal energy storage. Int Commun Heat Mass Transfer 34(5):534–543

Kirchstetter TW, Novakov T (2007) Controlled generation of black carbon particles from a diffusion flame and applications in evaluating black carbon measurement methods. Atmos Environ 41:1874–1888. doi:10.1016/j.atmosenv.2006.10.067

Kolokotsa D, Maravelaki-Kalaitzaki P, Papantoniou S, Vangeloglou E, Saliari E, Karlessi T, Santamouris M (2012) Development and analysis of mineral based coatings for buildings and urban structures. Sol Energy 86:1648–1659

Kolokotsa D, Santamouris M, Akbari H (2013) Advances in the development of cool materials for the built environment. Benthan E-books Editors.

Kotthaus S, Smith TEL, Wooster MJ, Grimmond CSB (2014) Derivation of an urban materials spectral library through emittance and reflectance spectroscopy. ISPRS J Photogramm Remote Sens 94:194–212. doi:10.1016/j.isprsjprs.2014.05.005

Kubelka P (1948) New contributions to the optics of intensely light-scattering materials. J Opt Soc Am 38:448–457. doi:10.1364/JOSA.44.000330

Kültür S, Türkeri N (2012) Assessment of long term solar reflectance performance of roof coverings measured in laboratory and in field. Build Environ 48:164–172

LBNL (2015) Heat Island group SRI calculator excel sheet: http://coolcolors.lbl.gov/assets/docs/SRI%20Calculator/SRI-calc10.xls

Levinson R, Akbari H (2002) Effects of composition and exposure on the solar reflectance of portland cement concrete. Cem Concr Res 32–11:1679–1698

Levinson R, Akbari H, Berdahl P (2010) Measuring solar reflectance—part I: defining a metric that accurately predicts solar heat gain. Sol Energy 84:1717–1744. doi:10.1016/j.solener.2010.04.018

Levinson R, Akbari H, Konopacki S, Bretz S (2005a) Inclusion of cool roofs in nonresidential Title 24 prescriptive requirements. Energy Policy 33:151–170. doi:10.1016/S0301-4215(03)00206-4

Levinson R, Berdahl P, Akbari H (2005b) Solar spectral optical properties of pigments—part II: survey of common colorants. Sol Energy Mater Sol Cells 89:351–389. doi:10.1016/j.solmat.2004.11.013

Levinson R, Berdahl P, Berhe AA, Akbari H (2005c) Effects of soiling and cleaning on the reflectance and solar heat gain of a light-colored roofing membrane. Atmos Environ 39:7807–7824

Levinson R, Akbari H, Reilly JC (2007a) Cooler tile-roofed buildings with near-infrared-reflective non-white coatings. Build Environ 42:2591–2605. doi:10.1016/j.buildenv.2006.06.005

Levinson R, Berdahl P, Akbari H et al (2007b) Methods of creating solar-reflective nonwhite surfaces and their application to residential roofing materials. Sol Energy Mater Sol Cells 91:304–314. doi:10.1016/j.solmat.2006.06.062

Levinson R, Akbari H, BanWeiss G, et al (2011a) Cool colored cars to reduce air conditioning energy use and reduce CO_2 emission. Berkeley, CA, USA

Levinson R, Pan H, Ban-Weiss G et al (2011b) Potential benefits of solar reflective car shells: cooler cabins, fuel savings and emission reductions. Appl Energy 88:4343–4357

Levinson R, Chen S, Berdhal P, Rosado P, Medina LA (2014) Reflectometer measurement of roofing aggregate albedo. Sol Energy 100:159–171

Lienhard JH (2010) Heat Transfer. J Heat Transfer 82:198. doi:10.1115/1.3246887

Lindberg JD, Douglass RE, Garvey DM (1993) Carbon and the optical properties of atmospheric dust. Appl Opt 32:6077–6081

Luís M, Goncalves L, Costa A, Santos CP (2015) Cool façades. Thermal performance assessment using infrared thermography, key engineering materials 634:14–21

Mainini AG, Poli T, Paolini R et al (2014) Transparent multilayer etfe panels for building envelope: thermal transmittance evaluation and assessment of optical and solar performance decay due to soiling. Energy Procedia 48:1302–1310. doi:10.1016/j.egypro.2014.02.147

Miller WA, Desjarlais A, Roodvoets DL (2004) Long term reflective performance of roof membranes. In: Proceedings of the 2004 roof consultants institute convention

Morse JW (1983) The kinetics of calcium carbonate dissolution and precipitation. Rev Mineral Geochemistry 11:227–264.

Morse JW, Arvidson RS (2002) The dissolution kinetics of major sedimentary carbonate minerals. Earth-Science Rev 58:51–84. doi:10.1016/S0012-8252(01)00083-6

ORNL SRI calculator: http://www.ornl.gov/sci/roofs+walls/calculators/sreflect/index.htm

Pacheco-Torgal F, Labrincha JA, Cabeza LF, and Granqvist CG (2011) Eco-efficient materials for mitigating building cooling needs, design, properties and applications. In: Woodhead Publishing Series in Civil and Structural Engineering (ed)

Pacheco-Tordal F, Diamanti MV, Nazari A, Granqvist CG (2013) Nanotechnology in eco-efficient construction. Woodhead Publishing Limited, Sawston

Paolini R, Sleiman M, Terraneo G, et al (2014a) Solar spectral reflectance of building envelope materials after natural exposure in Rome and Milano, and after accelerated aging. In: Muscio A (ed) Third international conference on countermeasures to Urban Heat Island, Venice, Italy, pp 498–509

Paolini R, Zinzi M, Poli T et al (2014b) Effect of ageing on solar spectral reflectance of roofing membranes: natural exposure in Roma and Milano and the impact on the energy needs of commercial buildings. Energy Build 84:333–343. doi:10.1016/j.enbuild.2014.08.008

Parameshwaran R, Deepak K, Saravanan R, Kalaiselvam S (2014) Preparation, thermal and rheological properties of hybrid nanocomposite phase change material for thermal energy storage. Appl Energy 115:320–330

Pisello AL (2015a) Thermal-energy analysis of roof cool clay tiles for application in historic buildings and cities. Sustain Cities Soc. doi:10.1016/j.scs.2015.03.003

Pisello AL (2015b) Experimental analysis of cool traditional solar shading systems for residential buildings. Energies 8:2197–2210. doi:10.3390/en8032197

Pisello AL, Cotana F (2014) The thermal effect of an innovative cool roof on residential buildings in Italy: results of two years of continuous monitoring. Energy Build 69:154–164

Pisello AL, Cotana F, Nicolini A, Brinchi L (2013) Development of clay tile coatings for steep-sloped cool roofs. Energies 6:3637–3653. doi:10.3390/en6083637

Pisello AL, Pignatta G, Castaldo VL, Cotana F (2014) Experimental analysis of natural gravel covering as cool roofing and cool pavement. Sustainability 6:4706–4722. doi:10.3390/su6084706

Pisello AL, Castaldo VL, Pignatta G, Cotana F, Santamouris M (2015a) Experimental in-lab and in-field analysis of waterproof membranes for cool roof application and urban heat island mitigation. Energy Build. doi:10.1016/j.enbuild.2015.05.026

Pisello AL, Castaldo VL, Piselli C, Pignatta G, Cotana F (2015b), Combined thermal effect of cool roof and cool façade on a prototype building, In: Proceedings of the 6th international conference of building physics for a sustainable built environment, Turin.

Revel GM, Martarelli M, Bengochea MÁ, Gozalbo A, Orts MJ, Gaki A, Gregou M, Taxiarchou M, Bianchin A, Emiliani M (2013) Nanobased coatings with improved NIR reflecting properties for building envelope materials: development and natural aging effect measurement Cement Concrete Compos 36(1):128–135

Revel GM, Martarelli M, Emiliani M, Celotti L, Nadalini R, De Ferrari A, Hermanns S, Beckers E (2014a) Cool products for building envelope—part II: experimental and numerical evaluation of ther-mal performances. Sol Energy 105:780–791

Revel GM, Martarelli M, Emiliani M, Gozalbo A, Orts MJ, Bengochea MA, Delgado LG, Gaki A, Ka-tsiapi A, Taxiarchou M, Arabatzis I, Fasaki I, Hermanns S (2014b) Cool products for building envelope—part I: development and lab scale testing. Sol Energy 105:770–779

Rossi F, Pisello AL, Nicolini A, Filipponi M, Palombo M (2014) Analysis of retro-reflective surfaces for urban heat island mitigation: a new analytical model. Appl Energy 114:621–631

Ryan M (2013) Lead is dead. Eur Coatings J 3:74–77

Santamouris M (2014a) Cooling the cities—a review of reflective and green roof mitigation technologies to fight heat island and improve comfort in urban environments. Sol Energy 103:682–703

Santamouris M (2014b) Cooling the citie—a review of reflective and green roof mitigation technologies to fight heat island and improve comfort in urban environments. Sol Energy 103:682–703

Santamouris M (2013) Using cool pavements as a mitigation strategy to fight urban heat island—a review of the actual developments. Renew Sustain Energy Rev 26:224–240

Santamouris M (2015) Regulating the damaged thermostat of the cities—status, impacts and mitigation challenges. Energy Build 91:43–56

Santamouris M, Kolokotsa D (2015) On the impact of urban overheating and extreme climatic conditions on housing, energy, comfort and environmental quality of vulnerable population in Europe. Energy Build 98:125–133

Santamouris M, Pavlou K, Synnefa A, Niachou K, Kolokotsa D (2007) Recent progress on passive cooling techniques. Advanced technological developments to improve survivability levels in low-income households. Energy Build 39:859–866

Santamouris M, Gaitani N, Spanou A, Saliari M, Giannopoulou K, Vasilakopoulou K, Kardomateas T (2012) Using cool paving materials to improve microclimate of urban areas—design realization and results of the flisvos project. Build Environ 53:128–136

Santamouris M, Cartalis C, Synnefa A, Kolokotsa D (2015) On the impact of urban heat island and global warming on the power demand and electricity consumption of buildings—a review. Energy Build 98:119–124

Shen H, Tan H, Tzempelikos A (2011) The effect of reflective coatings on building surface temperatures, indoor environment and energy consumption—An experimental study. Energy Build 43:573–580

Shirakawa MA, Werle AP, Gaylarde CC et al (2014) Fungal and phototroph growth on fiber cement roofs and its influence on solar reflectance in a tropical climate. Int Biodeterior Biodegradation 95:1–6. doi:10.1016/j.ibiod.2013.12.003

Sleiman M, Ban-Weiss G, Gilbert HE et al (2011) Soiling of building envelope surfaces and its effect on solar reflectance—part I: analysis of roofing product databases. Sol Energy Mater Sol Cells 95:3385–3399. doi:10.1016/j.solmat.2011.08.002

Sleiman M, Kirchstetter TW, Berdahl P et al (2014) Soiling of building envelope surfaces and its effect on solar reflectance—part II: development of an accelerated aging method for roofing materials. Sol Energy Mater Sol Cells 122:271–281. doi:10.1016/j.solmat.2013.11.028

Smithers Apex (2009) The future of titanium dioxide—market forecasts to 2016

Stazi F, Marinelli S, Di Perna C, Munafo P (2014) Comparison on solar shadings: monitoring of the thermo-physical behaviour, assessment of the energy saving, thermal comfort, natural lighting and environmental impact. Sol Energy 105:512–528

Steen AS, Steen B, Komatsu E (2003) Built by hand: vernacular buildings around the world. Gibbs Smith, Layton

Stieg Fred B (1989) Effect of extender on crowding of titanium pigment. J Coatings Technol 61 (778):67–70

Synnefa A, Santamouris M, Livada I (2006a) A study of the thermal performance of reflective coatings for the urban environment. Solar Energy Journal 80:968–981

Synnefa A, Santamouris M, Apostolakis K (2006b) On the development, optical properties and thermal performance of cool coloued coatings for the urban environment. Sol Energy 81:488–497

Synnefa A, Santamouris M, Apostolakis K (2007) On the development, optical properties and thermal performance of cool colored coatings for the urban environment. Sol Energy 81:488–497. doi:10.1016/j.solener.2006.08.005

Synnefa A, Dandou A, Santamouris M, Tombrou M, Soulakellis N (2008a) On the use of cool materials as a heat island mitigation strategy. J Appl Meteorol Climatol. doi:10.1175/2008JAMC1830.1

Synnefa A, Dandou A, Santamouris M, Tombrou M, Soulakellis N (2008b) Large scale albedo changes using cool materials to mitigate heat island in Athens. J Appl Meteorol Climatol 47 (11):2846–2856

Synnefa A, Karlessi T, Gaitani N, Santamouris M, Assimakopoulos DN, Papakatsikas C (2011) Experimental testing of cool colored thin layers asphalt and estimation of its potential to improve the urban microclimate. Build Environ 46(1):38–44

Synnefa A, Saliari M, Santamouris M (2012) Experimental and numerical assessment of the impact of increased roof reflectance on a school building in Athens. Energy Build 55:7–15

Taleghani M, Sailor DJ, Tenpierik M, Van den Dobbelsteen A (2014) Thermal assessment of heat mitigation strategies: the case of Portland State Unviersity, Oregon, USA. Build Environm 73:138–150

Thongkanluang T, Limsuwan P, Rakkwamsuk P (2010) Preparation and using of high near-infrared reflective green pigments on ceramic glaze. J Ceram Soc Jpn 18(1377):349–352

Thornbush MJ, Viles HA (2007) Simulation of the dissolution of weathered versus unweathered limestone in carbonic acid solutions of varying strength. Earth Surf Process Landforms 32:841–852. doi:10.1002/esp.1441

United Nations (2011) World urbanization prospects: the 2007 revision population database, panel 1: urban and rural areas. Last accessed 10 April 2011. http://esa.un.org/unup/

Wan WC, Hien WN, Ping TP, Aloysius AZW (2012) A study on the effectiveness of heat mitigating pavement coatings in Singapore. J Heat I Inst Int 7:2

Wang DS, Mingfeng Z (2014) Chromatic and near-infrared reflective properties of Fe^{3+} doped $KZnPO_4$. Sol Energy 110:1–6

Wypych J (1995) Weathering handbook (4thed.), Chemtec Publishing, Toronto, (Canada)

Zhang Z, Wang K, Mo B, Li X, Cui X (2015) Preparation and characterization of a reflective and heat insulative coating based on geopolymers. Energy Build 87:220–225

Zhao X, Zhang Y, Huang Y, Gong H, Zhao J (2015) Synthesis and characterization of neodymium doped yttrium molybdate high NIR reflective nano pigments. Dyes Pigm 116:119–123

Zinzi M (2015) Characterisation and assessment of near infrared reflective paintings for building facade applications. Energy Build. doi:10.1016/j.enbuild.2015.05.048

Zinzi M, Carnielo E, Agnoli S (2012) Characterization and assessment of cool colored solar protection devices for Mediterranean residential buildings application. Energy Build 50:111–119. doi:10.1016/j.enbuild.2012.03.031

Zinzi M, Carnielo E, Rossi G (2015) Directional and angular response of construction materials, solar properties: characterisation and assessment. Sol Energy 115:52–67

Chapter 10
Performance of Semi-transparent Photovoltaic Façades

L. Olivieri

Abstract This chapter shows the potential of the architectural integration of semi-transparent photovoltaic (STPV) systems for improving the energy efficiency of buildings. The research presented focuses on developing a methodology able to quantify the building energy demand reduction provided by these novel constructive solutions. At the same time, the design parameters of the STPV solution are analyzed to establish which of them have the greatest impact on the global energy balance of the building, and therefore which have to be carefully defined in order to optimize the building operation. In summary, this work contributes to the understanding of the interaction between STPV systems and buildings, providing both components manufacturers and construction technicians, valuable information on the energy-saving potential of these new construction systems and defining the appropriate design parameters to achieve efficient solutions in both new and retrofitting projects.

Acronyms

10	STPV element with a normal visible transmittance of about 10 %
20	STPV element with a normal visible transmittance of about 20 %
30	STPV element with a normal visible transmittance of about 30 %
40	STPV element with a normal visible transmittance of about 40 %
a-Si	Amorphous silicon
BAPV	Building added/adopted/attached photovoltaic
BIPV	Building-integrated photovoltaic
BOE	Boletín Oficial del Estado—Official Bulletin of the State
CED	Cooling energy demand
CENELEC	European Commission for Electrotechnical Standardization
CMP	Commercialization margin price
COP	Coefficient of performance
c-Si	Crystalline silicon

L. Olivieri (✉)
Instituto de Energía Solar, Universidad Politecnica de Madrid, Madrid, Spain
e-mail: lorenzo.olivieri@ies-def.upm.es

F. Pacheco Torgal et al. (eds.), *Nano and Biotech Based Materials for Energy Building Efficiency*, DOI 10.1007/978-3-319-27505-5_10

CTE	Spanish technical building code
DGI	Daylighting glare index
EBI	Energy balance index
EPC	Electricity production cost
g-value	Solar factor
HED	Heating energy demand
HVAC	Heating, ventilating, and air conditioning
IEA	International energy agency
IEA-SHC	IEA-Solar Heating and Cooling Program
IGDB	International glazing database
LBNL	Lawrence Berkeley National Laboratory
LED	Lighting energy demand
NIR	Near infrared
NPV	Net present value
PEG	Photovoltaic energy generation
PV	Photovoltaic
RG	Reference glass
SHGC	Solar heat gain coefficient
STC	Standard test condition
STPV	Semi-transparent photovoltaic
UV	Ultraviolet
U-value	Thermal transmittance
Vis	Visible
WWR	Window-to-wall ratio

10.1 Introduction

Within the general framework of studying the possibilities of incorporating the photovoltaic technology into the urban fabric and more precisely in the envelope of the buildings, the discipline that deals with the replacement of traditional passive construction elements with active components (Building-Integrated Photovoltaic, BIPV) is relatively recently and is attracting increasing attention due to several factors, including:

- The growing interest in improving the efficiency of buildings and maximizing the local energy generation, as suggested by the European Directive 2010/31 (European Commission 2010) which states that from January 2021 all newly constructed buildings have to be "nearly zero energy buildings";
- The growing interest for a progressive change of paradigm in the generation of electricity, from the present centralized system to a distributed approach, characterized by a significantly higher number of generation points and bidirectional energy flows at distributed levels;

- PV products from standardized and scarcely adaptable units, with limited and undesirable esthetic characteristics for building integration, have evolved into a very broad range of possibilities, providing the designers with suitable products to design well-integrated and architecturally pleasant systems. In many cases, this freedom has changed the perception of PV systems, which rather than being seen as a something "to hide" are usually now recognized as an added value of the architectural project. However, in spite of the BIPV products market expansion, a lack of knowledge about the actual behavior of these building solutions still exists. Likewise, tools and methodologies suitable to analyze the performance of these multifunctional products have not been yet proposed, hampering the diffusion of PV building product into the construction industry;
- The extraordinary price reduction that PV modules have experienced in recent years [around 85 % since 2007 (UBS 2014)], which have contributed to bringing this technology and the construction world closer. Furthermore, in the case of BIPV solutions that replace conventional building materials for photovoltaic elements, the differential cost only between the two alternative solutions has to be considered.

In this area, semi-transparent photovoltaic (STPV) elements, electricity-producing multifunctional products designed to replace traditional glazing systems, are one of the most promising BIPV solutions in the near future, as they have a central role in the global energy balance of a building. The importance of the glazing elements in the behavior of a building is easily explained by taking into account that the façade openings constitute the fraction of the building envelope more permeable to energy exchanges with the outside, and therefore, the constructive solutions intended for these applications affect deeply heating, cooling, and lighting demand.

However, rather than for the actual global energy efficacy, which is still under study, most of the STPV existing systems have been made mainly for esthetic reasons. In fact, BIPV elements convey the image of modern, efficient, and technologically advanced buildings and are generally used with the main objective of making visible the relationship of the project developer with renewable energy, receiving the positive influence of the "green touch" in terms of image.

In order for the integration of these elements in the building envelope to be fully efficient and provide an optimal comfort, it is firstly necessary to characterize how they affect the building energy balance. In fact, to design an efficient STPV system means sizing a system capable of achieving sometimes conflicting requirements, such as:

- Performing as a sunscreen in summer to avoid overheating;
- To provide solar gains and thermal insulation in winter to reduce heating loads;
- To ensure the maximum use of natural lighting providing luminous comfort conditions;
- To protect the users against possible glare;
- To allow a good outward view;
- To produce the maximum electricity output, compatibly with other aspects to be considered;

The added difficulty in the design of the system is that all these functions must be performed (and optimized) in transient state, since both the external (irradiance, sun position, temperature, etc.) and the indoor conditions (thermal loads, thermal and luminous comfort conditions, etc.) are subject to continuous variations.

To know how the constructive parameters of the STPV element (material, size, transparency, etc.) and the characteristics of the architectural integration (orientation, tilt, interaction with other elements, type of building, etc.) influence the operation of the building from an energy point of view, would provide:

- The manufacturers of the elements with valuable information on the energy-saving potential, not only related to the electricity production, provided by the STPV systems;
- The construction professional with the knowledge of the energy advantages of these new constructive solutions, including the appropriate design parameters to plan efficient systems in both new and rehabilitation projects.

Therefore, the methodology presented in this chapter contributes to the comprehension of the interaction between STPV systems and buildings analyzing how the energy behavior is modified when the design parameters vary and evaluating the energy advantages with respect to traditional glazing solutions.

10.2 State of the Art

10.2.1 Definitions and Classification

In the area of the photovoltaic systems installed in buildings, the distinction between two types of solutions is internationally accepted (CENELEC 2012; German Solar Energy Society 2013; IEA-SHC Task 41 2012a; Martín Chivelet and Fernandez Solla 2007; Montoro et al. 2011; Roberts and Guariento 2009):

- Additive (known as Building Added/Adopted/Attached Photovoltaics, BAPV);
- Integrative (known as BIPVs).

In an additive solution, conventional photovoltaic modules are secured to the roof or onto the façade using a dedicated mounting structure and the PV system is an additional technical element of the building. The building envelope is fully functional without the PV system and this is installed with the sole function of generating power.

In an integrative solution, building roof or façade components are replaced with photovoltaic components designed to be architecturally integrated in the building. The BIPV elements become part of the building envelope and, as well as having the function of generating electricity, perform one or more typical architectural functions such as heat and noise insulation, sun shading, weather protection, and safety. For this reason, the BIPV elements are also called multifunctional elements, since the power generation is always accompanied by other functionalities. Another difference

between BAPV and BIPV solutions is that the fixing systems usually used to install the BIPV elements in the building envelope are not additional metal structures as in the case of BAPV systems, but consist of solutions similar to those used to install conventional building elements, except that in this case not only the mechanical attachment of the units but also the electrical interconnection between them is implemented. In this sense, a variety of special PV components have been developed in the last years and is available on the market to match building integration needs (Cerón et al. 2013). Furthermore, compared to BAPV solutions, the integrated ones in general offer the intrinsic advantage of improving the profitability of a construction project from the substitution of traditional materials by the photovoltaic multifunctional elements.

Regarding the possibility of installing PV solutions in the built environment, most building surfaces reasonably free of shadows are suitable. Following a topological approach based on the placement of the PV elements in the building envelope, a possible categorization is shown in Table 10.1 (IEA-SHC Task 41 2012a).

As regards the semi-transparent products for roof integration, in most cases the BIPV elements are used in skylights as complete roof covering, fulfilling all its functions. In fact, these solutions provide thermal insulation and controlled daylighting while simultaneously the basic function of electricity generation is provided. The daylighting pattern provided by the semi-transparent BIPV element is very different depending on the PV technology used, and this is a fundamental aspect to be considered in designing roof and façade solutions. In fact, modules based in crystalline cells produce a dynamic light square pattern that may be appropriate in common or transit areas, but can be annoying in working zones in which the building users spend many hours (Fig. 10.1b). On the other hand, thin-film elements produce a much more uniform daylighting pattern, ensuring luminous comfort conditions compatible with most tasks (Fig. 10.1a). Beyond this, in both cases, when the BIPV element makes up the building thermal envelope itself, it is important to consider in detail the thermal characteristics of the product (such as the thermal transmittance and the solar factor), in order to avoid overheating and excessive thermal losses.

Although most BIPV systems have been developed for roof integration (IEA-SHC Task 41 2012a), due to the higher solar irradiation availability if compared with vertical planes, in the near future the utilization of roof surfaces only for capturing solar irradiance will not be enough to meet ambitious goals such as the nearly zero energy demand of the buildings established by the European policy (European Commission 2010; Voss and Musall 2012). Many studies (Chow et al. 2007; Corgnati et al. 2007; Eicker et al. 1999; Guardo et al. 2009; Quesada et al. 2012) point out that the huge solar integration potential of façades cannot be missed in order to reach the nearly zero energy balance.

Regarding semi-transparent elements for façades, the BIPV element itself always represents the whole-building façade system, so it has to meet additional requirements to the weather protection, such as thermal and noise insulation, sun shading, and light regulation. A constructive system that exemplifies this building solution is

Table 10.1 Integration typologies of PV elements into the building envelope (Olivieri 2015)

Roof elements			
	• Opaque		
		• Tilted roofs	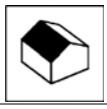
		• Flat roofs	
	• Semi-transparent		
		• Translucent roof and skylights	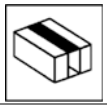
Façades elements			
	• Opaque		
		• External layer of the façades system	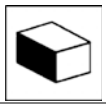
		• Whole façades system	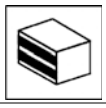
External devices			
	• Shading component (louvers and overhang)		
	• Safety devices (balconies parapets)		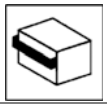

the curtain wall with both opaque and translucent zones, in which each zone has to perform specific functions. It is worth noting that in this case some of the capabilities required are opposed, meaning that inevitably the improvement of one impairs another. For instance, when a high daylighting capability is required (higher transparency), the solar protection is usually limited, as well as the electricity generation (due to a lower superficial power density). It is clear that the more architectural functions the BIPV element has to develop, most important is the balance between them in order to optimize the façade efficiency and consequently the building energy behavior (Fig. 10.2).

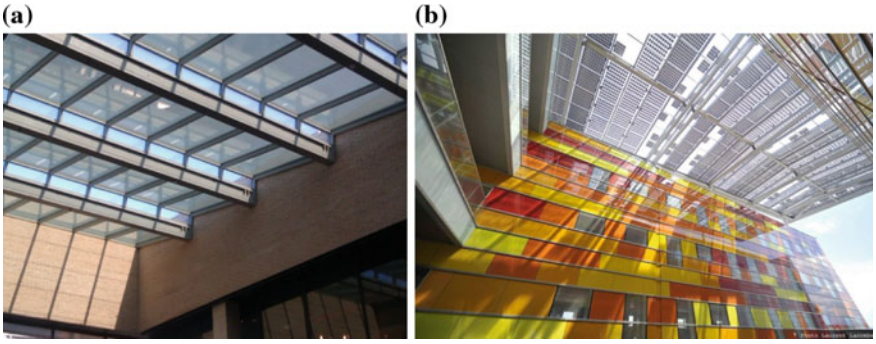

Fig. 10.1 Examples of skylights with a-Si semi-transparent BIPV modules (**a**) and crystalline ones (**b**). *Sources* **a** own work; **b** https://commons.wikimedia.org/wiki/File:Projet_BIPV_-_Gare_TGV_de_Perpignan.jpg by Issolsa, CC BY-SA 3.0

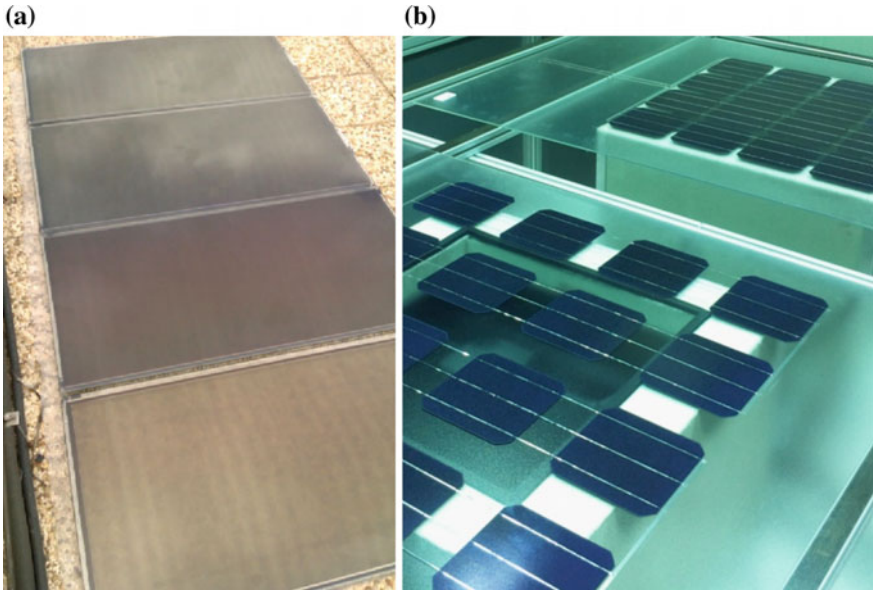

Fig. 10.2 Examples of semi-transparent PV elements with different transparency based on a-Si technology (**a**) and c-Si technology (**b**). *Source* own work

This chapter focuses on the performance of semi-transparent BIPV elements forming the whole-building façade system, since they have an interesting optimization potential related to the several roles (such as thermal insulation, solar gains control, and light regulation) played in the building energy balance.

10.2.2 Research on BIPV Systems

Building-integrated photovoltaics (BIPV) allow buildings to generate part of their electricity needs while one or several architectural functionalities are performed (Ban-Weiss et al. 2013; Oliver and Jackson 2001; Pagliaro et al. 2010; Petter Jelle et al. 2012). To minimize the final energy demand of buildings, it is firstly necessary to cut down the energy demand needed to guarantee thermal and lighting comfort and then to cover the residual demand using local efficient energy systems (Annunziata et al. 2013; European Commission 2010; Li et al. 2013). In this sense, due to the importance of the glazing elements in the building envelope to reduce energy demands for heating, cooling, and lighting loads, the relationship between façade design and building energy performance has been widely investigated (Bodart and De Herde 2002; Denton et al. 2007; Hien et al. 2005; Inanici and Demirbilek 2000; Iqbal and Al-Homoud 2007). If, on the one hand, the state-of-the-art best performing commercial fenestration products and future research opportunities have been extensively studied (Buratti and Moretti 2013a, b; Chow et al. 2009, 2010; Gil-Lopez and Gimenez-Molina 2013; Petter Jelle et al. 2012), then, on the other hand, the innovative and emerging technology consisting of using semi-transparent photovoltaic modules (STPV, transparency provided by separating individual solar cells within the module or by eliminating parts of the solar cells during their manufacturing process) integrated in façades has not been appropriately studied yet (Olivieri et al. 2014b; Quesada et al. 2012).

The lack of knowledge about STPV solutions in terms of global energy performance is particularly emphasized in view of the fact that the active building envelope is required to perform several and opposed requirements (solar shading in summer to avoid overheating, solar gains and thermal insulation in winter to reduce heat loads, daylighting provision to reduce lighting loads, outside view allowance to the occupants and maximum electrical output). Thus, to improve the building overall energy efficiency, the achievement of a balance between these functionalities is required. Nevertheless to date, research on the multifunctional effect of STPV solutions on the building energy balance has been limited.

In fact, research on STPV elements has been focused on three main approaches:

- Experimentally monitoring the energy performance of STPV elements and/or systems;
- Modeling the heat transfer process and fluid dynamics behavior of STPV elements and/or systems;
- Assessing the multifunctional effect of STPV solutions on the building energy balance, using simulation software and experimental analyses.

In the following sections, the most relevant studies in each approach will be briefly presented.

10.2.2.1 Experimentally Monitoring the Energy Performance of STPV Elements and/or Systems

Up to now, limited experimental research has been conducted on the energy performance of STPV modules. One of the studies on this issue was carried out by Park et al. (2010) who used an indoor setup (solar simulator) to analyze the variation of the I-V curve of a c-Si STPV module depending on the color of the glass on the backside and an outdoor setup to investigate the effects of solar radiation, ambient temperature, and glass used on the temperature and electrical performance of the STPV modules. The results showed that the power decreased about 0.5 % per the 1 °C increase of the PV module temperature. It was also found that the color of the glass used for the module affected the PV module temperature and consequently its electrical performance. Another related study was conducted by Li et al. (2009). They experimentally tested a-Si STPV modules to determinate the visible and solar transmittances and the daily mean conversion efficiency. The recorded results were then used to estimate the performance of the façade system applied to a generic reference office building in terms of energy, environmental, and economic issues. The electricity reduction represented about 12 % of the annual building demand. Han et al. (2013) compared the outdoor performance of a naturally ventilated STPV façade with a conventional clear glass façade. They demonstrated that the ventilated system reduces the possibility of potential overheating problems and that the conversion efficiency of a-Si PV modules slightly decreases from 4.7 to 4.4 % when its temperature increases about 16 °C. Robinson and Athienitis (2009) used an experimental setup to validate the simulated work plane illuminance values in an office with a c-Si STPV module. It was found that the optimal PV area ratio, defined as ratio of opaque PV cells coverage to fenestration area, was 80–90 % for all façade orientations studied from East through South through to West as well as for PV efficiencies of 6–16 %. Furthermore, it was demonstrated that the use of STPV over opaque PV modules can significantly increase the overall net electricity generation of the façade, due to an increased work plane illuminance and thus a reduced lighting load. Chen et al. (2012) developed a calorimetric hotbox (Chen and Wittkopf 2012) and a solar simulator to measure the solar heat gain coefficient (SHGC) of five different STPV glazing. They studied the angular effect of the incident solar radiation and of the electrical load on the SHGC values. They found that with an increasing angle of incidence, the SHGC and power generation are reduced significantly (up to 20 %). Furthermore, the influence of the electrical operation conditions can reduce the SHGC by 3–6 %. Olivieri et al. (2015) performed a similar study developing an indoor testing facility to analyze the solar factor of STPV elements under different measuring configurations. They showed that the electrical operating point actually modifies the solar control properties of the element, with a variation up to 11 % moving from the short circuit to the maximum power point condition.

10.2.2.2 Modeling the Heat Transfer Process and Fluid Dynamics Behavior of STPV Elements and Systems

Regarding the definition of heat transfer models to evaluate the heat gain given by STPV modules in building integrated applications, a significant contribution was provided by Fung and Yang (2008). They presented a one-dimensional heat transfer model and found that the area of solar cells in the PV module has significant effects on the total heat gain, since nearly 70 % of total heat gain can be reduced if the solar cell area ratio, defined as PV module area covered by solar cells, is 0.8. However, other parameters such as the solar cells efficiency and the PV module's thickness have only limited influence. The model was validated using a calorimeter box at steady-state conditions: A difference of 4.1 % was found between the experimentally measured heat gain and the simulated results. Wong et al. (2008) presented power generation, thermal balance, and daylight models of roof-integrated multicrystalline silicon STPV and incorporated them into EnergyPlus (Crawley et al. 2001) to carry out overall energy consumption analysis in five climate regions in Japan. It was concluded that with appropriate optimization measures (transparent insulation material and opaque movable insulation depending on the climate region) net energy savings in the range of 3.0–8.7 % could be achieved relative to the base case of BIPV roof. Another one-dimensional transient model of four different roofs including opaque BIPV was used by Wang et al. (2006) to assess the impacts of BIPV on buildings heating and cooling loads in Tianjin, China. It was found that the PV roof integration with ventilated air gap is appropriate for the application in summer (low cooling load and high PV conversion efficiency), whereas on the contrary in winter, non-ventilated (closed air gap) installation of PV elements is more effective mainly due to the reduced heating loads caused by the improved roof thermal resistance. A mathematical model and computer code were developed by Han et al. (2009) to study the heat transfer by natural convection of air in a novel type of a-Si STPV system. They analyzed the effect of cavity air thickness on the overall heat transfer through the window and concluded that the optimum thickness for the air layer in Hong Kong climate conditions is in the range of 60–80 mm. Chow et al. (2006) proposed a numerical model of four configurations of a ventilated solar screen window system. The heat flows were analyzed for office hours based on the TMY weather data of Hong Kong. A high saving potential was found in summer using the proposed ventilated window, whereas in winter the benefit of interchanging glass panes was not justified based on the numerical results obtained. Computational fluid dynamic simulation was used by Guardo et al. (2009) and Gan (2009) in order to evaluate the influence of construction and operation parameters of an active transparent facade on solar gain and to assess the effect of the size of air gap between the PV modules and the building envelope on the PV performance, respectively. According to the first study, the parameters that affect most of the reduction on solar load gain are related to the optical properties of the glass. In the second case, it was found that to reduce the overheating potential, a minimum air gap of 0.12 m between the PV module and the building envelope would be required. In the same research line, Infield et al. (2006) proposed a simplified

methodology, based on an extension of widely used the U- and g-values, for calculating the thermal impact on building performance of an integrated ventilated PV façade. They found that four parameters describing ventilation gains and transmission losses can be used to adequately characterize the thermal performance of partially transparent ventilated PV façades.

10.2.2.3 Assessing the Multifunctional Effect of STPV Solutions on the Building Energy Balance

In this context, most studies concerning energy performance assessment have been carried out using commercially available simulation software. Bahaj et al. (2008) compared the impact of electrochromic glazing, holographic optical elements, aerogel glazing, and thin-film PV on two highly glazed buildings in arid Middle Eastern climates using TRNSYS. They concluded that glazing integrated thin-film PV solutions are potentially the most promising solution providing an annual cooling load reduction of 31 %. The same software was used by Song et al. (2008) to calibrate the experimental power output data (DC output) of a commercialized single-plate STPV thin-film module modified into a double-glazed one. It was found that the experimental and simulated data fitted comparatively well, with a relative error of 8.5 % in terms of annual electricity output. de Boer and van Helden (2001) performed the optimization of the design of STPV modules for building integration taking into account the cooling and heating load, as well as the daylight distribution and the power output of a STPV system integrated in an office room in Madrid. Using different simulation software packages (TRNSYS, WINDOW, Adeline), they concluded that building-specific design parameters such as orientation, slope of PV surface, or internal gain intensity influence the building performance largely than the PV module properties. Miyazaki et al. (2005) expounded the effect of thin-film solar cell transmittance and window-to-wall ratio (WWR) (i.e., ratio of glazing area to wall area) on the energy consumption of office buildings in terms of heating and cooling loads, daylighting, and electricity production. The simulation was carried out using EnergyPlus and it was found that the total electricity consumption of the building could be reduced by 55 % using optimum STPV windows. The reduction in annual cooling energy as the result of applying a PV cladding system in a commercial building in United Arab Emirates was calculated by Radhi (2010). The analysis carried out using Energy-10 software shows that the cooling energy consumption declines by about 6 % due to the thermal insulation function provided by façade-integrated PV modules. Also concerning the total building energy demand, Ng et al. (2013) used the simulation tool EnergyPlus to examine six commercially available amorphous silicon STPV elements. They defined a new index to evaluate the overall energy performance in Singapore and found that BIPV glazing solutions provide an energy-saving rate of between 17 and 41 % compared to common window glazing for large façade openings. Olivieri et al. (2014a) defined a methodology to assess the overall energy performance of STPV elements, including thermal, luminous, and electrical aspects.

The study based on the experimental characterization of the optical properties of the elements and on the use of a package of specific software tools (DesignBuilder, EnergyPlus, PVsyst, and COMFEN) showed that in Madrid the use of STPV solutions for large façade openings can provide energy savings up to 59 % in comparison with code-compliant reference glasses. He et al. (2011) compared experimentally and numerically the performance of a-Si PV double- and single-glazing windows in east China. They found that the double-glazing solution can reduce to 46 % the indoor heat gains, improving the indoor thermal comfort level. An experimental study was performed by Peng et al. (2013) in order to assess the thermal performance of a ventilated PV double skin façade in Hong Kong. They studied the variation of the SHGC and U-value depending on the operation mode of the façade, defining the optimum strategy to improve its thermal behavior under different weather conditions. Lu and Law (2013) estimated the overall energy performance corresponding to five orientations of a STPV system installed in Hong Kong by integrating the simulation results of thermal, power, and visual behaviors. The main finding of the work was that the system would lead to an annual electrical benefit of about 1300 kWh in the best-case orientation (southeast).

In summary, various studies into STPV systems have focused on their energy performance and influence on the buildings energy balance based on existing simulation programs. However, global behavior of this type of PV modules could not be correctly represented by any of the commercial simulation tools because they do not implement specific models that properly and simultaneously reflect the singularities of these elements, such as the daylighting and power generation functions. At the same time, current research includes thermal modeling of STPV modules but the predictive models proposed have been validated by limited experimental data.

Furthermore, while recent years have seen an increasing number of building energy codes and standards focused on improving the energy efficiency of the construction sector (Asdrubali et al. 2008; CTE 2013; GmbH 2011), at present a specific standard that considers PV elements as constructive components does not yet exist or it is just starting to emerge (CENELEC 2012). In the specific case of glazing products, useful tools that enable designers to adopt energy-effective project solutions, i.e., the integration of simulation software with reliable and detailed optical data like the International Glazing Database (IGDB) (LBNL-IGDB 2014) or the newer Complex Glazing Database (CGDB) (LBNL-CGDB 2014) are being improved constantly, but STPV elements are still not properly considered.

Consequently, it is worth considering the performance of innovative STPV solutions in comparison with well-established constructive elements in order to assess the energy-saving potential of these novel construction products to move toward net zero energy buildings. Besides, a lack of research exists on the performance of multifunctional STPV façade in the Mediterranean region, characterized by a high annual solar irradiation and a wide range of ambient temperatures (Olivieri et al. 2014b). For these reasons, a performance comparison with conventional glazing in Mediterranean conditions is necessary in order to assess realistically the energy-saving potential that STPV solutions might provide.

10.3 Energy-Saving Potential of STPV Elements

Building integration of STPV elements deeply affects the building energy demand since it influences the heating, cooling, and lighting loads as well as the local electricity generation. Until it is unequivocally proven that using these novel solutions can reduce the building energy demand, these systems will not be considered a mainstream technology in building practice. To move forward in this respect, in this section, the overall energy performance of five double-glazing STPV elements, each one with a specific degree of transparency, is analyzed over different window-to-wall ratios, in order to assess the energy-saving potential compared to a conventional double-glazed code-compliant glass. The prior optical characterization, focused to measure the spectral transmittance and reflectance of the elements, was experimentally undertaken. Results obtained were used to perform simulations based on a reference office building using a package of specific software tools (mainly DesignBuilder, EnergyPlus, PVsyst, and COMFEN) to take proper account of the STPV peculiarities. To evaluate the global energy performance of the STPV elements, a new *Energy Balance Index* (EBI) was formulated and calculated. Finally, in order to cover a wide range of climatic conditions, a total of ten cities were analyzed.

10.3.1 Methodology

Due to the multifunctional role that STPV plays in the building envelope, which affects the heating, cooling, and lighting loads, the visual comfort as well as the power generation, a set of simulation tools has been used to correctly characterize the behavior of each element. In fact, none of the existing simulation tools, if used in a stand-alone manner, is capable of property taking into account all the effects of STPV integration on the building energy balance (IEA-SHC Task 41 2012b). This approach allows combining the results of state-of-the-art tools in their respective fields, such as EnergyPlus in thermal calculations, PVsyst in PV generation estimation, and Radiance-based software in visual comfort assessment. Taking into account that the façade integration of STPV elements is particularly interesting in commercial buildings (Bodart and De Herde 2002; Dubois and Blomsterberg 2011; Kapsis and Athienitis 2015), having considerable vertical surfaces, being normally occupied during daytime and having considerable lighting and internal loads, a model of a reference office space was considered.

10.3.1.1 Reference Building

The reference building, originally defined in the European Commission Joule projects REVIS and SWIFT (van Dijk 2001a) and further refined in the IEA Solar Heating and Cooling Program Tasks 25, 27, and 31 (van Dijk 2001b), is a middle-size office

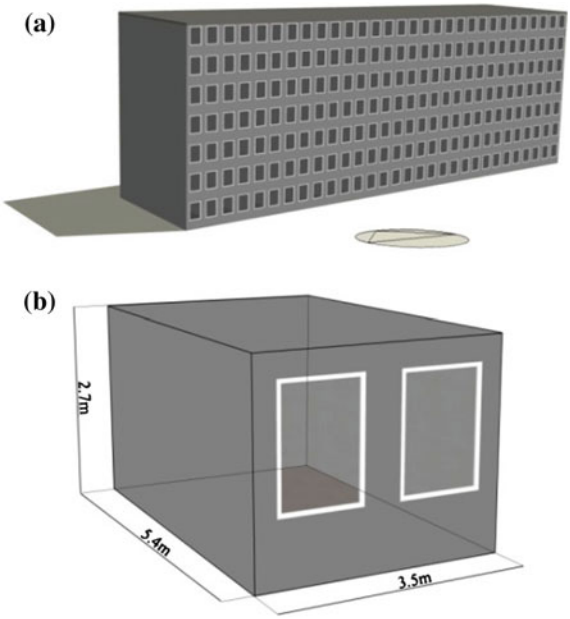

Fig. 10.3 Reference building (**a**) and dimensions of the office module used in simulations (**b**) (Olivieri et al. 2014a)

building with office modules aligned on two façades, separated by a central corridor. Figure 10.3 shows the whole building and the dimensions of the south-oriented office module used in simulations.

The building has an unshaded, south-facing façade with a WWR of 44 %. To properly assess the daylighting capability of the glazing materials, the space was simulated assuming a lighting control model continuously dimming the artificial light output to cover the daylight illuminance fluctuations and switching off completely when the target work plane illuminance of 500 lx is reached. In this way, the daylighting energy-saving potential is taken into account as a reduction of the artificial lighting load. The lighting power density in the office is 8 W/m^2 with an occupation on weekdays from 8 AM to 7 PM. Figure 10.4 summarizes the overall simulation approach.

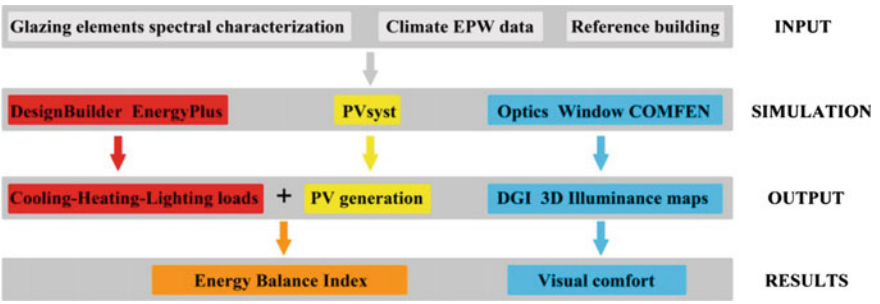

Fig. 10.4 Overall energy simulation approach (Olivieri et al. 2014a)

Table 10.2 Characteristics of the glazing elements analyzed

Glazing element	T_{vis}	g-value	U-value (W/(m^2 K))	STC power density (W/m^2)	PV-tech	Thickness (mm)	Density (kg/m^2)
0	0.003	0.145	2.783	62.0	a-Si	21	25.4
10	0.101	0.216	2.783	44.3	a-Si	21	25.4
20	0.158	0.253	2.783	37.9	a-Si	21	25.4
30	0.249	0.316	2.783	31.6	a-Si	21	25.4
40	0.324	0.367	2.783	25.3	a-Si	21	25.4
RG	0.461	0.473	2.783	–	–	20	25.0

The nomenclature used to define the STPV elements refers to the approximated value of the visible transmittance. *RG* refers to reference glass

10.3.1.2 Optical Characterization

According to EN410:2011 and EN673:2011 standards on glass in buildings (European Committee for Standardization 2011a, b), the basic optical properties required to accurately assess the thermal and daylighting behavior of STPV multifunctional elements are the spectral reflectance and transmittance. Normally only global characteristics as U-value and g-value as well as visible transmittance are specified by the manufacturers, whereas detailed spectral data are in general not available in the technical specifications of glazing systems. In this context, the IGDB (LBNL-IGDB 2014) is a valuable source of information about the performance of conventional glazing solutions but unfortunately at the present PV products for building integration such as STPV elements are not included in the database. Consequently, the experimental characterization of the optical characteristics of the STPV elements is required in order to perform accurate energy performance assessments. In this study, the spectral characterization of the STPV elements has been carried out using an UV/Vis/NIR spectrophotometer equipped with an integrating sphere (Olivieri et al. 2014a). Table 10.2 shows the main characteristics of the STPV elements considered in this study. It can be noted that the codes used to define the STPV elements (0, 10, 20, 30, 40) represent the approximate values of the visible transmittance.

10.3.1.3 Thermal Simulation

All thermal simulations were performed using the EnergyPlus-based DesignBuilder software (Designbuilder 2014). It was assumed that the space is bounded on five sides by similar spaces, therefore interior walls, floors, and ceilings were modeled adiabatically. The exterior wall has a U-value of 0.66 W/(m^{2}K), according to the limit established in the Spanish Technical Building Code for the corresponding climatic zone (CTE 2013). As regards the HVAC system, it was assumed that the space is conditioned by means of a fan-coil unit coupled to a reversible heat pump system. To convert the thermal loads to electricity consumptions, the simulation

program default data of the coefficient of performance (1.67 both in heating and in cooling mode, including distribution and control losses) are used (Designbuilder 2014; Reinhart and Wienold 2011). Heating and cooling setpoint temperatures are 20 and 26 °C, respectively, being typical values normally used in HVAC applications. The experimentally measured spectral data of the elements were included in the model to assess the expected performance of the façade-integrated systems. Climate EnergyPlus weather data (Typical Meteorological Year, a full set of 8760 hourly data composed from a data bank much longer than a year in duration to closely match the long-term average climatic conditions and at the main time to preserve the natural variability of the actual climatic conditions) were used to perform the simulation.

10.3.1.4 Daylighting Simulation

The visual comfort analyses were carried out using the Lawrence Berkeley National Laboratory (LBNL) daylighting software package consisting of Optics, Window, and COMFEN tools (LBNL-COMFEN 2014; LBNL-OPTICS 2014; LBNL-WINDOW 2014). In particular, Optics was used to import the experimental spectral data of the glazing materials. Next, in order to perform the radiance-based simulations the glazing systems were defined in Window and finally exported to COMFEN. To evaluate the visual comfort, both glare (based on the Daylighting Glare Index) and illuminance analysis (based on illuminance 3D contours maps and render visualizations) were carried out. In the first stage of the study, the reference model with a WWR = 44 % was analyzed, and in a later step the analysis was extended to a wide range of WWRs, with values comprised between 11 and 88 %.

10.3.1.5 Electrical Simulation

The photovoltaic electricity generation was estimated using PVsyst software (PVsyst 2014). This tool was selected because it accurately takes into account several loss factors, such as optical, irradiance, mismatch, and thermal losses, just to cite some examples. To perform the simulations, for each STPV element a base-case grid-connected photovoltaic system was defined, consisting of 5 modules (4 m^2 available area, corresponding to a WWR = 44 %) and an appropriate commercial inverter. The electrical characteristics of the STPV elements (Table 10.3) and inverter were imported from the Photon International database (Photon International 2014a, b) and with these data, five systems were simulated. Then, in order to estimate the electricity output corresponding to different WWRs, the base case was adjusted by means of linear interpolation to take into account the available area (and the corresponding power of the PV system) in each case.

Table 10.3 Electrical characteristics of the PV glazing elements analyzed

Glazing elem.	PV-tech	I_{SC} (A)	V_{OC} (V)	I_{MP} (A)	V_{MP} (V)	P_M (W)	α (%/°C)	β (%/°C)	γ (%/°C)
0	a-Si	1.05	64.5	0.95	51.7	48.9	+0.09	−0.28	−0.19
10	a-Si	0.89	59.5	0.77	45.4	34.9	+0.09	−0.28	−0.19
20	a-Si	0.79	59.5	0.68	44.1	30.0	+0.09	−0.28	−0.19
30	a-Si	0.64	59.5	0.56	44.6	25.0	+0.09	−0.28	−0.19
40	a-Si	0.52	59.5	0.44	45.2	19.9	+0.09	−0.28	−0.19

Parameters α, β, and γ refer to I_{SC}, V_{OC}, and P_M temperature coefficients, respectively

10.3.1.6 Integrated Energy Balance: The Energy Balance Index

To assess the overall energy performance of the glazing elements considering heating, cooling, and lighting loads as well as the PV generation (calculated on an annual basis and using hourly time step simulations), a new parameter is proposed. The parameter, named EBI, represents the building energy balance in terms of electricity and is calculated as shown in Eq. (10.1):

$$\mathrm{EBI} = \mathrm{CED} + \mathrm{HED} + \mathrm{LED} + \mathrm{PEG}\ (\mathrm{kWh/m^2}) \tag{10.1}$$

where CED is the annual cooling electricity demand, HED is the annual heating electricity demand, LED is the annual lighting electricity demand, and PEG is the annual photovoltaic electricity generation. Notice that the values corresponding to energy demand, i.e., CED, HED, and LED, are positive, whereas the energy generation value PEG is negative. The choice of the signs is necessary to ensure the consistency of the equation, since the energy flows (energy demand vs. energy generation) have opposed directions. All the values are expressed in kWh and normalized to the net space floor area. To determinate the values used to calculate the EBI, all the boundary conditions regarding the model characteristics (envelope properties, HVAC systems, internal gains, occupation schedules, etc.) are kept constant and only the WWR and the STPV elements are modified. Thus the EBI, which is an indicator of the building energy performance, is here used as a meter of the different façade STPV systems global performance, since the remaining building characteristics are invariant throughout the study. According to Eq. (10.1), the lower the value of the EBI, the more efficiently the glazing element performs in an annual basis. In this sense, the EBI complements other parameters used to assess the building energy performance, such as the *Energy Performance Index,* mainly used in Europe, or the *Energy Use Intensity* principally used in the USA (Pérez-Lombard et al. 2009), which are defined as the site energy consumption per unit of net floor area. The new balance index aims to reflect the increasingly electricity generation role required in buildings in order to minimize the residual demand of grid electricity. In this regard, the parameter, which includes both building electricity consumption and generation, is useful to compare the performance of alternative multifunctional solutions that integrate strategies focused to

reduce the energy demand and increase the on-site generation, such as STPV systems. Furthermore, the parameter allows us to estimate how close the building performance is to the net zero energy balance. For these reasons in the EBI calculation, not only the on-site energy consumption per unit of net floor area is taken into account, but also the local PV generation.

10.3.2 Results

To assess the glazing material performance, the EBI was calculated for the six glazing elements. As an example in Fig. 10.5, the results corresponding to one of the cases analyzed (Madrid, WWR = 44 %) are shown. Graphs (a) and (b) show the annual EBI as a function of the glazing material, with the difference that in (a) all the components of the energy balance are reported, while (b) represents only the net EBI values. By looking at graph (a), it can be noted that increasing the transparency degree of the glazing material: (i) the cooling demand increases (higher solar gains), (ii) the lighting demand decreases (less artificial lighting), and (iii) the PV generation decreases (because the superficial power density of STPV elements is inversely proportional to the transparency degree, as can be seen looking at Table 10.2). Concerning the heating demand, it can be noted that the values calculated, in the specific case analyzed (building located in Madrid, south-oriented and with the entire envelope modeled as adiabatic with the exception of the façade), are barely visible so in this case the heating demand can be considered negligible. On the other hand, graph (b) shows that the element 20 outperforms the other solutions (lower EBI value). This is due to the good performance of element 20 in combining opposed requirements, such as daylighting supply, solar shading, and electricity generation.

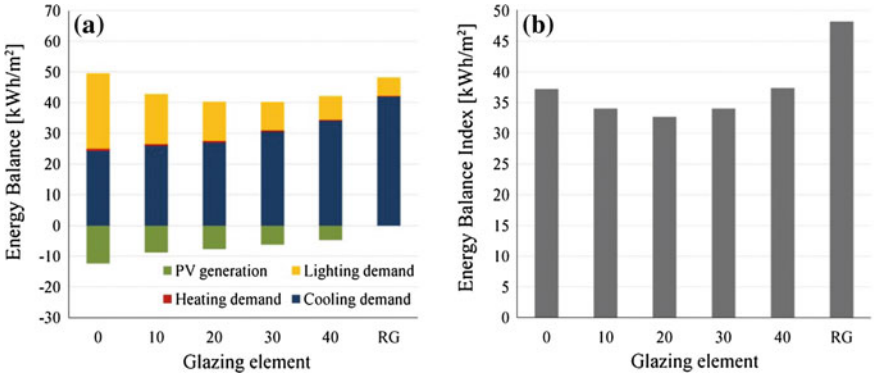

Fig. 10.5 Annual energy balance as a function of the glazing material in the case of the original reference office (WWR = 44 %). Graph **a** represents all the components involved in the balance, reporting as positive the energy consumption and as negative the energy generation. Graph **b** reports the net energy balance index (EBI) values

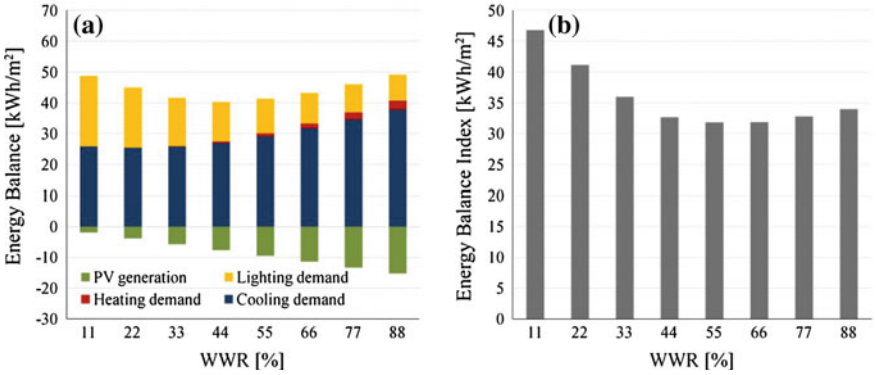

Fig. 10.6 Annual energy balance as a function of the WWR corresponding to element 20. Graph **a** represents all the components involved in the balance, reporting as positive the energy consumption and as negative the energy generation. Graph **b** reports the net energy balance index (EBI) values

Moreover, it can be noted that for elements 10, 20, and 30 (visible transmittance ranging between 10 and 25 %) the energy balance components vary appreciably (Fig. 10.5a) but the overall energy performance is almost constant (Fig. 10.5b). However, it is important to emphasize that all the STPV elements improve the building energy efficiency compared to the RG solution, providing a EBI reduction ranging between 22 % (element 40) and 32 % (element 20).

To evaluate not only the glazing material performance but also the effect of the façade openings dimensions, the EBI was calculated for the same glazing for WWR values ranging between 11 and 88 %. Figure 10.6 shows an example of the results, corresponding to glazing element 20. By looking at graph (a), it can be noted that increasing the WWR: (i) the cooling demand increases (higher solar gains), (ii) the lighting demand decreases (more daylighting), and (iii) the PV generation increases (bigger STPV active surface). Also in this case the heating demand, which increases with WWR, is considerably less significant than the other variables, being appreciable for high WWR only. By looking at the graph (b), it should be concluded that using the glazing material 20, the WWR that minimizes the EBI, i.e., which optimizes the building energy performance, is represented by 55 %. It can be also noted that the performances for WWR between 44 and 88 % are very similar, with a relative variation between them below 7 %.

10.3.2.1 Parametric Analysis on Glazing Material and Window-to-Wall Ratio

The annual EBI as a function of the glazing material for the WWRs analyzed (case of Madrid) is shown in Fig. 10.7. It can be noted that for reduced WWR the glazing material only irrelevantly affect the energy balance of the building, whereas marked

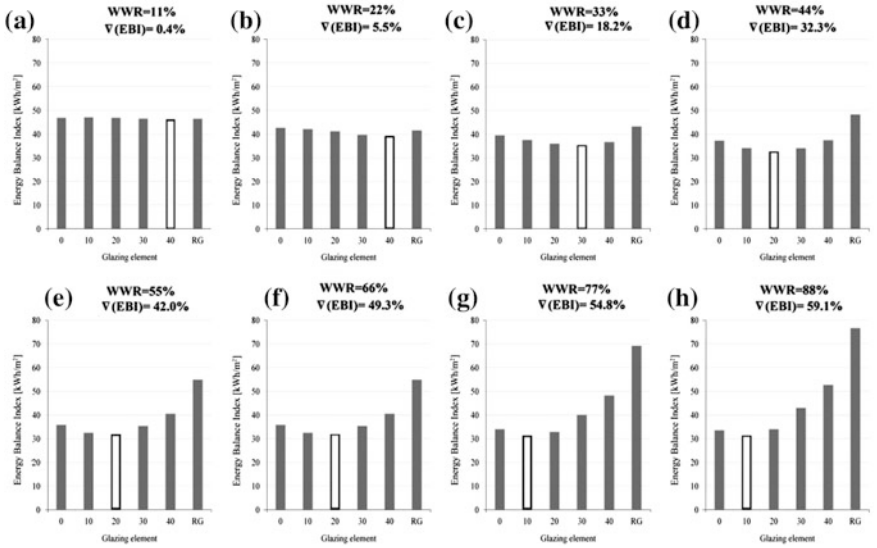

Fig. 10.7 Energy balance index as a glazing element function for WWR ranging from 11 to 88 %. The glazing element which minimizes the EBI for each WWR is black-outlined and the EBI percentage difference between the best solution and the RG is included

differences can be noticed for bigger façade openings. To highlight this behavior, the energy-saving potential between the most efficient STPV solution and the RG is computed and reported as ∇(EBI), reduction of EBI. As shown, for WWR ≤ 22 %, the energy behavior of all the elements is quite similar, being the saving potential provided by the best performing STPV solution compared to the RG lower than 6 % (Fig. 10.7b). For WWR ≥ 33 %, the energy-saving potential starts to increase appreciably and ranges between 18.2 % (WWR = 33 %, Fig. 10.7c) and 59.1 % (WWR = 88 %, Fig. 10.7h). Regarding the original reference office (WWR = 44 %), Fig. 10.7d shows that approximately one-third of the energy demand could be saved using the glazing element 20 instead of the RG.

Another point to consider when examining the glazing elements performance is to compare the STPV optimum solution not only with the RG, but also with the other STPV elements, in order to assess the relevance of choosing the appropriate degree of transparency of the element. As can be observed in Fig. 10.7, for WWR up to 33 % the energy performance of the five active elements is quite similar, with a maximum EBI difference between the most efficient (element 30) and the least efficient (element 0) of about 10.5 %. For intermediate values of the WWR (44–55 %), element 20 outperforms other solutions and the STPV elements performance begins to differ significantly, being the maximum EBI difference between the most and the least efficient element (element 40) of about 21.3 %. For WWR ≥ 66 %, element 10 seems to be the best solution, providing the lowest EBI value. In this case, choosing a suitable degree of transparency is critical, since the maximum energy balance difference between the best and the worst solution (element 40) rises up to 40.5 %.

Table 10.4 Normalized energy balance index to the best performance WWR-glazing element combination, corresponding to glazing element 10 and WWR = 77 %

		WWR							
		11	**22**	**33**	**44**	**55**	**66**	**77**	**88**
GLAZING ELEMENT	**0**	1.50	1.36	1.26	1.19	1.14	1.11	1.09	1.07
	10	1.50	1.35	1.20	1.09	1.04	1.00	1.00	1.00
	20	1.50	1.32	1.15	1.04	1.02	1.02	1.05	1.09
	30	1.49	1.27	1.13	1.09	1.13	1.19	1.28	1.37
	40	1.48	1.26	1.17	1.20	1.29	1.41	1.54	1.68
	RG	1.49	1.33	1.38	1.54	1.76	1.98	2.21	2.45

To summarize the previous results corresponding to the case of Madrid, in Table 10.4 the EBI has been normalized to the best WWR-glazing combination (WWR = 77 % combined with element 10). A color range from green to red (good and bad performance respectively) has been used to highlight the efficiency of the different solutions. As can be seen, the best solutions concentrate around the upper right-hand part of the diagonal, corresponding to elevate WWR values and low degree of transparency elements. It can be also noted that using the RG for WWR > 66 %, the building zone energy demand is at least twice the energy demands reached in the best case, i.e., using STPV 10.

10.3.2.2 Daylighting Analysis—Visual Comfort

The previous section presented a methodology to evaluate the overall energy performance of photovoltaic glazing systems. In this section, the visual comfort provided by the different solutions is analyzed. To this end, *Daylighting Glare Index (DGI)* and *Illuminance Contour Maps* are used. Three typical days are selected (spring equinox, summer and winter solstice, northern hemisphere) to perform DGI and illuminance calculations in order to cover average (equinox) and extreme (solstice) conditions. Also, three time slots (9 AM, 12 PM, 3 PM, official time) were selected to take into account different sun azimuth and elevation angles.

Daylight Glare Index (DGI)

DGI is a measure of glare based on the glare source luminance, glare source size, surround background luminance, and the location of the glare source relative to the occupant's field of view (Wienold and Christoffersen 2006). The DGI values corresponding to a subjective user assessment of glare are displayed in Table 10.5. To carry out the DGI calculations, the radiance utility tool included in COMFEN was used. Table 10.6 summarizes the results under clear and overcast sky conditions. It can be noted that under clear sky conditions in the spring equinox and summer solstice comfort conditions are provided by all the glazing systems, being the DGI

Table 10.5 Daylight glare index scale

DGI	Subjective glare assessment
16	Just perceptible
20	Just acceptable
22	Borderline between comfort and discomfort
24	Just uncomfortable
28	Just intolerable

lower than 22 (with a slightly increased glare probability for high transparency solutions). In the winter solstice, as expected, the highest DGI values are reached: In this case, uncomfortable conditions occur using all the glazing materials at midday. However, glazing element 10 seems to provide a considerably more comfortable daylighting than the other solutions, providing an effective sun-shading function as the close to comfort zone DGI value (DGI = 22.1) and the rendered view shown in Fig. 10.8a demonstrate. Under overcast sky conditions, no glare problems have been observed, being 18.9 the maximum DGI value registered and corresponding to the RG, at 3 PM in the summer solstice.

Illuminance Contour Maps

Illuminance contour maps for the camera position marked in Fig. 10.8c at noon (12 PM) under clear and overcast skies are shown in Figs. 10.9 and 10.10, respectively. Colored lines define nearly homogenous illuminance zones (illuminance variation less than 100 lx), ranging from 50 lx (violet) to 950 lx (yellow). Accordingly, this representation allows visualizing the daylighting pattern provided by the glazing elements pointing out the degree of transparency effect. It is interesting to observe that under clear skies in nearly all of the cases, the maximum illuminance value falls within the range 100 lx to 2000 lx considered as offering potentially useful illumination for the occupants of the space (Mardaljevic et al. 2009; Nabil and Mardaljevic 2006).

Regarding overcast sky conditions, the radiance visualizations shown in Fig. 10.10 suggest that the illuminance distribution can be considered to be practically invariant to the glazing element used. In this condition, in nearly all of the cases, the daylighting potential could be considered negligible, with maximum illuminance over the floor lower than 50 lx.

10.3.2.3 The STPV Performance in Spain and in Europe

In this section, the performance of the STPV solutions and the associated energy-saving potential are analyzed under different climatic conditions. With this aim, 9 European cities in addition to Madrid base case have been selected in order to cover the main characteristics of the European climate. The selection has been made taking into account not only the Köppen climate classification (Köppen 1936;

Table 10.6 COMFEN simulated DGI values for three representative days under clear and overcast sky conditions

Clear sky	10			20			30			40			RG		
	9 AM	2 PM	3 PM	9 AM	12 PM	3 PM	9 AM	12 PM	3 PM	9 AM	12 PM	3 PM	9 AM	12 PM	3 PM
21-3	6.6	4.1	0.0	12.7	9.7	0.0	14.3	10.4	0.0	16.4	12.0	0.0	17.7	13.0	0.0
21-6	8.6	3.3	0.0	15.9	17.2	15.4	17.6	18.2	16.0	19.3	19.9	17.7	17.0	20.7	18.4
21-12	0.0	**22.1**	13.5	5.6	**24.1**	16.9	9.7	**24.9**	18.1	11.6	**26.2**	19.6	13.4	**26.8**	20.2
Overcast sky	10			20			30			40			RG		
	9 AM	2 PM	3 PM	9 AM	12 PM	3 PM	9 AM	12 PM	3 PM	9 AM	12 PM	3 PM	9 AM	12 PM	3 PM
21-3	0.0	6.2	6.8	0.0	12.0	12.1	9.4	14.3	13.7	12.6	15.8	0.0	13.6	16.9	17.1
21-6	4.4	9.2	8.5	10.9	13.7	12.7	12.8	15.2	15.4	15.8	17.2	17.3	16.2	18.8	18.9
21-12	0.0	0.0	1.7	0.0	8.5	8.0	0.0	10.7	10.0	0.0	13.6	13.4	1.3	15.1	14.7

DGI values greater than 22 are reported in bold. Results refer to the base-case reference model (WWR = 44 %)

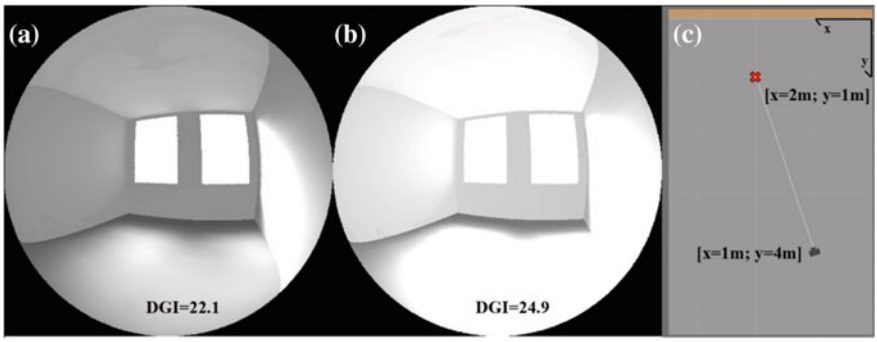

Fig. 10.8 Rendered views using glazing elements 10 (**a**) and 30 (**b**) under clear sky condition at noon in the winter solstice, **c** shows the camera position (Olivieri et al. 2014a)

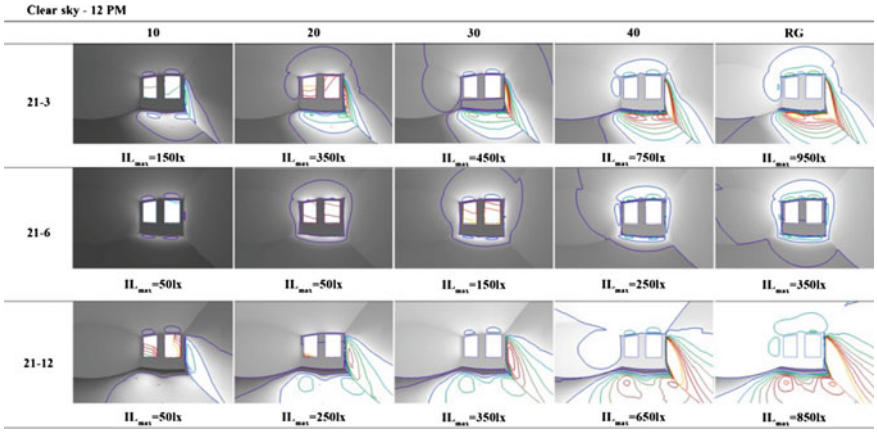

Fig. 10.9 Illuminance contour maps under clear sky at 12 PM and maximum illuminance value over the floor for three representative days. Lines show equal illuminance zones ranging from 50 lx (violet) to 950 lx (*yellow*) (Olivieri et al. 2014a)

Kottek et al. 2006) but also the climatic zones defined in the Spanish Technical Building Code (CTE 2013) in order to have a higher resolution about the influence of the Spanish climate peculiarities on the STPV behavior. In Table 10.7, the main geographical and climatic characteristics of the selected cities are summarized.

For each city, the energy performance of the reference building has been simulated varying both the WWR and the glazing element, as it was done in the case of Madrid. Considering that the combination of 8 WWRs and 6 glazing elements has been analyzed for each city (totally 9 excluding Madrid), a total of 432 hourly based annual simulations have been carried out to complete this study. Then, to evaluate the overall energy performance of the glazing elements, the corresponding EBI has been calculated using the results of the simulations.

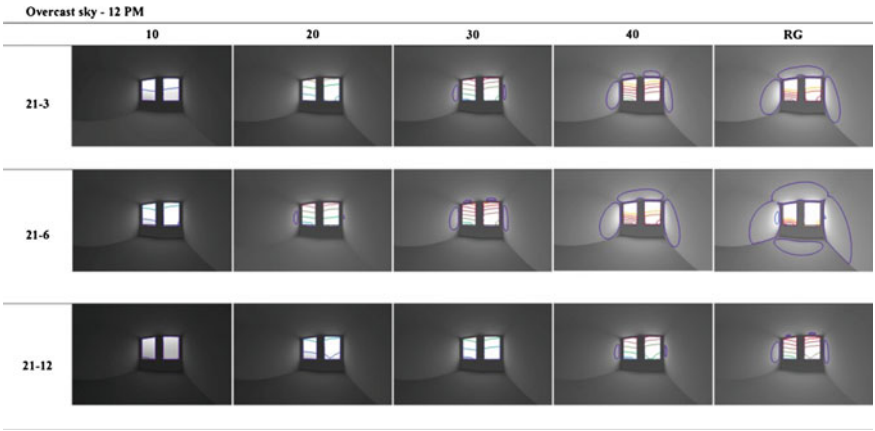

Fig. 10.10 Illuminance contour maps under overcast sky at 12 PM for three representative days. *Lines* show equal illuminance zones ranging from 50 lx (*violet*) to 950 lx (*yellow*) (Olivieri et al. 2014a)

Table 10.7 Main geographical and climatic characteristics of the selected cities

City	Country	AVG daily irradiation $\alpha = 0°$ $\beta = 90°$ (kWh/m^2)	AVG T (°C)	HDD	CTE C.Z.	Köppen C.Z.[a]
Castellón	Spain	3.73	17.5	796	B3	BSk
Sevilla	Spain	3.73	18.2	641	B4	Csa
Pontevedra	Spain	3.34	14.7	1260	C1	Csb
Vitoria-Gasteiz	Spain	2.92	11.5	1720	D1	Cfb
Guadalajara	Spain	3.56	13.5	1836	D3	Csa
Soria	Spain	3.51	10.6	2077	E1	Cfb
Ancona	Italy	3.10	15.5	1776	–	Cfa
Innsbruck	Austria	2.76	10.6	3173	–	Dfc
Oslo	Norway	2.73	6.7	4393	–	Dfb

The average daily irradiation values refer to the equator-orientated vertical plane. *HDD* means heating degree days, a parameter commonly used to describe the energy needed to heat a building (Kreith and Goswami 2004)

[a]According to the Köppen climate classification (Köppen 1936; Kottek et al. 2006), the first letter refers to the main climate, the second one refers to the precipitation, and the third one refers to the temperature

BSk = Arid-steppe-cold arid
Csa = Warm temperate–Summer dry–Hot summer
Csb = Warm temperate–Summer dry–Warm summer
Cfa = Warm temperate–Fully humid–Hot summer
Cfb = Warm temperate–Fully humid–Warm summer
Dfb = Snow–Fully humid–Warm summer
Dfc = Snow–Fully humid–Cool summer

To summarize the results, the EBIs and the values normalized to the best WWR-glazing element combination are shown in Table 10.8 (Spanish cities) and Table 10.9 (other European cities). To highlight the efficiency of the solutions, a color range from green (good performance) to red (bad performance) has been used.

As can be seen in Table 10.8, in general the best solutions in the Spanish climates concentrate around the upper right-hand part of the diagonal, corresponding to medium and elevate WWR values (from 44 to 88 %) and low degree of transparency elements (from 0 to 20). It is worth noting that in all cases using the RG for WWR ≥ 44 %, typical in commercial buildings in which the glazing materials are more and more extensively used, the building energy demand is at least 47 % higher (case of Sevilla) than those reached implementing the best solution for the city considered, i.e., using STPV 20. The difference in terms of

Table 10.8 Energy balance index (kWh/m^2) (a) and values normalized to the best WWR-glazing element combination (b)

Energy Balance Index [kWh/m^2] (a)

WWR - Castellón

GLAZING ELEMENT	11.1	22.2	33.3	44.4	55.5	66.6	77.7	88.8
0	48.5	44.7	40.9	37.4	34.5	31.7	29.4	27.5
10	48.7	44.5	39.4	35.1	32.6	30.4	29.1	28.0
20	48.6	43.7	38.4	34.7	33.3	32.3	32.3	32.5
30	48.3	42.4	38.7	37.3	38.2	39.7	41.8	44.2
40	48.1	42.4	40.6	41.4	44.4	47.8	51.6	55.7
RG	48.5	45.6	48.4	53.9	61.1	68.5	75.9	83.6

WWR - Sevilla

GLAZING ELEMENT	11.1	22.2	33.3	44.4	55.5	66.6	77.7	88.8
0	53.2	51.2	49.3	45.4	46.2	44.9	43.9	43.2
10	53.4	50.9	47.5	43.0	43.8	43.2	43.4	43.7
20	53.1	50.0	46.2	42.5	44.2	44.9	46.4	48.0
30	52.8	48.5	46.2	45.2	48.9	51.9	55.7	59.7
40	52.5	48.2	47.9	49.3	54.9	60.1	65.5	71.4
RG	52.8	50.9	55.1	62.4	71.3	80.5	89.4	98.6

WWR - Pontevedra

GLAZING ELEMENT	11.1	22.2	33.3	44.4	55.5	66.6	77.7	88.8
0	45.4	40.3	35.5	31.7	28.8	26.3	24.3	22.6
10	45.6	39.2	33.2	28.3	25.3	22.8	21.4	20.1
20	45.4	38.4	32.0	27.2	25.0	23.4	23.0	22.8
30	45.1	37.4	31.8	28.7	28.5	28.9	30.1	31.6
40	44.9	37.2	33.0	32.1	33.6	35.6	38.2	41.1
RG	45.1	39.5	39.7	43.1	48.2	53.6	59.2	65.1

WWR - Vitoria

GLAZING ELEMENT	11.1	22.2	33.3	44.4	55.5	66.6	77.7	88.8
0	38.4	32.4	29.2	27.5	26.6	26.0	25.7	25.7
10	38.5	31.3	26.5	23.2	21.5	20.3	19.9	19.6
20	38.3	30.3	24.6	21.0	19.5	18.8	18.9	19.2
30	38.0	28.8	22.9	20.0	19.7	20.2	21.3	22.8
40	37.8	28.0	22.9	21.2	22.1	23.5	25.5	28.0
RG	38.0	29.0	26.6	27.8	31.0	34.8	39.0	43.7

WWR - Guadalajara

GLAZING ELEMENT	11.1	22.2	33.3	44.4	55.5	66.6	77.7	88.8
0	42.8	37.0	33.6	31.4	30.0	29.0	28.2	27.7
10	43.0	36.5	31.3	27.8	25.9	24.5	23.8	23.5
20	42.8	35.6	29.8	26.0	24.5	23.6	23.7	24.1
30	42.5	34.4	28.7	26.1	26.0	26.5	28.0	29.7
40	42.3	34.0	29.5	28.3	29.5	31.5	34.1	37.0
RG	42.5	35.8	34.9	37.1	41.3	46.1	51.2	56.7

WWR - Soria

GLAZING ELEMENT	11.1	22.2	33.3	44.4	55.5	66.6	77.7	88.8
0	38.0	32.3	29.4	27.7	26.7	26.1	25.6	25.6
10	38.3	31.4	26.8	23.5	21.7	20.4	19.9	19.6
20	38.2	30.4	24.9	21.3	19.8	19.0	19.0	19.4
30	37.9	28.9	23.3	20.4	20.2	20.8	22.0	23.6
40	37.8	28.3	23.6	22.3	23.3	25.0	27.4	30.1
RG	38.1	29.8	28.5	30.5	34.5	38.8	43.5	48.6

Normalized Energy Balance Index (b)

WWR - Castellón

GLAZING ELEMENT	11.1	22.2	33.3	44.4	55.5	66.6	77.7	88.8
0	1.76	1.63	1.49	1.36	1.26	1.15	1.07	1.00
10	1.77	1.62	1.43	1.28	1.19	1.11	1.06	1.02
20	1.77	1.59	1.40	1.26	1.21	1.18	1.18	1.18
30	1.76	1.54	1.41	1.36	1.39	1.44	1.52	1.61
40	1.75	1.55	1.48	1.51	1.62	1.74	1.88	2.03
RG	1.77	1.66	1.76	1.96	2.22	2.49	2.76	3.04

WWR - Sevilla

GLAZING ELEMENT	11.1	22.2	33.3	44.4	55.5	66.6	77.7	88.8
0	1.25	1.20	1.16	1.07	1.09	1.05	1.03	1.02
10	1.25	1.20	1.12	1.01	1.03	1.01	1.02	1.03
20	1.25	1.17	1.09	1.00	1.04	1.06	1.09	1.13
30	1.24	1.14	1.09	1.06	1.15	1.22	1.31	1.40
40	1.23	1.13	1.13	1.16	1.29	1.41	1.54	1.68
RG	1.24	1.20	1.29	1.47	1.68	1.89	2.10	2.32

WWR - Pontevedra

GLAZING ELEMENT	11.1	22.2	33.3	44.4	55.5	66.6	77.7	88.8
0	2.26	2.01	1.77	1.58	1.43	1.31	1.21	1.13
10	2.27	1.95	1.65	1.41	1.26	1.14	1.07	1.00
20	2.26	1.91	1.59	1.36	1.25	1.16	1.14	1.13
30	2.25	1.86	1.58	1.43	1.42	1.44	1.50	1.58
40	2.24	1.85	1.65	1.60	1.67	1.78	1.90	2.05
RG	2.25	1.97	1.98	2.15	2.40	2.67	2.95	3.24

WWR - Vitoria

GLAZING ELEMENT	11.1	22.2	33.3	44.4	55.5	66.6	77.7	88.8
0	2.05	1.73	1.56	1.47	1.42	1.39	1.37	1.37
10	2.05	1.67	1.41	1.24	1.15	1.08	1.06	1.05
20	2.04	1.62	1.31	1.12	1.04	1.00	1.01	1.03
30	2.03	1.53	1.22	1.07	1.05	1.08	1.14	1.21
40	2.02	1.49	1.22	1.13	1.18	1.25	1.36	1.49
RG	2.03	1.54	1.42	1.48	1.65	1.85	2.08	2.33

WWR - Guadalajara

GLAZING ELEMENT	11.1	22.2	33.3	44.4	55.5	66.6	77.7	88.8
0	1.82	1.58	1.43	1.34	1.28	1.23	1.20	1.18
10	1.83	1.56	1.33	1.18	1.10	1.04	1.02	1.00
20	1.82	1.52	1.27	1.11	1.04	1.01	1.01	1.03
30	1.81	1.46	1.23	1.11	1.11	1.13	1.19	1.27
40	1.80	1.45	1.26	1.20	1.26	1.34	1.45	1.58
RG	1.81	1.53	1.49	1.58	1.76	1.96	2.18	2.42

WWR - Soria

GLAZING ELEMENT	11.1	22.2	33.3	44.4	55.5	66.6	77.7	88.8
0	2.00	1.70	1.55	1.46	1.41	1.37	1.35	1.35
10	2.02	1.65	1.41	1.23	1.14	1.08	1.05	1.03
20	2.01	1.60	1.31	1.12	1.04	1.00	1.00	1.02
30	1.99	1.52	1.22	1.08	1.06	1.09	1.16	1.24
40	1.99	1.49	1.24	1.17	1.23	1.32	1.44	1.58
RG	2.01	1.57	1.50	1.61	1.81	2.04	2.29	2.56

Spanish cities (Olivieri 2015)

Table 10.9 Energy balance index (kWh/m^2) (a) and values normalized to the best WWR-glazing element combination (b)

Energy Balance Index [kWh/m^2] (a)

WWR - Ancona

GLAZING ELEMENT	11.1	22.2	33.3	44.4	55.5	66.6	77.7	88.8
0	43.7	39.1	37.6	37.0	37.0	37.2	37.7	38.3
10	43.7	38.1	35.2	33.3	32.7	32.4	32.8	33.2
20	43.5	37.0	33.3	30.8	30.5	30.7	31.7	32.9
30	43.1	35.6	31.0	29.6	30.5	31.9	33.9	36.0
40	42.8	34.5	30.6	30.4	32.3	34.5	37.3	40.2
RG	42.7	34.1	33.0	34.9	38.7	42.8	47.2	51.9

WWR - Innsbruck

GLAZING ELEMENT	11.1	22.2	33.3	44.4	55.5	66.6	77.7	88.8
0	38.6	34.9	33.2	32.6	32.7	33.1	33.8	35.0
10	38.5	32.9	29.8	27.4	26.8	26.7	27.5	28.5
20	38.2	31.8	27.7	25.0	24.8	25.3	26.8	28.5
30	37.8	30.0	25.7	24.2	25.3	27.1	29.5	32.4
40	37.4	29.1	25.7	25.6	27.7	30.5	33.9	37.8
RG	37.3	29.9	29.4	31.8	36.3	41.3	46.8	52.7

WWR - Oslo

GLAZING ELEMENT	11.1	22.2	33.3	44.4	55.5	66.6	77.7	88.8
0	36.4	36.2	38.2	40.9	44.0	47.2	50.5	54.1
10	36.0	34.6	34.8	36.0	38.3	40.9	44.1	47.5
20	35.7	33.4	32.8	33.6	36.3	39.4	43.0	46.8
30	35.2	31.8	31.0	32.7	36.2	40.0	44.2	48.7
40	34.8	30.6	30.6	33.1	37.1	41.5	46.2	51.3
RG	34.4	30.6	32.3	36.1	41.4	47.2	53.2	59.8

Normalized Energy Balance Index (b)

WWR - Ancona

GLAZING ELEMENT	11.1	22.2	33.3	44.4	55.5	66.6	77.7	88.8
0	1.48	1.32	1.27	1.25	1.25	1.26	1.27	1.30
10	1.48	1.29	1.19	1.13	1.11	1.10	1.11	1.12
20	1.47	1.25	1.13	1.04	1.03	1.04	1.07	1.11
30	1.46	1.20	1.05	1.00	1.03	1.08	1.15	1.22
40	1.45	1.17	1.03	1.03	1.09	1.17	1.26	1.36
RG	1.44	1.16	1.12	1.18	1.31	1.45	1.60	1.75

WWR - Innsbruck

GLAZING ELEMENT	11.1	22.2	33.3	44.4	55.5	66.6	77.7	88.8
0	1.59	1.44	1.37	1.35	1.35	1.37	1.40	1.45
10	1.59	1.36	1.23	1.13	1.11	1.10	1.13	1.18
20	1.58	1.31	1.15	1.03	1.03	1.05	1.11	1.18
30	1.56	1.24	1.06	1.00	1.05	1.12	1.22	1.34
40	1.55	1.20	1.06	1.06	1.15	1.26	1.40	1.56
RG	1.54	1.24	1.21	1.31	1.50	1.71	1.94	2.18

WWR - Oslo

GLAZING ELEMENT	11.1	22.2	33.3	44.4	55.5	66.6	77.7	88.8
0	1.19	1.18	1.25	1.34	1.44	1.54	1.65	1.77
10	1.18	1.13	1.14	1.18	1.25	1.34	1.44	1.55
20	1.17	1.09	1.07	1.10	1.19	1.29	1.40	1.53
30	1.15	1.04	1.01	1.07	1.18	1.31	1.44	1.59
40	1.14	1.00	1.00	1.08	1.21	1.36	1.51	1.68
RG	1.12	1.00	1.06	1.18	1.35	1.54	1.74	1.95

No Spanish cities (Olivieri 2015)

façade and building performance using a code-compliant conventional glass instead of a correctly dimensioned STPV element rises up to 324 % in the case of Pontevedra, meaning that the building energy demand is more than three times those reached using the STPV element 10. Apart from this, even if the optimum solution in terms of glazing material and WWR combination has been highlighted, it can be noted that roughly the same building performance could be reached by choosing other combinations of these parameters. For instance, in the case of Sevilla, the lower energy demand is obtained with the combination WWR = 44 % and glazing element 20, but designing bigger façade openings (WWR = 66 %) and using a less transparent element (STPV 10) the building energy performance is worsened at only 1 %. Thus, it is evident that in such case not only the efficiency of the building should be taken into account to define the appropriate facade solution, but also other elements which may be critical such as the visual comfort conditions in the space or the building façade esthetic, to mention just a few examples.

Regarding the other European cities analyzed (Table 10.9), for Ancona and Innsbruck the best solutions concentrate around the center of the tables (medium WWR and degree of transparency). In case of Oslo, the best results fall around the lower left-hand part of the diagonal, corresponding to small façade openings and high transparency elements. Regarding the first two cities, it is interesting to note that even if they are characterized by highly diverse climates (see Table 10.7), the WWR-glazing element combination that ensures the best building performance is the same in both cases (WWR = 44 %, glazing element 30). This behavior is due to the good balance of this STPV element in both climates in terms of thermal performance, daylighting, and electricity generation. In case of Oslo, the severe climatic conditions make the heating loads more important than in the other sites, thus small façade openings reduce the heat losses and glazing elements with high degree

of transparency enhance the solar gains. In fact, this case is the only one of the analyzed in which the RG performs as well as the STPV elements, so probably in this case it would not be worth implementing the STPV solution from an energy balance point of view.

10.4 Economic Profitability of STPV Solutions

In this section, the economic viability of STPV façades is assessed. With this aim, for each Spanish city, the best performing STPV system has been compared with the façade solution with the same WWR but made up of the reference glass. For instance, in the case of Madrid, the most efficient design consisting of the use of element 10 with façade openings corresponding to WWR = 77 % was compared with the building with the same openings size in which the conventional reference glass has been used.

10.4.1 Methodology

To carry out the study, the first step was to estimate the annual expenditure that the building would pay in order to cover its global electricity demand. To do this, annual data of PV generation (in the case of STPV integrated solution) and electricity demand (in both cases) were hourly analyzed. In fact, according to the Spanish regulation (BOE 2014), the energy price consists of two components: the *power term*, which depends on the maximum power demanded (measured in commercial buildings through a maximum power meter) and the *energy term* that represents the price for the kilowatt-hour consumed. In addition, both factors depend on the billing period, having three different billing periods: peak, flat, and valley billing periods. Considering the characteristics of the reference building (a 7 floors midsize office building consisting of approximately 6500 m^2) power and energy terms corresponding to the contract rate 3.1A (medium voltage connection up to 36 kV) were assumed. In addition, to calculate the actual power and energy rates, two other terms have to be considered: the *Commercialization Margin Price* (*CMP*), which should be added to the annual power term and similarly the *Electricity Production Cost* (*EPC*), fixed on the basis of the electricity price in the market, which must be added to the energy term. The main characteristics of the contract rate 3.1A and the other costs to be taken into account are specified in Table 10.10.

On the basis of these specific costs, and using the hourly data of PV generation (PVsyst simulations) and global electricity demand for HVAC and lighting (EnergyPlus simulations), the annual electricity billing was calculated in each case. Regarding the setup of the PV system, it was assumed to be connected for instantaneous self-consumption, as the current Spanish legal framework about the

Table 10.10 Power and energy terms according to the contract rate 3.1A

Period	Peak	Flat	Valley
Annual power term (€/kW)	59.173468	36.49068	8.367731
Annual CMP (€/kW)	4	4	4
Energy term (€/kWh)	0.014335	0.012754	0.007805
EPC (€/kWh)	0.085033	0.073095	0.049492

Source BOE (2014)

grid connection of small power generating systems (RD 1699/2011) does allow (BOE 2011). Furthermore, it was assumed that the surplus energy not locally consumed is not compensated in anyway or, in others words, it has been assumed the implementation of a zero energy grid injection strategy. According to these suppositions, the annual billings for the electricity consumption have been calculated. Results are summarized in Table 10.11, which also includes the annual savings calculated as the difference between the energy billing to be paid using the STPV solution and the one resulting from using the reference glass. As it can be seen, the annual savings range between 7700 € corresponding to the case of Sevilla and more that 28,000 € achieved in the case of Pontevedra and Castellón. These differences can be explained by looking at the *Energy Balance Indices* provided by the best performing STPV solutions in comparison with those obtained with the reference glass for the same WWR (see Table 10.8). In case of Sevilla for instance, the conventional glazing performs relatively well, producing an increase in the building energy demand of about 47 %. On the contrary, in the case of Pontevedra the performances of the reference glass and of the STPV solution strongly diverge, being the building energy demand using the conventional systems more than three times those achieved using the PV façade system. This behavior causes that the annual savings are also significantly different from city to city.

To evaluate how profitable the STPV façade projects would be, the Net Present Value (NPV) has been calculated. This parameter is one of the most widely used

Table 10.11 Best performing STPV system, annual billing due to the power and energy terms, total annual electricity billing and annual savings

	Best STPV system		Power-term billing		Energy-term billing		Electricity billing		Annual savings	
	Element (–)	WWR (–)	STPV (k€)	RG (k€)	STPV (k€)	RG (k€)	STPV (k€)	RG (k€)	k€	%
Castellón	00	88.8	15.6	24.5	26.4	45.6	42.0	70.1	28.1	40.1
Sevilla	20	44.4	14.4	15.9	27.5	33.9	42.0	49.7	7.7	15.6
Pontevedra	10	88.8	13.6	23.9	17.8	35.7	31.4	59.6	28.2	47.3
Vitoria	20	66.6	10.5	16.8	13.7	19.2	24.2	36.1	11.9	32.9
Guadalajara	10	88.8	13.3	23.7	18.9	31.2	32.2	54.9	22.7	41.3
Madrid	10	77.7	16.0	22.7	23.5	37.9	39.5	60.6	21.1	34.8
Soria	20	66.6	11.3	17.7	14.5	21.5	25.7	39.2	13.4	34.3

measures in capital budgeting, since it gives the potential investor clear information of whether the project will be a valuable investment or not. NPV is simply defined as the present value of net cash inflows generated by a project minus the initial investment on the project. Accordingly, to be adequately profitable, an investment should have a NPV greater than zero. In the cases analyzed, the projects do not generate any cash inflows (since only energy-saving strategies are being considered), but the annual savings can be considered as inflows, as they represent cash outflows that will not have to be paid.

In order to calculate the NPV, the first step is to estimate the initial investment for the projects. This task is far from simple, mainly because the cost of STPV solutions depends on several factors related to the particular building in which the system will be integrated. For instance, aspects such as the size of the system or the opportunity of using standard elements instead of custom-made products have a big impact over the final cost of the project. The correlation between the specific project and the final price per square meter of the STPV element, besides the relative novelty of these building products, explain the fact that they are still not included in the price databases of the building industry materials. Because of these difficulties to find real prices representative of the STPV products in the particular projects analyzed, in this study three cost scenarios have been assumed on the basis of the reference glass price. In other words, the price of the conventional glass has been taken as a reference and on this basis the extra cost of the STPV products has been supposed according to the following scenarios:

(a) STPV products are 50 % more expensive than the conventional reference glass;
(b) STPV products are 100 % more expensive than the conventional reference glass;
(c) STPV products are 200 % more expensive than the conventional reference glass.

Next, to define the price of the conventional glazing element, several price databases of construction materials have been checked. As specified in Table 10.2, the reference glass is a double-glazing unit with a solar control coating, having U-value = 2.8 W/(m^2 K) and g-value = 0.47. Both glass panes have 6 mm thicknesses and the air gap has a thickness of 12 mm. The price of this products varies between 93.14 and 134.14 €/m^2 depending on the database consulted (COAATGU 2015; CYPE Ingenieros 2015; FIVE 2015; ITEC 2015). To cover all the range of prices, both extreme values have been taken into account in the analysis, defining two scenarios for the conventional glass:

(i) The minimum price of the conventional glass is 93.14 €/m^2;
(ii) The maximum price of the conventional glass is 134.14 €/m^2.

To summarize, on the basis of the assumptions made, prices per square meter used to carry out the analysis are shown in Table 10.12.

In Table 10.13, the maximum and minimum prices of the STPV elements, calculated according to the assumptions made and using the power density reported

Table 10.12 Prices of the reference glass and prices of STPV elements according to the scenarios assumed

Scenario	(€/m^2)	STPV element extra cost		
		(a) +50 %	(b) +100 %	(c) +200 %
RG glazing cost		Final STPV element price		
		(€/m^2)	(€/m^2)	(€/m^2)
(i) RG min. price	93.14	139.7	186.2	279.3
(ii) RG max. price	134.14	201.2	268.3	402.4

Table 10.13 Minimum and maximum prices of the STPV elements expressed in Euros per watt peak

STPV element	Final STPV element price	
	Minimum price (€/W$_P$)	Maximum price (€/W$_P$)
0	2.3	6.5
10	3.2	9.1
20	3.7	10.6
30	4.4	12.7
40	5.5	15.9

Values have been calculated according to the assumption made and considering the power density of the different elements

in Table 10.2, are expressed in Euros per watt peak. It can be noted that the specific price (€/W$_P$) rises by increasing the transparency degree, since the power density (W$_P$/m^2) decreases.

Next, the initial investments required to build the façade systems have been calculated using the specific prices defined in Table 10.12. Results are reported in Tables 10.14 and 10.15. In particular, Table 10.14 refers to the case in which the minimum price of the reference glass has been taken as starting point, whereas Table 10.15 reports the costs of the façades calculated using the maximum price of the reference glass.

Table 10.14 Costs of the façade systems calculated using the minimum price of the reference glass

	WWR	Façade system size	RG façade Max cost	STPV façade cost			STPV façade extra cost		
				+50 %	+100 %	+200 %	+50 %	+100 %	+200 %
	–	(m^2)	(k€)	(k€)	(k€)	(k€)	(k€)	(k€)	(k€)
Castellón	88.8	881	82.1	123.1	164.1	246.2	41.0	82.1	164.1
Sevilla	44.4	441	41.0	61.6	82.1	123.1	20.5	41.0	82.1
Pontevedra	88.8	881	82.1	123.1	164.1	246.2	41.0	82.1	164.1
Vitoria	66.6	661	61.6	92.3	123.1	184.7	30.8	61.6	123.1
Guadalajara	88.8	881	82.1	123.1	164.1	246.2	41.0	82.1	164.1
Madrid	77.7	771	71.8	107.7	143.6	215.4	35.9	71.8	143.6
Soria	66.6	661	61.6	92.3	123.1	184.7	30.8	61.6	123.1

Table 10.15 Costs of the façade systems calculated using the maximum price of the reference glass

	WWR	Façade System size	RG façade Max cost	STPV façade cost			STPV façade extra cost		
				+50 %	+100 %	+200 %	+50 %	+100 %	+200 %
	–	[m^2]	(k€)	(k€)	(k€)	(k€)	(k€)	(k€)	(k€)
Castellón	88.8	881	118.2	177.3	236.4	354.6	59.1	118.2	236.4
Sevilla	44.4	441	59.1	88.6	118.2	177.3	29.5	59.1	118.2
Pontevedra	88.8	881	118.2	177.3	236.4	354.6	59.1	118.2	236.4
Vitoria	66.6	661	88.6	133.0	177.3	265.9	44.3	88.6	177.3
Guadalajara	88.8	881	118.2	177.3	236.4	354.6	59.1	118.2	236.4
Madrid	77.7	771	103.4	155.1	206.8	310.3	51.7	103.4	206.8
Soria	66.6	661	88.6	133.0	177.3	265.9	44.3	88.6	177.3

In addition to the costs of the systems (Tables 10.14 and 10.15) and the annual savings (Table 10.11), to calculate the NPV other data such as the lifetime of the installation, the discount rate and the annual rate of increase in energy prices are required. Values used in the analysis are reported below:

- lifetime of the installation: 30 years (Creara 2015);
- discount rate: 5 % (Creara 2015);
- annual operation and maintenance costs: 5 €/kW_p plus the inverter replacement after 15 years. To estimate the cost of the inverter (in the range 15–50 kW), a conservative value of 150 €/kW has been used;
- annual inflation rate: 2 % (Creara 2015);
- Annual rate of increase in electricity prices: considering that annual increase in the price of commercial electricity is a difficult parameter to estimate accurately, two extreme scenarios have been proposed in order to cover the most likely developments of this parameter. In the first one, a moderate increase has been supposed with an annual rate I_e = 1 %; in the second one, a high increase has been supposed with an annual rate I_e = 5 %.

With these data, the NPV of the projects has been calculated for each city according to the suppositions made. A total of 12 scenarios obtained from the combination of six prices (see Table 10.12) and two annual rates of increase in electricity prices have been studied for each city. As an example, results corresponding to the case of Castellón are shown in Fig. 10.11, in which figure (a) represents the NPV calculated using the STPV prices refereed to the minimum price of the reference glass, for both the expected rates of increase in energy prices. Figure 10.11b analyzes the NPV when the higher prices of the STPV elements are considered, also in this case for both energy increases.

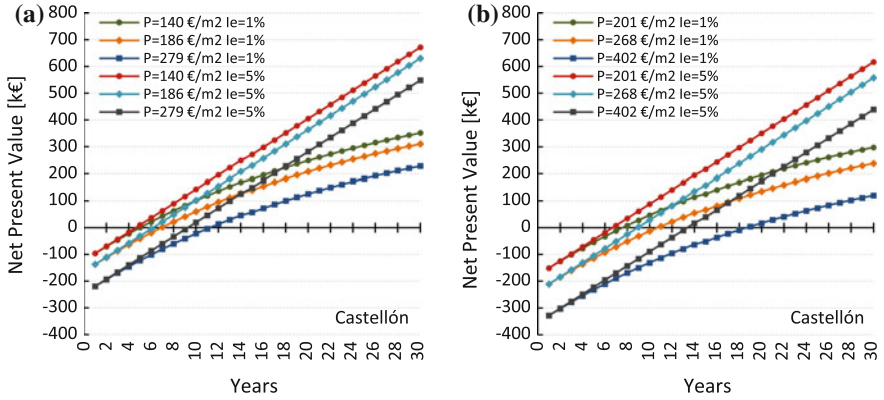

Fig. 10.11 NPV calculated according to the suppositions made: using the minimum (**a**) and the maximum (**b**) price of the reference glass, for low (I_e = 1 %) and high (I_e = 5 %) rise of electricity prices. Case of Castellón (Olivieri 2015)

10.4.2 Results

Looking at Fig. 10.11 corresponding to the case of Castellón, it can be seen that the NPV after 30 years ranges between nearly 670 k€ in the best scenario (low price of STPV elements being P = 140 €/m^2 and high energy price increase with I_e = 5 %) and approximately 100 k€ in the worst one (high initial investment with a price of STPV elements of 402 €/m^2 and low increase of the energy price, being I_e = 1 %). The payback period (defined as the period of time required to recoup the funds expended in an investment, i.e., the time in which the NPV changes from negative to positive) ranges between 5 and 19 years. The corresponding internal rate of return (IRR), namely the discount rate that makes the NPV equal to zero, ranges between 27.5 and 7.6 %.

To summarize the results of the economic study for all the cities analyzed, in Table 10.16 the NPV of all the projects has been summarized and in Table 10.17 the corresponding payback periods have been reported. Furthermore, in Table 10.18 projects deemed economically profitable have been indicated. This classification has been made by applying two conditions: a NPV at the end of the lifetime of the system (estimated in 30 years) greater or equal to 48,000 € (corresponding at about 13 % of the initial investment required to build the most cost-intensive STPV façade, Table 10.15) and a payback period lower or equal to 20 years. Projects that meet both conditions have been marked in green, the others in red.

To conclude, the economic study shows the price ranges among which the STPV façade solutions would be economically feasible. To carry out the analysis, the best performing STPV systems have been compared with solutions of the same dimensions based on conventional glazing. To estimate the annual energy expenditure, a contract rate has been supposed on the basis of the characteristics of the reference building. Since in Spain electricity billing depends on energy consumed, power

Table 10.16 Net present value of the projects after 30 years according to the assumptions made

	Energy prices rise I_e = 1 %						Energy prices rise I_e = 5 %					
	STPV element price (€/m^2)						STPV element price (€/m^2)					
	140	186	201	268	279	402	140	186	201	268	279	402
Castellón	351	310	297	238	228	120	670	629	616	557	547	439
Pontevedra	355	314	301	242	232	124	676	635	622	563	553	444
Guadalajara	261	220	206	147	138	29	519	478	464	405	396	287
Madrid	249	214	202	150	142	47	489	453	442	390	382	287
Soria	134	104	94	50	42	−39	287	256	246	202	195	114
Vitoria	107	77	67	22	15	−66	242	211	201	157	150	68
Sevilla	69	48	42	12	7	−47	157	137	130	100	96	41

Values in thousands of euros

Table 10.17 Payback periods of the projects according to the assumptions made

	Energy prices rise I_e = 1 %						Energy prices rise I_e = 5 %					
	STPV element price (€/m^2)						STPV element price (€/m^2)					
	140	186	201	268	279	402	140	186	201	268	279	402
Castellón	6	7	8	11	12	19	5	7	7	9	10	14
Pontevedra	5	7	8	11	12	19	5	7	7	9	10	14
Guadalajara	7	9	10	15	16	27	6	8	9	12	12	17
Madrid	6	9	10	13	14	24	6	8	8	11	11	16
Soria	9	12	14	20	22	>30	8	10	11	14	15	22
Vitoria	10	15	16	25	27	>30	9	12	12	17	17	24
Sevilla	10	15	17	26	27	>30	9	12	13	17	17	25

Values in years

Table 10.18 STPV projects deemed profitable, having e NPV greater or equal to 48,000 € and a payback period lower or equal to 20 years

	Energy prices rise I_e = 1%						Energy prices rise I_e = 5%					
	STPV element price [€/m^2]						STPV element price [€/m^2]					
	140	186	201	268	279	402	140	186	201	268	279	402
Castellón	YES	YES	YES	YES	YES	YES	YES	YES	YES	YES	YES	YES
Pontevedra	YES	YES	YES	YES	YES	YES	YES	YES	YES	YES	YES	YES
Guadalajara	YES	YES	YES	YES	YES	NO	YES	YES	YES	YES	YES	YES
Madrid	YES	YES	YES	YES	YES	NO	YES	YES	YES	YES	YES	YES
Soria	YES	YES	YES	YES	NO	NO	YES	YES	YES	YES	YES	NO
Vitoria	YES	YES	YES	NO	NO	NO	YES	YES	YES	YES	YES	NO
Sevilla	YES	YES	NO	NO	NO	NO	YES	YES	YES	YES	YES	NO

peaks demanded, and billing periods, hourly based simulations have been carried out to realistically estimate the energy bills and the expected annual savings provided by STPV solutions. Next, six price scenarios of STPV products have been formulated on the basis of the price of the conventional glass. These assumptions have been required due to the impossibility to surely establish the price of STPV products, since it depends on several factors mainly related to the particular project. With the expected annual savings and the prices assumed of the semi-transparent products, the NPV of the projects has been calculated considering two possible scenarios about the annual rate of increase of the energy price. A total of 84 cases have been analyzed, combining two annual rates of increase of energy prices, six price scenarios, and seven cities. Results show that in cases of Castellón and Pontevedra, the projects are profitable for all the scenarios. In fact, under the less favorable hypothesis (STPV price about 400 €/m^2, rate of increase of energy prices of 1 %), the NPV after 30 years is more than 120,000 €, the payback period is 19 years, and the IRR is about 8 %. As regards Madrid and Guadalajara, the profitability of the investment is similar for both cities and seems to be acceptable under all the scenarios excluding the worst one, which presents a NPV of about 46,000 €, a payback period of 24 years, and a IRR of about 6 %. Concerning Vitoria and Soria, considering an annual increase in the price of the electricity of 1 %, the cut-off prices seem to be about 200 and 270 €/m^2, respectively. In fact, with this initial costs of the projects, the NPV is nearly 66,000 € with a payback period of 16 years and a IRR of about 9 % in the case of Vitoria. In case of Soria, the NPV is about 50,000 €, the payback period is 20 years, and the IRR is about 7 %. Considering an annual increase in the price of the electricity of 5 %, including prices higher than 280 €/m^2 seems acceptable for the project, since the NPV after 30 years is higher than 150,000 €. Finally in the case of Sevilla, if the electricity price only rises 1 % yearly, the project seems profitable if the price of STPV products is lower than 185 €/m^2 approximately. In this case, in fact the NPV is about 50,000 €, the payback period is 15 years, and the IRR is about 9 %. If the electricity price annually rises 5 %, prices up to 280 €/m^2 seem acceptable, since the NPV would be 95,000 €, the payback period around 17 years, and the IRR about 9 %.

10.5 Conclusions

In this chapter, an integral energy simulation methodology of STPV elements, covering thermal, daylighting, and electrical performance has been presented. These products, born from the collaboration between the photovoltaic and the construction industries, are currently experiencing slow market diffusion (largely limited to prestigious architectonic projects with high-visibility) mostly because they have not yet been adequately studied and their potential for energy savings has not yet been clearly shown. The behavior of STPV systems cannot be simply expressed by specifying the performance ratio or the kilowatt-hours of electricity yearly produced because they are not just PV systems, but also integral parts of the building

envelope. Likewise, to reduce the performance description of the systems to the parameters typically used to express the properties of conventional glazing solutions, i.e., the thermal transmittance and the solar factor, is not a convenient approach because the electricity generation should be also taken into account. The variables involved in the characterization of the global energy performance of STPV solutions are numerous and require an articulated and multidisciplinary methodology.

To carry out the simulations, the glazing solutions have been previously experimentally characterized, using a spectrophotometer system coupled with an integrating sphere. The measures have allowed identifying the spectral transmittance (front) and reflectance (front and back) of the samples, necessary input data to perform detailed and reliable simulations. To complete the simulations, a reference office space has been considered and a package composed of a range of specific software tools has been used: DesignBuilder and EnergyPlus to carry out the thermal analysis, PVsyst to estimate the electricity generation, and LNBL daylighting programs (Optics, Window, and COMFEN) to evaluate the visual comfort. To assess the overall energy performance of the glazing elements, a parameter called EBI that takes into account annual heating, cooling, and lighting loads, as well as the electricity generation, has been proposed. This parameter, which expresses the building net electricity balance per unit of net floor area, is a useful indicator of the overall building energy performance and allows assessing the energy performance of STPV façade systems. According to the comparative analysis performed, the remarkable findings of this work are listed below.

Five different commercial STPV elements representative of the current marker (visible transmittance between 0 and 32 %) have been analyzed together with a reference glass complying with the local building regulations. Comparing the performance of the STPV elements with the code-compliant reference glass, to fully exploit the energy-saving potential of these glazing solutions it might be concluded that:

- For small façade openings (WWR ≤ 22 %), the energy-saving potential provided by the best performing STPV solution compared to the RG is lower than 5.5 %, so probably in this case it would not be worth implementing the STPV solution;
- For intermediate and large façade openings (WWR ≥ 33 %), the STPV solutions provide a promising energy-saving potential, ranging between 18 % (WWR = 33 %) and 59 % (WWR = 88 %) compared to the RG.

Comparing the performance of the STPV elements between them, to point out the degree of transparency effect and the importance of an adequate selection of this parameter, we can conclude that:

- For relative small façade openings (WWR ≤ 33 %), the energy performance of all STPV elements is reasonably similar, with a maximum EBI difference between elements of about 10 %;

- For intermediate façade openings (33 % < WWR < 66 %), the second less transparent STPV element (visible transmittance of 16 %) outperforms the other solutions being about 25 % more efficient than the least efficient STPV element (visible transmittance of 32 %);
- For large façade openings (WWR ≥ 66 %), the less transparent STPV element (visible transmittance of 10 %) provides the most efficient energy balance and in this case the performance of the different glazing materials diverges drastically, rising up to 68 % the difference between the best and the worst STPV solution (most transparent element, visible transmittance of 32 %).

To assess the STPV systems performance under different climatic conditions, the methodology has been applied in nine other cities in addition to the Madrid-based case. The selection of the cities has been made in order to cover both the climatic zones defined in the Spanish Technical Building Code (CTE 2013) and also the most diffused European climatic zones according to Köppen climate classification (Köppen 1936; Kottek et al. 2006). All the combination possibilities of window-to-wall ratios and glazing elements have has been analyzed for each city, performing a total of 432 hourly based annual simulations. The analysis of the associated *Energy Balance Indices* has allowed emphasizing that for the façade opening size of the reference building originally defined by IEA (WWR = 44 %), two STPV elements (elements 20 and 30) outperform the other solutions in all the climates, since they combine good annual thermal performance, daylighting supply, and electricity generation. In particular, the element with a lower degree of transparency (element 20) has proven to be the most efficient solution in the Spanish cities with a warmer climate, whereas the more transparent element 30 has proven to be the best option in more rigid climates.

Apart from this, the optimum solution (the one that minimizes the building annual energy demand), in terms of glazing material and WWR combination, has been point out for each city. This analysis has shown that although it is always possible to find the optimum configuration, a close to optimum building performance could be achieved by choosing other combinations of the design parameters. In these cases, it is evident that the design choice has to be taken considering also other factors, such as luminous comfort or the esthetics of the façade.

Regarding the glare and daylighting analysis, the main findings are that:

- Under clear skies in the spring equinox and summer solstice, no glare conditions occur at noon. In the winter solstice, uncomfortable conditions occur using all the glazing materials, although the least transparent STPV provides close to comfort conditions;
- Under clear skies, in nearly all of the cases the maximum illuminance value over the floor falls within the range 100–2000 lx considered as offering potentially useful illumination for the space users;
- Under overcast sky conditions, illuminance over the floor is lower than 50 lx. Accordingly, the daylighting potential in these conditions could be considered negligible.

Regarding the economic study, it has shown the price ranges among which the STPV façade solutions would be economically feasible. The annual electricity expenditures of the best performing buildings having a façade-integrated STPV system have been compared with those of the same building having façade solutions based on conventional glazing. The costs of the systems have been estimated formulating six price scenarios of STPV products. Next, the NPV, the payback period, and the IRR of the projects have been calculated using the construction costs and the annual savings considering two possible scenarios about the annual rate of increase of the electricity price. A total of 84 cases have been analyzed, showing that in the cases of Castellón and Pontevedra the projects are profitable for all the scenarios. As regards Madrid and Guadalajara, the profitability of the investment is similar for both cities and is acceptable under all the scenarios if a high annual increase in the price of the electricity of 5 % is assumed. With a low rise of the electricity price, the maximum STPV price that still makes profitable projects is about 280 €/m^2. Concerning Vitoria and Soria, considering an annual increase in the price of the electricity of 1 %, the cut-off prices are about 200 and 270 €/m^2, respectively. Considering a rise of the electricity price of about 5 %, including prices higher than 280 €/m^2 seems acceptable for the project. Finally in the case of Sevilla, if the electricity price only rises 1 % yearly the project is feasible if the price of STPV products is lower than 185 €/m^2 approximately. If the electricity price annually rises 5 %, prices up to 280 €/m^2 seem acceptable.

In summary, it has been shown that the use of active photovoltaic glazing systems is economically profitable in a wide range of projects and can significantly contribute to reduce the building energy demand. Moreover, it has been shown that a rigorous analysis methodology based on the STPV optical characterization and on the utilization of complementary software tools:

- Is an adequate approach in order to properly and realistically quantify the STPV elements potentiality, as well as provide guidance on optimization possibilities of these elements;
- Is hardly applicable in the real world due to the time consumption required.

On that score, a more integrated workflow would be required, both in terms of detailed optical data accessibility and simulation software interoperability, to encourage STPV elements use in the building sector.

To conclude, it would be expected that existing barriers for the introduction of active construction components into the urban fabric will be jointly faced by photovoltaic and building construction industries, as well as by architects and designers, in order to enable BIPV emerging technologies to contribute to the improvement of the building sector sustainability. In this sense, this work has aimed to contribute to removing the existing barriers for the diffusion of STPV elements within the energy-efficient building design and construction practices, defining a methodology to analyze the energy interaction between buildings and STPV elements and quantifying the interesting energy and economic savings that these building solutions, nowadays already available in the market, can provide in both new and retrofitting projects.

References

Annunziata E, Frey M, Rizzi F (2013) Towards nearly zero-energy buildings: the state-of-art of national regulations in Europe. Energy 57:125–133. doi:10.1016/j.energy.2012.11.049

Asdrubali F, Bonaut M, Battisti M, Venegas M (2008) Comparative study of energy regulations for buildings in Italy and Spain. Energy Build 40:1805–1815. doi:10.1016/j.enbuild.2008.03.007

Bahaj AS, James PAB, Jentsch MF (2008) Potential of emerging glazing technologies for highly glazed buildings in hot arid climates. Energy Build 40:720–731. doi:10.1016/j.enbuild.2007.05.006

Ban-Weiss G, Wray C, Delp W, Ly P, Akbari H, Levinson R (2013) Electricity production and cooling energy savings from installation of a building-integrated photovoltaic roof on an office building. Energy Build 56:210–220. doi:10.1016/j.enbuild.2012.06.032

Bodart M, De Herde A (2002) Global energy savings in offices buildings by the use of daylighting. Energy Build 34:421–429

BOE (2014) Orden IET/107/2014, de 31 de enero, por la que se revisan los peajes de acceso de energía eléctrica para 2014

BOE (2011) Real Decreto 1699/2011, de 18 de noviembre, por el que se regula la conexión a red de instalaciones de producción de energía eléctrica de pequeña potencia

Buratti C, Moretti E (2013a) Silica nanogel for energy-efficient windows. In: Pacheco-Torgal F, Diamanti MV, Nazari A, Granqvist C-G (eds) Nanotechnology in eco-efficient construction. Woodhead Publishing Limited, Cambridge, pp. 207–235. doi:10.1533/9780857098832.2.207

Buratti C, Moretti E (2013b) Nanogel windows. In: Pacheco-Torgal F, Mistretta M, Kaklauskas A, Granqvist C-G, Cabeza L-F (eds) Nearly zero energy building refurbishment. Springer, London. doi:10.1007/9781447155232

CENELEC, 2012. Photovoltaics in buildings - DRAFT prEN 50583

Cerón I, Caamaño-Martín E, Neila FJ (2013) "State-of-the-art" of building integrated photovoltaic products. Renew Energy 58:127–133. doi:10.1016/j.renene.2013.02.013

Chen F, Wittkopf SK (2012) Summer condition thermal transmittance measurement of fenestration systems using calorimetric hot box. Energy Build 53:47–56. doi:10.1016/j.enbuild.2012.07.005

Chen F, Wittkopf SK, Khai Ng P, Du H (2012) Solar heat gain coefficient measurement of semi-transparent photovoltaic modules with indoor calorimetric hot box and solar simulator. Energy Build 53:74–84. doi:10.1016/j.enbuild.2012.06.005

Chow TT, Lin Z, He W, Chan ALS, Fong KF (2006) Use of ventilated solar screen window in warm climate. Appl Therm Eng 26:1910–1918. doi:10.1016/j.applthermaleng.2006.01.026

Chow TT, He W, Ji J (2007) An experimental study of façade-integrated photovoltaic/water-heating system. Appl Therm Eng 27:37–45. doi:10.1016/j.applthermaleng.2006.05.015

Chow T-T, Qiu Z, Li C (2009) Potential application of "see-through" solar cells in ventilated glazing in Hong Kong. Sol Energy Mater Sol Cells 93:230–238. doi:10.1016/j.solmat.2008.10.002

Chow T, Li C, Lin Z (2010) Innovative solar windows for cooling-demand climate. Sol Energy Mater Sol Cells 94:212–220. doi:10.1016/j.solmat.2009.09.004

COAATGU (2015) Precio de la Construcción Centro (WWW Document). www.preciocentro.com. Accessed 20 Mar 2015

Corgnati SP, Perino M, Serra V (2007) Experimental assessment of the performance of an active transparent façade during actual operating conditions. Sol Energy 81:993–1013. doi:10.1016/j.solener.2006.12.004

Crawley DB, Lawrie LK, Winkelmann FC, Buhl WF, Huang YJ, Pedersen CO, Strand RK, Liesen RJ, Fisher DE, Witte MJ, Glazer J (2001) EnergyPlus: creating a new-generation building energy simulation program. Energy Build 33:319–331

Creara (2015) PV grid parity monitor—commercial sector

CTE (2013) Código Técnico de la Edificación. Boletín Oficial del Estado, BOE 12/09/13, Madrid, Spain

CYPE Ingenieros (2015) Generador de precios de la construcción

de Boer BJ, van Helden WGJ (2001) PV MOBI, PV modules optimised for building integration. In: 9th international conference on solar energy in high latitudes. Northsun, Leiden, The Netherlands

Denton JC, Rakopoulos CD, Tsatsaronis G, Frangopoulos CA, Stegou-Sagia A, Antonopoulos K, Angelopoulou C, Kotsiovelos G (2007) The impact of glazing on energy consumption and comfort. Energy Convers Manag 48:2844–2852

Designbuilder (2014) Designbuilder—Version 3.2.0.073

Dubois M-C, Blomsterberg Å (2011) Energy saving potential and strategies for electric lighting in future North European, low energy office buildings: a literature review. Energy Build 43: 2572–2582. doi:10.1016/j.enbuild.2011.07.001

Eicker U, Fux V, Infield D, Mei L, Vollmer K (1999) Thermal performance of building integrated ventilated PV facades. Proceedings of the ISES 1999 Solar World

European Commission (2010) Directive 2010/31/EU of the European Parliament and of the Council of 19 May 2010 on the energy performance of buildings. Off J Eur Union L153:13

European Committee for Standardization (2011a) EN 410:2011 glass in building. Determination of luminous and solar characteristics of glazing

European Committee for Standardization (2011b) EN 673:2011 glass in building. Determination of thermal transmittance (U value). Calculation method. EN 6732011

FIVE (2015) Instituto Valenciano de la Edificación (WWW document). www.five.es

Fung TYY, Yang H (2008) Study on thermal performance of semi-transparent building-integrated photovoltaic glazings. Energy Build 40:341–350. doi:10.1016/j.enbuild.2007.03.002

Gan G (2009) Effect of air gap on the performance of building-integrated photovoltaics. Energy 34:913–921. doi:10.1016/j.energy.2009.04.003

German Solar Energy Society (2013) Planning and installing photovoltaic systems. A guide for installers, architects and engineers, 3rd edn. Routledge, London

Gil-Lopez T, Gimenez-Molina C (2013) Influence of double glazing with a circulating water chamber on the thermal energy savings in buildings. Energy Build 56:56–65. doi:10.1016/j.enbuild.2012.10.008

GmbH E (2011) POLIS—solar urban planning—The National state of the art in Germany

Guardo A, Coussirat M, Egusquiza E, Alavedra P, Castilla R (2009) A CFD approach to evaluate the influence of construction and operation parameters on the performance of active transparent façades in mediterranean climates. Energy Build 41:534–542. doi:10.1016/j.enbuild.2008.11.019

Han J, Lu L, Peng J, Yang H (2013) Performance of ventilated double-sided PV façade compared with conventional clear glass façade. Energy Build 56:204–209. doi:10.1016/j.enbuild.2012.08.017

Han J, Lu L, Yang H (2009) Thermal behavior of a novel type see-through glazing system with integrated PV cells. Build Environ 44:2129–2136. doi:10.1016/j.buildenv.2009.03.003

He W, Zhang YX, Sun W, Hou JX, Jiang QY, Ji J (2011) Experimental and numerical investigation on the performance of amorphous silicon photovoltaics window in East China. Build Environ 46:363–369. doi:10.1016/j.buildenv.2010.07.030

Hien WN, Liping W, Chandra AN, Pandey AR, Xiaolin W (2005) Effects of double glazed facade on energy consumption, thermal comfort and condensation for a typical office building in Singapore. Energy Build 37:563–572

IEA-SHC Task 41 (2012a) Solar energy systems in architecture—integration criteria and guidelines

IEA-SHC Task 41 (2012b) Solar design of buildings for architects: review of solar design tools—Subtask B—Methods and Tools for Solar Design

Inanici MN, Demirbilek FN (2000) Thermal performance optimization of building aspect ratio and south window size in five cities having different climatic characteristics of Turkey. Build Environ 35:41–52

Infield D, Eicker U, Fux V, Mei L, Schumacher J (2006) A simplified approach to thermal performance calculation for building integrated mechanically ventilated PV facades. Build Environ 41:893–901. doi:10.1016/j.buildenv.2005.04.010

Iqbal I, Al-Homoud MS (2007) Parametric analysis of alternative energy conservation measures in an office building in hot and humid climate. Build Environ 42:2166–2177
ITEC (2015) Instituto de Tecnología de la Construcción (WWW Document). http://itec.es/. Accessed 20 Mar 2015
Kapsis K, Athienitis AK (2015) A study of the potential benefits of semi-transparent photovoltaics in commercial buildings. Sol Energy 115:120–132. doi:10.1016/j.solener.2015.02.016
Köppen W (1936) Das geographische system der klimate. Borntrager Verlag, Berlin
Kottek M, Grieser J, Beck C, Rudolf B, Rubel F (2006) World Map of the Köppen-Geiger climate classification updated. Meteorol Zeitschrift 15:259–263. doi:10.1127/0941-2948/2006/0130
Kreith F, Goswami DY (2004) The CRC handbook of mechanical engineering, 2nd edn. CRC Press, Boca Raton
LBNL-CGDB (2014) Complex glazing database (WWW document). http://windowoptics.lbl.gov/data/cgdb. Accessed 14 May 2014
LBNL-COMFEN (2014) COMFEN—version 4.1.25 (WWW document). http://windows.lbl.gov/software/comfen/comfen.html. Accessed 14 May 2014
LBNL-IGDB (2014) International glazing database (WWW document). http://windowoptics.lbl.gov/data/igdb. Accessed 14 May 2014
LBNL-OPTICS (2014) Optics—version 5.1 (WWW document). http://windows.lbl.gov/software/Optics/optics.html. Accessed 14 May 2014
LBNL-WINDOW (2014) Window—version 6.3.26.0 (WWW document). http://windows.lbl.gov/software/window/window.html. Accessed 14 May 2014
Li DHW, Lam TNT, Chan WWH, Mak AHL (2009) Energy and cost analysis of semi-transparent photovoltaic in office buildings. Appl Energy 86:722–729. doi:10.1016/j.apenergy.2008.08.009
Li DHW, Yang L, Lam JC (2013) Zero energy buildings and sustainable development implications—a review. Energy 54:1–10. doi:10.1016/j.energy.2013.01.070
Lu L, Law KM (2013) Overall energy performance of semi-transparent single-glazed photovoltaic (PV) window for a typical office in Hong Kong. Renew Energy 49:250–254. doi:10.1016/j.renene.2012.01.021
Mardaljevic J, Heschong L, Lee E (2009) Daylight metrics and energy savings. Light Res Technol 41:261–283. doi:10.1177/1477153509339703
Martín Chivelet N, Fernandez Solla I (2007) La Envolvente fotovoltaica en la arquitectura: criterios de diseño y aplicaciones. Editorial Reverté
Miyazaki T, Akisawa A, Kashiwagi T (2005) Energy savings of office buildings by the use of semi-transparent solar cells for windows. Renew Energy 30:281–304. doi:10.1016/j.renene.2004.05.010
Montoro DF, Vanbuggenhout P, Ciesielska J (2011) Building integrated photovoltaics: an overview of the existing products and their fields of application
Nabil A, Mardaljevic J (2006) Useful daylight illuminances: a replacement for daylight factors. Energy Build 38:905–913. doi:10.1016/j.enbuild.2006.03.013
Ng PK, Mithraratne N, Kua HW (2013) Energy analysis of semi-transparent BIPV in Singapore buildings. Energy Build 66:274–281. doi:10.1016/j.enbuild.2013.07.029
Oliver M, Jackson T (2001) Energy and economic evaluation of building-integrated photovoltaics. Energy 26:431–439. doi:10.1016/S0360-5442(01)00009-3
Olivieri L (2015) Integral energy behaviour of photovoltaic semi-transparent glazing elements for building integration. Ph.D thesis, Universidad Politécnica de Madrid, Madrid, Spain. http://oa.upm.es/37242/
Olivieri L, Caamaño-Martín E, Moralejo-Vázquez FJ, Martín-Chivelet N, Olivieri F, Neila-Gonzalez FJ (2014a) Energy saving potential of semi-transparent photovoltaic elements for building integration. Energy 76:572–583. doi:10.1016/j.energy.2014.08.054
Olivieri L, Caamaño-Martin E, Olivieri F, Neila J (2014b) Integral energy performance characterization of semi-transparent photovoltaic elements for building integration under real operation conditions. Energy Build 68:280–291. doi:10.1016/j.enbuild.2013.09.035

Olivieri L, Frontini F, Polo-López C, Pahud D, Caamaño-Martín E (2015) G-value indoor characterization of semi-transparent photovoltaic elements for building integration: new equipment and methodology. Energy Build 101:84–94. doi:10.1016/j.enbuild.2015.04.056

Pagliaro M, Ciriminna R, Palmisano G (2010) BIPV: merging the photovoltaic with the construction industry. Prog Photovoltaics Res Appl 18:61–72. doi:10.1002/pip.920

Park KE, Kang GH, Kim HI, Yu GJ, Kim JT (2010) Analysis of thermal and electrical performance of semi-transparent photovoltaic (PV) module. Energy 35:2681–2687. doi:10.1016/j.energy.2009.07.019

Peng J, Lu L, Yang H (2013) An experimental study of the thermal performance of a novel photovoltaic double-skin facade in Hong Kong. Sol Energy 97:293–304. doi:10.1016/j.solener.2013.08.031

Pérez-Lombard L, Ortiz J, González R, Maestre IR (2009) A review of benchmarking, rating and labelling concepts within the framework of building energy certification schemes. Energy Build 41:272–278. doi:10.1016/j.enbuild.2008.10.004

Petter Jelle B, Breivik C, Drolsum Røkenes H (2012) Building integrated photovoltaic products: a state-of-the-art review and future research opportunities. Sol Energy Mater Sol Cells 100:69–96. doi:10.1016/j.solmat.2011.12.016

Photon International (2014a) Photon international solar modules database (WWW document). http://www.photon.info/photon_site_db_solarmodule_en.photon. Accessed 14 May 2014

Photon International (2014b) Photon international solar inverters database (WWW document). http://www.photon.info/photon_site_db_wechselrichter_en.photon. Accessed 14 May 2014

PVsyst (2014) PVsyst—version 5.55 (WWW document). http://www.pvsyst.com. Accessed 14 May 2014

Quesada G, Rousse D, Dutil Y, Badache M, Hallé S (2012) A comprehensive review of solar facades. Transparent and translucent solar facades. Renew Sustain Energy Rev 16:2643–2651. doi:10.1016/j.rser.2012.02.059

Radhi H (2010) Energy analysis of façade-integrated photovoltaic systems applied to UAE commercial buildings. Sol Energy 84:2009–2021. doi:10.1016/j.solener.2010.10.002

Reinhart CF, Wienold J (2011) The daylighting dashboard—a simulation-based design analysis for daylit spaces. Build Environ 46:386–396. doi:10.1016/j.buildenv.2010.08.001

Roberts S, Guariento N (2009) Building integrated photovoltaics: a handbook. Birkhauser Verlag AG, Basel

Robinson L, Athienitis A (2009) Design methodology for optimization of electricity generation and daylight utilization for façade with semi-transparent photovoltaics. In: Proceedings of building simulation 2009. Glasgow, Scotland, pp. 811–818

Song J-H, An Y-S, Kim S-G, Lee S-J, Yoon J-H, Choung Y-K (2008) Power output analysis of transparent thin-film module in building integrated photovoltaic system (BIPV). Energy Build 40:2067–2075. doi:10.1016/j.enbuild.2008.05.013

UBS (2014.) Global utilities, autos & chemicals. Will solar, batteries and electric cars re-shape the electricity system?

Van Dijk HAL (2001a) The European project REVIS, daylighting products with redirecting visual properties. In: Proceedings of NorthSun conference

Van Dijk HAL (2001b) Reference office for thermal, solar and lighting calculations. Performance of solar facade components. IEA-SHC Tak27, IEA SHC Task27. Delft, The Netherlands

Voss K, Musall E (2012) Net zero energy buildings—international projects of carbon neutrality in buildings. Detail Green Books

Wang Y, Tian W, Ren J, Zhu L, Wang Q (2006) Influence of a building's integrated-photovoltaics on heating and cooling loads. Appl Energy 83:989–1003. doi:10.1016/j.apenergy.2005.10.002

Wienold J, Christoffersen J (2006) Evaluation methods and development of a new glare prediction model for daylight environments with the use of CCD cameras. Energy Build 38:743–757. doi:10.1016/j.enbuild.2006.03.017

Wong PW, Shimoda Y, Nonaka M, Inoue M, Mizuno M (2008) Semi-transparent PV: thermal performance, power generation, daylight modelling and energy saving potential in a residential application. Renew Energy 33:1024–1036. doi:10.1016/j.renene.2007.06.016

Chapter 11
Organic Photovoltaics for Energy Efficiency in Buildings

Cristina Cornaro and Aldo Di Carlo

Abstract Organic photovoltaics is now reaching a more mature stage and new applications are emerging to its direct use as active elements into buildings. This chapter illustrates the more recent developments of organic photovoltaic technology focussing on the description of semitransparent devices integrated into glazing systems for energy efficiency in buildings. It describes briefly the fundamental functioning principles of Hybrid and Organic (HOPV) devices that includes Dye Sensitized Solar Cells (DSC), polymeric cells as well as new emerging technologies, followed by a description of the actual studies carried on building integrated HOPV. Last section presents some showcases of HOPV integrated into buildings.

11.1 Introduction

Organic photovoltaics that includes dye-sensitized solar cells (DSC) and polymeric/small-molecule solar cells is occupying an important role in renewable energy research due to their low-cost manufacturing processes and their specific features. In particular, these devices appear very well suited for building integration applications with the aim of improving energy efficiency in buildings. Due to their intrinsic characteristic of transparency, colour tuning and, especially for DSC, their preferred manufacturing directly on glass substrates, the major application in buildings regards glazing systems. Glass can be considered one of the key materials in building architecture especially in recent years due to the great improvement achieved by the glass construction technology. Many architects consider not only glass as their preferred construction material for large facades and skylights but also for innovative architectonic elements as, for example, experienced by Frank Gehry in the magnificent building of the "Fondation Louis Vuitton" in Paris. From the point of view of the buildings occupants, glazing systems present many benefits but

C. Cornaro (✉) · A. Di Carlo
Center for Hybrid and Organic Solar Energy, University of Rome Tor Vergata, Roma, Italy
e-mail: cornaro@uniroma2.it

F. Pacheco Torgal et al. (eds.), *Nano and Biotech Based Materials for Energy Building Efficiency*, DOI 10.1007/978-3-319-27505-5_11

also some drawbacks. Daylight is proved to be preferable to perform visual tasks inside buildings contributing to improve visual and mental comfort. In addition, it reduces the artificial lighting demand during daytime improving lighting energy saving. However, the extensive use of glass in facades can increase heating loads in summertime and thermal losses in wintertime reducing thermal comfort and increasing cooling and heating demand of the building. Specific thermal and optical parameters are used to identify the effect of glazing on energy use in buildings. They are the *U*-value and solar heat gain coefficient (SHGC) for thermal aspects and the visible light transmittance (VLT) for optical ones. Controlling these parameters, it is possible to minimize heating and cooling loads and electrical lighting costs.

With the recent increment in the use of renewable photovoltaic energy, building-integrated photovoltaic (BIPV) has been developed rapidly. In this case, the photovoltaic module becomes part of the building envelope and can satisfy the double need of electricity production and structural functionality. In particular, when PV technology is integrated into glazing systems, it is possible to talk about building-integrated photovoltaic windows (BIPW). Semitransparent BIPW can reduce solar heat gain promoting shading with the advantage of producing electricity. Various PV technologies can be used for the implementation in glazing systems, and an extensive and complete review on the subject has been published very recently by Skandalos and Karamanis (2015). Consolidated PV materials such as crystalline silicon, named first-generation PV, and thin films (amorphous silicon, CIGS, and CdTe), known also as second-generation PV, have been already investigated for BIPW. For example, Park et al. (2010) presented an experimental study on the thermal and electrical performance of a system made of opaque polycrystalline PV cells laminated into glass and spaced so that some portion of light passed through the glass area. In general, one of the drawbacks of this arrangement is that it can drastically reduce the amount of daylight gained by the indoor environment depending on the cell spacing and it also compromises the external view. This device can reach quite high electrical efficiency due to the PV material used, but however high temperature of the glass can be a concern. Indeed, it is well known that polycrystalline silicon decreases its efficiency as temperature increases. Moreover, as also pointed out by the authors, the high temperatures reached by the system could increase heat gains of the room. Another related study was conducted by de Boer and van Helden (2001). They modelled the cooling and heating demand as well as the daylight distribution inside an office room that incorporates semitransparent silicon PV glazing in Madrid. In the designing of these devices, a good compromise has to be reached between the amount of daylight entering into the interior spaces, the solar heat gain and the electricity generation. Thin films, on the contrary, reduce the issues related to visual obstruction and daylight penetration maintaining acceptable electrical efficiency. This is because their transparency can be conveniently modulated uniformly over the glass. Various studies can be found in the literature regarding the use of such kind of BIPW. Miyazaki et al. (2005) analysed the effects of transmittance percentage of translucent type solar cell windows on daylighting utilization, electricity production, heating load, and cooling load of an office building. Chae et al. (2014) also

evaluated the potential benefits of using BIPW equipped with amorphous silicon semitransparent material in different climatic conditions. Thin films are promising materials for BIPW because of their homogeneous appearance even if the increase of transparency can deeply reduce electricity production.

First- and second-generation photovoltaics suffer from some drawbacks such as high cost, long paybacks, scarcity of materials, and low working capability in cloudy conditions and shade. For these reasons, third-generation devices appeared in the research stage to overcome these problems. Third-generation PV includes DSC and polymeric solar cells. These devices gained quite great interest on the PV scene principally due to their low cost and simple manufacturing process. Despite these advantages, they generally suffer from low efficiency and short-term outdoor stability compared to the other two generation devices (Fakharuddin et al. 2014). However, many improvements have been achieved in recent years so that they have been recently considered also good candidates for BIPW. In this chapter, we will examine these new technologies and we will try to give a perspective on the use of these devices for energy efficiency in buildings. The term hybrid (organic/inorganic) and organic photovoltaic (HOPV) will be used to identify both dye-sensitized and polymeric/small-molecule solar cells. In Sect. 11.2, a synthetic overview of the functioning principles of these devices will be given, while in Sect. 11.3 their performance related to the thermal, visual, and electric aspects will be described. Section 11.4 will be more focused on the application of HOPV in buildings principally as BIPW, paying attention also to the device behaviour in outdoor conditions, and finally,

11.2 Organic Photovoltaics Functioning Principles

11.2.1 Overview

In recent years, the progress in organic and hybrid photovoltaic has been remarkable. This emerging technology is based on the combination of a new class of a solution-processed materials and large area, high-volume deposition printing techniques able to reduce the manufacture cost of this PV technology and to open new application scenarios. DSC, polymeric solar cells, small molecule solar cells, and perovskite solar cells are all different flavours of HOPV technology.

HOPV is still considered as “emerging PV” class, and their increasing efficiency trend during the last two decades, as reported in the National Renewable Energy Laboratory chart (NREL 2015), underlines the strong efforts made to make these solar cells competitive with the other well-established inorganic technologies. In this respect, a breakthrough discovery has profoundly changed the HOPV field, namely the use of organometal halide perovskite for fabrication solution-processed photovoltaic solar cells (PSC). This new technology overcomed 20 % of certified efficiency in less than 4 years (NREL 2015), making these solar cells competitive with conventional silicon technologies.

DSCs, polymer solar cell, and small molecule-based solar cells are nearer to enter into the global market thanks to their low environmental impact, low cost, and their promising stability. Nowadays, several companies such as GCEL, 3GSolar, and Fujikura started the industrialization of DSC modules. Konarka Technologies (now Belectric) started production of polymer–fullerene solar cells (Belectric 2015), while, in January 2013, Heliatek (Heliatek 2015) announced a record breaking 12.0 % cell efficiency for its small molecule-based solar cells realized by means of high-vacuum deposition technique. The feasibility of a commercialization of these technologies requires an integrated overview that comprises efficiency, stability, costs, and environmental impact.

Regarding the costs, it is really difficult to forecast the impact of facilities, materials, and energy on the final product price, due to the larger differences between each organic and hybrid technologies. Mulligan et al. (2014) estimated a cost of about $\$7.85 \pm 2.35/m^2$ for the large-scale manufacture of OPV flexible modules incorporating bulk scale manufacture of all of the component materials, which is competitive with the typical values of the conventional flexible silicon or inorganic thin-film technologies.

The potential low cost of the new organic and hybrid photovoltaic technologies, even known as third-generation photovoltaic, is also accompanied by their versatility in term of tuning of colour and shape, transparency, flexibility, and roll-to-roll production. That makes these technologies very attractive and suitable for innovative applications such as the building integration (i.e. for photovoltaic windows), the consumer electronics (i.e. mobile phone or photovoltaic clothes), and even medical application as reported by Zygmanski et al. (2015).

Since the number of the application fields is so huge and the real working conditions for a solar cell are countless and so disparate, the chemical and electrical stability remains a key point to make this technology really attractive for the market. Each type of hybrid and organic solar cell in fact suffers typical degradation mechanisms under real working conditions that need enormous efforts in designing stable chemical compounds and solar cell architectures, in developing materials and procedures for the encapsulation of the active devices against the external moisture attack, and in defining standard ageing protocol to unequivocally certify the durability of each technology.

A consensus on stability testing protocols for organic photovoltaic materials and devices has been reached in 2011 as conclusions of the first 3 years of the international summit on OPV stability (ISOS). The authors agreed on some different categories of test protocols, in particular, dark, outdoor, simulated light and stress testing and thermal cycling, each of these subdivided in three levels: basic (Level 1), intermediate (Level 2) and advanced (Level 3), as detailed by Reese et al. (2011). The goal of this set of recommended procedures is to increase the amount of data that can readily be compared between different laboratories.

In the following, we will review the main aspects of HOPV technologies with special attention to the possible applications in BIPV.

11.2.2 Polymer Solar Cells and Modules

The polymeric solar cell structure, shown in Fig. 11.1, consists in an active organic polymer (of a mix o two polymers) sandwiched between two selective contacts where at least one of the two is transparent.

The working principle of the cell can be divided in four consecutive steps: (1) photoexcitation of electron and hole charges, (2) charge separation, (3) charge transport, and (4) charge collection at the contacts. The photoexcitation, contrary to the inorganic semiconductor, creates a strongly bonded electron–hole exciton which cannot be dissociated with the thermal energy. To enhance exciton dissociation before electron and hole recombine, an interface between two different polymers is required. This is obtained by creating a double layer formed by electron donor and an electron acceptor polymer. To increase the optical absorption of the active region and, at the same time, to reduce the e-h recombinations due to the short lifetime of the exciton, a three-dimensional blend of donor–acceptor polymers is used, forming the so-called *bulk heterojunction* (*BHJ*), as shown in Fig. 11.2 (Halls et al. 1995; Yu et al. 1995).

In the BHJ, the exciton formed after the photon absorption can easily find a donor/acceptor interface and consequently can be dissociated into the electron and hole before recombining.

The reference donor polymer used in the literature is the poly-(3-hexylthiophene) (P3HT). P3HT is characterized by high crystallinity, high hole mobility ($10^{-4} \div 10^{-2}$ cm^2/Vs) in its *regio-regular* form (Sirringhaus et al. 1999) and high absorption in the red spectral region ($E_{gap} = 1.68$ eV and $\lambda_{abs} < 650$ nm). Furthermore, the typical organic acceptor is *phenyl-C61-butyric acid methyl ester* (PCBM), a fullerene derivate. PCBM is characterized by good solubility (i.e. in chlorinated solvents), high electron mobility (close to pure C60), and an absorption spectrum in the UV ($\lambda_{abs} < 400$ nm). P3HT in the blend P3HT:PCBM is the layer that absorbs the greater fraction of incident visible light (Cook et al. 2009; Ding et al. 2008).

Organic layer could also be formed by small molecules which can sublimate onto the substrate by vacuum processes (Lin et al. 2012). The main advantages of

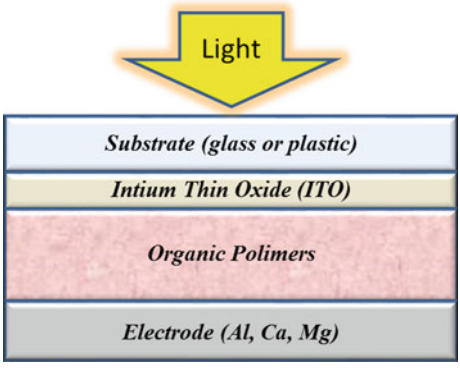

Fig. 11.1 Schematic drawing of the polymeric solar cells

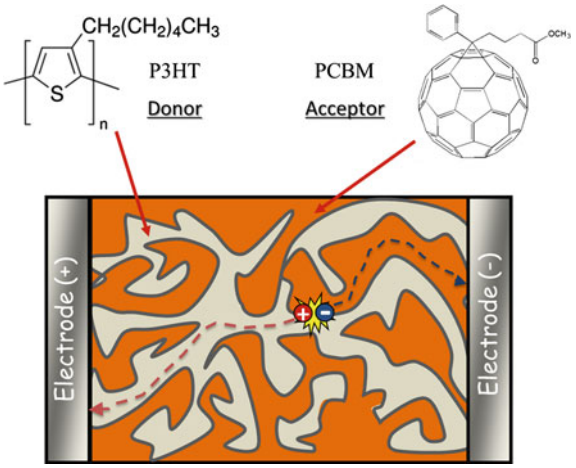

Fig. 11.2 Working principle of the bulk heterojunction polymeric solar cells

vacuum sublimation consist in the high purity of the deposited film that does not contain any remaining solvent and a controllable deposition of multi-layer structures by consecutive evaporations. Thus, small molecule-based photovoltaic technology seems to be the most promising in term of future feasibility perspective, easier to control in term of morphology, and more repeatable in term of performance. Furthermore, although vacuum processing is supposed to be more cost-intensive, considering initial investments, these costs should not be an issue for a high-throughput technology, where the main costs are given by the operation costs of the tools and the prices of the required raw material.

The conventional bulk heterojunction solar cell is the ITO/PEDOT:PSS/P3HT:PCBM/Al architecture, where ITO (indium-doped tin oxide) is the anode, poly (3,4-ethylenedioxythiophene) polystyrene sulfonate (PEDOT:PSS) is the hole-collecting layer, the blend P3HT:PCBM is the active layer, and aluminium (Al) is the top metallic electrode.

Although the conventional solar cell represented the most promising structure for several years (thanks to ease in fabrication), several barriers in the performance optimization (i.e. the stability) slowed the research and industrial developments. Mainly, the degradation mechanisms of the materials occur at the interfaces, i.e. ITO/PEDOT:PSS and P3HT:PCBM/Al, due to inevitable chemical reactions that limit strongly the stability of the solar cell. In particular, PEDOT:PSS is the most suitable hole-collecting layer (work function value, water solubility, etc.), but it is also a strongly acidic (pH $\sim$ 1) and hygroscopic compound (De Jong et al. 2000; Jørgensen et al. 2008). The oxygen exposure affects the PEDOT:PSS, disrupting the molecular structure. In particular, PSS (present in excess amount compared with PEDOT) diffuses to other parts of the device and can react with other components of the devices, i.e. the resistance of the PEDOT:PSS/active layer increases (Kawano et al. 2006). Recently, several promising materials alternative to the PEDOT:PSS have been studied, such as the vanadium (V_2O_5), molybdenum (MoO_3), and tungsten oxides (WO_X).

Fig. 11.3 Polymeric solar modules (Konarka)

Nowadays, organic solar cells based on conjugated polymer blend have achieved high performance. The P3HT:PCBM-based solar cells have achieved an efficiency up to 5 % (Huang et al. 2015). However, in last years, inverted structure solar cells and tandem architecture broke the η of 9 %. In particular, Yong Cao's research team of South China University Technology has published on Nature Photonics bulk heterojunction solar cells based on promising conjugated and electron donor polymers, as *poly-[(9,9-bis(3′-(N,N-dimethylamino)propyl)-2,7-fluorene)-alt-2,7-(9,9-ioctylfluorene)]* (PFN) and *thieno[3,4-b]thiophene/benzodithiophene* (PBT7), with conversion efficiency of 9.2 % (He et al. 2012). The state of art for tandem solar cell is achieved by Yang Yang's research group of UCLA in collaboration with Sumitomo Chemical in Japan that certified a power conversion efficiency of 10.6 ± 0.3 % at the National Renewable Energy Laboratory (NREL) (Dou et al. 2012). The tandem architecture is based on a spectrally matched low band gap, *the poly(2,6′-4,8-di(5-ethylhexylthienyl)benzo(1,2-b;3,4-b]dithiophene-alt-5-dibutyloctyl-3,6-bis (5-bromothiophen-2-yl)pyrrolo(3,4-c)pyrrole-1,4-dione)* (PBDTT-DPP), with conventional donor polymer, as P3HT (Dou et al. 2012). As far as large area devices (Fig. 11.3), a module efficiency of 5.5 % on a 16 cm^2 aperture area was achieved by collaboration between Imec and Solvay and certificated by Newport. In order to allow technology transfer from laboratory investigation to large area production, recent investigated deposition techniques are focused on roll-to-roll systems (Krebs 2009).

11.2.3 Dye-Sensitized Solar Cells and Modules

DSC (Kalyanasundaram et al. 2010) represents a class of solution process photovoltaic technology that able to combine aesthetical aspect, colour and transparency tuning, and superior response in low-light conditions which make them very suitable for architectonic integration (Yoon et al. 2011) and indoor use (Freunek and

Reindl 2013a, b). DSCs are photoelectrochemical devices which mimic very closely the photosynthetic system of plants. The active part of the cell is represented by a mesoporous semiconductor oxide (typically TiO_2) made of interconnected nanoparticles, a layer of sensitizing dye chemisorbed onto the oxide semiconductor surface, an electrolyte where both mesoporous oxide and dye are immersed, and a front-and-back electrode. The function of the sensitizer is to absorb the light and generate the electrical charge: light excites an electron from an occupied to an empty molecular orbital, and the electron is transferred from the excited state to the conduction band of the semiconductor. Several dyes have been considered as sensitizer for DSC, namely metalorganic molecule, organic molecules, and natural pigments (Calogero et al. 2015; Li and Diau 2012); nevertheless, the most studied dyes are based on Ru-complexes (Nazeeruddin et al. 1993, 2001) which also produced the largest certified efficiencies of 11.9 % (NREL 2015; Hinsch et al. 2013) and noticeable long-term stabilities (Hinsch et al. 2013).

The electron lost by the photoexcited dyes is regenerated via a REDOX process with the electrolyte. I^-/I_3^- is the typical redox couple used in the electrolyte which, if on the one hand has almost ideal kinetic properties, on the other hand has a considerable drawbacks (Gregg et al. 2001): 1) it is corrosive against the vast majority of metals and requires a Pt catalysts at the back electrode. For this reason, cobalt-based electrolyte has been considered (Elliott et al. 2005).

The DSC fabrication typically employs printing technology (Mariani et al. 2015). This makes the fabrication process low cost and easy to implement. Among the different techniques, we find (a) serigraphy (screen printing), (b) spray coating, (c) blade coating, and (d) inkjet printing. A great advantage of screen printing and spray coating resides in the fact that these are additive processes, which allow depositing only the needed amount of material and up to 90 % savings with respect to the other methods, also reducing impact on the environment. Furthermore, these methods are compatible with glass substrates and plastic roll-to-roll production methods, with further cost reduction with respect to silicon which is a rigid and fragile material. Scanning techniques are easily extensible to large area panel production, leading to lower production costs, integration, and installation for square metre. As opposed to silicon, the material processes for device realization may not need high temperatures, making it compatible with plastic substrates such as PEN or PET, with further advantages in terms of costs, integration over existing surfaces, and assembly (Zardetto et al. 2013; Mincuzzi et al. 2014).

As already discussed, DSC design can be optimized for specific architectonic requirements. In particular, colour and transparency can be tuned to achieve an optimal building integration of the DSC. Transparency tuning can be obtained by varying the oxide thickness, dye attachment, and thickness of the cell. Figure 11.4a shows (Tagliaferro et al. 2013) a typical plot of the transparency versus efficiency of DSCs realized by varying the TiO_2 thickness and dipping time into the dye (see Fig. 11.4b) for two different dyes. The red dye is the N719 molecule, while the orange dye is the Ru505 (Tagliaferro et al. 2013). The transparency of the cell can be larger than 30 % still keeping the efficiency around 5 %. This makes DSC one of the most promising PV technologies for building-integrated PV.

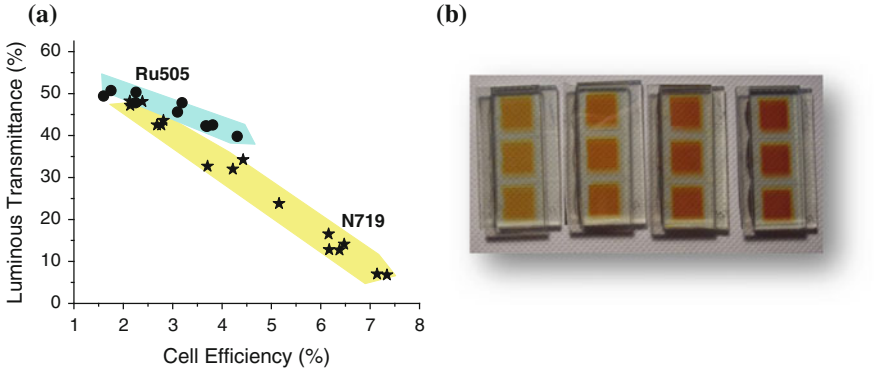

Fig. 11.4 **a** Luminous transmittance versus efficiency plot for DSC sensitized with a *red dye* (N719) and an *orange dye* (Ru505); **b** DSC photoanodes realized by varying the TiO_2 thickness and the dipping time with the *orange dye*.

Several research centres and companies, such as Dyesol, Aisin Seki, Fujikura, Solaronix, Dyepower, Dongjin Semichem, and Sony and Sharp, have undertaken DSC scaling up activities up to module and panel level (Fakharuddin et al. 2014). Gcell is already present on the market with a flexible DSC panel which has been applied to several consumer devices (Gcell 2015). Stability of the modules can be improved by proper sealing technologies and the right combination of dyes and electrolytes. To this end, ionic liquids and high-boiling solvents have been demonstrated to stabilize the cell characteristics (Jiang et al. 2013; Perganti et al. 2015).

Several procedures have been proposed to scale the solar cell from laboratory dimension to module size. In fact, due to the resistance of the transparent oxide conductor (TCO) which is of the order of 10 Ω/γ, enlarging the solar cell will induce a sever loss of efficiency. For this reason, modules are comprised of small width cells connected in a series or parallel way. Different architectures may be used to this end, namely W-connection, Z-connection, and monolithic and parallel connection (Calogero et al. 2015). A typical example of series-connected (*Z*-type) semitransparent module is shown in Fig. 11.5 with a panel of seven modules connected together. The module has a 20 cm × 30 cm with a transparency of 30 % and an efficiency on active area exceeding 4 % (Barolo et al. 2014).

11.2.4 Recent Developments

A new promising class of light harvesting materials, namely the hybrid organic halide-based perovskites, have been recently employed to realize high-efficiency photovoltaic solar cells (PSCs) (Kojima et al. 2009; Lee et al. 2012; Hui-Seon et al. 2012). This kind of (poly) crystalline material shows broad absorption in the visible

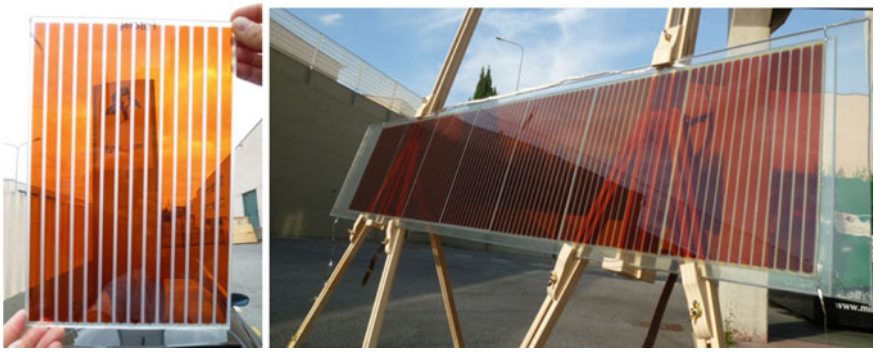

Fig. 11.5 On the *left* a semitransparent DSC module (size 20 cm x 30 cm) formed by 14 cells connected in series with the *Z*-type architecture. on the *right* DSC panel realized with 7 modules connected in series

spectrum, good electron and hole conductivities (Stranks et al. 2013; Xing et al. 2013), and high open-circuit voltages of photovoltaic devices. methylammonium lead iodite ($CH_3NH_3PbI_3$) (MAPI) perovskite is typically used as absorbing layer (direct energy gap down to 1.55 eV as reported by Ball et al. 2013). The energy gap can be tuned by mixing the Br and I in $CH_3NH_3Pb(I_{1-x}Br_x)_3$ perovskites (Noh et al. 2013) to cover almost the entire visible spectrum, enabling the realization of colourful solar cells.

Perovskite solar cells are usually fabricated with a *P-I-N* structure (Heo 2013) where *I* is the perovskite layer, *P* is a hole-transporting layer (HTL) such as Spiro-OMeTAD, PTAA, PEDOT, and P3HT (Di Giacomo et al. 2014), and *N* is the electron-transporting layer (ETL) such as TiO_2, ZnO, and PCBM. Moreover, PSC can also be realized in the solid-state DSC configuration where a thin layer (200–300 nm) of mesoporous TiO_2 is used as scaffold for perovskite crystallization.

Several techniques have been developed to grow perovskite thin films (Casaluci 2015) such as (i) direct deposition of the perovskite precursor solution (one-step solution deposition) on mesoscopic oxide (Hui-Seon et al. 2012; Kojima et al. 2009; Wang et al. 2014; Jeon et al. 2014; Lee et al. 2012a, b) or planar oxide (Eperon et al. 2014; Conings et al. 2014; Liu and Kelly 2014) and (ii) sequential deposition of PbI_2 and CH_3NH_3I (two step deposition) (Wu et al. 2014; Burschka et al. 2013; Bi et al. 2013; Chen et al. 2014; Casaluci 2015). Other strategies to produce the active layer are based on thermal sublimation of MAPI in vacuum (Liu and Kelly 2014; Hu et al. 2014).

For small area devices, a power conversion efficiency (PCE) of 18.4 % has been reached using a bilayer structure consisting of 85 % formamidinium lead iodide (FAPbI3) and 15 % of Methylammonium lead bromide (MAPbBr3) (Jeon et al. 2015), while the record efficiency has been certified to be 20.1 % by the National Renewable Energy Laboratory (NREL 2015).

Similarly, the development of large active area prototypes (Matteocci et al. 2014a, b) has evolved with an equal impressive pace, achieving η = 13 %

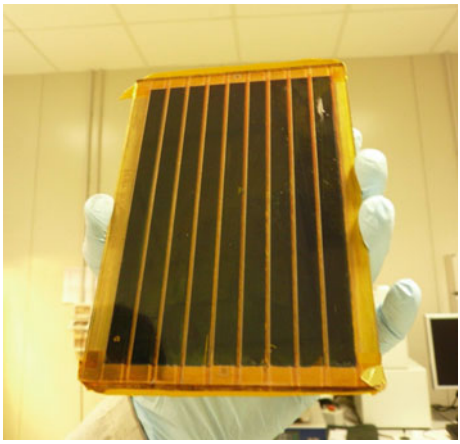

Fig. 11.6 Perovskite module realized at CHOSE. Active area of 100 cm^2

(Matteocci et al. 2014b) on 10 cm^2 and η = 9.6 % on an even larger active area (100 cm^2) (Razza et al. 2015a, b) (Fig. 11.6).

Due to the tunability of optical absorption, PSC can be considered for BIPV applications. Several semitransparent and coloured PSCs have been already demonstrated (Noh et al. 2013; Eperon et al. 2014; Roldán-Carmona et al. 2014; Zhang et al. 2015; Heo et al. 2015), and architectural integrations have been discussed. This technology may integrate the advantage of dye solar cells for what concern the aesthetical aspect and the efficiency of silicon PV. Nevertheless, the problems associated with the use of lead in a large PV manufactures together with the limited stability of the actual devices do not allow for an easy forecast of the penetration of this technology in the PV market.

11.3 Performance Assessment of Organic Photovoltaics

11.3.1 Overview

There are many factors that affect the good performance of BIPW, and their study is very important to understand the suitability of consolidated and emerging technologies for this application. First- and second-generation PV has been already extensively studied, while for organic photovoltaic, few works can be found in the literature, more related to DSC devices and less to polymeric ones. The main aspects of windows regard their visual characteristics that include transparency and their thermal behaviour that involves the study of thermal properties. Moreover, if PV material is used, also their electrical performance contributes to evaluate the overall performance of the system.

In general, all these factors define the energy performance of a semitransparent PV window so that it is possible to evidence several criteria to take into account for a complete characterization.

These are as follows:

- Optical and thermal properties of the window;
- Electrical properties of the PV material;
- Location of the building;
- Costs and environmental impact.

It has also to be considered that for these organic technologies, degradation is a main issue and also this factor should be taken into account to avoid transparency and electrical deterioration.

In the following paragraphs, the performance of organic photovoltaic under these various aspects will be examined focusing on the small amount of literature available.

11.3.2 Thermal Performance

Thermal performance of glazing systems is characterized by two important parameters: U-value that is the thermal transmittance of the system, evaluated knowing the materials' thermal conductivity and thickness and the solar heat gain coefficient (SHGC) that is defined as the amount of heat gained by the room due to solar irradiance transmission through the glazing. Many methods are available to evaluate these parameters such as test chambers, calorimetric hot boxes, and novel methods (Cornaro et al. 2015a). They use both indoor and outdoor measurements and provide absolute measurements or comparative analysis among different devices. It has to be noted that SHGC for BIPW depends on the electricity generation of the PV material since part of solar energy is converted into electricity. For this reason, a correct evaluation foresees that the system should generate electricity during the test. Unfortunately, very few works are available regarding organic photovoltaic, and more studies are desirable. Kang et al. in 2013 studied the optical and thermal characteristics of different kinds of DSC cells varying their colour (red or green) and TiO_2 thickness. First of all, they measured the optical properties of the samples using an optical spectrum analyser, and then, they used these parameters as input for the WINDOW 6.0 software that is able to evaluate both U-value and SHGC. They then compared these parameters with the standard parameters evaluated for a typical clear double glazing system. A reduction of about 60 % in SHGC was found compared to a typical double-layered clear glass. This result is particularly important to reduce cooling loads especially in office buildings at various locations in the world. Also, the TiO_2 thickness and colours play an important role demonstrating that red type with smaller thickness is more suitable for taking in more light, while the green type with higher thickness, having the lowest SHGC, is more suitable for reducing the cooling load of buildings. These results were

obtained considering DSC not generating electricity. More recently, Kapsis and Athienis (2015) built a model of BIPW using three different PV technologies: silicon, amorphous silicon, and organic (polymeric). They implemented three different models for daylight, thermal, and electrical aspects, and they evaluated *U*-value and SHGC using WINDOW and THERM softwares. In this case, the electrical generation was taken into account in the SHGC evaluation. The model was used to compare the performance of different technologies, and the results will be reported in the next paragraph.

11.3.3 Optical Performance

Optical characteristics of windows are related to visual comfort of the occupants and also on heating and cooling loads of the building through the SHGC. When using organic photovoltaic, the degree of transparency of the window can be modified. This parameter affects the electrical efficiency of the PV devices and also the above-mentioned aspects. Kang et al. (2013) evaluated the optical performance of different types of DSC, varying their colour (red and green) and thickness of TiO_2 layer. They measured absorbance, reflectance, and transmittance of the samples using a spectrometer. They reported that in the visible light spectrum, the transmittance varies according to the dye thickness. The red-type 1T (smaller thickness) has the highest transmittance of approximately 33 %, while the green type with higher thickness shows the lowest transmittance of 8 %. Reflectance is maintained at almost 10 % in the range between 300 nm and 1500 nm, and it varies with the cell colour; red type reflects slightly more than green type. Absorbance is quite high after 1200 nm, and it is dominant after 1800 nm. More recently, the same authors improved the DSC construction using an encapsulant, and they found an improvement in the average transmittance of approximately 4 % with respect to the previous configuration, mainly due to the reduction in reflectivity introduced by the encapsulant.

Yoon et al. (2011) evaluated the relationship between transparency and efficiency of BIPW equipped with DSC. They also measured the device transmittance varying the TiO_2 thickness. Using these measurements, they simulated an office building provided with DSC windows and they studied the relationship between transparency and energy consumption. It was found that due to excess of electricity production, the minimum energy consumption is obtained by a DSC with 25 % of transparency, while a simple window without DSC exhibits a minimum of consumption with a transparency of 60 %.

11.3.4 Electric Performance

Electric performance of PV devices is related to the response of the technologies to the environmental parameter variation such us irradiance and temperature and also to the orientation and tilt. Conventional PV technologies have been well studied and are highly affected by temperature and tilt and orientation. There are few studies on electrical performance of organic photovoltaic in building integration; some of them have been made on cells and others on modules, and the different configurations seem to affect the electrical response of the devices to the environmental variables. Moreover, these studies are focused on different variables representative of the electrical performance such as efficiency, power, and performance ratio, and for this reason, it is not easy to compare the results. It has also to be noted that the effects of the environmental variables on electrical performance are superimposed and attention has to be paid to data treatment and evaluation. Sometimes, methods to separate the effects of the different variables are omitted or not well described. Pierro et al. (2015) developed a semiempirical model of the performance ratio of PV modules in outdoor conditions to separate the contributions of the different environmental variables on the PV modules performance.

They applied it to polycrystalline and amorphous silicon technologies. More recently, they used the same approach to evaluate the dependence of electric performance of a DSM on the angle of incidence (AOI). A DSM was placed on an outdoor frame whose position could be varied in azimuth and tilt, as shown in Fig. 11.7. The test was carried out during a clear day fixing a suitable azimuth

Fig. 11.7 Experimental set-up for AOI measurements at ESTER laboratory

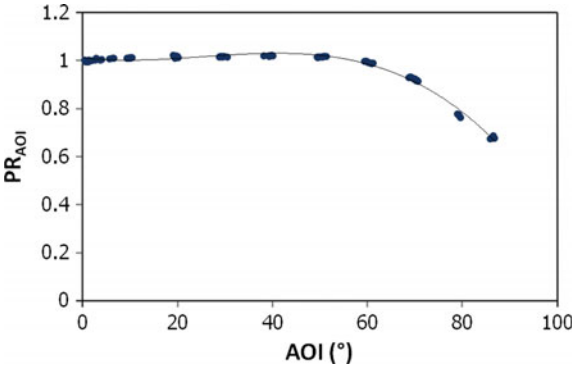

Fig. 11.8 PR_{AOI} versus angle of incidence for a DSM in outdoor conditions

position and varying the tilt angle during the day to get all possible angles of incidence from 0° (normal incidence) to 90°. Global irradiance was measured on the plane of the module together with back of the module temperature and electrical properties of the module. Short-circuit current (I_{sc}) was considered as main variable for the evaluation of the effect of AOI since it is directly proportional to irradiance. The parameter was also corrected for the effects of temperature, irradiance, and solar spectrum to isolate the sole AOI contribution. Figure 11.8 shows the trend of normalized Isc (PR_{AOI}) versus angle of incidence. DSM shows an increment of approximately 2 % with respect to normal incidence till 50° and a subsequent decrease till 86° (last angle tested).

In Fig. 11.9, the DSM power, corrected for temperature, irradiance, and spectrum influence is showed, versus AOI. In this case, the considered electric parameter is the power so that also influence of AOI on voltage is included. In this case, a maximum increment of approximately 3 % is observed with respect to normal incidence at 50°. Also, D'Ercole et al. (2011) observed a similar trend but with higher increases at higher AOI. DSC efficiency in indoor conditions exhibited an increase of 10 % at 60° for thick layer cells and of 16 % for thin layer cells.

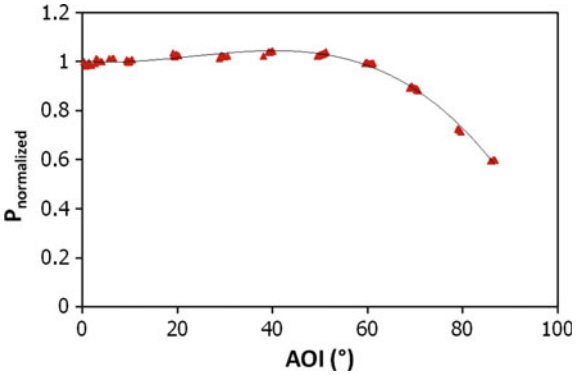

Fig. 11.9 DSM power corrected and normalized by nominal power versus AOI

A recent study conducted in outdoor conditions in Abu Dhabi (2014) on self-made DSC evaluated both temperature and angle of incidence influence. The authors evidenced an increasing power trend with increasing temperature, while cell efficiency was observed to increase logarithmically with the decrease of irradiance levels. This behaviour suggests better performance of DSC with respect to crystalline silicon especially for BIPW integration. In the same year, Reale et al. (2014) published a work on outdoor measurements for the characterization of a dye-sensitized module (DSM) for BIPW applications. They studied efficiency trend with respect to temperature and angle of incidence. In this case, they observed a decrease in efficiency with increasing temperature. This could be due to the type of electrolyte used and cell assemblies and also to other factors that can affect DSM such as internal series resistance and overall structure of the module. The same authors also studied the angle of incidence influence on the module efficiency in outdoor conditions. They found a performance increase (almost 60 % increase with respect to normal incidence) at high angles (75°). However, this result was not confirmed by Tian et al. (2012) and by what found by the authors of this chapter and reported in Fig. 11.9. What observed by various authors could confirm the better behaviour of organic photovoltaic on tilt configurations far from normal incidence as the case of integration into facades.

No works on these specific topics have been found for polymeric cells and modules.

11.3.5 Market Overview

DSMs have now reached a quite mature stage of development, and various companies can be found in the market that have emerged to develop this photovoltaic technology. Main applications are in indoor electronic and BIPV, with major focus on BIPW due to the characteristic of transparency of the devices (Asghar et al. 2014). Among the various companies, here we want to cite the ones that are mainly involved in BIPV applications evidencing their core business and major achievements in DSC. S Samsung SDI from Korea is a well-know company for electronic devices such as LCD and mobile phones; it is mainly involved in dye-sensitized panels for BIPV and smart windows with integrated storage. Dyesol, based in Australia, was born in 2004 as a leader in providing materials for DSC production. More recently, it is involved in the DSM production and integration in buildings thank also to a joint venture with Pilkington, a well-established company in glass manufacturing for construction applications. In Switzerland, Solaronix (Solaronix 2015) provides mainly DSC materials and commercial development. It produced DSM with active area of 200 m^2 that were installed as windows of Swiss Tech Convention Center at Ecole Polytechnique de Lausanne in 2014. In Italy, Dyepower, established in 2009, is a consortium of various Italian universities and a private company, Permasteelisa, for the development of DSMs for BIPV and more specifically for the application of facades. They are running an automated pilot line

for the production of A4 size DSMs and for larger area string panels. A4 DSMs successfully passed the IEC61646 humidity-freeze and damp-heat tests. Yingkou (2015) started its activity in China in 2009 developing products and materials for DSC. It is focused on the production of transparent DSMs in the form of glass windows. Exeger (2015), based in Sweden since 2009, has the main objective of the industrial production of DSMs for both building and automotive integration. It has a pilot plant installed for both applications. Apart from Solaronix, none of the cited companies has yet started mass device production.

All the above-mentioned companies are mainly involved in the development of DSM mass production. The start-up SBskin (2015) based in Palermo, Italy, is a spin-off of the University of Palermo that is focused on the design of construction products using innovative materials. They designed an active glass block in which DSC modules are integrated. The product is fit for installation in translucent roofs and facades (Buscemi et al. 2015).

Polymeric devices (PDs) have perhaps a less defined history. Only one extensive outlook on the market development of PD is available in the scientific literature, and it can be considered quite old since it is dated 2010 (Nielsen et al. 2010). At that time, PD market was dominated by Konarka that was then demised in 2012.

Currently, the leading manufacturer of polymeric devices is Heliatek (Germany) (Heliatek 2015) with their Heliafilm® technology that can be applied to every materials of a facade including glass. Belectric (2015), a solar developer and construction firm, acquired Konarka creating Belectric HOPV (Germany) in 2013 and made new partnership with flat glass processor BGT Bischoff Glastechnik to target BIPW market with the Solarte line. The results of their developments have been demonstrated at the German Pavilion at the World EXPO 2015 in Milan, where Belectric and its project partners have installed an HOPV system comprising hexagonal modules with a cell layout designed to be aesthetically pleasing.

Toshiba and Mitsubishi (Toshiba 2015; Mitsubishi 2015) in Japan have invested heavily and may well emerge as the first to manufacturing if the cell efficiency they have reached at laboratory level could be translated to the module level. Research activity in organic solar cells has exploded in the past 5 years. Big chemical companies such as BASF and MERCK (Basf 2015; Merk 2015) continue to have a strong presence particularly in material development. Konarka, Plextronics, and Princeton dominate the historical device, process and materials polymeric devices landscape although more recently new emerging companies in various part of the world are growing producing new patents such as Solamer (2015) and Nanoflex (2015) in USA. Polysolar (UK) (Polysolar 2015) develops, designs, and project-manages building-integrated photovoltaic (BIPV) solutions, in particular integrating new and emerging PV materials into glass. Polymeric photovoltaic development for this application is one of their main focuses. Also for polymeric devices, no massive production is yet in operation.

11.4 Organic Photovoltaics and Energy Efficiency in Buildings

11.4.1 Outdoor Performance and Stability

As already pointed out in the introduction, third-generation photovoltaics can overcome many issues of the previous two generations; however, these devices generally suffer from low efficiency and short-term outdoor stability. Great effort should be put to improve these aspects, and long-term outdoor monitoring is needed to verify the improvements. While in the last 10 years, many papers on outdoor measurements were published regarding the performance of the first two generation devices (PV Compare European project just to cite an example) (Jardine et al. 2001), few works on outdoor monitoring can be found in the literature regarding DSC and polymeric devices. The company AISIN SEKI (Toyoda et al. 2004) in Japan, in 2004, was the first to publish long-term outdoor tests over DSM made up of 64 series-connected DSC cells, tested for half a year. They made a comparative analysis of performance of DSM and silicon-based cell evidencing an improvement of 20 % in electricity production. They explained such result because of three factors: effect of light intensity, effect of temperature, and effect of angle of incidence of light. DSM, indeed, showed a better performance in low light, a better response of the electrolyte to high temperature, and a weak dependence on the angle of incidence. For what concern stability they reported monotonous decrease for 180 days probably due to trace of leakage of electrolyte in one of the modules. In a second work by Kato (Kato et al. 2009) in 2009, the same group investigated the degradation reasons using various experimental techniques during a 2.5 years outdoor test (the longest reported in the literature). The devices in this case showed good stability with no electrolyte leakage. However, the active tri-iodide concentration in the electrolyte showed a reduction due to an irreversible chemical reaction enhanced by UV light and temperature. From these studies, it can be inferred that long-term stability is achieved if good sealing and low humidity of the work environment are guaranteed during fabrication. Dai et al. (2008) presented a 354 daylong monitoring of the Isc and Voc on a 500-W DSC primary power station. They did not find any leakage and significant degradation of the devices. Few works have been published on the outdoor performance and stability of DSM with particular attention to building-integrated photovoltaics.

At the Fraunhofer Institute, outdoor test results on a glass facade prototype (70 × 200 cm) consisting of 10 modules (30 × 30 cm) were presented by Hinsch et al. (2009). Tests were carried out during 2 weeks of July and 2 weeks of October 2007. Later, Beucker et al. (2009) illustrated the capability of the upgraded prototype from Fraunhofer, made up of modules of 60 × 100 cm in size.

More recently, Asghar et al. (2014) and Cornaro et al. (2015a, b) presented comparative analysis of DSM with other technologies for possible integration in buildings in the MENA and Mediterranean regions. Asghar made different devices changing dye and electrolytes and exposed them in outdoor condition for over six

months on a rigid tilted stand in Abu Dhabi (UAE). The device performance was compared with a polycrystalline cell. They also tested a commercial G24i DSC device. They found that during the day the DSC devices produced more energy than the polycrystalline, and on a monthly basis, DSCs produced 20–30 % more energy with major differences during summer months due to higher temperatures and lower irradiance levels. Efficiency degradation was observed for all the self-made DSC devices mainly due to degradation of the electrolyte. Commercial module did not show major degradation probably due to a better sealing and to the use of a solid electrolyte. Cornaro et al. (2015b) made an outdoor monitoring campaign on a DSM minipanel, suitable for BIPV at the ESTER laboratory (Spena et al. 2008), University of Rome Tor Vergata.

They compared the device performance with a polycrystalline module and a double junction amorphous silicon module commercially available. The campaign lasted 3 months, from August till October 2011, and the devices were positioned on a vertical stand to simulate an application to facades, as shown in Fig. 11.10. The behaviour on a sunny day shows better performance of DSC device at low-light levels and high angles of incidence with respect to the other technologies. On a monthly basis, DSC performs better in August than in October due to its better response to high temperatures and high angles of incidence. On the whole period, for the configuration tested, the minipanel shows an energy yield which is 12 % higher than the a-Si device and comparable to m-Si within 3 %. Stability tests were carried out during the campaign. DSC showed a fluctuation of +5 %/–10 % with respect to the nominal peak power.

Fig. 11.10 Vertical configuration test bed for comparative analysis of DSM with other technologies

The same group made stability analysis on a DSC string made of 7 DSM in series exposed on a south-oriented tilted frame, from the middle of July till the end of October 2014. As shown in Fig. 11.11, also in this case an improvement in peak power was observed with an increment of 10 % obtained during the first 15 days of operation. A stable trend is observed for the month of August, and a subsequent decrease of 10 % with respect to the stable trend is achieved during almost 70 days of operation. From what it is known till now, DSC devices perform well with low light, high temperature, and high angle of incidence in real operating conditions proving to be suitable for integration into building facades. Stability is still an issue, and more research is needed at module level to improve duration. Main focus is the electrolyte and sealing that need to be improved.

Polymeric devices have been subjected to a more systematic investigation in outdoor conditions thank to the collaboration of various laboratories. Katz et al. (2006) performed an outdoor test of 32 days, during daylight hours, on polymeric devices reaching cell temperature values of 45°C and pointed out that Isc went down with the passing of time (the opposite for Voc). Later, Hauch et al. (2008) carried out a 1-year outdoor exposure of a flexible organic module at 42.6°N, in the USA, correlating the results with an accelerated indoor test under 1 sun at 65 °C for 1200 h.

A series of interlaboratory comparisons of performance of flexible roll-to-roll coated organic photovoltaic modules were carried out in 2011 (Gevorgyan et al. 2011) and 2013 (Gevorgyan et al. 2013), and more recently, investigation on the same device after 2.5 years of operation in Denmark has been presented (Angmo and Krebs 2015). Worldwide outdoor round robin study of organic photovoltaic devices was carried out and published in 2014. The studies revealed that the device terminals made up of a combination of metal snap fasteners and Cu tape produced deterioration of the barrier material generating paths for oxygen and water diffusion. This introduces significant variations in module lifetimes. The most stable modules exhibited a lifetime of more than ten thousand hours and a stability of up to 17 months. The long-term tests allowed also studying the effect of weather conditions on device behaviour.

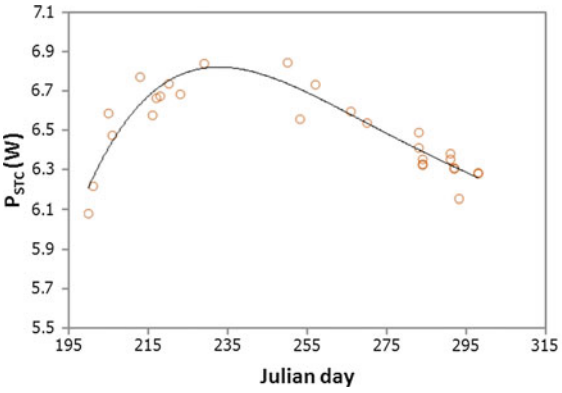

Fig. 11.11 Effect of outdoor deployment on DSM power at STC

Angmo and Krebs (2015) studied the stability of polymeric devices under illumination and dark conditions, and they confirmed that devices suited for long-term applications may require barrier materials with higher performance with respect to water vapour and oxygen transmission rates. Oxygen permeation could be the main responsible for the declining short-circuit current in outdoor conditions, while water vapour reactivity is lower under illumination with respect to dark conditions. The data of the best-performing module in dark conditions suggest that under the low-cost encapsulation conditions considered the module could last for 3–5 years in storage and perhaps even longer under outdoor conditions. The examined cases are however referred to opaque polymeric cells, while no investigations have been found on semitransparent materials for BIPW applications.

11.4.2 Energy Saving Potential

Various studies can be found in the literature about modelling and experiments regarding the evaluation of potential saving using PV windows.

Table 11.1 from the work of Skandalos and Karamakis (2015) well resumes the work done on first-generation photovoltaics (a-Si and c-Si). The references numbers listed in the table are referred to the original work. Still few works are available on organic photovoltaics, and surely, more research is requested on this issue. Yoon et al. studied the effect of DSC transparency on energy consumption simulating a standard rectangular floor plan layout of a reference building with a 50 % window–to-wall ratio (WWR) facing NW, NE, SW, and SE. Evaluation of energy consumption versus transparency for windows with and without DSC was carried out. They found that for windows without DSC, increasing heating loads is larger than decreasing cooling load as transparency decreases so that energy consumption increases as transmittance decreases. DSC windows act differently; indeed, lowest energy consumption is achieved with relative low transparency (25 %) due to the excess of electricity production compared to the energy use, for transmittance values between 60 and 25 %. Energy consumption rate for different efficiency of DSC has been also investigated. The study shows that when the efficiency is doubled the energy consumption is significantly reduced at various transmittance rate. For example, with 25 % of transmittance, a reduction in energy consumption of approximately 12 % is obtained. Reale et al. (2014) made a comparison of electricity production of DSC with respect to thin films and silicon technologies using a model of DSC efficiency with respect to environmental variables. They found that vertical position and orientation to north are more favourable configurations to DSC than to the other technologies and also that energy production on a vertical facade and all possible orientation is larger than other technologies.

More recently, Kapsis and Athienitis (2015) used an integrated simulation approach, involving thermal, electrical, and daylighting aspects to evaluate the performance of various PV technologies integrated into semitransparent PV windows. They considered polycrystalline silicon, amorphous silicon, and HOPV among

Table 11.1 List of works about potential saving in buildings using standard technologies PV in windows (from Skandalos and Karamanis 2015)

Type	Region	Study	Objectives	Outcomes	Reference
a-Si	(Middle East)	Tmsys simulations for highly glazed buildings	Performance investigation of BIPV integrated in high glazed buildings	31 % energy saving for cooling over a year	[175]
a-Si	(United Arab Emirates)	Energy-10 simulations	Interaction between PV modules and thermal performance of a building	1.1–2.2 % reduction in the building's total operational energy consumption. Reduced payback time	[176]
a-Si, c-Si		A brief overview of various advanced window technologies	Physical structure of window and energy performance evaluation	Best SHGC for single-glazed PV	[10]
				200 and 53 % heat gain reduction of double-glazed PV, compared with clear and low e-coating glass, respectively	
a-Si	(Brazil)	Simulations in Daysim/Radiance and energy plus software	Annual daylight estimation and energy performance	Building adaptation according to the climatic characteristics of the site reduce energy consumption for lighting and HVAC Low-E window present the overall best performance for the facades with less radiation and PV windows for all the others	[177]

(continued)

Table 11.1 (continued)

Type	Region	Study	Objectives	Outcomes	Reference
a-Si:H		Methodology for buildings' energy performance evaluation	Criteria affecting PV window and thus building's performance	Effective pathway to evaluate performance of semitransparent PV window in the perspective of an actual building scale	[19]
a-Si		Performance analysis for different window orientations	Energy saving investigation.	55 % energy savings for transparent (45–55 %) PV compared to standard glazing	[179]
mc-Si	5 regions in Japan (Temperate)	EnergyPlus simulations (experimentally validated)	Energy saving potential of STPV in a residential application	Up to 5.3 % energy savings for heating and cooling can be achieved with optimized STPV	[11]
a-Si	Hong Kong (Subtropical)	Daylight illuminance, solar irradiance, and power generation measurements for semitransparent a-Si PV	Investigation of the essential parameters affecting the thermal and optical characteristics of the PV	Reduced electric lighting and cooling energy requirements (12 % annually) and environmental benefits (CO_2, SO_2, NO_x decrease)	[143]
a-Si	Hong Kong (Subtropical)	Airflow analysis inside the cavity of ventilated STPV window	Factors affecting the heat transfer coefficients of vertical surfaces	Cooling loads can be reduced by 26 % and 61 % by using single-glazed and naturally ventilated PV windows, respectively	[178]
a-Si	Hong Kong (Subtropical)	Experimental study of PV window integrated on typical office building	Experimental validation of theoretical models developed in ESP-r platform	23 % electricity savings for cooling annually for the single-glazed and 28 % for ventilated PV system	[150]

(continued)

Table 11.1 (continued)

Type	Region	Study	Objectives	Outcomes	Reference
mc-Si a-Si	Singapore (Tropical)	EnergyPlus simulations for various STPV modules (10 % VLT)	Potential energy savings for various window-to-wall ratios	Potential to perform even to orientations which not receive direct solar gain	[153]

the devices. They used the software DAYSIM integrated with MATLAB and EnergyPlus to study BIPW system implemented in a standard office located in Toronto, Canada, studying two WWR configurations: WWR = 40 % and WWR = 60 %. DAYSIM was used to simulate the daylight modelling, while EnergyPlus was allowed to investigate the thermal and electrical behaviour of the devices. They found that the selection of BIPW technology has a small impact on the annual energy performance that is less than 8 % on heating and less than 4 % on cooling loads. However, the annual electricity generation varies significantly with technology resulting in major differences on end-use electricity consumption. HOPV showed an annual yield 49 % higher than amorphous silicon and 29 % less than polycrystalline. In general, BIPW with 10 % light transmittance appeared to be the best solution with respect to end-use energy consumption for all the PV technologies.

11.4.3 Showcases

Real operating plants made of HOPV and integrated into buildings are still few and are also recent developments. With the courtesy of Solaronix for DSM and Heliatek for polymeric modules, a description of two recently installed facilities could be included in this book.

11.4.3.1 Swiss Tech Convention Center

The Swiss Tech Convention Center as shown in Fig. 11.12 is a conference centre at the École polytechnique fédérale de Lausanne (EPFL), Switzerland. The biggest auditorium has a capacity of 3000 seats. The opening ceremony took place at the beginning of April 2014. It was designed by the architectural firm Richter Dahl Rocha & Associés of Lausanne and was financed by two Credit Suisse real estate funds. Financial support from the Swiss electricity supply company Romande Energie allowed the west facade of the building to be covered with panels made of DSC.

The façade, made by Solaronix, consists of 1410 DSM, each 35 × 50 cm in size, coming in 5 colours and shades.

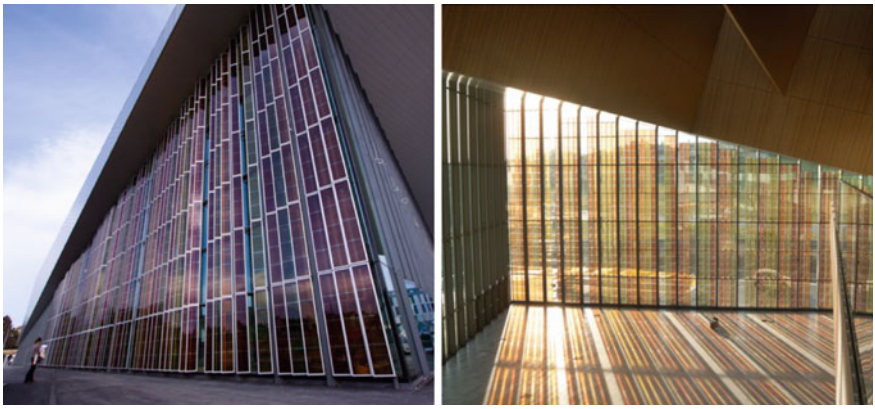

Fig. 11.12 Views of the Swiss Tech Convention Center and DSM façade (courtesy of Solaronix)

These DSMs are built into 358 glass/glass-laminated panels, the smallest panel has 2 modules, and the biggest consists of 5 modules. In figure 11.12, it is possible to recognize the panel metallic frames.

All the DSMs within a panel are in parallel connection, and each panel is equipped with a DC/DC converter adapting the ~6 V output to the common 48 VDC bus. All the panels are thus parallel mounted via these DC/DC converters.

The output of the façade is approximately 1.5kWp, as most of the modules were chosen to be fairly lightly coloured, and the power for each colour is reported in Table 11.2.

The transmission properties of the DSM were also measured for some kinds of composite cells, and the results are resumed in Table 11.3.

Table 11.2 Power characteristics of DSMs with respect to their colour

Colour	Average power (W)	Number of modules	Total power (W)
Dark red	1.33	382	508
Light orange	1.28	361	462
Light green	0.77	350	270
Dark green	0.67	220	147
Dark orange	1.12	97	109
Total		1410	1496

Table 11.3 Solar transmission properties of some DSM used for Swiss Tech facade

Sample description	SHGC	$T_{380–1100}$	Tv
Single 2.2-mm TCO glass	0.69	0.76	0.77
Dark red composite cell	0.27	0.41	0.15
Orange-red composite module	0.34	0.45	0.29
Olive-green module	0.36	0.47	0.37

The plant data collection started in April this year so that energy performance is not available at this moment.

11.4.3.2 Heliatek's Dresden Headquarter and Singapore Installation

In 2014, HeliaFilm® was installed for the first time at Heliatek's Dresden headquarters. It has been laminated into glass by AGC Glass Europe, the European branch of AGC (the world's largest producer of flat glass) and a long-term strategic business partner of Heliatek. The façade has a north-east orientation and a nominal peak power of 1 kWp. The installation demonstrates excellent low-light behaviour under non-optimal orientation and aesthetic integration into glass façade as shown in Fig. 11.13.

So it has produced far up more than 20 % higher energy yield than a comparable traditional solar installation.

In Table 11.4, some technical specification of the plant is listed.

In Fig. 11.14, the monthly energy production of the façade during the first year of operation is showed.

Fig. 11.13 View of the Heliafilm installation at Heliatek headquarter in Dresden (courtesy of Heliatek)

Table 11.4 Technical specifications of Heliatek façade in Dresden

Heliatek façade, Dresden	
Location	Dresden, Germany
Azimuth	−96° (North-East)
Inclination	80°
Operator	Heliatek GmbH
Initial commissioning	09.09.2014
System performance	0.962 kWp
Output per year	ca. 500 kWh (520 kWh/kWp)
CO_2 reduction	ca. 0.5 tons per year
Modules	Heliatek HeliaFilm opaque
Communication	SMA Sunny WebBox
Inverter	SMA Sunny Boy 1300TL-10
Sensors	SMA Sunny sensor box (module temperature + irradiation) SMA Ambient temperature sensor

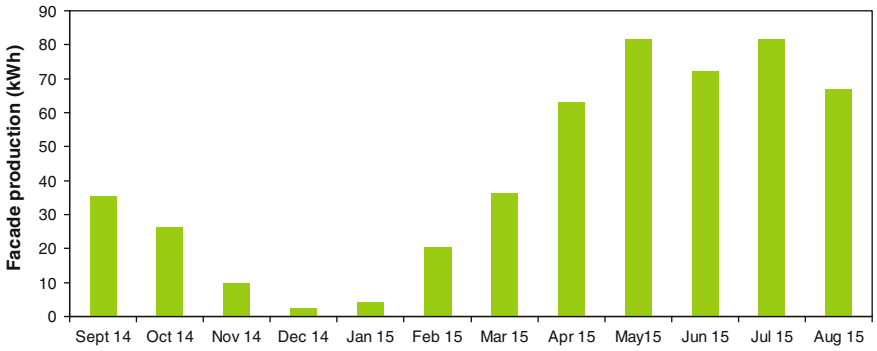

Fig. 11.14 Monthly energy production of Heliatek façade, Dresden

In Singapore, Heliatek, in collaboration with vTrium Energy, is working at the Asia's largest BIOPV installation. Heliatek's organic solar film, HeliaFilm®, will be the core part of this test-bed platform for investigation of new sustainable, urban-fit technologies. HeliaFilm® will be installed on more than 200 m^2 with a peak power of up to 10 kWp. Three different parts of buildings in JTCs Cleantech Park 1 and 2 (Fig. 11.15) and the Seletar Aerospace walkway will be covered with solar films. HeliaFilm® will be combined with various building materials: within and on glass and on metal. Several versions of HeliaFilm® will be used: full power opaque,

Fig. 11.15 Façade and entrance canopy of CleanTech Park 2, Singapore—© JTC (courtesy of Heliatek)

transparent, and different colours. The main orientation of the installation will be north and north-west. The work started in July 2015.

The installation demonstrates significant energy harvesting in tropical conditions and no special ventilation/cooling system required unlike conventional PV solutions.

The first phase of Heliatek's pilot project has been successfully completed in September 2015. 30 m^2 of Heliafilm with an average cell efficiency of 7 % has been installed on the Seletar walkway (Fig. 11.16). HeliaFilm® is fitting the walkway roof perfectly despite its uneven shaped aluminium top structure.

This project is funded and supported by Jurong Town Corporation (JTC, Singapore) and SPRING (Standards, Productivity and Innovation Board, Singapore). The independent monitoring of this pilot will be performed by the Solar Energy Research Institute of Singapore (SERIS), and the findings from this project will help to create a base for the future energy mix for Singapore.

Fig. 11.16 Installation of Heliafilm on the Seletar walkway (courtesy of Heliatek)

11.5 Conclusions

Hybrid and Organic photovoltaics have reached a certain stage of development to be considered a promising alternative to inorganic photovoltaic devices for some specific applications, due to easy manufacture, low production cost and acceptable efficiencies. Indeed, their characteristics are such that they can be easily adapted as active elements integrated into buildings. In particular the transparency characteristics of some of these devices make them suitable for integration into glazing systems. However, while a lot of research is carried out on improving laboratory scale devices little attention is devoted to the up-scaling process to large area products. Moreover, additional R&D is required to provide better results in terms of efficiency and stability. These are important issues to promote organic photovoltaics into the building market. The presented overview indicates that some attempts have been already made to characterize organic PV devices from the point of view of their electrical, thermal and optical performance, and to evaluate the effective advantage of using this technology to improve energy efficiency in buildings. Results are promising but we still have a long way to go to improve our knowledge in this field. Demonstration and pilot projects are also necessary to evaluate the real performance of the devices and their architectural features. At this stage and to our knowledge only few showcases are in operation but an increasing number of real installations will show up in the near future.

References

Angmo D, Krebs FC (2015) Over 2 years of outdoor operational and storage stability of ITO-free, fully roll-to-roll fabricated polymer solar cell modules. Energy Technol 3:774–783

Asghar A, Emziane M, Pak HK, Oh SY (2014) Outdoor testing and degradation of dye-sensitized solar cells in Abu Dhabi. Sol Energy Mater Sol Cells 128:335–342

Ball JM, Lee MM, Hey A, Snaith HJ (2013) Low-temperature processed meso-superstructured to thin-film perovskite solar cells. Energy Environ Sci 6:1739

Barolo C, Bignozzi C, Boaretto R, Brown TM, Bonandini L, Busatto E, Caramori S, Colonna D, De Angelis G, Di Carlo A, Guglielmotti A, Guidobaldi A, Lanuti A, Lembo A, Magistri D, Mariani P, Mirruzzo V, Penna S, Pietrantoni S, Prencipe D, Reale A, Riccitelli R, Smarra A, Soscia G, Tagliaferro R, Vesce L, Viscardi G (2014) Presented at HOPV. Lousanne, Switzerland

Basf (2015) https://www.dispersions-pigments.basf.com/portal/basf/ien/dt.jsp?setCursor=1_556381

Belectric (2015) www.belectric.com

Beucker S, Hinsch A, Brandt H, Veurman W, Flarup Jensen K, Lang-Koetz C, Stabe M (2009) Scaling-up of glass based DSC-modules for applications in building integrated photovoltaics. 34th IEEE photovoltaic specialists conference (PVSC)

Bi D, Moon SJ, Häggman L, Boschloo G, Yang L, Johansson EMJ, Nazeeruddin MK, Graetzel M, Hagfeldt A (2013) Using a two-step deposition technique to prepare perovskite ($CH_3NH_3PbI_3$) for thin film solar cells based on ZrO_2 and TiO_2 mesostructures. RSC Adv 3:18762

Burschka J, Pellet N, Moon S-J, Humphry-Baker R, Gao P, Nazeeruddin MK, Graetzel M (2013) Sequential deposition as a route to high-performance perovskite-sensitized solar cells. Nature 499:316

Buscemi A, Calabrò C, Corrao R, Di Maggio MS, Morini M, Pastore LP (2015) Optical performance evaluation of DSC-integrated Glassblocks for Activa Building Facade. J Modern Eng Res 5(2):17–22

Calogero G, Bartolotta A, Di Marco G, Di Carlo A, Bonaccorso F (2015) Vegetable-based dye-sensitized solar cells. Chem Soc Rev 44:3244–3294

Casaluci S, Cina L, Pockett A, Kubiak PS, Niemann RG, Reale A, Di Carlo A, Cameron PJ (2015) A simple approach for the fabrication of perovskite solar cells in air. J Power Sour 297:504–510

Chae YT, Kim J, Park H, Shin B (2014) Building energy performance evaluation of building integrated photovoltaic (BIPV) window with semi-transparent solar cells. Appl Energy 129:217–27

Chen Q, Zhou H, Hong Z, Luo S, Duan H-S, Wang H-H, Liu Y, Li G, Yang Y (2014) Planar Heterojunction perovskite solar cells via vapor-assisted solution process. J Am Chem Soc 136:622

Conings B, Baeten L, De Dobbelaere C, D'Haen J, Manca J, Hans-Gerd B (2014) Perovskite-based hybrid solar cells exceeding 10 % efficiency with high reproducibility using a thin film sandwich approach. Adv Mater 26:2041–2046

Cook S, Katoh R, Furube A (2009) Ultrafast studies of charge generation in PCBM:P3HT blend films following excitation of the fullerene PCBM. J Phys Chem C 113:2547–2552

Cornaro C, Bucci F, Pierro M, Bonadonna ME, Siniscalco G (2015a) A new method for the thermal characterization of transparent and semi-transparent materials using outdoor measurements and dynamic simulation. Energy Build 104:57–64

Cornaro C, Bartocci S, Musella D, Strati C, Lanuti A, Mastroianni S, Penna S, Guidobaldi A, Giordano F, Petrolati E, Brown TM, Reale A, Di Carlo A (2015b) Comparative analysis of the outdoor performance of a dye solar cell mini-panel for building integrated photovoltaics applications. Prog Photovolt 23(2):215–225

D'Ercole D, Dominici L, Brown TM, Michelotti F, Reale A, Di Carlo A (2011) Angular response of dye solar cells to solar and spectrally resolved light. Appl Phys Lett 99

Dai S, Weng J, Sui Y, Chen S, Xiao S, Huang Y, Kong F, Pan X, Hu L, Zhang C, Wang K (2008) The design and outdoor application of dye-sensitized solar cells. Inorganica Chimica Acta 361:786–791

De Boer B, Van Helden W (2001) PV-MOBI-PV modules optimized for building integration. In: Proceedings of the 9th international conference on solar energy in high latitudes, Netherlands

De Jong M, Van Ijzendoorn L, De Voigt M (2000) Stability of the interface between indium-tin-oxide and poly (3, 4-ethylenedioxythiophene)/poly (styrenesulfonate) in polymer light-emitting diodes. Appl Phys Lett 77:2255–2257

Di Giacomo F, Razza S, Matteocci F, D'Epifanio A, Licoccia S, Brown TM, Di Carlo A (2014) High efficiency CH3NH3PbI (3-x) Clx perovskite solar cells with poly (3-hexylthiophene) hole transport layer. J Power Sour 251:152

Ding Y, Lu P, Chen Q (2008) In optimizing material properties of bulk-heterojunction polymer films for photovoltaic applications, pp 709919–709919-8.

Dou L, You J, Yang J, Chen C-C, He Y, Murase S, Moriarty T, Emery K, Li G, Yang Y (2012) Tandem polymer solar cells featuring a spectrally matched low-bandgap polymer. Nat Photonics 6:180–185

Elliott CM, Caramori S, Bignozzi CA (2005) Indium Tin Oxide Electrodes Modified with Tris (2,2'-bipyridine-4,4'-dicarboxylic acid) Iron(II) and the Catalytic Oxidation of Tris(4,4'-di-tert-butyl-2,2'-bipyridine) Cobalt(II). Langmuir 21:3022–3027

Eperon GE, Burlakov VM, Docampo P, Goriely A, Snaith HJ (2014a) Morphological control for high performance, solution-processed planar heterojunction perovskite solar cells. Adv Funct Mater 24:151–157

Eperon GE, Burlakov VM, Goriely A, Snaith HJ (2014b) Neutral color semitransparent microstructured perovskite solar cells. ACS Nano 8(1):591–598

Exeger (2015) http://www.exeger.com

Fakharuddin A, Josè R, Brown TM, Fabregat-Santiago F, Bisquert J (2014a) A perspective on the production of dye-sensitized solar modules. Energy Environ Sci 7:3952

Fakharuddin A, Jose R, Brown TM, Fabregat-Santiago F, Bisquert J (2014b) A perspective on the production of dye-sensitized solar modules. Energy Environ Sci 7:3952–3981. www.gcell.com

Freunek M, Reindl LM (2013a) Maximum efficiencies of indoor photovoltaic devices. IEEE J Photovolt 3:54–69

Freunek M, Reindl LM (2013b) Maximum efficiencies of indoor photovoltaic devices. IEEE J Photovolt 4:1464-1464

Gcell (2015) www.gcell.com

Gevorgyan SA, Medford AJ, Bundgaard E, Sapkota SB, Schleiermacher H-F, Zimmermann B, Würfel U, Chafiq A, Lira-Cantu M, Swonke T, Wagner M, Brabec CJ, Haillant O, Voroshazi E, Aernouts T, Steim R, Hauch JA, Elschner A, Pannone M, Xiao M, Langzettel A, Laird D, Lloyd MT, Rath T, Maier E, Trimmel G, Hermenau M, Menke T, Leo K, Rösch R, Seeland M, Hoppe H, Nagle TJ, Burke KB, Fell CJ, Vak D, Singh T, Watkins SE, Galagan Y, Manor A, Katz EA, Kim T, Kim K, Sommeling PM, Verhees WJ, Veenstra SC, Riede M, Greyson Christoforo M, Currier T, Shrotriya V, Schwartz G, Krebs FC (2011) An inter-laboratory stability study of roll-to-roll coated flexible polymer solar modules, Solar Energy Mater. Sol Cell 95:1398–1416

Gevorgyan SA, Madsen MV, Dam HF, Jorgensen M, Fell CJ, Anderson KF, Duck BC, Mescheloff A, Katz EA, Elschner A, Roesch R, Hoppe H, Hermenau M, Riede M, Krebs FC (2013) Interlaboratory outdoor stability studies of flexible roll-to-roll coated organic photovoltaic modules: stability over 10,000 h. Sol Energy Mater Sol Cell 116:187–196

Gregg B, Pichot F, Ferrere S, Fileds CR (2001) Interfacial recombination processes in dye-sensitized solar cells and methods to passivate the interfaces. J Phys Chem B. 105:1422–1429

Halls J, Walsh C, Greenham N, Marseglia E, Friend R, Moratti S, Holmes A (1995) Efficient photodiodes from interpenetrating polymer networks. Nature 376:498.

Hauch JA, Schilinsky P, Choulis SA, Childers R, Biele M, Brabec CJ (2008) Flexible organic P3HT:PCBM bulkheterojunction modules with more than 1 year outdoor lifetime. Sol Energy Mater Sol Cell 92:727–731

He Z, Zhong C, Su S, Xu M, Wu H, Cao Y (2012) Enhanced power-conversion efficiency in polymer solar cells using an inverted device structure. Nat Photonics 6:593–597

Heliatek (2015) www.heliatek.com/

Heo JH, Im SH, Noh JH, Mandal TN, Lim CS, Chang JA, Lee YH, Kim H, Sarkar A, Nazeeruddin MK, Grätzel M, Seok SI (2013) Efficient inorganic–organic hybrid heterojunction solar cells containing perovskite compound and polymeric hole conductors. Nat Photon 7:486–491

Heo J, Han HJ, Lee M, Song M, Kim D, Im SH (2015) Stable semi-transparent $CH_3NH_3PbI_3$ planar sandwich solar cells. Energy Environ. Sci. doi:10.1039/C5EE01050K

Hinsch A (2013) Status of the Dye Solar Cell technology (DSC) as guideline for further research. In: Proceedings of the 28th European PV solar energy conference, Paris (France), 20 Sept–4 Oct 2013, available at https://www.ise.fraunhofer.de/de/veroeffentlichungen/konferenzbeitraege/konferenzbeitraege-2013/28th-eupvsec/hinsch.pdf

Hinsch A, Brandt H, Veurman W, Hemming S, Nittel M, Wurfel U, Putyra P, Lang-Koetz C, Stabe M, Beucker S, Fichter K (2009) Dye solar modules for facade applications: recent results from project ColorSol. Sol Energy Mater Sol Cell 93:820–824

Hu H, Wang D, Zhou Y, Zhang J, Lv S, Pang S, Chen X, Liu Z, Padture NP, Cui G (2014) Vapour-based processing of hole-conductor-free $CH_3NH_3PbI_3$ perovskite/C60 fullerene planar solar cells. RSC Adv 4:28964

Huang Hung-Lin, Lee Ching-Ting, Lee Hsin-Ying (2015) Performance improvement mechanisms of P3HT:PCBM inverted polymer solar cells using extra PCBM and extra P3HT interfacial layers. Org Electron 21:126–131

Hui-Seon K, Lee C-R, Im J-H, Lee K-B, Moehl T, Marchioro A, Moon S-J, Humphry-Baker R, Yum J-H, Moser JE, Grätzel M, Park N-G (2012) Lead iodide perovskite sensitized all-solid-state submicron thin film mesoscopic solar cell with efficiency exceeding 9%. Sci Rep 2:591

Jardine CN, Conibeer GJ, Lane K (2001) PV-COMPARE: direct comparison of eleven PV technologies at two lo- cations in northern and southern Europe. Seventeenth EU PVSEC

Jeon NJ, Noh JH, Chan Kim Y, Seok Yang W, Ryu S, Il Seok S (2014) Solvent engineering for high-performance inorganic–organic hybrid perovskite solar cells. Nat Mater 13:897

Jeon NJ, Noh JH, Yang WS, Kim YC, Ryu S, Seo J, Seok SI, Seok SI, Seok SI, Seok SI, Seok SI, Seok SI (2015) Compositional engineering of perovskite materials for high-performance solar cells. Nature 517:476

Jiang N, Sumitomo T, Lee T, Pellaroque A, Bellon O, Milliken D, Desilvestro H (2013) High temperature stability of dye solar cells. Sol Energy Mater Sol Cell 119:36–50

Jørgensen M, Norrman K, Krebs FC (2008) Stability/degradation of polymer solar cells. Sol Energy Mater Sol Cell 92:686–714

Kalyanasundaram K (2010) Dye-sensitized solar cells. EPFL Press, ISBN-13:978-1439808665

Kang J-G, Kim J-H, Kim J-T (2013) Performance evaluation of DSC windows for buildings. Int J Photoenergy 6

Kapsis K, Athienitis AK (2015) A study of the potential benefits of semi-transparent photovoltaics in commercial buildings. Sol Energy 115:120–152

Kato N, Takeda Y, Higuchi K, Takeichi A, Sudo E, Tanaka H, Motohiro T, Sano T, Toyoda T (2009) Degradation analysis of dye-sensitized solar cell module after long-term stability test under outdoor working condition. Sol Energy Mater Sol Cells 93:893–897

Katz EA, Gevorgyan S, Orynbayev MS, Krebs FC (2006) Outdoor testing and long-term stability of plastic solar cells. Eur Phys J Appl Phys 36:307–311

Kawano K, Pacios R, Poplavskyy D, Nelson J, Bradley DDC, Durrant JR (2006) Degradation of organic solar cells due to air exposure. Sol Energy Mater Sol Cell 90:3520–3530

Kojima A, Teshima K, Shirai Y, Miyasaka T (2009) Organometal Halide Perovskites as visible-light sensitizers for photovoltaic cells. J Am Chem Soc 131:6050–6051

Krebs FC (2009) Fabrication and processing of polymer solar cells: A review of printing and coating techniques. Sol Energy Mater Sol Cell 93:394–412
Lee MM, Teuscher J, Miyasaka T, Murakami TN, Snaith HJ (2012a) Efficient hybrid solar cells based on meso-superstructured organometal halide perovskites. Science 338:643–647
Lee MM, Teuscher J, Miyasaka T, Murakami TN, Snaith HJ (2012b) Efficient hybrid solar cells based on meso-superstructured organometal halide perovskites. Science 338:643
Li L-L, Diau EW-G (2013) Porphyrin-sensitized solar cells. Chem Soc Rev 42:291
Lin Y, Li Y, Zhan X (2012) Chem Soc Rev 41:4245–4272
Liu D, Kelly TL (2014) Perovskite solar cells with a planar heterojunction structure prepared using room-temperature solution processing techniques. Nat Photonics 8:133
Mariani P, Vesce L, Di Carlo A (2015) The role of printing techniques for large-area dye sensitized solar cells. Semicond Sci Technol 30:104003
Matteocci F, Razza S, Di Giacomo F, Casaluci S, Mincuzzi G, Brown T, D'Epifanio A, Licoccia S, Carlo AD (2014a) Solid-state solar module based on mesoscopic organometal halide perovskite: a route towards the upscaling process. Phys Chem Chem Phys 16:3918–3923
Matteocci F, Cinà L, Di Giacomo F, Razza S, Palma AL, Guidobaldi A, D'Epifanio A, Licoccia S, Brown TM, Reale A, Di Carlo A (2014b) High efficiency photovoltaic module based on mesoscopic organometal halide perovskite. Prog Photovolt Res Appl. DOI: 10.1002/pip.2557
Merc K (2015) http://www.merck-performancematerials.com/en/solar_and_energy/photovoltaics/
Mincuzzi G, Vesce L, Schulz-Ruhtenberg M, Gehlen E, Reale A, Di Carlo A, Brown TM (2014) Taking temperature processing out of dye-sensitized solar cell fabrication: fully laser-manufactured devices. Adv Energy Mater 4:1400421
Mitsubishi (2015) http://www.mitsubishichem-hd.co.jp/english/discover_kaiteki/kaiteki_value/detail01.html
Miyazaki T, Akisawa A, Kashiwagi T (2005) Energy savings of office buildings by the use of semi-transparent solar cells for windows. Renew Energy 30:281–304
Mulligan CJ, Wilson M, Bryant G, Vaughan B, Zhou X, Belcher WJ, Dastoor PC (2014) A projection of commercial-scale organic photovoltaic module costs. Sol Energy Mater Sol Cell 120:9–17
Nanoflex (2015) http://www.nanoflexpower.com/
Nazeeruddin MK, Kay A, Rodicio I, Humpry-Baker R, Muller E, Liska P, Vlachopoulos N, Graetzel M (1993) Conversion of light to electricity by cis-X2bis(2,2'-bipyridyl-4,4'-dicarboxylate)ruthenium(II) charge-transfer sensitizers (X = Cl-, Br-, I-, CN-, and SCN-) on nanocrystalline titanium dioxide electrodes. J Am Chem Soc 115:6382–6390
Nazeeruddin MK, Pechy P, Liska P, Renouard T, Zakeeruddin SM, Humphry-Baker R, Comte P, Cevey L, Costa E, Shklove V, Spiccia L, Deacon GB, Bignozzi CA, Gra¨tze M (2001) Engineering of efficient panchromatic sensitizers for nanocrystalline TiO(2)-based solar cells. J Am Chem Soc. 123:1613–1624
Nielsen TD, Cruickshank C, Foged S, Thorsen J, Krebs FC (2010) Business, market and intellectual property analysis of polymer solar cells. Sol Energy Mater Sol Cell 94:1553–1571
Noh JH, Im SH, Heo JH, Mandal TN, Seok SI (2013) Chemical management for colorful, efficient, and stable inorganic–organic hybrid nanostructured solar cells. Nano Lett 13(4):1764–1769
NREL, National Renewable Energy Laboratory (USA) http://www.nrel.gov/ncpv/images/efficiency_chart.jpg. Accessed on 1 Oct 2015
Park KE, Kang GH, Kim HI, Yu GJ, Kim JT (2010) Analysis of thermal and electrical performance of semi-transparent photovoltaic (PV) module. Energy 35:2681–2687
Perganti D, Kontos AG, Stergiopoulos T, Likodimos V, Farnell J, Milliken D, Desilvestro H, Falaras P (2015) Thermal stressing of dye sensitized solar cells employing robust redox electrolytes. Electrochimica Acta 179:241–249
Pierro M, Bucci F, Cornaro C (2015) Full characterization of PV modules in real operating conditions: theoretical model, measurement method and results. Prog Photovolt Res Appl 23 (4):443–461
Polysolar (2015) www.polysolar.co.uk

Razza S, Di Giacomo F, Matteocci F, Cinà L, Palma AL, Casaluci S, Cameron P, D'Epifanio A, Licoccia S, Reale A, Brown TM, Di Carlo A (2015a) Perovskite solar cells and large area modules (100 cm^2) based on an air flow-assisted PbI2 blade coating deposition process. J Power Sour 277:286–291

Razza S, Matteocci F, Di Giacomo F, Dianetti M, Palma AL, Brunetti F, Brown TM, Di Carlo A (2015b) Large area (100 cm^2) Perovskite modules with efficiency exceeding 9 %, presented at HOPV15, Rome, 10–13 May 2015

Reale A, Cinà L, Malatesta A, De Marco R, Brown TM, Di Carlo A (2014) Estimation of energy production of dye-sensitized solar cell modules for building-integrated photovoltaic applications. Energy Technol 2:531–541

Reese MO, Gevorgyan SA, Jørgensen M, Bundgaard E, Kurtz SR, Ginley DS, Olson DC, Lloyd MT, Morvillo P, Katz EA, Elschner A, Haillant O, Currier TR, Shrotriya V, Hermenau M, Riede M, Kirov KR, Trimmel G, Rath T, Inganäs O, Zhang F, Andersson M, Tvingstedt K, Lira-Cantu M, Laird D, McGuiness C, Jimmy Gowrisanker S, Pannone M, Xiao M, Hauch J, Steim R, DeLongchamp DM, Rösch R, Hoppe H, Espinosa N, Urbina A, Yaman-Uzunoglu G, Bonekamp J-B, van Breemen AJJM, Girotto C, Voroshazi E, Krebs FC (2011) Consensus stability testing protocols for organic photovoltaic materials and devices. Sol Energy Mater Sol Cell 95:1253

Roldán-Carmona C, Malinkiewicz O, Betancur R, Longo G, Momblona C, Jaramillo F, Camacho L, Bolink HJ (2014) High efficiency single-junction semitransparent perovskite solar cells. Energy Environ Sci 7:2968–2973

SBskin (2015) www.sbskin.it

Sirringhaus H, Brown PJ, Friend RH, Nielsen MM, Bechgaard K, Langeveld-Voss BMW, Spiering AJH, Janssen RAJ, Meijer EW, Herwig P, de Leeuw DM (1999) Two-dimensional charge transport in self-organized, high-mobility conjugated polymers. Nature 401:685–688

Skandalos N, Karamanis D (2015) PV glazing technologies. Renewe Sustain Energy Rev 49:306–322

Solamer (2015) http://www.solarmer.com

Solaronix SA (2015) www.solaronix.com

Spena A, Cornaro C, Serafini S (2008) Outdoor ESTER test facility for advanced technologies PV modules. In: Proceedings of the 33rd IEEE PV specialists conference, San Diego (CA), 11–16 May 2008

Stranks SD, Eperon GE, Grancini G, Menelaou C, Alcocer MJ, Leijtens T, Herz LM, Petrozza A, Snaith HJ (2013) Electron-hole diffusion lengths exceeding 1 micrometer in an organometal trihalide perovskite absorber. Science 342:341–344

Tagliaferro R, Colonna D, Brown TM, Reale A, Di Carlo A (2013) Interplay between transparency and efficiency in dye sensitized solar cell. Opt Express 21(3):3235–3242

Tian H, Yu X, Zhang J, Duan W, Tian F, Yu T (2012) The Influence of Environmental Factors on DSCs for BIPV. Int J Electrochem Sci 7:4686–4691

Toshiba (2015) http://www.toshiba.co.jp

Toyoda T, Sano T, Nakajima J, Doi S, Fukumoto S, Ito A, Tohyama T, Yoshida M, Kanagawa T, Motohiro T (2004) Outdoor performance of large scale DSC modules. J Photochem Photobiol A Chem 164:203–207

Wang J-W, Ball JM, Barea EM, Abate A, Alexander-Webber JA, Huang J, Saliba M, Mora-Sero I, Bisquert J, Snaith HJ, Nicholas RJ (2014) Low-temperature processed electron collection layers of graphene/TiO_2 nanocomposites in thin film perovskite solar cells. Nano Lett 14:724–730

Wu Y, Islam A, Yang X, Qin C, Liu J, Zhang K, Peng W, Han, L (2014) Retarding the crystallization of PbI2 for highly reproducible planar-structured perovskite solar cells via sequential deposition. Energy Environ Sci 7:2934–2938

Xing G., Nripan Mathews, Shuangyong Sun, Swee Sien Lim, Yeng Ming Lam, Michael Grätzel, Subodh Mhaisalkar, Tze Chien Sum, Long-Range Balanced Electron- and Hole-Transport Lengths in Organic-Inorganic CH3NH3PbI3, Science 2013, 342, 344-347

Yingkou (2015) http://www.opvtech.com/

Yoon S, Tak S, Kim J, Jun Y, Kang K, Park J (2011a) Application of transparent dye- sensitized solar cells to building integrated photovoltaic systems. Build Environ 46:1899–1904

Yoon S, Sehyun T, Jinsoo K, Yongseok J, Kisuk K, Jiyoung P (2011b) Application of transparent dye-sensitized solar cells to building integrated photovoltaic systems. Build Environ 46:1899–1904

Yu G, Gao J, Hummelen J, Wudl F, Heeger A (1995) Polymer Photovoltaic cells: enhanced efficiencies via a network of internal donor-acceptor heterojunctions. Science 270:1789

Zardetto V, Di Giacomo F, Garcia-Alonso D, Keuning W, Creatore M, Mazzuca C, Mazzuca C, Reale A, Di Carlo A, Brown TM (2013) Fully plastic dye solar cell devices by low-temperature UV-irradiation of both the mesoporous TiO_2 photo- and platinized counter-electrodes. Adv Energy Mater 3:1292–1298

Zhang W, Anaya M Lozano G, Calvo ME, Johnston MB, Míguez H, Snaith HJ (2015) Highly efficient perovskite solar cells with tunable structural color. Nano Lett 15:1698–1702

Zygmanski P, Abkai C, Han Z, Shulevich Y, Menichelli D (2015) Low-cost flexible thin-film detector for medical dosimetry applicationsm. J Appl Clin Med Phys 15:1

Chapter 12
Bio-Based Polyurethane Foams for Heat-Insulating Applications

Maria Kurańska and Aleksander Prociak

Abstract In this chapter, the sustainable development of rigid polyurethane foams for heat-insulating applications is described. Firstly, the most important aspects as the use of bio-based and environmentally friendly components in the formulations of polyurethane systems as well as requirements for heat insulating of buildings are presented. Next, the complex mechanism of heat transport in porous materials is discussed including the influence of cell structure on the thermal conductivity of final rigid polyurethane foams. In the two last parts of this chapter, the most important components used in various methods of polyurethane foam synthesis are described. Moreover, the effects of bio-components and foaming conditions on the cell structure and physical mechanical properties of rigid polyurethane foams are discussed.

12.1 Introduction

Currently, the idea of sustainable development played a significant role in shaping the thinking about the relationship between economy, society, and environment. One of the most significant factors influencing climate changes is an increase in the concentration of greenhouse gases (GHG—greenhouse gases), including carbon dioxide (CO_2).

In order to reduce GHG emissions, especially CO_2, it is necessary to identify the main areas of greenhouse gases production. One of the biggest sources of CO_2 emissions is burning of fossil fuels to produce energy for heating, cooling, or operation of buildings. CO_2 emissions from fossil fuel combustion and industrial processes contributed about 78 % to the total GHG emission increase between 1970 and 2010 (Intergovernmental Panel on Climate Change 2015).

M. Kurańska · A. Prociak (✉)
Department of Chemistry and Technology of Polymers,
Cracow University of Technology, Kraków, Poland
e-mail: aprociak@pk.edu.pl

F. Pacheco Torgal et al. (eds.), *Nano and Biotech Based Materials for Energy Building Efficiency*, DOI 10.1007/978-3-319-27505-5_12

Reduction of CO_2 emissions is possible by modernization of buildings and increase of their thermal insulation. The need to take such measures imposes changing legislative requirements. The most important changes concern a reduction of the maximum overall heat transfer coefficient for all types of buildings and the annual consumption of building by using non-renewable energy.

The growing requirement for thermal insulation of buildings makes the selection of a heat-insulating material increasingly important. The overriding factor for choosing insulation should be the value of thermal conductivity. Among the commercially available insulation materials, the lowest coefficient of thermal conductivity is offered by rigid polyurethane (PUR) and polyurethane-polyisocyanurate (PUR-PIR) foams. Additionally, rigid PUR foams have relatively good specific mechanical properties (strength to weight ratio) and good thermal ones (Kakroodi et al. 2015; Faruk et al. 2014; Gao et al. 2013; Lee et al. 2007). The thermal conductivity is declared by the producers of rigid PUR and PUR-PIR foams to be in the range of 0.022–0.028 W/m K (Rutowicz 2012).

Low thermal conductivity is associated with thinner insulation for any specified insulation level, and thinner insulation means that it is easier to fit it into the building cavity. Good mechanical properties and strong adhesion to other materials allow a broad field of applications from insulation boards for roofing, walls, floors, and ceilings to window frame insulation and foam sealants to metal-faced sandwich panels for industrial buildings. Rigid PUR foams can be applied using in situ method by spraying onto the desired surface or pouring into the mold. The application of PUR foams as heat-insulating materials is an ideal solution for the lightweight, low-energy, or zero-energy building.

The properties of the rigid polyurethane foams depend mainly on raw materials used in their synthesis as well as the cell structure and apparent density of final products. The low thermal conductivity of such foams allows relatively thin building envelopes with a high thermal resistance R-value (m^2 K/W) (Pargana et al. 2014; Petter 2011). Currently, in the synthesis of rigid foams, different types of vegetable oils, such as palm, rapeseed, soybean, linseed oil, and natural fillers have been used. In a large number of papers, the presented results confirm that PUR foams can be successfully made using natural oil-based polyols (NOPs). The properties of the foams modified with NOPs can be changed by controlling variables, such as water content, isocyanate index, catalysts and fillers (Kurańska et al. 2015a; Prociak 2008a, b; John et al. 2002).

12.2 Heat-Insulating Properties of Polyurethane Foams

Thermal conductivity (λ) represents the heat flow in watts (W) through a 1 m^2 surface and 1-m-thick flat layer of a material when the temperature difference between the two surfaces is 1 Kelvin (K). The unit of λ is W/(m K). Another parameter, described as thermal resistance (R), represents heat-insulating effect of a

constructional layer. This parameter is calculated as the ratio of the material layer thickness (d) and its λ-value: R = d/λ. The unit of R is (m^2 K)/W. In a heat-insulating material comprising several layers, the thermal resistances of the individual layers are added together. Thermal transmittance (U) is the heat flow in watts (W) through 1 m^2 of a building component when the temperature difference between the surfaces in the direction of the heat flow is 1 K. U-value is calculated as U = 1/R.

Due to the complex mechanism of heat transport in porous materials, total thermal conductivity of PUR foams λ_F can be written as a sum according to formula 12.1 (Prociak et al. 2000; Biedermann et al. 2001; Cunningham et al. 1989).

$$\lambda_F = \lambda_g + \lambda_s + \lambda_r \left(\frac{W}{m\,K}\right) \tag{12.1}$$

where

λ_g is the thermal conductivity contribution arising from cell gases,
λ_s is the thermal conductivity contribution arising from the polymer matrix,
λ_r is the thermal conductivity contribution arising from the radiative heat transfer within the foam.

The above values are not additives and therefore are considered as contributions in total λ_F. The transfer of heat by convection for foams with cell diameters smaller than 3 mm may be negligible. It was found that the thermal conductivity of the blowing agent contained in cells has the greatest effect on the coefficient of thermal conductivity of foam materials. The blowing agent in foams with an apparent density of 30–40 kg/m^3 constitutes 92–98 % of the material volume. The heat conduction coefficient according to the kinetic theory of gases increases with an increasing temperature and decreases with an increasing molar mass, but is independent of pressure in the range from 10^2 to 10^5 Pa (Prociak 2008a). The thermal conductivity of the blowing agent at a reference temperature of 10 °C is considerably lower than that of the air (λ_{air} = 0.024 W/m K).

Thermal conductivity of PUR foams depends also on the thermal conductivity of the solid material in struts and walls of cells. The heat transfer through a foamed material in the directions perpendicular and parallel to the foam rise may differ, and this is an effect of cell anisotropy. Park et al. (2013) examined the effect of water, cyclopentane, and mixtures thereof, as well as the size of cells on the thermal conductivity. A significant impact on the property of foams was related to the kind of the blowing agent. The use of cyclopentane gave the lowest thermal conductivity compared to water and a mixture of cyclopentane and water. The cell size and shape also affect thermal conductivity of foams (San 2007; Roux and Balme 1990). An increase in cell size affects the growth of thermal conductivity, irrespective of the blowing agent (Park et al. 2013). The heat-insulating properties can be improved by increasing the cell isotropy and reducing the radiative heat transfer within foam (Prociak et al. 2000).

12.3 Raw Materials for Synthesis of Bio-Polyurethane Foams

Properties of rigid PUR foams can be optimized for a wide range of applications through a well-designed formulation of polyols, isocyanates, catalysts, surfactants, and blowing agents. A change in a formulation could alter the properties of the foams by changing their chemical and cellular structure (Jin et al. 2002; Kurańska and Prociak 2012).

One of the main components in the synthesis of rigid PUR foams is polyols that largely determine the properties of final products. Polyols are chemical compounds containing in their structure hydroxyl groups. Rigid PUR foams are derived from highly branched polyols of low molecular weight. Suitable molar mass, hydroxyl group number, functionality, and stiffness of the chain macromolecules are the determining factors for the properties of PUR foam. Polyols with a lower molecular weight (having the same functionality) increase the exothermic effect of the reactions and improve the compressive strength and dimensional stability, however increase the friability of rigid foams. Increased functionality of a polyol while maintaining the same molar mass improves the heat resistance and mechanical strength as well as dimensional stability of foams. A higher hydroxyl group number of used polyols improves the compressive strength of the obtained foams (Seo et al. 2004).

Currently, rigid PUR-PIR foams are obtained mainly from polyester polyols, both aliphatic and aromatic, as well as high molecular weight polyether polyols. As far as thermal stability is concerned, it is preferable to use aromatic polyols in a synthesis of heat-insulating materials and these are used more and more due to their low viscosity and low price.

Nowadays, the polyols for PUR foams production are derived predominantly from a petrochemical feedstock. Fluctuations in oil prices and legislative requirements for environmental protection guide the chemical industry toward an introduction of new green technologies. One way to meet these requirements is an introduction of polyols based on vegetable oils into the synthesis of polyurethane (Gu et al. 2012). Bio-based polyols can be derived from several food and non-food crops such as soybean oil (Dai et al. 2009; Banik and Sain 2009; Mello et al. 2015), castor oil (Zhang et al. 2014), and cardanol derivatives from soybean oil (Kayode 2015), sunflower oil, cashew nut oil (Ionescu et al. 2012), linseed oil (Yadav et al. 2009), and rapeseed oil (Fridrihsone et al. 2013; Kurańska and Prociak 2012).

Natural oils have in their structure the reactive sites (ester bonds and double bonds) that can be modified to compounds containing hydroxyl groups. One of the vegetable oils, which can directly react with isocyanate, is castor oil. A production of bio-based polyols can be achieved by modifying unsaturated or ester bonds of triglycerides of higher fatty acids.

Several techniques have already been proposed for the production of bio-based polyols from vegetable oils, such as hydroformylation (Guo et al. 2002), hydrogenation, epoxidation and opening of oxirane rings (Kurańska et al. 2015a, b),

transesterification (Fridrihsone et al. 2013; Lubguban et al. 2009), amidization (Kirpluks et al. 2013; Stirna et al. 2013), ozonolysis (Ionescu et al. 2012), hydrogenation (Sonnenschein and Wendt 2013), and microbial conversion (Kakroodi et al. 2015; Gu et al. 2013; Lubguban et al. 2009).

The second important reactant in the synthesis of rigid PUR foams is an isocyanate component. The isocyanate compounds for polyurethane synthesis should contain at least two isocyanate groups capable of reacting with the hydroxyl groups of polyols. As a result of the reaction (12.2) between polyols and isocyanates, urethane bonds are formed. There are two basic types of isocyanates, aromatic and aliphatic. In the production of polyurethane foams, aromatic isocyanates are most commonly used because they have higher reactivity, which is required in such a type of products.

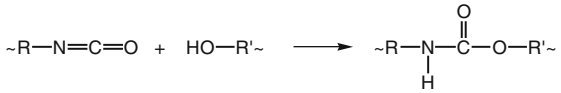

(12.2)

In practice, rigid PUR foams are produced using liquid polymeric diphenylmethane diisocyanate (PMDI), because diphenylmethane diisocyanate (MDI) at room temperature is a solid raw material. Rigid PUR foams based on PMDI have more favorable mechanical properties and lower flammability compared to foams received from other isocyanates such as toluene diisocyanate (TDI). Moreover, PMDIs have a reduced vapor pressure, which reduces the toxicity problem of these components, unlike the conventional isocyanate.

Generating a gas is an essential part in the synthesis of rigid PUR and PUR-PIR foams. The blowing agents may be obtained by a chemical reaction (chemical blowing agent) and physical evaporation (physical blowing agents). Carbon dioxide is an example of chemical blowing agent, which is generated by the reaction (12.3) of isocyanate groups with water (Prociak et al. 2014):

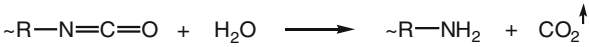

(12.3)

This strong exothermic reaction leads also to primary amines that in the next reaction with isocyanates create urea bonds. A too high content of urea groups may cause a higher friability of foams, as well as a deterioration of the foam adhesion to various substrates. Other disadvantages of the water use are the high viscosity of the reaction mixture and an increase of the polyurethane system cost due to a higher consumption of isocyanate.

The above-mentioned negative aspects of the water use as a chemical blowing agent are minimized by very important advantages. Currently, the most important issue in the field of PUR is the impact of blowing agents on the environment. Carbon dioxide has zero ozone depleting potential (ODP) and a very low value of global-warming potential (GWP). Moreover, carbon dioxide is not flammable.

A physical blowing agent should have possibly the lowest thermal conductivity because it most substantially determines the heat-insulating properties of foamed materials. In addition, physical blowing agents must have a boiling temperature of

30 °C, good solubility in polyol components, lack of toxicity and flammability. The choice of new physical blowing agents depends on environmental criteria, physical–chemical, and technological solutions.

Currently, there are two important environmental parameters which include a zero-ODP and a very low GWP. The main physical–chemical properties that are taken into account in the selection of physical blowing agents are the molar mass, volatility, reactivity, solubility in polyol and isocyanate components, the molar heat of vaporization, thermal conductivity, and the diffusion rate of foams. Technological requirements relate to flammability, toxicity, and prices (Kurańska et al. 2015a, b).

The requirements for a zero-ODP resulted in an increased interest in materials which do not contain chlorine atoms. Trichlorofluoromethane (CFC-11) was the primary blowing agent for the urethane industry. CFC-11 is one of the compounds suspected of damaging the Earth's ozone layer. It was initially replaced by compounds from the group of hydrocarbons (HCs) and hydrochlorofluorocarbons (HCFCs). In accordance with the 1987 Montreal Protocol, HCFCs have to be replaced by new generation blowing agents (Yu-Hallada et al. 1993). Among the new generation of blowing agents in use, there are pentane isomers (Pielichowski et al. 2003; Prociak et al. 2000), and fluorinated derivatives of ethane, propane, and butane. The blowing agents replacing HCFC-141b may be HFC-134a (1,1,1,2-tetrafluoroethane), HFC-356 mffm (1,1,1,1,3,3-hexafluorobutane), HFC-365mfc (1,1,1,3,3-pentafluorobutane), and HFC-245fa (1,1,1,3,3-pentafluoropropane).

Solvay Fluor developed Solkane 365/227, which is a mixture of two fluorinated hydrocarbons HFC-365mfc and HFC-227ea (Technical Datasheet. Solvay). This blowing agent allows obtaining PUR materials with a low apparent density and favorable thermal conductivity. The properties of Solkane 365/227 are similar to those of HCFC-141b. An introduction of at least 5 wt% HFC-227ea to HFC-365mfc allows obtaining a nonflammable product (HFC-365mfc is classified as a flammable product). The ignition energy of the described physical blowing agent is more than 50 times greater than that of n-pentane. Solkane 365/227 also meets the requirements of the Montreal Protocol.

Honeywell developed Fourth Generation Liquid Blowing Agent—Honeywell Solstice® 1233zd(E), trans-1-chloro-3,3,3-trifluoropropene is a liquid halogenated olefin (Technical Datasheet. Honeywell Solstice®). This component is marketed commercially as Honeywell Solstice® Liquid Blowing Agent (LBA). Solstice LBA has a low GWP and is a nonflammable replacement blowing agent for applications where hydrocarbons, HFCs, HCFCs, and other liquid blowing agents are currently used. Solstice LBA is a nonflammable liquid having a room temperature boiling point (Technical Datasheet. Honeywell Solstice®). In the case of pentane, its isomers require additional protection against the flammability of a polyurethane foam through the use of various types of flame retardants (Król 2009, 2010).

In the synthesis of PUR, there is a series of chemical reactions. Catalysts may affect the formation kinetics of bonds, which are characteristic of polyurethane foams as well as the release rate of CO_2. A suitable gelling time of a PUR system affects the apparent density of foams and their cellular structure, which importantly

influences the properties of final products. The catalysts are used primarily to increase the rate of isocyanate reaction with water, often referred to as foaming catalysts. The compounds preferring the reaction of hydroxyl groups with isocyanates are defined as gelling catalysts.

One group of catalysts used in the synthesis of PUR is amine catalysts. The most common group includes compounds containing a tertiary amine. These compounds are characterized by the presence of a free electron pair in the nitrogen atom, which affects the activation of both hydroxyl groups and isocyanate groups. Tertiary amines are often used in the production of rigid PUR foams. The use of such catalysts allows controlling the balance of foaming and gelling reactions. However, the main disadvantage of catalysts based on tertiary amines is their unpleasant smell, which is problematic in the production.

One of the challenges for manufacturers of the components for the polyurethane foams and finished products is to improve recipes with regard to the reduction of the volatile organic compounds (VOC) content. Among the proposed solutions are the use of reactive tertiary amines having a hydroxyl group. Use of these compounds, due to their ability to build in the polymer chain, reduces the emission of VOC.

Another solution leading to reducing VOC emissions is the use of polyols with improved reactivity. Such polyols are obtained by incorporating a tertiary amine in the polyol chain (Prociak et al. 2000). Another group of catalysts used in the synthesis of rigid polyurethane foams are organometallic catalysts. These compounds mainly catalyze the reaction of hydroxyl groups with isocyanate groups. In the case of rigid PUR-PIR foams, it is necessary to use catalysts for the trimerization of isocyanate groups. In industry, potassium salts of carboxylic acids (potassium acetate, potassium octoate), tertiary amine (pentamethyldiethylenetriamine—PMDETA), and quaternary ammonium derivatives are mostly used. These catalysts have a different nature of their action; therefore, their mixtures are most frequently used.

The cellular structure of the PUR foams affects their basic properties including heat conductivity and mechanical strength. Surfactants play an important role in each stage of the polyurethane foam synthesis. In the first stage, surfactants facilitate mixing of the components and then stabilize the resulting bubbles in the liquid reaction mixture, preventing them from merging into larger bubbles as well as allowing a control over the time and degree of cells opening. Currently, the surfactants are mainly polyether-polysiloxane copolymers.

For the use of rigid PUR and PUR-PIR foams in the construction industry, these materials are modified by various types of additives, flame retardants, organic and inorganic fillers, reinforcing fibers, and pigments.

12.4 Synthesis and Properties of Bio-Polyurethane Foams

The term “polyurethanes” covers a wide range of materials produced by the reaction of multifunctional isocyanates with components containing at least two hydroxyl groups. The basic reactions have been described in the previous parts of

this chapter. Depending on the process conditions and catalysts used, other reactions can also take place, leading to such bonds as urea, biuret, and allophanate.

The foamed polyurethane materials are obtained mainly using two-component systems (A + B). Component A contains a mixture of polyols, catalysts, stabilizers, auxiliaries, and blowing agents, and the component B is an isocyanate.

On an industrial scale, high-speed mixing-dosing devices of low or high pressure are used to produce rigid PUR foams. It is also possible to use mobile equipment that enables the production and application of a PUR foam "in situ," which allows meeting the need for thermal insulation. This method is also used to synthesize heat-insulating PUR-PIR foams in the production of sandwich boards and pipelines (Żabski and Papiński 2010).

Another increasingly popular method for producing heat-insulating layers is spraying PUR foams on roofs, walls, and ceilings. This method allows obtaining PUR foams having accurate thickness of heat-insulating layer in the place of application.

Rigid PUR foams may also be prepared in the form of blocks which are then processed into plates. Heat-insulating materials are evaluated primarily in terms of thermal conductivity—λ, thermal resistance—R, as well as the heat transfer coefficient "U" of the obtained layer. However, in spite of very good insulating properties, rigid PUR foams sometimes do not pass the actual flammability tests demanded by insurance companies (Żabski and Papiński 2012). Improving the fire resistance can be achieved by increasing the amount of the flame retardants content in PUR system, but such a solution may increase the emissions of toxic gases during material combustion. In addition, flame retardants significantly worsen the heat resistance and mechanical strength of PUR.

One of the solutions to this problem is to modify the formulation of a foam material and the use of an unconventional reaction of isocyanates. In the middle of the twentieth century, studies were conducted on reactions of aromatic isocyanates and showed that these compounds may be suitable catalysts forming a group called isocyanurate having higher heat resistance than the urethane linkages.

The first patent for manufacturing polyisocyanurate (PIR) foams was published in 1964. Rigid foams containing isocyanurate groups significantly affected the development of insulating materials with higher thermal stability, flame retardancy, chemical resistance, and dimensional stability.

High thermal stability isocyanurate groups made PIR foams commercially available materials for insulation of roofs which meet the highest standards of fire resistance. Nowadays, a large part of the market of rigid foams belongs to the rigid PUR-PIR characterized by improved fire resistance with respect to traditional rigid PUR foams. Rigid PUR-PIR foams are prepared by reaction of the polyol with excess of isocyanate in the presence of suitable catalyst. Excessive isocyanate groups react with each other to form isocyanurate rings (12.4). The presence of the isocyanurate groups in PUR-PIR foams allows the production of heat-insulating materials with good fire resistance using cheaper flame retardants.

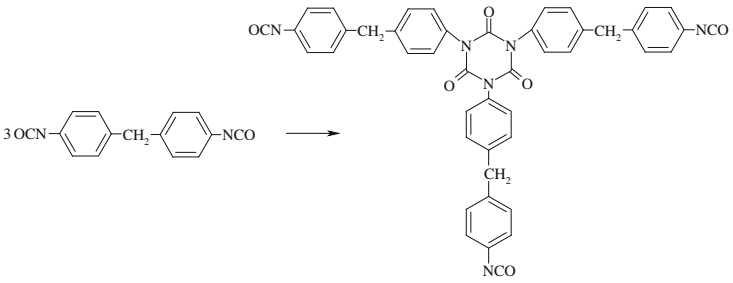

(12.4)

In the last years, an increasing interest in PUR and PUR-PIR materials has led to the development of research aimed to introduce renewable raw materials in foam formulations (Mosiewicki and Aranguren 2013; Kakroodi et al. 2015). The research concerns mainly the replacement of partially or totally petrochemical polyols by bio-polyols based on natural oils (Gu et al. 2011, 2013; Fan et al. 2013).

When designing an insulating layer, one should take into account the fact that the method of foaming significantly affects the cellular structure of produced foam materials. The cellular structure has a decisive influence on the thermal insulation and mechanical properties of rigid PUR and PUR-PIR foams.

Conditions and a properly selected catalyst system, especially when bio-polyols are used, also have a very significant impact on the cell structure of PUR foams. While obtaining rigid PUR-PIR, two-stage growth behavior of the material can be observed. This is due to the fact that trimerization catalysts operate at higher temperatures.

The phenomenon of open cells is disadvantageous in the case of rigid PUR foams that are used as heat-insulating materials because dry materials should have closed cell content greater than 90 % (Prociak 2008a). Choe et al. (2004) analyzed the influence of gelation and foaming catalysts, as well as the chemical and the physical blowing agents on the foaming reaction rate, which determined the physical characteristics of foam materials.

Changing the content of the catalysts has a direct impact on the cellular structure of obtained foamed materials. Increasing the amount of gelling catalyst resulted in a decrease in the mean cell size of the cells from 307 to 132 μm. The analysis of the structure carried out by Choe et al. (2004) showed that the rate of gas bubbles formation increases with increasing amounts of the catalyst, and the type of catalyst is not critical.

The rate of expansion affects the shape of the cells. If the foaming reaction takes place slowly, the cells are characterized by an isotropic shape, which in turn affects the mechanical properties of the foamed materials, they exhibit the same characteristics regardless of the direction of measurement. In the case of fast processes, it is very important to analyze the cellular structure of the foam and to correlate its properties measured in parallel and perpendicular to the foam rise direction. The cellular structure also depends on the apparent density, viscosity, and the reactivity of the components used for the synthesis of porous material (Prociak et al. 2014).

The most important stage in the synthesis of rigid PUR foams is the foaming process. The effect of introducing new components into a PUR formulation can be analyzed using the FOAMAT device, which allows determination of characteristic parameters, such as the foam rise height, reaction mixture temperature, pressure, dielectric polarization, and mass loss during foaming.

Generally, bio-polyols have lower reactivity compared to petrochemical polyols as described in the works (Yang et al. 2012; Ionescu et al. 2010; Tan et al. 2011; Ionescu 2008). It is confirmed by the results shown in Fig. 12.1.

The lower reactivity of the bio-polyol is evidenced by a slower decrease of dielectric polarization, which is a measure of the reaction progress, as well as by a lower maximum temperature during the foaming process of PUR systems modified with the bio-polyol replacing 30, 50, and 70 wt% of the petrochemical polyol.

Prociak (2008a, b) analyzed the effect of bio-polyols based on natural oil (rapeseed, soybean, sunflower, linseed) on the thermal insulation properties of rigid PUR foams. Studies have shown that a partial replacement of a petrochemical polyol by a polyol based on rapeseed oil (30 wt%) in a PUR has a beneficial effect on the cell structure and thermal insulation properties of rigid PUR foams. It has been found that a PUR foam modified with bio-polyols (30 wt%) is characterized by lower values of thermal conductivity in comparison with the reference material.

A significant part of the published works concerns the modification of polyurethane foams with polyols based on soybean oil (Tu et al. 2007, 2008, 2009; Guo et al. 2000). Fan et al. (2013) examined the impact of a polyol from soybean oil with different viscosities on the physical properties of PUR foamed with carbon dioxide generated by the reaction of isocyanate groups with water. The content of the bio-polyol based on soy oil in the formulation of rigid PUR foams was 10, 20, 30, 40, and 50 % of the weight of polyols premix. The apparent density of the obtained materials decreased with increased amounts of the bio-polyol in the formulations. Decreasing hydroxyl number of polyol premix by an addition of a bio-polyol resulted in a reduction in the apparent density of the foams and the content of closed cells which influenced an increase of the coefficient of thermal conductivity (Fan et al. 2013). Rigid PUR foams modified with 30 wt% of

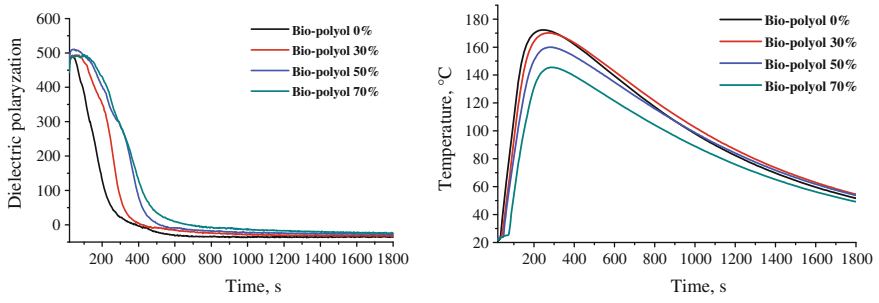

Fig. 12.1 The influence of a rapeseed oil-based polyol on the dielectric polarization and temperature during the foaming process

bio-polyols were characterized by lower compressive strength. However, a higher content of catalyst or higher functionality of a bio-polyol makes it possible to obtain foam structures with better mechanical properties. Banik and Sain (2008) have shown that the application of soybean oil-based polyols (SOP) with similar OH-values but with various viscosities has a different influence on the mechanical properties of final products. The foams prepared using SOP with higher viscosity had higher compressive strength.

Tan et al. (2011) modified rigid PUR foams with a soybean-based bio-polyol in a content of 25, 50, 75, and 100 wt%. The materials obtained with this bio-polyol were characterized by a smaller cell size than the reference foam. The apparent densities of the foams were at similar levels with the exception of the foam, wherein the petrochemical polyol had been completely replaced by SOP. The glass transition temperature of the obtained materials increased from 98 to 142 °C with an increasing content of the bio-polyol in the foam. Moreover, increasing the content of SOP led to a reduction of the cell size and improvement of the mechanical strength of foams. The closed cell content of the obtained rigid PUR foams remained at a similar level as in the case of the reference foam which resulted in a similar coefficient of thermal conductivity.

Veronese et al. (2011) modified PUR foams using bio-polyols from soy oil and castor oil. The bio-polyol from soybean oil was obtained by oxidation of double bonds followed by oxirane ring opening using a formic acid. In order to increase the hydroxyl number, the bio-polyol was subject to transesterification triethanolamine (SO1). Castor oil also reacted with triethanolamine (CO1) and glycerol (CO2). The cell structure of the foams synthesized with polyols CO1 and CO2 was homogeneous, unlike that of the foams synthesized with polyol SO1.

The mechanical properties of the foams involving bio-polyols deteriorated by approx. 30 % compared with the reference material, and the material synthesized with the participation of polyol SO1 have less compressive strength by approx. 50 %. Lower values of compressive strength of the material with polyol SO1 may be related to the plasticizing effect of the side chains within the structure of the organic polyol and uniform cell structure. Furthermore, it was found that the reference material when compared to the modified one had the highest thermal stability in the early stages of degradation (Veronese et al. 2011).

An analogous method for the preparation of a bio-polyol was used by Hu et al. (2002), but they used in the synthesis a derivative of rapeseed oil. A petrochemical polyol was replaced by a rapeseed oil-based polyol. The obtained foams were characterized by an apparent density of approx. 40 kg/m^3 and properties comparable to the reference material.

Narine et al. (2007) also showed that rigid PUR foams based on castor oil have favorable mechanical properties than foam materials prepared from polyols produced from the rapeseed and soybean oils. The changes of the foam properties were associated with different values of the hydroxyl group number and the position of the hydroxyl groups in the molecule chain of bio-polyols.

The literature also describes the effect of bio-polyols on the properties of rigid PUR-PIR foams. Kurańska et al. (2015a, b) have obtained rigid PUR-PIR foams

with three different isocyanate indices (150, 200, and 250) and three types of rapeseed oil-based polyols. The bio-polyols were synthesized using the epoxidation and opening of oxirane rings method (EP), as well as transesterification with triethanolamine (TE) and transamidization with diethanolamine (DE). They found that mechanical and thermal properties of rigid PUR-PIR foams depended on the isocyanate index and the type of bio-polyols. Increasing the isocyanate index gave rigid foams with increased thermal stability, improved mechanical properties, and decreased flammability (Fig. 12.2).

The PUR-PIR systems modified with bio-polyol synthesized in the reaction of epoxidation and oxirane ring opening had the largest number of isotropic cells which beneficially influenced on compressive strength and heat-insulating properties of the rigid PUR-PIR foams (Table 12.1).

Stirna et al. (2008) found that it is possible to obtain foams based on bio-polyols having good dimensional stability and mechanical strength. Javni et al. (2004) synthesized rigid PUR-PIR foams based on the bio-polyol from soybean oil. The aim of that study was to analyze the impact of the structure of the bio-polyol and isocyanate index on selected properties of rigid PUR-PIR foams. The isocyanate index of the obtained rigid PUR-PIR foams ranged from 110 to 350. Increasing the isocyanate index improved thermal stability, resistance to flammability, and compressive strength of the modified foams as compared to the reference PUR-PIR foams based on a petrochemical polyol.

The content of biodegradable components in the PUR matrix can be increased also by introducing different types of natural fillers such as flax fibers (Kurańska and Prociak 2012), wood fibers (Kurańska et al. 2015a; Cabulis et al. 2012; Yuan and Shi Sheldon 2009; Casado et al. 2009), lignin (Luo et al. 2013; Paberza et al. 2014), and microcellulose (Luo et al. 2012; Zhu et al. 2012) (Table 12.2).

Zhu et al. (2012) obtained rigid PUR foams based on a soy polyol and then modified them with cellulose microfibers. The authors analyzed the effect of the filler on the thermal properties, cellular structure, and the related compressive strength of the foams. The modification of the PUR with microcellulose caused a decrease in the cell size which had an effect of increasing the compressive strength by more than 40 %. Luo et al. (2013) showed that the most favorable properties

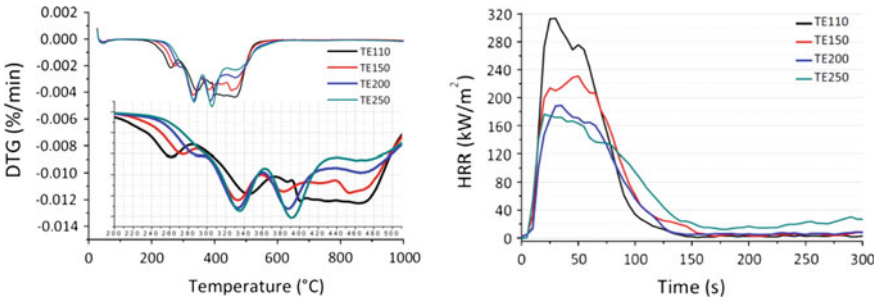

Fig. 12.2 The influence of the isocyanate index on the thermal stability and heat release rate of the PUR-PIR foams based on bio-polyol TE (Kurańska et al. 2015a, b)

Table 12.1 Selected properties of rigid PUR-PIR foams modified with different bio-polyols based on rapeseed oils (Kurańska et al. 2015a, b)

Foam symbol	Apparent density (kg/m$^{3)}$	Water absorption (vol.%)	Brittleness (%)	Coefficient of thermal conductivity (m W/m K)	Content of closed cells (%)
EP150	37.5	0.84	27.1	23.1	87.9
TE150	34.7	0.53	48.5	24.1	91.9
DE150	39.1	0.57	35.7	24.5	88.1
EP200	35.0	0.87	49.4	24.0	87.3
TE200	38.1	0.46	42.6	24.1	94.0
DE200	34.9	0.57	46.6	23.8	87.8
EP250	37.0	0.99	75.0	23.9	88.7
TE250	35.3	0.60	58.3	24.3	90.8
DE250	38.2	0.45	46.1	24.2	86.8

Table 12.2 Selected properties of rigid foams modified with bio-components

Natural filler type	Properties of rigid foams modified with bio-components			
	Content of natural filler	Apparent density (kg/m^3)	Compressive strength (kPa)	Thermal conductivity (m W/m K)
Flax fiber (Kurańska and Prociak 2012)	5 php	40	190	20.15
	10 php	40	200	20.70
	15 php	44	215	20.75
Hemp fiber (Kurańska and Prociak 2012)	10 php	47	230	21.75
Lignin (Paberza et al. 2014)	2.4 wt%	48	320	32.40
	6.3 wt%	49	280	29.80
Lignin (Luo et al. 2013)	5 php	65	400	–
	10 php	76	460	–
	15 php	86	320	–
Wood fiber (Kurańska et al. 2015a)	3 wt%	46	260	23.46
	6 wt%	45	210	23.63
Microcrystalline cellulose (Luo et al. 2012)	1 wt%	68	310	–
	5 wt%	50	170	–
	10 wt%	53	160	–
Cellulose microfibers (Zhu et al. 2012)	0.5 php	73	110	–
	1 php	70	151	–
	2 php	85	170	–

Note php is per hundred polyol

were observed for materials with such a natural filler in an amount of 10 wt%. The glass transition temperature of foams was increased with an increase in the lignin content from 5 to 15 % by weight. Luo et al. (2013) observed (like Zhu et al.) an

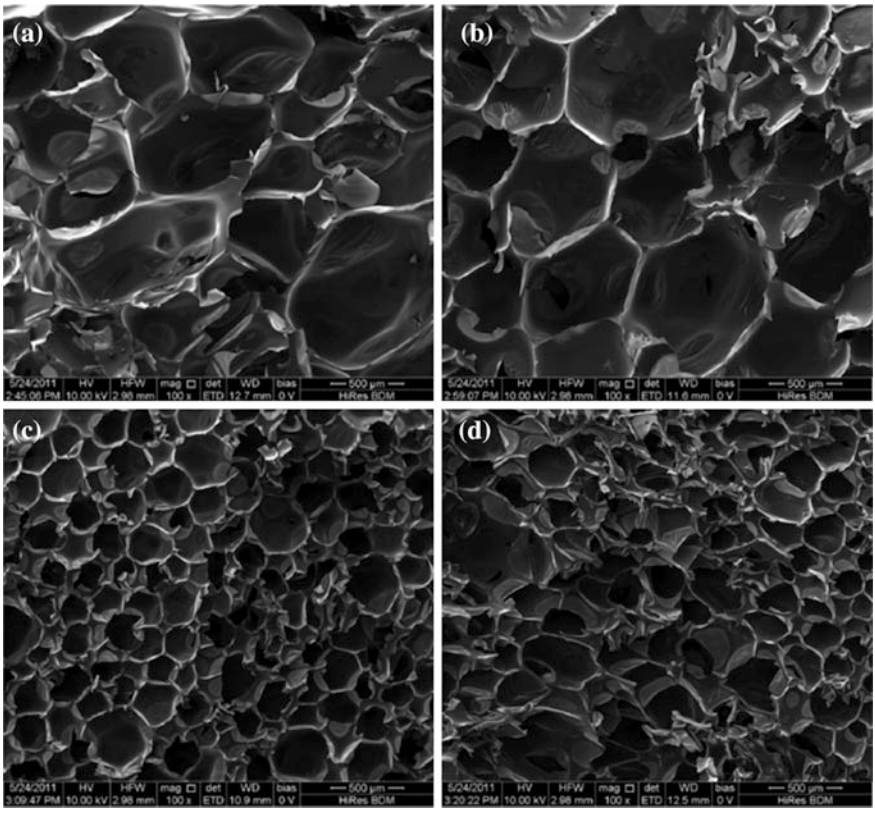

Fig. 12.3 SEM images of foam unmodified (**a**) and modified with lignin in amount 5 (**b**), 10 (**c**), and 15 wt% (**d**) (Luo et al. 2013)

effect of a cell size reduction in the case of foams modified with microfiller as shown in Fig. 12.3.

In other published works related to the modification of the PUR matrix using bio-polyols, authors found similar relationships, mechanical strength, and thermal properties (Khazabi et al. 2011; Kurańska et al. 2013; Gu et al. 2011). It was shown that suitable filler content allows to improve the mechanical and thermal properties of the foams.

References

Banik I, Sain MM (2009) Water-blown soy polyol based polyurethane foams modified by cellulosic materials obtained from different sources. J Appl Polym Sci 112:1974–1987

Banik I, Sain MM (2008) Water blown soy polyol-based polyurethane foams of different rigidities. J Reinf Plast Compos 27:357–373

Biedermann A, Kudoke C, Merten A, Minogue E, Rotermund U, Ebert HP, Heineman U, Fricke J, Seifert H (2001) Analysis of heat transfer mechanisms in polyurethane rigid foam. J Cell Plast 37:467–481

Cabulis U, Kirpluks M, Stirna U, Lopez MJ, Carmen Vargas-Garcia M, Suarez-Estrella F, Moreno J (2012) Rigid polyurethane foams obtained from tall oil and filled with natural fibers: application as a support for immobilization of lignin-degrading microorganisms. J Cell Plast 48:500–515

Casado U, Marcovich NE, Aranguren MI, Mosiewicki MA (2009) High-strength composites based on tung oil polyurethane and wood flour: effect of the filler concentration on the mechanical properties. Polym Eng Sci 49:713–721

Choe KH, Lee DS, Seo WJ (2004) Properties of rigid polyurethane foams with blowing agents and catalysts. Polym J 36:368–373

Cunningham A, Jeffs GMF, Rosbotham ID, Sparrow DJ (1989) Recent advances in the development of rigid polyurethane foams of improved thermal insulation efficiency. J Therm Insul 12:209–222

Dai H, Yan L, Lin B, Wang C, Shi G (2009) Synthesis and characterization of the different soy-based polyols by ring opening of epoxidized soybean oil with Methanol, 1,2-Ethanediol and 1,2-Propanediol. J Am Oil Chem Soc 86:261–267

Fan H, Tekeei A, Suppes GJ, Hsieh FH (2013) Rigid polyurethane foams made from high viscosity soy-polyols. J Appl Polym Sci 127:1623–1629

Faruk O, Sain M, Farnood R, Pan Y, Xiao H (2014) Development of lignin and nanocellulose enhanced bio PU foams for automotive parts. J Polym Environ 22:279–288

Fridrihsone A, Stirna U, Lazdina B, Misane M, Vilsone D (2013) Characterization of polyurethane networks structure and properties based on rapeseed oil derived polyol. Eur Polym J 49:1204–1214

Gao L, Zheng G, Zhou Y, Hu L, Feng G, Xie Y (2013) Synergistic effect of expandable graphite, melamine polyphosphate and layered double hydroxide on improving the fire behavior of rosin-based rigid polyurethane foam. Ind Crops Prod 50:638–647

Gu R, Sain MM, Konar SK (2013) A feasibility study of polyurethane composite foam with added hardwood pulp. Ind Crops Prod 42:273–279

Gu R, Konar S, Sain M (2012) Preparation and characterization of sustainable polyurethane foams from soybean oils. J Am Oil Chem Soc 89:2103–2111

Gu R, Khazabi M, Sain M (2011) Fiber reinforced soy-based polyurethane spray foam insulation. Part 2: thermal and mechanical properties. BioResources 4:3775–3790

Guo A, Demydov D, Zhang W, Petrovic ZS (2002) Polyols and polyurethanes from hydroformylation of soybean oil. J Polym Environ 10:49–52

Guo A, Javni I, Petrovic Z (2000) Rigid polyurethane foams based on soybean oil. J Appl Polym Sci 77:467–473

Hu YH, Gao Y, Wang DN, Hu CP, Zu S, Vanoverloop L, Randall D (2002) Rigid polyurethane foam prepared from a rape seed oil based polyol. J Appl Polym Sci 84:591–597

Intergovernmental Panel on Climate Change (2015) Synthesis report climate change

Ionescu M, Wan X, Bilic N, Petrovic ZS (2012) Polyols and rigid polyurethane foams from cashew nut shell liquid. J Polym Environ 20:647–658

Ionescu M, Petrovic ZS, Wan X (2010) Ethoxylated soybean polyols for polyurethanes. J Polym Environ 18: 1–7

Ionescu M (2008) Chemistry and technology of polyols for polyurethanes. Rapra Technology Ltd, Shawbury

Javni I, Zhang W, Petrovic ZS (2004) Soybean-oil-based polyisocyanurate rigid foams. J Polym Environ 12:123–129

Jin JF, Chen YL, Wang DN, Hu CP, Zhu S, Vanoverloop L, Randall D (2002) Structures and physical properties of rigid polyurethane foam prepared with rosin-based polyol. J Appl Polym Sci 84:598–604

John J, Bhattacharya M, Turner RB (2002) Characterization of polyurethane foams from soybean oil. J Appl Polym Sci 86:3097–3107

Kakroodi AR, Khazabi M, Maynard K, Sain M, Kwon O (2015) Soy-based polyurethane spray foam insulations for light weight wallpanels and their performances under monotonic and static cyclicshear forces. Ind Crops Prod 74:1–8
Kayode AF (2015) A review of vegetable oil-based polymers: synthesis and applications. Open J Polym Chem 5:34–40
Khazabi M, Gu R, Sain M (2011) Fiber reinforced soy-based polyurethane spray foam insulation. Part 1: cell morphologies. BioResources 6:3757–3774
Kirpluks M, Cābulis U, Kurańska M, Prociak A (2013) Three different approaches for polyol synthesis from rapeseed oil. Key Eng Mater 559:69–74
Król P (2010) Ekologiczne uwarunkowania rozwoju technologii wytwarzania i stosowania tworzyw poliuretanowych. Przemysł Chemiczny 89:923–926
Król P (2009) Poliuretany- Przegląd 60-letniego rozwoju ich syntezy i zastosowań. Polimery 54:489–499
Kurańska M, Prociak A, Kirpluks M, Cabulis U (2015a) Polyurethane–polyisocyanurate foams modified with hydroxylderivatives of rapeseed oil. Ind Crops Prod 74:887–897
Kurańska M, Prociak A, Cabulis U, Kirpïuks M (2015b) Water-blown polyurethane-polyisocyanurate foams based on bio-polyols with wood fibers. Polimery 60:35–42
Kurańska M, Prociak A, Kirpluks M, Cabulis U (2013) Porous polyurethane composites based on bio-components. Compos Sci Technol 75:70–76
Kuranska M, Prociak A (2012) Porous polyurethane composite with natural fibres. Compos Sci Technol 72:299–304
Lee CS, Ooi TL, Chuah CH, Ahmad S (2007) Synthesis of palm oil-based diethanolamides. J Am Oil Chem Soc 84:1161–1167
Lubguban AA, Tu YC, Lozada ZR, Hsieh FH, Suppes GJ (2009) Functionalization via glycerol transesterification of polymerized soybean oil. J Appl Polym Sci 112:19–27
Luo X, Amar M, Misraa M (2013) Lignin as a reactive reinforcing filler for water-blown rigid biofoam composites from soy oil-based polyurethane. Ind Crops Prod 47:13–19
Luo X, Mohanty A, Misra M (2012) Water-blown rigid biofoams from soy-based biopolyurethene and microcrystalline cellulose. J Oil Chem Soc 89:2057–2065
Mello VM, Martins GBC, Montenegro MA, Suarez PAZ (2015) Thermal processing of soybean oil to obtain bio-based polymers and bio-oil. Ind Crops Prod 66:255–261
Mosiewicki MA, Aranguren MI (2013) A short review on novel biocomposites based on plant oil precursors. Eur Polym J 49:1243–1256
Narine SS, Kong X, Bouzidi L, Sporns P (2007) Physical properties of polyurethanes produced from polyols from seed oils: II. Foams. J Am Oil Chem Soc 84:65–72
Paberza A, Cabulis U, Arshanitsa A (2014) Wheat straw lignin as filler for rigid polyurethane foams on the basis of tall oil amide. Polimery 59:477–481
Pargana N, Pinheiro MD, Silvestre JD, Brito J (2014) Comparative environmental life cycle assessment of thermalinsulation materials of buildings. Energy Buildings 82:466–481
Park DH, Park GP, Kim SH, Kim WN (2013) Effects of isocyanate index and environmentally-friendly blowing agents on the morphological, mechanical, and thermal insulating properties of polyisocyanurate-polyurethane foams. Macromol Res 21:852–859
Petter JB (2011) Traditional, state-of-the-art and future thermal building insulation materials and solutions—properties, requirements and possibilities. Energy Buildings 43:2549–2563
Pielichowski K, Kulesza K, Pearce EM (2003) Thermal degradation studies on rigid polyurethane foams blown with pentane. J Appl Polym Sci 88:2319–2330
Prociak A, Rokicki G, Ryszkowska J (2014) Materiały poliuretanowe, Wydawnictwo naukowe PWN
Prociak A (2008a) Właściwości termoizolacyjne sztywnych pianek poliuretanowych syntetyzowanych z udziałem polioli z olejów roślinnych. Polimery 53:195–200
Prociak A (2008b) Poliuretanowe materiały termoizolacyjne nowej generacji. Wydawnictwo Politechniki Krakowskiej, Kraków
Prociak A, Pielichowski J, Sterzyński T (2000) Thermal diffusivity of rigid polyurethane foams blown with different hydrocarbons. Polym Test 19:705–712

Roux GA, Balme AL (1990) The Improvement of the effective R-value of rigid polyurethane foams. J Therm Insul 14:98–106

Rutowicz M (2012) Wykonywanie izolacji cieplnych z pianki poliuretanowej. Materiały Budowlane 7:1

San RV (2007) Fluoro-olefine additives to reduce thermal conductivity of rigid foams. PU Magazine 4

Seo WJ, Park JH, Sung YT, Hwang DH, Kim WN, Lee HS (2004) Properties of water-blown rigid polyurethane foams with reactivity of raw materials. J Appli Polym Sci 93:2334–2342

Sonnenschein MF, Wendt BL (2013) Design and formulation of soybean oil derived flexible polyurethane foams and their underlying polymer structure/property relationships. Polymer 54:2511–2520

Stirna U, Fridrihsone A, Lazdiņa B, Misāne M, Vilsone D (2013) Biobased polyurethanes from rapeseed oil polyols: structure, mechanical and thermal properties. J Polym Environ 21:952–962

Stirna U, Cabulis U (2008) Water-blown polyisocyanurate foams from vegetable oil polyols. J Cell Plast 44:139–160

Tan S, Abraham T, Ference D, Masocko CW (2011) Rigid polyurethane foams from a soybean oil-based polyol. Polymer 52:2840–2846

Technical Datasheet SolvaySOLKANE® 365/227 Blends. Solvay

Technical Datasheet Honeywell Solstice® 1233zd(E). Honeywell Solstice®

Tu YC, Fan H, Suppes GJ, Hsieh FH (2009) Physical properties of water-blown rigid polyurethane foams containing epoxidized soybean oil in different isocyanate indices. J Appl Polym Sci 114:2577–2583

Tu YC, Suppes GJ, Hsieh FH (2008) Water-blown rigid and flexible polyurethane foams containing epoxidized soybean oil triglycerides. J Appl Polym Sci 109:537–544

Tu YC, Kiatsimkul P, Suppes G, Hsieh FH (2007) Physical properties of water-blown rigid polyurethane foams from vegetable oil-based polyols. J Appl Polym Sci 105:453–459

Veronese VB, Menger RK, Forte MMC, Petzhold CL (2011) Rigid polyurethane foam based on modified vegetable oil. J Appl Polym Sci 120:530–537

Yadav S, Zafar F, Hasnat A, Ahmad S (2009) Poly (urethane fatty amide) resin from linseed oil—a renewable resource. Prog Org Coat 64:27–32

Yu-Hallada LC, McLellan KP, Wierzbicki RJ, Reichel CJ (1993) Improved rigid insulating polyurethane foams prepared with HCFCs and perfluoroalkanes. J Cell Plast 29:589–596

Yang LT, Zhao CS, Dai CL, Fu LY, Lin SQ (2012) Thermal and mechanical properties of polyurethane rigid foam based on epoxidized soybean oil. J Polym Environ 20:230–236

Yuan J, Shi Sheldon Q (2009) Effect of the addition of wood flours on the properties of rigid polyurethane foam. J Appl Polym Sci 113:2902–2909

Zhang L, Zhang M, Hu L, Zhou Y (2014) Synthesis of rigid polyurethane foams with castor oil-based flame retardant polyols. Ind Crops Prod 52:380–388

Zhu M, Bandyopadhyay-Ghosh S, Khazabi M, Cai H, Correa C, Sain M (2012) Reinforcement of soy polyol-based rigid polyurethane foams by cellulose microfibers and nanoclays. J Appl Polym Sci 124:4702–4710

Żabski, L.; Papiński, J. (2012) Panki PIR-nowy typ izolacji typu sztywna pianka poliuretanowa. Izolacje 6, 54-60.

Żabski L, Papiński J (2010) PUR i PIR, czyli o efektywnym izolowaniu. Izolacje 4:34–35

Chapter 13
Biorefinery-Derived Bioplastics as Promising Low-Embodied Energy Building Materials

V. Ivanov and L. Christopher

Abstract Petrochemical-based plastics that are used in building construction produce hazardous non-biodegradable wastes after demolition of the buildings or temporal constructions that create logistics and disposal problems. Recent investigations on bio-based plastics reveal opportunities for a new and sustainable construction material made from the renewable organic sources that due to biodegradability can be left in soil or composted after demolition because of biodegradability. Bioplastics also have the potential to lead to the rise of new building materials with low-embodied energy, thus contributing to energy building efficiency. However, the current cost of pure bioplastics is higher than the cost of petrochemical plastics. To improve the cost efficiency of bioplastics, inexpensive raw materials are needed. Potential feedstocks for bioplastics production include negative-, zero- or low-cost by-products of acidogenic fermentation, pyrolysis oil from lignocellulosic biomass and waste, organic fractions of municipal solid waste, reject waters, primary and secondary sludges from wastewater treatment plants, to mention a few. Cost reduction can be achieved through cost-efficient fermentation technologies based on continuous and septic cultivation of mixed bacterial cultures and production of crude composite bioplastics as construction material with low-embodied energy.

V. Ivanov (✉)
Department of Civil and Environmental Engineering,
Nanyang Technological University, Singapore, Singapore
e-mail: cvivanov@ntu.edu.sg

L. Christopher
Biorefining Research Institute, Lakehead University, Thunder Bay, Canada
e-mail: lchristo@lakeheadu.ca

F. Pacheco Torgal et al. (eds.), *Nano and Biotech Based Materials for Energy Building Efficiency*, DOI 10.1007/978-3-319-27505-5_13

13.1 Introduction

13.1.1 Bioplastics and Their Types

Historically, biopolymers of timber were the first construction materials replaced later for stronger and durable concrete and bricks. Petrochemical plastics are also important construction materials at present. The building and construction market consumes about 23 % of produced plastics (Storz and Vorlop 2013). However, concrete, bricks, and construction plastics consume a large quantity of energy for their production thereby creating construction waste that requires additional land for disposal. Therefore, there is a growing demand for production and use of bio-based or biodegradable materials, biopolymers and bioplastics in the construction industry (Plank 2003, 2004; Ramesh et al. 2010; Pacheco-Torgal and Labrincha 2013; Ivanov 2015). Due to their renewable origin, the application of bio-based plastics such as composites of starch, lignin, lignosulfonates, and natural cellulose-containing fibers can increase the environmental and economic sustainability of the construction industry. Furthermore, bioplastics can be composted to produce soil fertilizers instead of landfilling and incineration. This would lead to waste diversion from landfilling and save additional ciosts related to demolition and hauling of construction waste. However, in some instances production of biodegradable composites (e.g. starch-based) consumes substances, which can be used as food or feed. Also, lignin-based plastic composites, for example ARBOFORM® and ARBOBLEND®, (Nagele et al. 2002), are not biodegradable so they must be incinerated or landfilled after use.

The most abundant microbially produced biodegradable bioplastics (further bioplastics) with potential use in the construction industry are the polyhydroxyalkanoates (PHAs), especially poly-3-hydroxybutyrate (PHB) with monomer formula (–OCH(CH_3)–CH_2–C(O)–) and polyhydroxyvalerate (PHV) with monomer formula (–OCH(CH_2CH_3)–CH_2–C(O)–). The content of PHAs in dry biomass of some microorganisms can be up to 80 % (w/w). These PHAs can be extracted from the bacterial biomass and used in practice as bioplastics. The melting temperature of PHAs is 160–180 °C and tensile strength is 24–40 MPa. Elasticity of the PHAs, which is expressed as elongation at break, is from 3 to 142 % and depends on the content of PHV in PHAs. These mechanical properties are comparable with the properties of petroleum-based thermoplastics (Braunegg et al. 1998; Castilho et al. 2009; Steinbuchel et al. 2003; Sudesh et al. 2000; Sudesh and Abe 2010; Volova 2004; DeMarco 2005; Khanna and Srivastava 2005; Lenz and Marchessault 2005).

Polylactic acid (PLA) is another type of commercially available bioplastics for the construction industry. PLA is manufactured by chemical polymerization of lactic acid—a product of anaerobic fermentation of lactic acid bacteria on

carbohydrates and other carbon sources. PLA is applicable in many industries and medicine (Ebnesajjad 2012). However, PLA as a pure product is more expensive than crude PHAs and polypropylene (PP) or polyvinylchloride (PVC) but cheaper than pure PHAs.

Currently, the use of bio-based plastics in construction is just 2,500 tons while agriculture and horticulture consume 84,000 tons; catering requires 101,000 tonnes; automotive applications consume 130,000 tonnes, bottles production and packaging materials are the major consumers of bio-based plastics: 450,000 and 510,000, respectively (European Bioplastics, Institute of bioplastics & Biocomposites; http://en.european-bioplastics.org; Gkaidatzis 2014). The reason for the low-scale applications of bio-based plastic in construction is the high cost of the bioplastics presently available on the market.

13.1.2 Biodegradability of Bioplastics

The complete biodegradation of PHAs to carbon dioxide and water varies depending on the environment—1.5 months in anaerobic sewage, 1.5 years in soil, and 6.5 years in seawater (Reddy et al. 2003; Castilhio et al. 2009). In addition to PHA, dead bacterial biomass contains cell wall polysaccharides, proteins, polynucleotides, and phospholipids, that represents 15, 50, 25, and 10 % of the dry cell biomass (excluding PHA), respectively. Most importantly, the biodegradation rate of the PHA-containing microbial biomass is higher than that of the extracted PHAs. Therefore, from the point of view of biodegradability of PHA-based bioplastics and their economics, extraction of PHAs from the cell biomass is not desirable. Instead, the microbial biomass can be directly utilized as a crude nanocomposite consisting of PHA granules and interlayers of other cellular biopolymers. Such nanocomposites would be more flexible and biodegradable than isolated PHAs.

Biodegradation of PLA in soil or compost normally takes several weeks (Fukushima et al. 2000) whereas bars of PLA with nanocomposites can be degraded with up to 50 % a year (Shogren et al. 2003). The addition of nanocomposites such as montmorillonites (Fukushima et al. 2000), starch or poly(hydroxyester-ether) (Shogren et al. 2003), or just a source of protein (Yang et al. 2015) facilitated biodegradation of PLA. In contrast, addition of PHAs to PLA can improve the mechanical stiffness and increase the film stretchability of the biocomposite mix, but at the same time reduce the biodegradation rate of both bioplastics (Arrieta et al. 2014).

13.2 Biorefinery-Derived Bioplastics

13.2.1 Biorefinery as a Facility Producing Bioplastics for Construction Industry

The production of biodegradable plastics can provide many socioeconomic and environmental benefits to our society. The embodied energy and cost of the bioplastics depend on the choice of raw materials and production methods. Use of cheap raw materials, such as cellulose- and starch-containing biomass, is the most essential factor for cost reduction. Globally, 140 billion metric tons of biomass is generated every year from agriculture alone, which is energy-equivalent to approximately 50 billion tons of oil. Therefore, as a raw material, biomass has attractive potential for biorefineries of large-scale and community-level enterprises. Lignocellulosic biomass as a feedstock for production of bioplastics can be classified as follows:

- wood, wood-processing waste, forestry wastes, short rotation poplar containing mainly cellulose, hemicellulose, and lignin (Christopher 2012, 2013; Golden et al. 2015); about 131 million m^3 of wood residues are generated in the world including 40 mln in Europe, 27 mln in East Asia, 22 mln in USA and Canada, and 14 mln in Brasil (Koutinas et al. 2014);
- agricultural wastes such as unbaled straw; corn cobs, stalks, and leaves (corn stover); silage effluent; horticulture residuals; farm yard manure; coconut fronds, husks, and shells; coffee hulls and husks; cotton (stalks), nut shells; rice hull, husk, straw, and stalks; sugarcane bagasse; and perennial grasses (Golden et al. 2015);
- food-processing wastes such as molasses, whey, different starch-containing waste, potato peels, and vegetable oil-containing wastes (Arancon et al. 2013; Girotto et al. 2015);
- wastes from pulp and paper factories (Bajpa 2013; Christopher 2013).

The organic fraction of municipal solid waste or liquid waste ("reject water") of municipal wastewater treatment plants also can be used as the raw materials for the bioplastic production (Ivanov et al. 2015) but the incorporation of the biotechnological line for the production of value-added materials on these municipal plants is still a problem. Hypothetically, biotechnological production of bioplastic on municipal solid or liquid waste treatment facilities as a public–private partnership can reduce waste treatment costs and generate revenue for the waste treatment facilities. However, no such examples are known at present.

The simultaneous production of biofuels, biochemicals, and bioplastics will maximize the value extracted from plant biomass and certainly reduce the capital and operating costs at the Lignocellulosic Biorefinery. Production of bioplastics can be integrated within the biorefinery production platforms through both the biochemical and the thermochemical conversion routes with the objective to valorize the lignocellulosic biomass in the most cost-efficient and environmentally friendly way (Christopher 2012, 2013; Christopher and Kumar 2015; Liguori et al. 2013).

Aseptic cultivation of microorganisms requires thermal sterilization of all materials and equipment and is energy-consuming process. The septic cultivation of mixed bacterial cultures accumulating PHAs or lactic acid, however, is a cost-effective alternative for production of construction bioplastics. Further cost reduction can be achieved by the use bioplastics in situ without their prior extraction using chemical treatment, filtration, centrifugation, or flotation of the microbial biomass. Additional cost and environmental benefits can be gained by: (1) using low-cost feedstock such as waste biomass and (2) placing the Lignocellulosic Biorefinery in proximity to the feedstock. All above would facilitate the feedstock supply and logistics, and minimize the overall carbon footprint and associated greenhouse gas (GHG) emissions.

13.2.2 Biotechnological Production of Bioplastics

In case when lactose of whey, saccharose of molasses or glucose of chemically or enzymatically hydrolyzed starch, agro-industrial or wood-processing residues are the major components of feedstock for PLA bioplastic production, these substances can be used for the homofermentative lactic acid fermentation by *Lactobacillus acidophilus*, *L. amylophilus*, *L. bulgaricus*, *L. helveticus, and L. salivarius* (Koutinas et al. 2014). Yield of lactic acid could be from 129 to 215 g/L with productivity of 8 g/L h^{-1} or higher and cost of 0.47 Euro kg^{-1} or lower. Production process combines continuous systems of lactic acid fermentation with an electrodialysis membrane separation for lactic acid recovery (Koutinas et al. 2014). The purified lactic acid is further chemically transformed via direct condensation or via its cyclic lactide form to PLA (Sin et al. 2012). The current production of PLA by NatureWorks alone is 136,000 metric tons per year (Cargill-PTT Global Chemical) with estimated annual growth of nearly 20 %. Economies of scale should decrease the production costs, but new technical approaches are needed to reach these figures. In typical lactic acid fermentation methods, the raw material cost constitutes between 40 and 70 % of the total production cost (Tejayadi and Cheryan 1995). It is therefore very expensive to use starch and refined sugars as feedstock for lactic acid production. As polymer producers and other industrial users usually require large quantities of lactic acid at a relatively low cost, inexpensive raw materials including biomass waste are essential for the economic feasibility of the lactic acid microbial process (Upadhyaya et al. 2014). Based on a PLA price of 2.2 $/kg, the estimated target price of lactic acid in a captive should be less than 0.55 $/kg (Golden et al. 2015).

Another bioplastic option is the conversion of carbohydrates to organic acids and hydrogen by acidogenic fermentative bacteria on biorefinery (Surendra et al. 2015). Organic acids must be used for septic cultivation of mixed cultures to ensure selective conditions for growth of PHA-accumulating bacteria (Yu 2006). Alternatively, oxidation of cellulosic bioethanol with microaerophilic bacteria can produce acetic acid, which is further converted to PHAs with aerobic

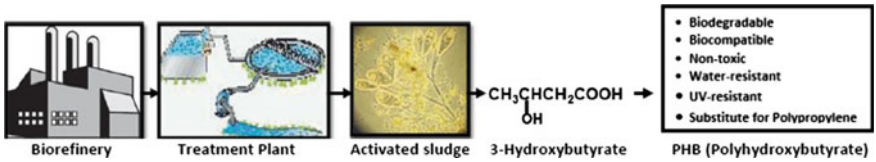

Fig. 13.1 Schematics of biotechnological production of PLA and PHA bioplastics at a lignocellulosic biorefinery

PHA-accumulating bacteria. Examples for biotechnological production of bioplastics (PLA and PHAs) are illustrated in Fig. 13.1.

A typical material balance of acidogenic fermentation of carbohydrates is as follows: (molar ratios of volatile fatty acids (VFA)—formic, acetic, and butyric acids—were taken from Madigan et al. 2012):

$C_6H_{12}O_6 + 0.82\ H_2O \rightarrow 1.13\ CH_3COOH + 0.35\ C_2H_5COOH + 0.26\ C_3H_7COOH + 1.67\ CO_2 + 2.47\ H_2$, where $C_6H_{12}O_6$ is a monomer of cellulose (glucose); CH_3COOH, C_2H_5COOH, C_3H_7COOH are acetic, propionic, and butyric acids, respectively. In one example, batch acidogenic solid-state fermentation of maize silage produced 3.3 g/L of acetic acid, 0.3 g/L of propionic acid, 0.4 g/L of iso-butyric acid, 4.0 g/L of n-butyric acid, 0.1 g/L of iso-valeric acid, 0.2 g/L of n-valeric acid, 2.8 g/L of caproic acid, and 0.2 g/L of lactic acid. Produced gas contained 35 % of hydrogen and 69 % of carbon dioxide (Strauber et al. 2012). However, pH can drop below 5.5 during acidogenic fermentation (Barlaz et al. 2010); while the optimal pH for acidogens is above 6.0 (Moosbrugger et al. 1993). To maintain optimal pH during acidogenic fermentation of lignocellulosic biomass, pH must be controlled automatically by titration with alkali or using codigestion with the wastes with high content of protein (Ahring et al. 1992; Macias-Corral et al. 2008). If there is additional source of protein-containing waste, mixing of carbohydrate- and protein-containing waste could balance the concentration of the carbohydrate-derived protons with that of the hydroxide ions released during ammonification of protein. If the biorefinery is using starch or hydrolyzed cellulose for fermentation of ethanol biofuel, part of this ethanol can be easily converted to acetate (Lin and Tanaka 2006). Another source of acetate can be pyroligneous acids, especially acetic acid derived from the acetyl groups of hemicelluloses in the pyrolysed lignocellulosic biomass(Yaman 2004). Using organic acids produced by acidogenic fermentation or pyrolysis of lignocellulosic biomass, PHAs can be accumulated in cells of pure cultures of the species from genera *Acinetobacter*, *Alcaligenes*, *Alcanivorax*, *Azotobacter*, *Bacillus*, *Burkholderia*, *Delftia*, *Klebsiella*, *Marinobacter*, *Pseudomonas*, *Ralstonia*, *Rhisobium* or mixed bacterial cultures using batch, semicontinuous, or continuous cultivation (Ben Rebah et al. 2004; Beun et al. 2006; Lu 2007).

PHA production by activated sludge-treating municipal wastewaters or pulp and paper mill effluents is affected by their nutrient composition, in particular carbon and nitrogen sources, sludge retention time, pH, temperature, etc., with typical

values between 20 and 30 % PHA by weight. To stimulate accumulation of PHA in activated sludge, a feast/famine strategy (aerobic dynamic feeding) with alternating high- and low-organic load is normally applied (Arcos-Hernandes et al. 2013; Albuquerque et al. 2007; Bengtsson et al. 2008; Dias et al. 2006; Ivanov et al. 2015). These dynamic conditions generate unbalanced cell growth and favor production of intracellular storage polymers (such as PHAs) during the high-carbon load phase. Acclimation and optimization of PHA production is normally carried out as a two-step process: (1) selection of PHA-accumulating cultures under feast/femine conditions; (2) batch PHA accumulation using selected cultures and substrate (wastewaters). However, as mixed cultures do not store carbohydrates as PHAs, carbohydrate-rich substrates such as those from the Lignocellulosic Biorefinery (biomass hydrolysates, pre-hydrolysates, pulping effluents, etc.) need to be first converted to VFA using anaerobic acidogenic fermentation. As mixed cultures can store VFA as PHAs, this additional step will further increase the PHA yield reaching levels of around 70 % by weight, which is competitive with PHA production using pure cultures. However, the use of pure cultures (wild and recombinant) and pure substrates for PHA production is inherently expensive. As the substrate cost accounts for about 40 % of the total PHA production costs, the use of mixed cultures (as in the activated sludge) and mixed organic matter contained in the biorefinery effluents with a negative cost (Fig. 13.2) is expected to diminish additionally the cost barriers to a widespread use of the PHA bioplastics.

Major technical challenges associated with the PHA fermentation process using cellulosic biomass waste include: (1) complete utilization of all fermentable sugars including C5 (pentose) sugars such as xylose and arabinose; PHA producers such as *Ralstonia eutropha* however cannot utilize pentose; (2) incompatibility of pH for

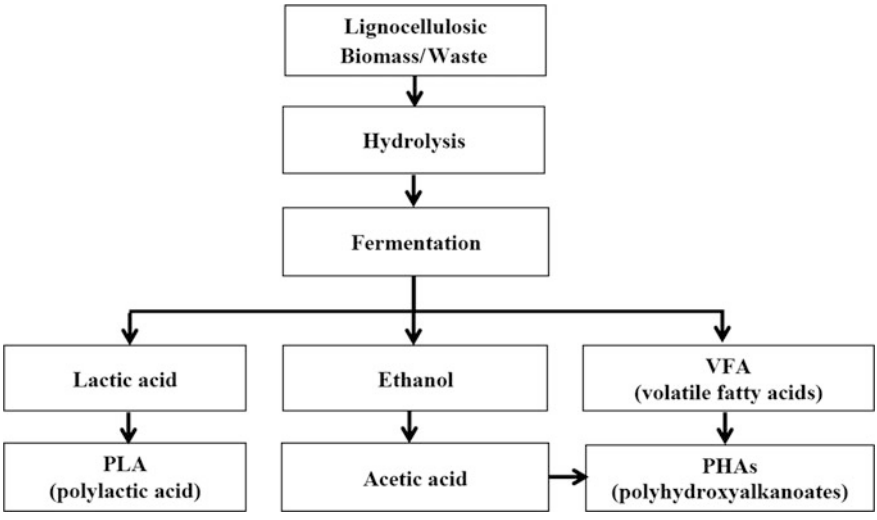

Fig. 13.2 Accumulation of PHB by activated sludge at the effluent treatment plant of a lignocellulosic biorefinery

enzymatic hydrolysis of cellulosic biomass to fermentable sugars (acidic) with the pH for optimal PHA production (neutral to alkaline); (3) PHA recovery from a complex solid mixture of PHA-containing cells, residual biomass containing lignin and undigested fibers, etc. (Wang et al. 2014).

PHAs are commonly extracted from cells after their accumulation in bacterial biomass. Microbial cells can accumulate up to 80 % PHA of their dry cell weight. Due to the solid state of the PHA particles, PHA recovery from microbial biomass is challenging and requires dissolution of either the PHA polymer or the non-PHA biomass. The former method employs organic solvents such as chloroform and dichloromethane (chlorinated hydrocarbons). The extracted PHA is then precipitated with methanol to give very pure and intact PHA macromolecules. The PHA extraction method however suffers from some major drawbacks such as use of large quantities of organic solvent and associated recovery costs, lengthy extraction and filtration procedures, etc. The alternative method for PHA recovery is by centrifugation which separates the solubilized non-PHA cell biomass (proteins, nucleic acids, lipids, peptidoglycans) from the high-density PHA granules which remain in the solid phase. For dissolution of the cell organelles and fragment, both nonselective (alkali, alkaline hypochlorite) and selective (anionic surfactants, proteases) have been used (Madkour et al. 2013). However, all methods of extraction suffer from high cost, environmental pollution, and increase of embodied energy. Therefore, to reduce costs, crude bioplastic, without extraction of PHAs, could be used for construction applications.

Bioplastics are entirely compatible with the production of other biochemicals, ethanol, and advanced drop-in biofuels from lignocellulosic biomass (Yu and Chen 2008; Snell and Peoples 2009). The Lignocellulosic Biorefinery provides the optimal platform for process and product integration (Pervaiz and Sain 2006; Bohlmann 2007). Biofuel by-products can be used for the production of bioplastic, for example, xylose remaining after ethanol fermentation of sugarcane bagasse hydrolysate (Silva et al. 2014) or lignin remaining after processing of wood can be used in PLA-lignin composites (Spiridon et al. 2015). A proof-of-concept biorefinery technology for the production of PHAs has already been demonstrated (Snell and Peoples 2009).

Currently, PHAs are produced on a pilot scale at 50–500,000 tons per year with a cost that ranges from 1.5 to 13 Euro kg^{-1} by Mitsubishi Gas Chemical Company Inc. (Japan), Telles (USA), PHB Industrial Company (Brazil), Biomer Inc. (Germany), Tianan Biologic, P&G (USA), Ningbo (China), Lianyi Biotech (China), Kaneka Corporation (Japan) (Koutinas et al. 2014). The biorefinery technology and the utilization of waste and by-product streams are most essential factors in order to develop cost-competitive PHA production (Koutinas et al. 2014).

PLA is produced on industrial scale at about 136,000 metric tons per year by NatureWorks, Cargill-PTT Global Chemical (Golden et al. 2015). It will be produced also in Germany, Russia, India, and other countries. The global demand for PLA is about 50 million tons/year. However, the selling price of PLA is about $2.20/kg (Golden et al. 2015), which could be too high for construction applications. Therefore, the technology of lactic acid fermentation must be enhanced or

cheaper raw materials must be used for the production of PLA as a construction material. The production cost of PHA varied by different evaluations from 1.5 to 6 Euro kg^{-1}, while the market price of petrochemical plastic polyethylene terephthalate (PET) is 1.3 Euro kg^{-1} (Dacosta et al. 2015). As discussed previously, price compatibility of crude composite PHAs with PET should be aimed through septic production from low-cost biomass feedstock using mixed bacterial cultures.

13.3 Bioplastics as New Building Materials

13.3.1 Embodied Energy, Greenhouse Emissions, the Nonrenewable Energy Use, and Carbon Footprint of Bioplastics

The use of eco-efficient building materials is one of the most important aspects in construction industry (Pacheco-Torgal and Jalali 2013). PHAs are a promising eco-friendly bioplastic that can be produced from lignocellulosic biorefinery as a value-added coproduct. Life cycle assessment (LCA), performed with the GHG emissions and fossil energy requirement per kg of bioplastics produced, showed that PHAs contribute 0.49 kg CO_2/kg, while petrochemical plastics contribute 2–3 kg CO_2/kg to the greenhouse gas (GHG) emissions. The fossil energy requirement per kg of bioplastic is 44 MJ, while for the petrochemical plastics this parameter is 78−88 MJ/kg (Yu and Chen 2008).

LCA, performed according to ISO 14040 and ISO 14044 standards and supported by EcoInvent 2.2 database, revealed that the GHG and the nonrenewable energy use (NREU) for PHB production were 1.97 kg CO_2 eq/kg of PHB and 109 MJ/kg of PHB, respectively (Dacosta et al. 2015), while for production of the petrochemical plastic PET the total GHG emissions were 2.15 kg CO_2 eq/kg and NREU 69 MJ/kg. However, steam for sterilization of the facility of PHB production presented a 15 % share of the total GHG emissions and a 12 % of the share of the total NREU, the sources of N and P presented a 20 % share of the total GHG emissions and a 15 % of the share of the total NREU, and materials for PHB extraction (NaOCl and SDS) from biomass presented a 25 % share of the total GHG emissions and a 26 % share of the total NREU (Dacosta et al. 2015). Hence, nonaseptic production of PHB using waste sources of N and mixed bacterial cultures without extraction of PHB from bacterial biomass will be characterized by the GHG emissions of 0.9 kg CO_2 eq/kg of crude PHB (46 % of GHG emissions for pure PHB) and the nonrenewable energy use (NREU) of 51 MJ/kg of PHB, which are 42 and 74 % of the respective values for PET. Therefore, partial replacement of petrochemical plastics with bioplastic PHAs could mitigate global warming.

The eco-inventory carried out during a pilot plant trial suggested that the PHA production resulted in an aggregated ecological footprint of 10.4 m^2/kg of PHAs compared to 1.7 m^2/kg for polypropylene. The major contribution to this large

footprint of PHAs came from the use of electricity in the fermentation step (Narodoslawsky et al. 2015).

The embodied energy (energy input) for production of pure PHB is 80 MJ/kg (Dicker et al. 2014). Considering a linear correlation between embodied energy and the GHG emissions, the embodied energy of crude PHAs is about 46 % of the value of pure PHB, i.e., about 37 MJ/kg of the crude PHAs. This is higher than the embodied energy for timber (9.4 MJ/kg) but significantly lower than that of petroplastics (70–160 MJ/kg) (Hammond and Jones 2008). Based on above comparison, the crude PHAs can be considered as a low-embodied energy construction material.

On the other hand, PLA produced by NatureWorks™ (Cargill Dow LLC) has a gross fossil energy requirement of 54 MJ/kg and GHG emissions of 1.8 kg CO_2 eq/kg (Vink et al. 2003). The embodied energy of pure PLA is about 80 MJ/kg (Dicker et al. 2014), which is comparable with the values of petrochemical plastics.

13.3.2 Applications of Bioplastics in Construction

The major application of bioplastics is in the temporarily constructions. The bioplastic materials can be used as sealants and insulants, solid foam (Willke and Vorlop 2004), silt and dust fences, for construction of nonstructural (internal) elements such as separating walls and partitions, and manufacturing of biocomposite packaging films. PLA can be used for manufacturing of: (1) composite biodegradable fibers for reinforcement of the construction materials (Huda et al. 2006; John and Thomas 2008; Bajpai et al. 2013; Faludi et al. 2013; Saba et al. 2015); (2) biocomposite sheets for construction and packaging; (3) biodegradable resins for construction molds (Tokiwa and Tsuchiya 2003); and (4) environmentally friendly flooring material that is recycled or rapidly decomposed upon the discarding (Ko et al. 2014).

Pure PLA and PHA bioplastics cannot be used in construction industry because of their brittleness. Elongation at failure for PLA and PHB is about 2–6 %, while for PP and PET is 28–320 % (Peelman et al. 2013). So, natural fibers and plasticizers need to be used in combination with PLA and PHAs in the composites. Natural fiber-reinforced bioplastics can be strong and rigid composite materials and at the same time more biodegradable, elastic, and stronger than pure bioplastics. The bio-based fiber and particles that are used for the reinforcement of petrochemical plastics—wood, bark, straw, coconut, kenaf, flax, jute, hemp or the particles of lignin, and lignosulfonate—can also be used as the composite material for bioplastics. Probably, different types of the biodegradable textile can be used on the construction sites as silt fence, sediment trap, drainage pipe, biodegradable cover, and erosion control blanket, or as a geotextile for the temporarily slope stabilization. These materials do not require post-construction extraction and can remain in soil for biodegradation after construction.

The bioplastics can also be used in the production of novel bio-nanocomposites with improved or unique properties. For example, addition of 5 % (v/v) clay to PLA improved the tensile strength, break elongation, scratch resistance, and other mechanical properties (Ray 2012). A PLA nanocomposite containing 0.15 % (w/w) multi-walled carbon nanotubes and 6 % (w/w) of the plasticizer polyethylene glycol (PEG) had tensile and flexural strength characteristics of up to 43.8 MPa and 81.4 MPa, respectively, that are suitable for many industrial applications including construction industry (Maizatulnisa et al. 2013). Bioplastics and petrochemical plastics can be used together. Blending of PLA and PHAs with petrochemical plastics could reduce brittleness and increase durability of bioplastic composites so such composites can also find their applications in construction industry.

It is important that biodegradable plastic composites can be composted following verification of their compostability by standards, such as the European Standards EN 13432 and EN 14995, US Standards ASTM D6400 and ASTM 5338, and international standard ISO 14855. The key requirements are usually as follows: There are limits for toxic volatile and nonvolatile organic compounds, heavy metals, and fluorine; breakdown at least 90 % of material to CO_2, water, and minerals for 6 months; physical decomposition of at least 90 % of material to tiny pieces less than 2 × 2 mm for at least 12 weeks; there must be no negative effect of this compost on seeds germination and plant biomass growth.

In conclusion, the bioplastics are sustainable construction materials that can be produced from renewable organic sources. Their major advantages over the petroplastics include the following:

1. increased energy building efficiency because of low-embodied energy of crude bioplastics;
2. diminished cost for extraction and disposal of construction wastes because bioplastic materials can be left in the soil for their biodegradation in situ;
3. reduced area of land used for the landfilling of construction waste;
4. bioplastics do not require incineration after demolition of construction materials due to their biodegradability;
5. bioplastic construction waste can be used for composting and soil fertilization.

References

Ahring BK, Angelidaki L, Johansen K (1992) Anaerobic treatment of manure together with industrial waste. Water Sci Technol 30:241–249

Albuquerque MGE, Eiroa M, Torres C, Nunes BR, Reis MAM (2007) Strategies for the development of a side stream process for polyhydroxyalkanoate (PHA) production from sugar cane molasses. J Biotechnol 130:411–421

Arancon RAD, Lin CSK, Chan KM et al (2013) Advances on waste valorization: new horizons for a more sustainable society. Energy Sci Eng 1:53–71

Arcos-Hernandes MV, Pratt S, Laycock B, Johansson P, Werker A, Lant PA (2013) Waste activated sludge as biomass for production of commercial-grade polyhydroxyalkanoate (PHA). Waste Biomass Valorization 4:117–127

Arrieta MP, Fortunati E, Dominici F et al (2014) PLA-PHB/cellulose based films: mechanical, barrier and disintegration properties. Polym Degrad Stab 107:139–149
Bajpa P (2013) Biorefinery in the pulp and paper industry. Academic Press, Waltham
Bajpai PK, Meena D, Vatsa S, Singh I (2013) Tensile behavior of nettle fiber composites exposed to various environments. J Nat Fibers 10:244–256
Barlaz MA, Staley BF, De Los Reyes III FL (2010) Anaerobic biodegradation of solid waste. In: R. Mitchell and J.-D. Gu (eds) Environmental Microbiology, 2nd edition, John Wiley & Sons, Inc., Hoboken, NJ, USA, pp 281–299
Ben Rebah F, Yan S, Filali-Meknassi Y, Tyagi RD, Surampalli RY (2004) Bacterial production of bioplastics. In: RY Surampalli, R D Tyagi (eds) Advances in Water and Wastewater Treatment, ASCE Publications, pp 42–71
Bengtsson S, Werker A, Sristensson M, Welander T (2008) Production of polyhydroxyalkanoates by activated sludge treating a paper mill wastewater. Bioresour Technol 99:509–516
Beun JJ, Dircks K, van Loosdrecht MCM, et al. (2006) Poly-β-hydroxybutyrate metabolism in dynamically fed mixed microbial cultures. Water Res 36:1167–1180
Bohlmann GM (2007) Bioplastics & biofuels: pricing and production trends. Ind Biotechnol 3:25–28
Braunegg G, Lefebvre G, Genser KF (1998) Polyhydroxyalkanoates, biopolyesters from renewable resources: physiological and engineering aspects. J Biotechnol 65:127–161
Castilho LR, Mitchell DA, Freire DMG (2009) Production of polyhydroxyalkanoates (PHAs) from waste materials and by-products by submerged and solid-state fermentation. Bioresour Technol 100:5996–6009
Christopher L (2012) Adding value prior to pulping: bioproducts from hemicellulose. In: Okia CA (ed) Global perspectives on sustainable forest management. InTech
Christopher L (2013) Integrated forest biorefineries: current state and development potential. In: Christopher L (ed) Integrated forest biorefineries. The Royal Society of Chemistry, Cambridge, pp 1–58
Christopher LP, Kumar H (2015) Clean and sustainable biodiesel production. In: Handbook of clean energy systems. John Wiley & Sons Ltd., pp 1–16
Dacosta CF, Posada JA, Ramirez A (2015) Large scale production of polyhydroxyalkanoates (PHAs) from wastewater: a study of techno-economics, energy use and greenhouse gas emissions. Int J Environ Chem Ecol Geol Geophys Eng 9:422–427
DeMarco S (2005) Advances in polyhydroxyalkanoate production in bacteria for biodegradable plastics. Basic Biotechnol eJ 1:1–4
Dias JML, Lemos PC, Serafin LS, Oliveira C, Eiroa M, Albuquerque MGE, Ramos AM, Oliveira R, Reis MAM (2006) Recent advances in polyhydroxyalkanoate production by mixed aerobic cultures: from the substrate to the final product. Macromol Biosci 6:885–906
Dicker MPM, Duckworth PF, Baker AB et al (2014) Green composites: a review of material attributes and complementary applications. Compos Part A 56:280–289
Ebnesajjad S (ed) (2012) Handbook of biopolymers and biodegradable plastics: properties, processing and applications. Elsevier, USA, p 447
European Bioplastics, Institute of bioplastics & Biocomposites, http://en.european-bioplastics.org
Faludi G, Dora G, Renner K, MoczoJ, Pukanszky B (2013) Biocomposite from polylactic acid and lignocellulosic fibers: structure–property correlations. Carbohydr Polym 92:1767–1775
Fukushima K, Abbate C, Tabuani D et al (2000) Biodegradation of poly (lactic acid) and its nanocomposites. Polym Degrad Stab 94:1646–1655
Girotto F, Alibardi L, Cossu R (2015) Food waste generation and industrial uses: a review. Waste Manage. doi:10.1016/j.wasman.2015.06.008
Gkaidatzis R (2014) Bio-based FRP structures: a pedestrian bridge in Schiphol Logistics Park. MSc Architecture, Urbanism and Building Sciences thesis, Delft University of Technology, Delft, The Netherlands
Golden JS, Handfield RB, Daystar J, McConnell TE (2015) An economic impact analysis of the US biobased products industry: a report to the Congress of the United States of America. A Joint Publication of the Duke Center for Sustainability & Commerce and the Supply Chain Resource

Cooperative at North Carolina State University. http://wrrfdata.org/NBP/Newsletter/wp-content/uploads/2015/06/USDA-Economic-Analysis-of-Biobased-Products-12-JUN-2015.pdf
Hammond G, Jones C (2008) Embodied energy and carbon in construction materials. Proc Inst Civil Eng Energy 161:87–98
Huda MS, Drzal LT, Mohanty AK, Misra M (2006) Chopped glass and recycled newspaper as reinforcement fibers in injection molded poly (lactic acid) (PLA) composites: a comparative study. Compos Sci Technol 66:1813–1824
Ivanov V, Stabnikov V, Ahmed Z, Dobrenko S, Saliuk A (2015) Production and applications of crude polyhydroxyalkanoate-containing bioplastic from the organic fraction of municipal solid waste. International Journal of Environmental Science and Technology 12, 725–738
Ivanov V (2015) Environmental Microbiology for Engineers, 2nd ed. CRC Press, Taylor & Francis Group. Boca Raton. 400 p
John MJ, Thomas S (2008) Biofibres and biocomposites. Carbohydrate Polymers 71, 343–364
Khanna S, Srivastava AK (2005) Recent advances in microbial polyhydroxyalkanoates, Process Biochemistry 40, 607–619
Ko HS, Kwon JH, Park SS (2014) Flooring material using poly lactic acid resin and construction methods of the same. US Patent 20140370225
Koutinas AA., Vlysidis A., Pleissner D. et al. (2014) Valorization of industrial waste and by-product streams *via* fermentation for the production of chemicals and biopolymers. Chemical Society Reviews 43, 2587–2627
Lenz RW, Marchessault RH (2005) Bacterial polyesters: biosynthesis, biodegradable plastics and biotechnology. Biomacromolecules 6, 1–8
Liguori R, Amore A, Faraco V (2013) Waste valorization by biotechnological conversion into added value products. Applied Microbiology and Biotechnology 97, 6129–6147
Lin Y, Tanaka S (2006) Ethanol fermentation from biomass resources: current state and prospects. Applied Microbiology and Biotechnology 69, 627–642
Lu Y (2007) Advance on the production of polyhydroxyalkanoates by mixed cultures. Frontiers of Biology in China 2, 1673–3509
Macias-Corral M, Samani Z, Hanson A (2008) Anaerobic digestion of municipal solid waste and agricultural waste and the effect of co-digestion with dairy cow manure. Bioresource Technol 99:8288–8293
Madigan MT, Martinko JM, Stahl D, Clark DP (2012) Brock Biology of Microorganisms. 13th ed. Benjamin Cummings
Madkour MH, Heinrich D, Alghamdi MA, Shabbaj II, Steinbüchel A (2013) PHA recovery from biomass. Biomacromolecules 14, 2963–2972
Maizatulnisa O, Tan KH, Yusof HM et al (2013) Effects of multi-walled carbon nanotubes (MWCNTS) on the mechanical and thermal properties of plasticized polylactic acid nanocomposites. Advanced Material Research 812, 181–186
Moosbrugger RE, Wentezel MC, Ekama GA, Marais GV (1993) Weak acid/bases and pH control in anaerobic systems: a review. Water South Africa 19:1–10
Nagele H, Pfitzer J, Nagele E. et al. (2002) Arboform® - a thermoplastic, processable material from lignin and natural fibers. In: Chemical Modification, Properties, and Usage of Lignin (Hu, Thomas Q, eds.). Kluwer Academic/Plenum Publishers, New York, pp 101–119
Narodoslawsky M, Shazad K, Kollmann R, Schnitzer H (2015) LCA of PHA production—identifying the ecological potential of bio-plastic. Chemical and Biochemical Engineering Quarterly 29, 299–305
Pacheco-Torgal F, Labrincha JA (2013) Biotechnologies and bioinspired materials for the construction industry: an overview. International Journal of Sustainable Engineering 7, 235–244
Pacheco-Torgal F, Jalali S (2013) Eco-efficient construction and building materials. Springer, London. p 247
Peelman N., Ragaert P.' Bruno De Meulenaer B. (2013) Application of bioplastics for food packaging. Trends in Food Science & Technology 32, 128–141

Pervaiz M, Sain M (2006) Biorefinery: opportunities and barriers for petro-chemical industries. Pulp and Paper Canada 107, 31–33

Plank J (2003) Applications of biopolymers in construction engineering. In: Biopolymers, V.10. General Aspects and Special Applications (Alexander Steinbüchel, ed.). Wiley-VCH Verlag GmbH, Weinheim

Plank J (2004) Application of biopolymers and other biotechnological products in building material. Applied Microbiology and Biotechnology 66, 1–9

Ramesh BNG, Anitha N, Rani HKR (2010) Recent trends in biodegradable products from biopolymers. Advanced Biotechnology 9, 30–34

Ray SS (2012) Polylactide-based bionanocomposites: a promising class of hybrid materials. Accounts of Chemical Research 45, 1710–1720

Reddy CSK, Ghai R, Rashmi, Kalia VC (2003) Polyhydroxyalkanoates: an overview. Bioresourse Technology 87: 137–146

Saba N, Paridah MT, Jawaid M (2015) Mechanical properties of kenaf fibre reinforced polymer composite: a review. Construction and Building Materials 76, 87–96

Shogren RL, Doane WM, Garlotta D, Lawton JW, Willett JL (2003) Biodegradation of starch/polylactic acid/poly(hydroxyester-ether) composite bars in soil. Polymer Degradation and Stability 79, 405–411

Silva LF, Taciro MK, Raicher G et al (2014) Perspectives on the production of polyhydroxyalkanoates in biorefineries associated with the production of sugar and ethanol. International Journal of Biological Macromolecules 71, 2–7

Sin LT, Rahmat AR, Rahman WA (2012) Polylactic Acid: PLA Biopolymer Technology and Applications. Elsevier, p 329

Snell KD, Peoples OP (2009) PHA bioplastic: a value-added coproduct for biomass biorefineries. Biofuels, Bioproducts and Biorefining 3, 456–467

Spiridon I, Leluk K, Resmerita AM, Darie RN (2015) Evaluation of PLA–lignin bioplastics properties before and after accelerated weathering. Composites Part B: Engineering, 69, 342–349

Storz H, Vorlop KD (2013) Bio-based plastics: status, challenges and trends. Applied Agriculture and Forestry Research 63, 321–332

Strauber H, Schroder M, Kleinsteuber S (2012) Metabolic and microbial community dynamics during the hydrolytic and acidogenic fermentation in a leach-bed process. Energy, Sustainability and Society 2:13. http://www.energsustainsoc.com/content/2/1/13

Sudesh K, Abe H, Doi Y (2000) Synthesis, structure and properties of polyhydroxyalkanoates: biological polyesters. Progress in Polymer Science 25, 1503–1555

Sudesh K, Abe H (2010) Practical Guide to Microbial Polyhydroxyalkanoates. Smithers Rapra Technology, p 160

Surendra KC, Chayanon S, Shilva S et al (2015) Anaerobic digestion-based biorefinery for bioenergy and biobased products. Industrial Biotechnology 11, 103–112

Tejayadi S, Cheryan M (1995) Lactic acid from cheese whey permeate—Productivity and economics of a continuous membrane bioreactor. Applied Microbiology and Biotechnology 43, 242–248

Tokiwa Y, Tsuchiya A (2003) Biodegradable resin compositions. US Patent 666977

Upadhyaya B, DeVeaux LC, Christopher LP (2014) Metabolic engineering as a tool for enhanced lactic acid production. Trends in Biotechnology 32, 637–644

Vink ETH, Rabago KR, Glassner DA, Gruber PR (2003) Applications of life cycle assessment to NatureWorks™ polylactide (PLA) production. Polymer Degradation and Stability 80, 403–419

Volova TG (2004) Polyhydroxyalkanoates—Plastic Materials of the 21st Century. Nova Publishers, 282 p

Wang Y, Yin J, Chen GQ (2014) Polyhydroxyalkanoates, challenges and opportunities. Current Opinion Biotechnology 30, 59–65

Willke T, Vorlop KD (2004) Industrial bioconversion of renewable resources as an alternative to conventional chemistry. Applied Microbiology and Biotechnology 66, 131–142

Yaman S (2004) Pyrolysis of biomass to produce fuels and chemical feedstocks. Energy Conversion and Management 45, 651–671

Yang S, Madbouly SA, Schrader JA et al. (2015) Characterization and biodegradation behavior of bio-based poly(lactic acid) and soy protein blends for sustainable horticultural applications. Green Chemistry 17, 380–393

Yu J, Chen LXL (2008) The greenhouse gas emissions and fossil energy requirement of bioplastics from cradle to gate of a biomass refinery. Environmental Science and Technology 42, 6961–6966

Chapter 14
Bio-inspired Lightweight Structural Systems: Learning from Microcomponents in the Nature for the Energy Efficiency in the Architecture

Rosa Cervera Sardá and Javier Pioz

Abstract The increasing interest about reaching a zero net balance energy building has mainly been focused on issues such as insulation, facades and smart and productive envelopes, and mechanical systems, that is, on the operational energy saving. Nevertheless, recent studies prove that the construction stage of a building is responsible for a significant amount of the total energy consumed by the same along its life. There are several open research lines starting from the interest in the embodied energy, and we may summarize the main ones in the following: scientific criteria to decide the material with less impact; improvements in the production of existing materials; advanced, intelligent, and composite materials, etc. Within these lines, it has taken special importance that related to bio-inspired materials. The work carried out by our team has investigated in the geometric patterns of the natural forms instead of the before-mentioned lines, and it has investigated how the physical configuration of the matter contributes to its reduction. Our work analyses how nature organizes its bearing systems and how nature uses the minimum energy possible, having developed, along millions of years, strategies to reach the most efficient, lightweight, and cooperative systems. Our work deals about how nature reaches the appropriate embodied energy lightening material in its structural forms at all scales, macroscopic and microscopic using emptiness. The tree's vascular bundle structure, the cellulose cell morphology, and the bird's pneumatic bone constitution show how vacuum or emptiness is as important as matter in structural resistance and stability. Application of this knowledge can be done for building technologies, with procedures to reduce weight and structural material as a way of saving energy.

R. Cervera Sardá (✉) · J. Pioz
Cervera and Pioz Architects, Alcalá University and Polytechnic University, Madrid, Spain
e-mail: rcervera@cerveraandpioz.com

F. Pacheco Torgal et al. (eds.), *Nano and Biotech Based Materials for Energy Building Efficiency*, DOI 10.1007/978-3-319-27505-5_14

14.1 Introduction

The current situation at the level of excessive energy consumption and the unstoppable growing process of the urban phenomenon demands new approaches for saving energy in a sustainable future. Today, buildings are demanding a great part of the energy consumed in the world. For this reason and given the inevitable growth of buildings because both the growth of the world population and the continuous process of migration from rural to urban areas, the reduction of energy in the construction industry is crucial. Until not long ago, the most relevant advances to reach a building with a zero net balance have mainly been focused on the consumption performance of the building.

The construction industry has developed in a record time important improvements in isolating and closing systems; in heating, ventilation, and air-conditioning installations; in the use of energy from renewable sources; and even in the behavior of users.

However, little attention was paid to the energy consumed in the construction process on the idea that its impact was small compared to the consumption of energy during the useful life of buildings. Recent studies prove the contrary and arrive to the conclusion that the construction stage of a building is responsible for a significant amount of the total energy consumed by the same along its life. For example, studies carried out by Sarkisian et al. (2014) have shown that the energy consumed by a great skyscrapper during the construction process is equivalente to the operational energy consumed by it during 20 years.

Studies done in Australia by Crawford et al. (2003) reach up to periods of 20–50 years. Pacheco-Torgal et al. (2013), analyzing the operational and the embodied energy of 97 different apartments in Portugal, reached the conclusion that the last one represents about 25.3 % of the former for a life of 50 years. That is, the impact of the construction, in the zero day of its activity, is equivalent to the energy that such building will consume during the following decades.

This has led to a growing number of researches about the ways to reduce the energetic cost during the construction process. When currently talks about the energy of buildings, it already handles a clear distinction between the energy consumed by the performance thru the time of use of a construction—operational energy—and the energy consumed during the construction process-embodied energy. That is why the life cycle energy of a building must consider both operational and embodied energy. With regard to the term "embodied energy," we must say that there is not yet a common interpretation of such term. Cabeza et al. (2013), reviewing proposals of different authors, expose us some interpretations that are handled as, for example, the energy consumed producing the material or the total energy consumed, direct and indirect, during the construction of a building, or energy consumed as well as during the extraction, transformation, and transportation of raw material. Table 14.1 presents the embodied energy of several construction systems.

Table 14.1 Embodied energy in various wall, floor, and roofing systems (Cabeza et al. 2013)

Type of building element	Energy per unit (GJ)
Burnt clay brick masonry (m^3)	2.00–3.40
SMB masonry (m^3)	0.50–0.60
Fly ash block masonry (m^3)	1.00–1.35
Stabilized rammed earth wall (m^3)	0.45–0.60
Non-stabilized rammed earth wall (m^3)	0.00–0.18
Reinforced concrete slab (m^2)	0.80–0.85
Composite SMB masonry jack-arch (m^2)	0.45–0.55
SMB filler slab (m^2)	0.60–0.70
Non-reinforced masonry vault roof (m^2)	0.45–0.60

There are several open research lines starting from the interest in the embodied energy, and we may summarize the main ones in the following: scientific criteria to decide the material with less impact; improvements in the production of existing materials; advanced, intelligent, and composite materials; bio-inspired materials, etc. Within these lines, it has taken special importance that related to bio-inspired materials with crossed researches which combine biology, chemistry, and engineering. As Chen et al. (2012) says disciplines that before were separated actually overlap generating a knowledge that it can bear solutions to obtain more than actual efficient construction and fabrication systems.

The work carried out by our team, formed mainly by architects, has investigated in the geometric patterns of the natural forms instead of the before-mentioned lines, and it has investigated how the physical configuration of the matter contributes to its reduction, so finding a new research line is not so concerned with the materials and its chemical specifications as in the reduction of matter in the constructive process from the study of nature. As a difference to those researches that try the reduction of materials based on their characteristics, we research reduction by the formal geometric patterns.

So, facing the issue from alternative points of view like, for example, the exposed by Chen et al. (2013), refered to the concrete and the use of clinker and how this can now be substituted, we investigate the processes and strategies of nature on its morphogenesis to become efficient by the minimum use of material. Extending this concrete example, our position complements the reduction of volume in a given construction process by enhancing the concrete performance, as Chen says, with a reduction of volume because of a more effective form and geometry.

14.2 Reaching Efficiency Through Bio-inspired Materials

The intersection between biology and sciences is becoming a field of growing interest for researchers. Most of the works deal with the composition of natural materials and how it is possible to translate this knowledge to the fabrication of new

man-made materials. The interest has exponentially grown having produced in the last five years a broad literature about nanostructure and microstructure of nature and having investigated in the properties derived from this microorganization: great resistance with fragile materials, self-organization, self-repair, self-cleaning, anti-reflection, water proof, etc.

To cite only some cases of the contemporary instigation, Shahinpoor (2013) discussed the properties and characteristics of biopolymer–metal nanocomposites and Ellison (2013) reviewed the current state of the investigation in the field of biomimetic textiles. The work on natural fibers and their microscopic constitution and then the consecutive scales of yarns and threads and finally fabrics is resulting fruitful in the application to the textile industry. Jiang (2010) treats smart nanoscale interfacial materials. Optical capacities to produce different colors, not due to pigments but due to the scattering microstructure of wings, is a field of research that has produced results in the combination of microstructure and light with the hope to produce what is known as structural colors without pigments in bio-replication for art and industry. Dushkina et al. (2013) and Wilts et al. (2015) have reviewed the photonic structure in the animal kingdom as inspirations for biomimetic applications. One aspect that has brought enormous attention in last years is related to self-cleaning materials considering as the starting point for many authors the lotus leaf. Many recent studies repeat their interest in a range of living organisms of amazing properties, so is investigated on spiders and the silk fabricated by them, on mollusks and seashells and their massive resistance, the gecko lizard and its capacity for sticking to the walls defying gravity and also on feathers, bones, thorns, etc.

Within the field of materials, a part of the investigations has been focused in the structural properties of certain natural forms due to its nano or microscale organization. For example, Mirkhalaf et al. (2013) deal with the inner microstructure of natural materials. They remark the exceptional performance of bones, seashells, teeth, etc. These forms are thousand times tougher than the brittle material they are made of. This capacity is due to the layout of their microstructure. The staggered disposition is similar to a microscopic brick and mortar in such a way that this structure generates a universal method to increase the strength, stiffness and toughness in natural materials. About the same issue Chen et al. (2012) write, when analyzing the components of shells or jaws of insects. According to his description, the minerals provide strength and stiffness, while the biopolymers provide toughness and ductility.

Yang et al. treat about the resistance of the procupones quills. They are extremelly lightweight but strong enough to support compression and flexure loads for defense. For Fratzl (2007), an analysis of structure–function relations in natural tissues must precede the engineering of new bio-inspired materials and remark the fact that natural materials consist of few constituent elements using very little energy for their fabrication. On the contrary, the man-made materials use many more elements than usually require high temperatures and therefore a great quantity of energy for their fabrication.

What we can conclude is that the investigations of the microscopic scales of nature are providing new visions for improving the structural performance of materials. Somehow the work initiated by the biologist Dàrcy Thompson is being

continued, but the current means and interests are focusing in how to describe mathematically these natural sttuctures. As Chattopadhyay (2015) says, most of these studies are centered in the materials, and as stated by Jiang et al., the progress of human society is based on the progress of materials.

14.3 Toward New Lightweight Structural Systems Through Emptiness and Microcomponents

The role of the structural systems in the overall energy consumption of a building has often been underestimated, or even neglected as Griffin (2014) says, and the up-to-now discussion about how to find efficient structural models or about how to reach lightweight material in architecture refers mainly to the decision of using the most efficient material: reinforced concrete, advanced concrete, steel, wood, or composite, but rarely about the geometrical patterns and forms of the structural elements or about the balance between porosity and material of the same. The mechanically aided industry, accepted without any question by the modern architecture, has contributed to a divorce between forms needed and materials used. Uniform sections of the structural elements produced industrially help to a systematical construction but do not consider the amount of material really required, using most of the time more material than what is really needed. Recent discussions show that arguments about the material choice and their effect on embodied CO_2 are not enough. Structural design, geometrical patterns, sections, dimensions, and vacuum are definitive in the embodied energy.

In order to give a different point of view, our work analyses how nature organizes its bearing systems and how nature uses the minimum energy possible, having developed, along millions of years, strategies to reach the most efficient, lightweight, and cooperative systems. At this point, we can wonder if is it possible that the study of bone structures of animals and patterns of organization of the material or matter in plants brings conclusions that improve the effectiveness of structural systems in architecture and engineering. Our objective is to establish bridges between what we could call biotechnology in nature and the construction building technology to reduce the energy used, always with the objective of reducing structural material.

In nature, the process of internal management of the material or matter requires that this matter, to take a form, to be capable of supporting efforts such as the derivatives of its own weight and pull of gravity, of added external loads, wind, thrust, etc. The way of organization of matter is dual or double, covering both the formal and the functional aspects such as structural. Therefore, shape and structure, in natural reality, they are the two aspects of the same issue. We can say that both notions are as independent as interdependent. The big difference between natural materials and artificial or man-made materials is that the first grow. In nature, form and structure grow at the same time, becoming intimately related. Nature uses codes

and laws, but not permanent or fix forms. The dynamic forms in nature have their design in the cells. And the geometrical instructions are, as well, inherent in the cells self-organization as Lenau et al. (2013) report. And precisely because in the morphogenesis of the natural forms there are codes, they can be read by algorithms, what opens the path to the parametric design.

The structures of natural forms, such as the architectural or engineering forms, face similar problems of stability, resistance, and resilience. Therefore, the conviction and the opportunity look at nature as a sophisticated and an efficient biotechnology. In the configuration of the natural structures are combined, in a repetitive manner, different strategies which together form a highly efficient system. Such strategies could be condensed into the following points:

(a) Prevalence of geometry over the material, where dynamic patterns and fractal geometry allow the variation according to the necessities due to structure, growing or external conditions.
(b) Fragmentation of the loads and forces, weakening loads and fragmenting them into smaller efforts to which, in turn, small-scale structural elements resist. Fragmentation of efforts to address major structural work avoids large gestures and therefore massive energy consumption.
(c) Structuring networked systems, diversifying work in multiple engaging elements where greater burden to bear more but smaller elements, in a permanent reduction of material and energy expenditure, through collaboration systems.
(d) Lightening structures by microstructuring and vacuum, with emptiness as the key characteristic of the material for the strength and stability of natural forms. Thanks to the above-mentioned process, natural forms reach the perfect embodied energy.

Cervera et al. (2014) reached a very significant conclusion: Nature does not build structures the way human beings do. In conventional construction, when we have a load or large weight, we use columns and beans to support it. If the load increases, we proportionally increase the size of the parts that support it, which also increases the weight. If there is a load to be supported in the natural world, a net is built. And if the load increases, then the number of elements increases but not its dimension; in fact, sometimes its dimension can even decrease. So nature is more successful and efficient in supporting increasingly heavier loads and in saving materials. This is made possible thanks to the cooperation of all its elements and the minimization process of is matter through microvacuum. We can summarize the differences between strategies of construction of natural forms and man-made structures in the following schemes (Fig. 14.1a, b, and c).

In the research developed by our team, we have work on these four subjects with surprising results. For example in the case of the importance of the geometry, we refer to the structural analysis of a water lily leaf known because of its large heavy-duty capacity, we considered it as a corbel structure with a holding central point, and we compared the leaf with a conventional model of structures distribution, with the following result (Fig. 14.2).

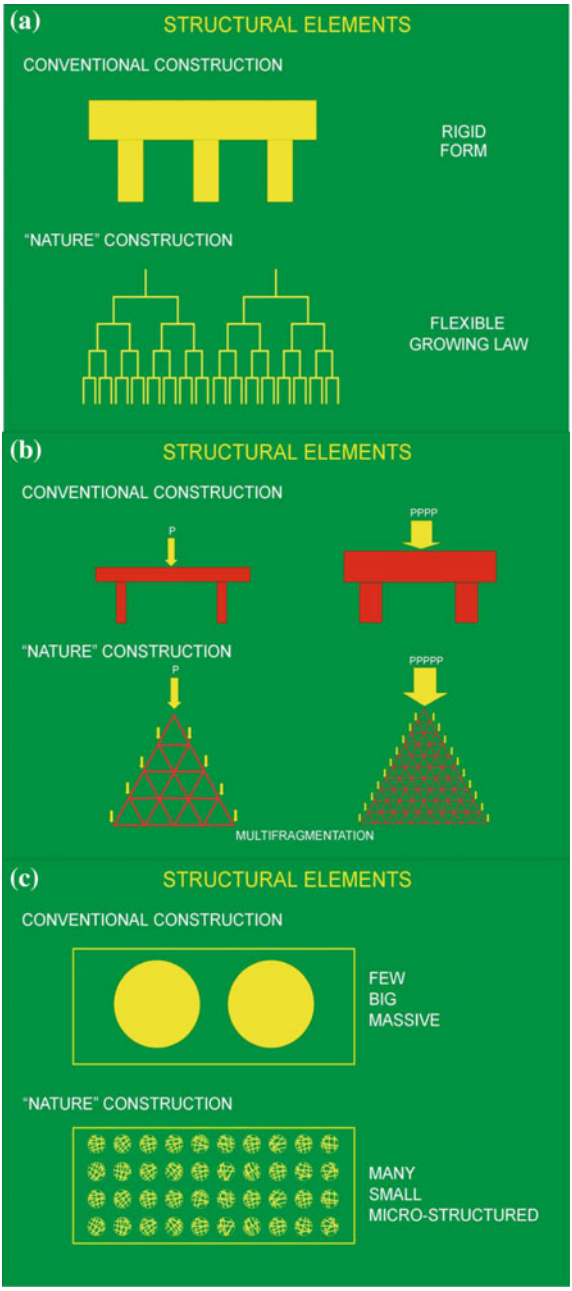

Fig. 14.1 **a** Comparison between standard rigid forms and dynamic geometrical patterns. **b** Comparison between dense and lightweight and cooperative structures. **c** Comparison between massive and not massive structures

In the work here present, we are centered in paragraph (d) focused in the permanent processes in nature for reducing material at all scales, macro, micro and nano and how the materia and the emptiness, or air inside the materia, cooperate for

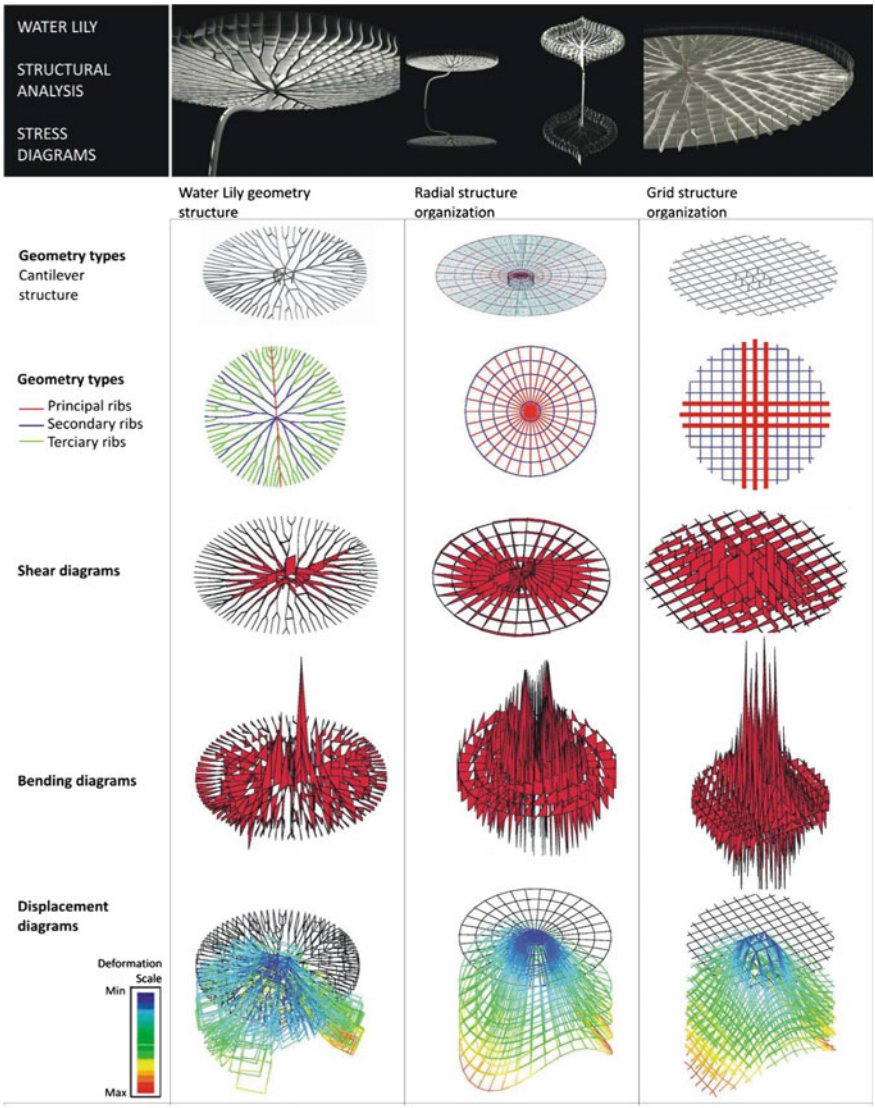

	Cantilever hypothesis			
	Maximum moment Mt (m.T)		Maximum Shear Vy (T)	
Nenuphar type geometry	15,95 L	1,69 Q	5,01 L	0,53 Q
Radial type geometry	16,53 L	1,75 Q	4,50 L	0,47 Q
Grid type geometry	28,52 L	7,00 Q	3,01 L	0,74 Q

Fig. 14.2 Water lily: structural analysis and stress diagrams. Comparative study with typical patterns and maximum moment and maximum shear

a better performance using minimun energy. Just because the hollow does not use matter, the embodied energy reduces clearly. It is not to seek new or smart or efficient materials. It is to analyze how the no matter is converted in a cooperating of strength, stiffness, and toughness as important as the own matter. This thesis may be studied from the point of view of the own physical geometry of the natural forms in all scales and clearly in nano- and microscales and be applied to the construction industry in architecture and engineering.

The minimization process of material in structural elements is general in nature. The porosity and microstructure are constant in all natural living forms and, like a permanent strategy, can be found both in the animal kingdom as well as the plant kingdom. The discovery of this "spongy" system took us to stablish the trascendental importance of the emptiness ("micro-emptiness") in natural structures, for both the configuration of the resistant systems and the adjustment of the hierarchical structural orders derived from their growth. That is, the paper that emptiness plays in the growth and in the structural stability of the living species is so important that becomes necessary to redefine the concept of "emptiness" when we try to understand the structures, being more appropriate to speak of "dynamic emptiness."

14.3.1 Pneumatic Structure of Bird's Bones

If we analyse the bones of animals, we observe that the concept of inner void and fragmentation into multiple parts is present in all cases. Of course, significant differences related to composition, density, and sponginess are obvious according to different species. For example, the skeleton of birds is much lighter than the skeleton of large land mammals. Both maintain the concept of porosity, but in the case of birds, the bone contains air instead of bone marrow. Bone cavities are in communication with the respiratory system to lighten matter. This pneumatic structure has the goal of reducing weight to improve flight. With this mechanism of sponginess, material and non-material cooperate to withstand the forces when moving through the air. It is relevant to the weight of the skeleton of birds in comparison with their total weight. For example, the Bald Eagle, about 4 kg, its skeleton weighs about 300 g, less than 1/13, while the plumage reaches up to 600 g.

The structure of a bird transforms the skeleton of the vertebrate animal and adapts it to the aerial environment and to flight by means of a series of useful "deformations" that minimize the weight, increase the resistance, and facilitate the navigation through air: hypertrophy of the sternum in the shape of a large keel to withstand the forces of the wind and of the powerful pectoral muscles; fusing or welding of the clavicle and all the ribs to the keel strengthening the thoracic cage; reinforcing of the ribs with uncinate processes in the form of spurs; aerodynamic lengthening of the hip and pelvis bones; ossification of the last tail bones strengthening the caudal vertebrae forming a rudder, etc. But one of the most

interesting strategies that the birds use to move opposing to the gravity is a process of minimization. If we study the wings of birds, we reach to understand this intelligent system. The wing of a bird is not a laminar surface or a single plane, but a surface composed of numerous very lightweight parts: feathers. A wing is no element of colossal size, such as a large plane wing, that would oppose to the great forces of wind. On the contrary, the resistance to air is fragmented when breaking up the surface of a wing in multiple parts that are permeable to wind with a fully efficient result. This is the first step to lighten matter.

If we take a closer look at a wing structure, we found that a relatively compact and solid outer crown and a large inner void form the bird's wing bones including the radius and the ulna. They adopt the form of hollow tubes with criss-crossing struts for structural strength. This is the case of the mentioned bones, which are relatively long and need to withstand the stresses of flying. These trabeculae or diagonal projections of osseous tissue work as braces of a structure and are arranged in all directions creating an interesting three-dimensional network. The hollow bone is also called pneumatic bone as mentioned previously (Fig. 14.3). If we take a feather and cut through its pen, we will find the same bone formation mentioned before: a structural hollow tube with an inner three-dimensional network where void has an important role. If we repeat the process on a barb with a 3 mm section, on a barbule with a 1.5 mm section or on the very tip of a barbule (0.5 mm), we will find the same formation. All in all, it is a fractal process that seeks to lower weight at all scales. Our findings confirm some of the investigations carried out up to date. Many biological systems with outstanding mechanical properties have hierarchically structures over multiple layers that cooperate among them to increase strength (Chen et al. (2012)), and others have multiscale structures with a great versatility. No wonder that the skeleton of a bird weighs less than all of its feathers.

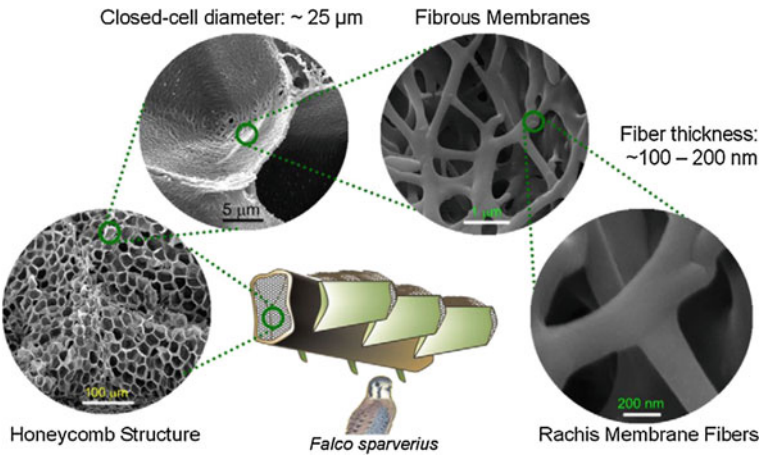

Fig. 14.3 Schematic of falcon (*Falco sparverius*) feather internal foam along with scanning electron micrographs of the medullary core (Chen et al. 2012)

14.3.2 The Trunk Tree: A Spongy Bio-Structure to Conquest the Verticality

Trees have a lineal structure with one of its extremities set into the ground. Their highest loads are the effect of wind forces on the tree crown. Its structural response is equivalent to that of a point load on a trampoline. The minimum height of mature trees in the smallest species is around 3 m and the maximum somewhere over 100 m. Sequoias are among the tallest of trees, with a trunk diameter ranging between a few centimetres and several meters. In mature specimens, the diameter can reach 10 m. Their crowns may reach a diameter of 30–40 m, which can be doubled in the case of very large specimens. Their slenderness ratio ranges from 1/13 (diameter/height) to 1/30, sometimes even 1/60. The most extreme case of slenderness is bamboo, which reaches a ratio of 1/200. There is no doubt that these plants are the structures of greatest slenderness in nature, far outstripping the slenderness of architectural forms.

In sight of the above, and considering that skyscrapers hardly reach the maximum ratio of 1/14, being the average around 5–10, two questions arise: How nature performs to reach such slenderness? And, how can we get some conclusions able to be applied to the constructive technology? The answer comes both from the macroscopic organization of the matter and from the microscopic and even cellular-scale structure (Fig. 14.4).

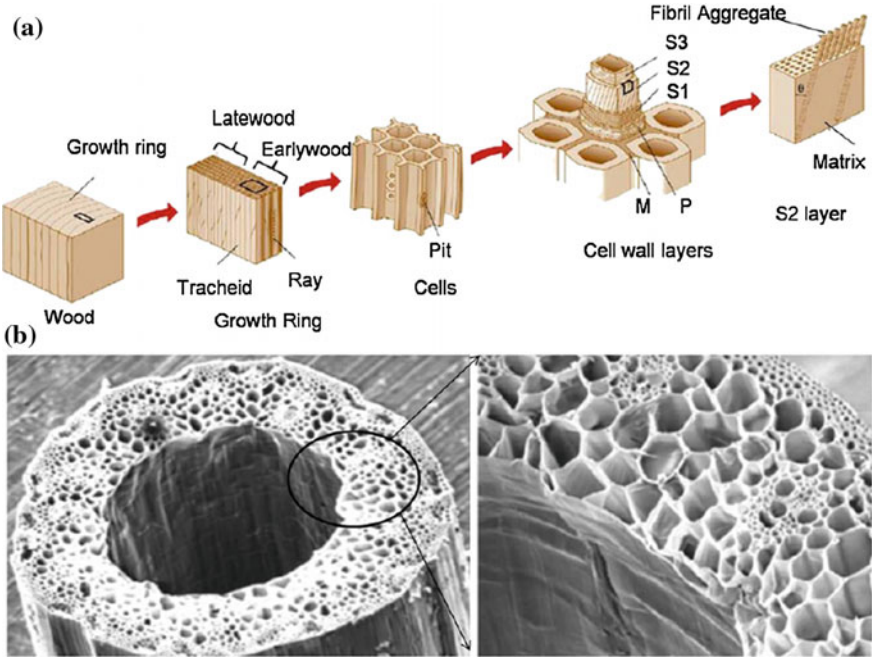

Fig. 14.4 **a** Schematic of hierarchical structure of wood; **b** structure of grass stem (Chen and Pugno 2013)

One of the clarifying discoveries of the bionic analysis made in the vegetal structures of vertical development is the mechanism of growth by sponginess. And it shows us that whichever greater it was the height of the organism, greater was also the proportion of inner emptiness, i.e., to say, for greater height, greater necessity of emptiness, and it is, indeed, the structural reorganization, internal and external, of "emptiness" which makes possible to the vegetal species to be surpassing its borders of the height. In a stem of young tree of 4 mm of diameter, the proportion of "sponginess" is of 29 %; in the same stem, but already simply with 8 mm of diameter, the proportion of "sponginess" is of 46 %. The vegetal species obtains this effect of sponginess, structuring and hollowing its conduits of flowed or "veins." The growth of vertical plants and trees happen alternating "layers" of elements of the radial family and "layers" of elements of the linear family; this is, combining layers specialized in structural fibrous behavior and layers specialized in conduction of fluids. Usually, the simple observation of a cut tree allows a better understanding of its horizontal growth with concentric layers. But since we rarely have the opportunity to observe the complete fibrous structure of a tree, the common assessment that a tree grows "wrapping itself" and "stretching" is not completely accurate. There are important mechanisms that apply to its vertical growth, such as the double helical arrangement of its fibers, which are indispensable in resisting torsion forces. The effect of wind on the structure of a tree's crown puts it under enormous bending and torsion forces. The fibers of the tree are organized into two helical fibrous structures that cross each other acting as braces. It is possible to affirm that all the elements of these two families, veins and fibers, participate simultaneously in the missions of the resistance and of the conduction of fluids. However, these two families can be identified like two subfamilies. On the one hand, the one of those elements is specifically specialized to absorb efforts, although they can lead fluids. In spite of its helicoidal spatial growth, its disposition in a horizontal section is fundamentally radial, as the radii of a bicycle wheel were. On the other hand, it is also easy to identify the subfamily of those elements which are specialized in the conductions of fluids, although they can develop missions of resistant structure. These elements also grow helically in the space but, in a vertical section, its configuration is fundamentally linear, similar to the system of pipes of a construction. Both subfamilies, besides to participate in the mentioned helical rule of growth, have a geometric fractal order, rule of common growth to all the vegetal species, which has very much important advantage from the point of view of their capacities of transformation and for their resistant and insulating qualities. This concept is easily understandable if we analyzed it comparatively with the fragility of an isolated hair and its enormous resistance if it is grouped and interlaced with the structure of braided hair (Fig. 14.5).

If we add the proportion of existing micro-emptiness inside each vein of the tree, along with the micro-emptiness that is located between the connections of the different layers, we reached the important conclusion that, approximately, 65 % of the structure of a tree is formed by void. This emptiness is the authentic protagonist of its enormous resistant behavior in spite of his reduced diametrical dimensions (Fig. 14.6). This is why we consider appropriate the qualifying of "dynamic

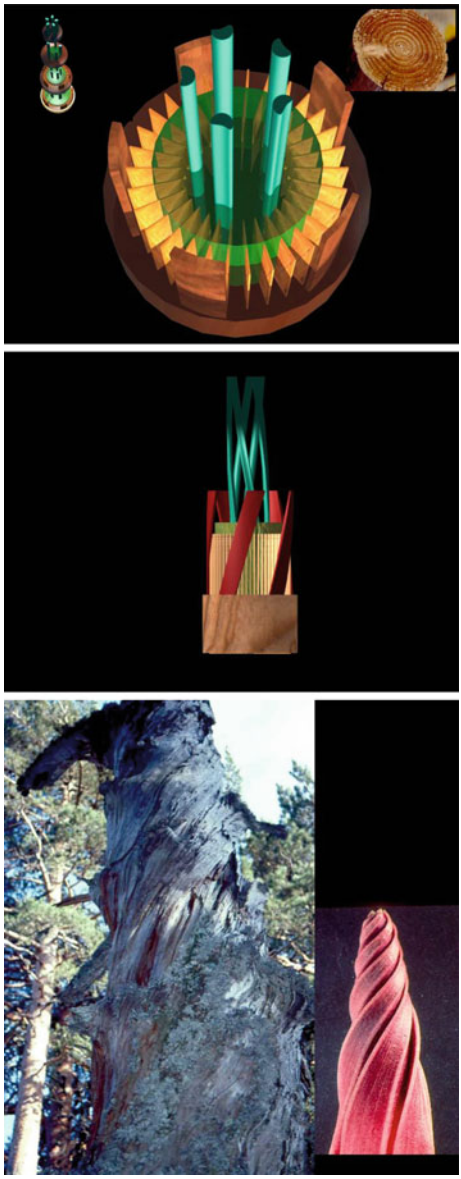

Fig. 14.5 Inner structure of trees

emptiness" to which we made reference. However, when we look at the cutting of a tree we reach the impression of a massive and dense object, being almost unable to appreciate the presence of air or vacuum inside of its micro structure. But this is an erroneous appreciation (Fig. 14.7). Also, the 60 % of the human body is made up of water molecules.

Fig. 14.6 Porosity of wood tissue

Let us analyze the fibrous microstructure. As the tree grows, the conduits of internal fluids gradually multiply the number of micromembranes forming its inner structure and producing the hard and solid woody core. In turn, the vertical conduits along the perimeter increase in number, while decreasing in size. Therefore, we can say that these conduits (vascular bundles) form a second skin, parallel to the bark of the stem, very resistant thanks to an effective microstructure, and highly insulating thanks to the amount of void space in the microstructure. This is the real fireproof defense mechanism of the large plant structures. As a structural element, the skin or bark forms a resistant membrane that ties all the perimeter container conduits of the vertical space contributing to the overall stability. The structure of a tree vein is formed by thousands of very thin membranes (similar to a puff pastry structure) (Fig. 14.8). And as the tree grows, each vein is capable of increasing the number of membranes in its interior, every so thin, without increasing its volume. This compacting/sponging capacity allows the different parts of the wood to be of higher or lower density and therefore of greater or lesser resistance. The result is a highly resistant structure that has a high percentage of microvoid space. It is to say that a vein of a vegetal species is, in addition to a conduit of fluids, a most effective "column" to hold the pressure of its weight and an extraordinary "brace" to absorb the tensions of traction and torsion due to the mobile battle of the wind and of the

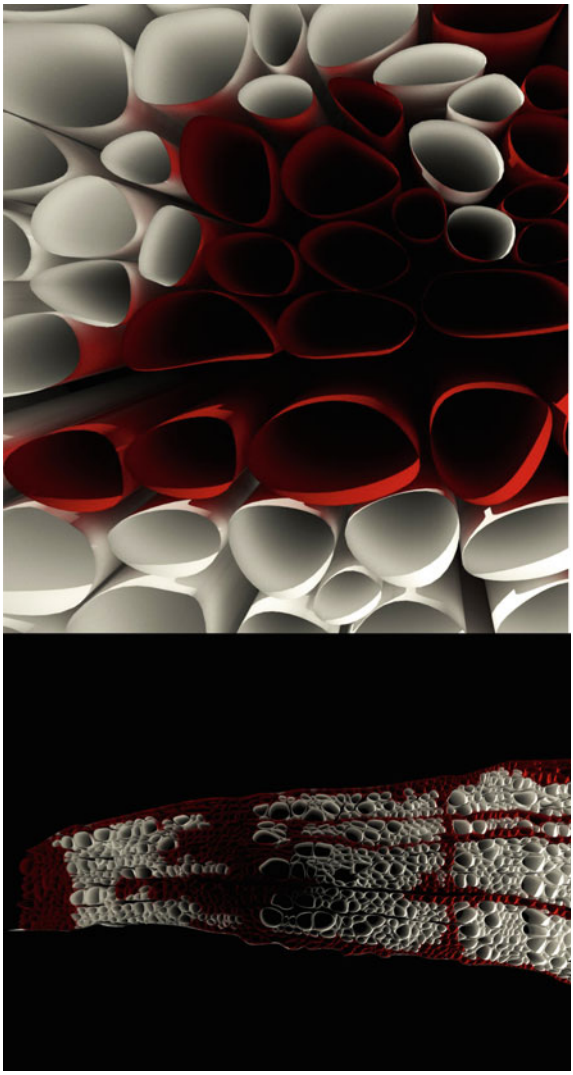

Fig. 14.7 Microstructure of vegetal fibers with a high percentage of air in the hollow volumes composition

expansions and compressions by changes of temperature. This effect of density reduction has a beneficent quality added when reducing the excessive weight derived from the increase of volume. And besides that, membrane, similar to a puff pastry, consists the way to channel fluids vertically without external input of energy.

If the construction technology develop formwork systems and sections for pillars that instead of being massive formed by sheets stuck together or cooperating, the resistance would increase, while the weight would reduce generating an important energy saving.

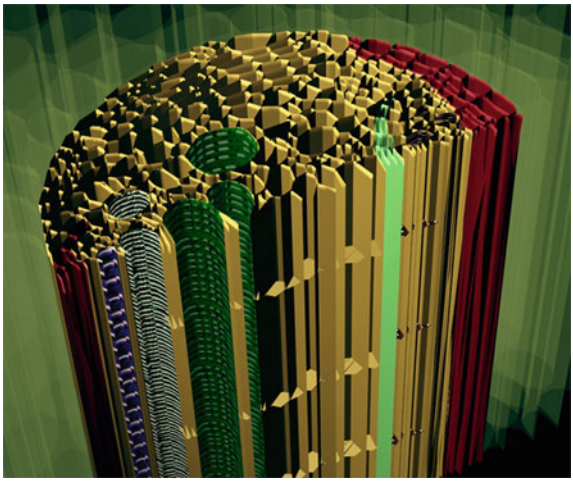

Fig. 14.8 Detail of the microstructure of a tree vein reducing weight at microscopic level

14.3.3 The Microstructure of the Cellulose Cell and Other Examples in Nature

Cellulose cell has a hollow tubular composition. A big number of nanopipes or nanotubes cooperate to increase resistance and decrease weight. It is extraordinary than the same configuration that can be found at the macroscopic scale in the plan structure is now showed in the microscopic level of a cell, i.e., co-operation of elements that work together with minimum matter reaching maximum strength. The tension force of cellulose is 10,000 kg/cm^2 greater than that of steel. Lignin has compression strength of 2400 kg/cm^2 greater than that of concrete that makes it lightweight in relative to its strength. We cannot compete with natural material for the moment, but we can learn from their display and geometrical disposition and from the mechanism of lighten matter.

The different families of elements inside the cellulose cells or consecutive layers that construct it use the same wall mechanism of alternating direction to absorb compression and tension forces. Similar to what is said in above sections, the cellulose cells, at their microscopic scale, use the same wall mechanism of alternating direction to absorb compression and tension forces (Fig. 14.9). So we can conclude that nature performs the same at all scales, even at cellular scale.

Not only cellulose cells but every element of the living forms tends to reduce material, or tends to be constructed through tissues. That is, what we consider massive is, in fact, a network where the amount of matter is less than the 50 % of the total area or volume. For example, the delicate wings of a butterfly, composed by silk-like tiles, have a microstructure formed by chitin ribs that are held apart by intricate crossbars generating a tissue (Fig. 14.10). Air is again the protagonist of the composition and improves the performance in flight, in isolation, in noise reduction, and in light absorption and refraction. So a miracle can be explored to be

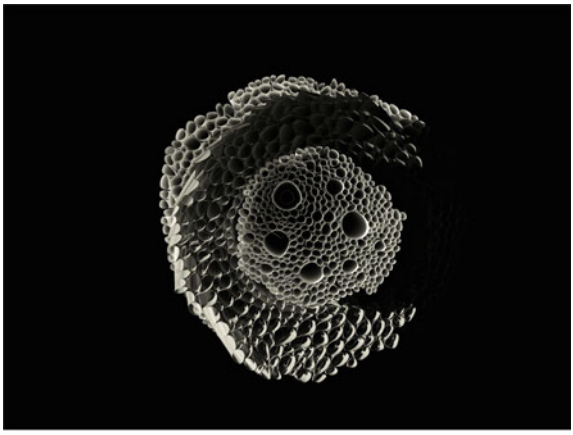

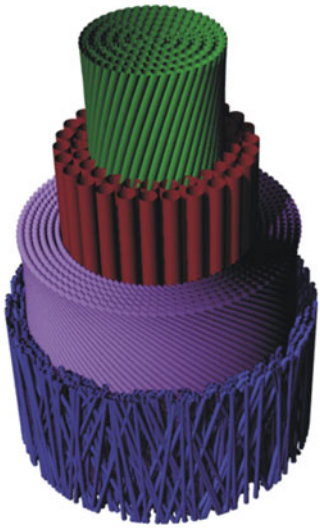

Fig. 14.9 Microstructure of the cellulose cell. The consecutive layers that form it alternate direction to absorb compression and tension forces

applied to the contemporary technology. But the aspect that we are working on, i.e., the structural behavior, shows once more that natural living forms are generated by means of cooperating grids with many small elements and vacuum in the interstices.

In the case of the eggshell, its extraordinary mechanical properties are due to both the material, bioceramic calcite crystals, and the microstructure of the thin membrane that protects the chick and, at the same time, allow it to breathe and to break the shell to emerge. It is not our aim to focus on the mineral and chemical properties of natural materials but to focus on geometrical patterns and structural configuration. So the fine membrane is in fact a three-dimensional-like net structure or an overlapped complex of layers that cooperate for the maximum efficiency for both a great physical force and a sufficient fragility (Fig. 14.11).

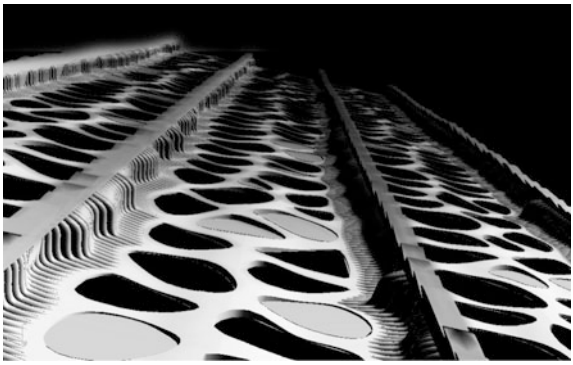

Fig. 14.10 Structure of a butterfly wing's ribs where the silk tiles are inserted

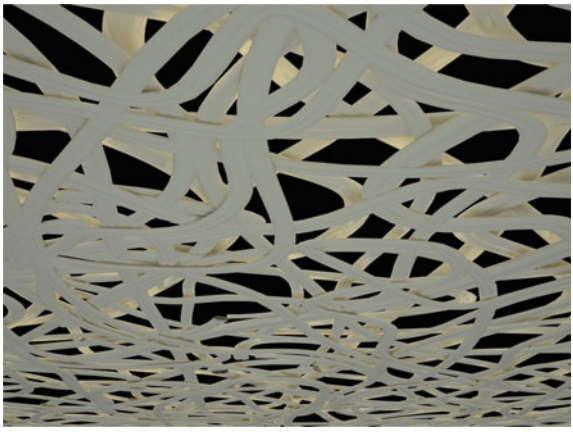

Fig. 14.11 Microstructure of the eggshell

14.4 Conclusions

The way in which nature organizes the structure of living forms to bear loads, gravity, movement, etc., is based in a permanent cooperation between matter and emptiness or void volumes in such a manner that material is as much important as no material is. And this strategy happens at all scales in such a way that the microstructure of the elements is mainly conformed by hollow volumes improving the energy consumption required to produce material. By means of this strategy, nature is able to reduce weight, to increase structural performance, to reach proper insulation, and to produce a large variety of shapes and forms to adapt to different environments. And the most significant issue is that by using small and light elements, structures in nature can produce each of those elements in the environmental conditions. That is, they do not need high temperatures or great energy to be produced. Multilayer thin structures and grids are permanent at all scales, macro, micro, and nano, in a fractal process of lightening material and improving behavior.

When talking about conventional construction, the structural strategies are, usually, the contrary, i.e., few, big, and massive elements. This way is the most simple and effective according to the traditional and contemporary constructive systems. But new proceedings are coming, such as the 3D printers that will transform the concept of construction. We are, likely, close to a radical change in the constructive world. New materials inspired by nature, joining biology, architecture, and engineering, will bring innovative and ecological solutions for the contemporary world.

References

Cabeza LF, Barreneche C, Miró L, Morera JP, Bartolí E, Fernández AI (2013) Low carbon and low embodied energy materials in buildings: a review. Renew Sustain Energy Rev 536–542

Cervera R, Gomez Pioz J (2014) Learning from nature as a tool for innovation in architecture. In: Madrid IABSE symposium engineering for progress, nature and people proceedings

Chattopadhyay S (2015) Biomimetic architectures by plasma processing, fabrication and applications. Standford publishing, Stanford

Chen Q, Pugno N (2013) Bio-mimetic mechanisms of natural hierarchical materials: a review. J Mech Behav Biomed Mater 19:3–33

Chen PY, McKittrick J, Meyers MA (2012) Biological materials: functional adaptations and bioinspired designs. Prog Mater Sci 57(8):1492–1704

Crawford RH, Treloar GJ (2003) Validation of the use of Australian input output data for building embodied energy simulation. In: Proceedings of the 8th international IBPSA conference. Eindhoven

Dushkina N, Lakhtakia A (2013) Structural color in engineered biomimicry. Elsevier, Amsterdam

Ellison MS (2013), Biomimetic textiles in engineered biomimicry. Elsevier, Amsterdam

Fratzl P (2007) Biomimetic materials research: what can we really learn from nature's structural materials? J Roy Soc Interface 4(15):637–642

Griffin C (2014) Sustainable structures: the intersections of structural systems and green buildings. In: The proceedings of the 5th annual school of architecture symposium

Jian L, Feng L (2010) Bioinspired intelligent nanostructured interfacial materials. Chemical Industry Press, Beijing

Lenau T, Hesselberg T (2013) Biomimetic self-organization and self-healing, in engineered biomimicry. Elsevier, Amsterdam

Mirkhalaf M, Zhu D, Barthelat F (2013) Biomimetic hard materials in engineered biomimicry. Elsevier, Amsterdam

Pacheco-Torgal F, Faria J, Jalaia S (2013) Embodied energy vs. operational energy. Showing the shortcomings of the energy performance building directive (EPBD). Mater Sci Forum 730–732:587–591

Sarkisian M, Shook D (2014) Embodied Carbon in our future cities, in CTBUH, ctbuh.org/papers

Shahinpoor M (2013) Muscular biopolymers in engineered biomimicry. Elsevier, Amsterdam

Wilts BD, Stavenga DG (2015) Photonic structures in the animal kingdom: valuable inspirations for biomimetic applications in biomimetic architectures by plasma processing, fabrication and aplications. Standford publishing, Stanford

Chapter 15
Nanocellulose Aerogels as Thermal Insulation Materials

Hai M. Duong and Son T. Nguyen

Abstract There is a high demand of energy consumption due to the increasing population, industrial expansion, and development plans. However, the increasing cost of energy and the negative impact on the environment by energy production plants have resulted in the need to find means to substantially reduce energy consumption. Buildings are one of the main factors contributing to the world energy consumption. About two-thirds of the total energy is used for the buildings. It is essential to reduce energy consumption of buildings by finding more effective thermal insulation materials. Cellulose is a green, cheap, and abundant material with low thermal conductivity. Its combination with aerogel structure forms a novel and effective heat insulation material known as cellulose aerogel. Cellulose aerogels can be fabricated from bacterial cellulose, wood/paper pulps, or cellulosic wastes. The aerogels become water-repellent after being treated with silane reagents via a chemical vapor deposition (CVD) method. They show highly porous structures with good flexibility, high stability, and extremely low thermal conductivities. These characteristics make them promising for thermal insulation applications.

15.1 Introduction

Cellulose is one of the most common and abundant polymers on the planet. It is widely used in industry and normal life. Cellulose is a non-branched macromolecule containing ringed glucose molecules. Its repeat unit consists of two anhydroglucose rings linked together through oxygen covalently bonded to C1 of one glucose ring and C4 of the adjoining ring. This bond is known as the β 1–4 glucosidic bond. Intra- and interchain hydrogen bonding makes cellulose a relatively stable polymer (Cai et al. 2008; Cervin et al. 2012; Chang and Zhang 2011;

H.M. Duong (✉) · S.T. Nguyen
Department of Mechanical Engineering, National University of Singapore, Singapore 117575, Singapore
e-mail: mpedhm@nus.edu.sg

F. Pacheco Torgal et al. (eds.), *Nano and Biotech Based Materials for Energy Building Efficiency*, DOI 10.1007/978-3-319-27505-5_15

Kalia et al. 2011; Wicklein et al. 2015; Pour et al. 2015). Van der Waals and intermolecular hydrogen bonds promote parallel stacking of multiple cellulose chains forming elementary fibrils. These fibrils then aggregate to form larger microfibrils in the plant cell wall, which also aggregate into macroscopic fibers. These microfibrils have typically a diameter of about 10–30 nm and are made up of 30–100 cellulose molecules in extended chain conformation and provide mechanical strength to the fiber (Eichhorn et al. 2010; Mieck et al. 1994; Moon et al. 2011).

Cellulose fibers have many potential applications because they are abundantly available, low weight, biodegradable, cheaper, renewable, low abrasive nature, and good mechanical properties. The cellulose fibers can be classified according to their origin and grouped as follows: (1) leaf: abaca, pineapple, sisal, banana, etc.; (2) seed: cotton; bast: flax, hemp, etc.; (3) fruit: coir, kapok, etc.; (4) grass: bagasse, bamboo, etc.; and (5) stalk: straw (cereal) (Eichhorn et al. 2010; Kalia et al. 2011; Klemm et al. 2011; Mieck et al. 1994; Moon et al. 2011; Oshima et al. 2014). Commonly used plant fibers are cotton, jute, hemp, flax, ramie, sisal, coir, henequen, and kapok. Properties of cellulose fibers are affected by many factors such as variety, climate, harvest, maturity, retting degree, decortications, disintegration (mechanical, steam explosion treatment), fiber modification, textile, and technical processes (spinning and carding). Cellulose fibers with moduli up to 40 GPa can be separated from wood by chemical-pulping process. Such fibers can be further subdivided into microfibrils with elastic modulus of 70 GPa.

Cellulose nanofibers (CNFs) have a high potential to be used in many different areas such as reinforcement in development of nanocomposites. Many studies have been done on isolation and characterization of CNFs from various sources. Cellulose nanofibers can be extracted from the cell walls by simple mechanical methods or by a combination of both chemical and mechanical methods (Eichhorn et al. 2010; Kalia et al. 2011; Klemm et al. 2011; Mieck et al. 1994; Moon et al. 2011; Oshima et al. 2014). Cellulose nanofibers are extracted from the agricultural residues, wheat straw, and soy hulls, by a chemomechanical technique. The wheat straw nanofibers have diameters in the range of 10–80 nm and lengths of a few thousand nanometers. By comparison, the soy hull nanofibers have diameters of 20–120 nm and shorter lengths than the wheat straw nanofibers. Zimmermann et al. (2004) separated nanofibrillated cellulose at the greatest possible lengths and diameters below 100 nm from different starting cellulose materials by mechanical dispersion and high-pressure (up to 1500 bar) homogenization processes. The treatment resulted in nanoscaled fibril networks.

Aerogels have been well known as highly porous solids that hold air within their pores. As a result, their lightness, low heat conductivity, and large surface area make them ideal for possible applications as heat insulators, particle filters, particle trappers, and catalyst supports (Innerlohinger et al. 2006; Gesser and Goswami 1989; Bheekhun et al. 2013; Bryning et al. 2007; Pierre and Pajonk 2002; Nguyen et al. 2012). The combination of aerogel structure and cellulose fibers forms cellulose aerogel, a new kind of aerogel, which is green, cheap, and abundant. Cellulose-based aerogels were developed during the 1950s by Stamm and coworkers (1950). However, little further development occurred until the 2000s.

Most research efforts have been in aerogel processing and in some isolated cases the subsequent functionalization of the aerogel via coatings. The environmentally friendliness, low thermal conductivity (0.040–0.050 W/m K) of cellulose fibers, and the highly porous aerogel structure facilitate the heat insulation property of cellulose aerogels and thus open a new chapter in thermal insulation (Baetens et al. 2011; Fan et al. 2014; Al-Homoud 2005; Briga-Sá et al. 2013; Jelle 2011). The total global aerogel market is forecast to grow at a very high rate of 19.3 % from 2012 to 2017 and reach global revenues of US $332.2 million by 2017 (Nguyen et al. 2014). In particular, the thermal and acoustic insulation sector accounted for 82.3 % of all revenues in 2012 and shows the most potential growth with a five-year compound annual growth rate of 20.2 % from 2012 through 2017. Therefore, cellulose aerogels will have a very bright future in the global insulation market.

15.2 Advanced Cellulose Aerogels for Heat Insulation of Buildings

There have been several works on cellulose aerogels. Based on the cellulose source, cellulose aerogels can be synthesized from bacterial cellulose, wood/paper pulp, or wastes.

15.2.1 Cellulose Aerogels Prepared from Bacterial Cellulose

15.2.1.1 Fabrication Methods

Bacterial cellulose (BC) was first reported by Adrian Brown while working with *Bacterium aceti* in 1886 (cited from https://en.wikipedia.org/wiki/Bacterial_cellulose). A solid mass is formed at the surface of vinegar fermentation medium and is commonly used in homemade vinegar production (Oshima et al. 2014; Cai et al. 2012; Sai et al. 2013, 2014; Pircher et al. 2014; Liebner et al. 2010). The constituent was later identified as cellulose, and the name *Bacterium xylinum* was assigned to the microorganism responsible for its synthesis. Since its discovery, several names were given to this bacterium including *Acetobacterium xylinum* and *Bacterium xylinodes*. It was later named as *Acetobacter xylinum* and became the official name according to the International Code of Nomenclature of Bacteria (Cannon and Anderson 1991; Yamanaka et al. 1989). Now, this Gram-negative, strictly aerobic bacteria are referred to as species *Gluconacetobacter xylinus.* Although BC can be produced from the species of genera *Achromobacter, Alcaligenes, Aerobacter, Agrobacterium, Azotobacter, Gluconacetobacter, Pseudomonas, Rhizobium, Sarcina, Dickeya, and Rhodobacter,* only *species from genus Gluconacetobacter* can produce cellulose at commercial levels.

Bacterial cellulose is produced by acetic acid bacteria in both synthetic and non-synthetic media through partial oxidation of ethanol. As mentioned above, *Acetobacter xylinum* is the most studied and the most efficient BC producer that manages to assimilate various sugar sources such as glucose, sucrose, and coconut milk and yields high level of cellulose in liquid media. It needs to be given the optimal conditions in terms of temperature, oxygen supply, and nutrients to be able to synthesize cellulose (Liebner et al. 2010; Liang et al. 2015; Keshk 2014; Sai et al. 2014; Pircher et al. 2014). As a nutrient source, several growth media exist, one that is very common is a mixture introduced by Schramm and Hestrin in 1954, which consists of 20 g l^{-1} glucose, 5 g l^{-1} peptone, 5 g l^{-1} yeast extract, 1.15 g l^{-1} citric acid monohydrate, and 6.8 g l^{-1} Na_2HPO_4 12 H_2O (Hestrin and Schramm 1954). Process is active at pH 3–7 and at temperature between 25 and 30 °C. It was reported that almost 30 % of bacterial fermentation cost belongs to the cost of fermentation medium. High cost and low-yield production have limited the industrial production of BC and its commercial application (Liebner et al. 2010; Liang et al. 2015; Keshk 2014; Sai et al. 2014; Pircher et al. 2014). Therefore, it is important to look for a new cost-effective carbon source with shorter fermentation process for high-yield BC production. The BC hydrogel then undergoes a drying process to be converted to BC aerogel. To maintain the porous structure of the BC hydrogel, two drying ways are usually used: freeze drying and supercritical point drying. In the first method, the hydrogel is frozen by liquid nitrogen or a refrigerator, and then, the ice in the sample is removed by sublimation directly with vacuum. In the supercritical drying method, the BC hydrogel is subject to thorough solvent exchange with ethanol to form BC alcogel. Then, ethanol is replaced by liquid CO_2. After that, CO_2 is converted into the supercritical state and slowly released to ambient pressure. Unlike plant cellulose, BC does not require extra processing to remove unwanted impurities and contaminants such as lignin, pectin, and hemicellulose, thus being able to retain a greater degree of polymerization.

15.2.1.2 Morphology

Scanning electron micrographs (SEM) of the BC aerogels (Fig. 15.1) reveal a hierarchical order of the open-porous network, which consists of a well-developed macropore system formed from disorderly dispersive 20–80 nm cellulose fibers. Apart from macropores, Liebner et al. (2010) found that BC aerogels also have a mesoporous substructure (Liebner et al. 2010). Nitrogen sorption experiments show that the mesopores considerably contribute to the total pore volume as the obtained isotherms are of type IV. The mesopore diameter is about 10 nm, and the surface area and pore volume are about 160–200 m^2 g^{-1} and 0.5 cm^3 g^{-1}, respectively. The BC aerogels possess very low densities of around 6.7–8.3 mg cm^{-3}. Their porosity is about 99.6 %. X-ray diffraction (XRD) spectra of the BC aerogels show three characteristic peaks centered at 14.78°, 16.98°, and 22.78°, corresponding to the typical $(1\bar{1}0)$, (110), and (020) planes of cellulose I, respectively.

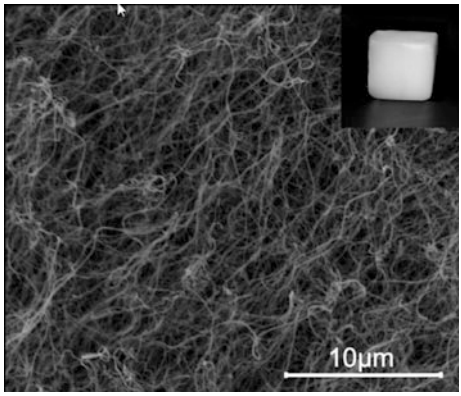

Fig. 15.1 The BC aerogel (Pircher et al. 2014)

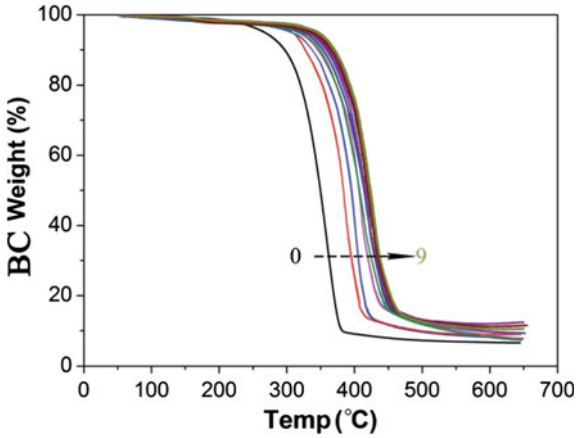

Fig. 15.2 TGA result of BC aerogels (Sai et al. 2014)

15.2.1.3 Thermal Properties

Thermogravimetric analysis (TGA) results (Fig. 15.2) show that BC aerogels start to decompose at 250 °C. They lose 5 % of their weight at 265 °C, 10 % of their weight at 290 °C, and completely degrade at about 380 °C. They exhibit an extremely low thermal conductivity of 0.0295 W m^{-1} K^{-1} (Sai et al. 2014), almost the same as that of silica aerogels, indicating that they are promising for thermal insulation applications.

15.2.1.4 Mechanical Properties

The BC aerogels have a 3D web-like morphology formed from a large number of hydrogen bonds between the BC nanofibers. This makes them strong and flexible. Figure 15.3 shows compressive curves of the BC aerogels. It was found that they

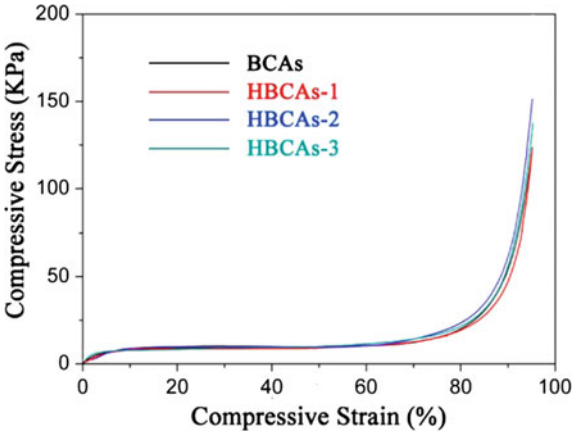

Fig. 15.3 Compressive curves of the BC aerogels (Sai et al. 2013)

possess a compression modulus of 0.27 MPa in Sai et al.'s work (Sai et al. 2013). Pircher et al. (2014) found that the BC aerogels have specific modulus values of 19–25 MPa $cm^3\ g^{-1}$, which are remarkably high compared to other porous materials. For example, for a polyurethane foam of a density of 90 mg cm^{-3}, a specific modulus of 7.8 MPa $cm^3\ g^{-1}$ was previously reported. A lower specific modulus of about 4 $cm^3\ g^{-1}$ was reported for silica aerogel.

15.2.2 Cellulose Aerogels Prepared from Wood/Paper Pulp

15.2.2.1 Fabrication Methods

Cai et al. (2008) fabricated cellulose aerogels from filter paper pulp, Whatman cellulose powder, cotton linter pulp, and tunicate cellulose. The solvent mixtures NaOH/urea/H_2O (7:12:81 w/w) and LiOH/urea/H_2O (4.6:15:80.4 w/w) were precooled to −12 °C. Then, the desired amount of the cellulose sample was immediately dispersed into the solvent system under vigorous stirring for 10 min at ambient temperature to obtain a transparent cellulose solution (0.5–7 wt%). The cellulose solution was subjected to centrifugation at 5000 rpm for 10 min at 5 °C to remove air bubbles. The resulting solution was cast on a glass plate to give a 0.5-mm-thick layer and immersed into various coagulation baths for regeneration. The regeneration conditions were wt% H_2SO_4 aqueous solution at 0–60 °C for 5 min, ethanol–H_2O with different volume ratios at 20 °C for 2 h, methanol at 20 °C for 2 h, acetone at 20 °C for 2 h, isopropanol at 20 °C for 2 h, and tert-butanol at 20 °C for 2 h. The regenerated cellulose films were washed with excess deionized (DI) water to remove the residual chemical reagents. The cellulose hydrogels were then dried by supercritical drying or freeze-drying methods.

Wang et al. (2012) pretreated microcrystalline cellulose, filter paper pulp, bleached sulfite pulp, cellulose I, and cellulose II (from beech wood holocellulose) with ethylene diamine (EDA) for 24 h at room temperature, and filtered and freeze-dried to get the cellulose-EDA complex. This complex was added into a 8 % LiCl/dimethyl sulfoxide (DMSO) solution. The mixture was stirred at room temperature for 24 h, followed by stirring at 75 °C for several hours to give clear solution. The cellulose solution was poured into a glass dish to form 1-mm-thick layer and immersed in ethanol for regeneration–gelation. The gel was thoroughly washed by ethanol, then by water to remove LiCl, DMSO, and EDA. The hydrogel was solvent-exchanged to ethanol and freeze-dried to form the final aerogel.

Instead of using NaOH/urea/H_2O, LiOH/urea/H_2O, or LiCl/DMSO solutions, Liebner et al. dissolved cellulose in a melting N-methylmorpholine-N-oxide (NMMO) and N-benzyl-morpholine-N-oxide (NBnMO) mixture (Liebner et al. 2007, 2008). The cellulose dope was poured into the desired form by molds and cooled to room temperature. NMMO/cellulose moldings were regenerated by adding ethanol or DMSO or mixtures of both in an end-over-end mixer for 24 h. Then, the regeneration was repeated with another 10 ml of the corresponding solvent for another 24 h. Supercritical drying was used to convert the gel to aerogel.

Cellulose can also be dissolved in hydrophilic ionic liquids, such as 1-allyl-3-methylimidazolium chloride (AMImCl). In Li et al.'s work (2011), wood flour was mixed with AMImCl in a 500-mL beaker. The beaker was immersed in an oil bath at 80 °C under constant stirring for 4 h to form a brownish homogeneous mixture. The homogeneous viscous solution was transferred to appropriate molds and sealed individually. All samples underwent cyclic freeze–thaw (FT) treatment. The typical FT process is described as follows: The sample was frozen at −20 °C for 10 h; then, it was vacuum-thawed for 6 h to room temperature. After undergoing several FT cycles, all samples were immersed in the first coagulation bath with deionized water. The bath was replenished at least three times until no chloride ion Cl^- was detected using $AgNO_3$ solution. The samples were then dried using supercritical drying with CO_2.

In Chen's group's research (Chen et al. 2011), wood fibers were dewaxed with a mixture of benzene and ethanol. Then, the lignin in the sample was removed using an acidified sodium chlorite solution at 75 °C for 1 h. Hemicellulose, residual starch, and pectin were removed by KOH treatment. Highly purified cellulose fibers were prepared by further treating the samples with a 1 wt% HCl solution at 80 °C for 2 h and thoroughly washing them with distilled water. Finally, about 100 ml of a solution containing purified cellulose fibers was placed in a common ultrasonic generator with a frequency of 19.5–20.5 kHz and equipped with a cylindrical titanium alloy probe tip 2.5 cm in diameter. The subsequent ultrasonication was conducted for 30 min at an output power of 1200 W, resulting in the cellulose hydrogels. The samples were then placed in a refrigerator at −18 °C for more than 24 h. Afterward, the samples were subjected to freeze-drying to allow frozen water in the materials to sublime directly from the solid phase to the gas phase.

15.2.2.2 Morphology

Cai et al. found that the cellulose aerogels fabricated from NaOH/urea or LiOH/urea had porosities of 73.9–98.0 % with Brunauer–Emmett–Teller (BET) surface areas of 260–495 m^2/g (Cai et al. 2008). For the NaOH/urea method, the porosity of the aerogels increased slightly from 85.5 to 88.7 % when increasing regeneration temperature (0–60 °C) in a regeneration bath of 5 wt% H_2SO_4. The LiOH/urea system exhibited a similar behavior. All the nitrogen adsorption/desorption isotherms obtained were of type IV (Fig. 15.4). BET surface areas of samples dried by water freeze-drying were smaller than those of samples dried with tert-butanol and CO_2. As shown in Fig. 15.5, the aerogels obtained by freeze-drying from water and tert-butanol showed differences in morphology between the surface and the inside cross sections. These aerogels had highly porous networks on the surface, consisting of fibrils less than 100 nm wide, but some parts of the sample obtained from water contained film-like structures spanning between the fibrils (Fig. 15.5b). These films could have resulted from the growth of relatively large ice crystals expelling fine fibrils of cellulose. This may be the cause of the small BET surface area value of the water freeze-dried material as compared with the other two samples. On the other hand, the inner parts of all the aerogel samples viewed on the cross sections displayed more uniform, nanometer-sized pore structures composed of fibrillar networks (Fig. 15.5d, h and l). The supercritical CO_2-dried material had a more homogenous structure, being the same on the surface and the cross section. These features confirm that the supercritical CO_2 drying is the best method in preserving the liquid-swollen gel structure upon drying.

For the cellulose aerogels synthesized with the LiCl/DMSO system, the surface of the aerogels showed somewhat collapsed structure; in contrast, the fractured cross sections showed cellulose networks of unique structure. The bulk of aerogel was composed of long and fairly straight fibrils interconnected with one another to form three-dimensional networks with large interstitial spaces (Wang et al. 2012). The difference between the surface and the cross section is likely to result from the

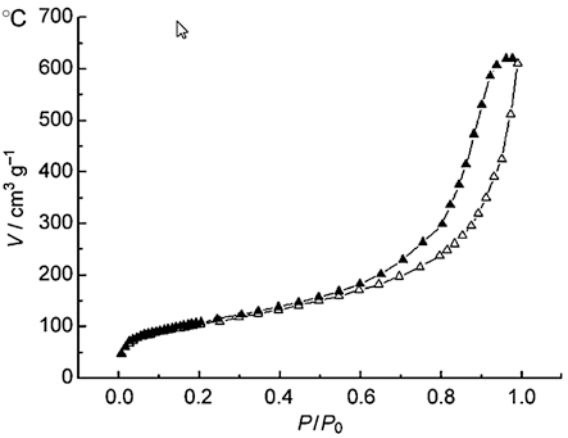

Fig. 15.4 Nitrogen adsorption/desorption isotherm of the cellulose aerogels (Cai et al. 2008)

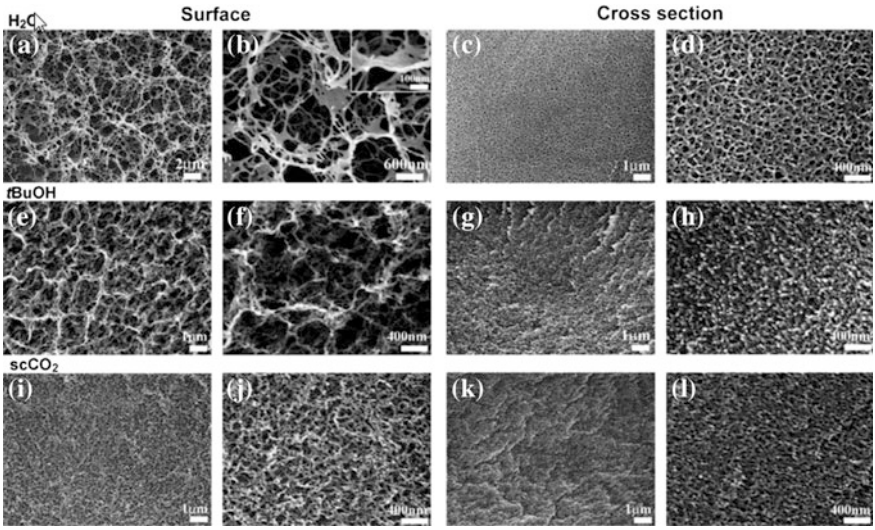

Fig. 15.5 SEM images of aerogels prepared from 4 wt% cellulose in aqueous LiOH/urea solution, regenerated with EtOH, and either freeze-dried from H_2O (**a**–**d**) or tBuOH (**e**–**h**) or dried from CO_2 (**i**–**l**) as indicated. (**a**), (**e**), (**i**) Low-magnification and (**b**), (**f**), (**j**) high-magnification images of the surface; (**c**), (**g**), (**k**) low-magnification and (**d**), (**h**), (**l**) high-magnification images of the cross sections of the aerogels. The inset in part (**b**) shows the SEM image of a tilted sample (Cai et al. 2008)

difference in regenerating condition; i.e., the surface was subjected to a drastic change in liquid composition, whereas the cross section should have experienced gradual composition changes, leading to slow coagulation. XRD diagrams of the aerogels showed that the cellulose I structure was completely lost by dissolution–regeneration, and the pattern of aerogels was that of a poorly crystalline cellulose II. BET analysis of the aerogels gave surface area of around 200 $m^2\ g^{-1}$. The mesopore analysis by Barret–Joyner–Harrenda (BJH) method gave wide mesopore size distributions, mostly in the range of 10–100 nm. The average mesopore diameter of the aerogels was 13–20 nm determined by the BJH method.

Cellulose aerogels produced by NMMO/NBnMO method displayed porous structures with specific density and surface area ranged 0.05–0.26 g cm^{-3} and 172–284 $m^2\ g^{-1}$, respectively, with increasing density at higher cellulose contents (Liebner et al. 2007, 2008). Among the tested regenerating solvents, ethanol gave the lowest specific densities upon supercritical drying at 40 °C and 100 bars and the highest retaining volume of about 70 %.

In the ionic liquid method, the morphology of the aerogels was changed with the number of FT treatment cycles (Li et al. 2011). With one FT treatment, the aerogel showed a porous structure. The distribution of the pores became denser with the increase in the FT treatment cycles. However, the microporous structure disappeared, and a dense film-like structure, which was associated with common open-pore web structure, was observed from the samples after quintuplicate FT

treatment. The film-like structure rather than a network structure was observed for the samples after septuplicate and decuplicate FT treatment. The construction of cellulose fibril networks was ascribed to the formation of the ionic liquid crystal during the freezing process. Despite the influence of the wood/ionic liquid solution concentration on the density of the network, the frequency of crystallization was considered as the vital parameter to form the mesh structure.

Cellulose aerogels prepared via ultrasonication exhibited extremely low bulk densities in the range of 1.3×10^{-3}–17.0×10^{-3} g cm^{-3} (Chen et al. 2011) and porosities of 98.94–99.91 %. They had a 3D open-porous fibrillar network structure of continuous nanofibers (approximately 30–150 nm in width and several hundred microns long), indicating that the CNFs self-assembled via hydrogen bonding during the freeze-drying process, thus organizing them into long nanofibers and formation a porous network structure. The distribution of the pores became denser with the increase in the solid content of the hydrogels. Most of the microporous structure disappeared when the CNF content was higher than 0.5 %, and a dense 2D sheet-like structure, organized by small CNFs (around 20–30 nm wide and several microns long) with only a few aggregates, was observed.

15.2.2.3 Thermal Properties

Thermogravimetric analysis showed the degradation temperature of cellulose aerogels synthesized by the alkali/urea method was about 300–310 °C (Cai et al. 2012). The degradation point of the aerogels fabricated by the sonication method was in the range of 325–337 °C. This degradation point was much higher than that of original wood fibers (210 °C) (Chen et al. 2011). The cellulose aerogels showed a very low thermal conductivity of 0.025 W m^{-1} K^{-1}, which was slightly lower than that of 0.0295 W m^{-1} K^{-1}, (Sai et al. 2014) of BC aerogels (Cai et al. 2012).

15.2.2.4 Mechanical Properties

In Cai et al.'s work (Cai et al. 2012), the tensile modulus and strength of the cellulose aerogels were determined as 72.0 and 12.4 MPa, respectively, which was much higher than the compression modulus, 0.27 MPa (Sai et al. 2013), of BC aerogels. Chen et al. found that their cellulose aerogels exhibited high flexibility and ductility because of the high aspect ratio, high crystallinity, high CNF mechanical properties, and an entangled 3D or 2D microstructure (Chen et al. 2011). As shown in Fig. 15.6a–c, an aerogel with approximate dimensions of $5.44 \times 5.44 \times 0.59$ cm^3 and a bulk density of 2.6×10^{-3} g cm^{-3} could be repeatedly bent without destroying its structural integrity. The compression property of the aerogels was also tested (Fig. 15.6d–f). A cylindrical aerogel with an approximate radius of 1.05 cm, a height of 1.67 cm, and density of 9.2×10^{-3} g cm^{-3} could be easily compressed by hand into a sheet about 0.09 cm thick without disintegrating. The obtained dense sheet with a bulk density of 0.17 g cm^{-3} could also be folded easily.

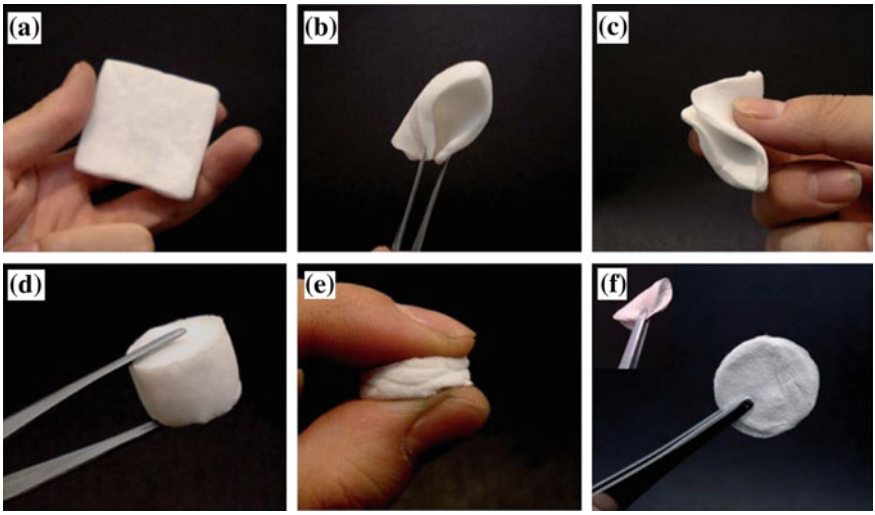

Fig. 15.6 A demonstration of the flexibility and deformability of the aerogels. **a–c** The aerogel with dimensions of about 5.44 × 5.44 × 0.59 cm^3 can be repeatedly bent as foldable as conventional paper. **d–f** An aerogel with a diameter of 2.10 cm and height of 1.67 cm can be compressed into a circuit sheet about 0.09 cm thick by hand; the obtained sheet can also be folded easily (Chen et al. 2011)

15.2.3 Cellulose Aerogels Prepared from Wastes

15.2.3.1 Fabrication Methods

In Nguyen et al.'s work (Nguyen et al. 2013, 2014), recycled cellulose fibers from paper waste were dispersed into a NaOH/urea solution by sonicating for 6 min. Thereafter, the solution was placed in a refrigerator for more than 24 h to allow gelation of the solution. After the solution was frozen, it was then thawed at room temperature and then followed by immersing into ethanol (99 vol.%) for coagulation. After the coagulation, solvent exchange was carried out by immersing the gel in DI water for 2 days. The sample was then frozen in a freezer at −18 °C for 12 h. After that, freeze drying is carried out for 2 days with a freeze dryer to obtain the desired aerogel.

Feng et al. dispersed recycled cellulose fibers and Kymene cross-linker in 30 ml DI water by sonicating for 10 min (Feng et al. 2015). The suspension was then placed in a refrigerator at −18 °C for more than 24 h to allow the gelation. The cellulose aerogel was obtained by freeze-drying the gel at −98 °C for 2 days using a freeze dryer. Thereafter, the cellulose aerogel was further cured at 120 °C for another 3 h to cross-link completely the Kymene molecules.

In Jin's work (Jin et al. 2015), waste newspaper (WNP) pieces were dispersed into 1-allyl-3-methyimidazolium chloride (AMImCl) in a 20-mL beaker. The beaker

was immediately immersed in an oil bath at 80 °C under vigorous stirring for 4 h to form a homogeneous mixture. Finally, a dark, amber-colored, viscous WNP suspension was obtained. The resultant WNP solution was completely cast in Teflon molds, took off air bubble in a vacuum oven, and then immediately coagulated in the water to obtain a regenerated cellulose hydrogel. It was washed with excess deionized water until the residual chemical reagents were absolutely removed. Then, the prepared hydrogels were freeze-dried in a vacuum freeze dryer at −50 °C for 48 h.

Li et al. used waste wheat straw powder to synthesize cellulose aerogels (Li et al. 2014). Wheat straw was first treated by a mixed solution of benzene/absolute ethanol (2:1 v/v) in a Soxhlet extractor at 90 °C for 6 h. Then, the treated sample was air-dried and treated with a 10 % $NaClO_2$ solution at 75 °C for 5 h. The next step was to collect the sample by filtration, wash it three times with DI water, and then immediately treat it with 2 % NaOH at 90 °C for 2 h. The product was again collected by the filtration and washed three times with DI water before treating it with 1 % HCl at 80 °C for 2 h. Finally, the purified cellulose was collected by the filtration, washed three times the deionized water, and dried at 60 °C for 24 h. The purified cellulose was added to a 10 % aqueous solution of NaOH/polyethylene glycol (PEG) (9:1 wt/wt) with magnetic stirring for 5 h to form a homogeneous solution. The solution was frozen for 12 h at −15 °C and then subsequently thawed at ambient temperature with vigorous stirring for 30 min. This process was repeated at least 3 times. The product was successively regenerated by 1 % HCl solution, DI water, and tert-butanol until the formation of an amber-like hydrogel. Finally, the resultant cellulose hydrogel samples were freeze-dried at −30 °C for 48 h.

15.2.3.2 Hydrophobic Coating Methods

As the cellulose aerogels developed in Sect. 15.2.3.1 were hydrophilic, the as-prepared cellulose aerogels were coated with a hydrophobic coating agent on their highly porous networks to form super-hydrophobic cellulose aerogels. Silane reagents such as methyltrimethoxy silane (MTMS) and trimethylchlorosilane (TMCS) were usually used as the coating agents via a CVD method (Feng et al. 2015; Jin et al. 2015; Li et al. 2014; Nguyen et al. 2013, 2014). The cellulose aerogel sample and an open glass vial containing MTMS/TMCS were placed in a big container. The container was then capped and heated at 70 °C for 3 or 12 h for the silanation reaction. Thereafter, the coated sample was placed in a vacuum oven to remove the excess coating reagent until the pressure reaches 0.03 mbar.

15.2.3.3 Environmental Stability

The MTMS-coated cellulose aerogels had super-hydrophobicity on both their external and internal structures. Large water contact angles of 153.5° and 150.8° of the surface and the cross section were obtained, respectively, thus proving that the

hydrophobic coating was successfully covered the whole aerogel networks. The cellulose aerogel samples were then exposed in normal ambient atmosphere for five months. The water contact angles on the external surface and the cross section did not show any obvious change within five months, confirming the excellent hydrophobicity stability of the MTMS-coated recycled cellulose aerogels (Feng et al. 2015).

15.2.3.4 Morphology Control

Figure 15.7 showed photographs and SEM images of the developed recycled cellulose aerogels (Feng et al. 2015; Nguyen et al. 2013; Nguyen et al. 2014). The recycled cellulose aerogels were formed via hydrogen bonding between the self-assembled cellulose fibers (Isobe et al. 2012). Besides, Kymene molecules could diffuse and react with the cellulose fiber surface to form the hydrogen bonding and also cross-linked with the surrounding Kymene molecules. The utilization of Kymene as a cross-linker combined the reinforcement and protection mechanisms (Nordell 2006) during the gelation process, which thus ensured the resultant aerogels with a robust structure and good flexibility. In contrast to the mesopores (2–50 nm) of the aerogels formed by the cellulose nanofibers, highly porous structures of the cellulose aerogels with macropores (>50 nm) could be clearly observed in SEM images of Fig. 15.7c–f. Their macropores were possibly caused by the larger length and diameter of the recycled cellulose fibers, obtained from the paper waste. Figure 15.7c, d shows the morphologies of the cellulose aerogels with cellulose concentrations of 0.25 and 1.00 wt%, respectively. The aerogel with the larger cellulose concentration (1.0 wt%) had a more compacted

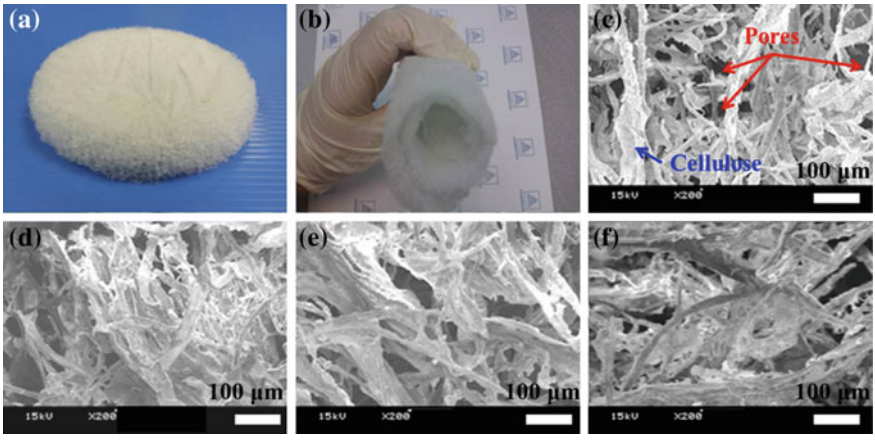

Fig. 15.7 **a** A super-hydrophobic recycled cellulose aerogel, **b** flexibility of the large-scale cellulose aerogel (38 × 38 × 1 cm) containing 0.60 wt% of the cellulose fibers, SEM images of the cellulose aerogels with different ratios of cellulose fibers (wt%) and kymene (µl): **c** 0.25:5, **d** 1.00:5, **e** 0.60:5 and **f** 0.60:20 (Feng et al. 2015)

network and lower porosity. However, an increase of Kymene from 5 to 20 μl did not significantly impact the aerogel structures as shown in Fig. 15.7e, f.

In Jin et al.'s study, the aerogels exhibited a highly open-porous structure (porosity of approx. 96.8 %) consisting of uniformly-interconnected cellulose fibers. The densities of the aerogels without and with silane modification were 0.020 and 0.029 g cm^{-3}, respectively (Jin et al. 2015). Li et al. found that the bulk densities of the cellulose aerogel samples increased with the enhanced cellulose concentrations (Li et al. 2014). The samples were referred as C1, C2, C4, and C8 with mass ratios of 1/100, 2/100, 4/100, and 8/100 cellulose to the NaOH/PEG solution, respectively. The bulk densities of C1, C2, C3, and C4 were 44.9, 56.7, 80.7, and 148.0 mg cm^{-3}, respectively. The pore configurations of C1 and C2 were dense, anfractuous, and multilayered, while the pore distributions of C3 and C4 were relatively uniform. Some larger sheet and blocky regions surrounding with the pore structures were observed. This might be attributed to the existence of undissolved fractional cellulose fibers at high concentrations. It was concluded that the concentration had a significant influence on the pore structures of the aerogels. Specific surface areas and mean pore diameters of the samples were in the ranges of 36.5–101 m^2 g^{-1} and 16.2–18.3 nm, respectively.

15.2.3.5 Thermal Properties

Thermal conductivity of the recycled cellulose aerogel was 0.032 W m^{-1} K^{-1} (Nguyen et al. 2014), which was comparable to those of good insulation materials such as silica aerogel (0.026 W m^{-1} K^{-1}), wool (0.03–0.04 W m^{-1} K^{-1}), and Aspen Aerogels products (0.021 W m^{-1} K^{-1}) (Sequeira et al. 2009; Nguyen et al. 2014). A TGA test was performed for the sample in air. There was a weight loss of 23 % in the temperature range of 25–230 °C due to the removal of absorbed water and some urea trace left in the cellulose aerogel sample. Then, a weight loss of 42 % occurred in the range of 230–330 °C due to the degradation and burning of the cellulose aerogel structure. There was small drop of the sample weight at 550–630 °C due to the oxidation of some stable local structures of the aerogel.

15.2.3.6 Mechanical Properties

As shown in Fig. 15.7b, the large-scale cellulose aerogel could be easily bent or rolled without damaging its structure. The flexibility of the recycled cellulose aerogel was comparable to that of nanocellulose aerogels (Chen et al. 2011). A qualitative test was performed for the sample to investigate its mechanical strength by loading a 200 g weight on the sample for 1 h, 5 h, 1 day, and 5 days. No structure damage of the aerogel was found after the test durations. Tensile and compression tests were also performed for the aerogel samples. The yield and tensile strengths of the aerogel were 1080 and 1470 N/m^2, respectively, with a Young's modulus of 11 kPa (Nguyen et al. 2014).

15.3 Conclusions and Future Perspectives

High energy consumption, climate changes, and the exhaust of fossil fuels require more sustainable and energy efficient construction solutions. In order to meet the demand of improved energy efficiency, the thermal insulation of the buildings has an important role. As a result, it is essential to develop new insulation materials with low thermal conductivity for the construction applications. The cellulose material is a green, non-toxic, cheap, and abundant material. The property combination of cellulose and aerogel structure has formed a novel and effective cellulose aerogel material. The extremely low thermal conductivity of 0.025–0.032 W m^{-1} K^{-1} and good flexibility of cellulose aerogels make them a promising material for building heat insulation. The thermal stability limitation of the cellulose aerogels can be overcome by combining with fire retardants or other heat insulation materials such as flexible silica aerogels.

References

Al-Homoud DMS (2005) Performance characteristics and practical applications of common building thermal insulation materials. Build Environ 40(3):353–366. doi:10.1016/j.buildenv.2004.05.013

Baetens R, Jelle BP, Gustavsen A (2011) Aerogel insulation for building applications: a state-of-the-art review. Energy Build 43(4):761–769. doi:10.1016/j.enbuild.2010.12.012

Bheekhun N, Abu Talib AR, Hassan MR (2013) Aerogels in aerospace: an overview. Adv Mater Sci Eng 2013:18. doi:10.1155/2013/406065

Briga-Sá A, Nascimento D, Teixeira N, Pinto J, Caldeira F, Varum H, Paiva A (2013) Textile waste as an alternative thermal insulation building material solution. Constr Build Mater 38:155–160. doi:10.1016/j.conbuildmat.2012.08.037

Bryning MB, Milkie DE, Islam MF, Hough LA, Kikkawa JM, Yodh AG (2007) Carbon nanotube aerogels. Adv Mater 19(5):661–664. doi:10.1002/adma.200601748

Cai J, Kimura S, Wada M, Kuga S, Zhang L (2008) Cellulose aerogels from aqueous alkali hydroxide-urea solution. ChemSusChem 1(1–2):149–154

Cai J, Liu S, Feng J, Kimura S, Wada M, Kuga S, Zhang L (2012) Cellulose-silica nanocomposite aerogels by in situ formation of silica in cellulose gel. Angew Chem Int Ed Engl 51(9):2076–2079. doi:10.1002/anie.201105730

Cannon RE, Anderson SM (1991) Biogenesis of bacterial cellulose. Crit Rev Microbiol 17(6):435–447. doi:10.3109/10408419109115207

Cervin NT, Aulin C, Larsson PT, Wågberg L (2012) Ultra porous nanocellulose aerogels as separation medium for mixtures of oil/water liquids. Cellulose 19(2):401–410

Chang C, Zhang L (2011) Cellulose-based hydrogels: present status and application prospects. Carbohydr Polym 84(1):40–53

Chen W, Yu H, Li Q, Liu Y, Li J (2011) Ultralight and highly flexible aerogels with long cellulose I nanofibers. Soft Matter 7(21):10360–10368

Eichhorn SJ, Dufresne A, Aranguren M, Marcovich NE, Capadona JR, Rowan SJ, Weder C, Thielemans W, Roman M, Renneckar S, Gindl W, Veigel S, Keckes J, Yano H, Abe K, Nogi M, Nakagaito AN, Mangalam A, Simonsen J, Benight AS, Bismarck A, Berglund LA, Peijs T (2010) Review: current international research into cellulose nanofibres and nanocomposites. J Mater Sci 45(1):1–33

Fan Z, Marconnet A, Nguyen ST, Lim CYH, Duong HM (2014) Effects of heat treatment on the thermal properties of highly nanoporous graphene aerogels using the infrared microscopy technique. Int J Heat Mass Transf 76:122–127. doi:10.1016/j.ijheatmasstransfer.2014.04.023

Feng J, Nguyen ST, Fan Z, Duong HM (2015) Advanced fabrication and oil absorption properties of super-hydrophobic recycled cellulose aerogels. Chem Eng J 270:168–175. doi:10.1016/j.cej.2015.02.034

Gesser HD, Goswami PC (1989) Aerogels and related porous materials. Chem Rev 89(4):765–788. doi:10.1021/cr00094a003

Hestrin S, Schramm M (1954) Synthesis of cellulose by *Acetobacter xylinum*. 2. Preparation of freeze-dried cells capable of polymerizing glucose to cellulose. Biochem J 58(2):345–352

Innerlohinger J, Weber HK, Kraft G (2006) Aerocellulose: aerogels and aerogel-like materials made from cellulose. Macromol Symp 244(1):126–135. doi:10.1002/masy.200651212

Isobe N, Kimura S, Wada M, Kuga S (2012) Mechanism of cellulose gelation from aqueous alkali-urea solution. Carbohydr Polym 89(4):1298–1300. doi:10.1016/j.carbpol.2012.03.023

Jelle BP (2011) Traditional, state-of-the-art and future thermal building insulation materials and solutions—properties, requirements and possibilities. Energy Build 43(10):2549–2563. doi:10.1016/j.enbuild.2011.05.015

Jin C, Han S, Li J, Sun Q (2015) Fabrication of cellulose-based aerogels from waste newspaper without any pretreatment and their use for absorbents. Carbohydr Polym 123:150–156. doi:10.1016/j.carbpol.2015.01.056

Kalia S, Dufresne A, Cherian BM, Kaith BS, Avérous L, Njuguna J, Nassiopoulos E (2011) Cellulose-based bio—and nanocomposites: a review. Int J Polym Sci. doi:10.1155/2011/837875

Keshk SM (2014) Bacterial cellulose production and its industrial applications. J Bioprocess Biotech 04(02). doi:10.4172/2155-9821.1000150

Klemm D, Kramer F, Moritz S, Lindström T, Ankerfors M, Gray D, Dorris A (2011) Nanocelluloses: a new family of nature-based materials. Angew Chem Int Ed 50(24):5438–5466

Li J, Lu Y, Yang D, Sun Q, Liu Y, Zhao H (2011) Lignocellulose aerogel from wood-ionic liquid solution (1-allyl-3- methylimidazolium chloride) under freezing and thawing conditions. Biomacromolecules 12(5):1860–1867

Li J, Wan C, Lu Y, Sun Q (2014) Fabrication of cellulose aerogel from wheat straw with strong absorptive capacity. Front Agric Sci Eng 1(1):46. doi:10.15302/j-fase-2014004

Liang H-W, Wu Z-Y, Chen L-F, Li C, Yu S-H (2015) Bacterial cellulose derived nitrogen-doped carbon nanofiber aerogel: an efficient metal-free oxygen reduction electrocatalyst for zinc-air battery. Nano Energy 11:366–376. doi:10.1016/j.nanoen.2014.11.008

Liebner F, Potthast A, Rosenau T, Haimer E, Wendland M (2007) Ultralight-weight cellulose aerogels from NBnMO-stabilized lyocell dopes. Res Lett Mater Sci 2007:1–4. doi:10.1155/2007/73724

Liebner F, Potthast A, Rosenau T, Haimer E, Wendland M (2008) Cellulose aerogels: highly porous, ultra-lightweight materials. Holzforschung 62(2):129–135

Liebner F, Haimer E, Wendland M, Neouze MA, Schlufter K, Miethe P, Heinze T, Potthast A, Rosenau T (2010) Aerogels from unaltered bacterial cellulose: Application of $scCO_2$ drying for the preparation of shaped, ultra-lightweight cellulosic aerogels. Macromol Biosci 10(4):349–352

Mieck KP, Nechwatal A, Knobelsdorf C (1994) Potential applications of natural fibres in composite materials. Melliand Textilberichte 75(11):892–898 + E228

Moon RJ, Martini A, Nairn J, Simonsen J, Youngblood J (2011) Cellulose nanomaterials review: Structure, properties and nanocomposites. Chem Soc Rev 40(7):3941–3994

Nguyen ST, Nguyen HT, Rinaldi A, Nguyen NPV, Fan Z, Duong HM (2012) Morphology control and thermal stability of binderless-graphene aerogels from graphite for energy storage applications. Colloids Surf A 414:352–358. doi:10.1016/j.colsurfa.2012.08.048

Nguyen ST, Feng J, Le NT, Le ATT, Hoang N, Tan VBC, Duong HM (2013) Cellulose aerogel from paper waste for crude oil spill cleaning. Ind Eng Chem Res 52(51):18386–18391. doi:10.1021/ie4032567

Nguyen ST, Feng J, Ng SK, Wong JPW, Tan VBC, Duong HM (2014) Advanced thermal insulation and absorption properties of recycled cellulose aerogels. Colloids Surf A 445:128–134. doi:10.1016/j.colsurfa.2014.01.015

Nordell P (2006) Wet strength development of paper. Lulea University of Technology

Oshima T, Sakamoto T, Ohe K, Baba Y (2014) Cellulose aerogel regenerated from ionic liquid solution for immobilized metal affinity adsorption. Carbohydr Polym 103:62–69. doi:10.1016/j.carbpol.2013.12.021

Pierre AC, Pajonk GM (2002) Chemistry of Aerogels and Their Applications. Chem Rev 102 (11):4243–4266. doi:10.1021/cr0101306

Pircher N, Veigel S, Aigner N, Nedelec JM, Rosenau T, Liebner F (2014) Reinforcement of bacterial cellulose aerogels with biocompatible polymers. Carbohydr Polym 111:505–513. doi:10.1016/j.carbpol.2014.04.029

Pour G, Beauger C, Rigacci A, Budtova T (2015) Xerocellulose: lightweight, porous and hydrophobic cellulose prepared via ambient drying. J Mater Sci 50(13):4526–4535. doi:10.1007/s10853-015-9002-4

Sai H, Xing L, Xiang J, Cui L, Jiao J, Zhao C, Li Z, Li F (2013) Flexible aerogels based on an interpenetrating network of bacterial cellulose and silica by a non-supercritical drying process. J Mater Chem A 1(27):7963. doi:10.1039/c3ta11198a

Sai H, Xing L, Xiang J, Cui L, Jiao J, Zhao C, Li Z, Li F, Zhang T (2014) Flexible aerogels with interpenetrating network structure of bacterial cellulose–silica composite from sodium silicate precursor via freeze drying process. RSC Adv 4(57):30453. doi:10.1039/c4ra02752c

Sequeira S, Evtuguin DV, Portugal I (2009) Preparation and properties of cellulose/silica hybrid composites. Polym Compos 30(9):1275–1282

Stamm AJ, Tarkow H (1950) Penetration of cellulose fibers. J Phys Colloid Chemistry 54(6):745–753

Wang Z, Liu S, Matsumoto Y, Kuga S (2012) Cellulose gel and aerogel from LiCl/DMSO solution. Cellulose 19(2):393–399. doi:10.1007/s10570-012-9651-2

Wicklein B, Kocjan A, Salazar-Alvarez G, Carosio F, Camino G, Antonietti M, Bergstrom L (2015) Thermally insulating and fire-retardant lightweight anisotropic foams based on nanocellulose and graphene oxide. Nat Nanotechnol 10(3):277–283. doi:10.1038/nnano.2014.248

Yamanaka S, Watanabe K, Kitamura N, Iguchi M, Mitsuhashi S, Nishi Y, Uryu M (1989) The structure and mechanical properties of sheets prepared from bacterial cellulose. J Mater Sci 24 (9):3141–3145. doi:10.1007/BF01139032

Zimmermann T, Pöhler E, Geiger T (2004) Cellulose fibrils for polymer reinforcement. Adv Eng Mater 6(9):754–761. doi:10.1002/adem.200400097

Chapter 16
Photobioreactor-Based Energy Sources

Scott N. Genin, J. Stewart Aitchison and D. Grant Allen

Abstract Microalgae are a potential candidate as a feedstock for biofuels and bioproducts in addition to remediate flue gas streams and wastewater. On an industrial scale, algae are grown in photobioreactors of which there are currently three styles: open, closed, and algal film. Open photobioreactors have the lowest capital cost, but suffer from lower productivity and contamination issues, while closed photobioreactors have high capital cost, but culture conditions are easier to control. Algal film photobioreactors are still in the developing phase, but show promise in reducing downstream processing costs due to their high algal biomass concentration. Algae are used to produce fuel products such as biodiesel, biocrude, ethanol, and biogas as well as producing high-value-added products. There are challenges with growing algae for fuel products associated with the high capital cost and processing costs of algae. To mitigate the high capital costs, building-integrated photobioreactor is a promising solution since the photobioreactor can serve multiple functions such as dissipating heat and removing CO_2 from the flue gas stream. In these applications, closed photobioreactors are the most promising since they have a wide range of configurations and culture control.

S.N. Genin · J.S. Aitchison · D.G. Allen (✉)
Department of Chemical Engineering and Applied Chemistry, University of Toronto, Toronto, Canada
e-mail: allendg@ecf.utoronto.ca

S.N. Genin
e-mail: scottnicholas.genin@mail.utoronto.ca

J.S. Aitchison
Department of Electrical and Computer Engineering, University of Toronto, Toronto, Canada
e-mail: stewart.aitchison@utoronto.ca

F. Pacheco Torgal et al. (eds.), *Nano and Biotech Based Materials for Energy Building Efficiency*, DOI 10.1007/978-3-319-27505-5_16

16.1 Introduction

There is an increasing effort to develop alternative fuels and technologies capable of reducing the human ecological foot print. Microalgae are a promising solution since they are a feedstock for biofuels and used for treatment of waste streams (i.e., flue gas and wastewater). Compared to terrestrial crops, microalgae have multiple advantages: (1) they grow significantly faster, (2) consume less land, (3) do not compete with the global food supply, and (4) can be collocated with wastewater treatment facilities. Wastewater streams from municipal and industrial sources are rich in nutrients (such as nitrogen and phosphorus) which when released into the environment often cause eutrophication of the water system. Algae can remove these nutrients during the water treatment processes and have it produce many value-added compounds such as nutraceuticals, livestock feed, proteins, lipids, and pigments (Barowitzka 1992; Pate et al. 2011; Lam and Lee 2012).

Microalgae are photosynthetic autotrophs (eukaryotes and prokaryotes) which convert water and carbon dioxide (CO_2) into glucose and oxygen (O_2) via the light reactions and Calvin cycle represented by the simplified chemical reaction found in Eq. (16.1). They use the glucose or other carbohydrates as an energy source for growth.

$$CO_2 + H_2O + \text{Light} \rightarrow O_2 + C_6H_{12}O_6 \tag{16.1}$$

Microalgae are found in both freshwater and saltwater ecosystems. They have growth rates 100 times faster than agricultural crops such as soybean and corn and some strains accumulate large quantities of lipids, usually inside their cells for energy storage, between 15 and 77 % dry weight depending on the conditions and species (Chisti 2007; Lam and Lee 2012). Some algal species such as *B. Braunii* are capable of storing lipids and oils outside of their cells (Hillen et al. 1982). Unicellular algae use sunlight more efficiently than terrestrial plants. As an example, Cyanobacteria are capable of converting 2–3 % of sunlight into biomass (Tredici and Zittelli 1998) in comparison with 0.2–2 % for plants (Melis 2009; Formighieri 2015). The approximate stoichiometric elemental composition of algae based on the Redfield ratio (elemental stoichiometric ratio for algae) is $C_{106}H_{181}O_{45}N_{15}P$ (Clarens et al. 2010).

Photobioreactors are used to grow algae in controlled environments. The definition of a photobioreactor is broad and includes designs such as the open raceway pond to complex vertical plate photobioreactors. Design principles and applications of photobioreactor are still relatively new compared to traditional bioreactors which grow heterotrophic organisms (i.e., yeast and *E. coli*). This chapter will give an overview of the types of photobioreactors used to produce energy and the possible energy types which can be derived from photobioreactors. This chapter begins with a discussion on the types of photobioreactors (open raceway, closed, and algal film) and then discusses the various fuels and products which can be produced from photobioreactors (ethanol, biodiesel, and biocrude). When discussing the

photobioreactors, there will be an emphasis on the material/design aspects of photobioreactors, and how they might be incorporated into buildings and factories. The final section of this chapter discusses the application of co-locating photobioreactors with buildings and other facilities.

16.2 Photobioreactors

16.2.1 Introduction and History

The first prototypes of photobioreactors were started in the 1950s (Cook 1953; Walter 1958; Kathrein 1960) and has continued into the twenty-first century. While these were the first devices to be patented with the explicit intention of growing microalgae, controlling the growth of algae has been a concern in aquaculture before these inventions (Herman and Anderson 1947). The early industrialization of algae was first conceived by Germans in late World War II for food production (Ugwu et al. 2008), and then, the Carnegie Institute at Washington implemented mass cultivation of algae for CO_2 sequestration (Berlew 1953). Cultivation of algae in photobioreactors continued to grow as applications for algal biomass were expanded. Production of algae has been important in food and aquaculture applications since the 1960s (Muller-Feuga 2000), but recently, algae have received attention for their potential to produce biochemical and biofuels (Borowitzka 1999; Dallaire et al. 2007; Chisti 2007).

The most common method of growing algae on a pilot or commercial scale is using a photobioreactor (PBR) such as raceway pond or a variation of a closed photobioreactor (Chisti 2007; Ugwu et al. 2008; Bitog et al. 2011; Wang et al. 2012). New unconventional reactors such as algal film photobioreactors have been demonstrated on the laboratory scale (Johnson and Wen 2010; Ozkan et al. 2012; Schnurr et al. 2013; Gross et al. 2013; Genin et al. 2014) and the pilot scale (Christenson and Sims 2012; Gross and Wen 2014), but the focus of these reactors is for wastewater treatment (Mulbry et al. 2008; Christenson and Sims 2012). This section of the chapter will outline the different types of photobioreactors and outline some design principles.

16.2.2 Open Photobioreactors

Open raceway ponds are the oldest and simplest systems for algal cultivation (Herman and Anderson 1947). Typical designs for algal raceway ponds include a single loop (Fig. 16.1a) or a loop with baffles (Fig. 16.1b). Baffles are added to either improve mixing and/or to help ensure that the water entering the pond travels the maximum length (e.g., plug flow). Water is circulated in the pond by using

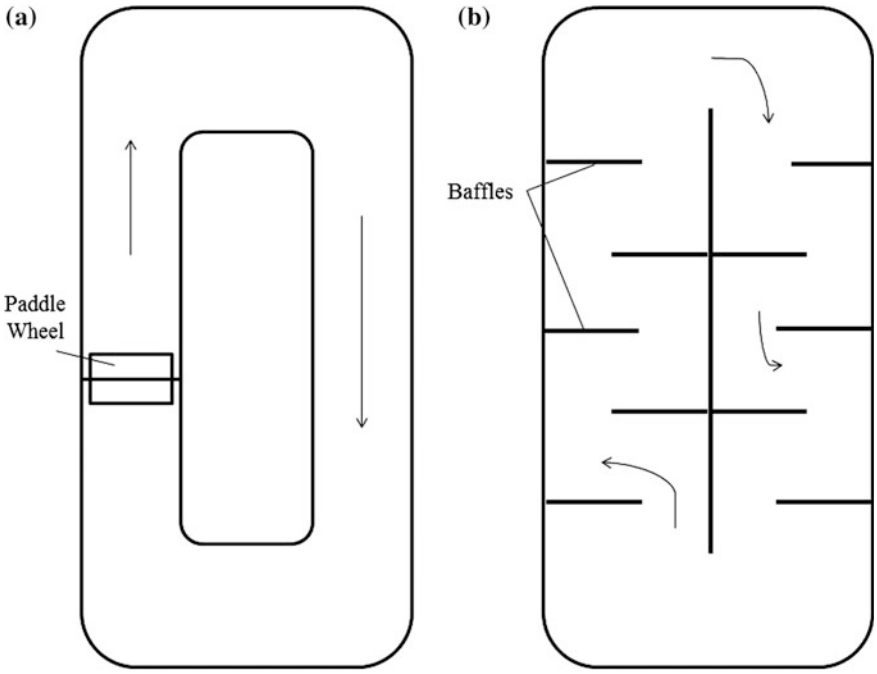

Fig. 16.1 schematics of **a** single-loop raceway pond, **b** raceway pond with baffles

paddle wheels or pumps, and sometimes, air is sparged into the pond to help with mixing (Boussiba et al. 1988; Hase et al. 2000; Doucha and Livansky 2006). An open raceway pond is usually constructed by building low walls (usually poured concrete) or are dug into the ground and lined with a plastic liner. The depth of a raceway pond ranges from 20 to 50 cm due to light limitations (Doucha and Livansky 2006; Chisit 2007), but the length and width are dependent on scale.

Open photobioreactors tend to have volumetric productivities which range from 0.05 to 0.32 g/L day and aerial productivities which range from 11.1 to 35 g/m^2 day) (Pushparaj et al. 1997; Jimenez et al. 2003; Doucha and Livansky 2006). Depending on the lipid content of the algae grown (5–30 w%/w), this results in an aerial lipid productivity range of 0.55 to 10.5 g/m^2 day, which is higher than most terrestrial crops (0.25 g/m^2 day) (Mata et al. 2010). Biomass productivity in open pond systems is less land efficient when compared to closed photobioreactors (Chisti 2007; Ugwu et al. 2008). This is often attributed to several factors such as temperature fluctuations, insufficient mixing, evaporation losses, and contamination. Open photobioreactors exposed to the atmosphere are susceptible to variations in weather conditions which can cause shocks to the algal cultures (Benemann 2008). Since the productivity in an open photobioreactor is lower than in a closed photobioreactor, they require more land to reach the same overall productivity. Open photobioreactors are also prone to infection by microorganisms which prey upon algae, which can reduce the long-term productivity (Benemann 2008).

Maintaining a homogeneous algae culture is difficult in an open raceway pond, which can result in the final product being off specification. This in turn can increase downstream processing costs.

The material considerations for open photobioreactors are based on the following criteria: (1) cost and (2) water permeability. An advantage that open photobioreactors have over closed photobioreactor are their reduced capital cost, so selecting materials which are as inexpensive is a priority to maintain this advantage. The materials for open photobioreactors have to be water impermeable to prevent water loss to the ground. Based on these considerations, plastics, such as PVC, and concrete are often chosen as materials of choice.

16.2.3 Closed Photobioreactors

Closed photobioreactors are often characterized according to their geometry. Common geometries are vertical column (bubble column or airlift), horizontal tubular, and flat plate (Ugwu et al. 2008; Bitog et al. 2011; Wang et al. 2012). In these configurations, the photobioreactors can be illuminated either from solar light, generated light, or both. The general design considerations for photobioreactors are as follows: (1) light transport, (2) CO_2 delivery, (3) oxygen gas removal, and (4) temperature and pH control. These design considerations need to be optimized to maximize the production of algae. Productivities of closed photobioreactors range from 0.05 to 2.7 g/L day depending on design, operating conditions, and algae species (Chisti 2007; Ugwu et al. 2008; Bitog et al. 2011). These volumetric productivities are significantly higher than those reported for open raceway ponds (Pushparaj et al. 1997; Jimenez et al. 2003; Doucha and Livansky 2006). Key operating parameters which influence the productivity in a closed photobioreactor are diffusion of CO_2, pH, light intensity, temperature, O_2 removal, and nutrient concentration (nitrogen and phosphorous) (Dauta et al. 1990; Takeuchi et al. 1992).

Light transport and illumination is a unique challenge in photobioreactors, since light does not follow conventional transport phenomena (heat, mass, and momentum) that are normally the main considerations for bioreactors that do not require light. Light intensity in a photobioreactor decays according to the Beer–Lambert law (Grima et al. 1999), which causes algae closer to the light source to have excess light and shade algae cells farther away from the light source. Shading within a photobioreactor is considered to be one of the main barriers to improved productivity (de Vasconcelos Barbosa 2003; Chisti 2007; Ugwu et al. 2008; Erickson et al. 2011; Chen et al. 2011a, b). It is possible to reduce shading and dark zones by constructing thinner reactors, improving mixing or adding internal light sources (de Vasconcelos Barbosa 2003; Ono and Cuello 2004; Posten 2009). Improving mixing by creating artificial dark and light zones within the bioreactor has shown to improve productivity so long as the frequency of mixing is appropriate for the algae (Kok 1956; Degen et al. 2001).

Efficient addition of CO_2 and removal of O_2 are dependent on the hydrodynamics and mass transport characteristics of the photobioreactor. The important hydrodynamic and mass transport characteristics in photobioreactors are the overall mass transport coefficient (k_La), mixing, liquid velocity, and gas bubble velocity, and holdup. In bioreactors, the overall volumetric mass transport of a gas into the liquid phase is dependent on the overall mass transport coefficient (k_La). This parameter is commonly used to assess the performance of bioreactors and to design them. It is dependent on the agitation rate, chemical additives such as surfactants, temperature, and the design of the sparger (de Vasconcelos Barbosa 2003; Ugwu et al. 2002). Mixing within a photobioreactor can be achieved through aeration or mechanically through the use of an impeller. Good mixing in helps keep the algal cell concentration high, keeps cells in suspension, improves nutrient distribution, enhances gas exchange, reduces shading, and eliminates thermal stratification, all of which can enhance the productivity of the photobioreactor (Posten 2009; Chen et al. 2011a, b).

An important design consideration is material selection for the closed photobioreactors. Unlike open photobioreactors, the materials for fabrication are dependent on the design. A closed photobioreactor using external solar light without a solar collector will need transparent walls to allow light to pass through, while a photobioreactor with internal light may want to have the inside walls coated with reflective material. In these cases, plastics with the highest optical transparency—especially in the red wavelength range (590–670 nm)—are desirable. Materials which prevent biofouling and the formation of algal biofilms are desirable in closed photobioreactors. Biofilm formation in these systems reduces the light transmission, competes for nutrients, and is difficult to clean. Material properties such as surface energy and roughness are known to affect algal biofilm attachment (Finlay et al. 2002; Sekar et al. 2004; Palmer et al. 2007; Genin et al. 2014). Nano- and micromaterials can be designed to reduce attachment (Schumacher et al. 2007).

The three common geometries for closed photobioreactors are flat-plate, tubular, and vertical column photobioreactors (Fig. 16.2a–c). Flat-plate photobioreactors are considered to be the most efficient design for photobioreactors due to their large illumination surface and thin construction (Ugwu et al. 2008). It has been reported that these photobioreactors are able to achieve very high photosynthetic efficiencies compared to other designs (Hu et al. 1996; Richmond 2000). A flat-plate photobioreactor is built from transparent plastic and can be either bubble column or airlift configurations. They are designed to be thin as to balance the light illumination area, transmission, and the algal productivity.

Tubular photobioreactors are commonly cited in the literature for potential design and application (Grima et al. 1999; Chisti 2007; Ugwu et al. 2008; Maor and Appelbaum 2011). These are usually constructed with glass or plastic tubes which are arranged in rows which are attached to a central sparging system. A pump circulates the media in the tubes. Some horizontal tubular photobioreactors suffer from high levels of dissolved oxygen (DO), which becomes inhibitory to algal growth (Richmond et al. 1993). The light in a tubular photobioreactor can be provided by a solar or generated light source (electrical sources such as fluorescent or LEDs), but the trend is that most laboratory-scale tubular photobioreactors use a

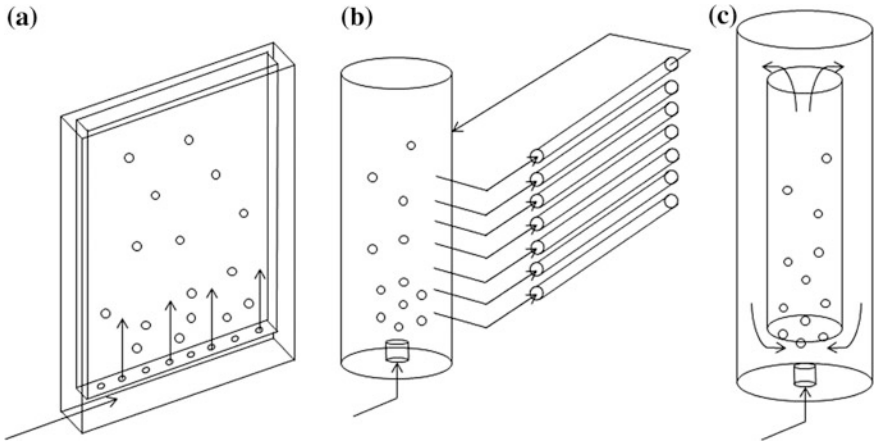

Fig. 16.2 Photobioreactor schematics of **a** flat plate, **b** horizontal tubular and **c** annular airlift

generated light source, while pilot-scale photobioreactors use sunlight. A study by Grima et al. (1999) suggested that tubular reactors should be designed in such that the pipe diameter is no greater than 0.1 m and a continuous length of 80 m with a flow velocity of 0.3–0.5 m/s.

Vertical photobioreactors take the form of bubble columns or airlifts. Rising gas bubbles induce mixing in the reactor or to generate currents. Baffles are added to enhance mixing, which in turn enhances diffusion of gasses (Ugwu et al. 2008). Airlift reactors have an added advantage over bubble columns in that they can simulate a light–dark cycle which has been shown to enhance the growth of algae. A study by Chui et al. (2009) showed that algae grown in concentric airlift reactors had a higher specific growth rate (0.226 day^{-1}) compared to concentric bubble columns (0.180 day^{-1}).

16.2.4 Algal Film Photobioreactors

Algal film photobioreactors produce algal film biomass. Algal biofilms are phototrophic algae embedded in a biofilm which is comprised of other microorganisms, such as bacteria and fungi, and extra cellular polymeric substance (EPS) (Lawrence et al. 1998; Hodoki 2005; Johnson and Wen 2010). EPS is a matrix comprised of nucleic acids, polysaccharides, proteins, glycoproteins, and glycolipids produced by the microorganisms embedded in the biofilm (Flemming et al. 2007). It bonds the cells to each other and the attachment material which helps immobilize the embedded cells. Microalgae grown as a biofilm present an opportunity to reduce dewatering costs since the biomass is more concentrated (90–150 g/L) (Christenson and Sims 2012; Ozkan et al. 2012; Gross et al. 2013) compared to suspended algae produced in raceway ponds (0.5–1 g/L) or photobioreactors (1–4 g/L) (Chisti 2007). This has the

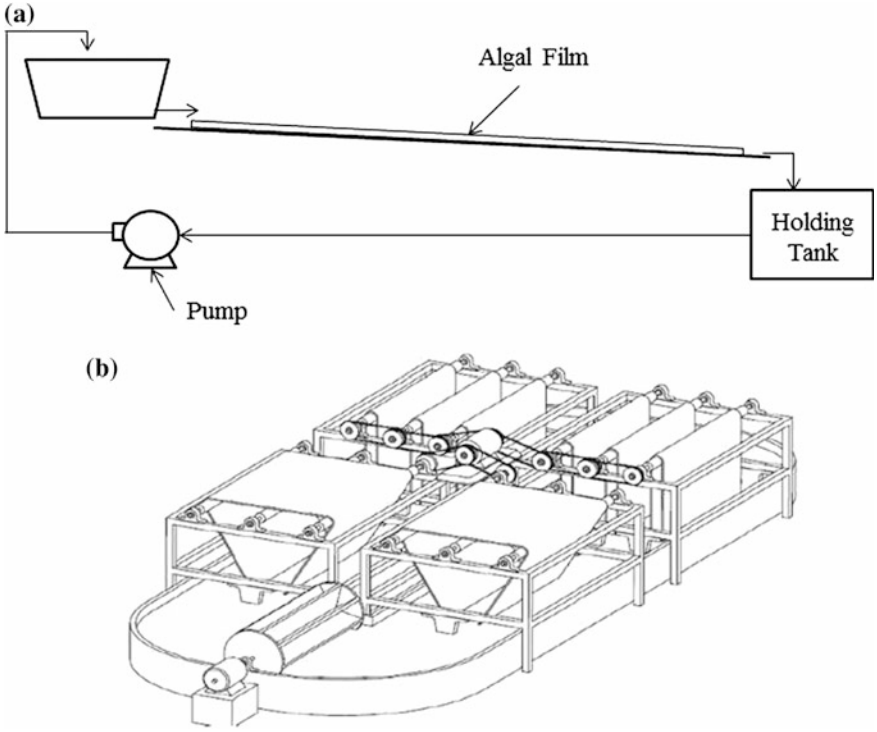

Fig. 16.3 Schematics of **a** ATS system and **b** a modified raceway pond with triangular and vertical RAB systems (Gross and Wen 2014, *Bioresource technology*, permission obtained from Elsevier)

potential to reduce dewatering costs, which contribute 20–30 % of the overall costs in suspended algal systems (Gudin and Therpenier 1986; Uduman et al. 2010).

Algal film photobioreactors from the literature take the form of either algal turf scrubbers (ATS) or rotating algal biofilm (RAB) systems (Fig. 16.3a, b). In an ATS system, shallow water is passed over a suitable attachment material (Craggs et al. 1996; Mulbry et al. 2008). Water is recycled and the entire system is exposed to the atmosphere. In a RAB system, the algal film is attached to a partially submerged mobile sheet usually made of cotton fabrics (Christenson and Sims 2012; Gross et al. 2013; Gross and Wen 2014). Algal biomass is harvested from the material at regular intervals.

RAB systems have demonstrated high algal biomass productivity. Christenson and Sims (2012) developed a RAB system, in which an algal biofilm was grown on a cotton rope and reported an aerial productivity of 21–30 g/m^2 day, at a dry biomass concentration of 120–160 g/L. This is comparable to productivities reported by open raceway ponds and lower than productivities reported by closed photobioreactors, but the algal biomass is significantly more concentrated than suspended algae. A pilot-scale algal film photobioreactor built by Gross and Wen (2014) demonstrated

surface area productivities of 5.8 g/m^2 day and had a maximum aerial productivity of 21.5 g/m^2 day, which was significantly higher than the maximum productivity of the control raceway pond (6 g/m^2 day) used in the same experiment.

Algal film reactors have been developed based on the active immobilization of algae with the use of flocculating agents, chemical attachment, and gel entrapment (Shi et al. 2007; Morendo-Garrido 2008). Flocculating agents are used for harvesting suspended algae, but have the additional effect of forming algal flocs which are similar in structure to algal biofilms. Gel entrapment of algae is less widely used for immobilization since entrapped algal cells are not able to grow, but still remain viable (Morendo-Garrido 2008; Lam and Lee 2012). In addition to gel structures, algal biofilms have also been immobilized on zeolite structures, which have successfully displayed the ability to help negate the toxic effect of high ammonia concentrations (Young 2011).

The mass transport and mixing properties of algal film photobioreactors is not well understood compared to closed photobioreactors. Studies on closed photobioreactors show a strong correlation between the partial pressure and mass transport of CO_2 in the gas stream and growth rate (Takeuchi et al. 1992), but in algal film photobioreactors, the relationship is not as well understood. A study by Gross et al. (2013) showed that increasing the partial pressure of CO_2 from 0.03 to 1 % in an RAB system did not increase productivity significantly. This could due to the different hydrodynamic environment that RAB systems experience, since the biofilm is only partially submerged.

Attachment material for algal film photobioreactors is a critical parameter for algal biofilm growth and is correlated to algal film productivity (Johnson and Wen 2010; Christenson and Sims 2012; Gross et al. 2013; Genin et al. 2014). Critical material properties which affect algal biofilm productivity are surface energy and roughness (Ozkan and Berberoglu 2013; Sathananthan et al. 2013; Genin et al. 2014). Material polar surface energy has been shown to affect the colonization time of algal biofilms, which in turn affects the overall productivity (Genin et al. 2014). Water–material contact angle has been shown to influence algal spore and cell attachment (Finlay et al. 2002; Sekar et al. 2004), but other research shows that algal biofilm productivity does not correlate to water–material contact angle (Irving and Allen 2011; Genin et al. 2014). Materials which have a greater roughness tend to have high algal film productivities and faster regrowth (Johnson and Wen 2010; Christenson and Sims 2012).

Micro-, nano-, and biological materials present an interesting avenue for enhancing productivity. By adding nano- and micro-features onto surfaces, it may be possible to enhance algal biofilm growth and productivity (Sathananthan et al. 2013). Algal biofilm growth is enhanced in the presence of bacteria (Hodoki 2005; Irving 2010). Designing a biomaterial to encourage initial bacterial growth would in principle enhance the long-term algal biofilm productivity. Materials such as cellulose acetate can be consumed by bacteria which can lay the foundation for an algal biofilm, but the trade-off is whether the biofilm will still be attached after the bacteria has consumed the biomaterial.

Table 16.1 Comparison between photobioreactors

	Open raceway pond	Closed photobioreactor	Algal film photobioreactor
Productivity (g/m^2 day)	11.1–35	20–72	2.1–35
Capital cost	Low	High	Variable
Species control	Poor	Good	Very poor
Temperature control	Poor	Good	Poor
Mass transfer and mixing	Poor	Good	Unknown

16.2.5 Photobioreactor Discussion and Comparison

A general comparison of the three types of photobioreactors is presented in Table 16.1. These parameters are important considerations in determining which photobioreactor is best suited for the application.

The end product from the photobioreactor is likely to drive the selection of the photobioreactor. Open photobioreactors are preferred for low-value products such as fuel, whereas high-value products which require strict control and operating conditions will favor closed photobioreactors. Algal film photobioreactors are often applied in wastewater treatment processes (Craggs et al. 1996; Mulbry et al. 2008; Christenson and Sims 2012).

Capital costs of photobioreactors are often the largest source of expenses in producing fuel products (Alabi et al. 2009; Davis et al. 2011). The materials that photobioreactors are constructed from make up a large portion of this cost. Advances in nano- and biomaterials could have a profound impact on the capital costs of photobioreactors if they are cheaper than current preferred materials, or if they can improve the reactor productivity.

Algal film photobioreactors have the greatest potential to be affected by improvements in nano-, micro-, and biomaterials. The literature has shown that the attachment materials have a significant impact in algal biofilm productivity (Johnson and Wen 2010; Christenson and Sims 2012; Gross et al. 2013; Genin et al. 2014). Recent advances have demonstrated the effects material surface energy and microstructure patterning has on algal biofilm growth (Sathananthan et al. 2013; Genin et al. 2014) in such that overall algal biofilm productivity is correlated to the polar surface energy of the attachment material and that embossing attachment materials can improve algal biofilm productivity.

16.2.6 Conclusions

Photobioreactor performance is affected by the operating conditions and the configuration, with the two often being intertwined. Compared to conventional fermenters and bioreactors, photobioreactors have additional challenges and requirements due to light transport, which is strongly affected by the design.

16.3 Energy-Based Products from Photobioreactors

16.3.1 Introduction

Algae have been investigated as a potential feedstock for biodiesel due to its high lipid content and fast growth rates. Multiple fuel products can be produced from algae, such as biodiesel, biocrude, ethanol, biomass, and biogas. These fuels are processed through different methods and some require non-conventional photobioreactors to produce. Growing algae for fuel production has recently attracted a lot of attention, but it still has not been commercialized.

16.3.2 Hydrocarbon-Based Energy Products

Biodiesel in the form of fatty acid methyl esters (FAME) produced from algae is derived from the lipids found in algal biomass (Ma and Hanna 1999; Demirbas and Demirbas 2011; Lam and Lee 2012). Neutral lipids in the form of triglycerides are reacted with alcohols—usually methanol—in the presence of an acidic or alkali catalyst to produce methyl esters (Fig. 16.4). Alkali-catalyzed transesterification is preferred over the acid version because it is 4000 times faster (Fuduka et al. 2001), but industrial processes often use both acid- and alkali-catalyzed methods (Meher et al. 2006). In addition to the methyl esters, the reaction produces glycerol which can be sold as a coproduct. The remaining biomass which now contains proteins, carbohydrates, and inorganics, can be either sold as an agricultural product such as

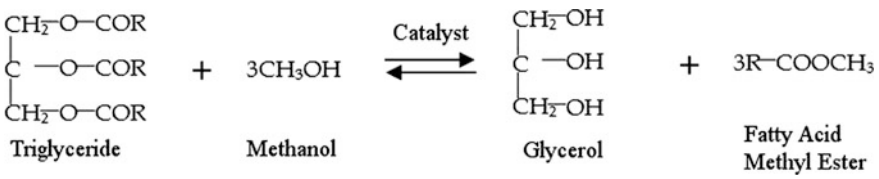

Fig. 16.4 Transesterification of triglycerides (Modified from Ma and Hanna 1999)

fertilizer or can be further processed to extract other products (Demirbas and Demirbas 2011).

A study by Chisti (2007) estimated that to meet 50 % of all transport fuel needs in the USA in 2007 with biodiesel, it would require 2–4.5 M ha (1.1–2.5 % of total US crop land) for algal cultivation depending on the lipid content of the algae. This is significantly better than the estimated land area for corn (1540 M ha), soybean (594 M ha), and oil palm (45 M ha). Despite this, biodiesel production from algae has not yet been commercialized due to the high capital investment required and high operational costs associated with nutrients (Davis et al. 2011).

An alternative to biodiesel is to process the algal biomass into biocrude via hydrothermal liquefaction (HTL) or pyrolysis. In HTL, algal biomass is subjected to high pressures (10–12 MPa) and temperatures (250–300 °C) along with sodium carbonate as a catalyst, whereas in pyrolysis the operating conditions depend on the desired products. HTL produces biocrude oil which has a nitrogen and oxygen content along with a wastewater stream (Minowa et al. 1995; Sawayama et al. 1999; Brown et al. 2010; Vardon et al. 2012). Pyrolysis produces a combination of syngas, biocrude, and char (Vardon et al. 2012). The main benefit HTL is that the biomass does not need to be dewatered entirely (20 w%/w dry biomass is sufficient) and does not require solvent extraction, but the end product does need to be refined to produce fuel or other products. This has several advantages, since the biocrude can be used to produce high-value-added products such as lubricants which can be sold as significantly higher prices than diesel, and the biocrude can be refined to produce expensive fuel products such as jet fuel. Conversion of algal biomass via HTL has been shown to be more energy efficient compared to pyrolysis (Bennion et al. 2015), although the two methods to produce biocrude with different physical properties (Vardon et al. 2012).

16.3.3 Ethanol and Other Alcohols

Ethanol and other alcohols produced from algae are an unconventional energy product since algae do not produce it naturally. Recent innovations in genetic modification enable genetically modified cyanobacteria to produce ethanol and other alcohols such as 1-butanol, isobutanol, and 2,3-butanediol (Formighieri 2015). The first example of ethanol-producing cyanobacteria was demonstrated by Deng and Coleman (1999) where ethanol-producing genes from *E. coli* were inserted into a cyanobacterium. Recent improvements in the genetic modification of the cyanobacterium have enabled it to reach productivity values of 212 mg/L day of ethanol (Gao et al. 2012). Algenol Inc. is currently further developing this technology to produce ethanol and other various products (Algenol Inc. website).

Ethanol has several advantages over biodiesel as an energy product. Ethanol is excreted from the cyanobacteria, which means that the bioreactor can be integrated with continuous extraction such as two-phase partitioning or membrane separation. This also has the added benefit of not requiring the destruction of the cyanobacteria.

The ethanol needs to be refined from the aqueous media, whereas biodiesel needs to be produced from the transesterification process, which requires methanol and catalysts as inputs. Ethanol has a lower heating value compared to FAME biodiesel (29.7 MJ/kg compared to 39.5–41 MJ/kg). Another disadvantage of growing genetically modified organisms is they often require special containment as prescribed by law (The Canadian Environmental Protection Act), thus growing genetically modified cyanobacteria requires regulatory permission and must be grown in closed photobioreactors, which significantly increases the capital cost of the process.

16.3.4 Biomass-Conversion-Based Energy Products

An alternative to processing algal biomass into fuel products is to directly combust it. Direct combustion produces heat along with CO_2, water, and other combustion products such as carbon monoxide (CO) and nitrogen oxides (NOx) depending on conditions and quality of the feedstock. This has the added advantage of not requiring downstream chemical processing, but reported heating values for algal biomass are lower than those for biodiesel or ethanol (Sturm and Lamer 2011) (algal biomass heating value is estimated to be 21.1–25.1 MJ/kg depending on strain). However, a study by Sturm and Lamer (2011) estimated that direct combustion of algal biomass is a more efficient energy source on an overall energy balance compared to using the algal biomass to produce biodiesel (based on the assumption of a lipid content of 10 w%/w). A direct combustion of algal biomass prevents the generation of coproducts.

A commonly referenced method to producing energy from algae is to anaerobically digest the biomass into biogas (Samson and LeDuy 1986; Chen 1987; Yen and Brune 2007; Sialve et al. 2009; Collet et al. 2011). In this process, algal biomass or residue is added to an anaerobic digester and converted into biogas. The algal biomass fed into the anaerobic digester does not need to be dewatered, which is a major advantage. The quality of the biogas—the volume fraction of methane in the gas—is dependent on the composition of the algal biomass and ranges from 46 to 76 % (Samson and LeDuy 1986; Chen 1987; Yen and Brune 2007). The lipid content of the algal biomass is positively correlated to the biogas quality; however, a theoretical study by Sialve et al. (2009) estimated that if the lipids were converted into biodiesel and the remained anaerobically digested, the total energy from the biodiesel and biogas would be greater than anaerobic digestion alone. Multiple life cycle analyses have demonstrated that anaerobic digestion of algal biomass or residue is a critical process in a biorefinery (Collet et al. 2011; Davis et al. 2011). This would enable to algal biorefinery to recycle nutrients/water from the anaerobic digester back into the algal growth medium and to produce biogas to generate electricity for the process or sold to the electrical grid.

16.3.5 Artificial Photosynthesis

All energy sources discussed above can be accomplished by using the naturally occurring photosynthesis in algae and cyanobacteria. An alternative method is to use artificial photosynthesis, in which sunlight is converted into electricity to produce hydrogen gas (H_2) which is then fed into a dark fermenter, which contains autolithotrophic H_2-oxidizing bacteria (Yu 2014). The reaction which the bacteria perform is shown in Eq. (16.2)

$$CO_2 + 2H_2 \rightarrow CH_2O + H_2O \tag{16.2}$$

The carbon dioxide is processed and stored in the bacteria cells as polyhydroxybutyrate (PHB), a polymer which contains approximately 50 % more energy than the same amount of starch (Yu and Chen 2006). PHB is an example of a polymer product which can be produced using the autolithotrophic H_2-oxidizing bacteria, which can be converted through further chemical processing into other compounds such as 1,3-butanediol. Artificial photosynthesis has an estimated theoretical energy conversion. Solar to chemical energy stored in biomass is between 9 and 10 %, which is higher than that of photosynthetic microalgae (2–3 %) (Tredici and Zittelli 1998; Yu 2014; Formighieri 2015).

The challenges that artificial photosynthesis faces are cost of generating H_2 gas, high capital costs associated with solar panels, and the high energy required to dissolve H_2 gas. In an industrial setting, there is an incentive to produce H_2 gas using natural gas reformation since it is cheaper than using an electrolyzer (Stoll and von Linde 2000; EIA and DOE 2013). This would defeat the purpose of artificial photosynthesis since the process would not rely on any solar energy. Another challenge is the energy required to dissolve H_2 gas in the dark fermenter and the challenges associated with mass transport of gasses into fermenters. These pose several challenges since H_2 has a low Henry's constant (1.26 mmol/L/atm at 25 °C), which will require a high partial pressure of H_2 to reach the desired dissolved H_2 concentration.

16.3.6 Discussion on Energy Sources and Products

Using algae to produce fuel is arguably the most discussed and researched field in terms of algal bioprocessing (Chen 1987; Yen and Brune 2007; Chisti 2007; Mata et al. 2010). While algae for biodiesel have demonstrated high land efficiency (Chisti 2007; Mata et al. 2010), there is minimal support for the full commercialization of algae as a source for biodiesel (Benneman 2008; Alabi et al. 2009; Davis et al. 2011). The cost to produce biodiesel from algae is too high (estimated cost of 3–6 $/L) to compete with the current gasoline and diesel prices (as of early 2015), even when coproduct generation/selling is included in the cost estimates (Alabi et al. 2009; Davis et al. 2011). A life cycle analysis by Quinn et al. (2014) showed

that the net energy ratio (NER)—defined as the ratio of the energy used to produce the fuel divided by the energy the fuel contains—for biodiesel production was 0.65, greater than that of conventional diesel fuel (NER of 0.2). Assessments on producing biocrude from algae through HTL and pyrolysis have shown that the NER is greater than 1 for both processes, which is unfavorable from an economical and energy perspective (Bennion et al. 2015). This net energy loss presents a problem for the energy effectiveness of biocrude.

The current barriers to commercialization of biodiesel from algal biomass are the high capital costs of photobioreactors and the relatively high cost of inputs such as fertilizer and CO_2 (Benneman 2008; Davis et al. 2011). Improvement in photobioreactor technology will be required to reduce the capital and operational costs. Capital costs of open raceway ponds are likely to be near their lowest in terms of materials and construction techniques since these are well established. Reduction of inputs such as CO_2 and phosphorous can be achieved by collocating photobioreactors near the sources of fuel gas or wastewater.

The most economically viable products from algal biomass would be high-value products such as astaxanthin (in 2000, astaxanthin sold for US$2500 per kg), which can be sold as a food supplement (Yoo et al. 2013). These products sell for a relatively high value which overcomes the high capital and operational costs required to produce them from algae. The remaining biomass could then be converted into fuel through any of the other methods (HTL, biogas, etc) and be sold as a coproduct. The main downside with this approach is that market for high-value-added products is not nearly as large as the market demand for fuel. An alternative approach is to grow algae for wastewater treatment and harvest the biomass to produce fuel. Algae have shown promise in this field, in particular, algal film photobioreactors such as the ATS and RAB system (Mulbry et al. 2008; Christenson and Sims 2012). A pilot-scale RAB system developed by Christenson and Sims (2012) was capable of removing 90 % of the total phosphorous.

16.3.7 Conclusions

There is potential to produce fuels and other products from photobioreactors and algal biomass. The main advantage that phototrophic biomass has over terrestrial crops (i.e., corn and soybean) is their land efficiency and that they do not compete directly with food sources. There are many challenges which prevent the full commercialization of energy products from photobioreactors such as the high capital and operational costs associated with photobioreactors. In the short term, it is likely that photobioreactors will be used to produce high-value-added products, which then the remaining biomass can then be converted into an energy product. New technological developments such as the genetic modification of cyanobacteria for ethanol production present new opportunities for photobioreactors to be used in energy production.

16.4 Integrated Photobioreactor Systems for Buildings

16.4.1 Introduction and the Biorefinery Concept

Biorefineries and collocation of photobioreactors with other processes are discussed as strategies to alleviate the capital and operational barriers for mass algal cultivation (Collet et al. 2011; Demirbas and Demirbas 2011). The main challenges which face algae photobioreactors as discussed earlier are the capital costs, cost of nutrients (CO_2, nitrogen, and phosphorus), and the selling price of the fuels. Integrating a photobioreactor into larger biorefinery can resolve the cost of nutrients and CO_2. A biorefinery is a series of processes in which biomass is grown, processed, and refined to produce multiple products. By producing multiple products with varying price ranges, the higher-value-added products can offset the cost to produce the fuel products.

Collocation of algal systems has several benefits: (1) waste products from other processes can be used as inputs, (2) centralized operation, and (3) cost offset by making multiple products. In this sense, the waste treatment can be turned into a revenue producing stream opposed to being a pure expense. Municipal wastewater treatment plants and livestock facilities have been the focus of studies examining the potential to remove nitrogen and phosphorous from these waste streams (Mulbry et al. 2008; Christenson and Sims 2012). These systems are excellent candidates for integration with algal biorefineries, since they provide important nutrients for the photobioreactors.

Residential and commercial buildings present another potential candidate for algal photobioreactor integration. Currently, some buildings have green roof or green wall systems which are used to reduce dissipate heat or to remove CO_2 from the building. It is quite common for large commercial and residential buildings to have central heating through combustion of natural gas, which produces a source of CO_2 that could be used for growing algae.

16.4.2 Examples of Building-Integrated Photobioreactors for Commercial, Industrial, and Residential Structures

A current application and example of algal photobioreactors in residential architecture is by the International Building Exhibition (IBA) Hamburg 2013 with the Smart Material House "BIQ" project in Hamburg (Smart Material House BIQ white paper 2013; Wolff et al. 2015). The BIQ building is located in Hamburg, Germany, and is one of the first apartments which include photobioreactors. The building contains 15 apartments and uses the photobioreactors to capture heat and produce electricity (Fig. 16.5).

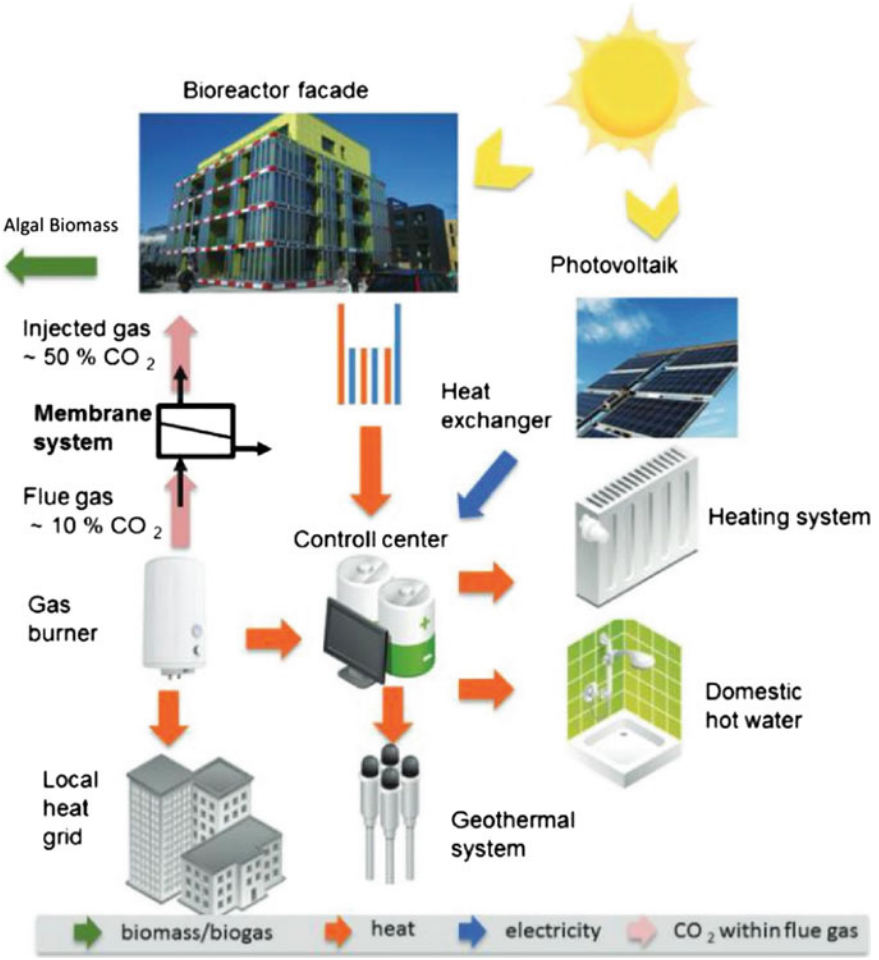

Fig. 16.5 Schematic concept of the integrated bioreactor façade system (Modified from Wolff et al. 2015, *Greenhouse gases: science and technology*, in-press, permission obtained from John Wiley and Sons)

The Smart Material House in Hamburg has bioreactor facades on the southeast and southwest side of the building. Each façade contains 129 photobioreactor modules which each reactor is configured as an airlift, which prevents the settling of the algal culture. The photobioreactors are supplied with culture medium, and enriched CO_2 is provided from the flue gas of the combined heat and power unit. The algal biomass is filtered out in the building and converted into biogas at an external plant. The energy from the biogas plant is used to power the city. The provisional forecast for algal biomass production in this building is estimated to be 15 g/m^2 day, which is expected to produce approximately 4541 kWh/year of net energy as methane after factoring energy losses and conversion. This is greater than

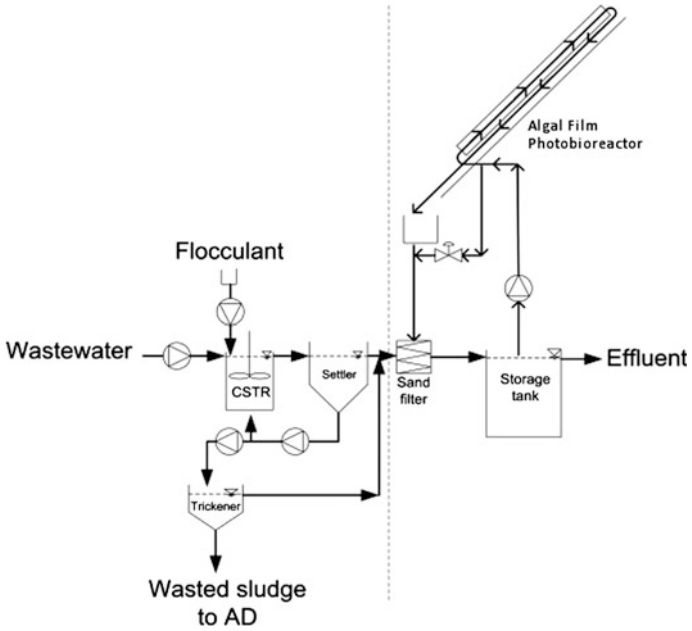

Fig. 16.6 Decentralized wastewater treatment system with an algal film photobioreactor (Modified from Zamalloa et al. 2013, *Bioresource Technology,* 130, used with permission from: Elsevier)

the estimated average German household electrical consumption (3500 kWh/year), so the electrical energy would only be able to provide enough power to one of the apartments (Smart Material House BIQ white paper 2013).

A comprehensive academic study has been conducted on integrating an algal film photobioreactor into a decentralized domestic waste treatment system by Zamalloa et al. (2013) (Fig. 16.6). While the system was designed and conducted in a laboratory, the system was intended to be integrated into a building. The overall treatment process involved a chemical and biological adsorption/flocculation to remove organic carbon. This was then followed by a sand filter combined with a photobioreactor to remove nitrogen and phosphorous from the stream. The sand filter combined with photobioreactor was able to remove up to 75 % of the TSS, 40 % of the total chemical oxygen demand (COD), and 90 % of the total phosphorus. The total nitrogen removed was calculated to be only 40 %. The aerial productivity of the algal film photobioreactor was on average 2.5 g/m^2 day. The preliminary economic evaluation for the integrated algal film photobioreactor and decentralized domestic wastewater treatment system was estimated to be 0.25 €/m^3, excluding the cost to treat the anaerobic sludge produced form the system. The system as constructed by Zamalloa et al. (2013) was not fully optimized, and it is estimated that additional optimization will increase the cost to 0.5 €/m^3. This is comparable to large-scale

conventional activated sludge treatment systems (Van Houtte and Verbauwhede 2010), which suggest there is potential for implementation of these systems.

16.4.3 Integrating Photobioreactors into Buildings

In order to integrate photobioreactors into buildings, some of the critical issues which will need to be addressed are: the light source, CO_2, nutrients, aesthetics, function, and monitoring/control system. Application of photobioreactors in building environments will be dependent on other non-reactor engineering factors such as local building codes and customer demand. In residential buildings, for example, the photobioreactors and supporting equipment (such as a biodigester) would need to be built in accordance with legal requirements, which will be more stringent than an industrial building. Currently, there are not many laws which have direct allowance of algal photobioreactors in buildings; however, some municipalities do have stringent rules on the construction of green roofs (Toronto Municipal Code: 492), and there is an ASTM standard for building green roofs (ASTM E2399.05). This implies there is potential for new regulations and standards for photobioreactor to be integrated into buildings.

A photobioreactor integrated into a building needs to be designed taking into account for the incident light direction and intensity. The incident radiation from the Sun on an outdoor reactor is a function of time, geographic location of the reactor, and environmental factors (Incropera and Thomas 1978). The incident photon flux anywhere on the surface of the Earth can be estimated (Liu and Jordan 1960). After calculating these values, it would be possible to calculate the optimal location for a photobioreactor on a building given the location of the building. Using a non-solar light source for a photobioreactor is not economically favorable (Benemann 2008; Chen et al. 2011a, b), so integrated photobioreactors should be designed to utilize the available sunlight.

Obtaining a CO_2 source for an integrated photobioreactor can be challenging. In a commercial or residential setting, biomass production may not be the main function of the bioreactor, but in an industrial setting, growing algae on atmospheric carbon dioxide is not desirable since the algae will be carbon limited and the productivity will be low. An ideal CO_2 partial pressure in the fluid phase of 0.1–0.2 kPa is required to prevent carbon limitation (Doucha et al. 2005; Spalding 2008). Photobioreactors integrated into industrial buildings should be supplied CO_2 through the flue gas, which means that CO_2 emitting processes can benefit from integrated photobioreactors.

CO_2 delivery to such photobioreactors needs to be carefully designed if removal of CO_2 from a flue gas stream is desired. A study by Lakaniemi et al. (2015) showed that *Chlorella Vulgaris* grown on air mixed with CO_2 in a bubble column, the percent utilization of CO_2 for biomass production decreased from 61.3 to 2.6 % when the percent CO_2 supplied increased from 0.04 to 12 % at a sparging rate of 0.096 L/min, which translates into 1.41 mL CO_2/h and 17.91 mL CO_2/h at STP

removed, respectively. While the efficiency decreased with increase CO_2 concentration, the total CO_2 absorbed per hour increased which presents a trade-off between total CO_2 removal and percent CO_2 removal. This will need to be carefully considered in an integrated building application, but more advanced photobioreactor design or unique sparging systems will be required to improve the CO_2 removal efficiency at these concentrations.

The source of nutrients such as nitrogen (in the form of nitrate, ammonium, or ammonia) and phosphorous will need to be carefully considered for photobioreactors integrated into buildings. The nutrient source for building-integrated photobioreactors is a critical parameter which needs to be addressed. Using synthetic media has not shown great promise in techno-economic studies (Davis et al. 2011). In industrial setting such as a waste treatment facility, nutrient sources are available from the processing of the waste itself. A biofacade photobioreactor system by AlgoSource Technologies for a waste processing plant in Nantes, France, has been proposed as a test case for integrated photobioreactor systems (Le Borgne et al. 2014). Nutrient sources from residential or commercial buildings can be from the wastewater generated, but this will require extra wastewater treatment processes before being supplied to the algae such as a decentralized wastewater treatment systems for buildings (Zamalloa et al. 2013). In countries where centralized wastewater treatment plants exist, there may be little incentive for these systems, but some municipalities such as the city of Toronto, Ontario, Canada, does offer sewage processing rebates for industrial and commercial buildings which discharge less sewage than water consumed (Toronto municipal code, 849-5), thus providing some economic incentive for decentralized wastewater treatment systems.

An advantage and potential downside of building-integrated photobioreactors is the requirement for aesthetics. In an industrial setting, the photobioreactor needs to be designed to be as efficient as possible, whereas aesthetics and design of the photobioreactor are very important in a building-integrated setting. It is likely that customers may be more willing to front the high capital costs for photobioreactors if they are aesthetically pleasing and are capable of serving some building utility functions such as helping heat or cool the building. This could be an economically viable option if engineering and design are well integrated to produce a viable photobioreactor product.

An algae textile photobioreactor has been proposed as a way to merge the engineering and aesthetics of photobioreactors in buildings (Boglas 2014). The algae textile is a photobioreactor organized as a flexible membrane, whose form can be adjusted depending on conditions. The main design objective of the textile was to balance aesthetics and building functions, while maintaining modern architectural design. Unique features of the algae textile are its proposed soft polymer construction and tapering walls. This construction allows a flexible reactor of which the light path through the walls decreases with the height of the photobioreactor. Aesthetical considerations are important in ensuring that there is a demand for these photobioreactors in buildings.

Photobioreactors integrated into buildings can serve multiple functions. A building-integrated photobioreactor can serve some of the building utility

functions. Depending on what utilities the building has, integrated photobioreactors can potentially serve the following functions: (1) heat dissipation, (2) wastewater treatment, and (3) co-product generation. Heat dissipation has been prosed and tested by the Smart Material House in Hamburg in a residential application (Smart Material House BIQ white paper 2013) and reducing the CO_2 emissions and removing nitrogen and phosphorus from waste streams is still being investigated (Zamolloa et al. 2013; Le Brogne et al. 2014). Coproduct generation is one of the more difficult potential synergies to address in non-industrial settings. Some products such as HTL and biodiesel will not be allowed to be processed onsite in a residential or commercial building due to laws, etc. This means that the biomass will have to be transported to another processing facility, which will increase costs.

Algae grown in building-integrated photobioreactors will require intelligent monitoring systems to respond to the various conditions the algae could be exposed to. Process control systems are already often designed for algal photobioreactors, but they are monitored on site by staff, where in a commercial or residential setting, current maintenance staff may not be well suited to maintaining photobioreactors. This will either require new training, new staff dedicated to the photobioreactor, or more advanced control systems.

If building-integrated photobioreactors are to be implemented in more industrial settings, closed photobioreactors are the preferred choice, with the flat-plate design being the best. Open raceway ponds and algal film photobioreactors are unlikely to be ideal candidates for integration in the short term. Open raceway ponds cannot be built vertically, so the simplest configuration would be to mount the pond on the top of a building, similar to a rooftop swimming pool. The current designs for algal film photobioreactors (ATS and RAB systems) are currently not suited for building integration, without further design refinement. These systems have been proven to be effective in applications of wastewater treatment (Mulbry et al. 2008; Christenson and Sims 2012) and on pilot-scale cultivation (Gross and Wen 2014), but the current proposed designs tend to resemble open raceway ponds with an attachment surface. Other designs of algal film photobioreactors, such as the parallel plate airlift reactor (Genin et al. 2014), have not been demonstrated on a sufficiently large scale.

It is expected that flat-plate photobioreactors would be the optimal photobioreactor based on the current literature and demands for integration into buildings. Flat-plate photobioreactors can have the highest directly illuminated surface area to volume ratio without high pumping costs that are problematic in tubular photobioreactors (Posten 2009). The removal of O_2 from flat-plate photobioreactors is better than in tubular photobioreactors (Chen et al. 2011a, b), and their CO_2 mass transport capabilities are similar to tubular (Ugwu et al. 2008). Flat-plate photobioreactors also have similar features as windows, so installation may be more familiar, some buildings are designed to have well illuminated rooms.

16.5 Conclusions

Microalgae have potential for production of many biofuels and biochemicals and for the treatment of waste streams. There are examples of pilot demonstrations of the potential biofuel production and treatment of wastewater. Fuels which can be produced from microalgae are biodiesel, biocrude, biogas, biomass for combustion, and ethanol. Biodiesel has the best NER compared to biocrude, but techno-economic studies show that biodiesel from algae is not economically feasible. The other fuels such as biogas and ethanol are still being researched and technology to make them economically feasible is still under development.

There are three general types of photobioreactors used to cultivate algae: open photobioreactors, closed photobioreactors, and algal film photobioreactors. Each one has distinct advantages over the others. When selecting which photobioreactor to use, common considerations are capital costs, value of end product, and source of nutrients. Open photobioreactors have the lowest capital cost, but lowest volumetric productivity and productivity is affected by weather and environmental conditions. Closed photobioreactors have high volumetric productivities and controlled environments, but have high capital costs. Algal film photobioreactors producing algal film biomass have the most concentrated biomass (50–100 times more than suspended algae) and productivities comparable to open raceway ponds, but the technology is still in development.

For the integration of photobioreactors into buildings, closed photobioreactors are the preferred choice due to their control and wider range of configurations opposed to open and algal film photobioreactors. When designing photobioreactors for buildings, multiple considerations have to be taken into account such as light source, nutrient source, aesthetics, cost, and functions. Integrating photobioreactors into buildings has been demonstrated in Hamburg with some success, but more research and engineering will be required to make building-integrated photobioreactors feasible on a wider scale.

References

Algenol website: www.algenol.com. Accessed on 21 May 2015

Alabi AO, Tampier M, Bibeau E (2009) Microalgae technologies and processes for biofuels/bioenergy production in British Columbia. Report prepared for the British Columbia Innovation Council.

ASTM E2397.05—Standard Practice for Determination of Dead Loads and Live Loads Associated with Green Roof Systems

Barowitzka MA (1992) Algal biotechnology products and processes—matching science and economies. J Appl Phycol 4:267–279

Benemann JR (2008) Open ponds and closed photobioreactors—comparative economics (Slide presentation). Paper presented at the 5th Annual World Congress on Industrial Biotechnology and Bioprocessing, April 27–30, Chicago, Illinois.

Bennion EP, Ginosar DM, Moses J, Agblevor F, Quinn JC (2015) Lifecycle assessment of microalgae to biofuel: comparison of thermochemical processing pathways, Applied Energy, In-press

Berlew JS (1953) Algal culture from laboratory to pilot plant. Carnegie Institution of Washington, Washington, DC, p 357

Bitog JP, Lee I-B, Lee C-G, Kim K-S, Hwang H-S, Hong S-W, Seo I-H, Kwon K-S, Mostafa E (2011) Application of computational fluid dynamics for modeling and designing photobioreactors for microalgae production: a review. Comput Electron Agric 76:131–147

Boglas P (2014) Algae textile: a lightweight photobioreactor for urban buildings. Master's Thesis, University of Waterloo, Waterloo

Borowitzka MA (1999) Commercial production of microalgae: ponds, tanks, tubes and fermenters. J Biotechnol 70:313–321

Boussiba S, Sandbank E, Shelef G, Cohen Z, Vonshak A, Ben-Amotz A, Arad S, Richmond A (1988) Outdoor cultivation of the marine microalga Isochrysis galbanna in open reactors. Aquaculture 72:247–253

Brown TM, Duan P, Savage PE (2010) Hydrothermal liquefaction and gasification of nannochloropsis sp. Energy Fuels 24:3639–3646

Chen PH (1987) Factors influencing methane fermentation of micro-algae. PhD. Thesis, University of California, Berkeley, CA, USA.

Chen C-Y, Yeh K-L, Aisyah R, Lee D-J, Chang J-S (2011a) Cultivation, photobioreactor design and harvesting of microalgae for biodiesel production: a critical review. Bioresour Technol 102:71–81

Chen X, Goh QY, Tan W, Hossain I, Chen WN, Lau R (2011b) Lumostatic strategy for microalgae cultivation utilizing image analysis and chlorophyll a content as design parameters. Bioresour Technol 102:6005–6012

Chisti Y (2007) Biodiesel from microalgae. Biotechnol Adv 25:294–306

Christenson LB, Sims RC (2012) Rotating algal biofilm reactor and spool harvester for wastewater treatment with biofuels by-products. Biotechnol Bioeng 109(7):1674–1684

Chui S-Y, Tsai M-T, Kao C-Y, Ong S-C, Lin C-S (2009) The air-lift photobioreactors with flow patterning for high-density cultures of microalgae and carbon dioxide removal. Eng Life Sci 9(3):254–260

Clarens AF, Resurreccion EP, White MA, Colosi LM (2010) Environmental life cycle comparison of algae to other bioenergy feedstocks. Environ Sci Technol 44:1813–1819

Collet P, Helias A, Lardon L, Lardon L, Goy R-A, Steyer J-P (2011) Life-cycle assessment of microalgae culture coupled to biogas production. Bioresour Technol 102:207–214

Cook PM (1953) U.S. Patent No. 2,658,310. U.S. Patent and Trademark Office, Washington, DC

Craggs RJ, Adey WH, Jenson KR, St John MS, Green FB, Oswald WJ (1996) Phosphorus removal from wastewater using an algal turf scrubber. Water Sci Technol 33(7):191–198

Dallaire V, Lessard P, Vandenberg G, de la Noue J (2007) Effect of algal incorporation on growth, survival and carcass composition of rainbow trout (Oncorhynchus mykiss) fry. Bioresour Technol 98:1433–1439

Dauta A, Devaux J, Piquemal F, Bouminch L (1990) Growth rate of four freshwater algae in relation to light and temperature. Hydrobiologia 207:221–226

Davis R, Aden A, Pienkos PT (2011) Techno-economic analysis of autotrophic microalgae for fuel production. Appl Energy 88:3524–3531

de Vasconcelos Barbosa MJ (2003) Microalgal photobioreactors: scale-up and optimization. Ph.D. Thesis, Wageningen University, Wageningen, The Netherlands

Degen J, Uebele A, Retze A, Schmid-Staiger U, Walter T (2001) A novel airlift photobioreactor with baffles for improve light utilization through the flashing light effect. J Biotechnol 92(2):89–94

Demirbas A, Demirbas MF (2011) Importance of algae oil as a source of biodiesel. Energy Convers Manage 52:163–170

Deng M-D, Coleman JR (1999) Ethanol Synthesis by genetic engineering in cyanobacteria. Appl Environ Microbiol 65(2):523–528

Doucha J, Livansky K (2006) Productivity, CO_2/O_2 exchange and hydraulics in outdoor open high density microalgal (Chlorella sp.) photobioreactors operated in a middle and southern European climate. J Appl Phycol 18(6):811–826

Doucha J, Straka F, Livansky K (2005) Utilization of flue gas for cultivation of microalgae (Chlorella sp.) in an outdoor open thin-layer photobioreactor. J Appl Phycol 17(5):403–412

Erickson D, Sinton D, Psaltis D (2011) Optofluidics for energy applications. Nat Photonics 5:583–590

Finlay JA, Callow ME, Ista LK, Lopez GP, Callow JA (2002) The influence of surface wettability on the adhesion strength of settled spores of the Green Alga Enteromorpha and the Diatom Amphora. Integr Comp Biol 42:1116–1122

Flemming H-C, Neu TR, Wozniak DJ (2007) The EPS matrix: the "house of biofilm cells". J Bacteriol 189(22):7945–7947

Formighieri C (2015) Cyanobacteria as a platform for direct photosynthesis-to-fuel conversion. In: Development of microalgae cultivation and biomass harvesting systems for biofuel production, (Chapter 7). Springer International Publishing, Switzerland

Fuduka H, Kondo A, Noda H (2001) Biodiesel fuel production by transesterification of oils. J Biosci Bioeng 92(5):405–416

Gao Z, Zhao H, Li Z, Tan X, Lu X (2012) Photosynthetic production of ethanol from carbon dioxide in genetically engineered cyanobacteria. Energy Environ Sci 5:9857–9865

Genin SN, Aitchison JS, Allen DG (2014) Design of algal film photobioreactors: material surface energy effects on algal film productivity, colonization and lipid content. Bioresour Technol 155:136–143

Grima EM, Fernandez FGA, Camacho FG, Chisti Y (1999) Photobioreactors: light regime, mass transfer, and scaleup. J Biotechnol 70:231–247

Gross M, Wen Z (2014) Yearlong evaluation of performance and durability of a pilot-scale revolving algal biofilm (RAB) cultivation system. Bioresour Technol 171:50

Gross M, Henry W, Michael C, Wen Z (2013) Development of a rotating algal biofilm growth system for attached microalgae growth with in situ biomass harvest. Bioresour Technol 150:195–201

Gudin C, Therpenier C (1986) Bioconversion of solar energy into organic chemicals by microalgae. Adv Biotechnol Process 6:73–110

Hase R, Oikawa H, Sasao C, Morita M, Watanabe Y (2000) Photosynthetic production of microalgal biomass in a raceway system under greenhouse conditions in Sendai City. J Biosci Bioeng 89:157–163

Herman EF, Anderson W (1947) Control of algal growths in hatching ponds and raceways. The Progressive Fish-Culturist 9(4):211–212

Hillen LW, Pollard G, Wake LW, White N (1982) Hydrocracking of oils of Botryococcus braunii to transport fuels. Biotechnol Bioeng 24:193–205

Hodoki Y (2005) Bacteria biofilm encourages algal immigration onto substrata in lotic systems. Hydrobiologia 539:27–34

Hu Q, Guterman H, Richmond A (1996) A flat inclined modular photobioreactor for outdoor mass cultivation of phototrophs. Biotechnol Bioeng 51:51–60

Incropera FP, Thomas JF (1978) A model for solar radiation conversion to algae in a shallow pond. Solar Energy 20(2):157–165

International Building Exhibition (IBA) Hamburg (2013) Smart Material House "BIQ" white paper

Irving TE (2010) Factors influencing the formation and development of microalgal biofilms. Thesis.

Irving TE, Allen DG (2011) Species and material considerations in the formation and development of microalgal biofilms. Appl Microbiol Biotechnol 92:283–294

Jimenez C, Cossio BR, Labella D, Xavier Niell F (2003) The feasibility of industrial production of Spirulina (Arthrospira) in southern Spain. Aquaculture 217(1–4):179–190

Johnson MB, Wen Z (2010) Development of an attached microalgal growth system for biofuel production. Appl. Microbiol. Biotechnol. 85:525–534

Kathrein HR (1960) U.S. Patent No. 2,949,700. U.S. Patent and Trademark Office, Washington, DC

Kok B (1956) Photosynthesis in flashing light. Biochim Biophys Acta 21:245–258

Lakaniemi AM, Hulatt CJ, Thomas DN, Puhakka JA (2015) Carbon dioxide utilization in gas-sparge microalgal photobioreactors. Conference paper presented at: Asian biohydrogen, bioproducts symposium. Chongqing, China.

Lam MK, Lee KT (2012) Microalgae biofuels: a critical review of issues, problems and the way forward. Biotechnol Adv 30:673–690

Lawrence JR, Neu TR, Swerhone GDW (1998) Application of multiple parameter imaging for the quantification of algal, bacterial and exopolymer components of microbial biofilms. J Microbiol Methods 32:253–261

Liu BYH, Jordan RC (1960) The interrelationship and characteristic distribution of direct, diffuse and total solar radiation. Solar Energy 4(3):1–19

Le Borgne F, Lepine O, Pruvost J, Le Gouic B, Legrand J (2014) Symbiotic integration of photobioreactors in a factory building façade for mutual benefit between building and microalgae needs. Presented at the 21st international congress of chemical and process engineering.

Ma F, Hanna MA (1999) Biodiesel production: a review. Bioresour Technol 70(1):1–15

Maor T, Appelbaum J (2011) Solar radiation on horizontal tubular microalgae photobioreactor: direct beam radiation. J Solar Eng 133:024502

Mata TM, Martins AA, Caetano NS (2010) Miroalgae for biodiesel production and another appliactions: a review. Renew Sustain Energy Rev 14:217–232

Meher LC, Vidya Sagar D, Naik, SN (2006) Technical aspects of biodiesel production by transesterification—a review. Renew Sustain Energy Rev 10(3):248–268

Melis A (2009) Solar energy conversion efficiencies in photosynthesis: minimizing the chlorophyll antennae to maximize efficiency. Plant Sci 177:272–280

Minowa T, Yokoyama S, Kishimoto M, Okakura T (1995) Oil production from algal cells of Dunaliella tertiolecta by direct thermochemical liquefaction. Fuel 74:1735–1738

Morendo-Garrido I (2008) Microalgae immobilization: current techniques and uses. Biosource Technol 99:3949–3964

Mulbry W, Kondrad S, Pizarro C, Kebede-Westhead E (2008) Treatment of dairy manure effluent using freshwater algae: algal productivity and recovery of manure nutrients using pilot-scale algal turf scrubbers. Bioresour Technol 99:8137–8142

Muller-Feuga A (2000) The role of microalgae in aquaculture: situation and trends. J Appl Phycol 12:527–534

Ono E, Cuello JL (2004) Design parameters of solar concentrating systems for CO_2-mitigating algal photobioreactors. Energy 29:1651–1657

Ozkan A, Berberoglu H (2013) Cell to substratum and cell to cell interactions of microalgae. Colloids Surf B Biointerfaces 112:302–309

Ozkan A, Kinney K, Katz L, Berberoglu H (2012) Reduction water and energy requirement of algae cultivation using an algae biofilm photobioreactor. Bioresour Technol 114:542–548

Palmer J, Flint S, Brooks J (2007) Bacterial cell attachment, the beginning of a biofilm. J Ind Microbiol Biotechnol 34:577–588

Pate R, Kilse G, Wu B (2011) Resource demand implications for US algae biofuels production scale-up. Appl Energy 88(10):3377–3388

Posten C (2009) Design principles of photo-bioreactors for cultivation of microalgae. Eng Life Sci 9(3):165–177

Pushparaj B, Pelosi E, Terdici M, Pinzani E, Materassi R (1997) As integrated culture system for outdoor production of microalgae and cyanobacteria. J Appl Phycol 9(2):113–119

Quinn JC, Smith TG, Downes CM, Quinn C (2014) Microalgae to biofuels lifecycle assessment—multiple pathway evaluation. Algal Res 4:116–122

Richmond A (2000) Microalgal biotechnology at the turn of the millennium: a personal view. J Appl Phycol 12:441–451

Richmond A, Boussiba S, Vonshak A, Kopel R (1993) A new tubular reactor for mass production of microalgae outdoors. J Appl Phycol 5:327–332
Samson R, LeDuy A (1986) Detailed study of anaerobic digestion of Spirulina maxima algae biomass. Biotechnol Bioeng 28:1014–1023
Sathananthan S, Genin SN, Aitchison JS, Allen DG (2013) Micro-structured surfaces for algal biofilm growth. Proc. SPIE 8923, micro/nano materials, devices, and systems, 892350
Sawayama S, Minowa T, Yokoyama S (1999) Possibility of renewable energy production and CO_2 mitigation by thermochemical liquefaction of microalgae. Biomass Bioenergy 17:33–39
Schnurr PJ, Espie G, Allen DG (2013) Algae biofilm growth and the potential to stimulate lipid accumulation through nutrient starvation. Bioresour Technol 136:337–344
Schumacher JF, Carman ML, Estes TG, Feinberg AW, Wilson LH, Callow ME, Callow JA, Finlay JA, Brennan AB (2007) Engineered antifouling microtopographies—effect of feature size, geometry, and roughness on settlement of zoospores of the green alga ulva. Biofouling 23:55–62
Sekar R, Venugopalan VP, Satpathy KK, Nair KVK, Rao VNR (2004) Laboratory studies on adhesion of microalgae to hard substrates. Hydrobiologia 512:109–116
Shi J, Podola B, Melkonian M (2007) Removal of nitrogen and phosphorous from wastewater using microalgae immobilized on twin layers: an experimental study. J Appl Phycol 19:417–423
Sialve B, Bernet N, Bernard O (2009) Anaerobic digestion of microalgae as a necessary step to make microalgal biodiesel sustainable. Biotechnol Adv 27:409–416
Spalding MH (2008) Microalgal carbon-dioxide-concentration mechanisms: Chlamydomonas inorganic carbon transporters. J Exp Bot 59:1463–1473
Stoll RE, von Linde F (2000) Hydrogen—what are the costs? Hydrocarbon Process 79:42–46
Sturm BSM, Lamer SL (2011) An energy evaluation of coupling nutrient removal from wastewater with algal biomass production. Appl Energy 88(10):3499–3506
Takeuchi T, Utsunomiya K, Kobayashi K, Owada M, Karube I (1992) Carbon dioxide fixation by a unicellular green algal Oocystis sp. J Biotechnol 25:261–267
Toronto municipal code chapter 492: green roofs (adopted as of 2009–05-27) articles: IV, VII
Toronto municipal code chapter 849: water and sewage services and utility bill (amended as of 2009-03-31) section; 849-5
Tredici MR, Zittelli GC (1998) Efficiency of sunlight utilization: tubular versus flat photobioreactors. Biotechnol Bioeng 57:187–197
Uduman N, Qi Y, Danquah MK, Forde GM, Hoadley A (2010) Dewatering of microalgal cultures: a major bottleneck to algae-based fuels. J Renew Sustain Energy 2:012701–012715
Ugwu CU, Ogbonna JC, Tanaka H (2002) Improvement of mass transfer characteristics and productivities of inclined tubular photo bioreactors by installation of internal static mixers. Appl Microbiol Biotechnol 58:600–607
Ugwu CU, Aoyagi H, Uchiyama H (2008) Photobioreactors for mass cultivation of algae. Bioresour Technol 99:4021–4028
U.S. Energy Information Administration (EIA) and the U.S. Department of Energy (DOE) (2013) Levelized cost of new generation resources in the annual energy outlook 2014.
Van Houtte E, Verbauwhede J (2010) Long-time membrane experience at Torreele's water re-use facility in Belgium. In: Proceedings of membranes in drinking and industrial water treatment. Trondheim, Norway
Vardon DR, Sharma BK, Blazina GV, Rajagopalan K, Strathmann TJ (2012) Thermochemical conversion of raw and defatted algal biomass via hydrothermal liquefaction and slow pyrolysis. Bioresour Technol 109:178–187
Walter J (1958) U.S. Patent No. 2,854,792. U.S. Patent and Trademark Office, Washington, DC
Wang B, Lan CQ, Horsman M (2012) Closed photobioreactors for production of microalgal biomasses. Biotechnol Adv 30:904–912
Wolff T, Brinkmann T, Geesthacht H-Z, Kerner M, Hindersin S (2015) CO_2 enrichment from a flue gas for the cultivation of algae—a field test. Greenhouse Gases Sci Technol 5:1–8
Yen HW, Brune DF (2007) Anaerobic co-digestion of algal sludge and waste paper to produce methane. Bioresour Technol 98:130–134

Yoo JJ, Choi SP, Kim JYH, Chang WS, Sim SJ (2013) Development of thin-film photobioreactor and its application to outdoor culture of microalgae. Bioprocess Biosyst Eng 36:729–736

Young AM (2011) Zeolite-based algae biofilm rotating photobioreactor for algae and biomass production. Masters Thesis, Utah State University, Logan, UT, USA.

Yu J (2014) Bio-based products from solar energy and carbon dioxide. Trends Biotechnol 32(1):5–9

Yu J, Chen L (2006) Cost effective recovery and purification of polyhydroxyalkanoates by selecting dissolution of cell mass. Biotechnol Progress 22:547–553

Zamalloa C, Boon N, Verstraete W (2013) Decentralized two-stage sewage treatment by chemical–biological flocculation combined with microalgae biofilm for nutrient immobilization in a roof installed parallel plate reactor. Bioresour Technol 130:152–160

Chapter 17
Case Studies on the Architectural Integration of Photobioreactors in Building Façades

Rosa Cervera Sardá and Cristina Alvarez Vicente

Abstract The research presented addresses the production of biomass in architectural facade, making these facades photobioreactors, PBRs, of micro algae cultivation. These aquatic microorganisms and simple structures grow from the process of photosynthesis and absorption of CO_2. The integration of what up to now was an industrial system in the architectural envelope opens new and interesting alternatives to renewable energies. We present different cases of PBRs on façades, with both new construction and renovation or energy-efficient rehabilitation. In all the examples, currently under development, it has sought a central objective economic feasibility and energy productivity. The designs range from simple and easily standard proposals done with existing materials in the market and economic assembly, to unique designs, with manufacturing singled out, which bring high representative value. The entire catalog of architectural design solutions is accompanied by industrial systems similar to those described for operation as PBR. In the study costs of façades transformed into PBRs are compared to standard façades achieving highly competitive values at a certain scale factor. Other factor developed is the increase of thermal regulation in the interior of a building because of the isolation produced by the inclusion of architectural PBRs and circulating water with microorganisms in the constructive elements of the models. Again the results open a promising future to this new concept of facades increasing both passive and active energetic values.

R. Cervera Sardá (✉)
Alcala University, Cervera & Pioz Architects Slp, Madrid, Spain
e-mail: rcervera@cerveraandpioz.com

C.A. Vicente
Alcala University, Alcalá de Henares, Spain

F. Pacheco Torgal et al. (eds.), *Nano and Biotech Based Materials for Energy Building Efficiency*, DOI 10.1007/978-3-319-27505-5_17

17.1 Energy for the Future: MicroAlgae Biomass as a Renewable Energy

One of the main problems that humankind has to face is the scarcity of energy. It is mandatory to reduce the dependency on fossil-based products to meet climate change objectives and make an eco-friendly world. Sun and wind, as renewable energies, have been in continuous development during last decades and have reached a high level of technology. But a few years ago, another renewable energy came up: biomass. Biomass is a biological material from living organism or recently living organism. Biomass can proceed from both the animal and the plant kingdom. It is generally associated with waste from plants and vegetables, and also, waste from animals can be used to produce bioenergy. In our case, we focus our research on the potentiality of microalgae biomass. Microalgae are aquatic organisms with a simple cell structures. They can grow in different environments such as freshwater, saline, or seawater and even in contaminated water. The characteristics that make them an optional sustainable source of energy are that, on the one hand, they are photoautotrophic, or in other words, they can convert solar energy into chemical forms through photosynthesis, and on the other hand, they need to capture CO_2 for their growing process. It means that with the sun, they can "provide" biomass that can be processed into different final products: biofuel, biogas, electricity through cogeneration and, besides that, value-added goods, such as food, medicines, pigments and cosmetics. Microalgae organisms "absorb" carbon dioxide from the atmosphere to produce biomass contributing to the sink effect that we need to improve the climate change conditions.

So due to their multiple potential capacities and benefits obtained from them, the microalgae have received great interest. The long-term and profitable microalgae industries developed are related to the production of food for both human beings and animals, and pharmaceuticals and other valuable compounds due to their proteins generation. In the field of renewable energies, considerable interest has been focused on the production of biofuel. Microalgae can produce big quantities of sugars (polysaccharides) and fats (triglycerides), being these the raw materials for producing biodiesel and bioethanol. Nevertheless, the research done up to now is questionable considering the net energy balance, i.e., the balance between energy obtained in production and energy used for cultivation, harvesting, and processing the biomass. More simple and cheaper way of generating microalgal biomass is just to obtain non-specialized biomass that can be used to produce biogas and electricity, in this case coming from biogas through cogeneration, and biofertilizers for watering gardens.

The starting point of our research considers the ultimate fate of the algal mass. It is said, biomass that has a low level of processing can be used for bioenergy and hundred percent biofertilizers, reducing the energy production of nitrate in chemical fertilizers[1]. And from there, we envision an entirely new stage of photobioreactors

[1]Micro-algae biofertilizers are 100 % natural and harmless product, produce higher assimilation capacity and higher crop yield, promote root development, increase the leaf vigor and the

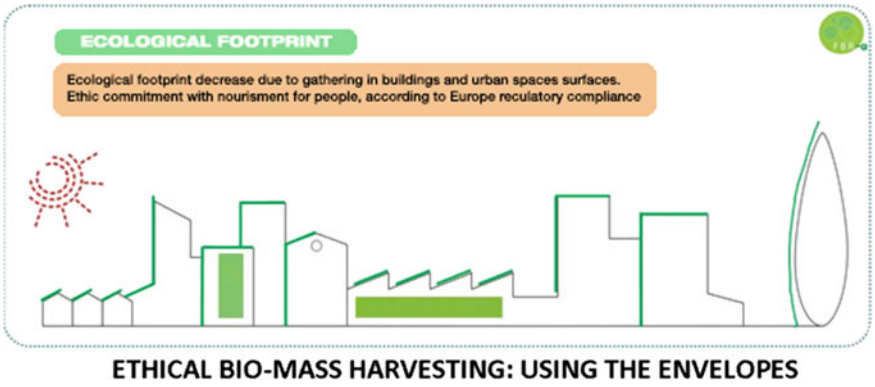

Fig. 17.1 Biomass cultivation using the architectural surfaces

closely linked to architecture. This is the innovative contribution of our proposals, using architecture as support surface for the cultivation of algae. Thus, we do not compete with land used for growing food products and thus avoid the price increase of the latter. A topic that always accompanies biomass is the controversy of the large amount of land used for cultivation; that is why, beyond research and technology developed for biomass from agriculture and forestry, alternative bio-based energies from those single microscopic organisms that live in water and grow hydrophonically are really high. A relevant aspect of microalgae for biomass is the fact of its rapid growth. It can double its volume in a day. Their fast growth rates brought the attention as a renewable source of energy, mainly after the energy crisis in the 1970s. So if we compare the cubic meters of oil produced per square kilometer of cultivation of different raw materials, we found that rapeseed, mustard, or pinion produce 100–160 m^3 per Km^2, while algae come to generate 10,000–20,000 m^3 per km^2. By using the constructed surfaces that receive sunlight we are able to save cropland factor improving environmental balance.

In summary, microalgae "are able to biofixate via photosynthesis up to 2 kg of CO_2 per kg of biomass produced, are inexhaustible, can be daily harvesting (up to 30 % of the total cultured volume), do not need fertile lands, not competing with human nutrition, and they grow in sea, fresh, brackish, and waste waters"[2] (Figs. 17.1 and 17.2).

(Footnote 1 continued)

flowering and fruit-setting, promote the regeneration of the damaged tissues, etc., http://www.algaenergy.es/en/sectors-products/agriculture-agrialgae/. For more information about biofertilizers, see Shannon B. Andrews, Quantifying the Fertilizer Value of Algal Meal: An Evaluation of an Integrated Dairy-Anaerobic Digester-Algae Production Facility, Master thesis in Soil Science, May 10, 2013, https://ir.library.oregonstate.edu/xmlui/bitstream/handle/1957/40443/AndrewsShannonB2013.pdf?sequence=1.

[2]http://www.algaenergy.es/en/about-us/what-are-microalgae/.

Raw material	m3 oil /km2 crop
COLZA	100-140
MUSTARD	130
PINION	160
PALM OIL	610
ALGAE	10000-20000

Fig. 17.2 Comparative of biomass production of different raw materials

17.2 Envelopes for Future-Oriented Architecture: From Passive Façades to Active BioFactories of Energy

According to our history and experience, architectural façades have the role of protecting the users from external conditions and limiting the construction building a shelter for life of human beings. Through façades, we recognize architectural styles, we learn about materials and technologies, and most importantly, we sense the dreams and aspirations of a society. The fundamental goal of providing comfort has made the façades of the buildings always an interface between exterior and interior, from the circumstances of the climate and culture, generating adaptive building system. Until recent times, the façade has faced the same function of protecting from the environment. This has meant that historically it has developed highly effective insulation and protection both in the monumental building and in the common buildings. Beyond the expression of sociocultural interests, cold insulation, heat protection, control of the solar impact, and permeability for ventilation have been key features of the façades in architecture until the twentieth century. The emergence of energy has fully transformed the role of the façade in architecture. The gas, electricity, and fossil resources provided the comfort required for the habitability of buildings. Today, in our already full and clear awareness of the excessive consumption of energy and the search for alternative sources, it has been granted to the façades the capacity to intervene in generating it. It is not surprising that architecture has assumed a new role, which is to generate part of the energy it consumes. To this end, it has focused on the envelope of buildings to harness energy from the sun. And the technology of solar collectors and photovoltaic panels has developed integrated elements in the architecture as a new language in response to the needs of our time. That is it, which has transformed the concept of architectural elements as "passive" thermal control agents to become "active" agents of power generation. Now, with the algae biomass, we can go one step further in energy generation with the construction elements themselves.

17.3 Architecture and MicroAlgae: State of Art

In last years, it has been produced diverse approaches to integrate the algae growing in the architecture. After a period of projects at the edge of fantasy and with almost null scientific base that imagined futuristic architecture with algae conquering façades and interstices, it is coming to first projects built and first prototypes that give a more realistic role to the incorporation of microorganisms in the construction.

Those projects of visionary character glimpsed what today starts to be a feasible option to generate biomass and to capture CO_2 in built patrimony. The first example built at the level of buildings is the Bio Intelligent Quotient building (BIQ building), Hamburg, Germany, 2013. The PBRs consist in sun-shading panels around 2.5 m × 0.7 m formed by a two monolithic glass layers with a cavity where water with microalgae circulates. These sun-shading panels, installed on the southeast and southwest sides, constitute like an outer façade protecting the building from sun radiation. The total area of PBRs is around 200 m^2. According to the words of Jan Wurm, Arup's architect and research leader, "we've done the research. We've got the units in place. Now as we add the microalgae we will see for the first time how the bioreactor façade operates in a real life situation. It is a test for the technology, but it also represents a huge step forward. If we can demonstrate that microalgae bio façades can become a viable new source of sustainable energy production, we can transform the urban environment, as well as providing architects with a new source of inspiration."[3]. After one year of running, and after some improvements in the installation, they consider that around 50 % of the energy consumed in the building is either saved or produced thanks to the PBRs. Nevertheless, the economic impact of the panel on the cost of the construction square meter is still really high.[4]

More samples of façades are being developed in different countries. In France, there are several proposals like the biofaçade in a waste processing plant in Nantes, consisting in a double PBRs contributing to the thermal regulation and the production of bioenergy,[5] and the L'Algo-Nomad Pavilion, a small prototype with four PBRs in one of the façades, presented in the Arsenal Pavilion in Paris, 2014 (Fig. 17.3).[6]

In USA, the Grow Energy, a young start-up company in the area of San Diego, has developed some PBRs integrated in the architecture. They are announced to be

[3] http://www.arup.com/News/2013_04_April/25_April_World_first_microalgae_facade_goes_live.aspx.

[4] http://www.fastcoexist.com/3033019/this-algae-powered-building-actually-works.

[5] J. Pruvost et al., Symbiotic Integration of Photobioreactors in a factory building façade for mutual benefit between buildings and microalgae needs. For Mutual Benefit Between Buildings And Microalgae Needs. http://www.researchgate.net/profile/Jeremy_Pruvost/publications.

[6] http://www.lemoniteur.fr/article/en-attendant-la-facade-a-micro-algues-grandeur-nature-un-prototype-s-expose-a-paris-23587916.

Fig. 17.3 Biofaçade in a waste processing plant in Nantes and the L'Algo-Nomad Pavilion, with 4 PBRs in one façcade

used in homes and buildings. Their Verde system can be installed in already existing architecture, and the Hydral system has been designed to culture algae for hydrogen as energy source that can be used for small constructions and homes. In both cases, the PBRs are again designed with two flat panels with liquid, CO_2 and nutrients circulating inside (Fig. 17.4).[7]

As we can see, there is a promising future in the synergy between microalgae culture and architecture. The buildings became alive because of the living organisms and increase their passive and active role related to energy saving and production. Besides that, the main advantage of using algae biomass is the storage of energy. But there is not enough experience yet and most of the built samples are done at laboratory scale. So, in terms of investments, it is still pendant the debate about the feasibility. That is why our research here presented has as a main goal the viability in all senses, i.e., energetically and economic speaking.

[7] http://www.growenergy.org/.

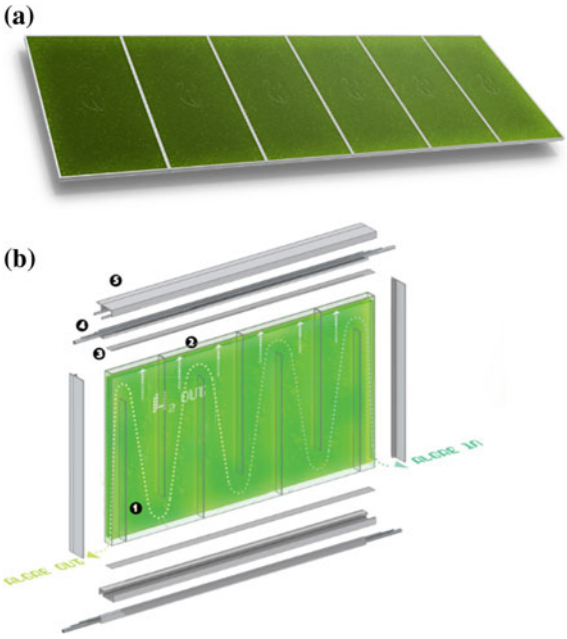

Fig. 17.4 Verde system and Hydral system by Grow Energy

17.4 Photobioreactors Integrated in Building Façades: Case Studies

In the research, we have overcome the challenge of incorporating organic matter into the architectural elements themselves to benefit from the advantage they bring of providing energy. Thus, a new material appears to intervene in the buildings, a living material that generates biomass, absorbs CO_2, and contributes to the insulation of the building. As added benefits of microalgae, it can contribute to the cycle of water being fed with sewage due its components generating a closed cycle and purifying industrial or contaminated water according to species or strains of microalgae. Besides the above, the fact of making the architectural façade into a photobioreactor or integrated photobioreactors minimizes the impact on façades of crop biomass by use of the surface with its now added traditional use. By this, the former industrial photobioreactors constitute a new type of outer layer of the architectural envelope with important additions to energy level and environmental values. The industrial type of photobioreactors is classified into two families: the raceway or pond that is open like a pool or pond very shallow where the water with microalgae is permanently moving at low speed, taking the carbon dioxide directly from the atmosphere, and the PBR in a closed circuit with water with microalgae circulating either by tubes or between the plates or panels, in both cases of transparent or translucent materials

which permit the passage of light. PBRs need both CO_2 injection as well as the evacuation of oxygen. For façades, due to its vertical conditions, only the photobioreactors of the closed circuit type are indicated being pond unfeasible. In this case, for the cultivation and collection of algae, PBRs need, at its input, pipes for water with microorganisms plus nutrients and CO_2 supply, a nutrients tank, and a preparation tank. Harvesting is also performed in a tank or reservoir, and a centrifuge machine for drying the biomass, thereby preventing the rot, is needed. If the product obtained is a biofertilizer further processing is not required and the water with microalgae can be used directly for irrigation. If you want to get biomass to produce energy, then a biodigester to transform matter into biogas is needed. Besides a heat exchanger, a unit of gas treatment and other wastewater is necessary. If the final product is electricity, a cogeneration equipment is required. As auxiliaries, centrifugal pump, air blower, control system, and PLC are requested. For the proper functioning of the PBR, an element is necessary for the release into the atmosphere of dissolved oxygen, maximum 400 m of conduit. The kind of microalgae will depend on local conditions because for their performance varies according to climate, water, nutrients, etc. The productivity of PBR for closed loop can be estimated as a realistic average 8 or 9 g/l/d, considering greater control to higher productivity, with a dilution rate of 15 %.

We present different cases of PBRs on façades, both with new construction and with renovation or energy-efficient rehabilitation. In all the examples, currently under development, it has sought a central objectives: economic viability and energy productivity. The designs range from simple and easily standard proposals done with existing materials in the market and economic assembly, to unique designs, with manufacturing singled out, which bring high representative value. The entire catalog of architectural design solutions is accompanied by industrial systems similar to those described for operation as PBR (Fig. 17.5).

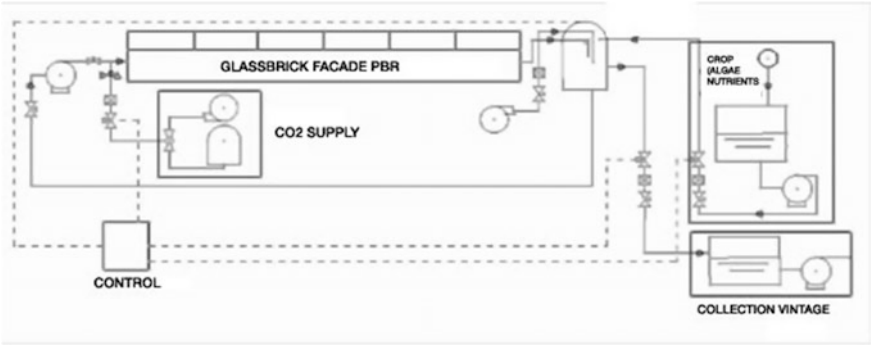

Fig. 17.5 Vertical photobioreactor of closed cycle for integrated in a glass block wall

17.4.1 Case Study 1: Architectural PBRs Overlapped on Existing Façades for an Energy-Efficient Renovation

Adapting existing building park to the new requirements of energy efficiency is a priority to address environmentally friendly future goal. This requires a renovation with attention focused on reducing energy consumption. This issue is especially important in regard to much of the built structures in the middle decades of the century, when the building heritage was based on energy consumption, low insulation, and also with their degradation of the building materials. There are already many actions taken in European cities, and these actions are based, in general, on the externally coated façades of little architectural value, with various types of insulation panels wrapping the building to protect from the cold.

Our research has led us to develop an outer envelope for existing buildings by varying PBR easily integrated into facades with the dual mission of both "passive" improvement aforementioned insulation and "active" contribution to power generation through microalgal biomass. Our goal is to generate architectural PBR that, beside fulfills the above, is easy to install, has low construction costs and maintenance and introduces new aesthetic expectations due to the inclusion of living organisms in architecture (Fig. 17.6).

To design this type of PBR, we begin with the sandwich concept in such a way that the existing façade to be coated constitutes the inner face of the PBR, reducing its cost by using already existing material. Attached to that support, an outer layer, which must be made of transparent or translucent material to allow pasaage of light, is fixed. In-between both, facade and exterior panel, the liquid with microalgae circulates. Starting with this simple scheme, we have considered various types of support and various exterior finishes. The various types of support considered generically cover the usual spectrum of façades in no historical or monumental building value. On one side, they are considered solid such as brick, concrete blocks or thermoclay, and on the other, light panel walls. As regards the outer material, they have been considered finished U-Glass with structure or frame mounted on glass. Between both layers, the flow of green water generates space acting as insulation. Either you can choose to drive the microalgal for transparent rubber hoses, easily replaceable which also prevent the leaks with fluid water. In any of these cases, it could be enough, with simple transparent rubber tube circuit; however, we understand that the outer sheet protects them well and gives them an appearance of greater architectural quality (Figs. 17.7,17.8 and 17.9).

Another group of PBRs attached to façades and using the existing walls or panels as the inner layer of the sandwich are those that allow the water to circulate freely, although directed. We have developed two models: PBR with the outer layer of cellular polycarbonate and PBR of ETFE or of plastic. In the first case, the cell structure of the polycarbonate itself makes conduits for water and microorganism.

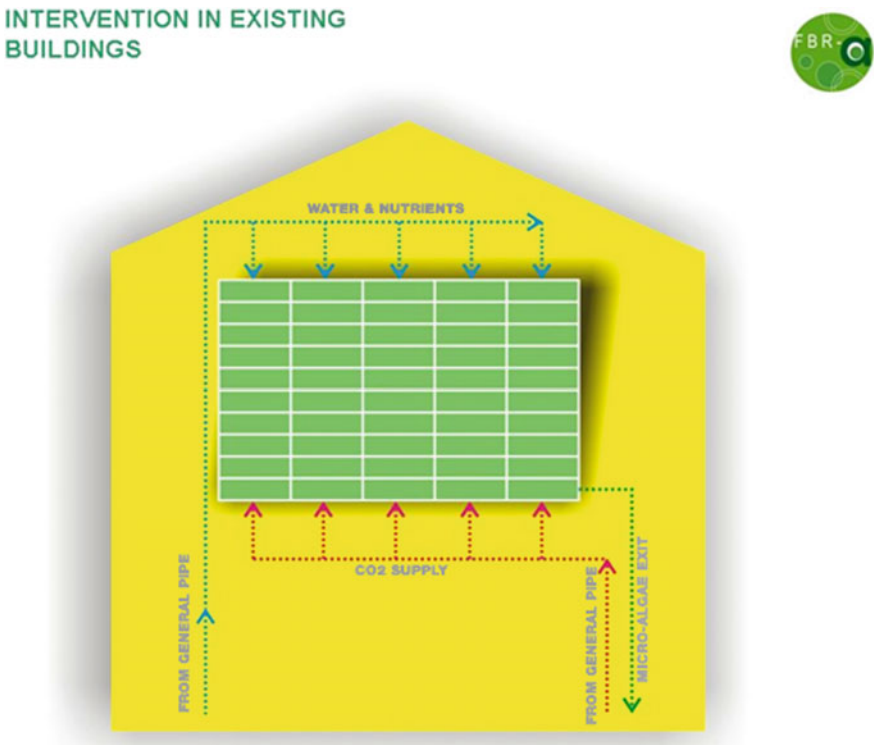

Fig. 17.6 Scheme of a PBR attached to an existing façade

The support may be both lightweight or heavy type. The external layer acts as an insulation buffer.(Fig. 17.10).

In this second case, the flexible structure of the outer membrane, ETFE and plastic or PVC, produces a pneumatic-like structure, forming large bags with padded compartments. To protect their vulnerability, some type of mesh or network containment is recommended (Fig. 17.11).

17.4.2 Case Study 2: Architectural PBRs Constituting Façades

If we now consider new constructions, there are interesting options transforming the façades itself into the PBR. In this case, the façade itself integrates the liquid component of living microalgae. The sandwich constituting the PBR has two transparent or translucent membranes with biomass therein. And the integrated organic material generates a translucent wall with a large variety of green and red colors, depending on the microalgae species. There are two large families that have

NEW ADITION LAYER FOR EXISTING FACADES	ORIGINAL SUPPORT	DRAWINGS
TUBULAR PBR WITH EXTRACLEAR CURTAIN WALL PROTECTION	SANDWICH FACADES.There are several types of facades with this designation: metallic, plastic, concrete exterior layers.	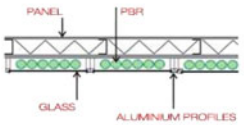
	TRADITIONAL BRICK WALL OR CONCRETE BLOCK WITH INSUALTION AT OUTTER FACE	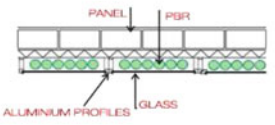
	HONEYCOMB CLAY BLOCK WALL	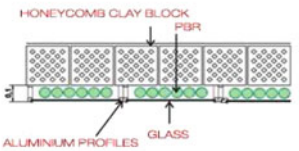

Fig. 17.7 Different solutions of PBRs made of glass attached to existing exterior walls

NEW ADITION LAYER FOR EXISTING FACADES	ORIGINAL SUPPORT	DRAWINGS
TUBULAR PBR WITH ONE FACE EXTRACLEAR U-GLASS PROTECTION	SANDWICH FACADES.There are several types of facades with this designation: metallic, plastic, concrete exterior layers.	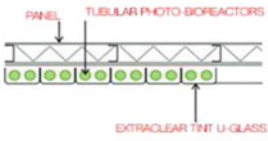
	TRADITIONAL BRICK WALL OR CONCRETE BLOCK WITH INSULATION AT OUTTER FACE	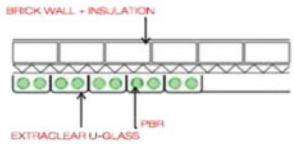
	HONEYCOMB CLAY BLOCK WALL	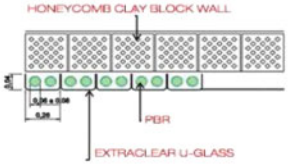

Fig. 17.8 Different solutions of PBRs made of U-Glass attached to existing exterior walls

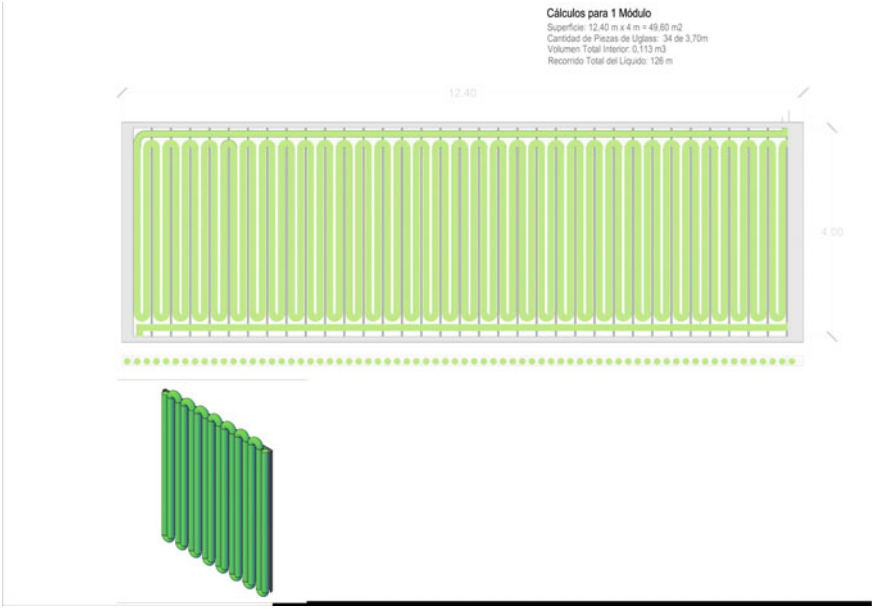

Fig. 17.9 PBR attached to an existing support with water hoses and U-Glass final exterior layer

NEW ADITION LAYER FOR EXISTING FACADES	ORIGINAL SUPPORT	DRAWINGS
FREE CIRCULATING WATER PBR INSIDE CELLULAR POLYCARBONATE	SANDWICH FACADES.There are several types of facades with this designation: metallic, plastic, concrete exterior layers.	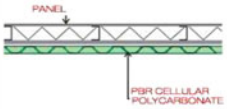
	TRADITIONAL BRICK WALL OR CONCRETE BLOCK WITH INSULATION AT OUTTER FACE	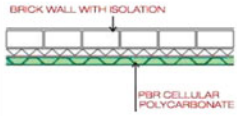
	HONEYCOMB CLAY BLOCK WALL	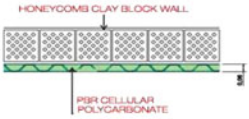

Fig. 17.10 Different solutions of PBRs made of polycarbonate panels attached to existing exterior walls

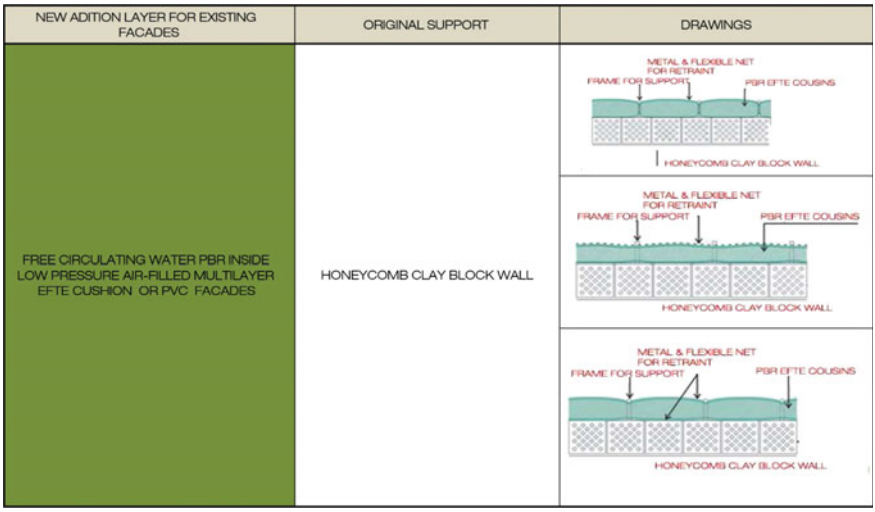

Fig. 17.11 Different solutions of PBRs made of ETFE or plastics attached to existing exterior walls

been developed in our research. One is consisting of modular system with double-sided hollow glass and translucent molding and high mechanical strength, forming a system for ducts with closed loop. Depending on its size, the modules form a single duct or, by mean of inner plates made of plastic or glass, multiple conduits. This system has been designed to allow the modular coupling of the glass blocks by bayonet fasteners. The liquid and seaweed solution passes from each piece to the other generating a continous circuit. The circuit allows the entry of essential nutrients and carbon dioxide for photosynthesis and the uoutput of liquid, seaweed biomass and oxygen. These modules can be built in a standardized way, reducing costs. And due to its high mechanical strength, it can be used to build walls, façades and even pavements[8] (Fig. 17.12).

The second family of PBRs acting as façades is referred as structural curtain walls. We consider three types according to the sandwich sheets forming the PBR. The first type is formed on the inner face of glass and on its outer face by cell polycarbonate. The water with microorganisms and nutrients flows inside the polycarbonate inner structure. In the second type, both sheets are made of glass and in the third case of U-Glass. In these two last cases, the liquid is preferable conducted inside flexible transparent pipes to avoid leaking, although it could circulate freely between the glass panels without water hoses (Fig. 17.13).

[8]For more information: R. Cervera et al.,.

NEW FACADE	DESCRIPTION	DRAWINGS
GLASS BLOCK WALLS	GLASS BLOCK WALLS, MODULAR SYSTEM WITH DOUBLE FACE SEPARATED BY AIR WHICH CAN REFILL WITH THE MICROALGAE CIRCUIT.	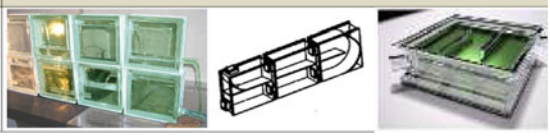

Fig. 17.12 PBRs integrated in a molded glass block façade

NEW FACADE	DESCRIPTION	DRAWINGS
CURTAIN WALL	FREE MICROALGAE FACADE IN POLYCARBONATE	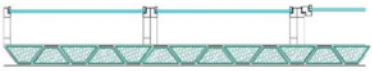
	TUBULAR PBR INSIDE TWO GLASS LAYERS CURTAIN WALL	
	TUBULAR PBR INSIDE DOUBLE U-GLASS FACADE	

Fig. 17.13 PBRs integrated in glass curtain façade and U-Glass facade

17.4.3 Case Study 3: Architectural PBRs Constituting Louvers and External Layers Protecting Façades

Generating parasols or louvers in front of the façade itself, like a double-skin façade, is a system that allows a wide range of feasible designs of PBRs. In fact, the up to now built samples have chosen this option, as mentioned above. In this case, the louvers are the PBRs, generally constituted by double panels of glass or transparent or translucent material with water and microalgae and nutrients and CO_2 inside. The input and output pipes run along the structures that sustain the parasols. The panels can also be movable to suit the different conditions of the sun or of the need to view from the inside. Presenting few examples developed by our group, some of them inspired in nature in our biomimicry research (Fig. 17.14).

Fig. 17.14 Different patterns of PBRs acting as an external parasol façade

17.4.4 Case Study 4: Singular Designs

Finally, we present most unique character design façades that generate high architectural added value due to its spectacular feature. Here, we present an elastic ETFE façade structured with stainless steel rings which allow to tighten and loosen

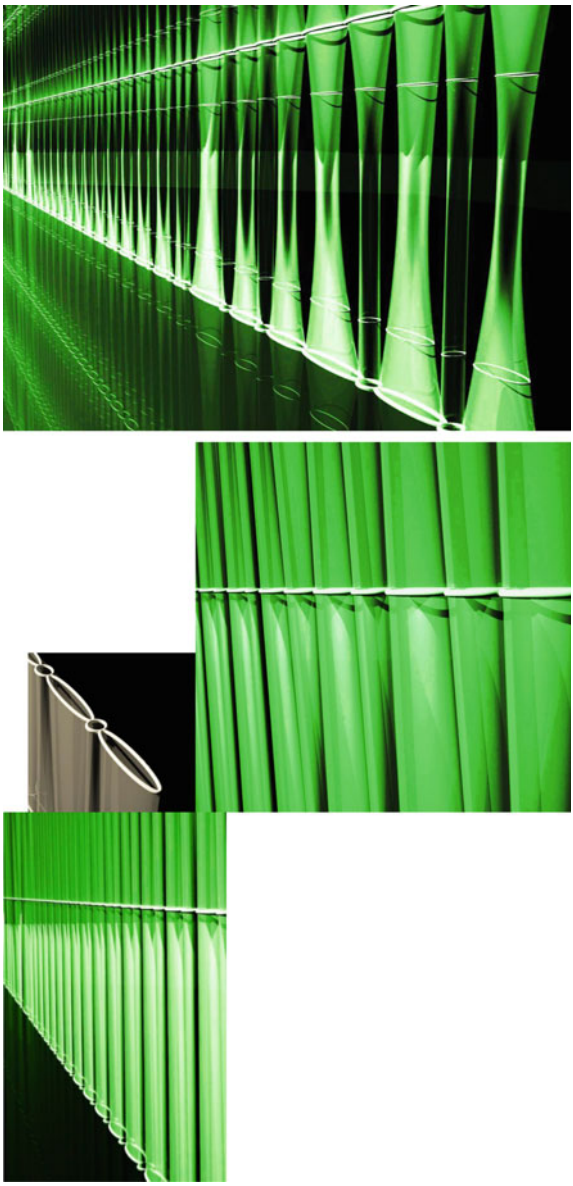

Fig. 17.15 PBR façade made of ETFE

the membrane so that the façade can be completely covered with the fabric or partially open in combination with various openings according to the sections. Filling these membranes of ETFE, the water and microalgas circulate constituting a PBR (Fig. 17.15).

17.5 Economic and Energetic Feasibility Analysis

One of the subjects more questioned in growing microalgae is its economic and energetic balance. Although algae biomass is seen as a powerful option for the future, current production schemes have not been able to prove a sustainable energy return on investment due in part to the high costs of nutrient addition, the energy required for drying and processing the biomass, and the land needed for growing them.

Leaving aside the food and value-added products where the industry has reached maturity, the experiences with algae to produce energy and biofuel are still uneconomic. In the case of the integration of its cultivation in the architecture, what has been built up to date are very experimental cases and at a very small scale, almost a laboratory essay. Beacuse of this the data are not sufficient yet to determine its efficiency. However, we can affirm that its profitability is guaranteed based on three basic questions: The first one is the minimization of the impact due to area of cultivation, the second is the improvement of the insulation of buildings where they are installed, and the third is the low economic impact due to adapt or use a façade or its elements as PBR.

We are dedicating to these two last questions a detailed study to compare profits. In any case, the profitability is also related to the final product and therefore to the control level of production. The larger the profitability of the cultivation is, the harder control of it will be demanded. In the case of the integration of the cultivation in buildings being a part of the urban panorama, to be realistic, a maintenance and control system in the basement level equivalent to a common garden has been proposed. Therefore, the final products that are considered feasible in the algae cultivation in architecture are the following:

Biofertilizers: Do not require more control than in landscaping and they may be used directly in the irrigation of parks and gardens avoiding chemical fertilizers and therefore saving energy.
Bioagricultural stimulators: Request a medium-level process and they are used as enhancers hundred per cent organic for agricultural growing.
Biomass for the production of gas and electricity: Request a low control level, but they must have installed a biodigestor to obtain biogas and a cogeneration system to produce electricity.

17.5.1 Cost Comparation of PBRs Integrated in Type Façades of Buildings

As the PBR is an integral part of the architecture, we can say, in general terms, that alternative proposals for PBRs, despite of the added costs for living organisms and industrial equipment, are still highly competitive with respect to the total spectrum for walls and roofs in the market.

In analyzing their integration into facades we must first consider the scale factor. The impact of the installations that transform a facade in PBR, according to our analysis, is competitive in terms of exceeding a minimum threshold m^2, being the scale factor determining profitability.

- High impact up to 200 m^2
- Average impact to 500 m^2
- Low impact to 1000 m^2
- No significant repercussion to the upper surfaces 2000 m^2

We have proceeded to study the average impact per square meter of needed installations and equipment for transforming a façade in PBR built as obtained final product and as scale factor getting the following indicative table (Fig. 17.16).

As we can see, a PBR over 500 m^2 area the economic impact of transforming the façade is around 30 €/m^2, what is not relevant and almost insignificant when the surface is over 5000 m^2. To have a complete vision of the total investment, impact maintenance and control cost must be evaluated. We are currently proceeding with some prototypes in order to quantify it. If now we move to analyze the economic competitiveness among façades, we must consider the range of different constructive surfaces and we can organize a list depending on technology and price of construction per square meter.

The most simple and common façades are built with bricks or concrete blocks plus attached isolation cameras. Its price under the standards of Spain is between 100 and 200 €/m^2. The following grade of façades is that of translucent built in U-Glass and in molded glass block. In this case, its price may reach 250 €/m^2. The facades that have facings of relevant quality, such as curtain walls of aluminum or

PBR-A FACILITIES COST. CLOSED VERTICAL TYPE	SCALE FACTOR: FACILITIES COST VARIANCE ACCORDING TO M2 BUILT					
	Square meters: M2	100	200	500	1.000	5.000
APPLICATION 1. Bio-Fertilizer & Irrigation	Total Cost	6.695,5	8.535,9	11.296,4	15.897,3	52.704,5
	Cost per m2	67,0	42,7	22,6	15,9	10,5
APPLICATION 2. Heat Generation	Total Cost	9.060,5	11.373,9	14.843,9	20.627,3	66.894,5
	Cost per m2	90,6	56,9	29,7	20,6	13,4
APPLICATION 3. Electricity & Heat Generation	Total Cost	10.060,5	12.573,9	16.343,9	22.627,3	77.894,5
	Cost per m2	100,6	62,9	32,7	22,6	15,6

Fig. 17.16 Analysis of cost of PBRs integrated in the architecture depending on the scale factor and the final product

stainless steel, reach up to 650 €/m^2. Finally, façades of very singular and iconic design or the intelligent façades move around 900–1000 €/m^2.

The cost of PBR facades is comparable to facades of low economic impact. If the proposed PBRs are compared to curtain wall facades or unique design facades, are extremely competitive because both, on the one hand, the highly innovative design and added value and, on the other, the much lower price. So the returns are immediate and the amortization starts from the outset. In any case, construction and installation of architectural PBRs, from areas exceeding 1000 m^2, have a transcendence of no impact on the total cost of construction of the building, and from 5000 m^2, the impact can be dismissed (Fig. 17.17).

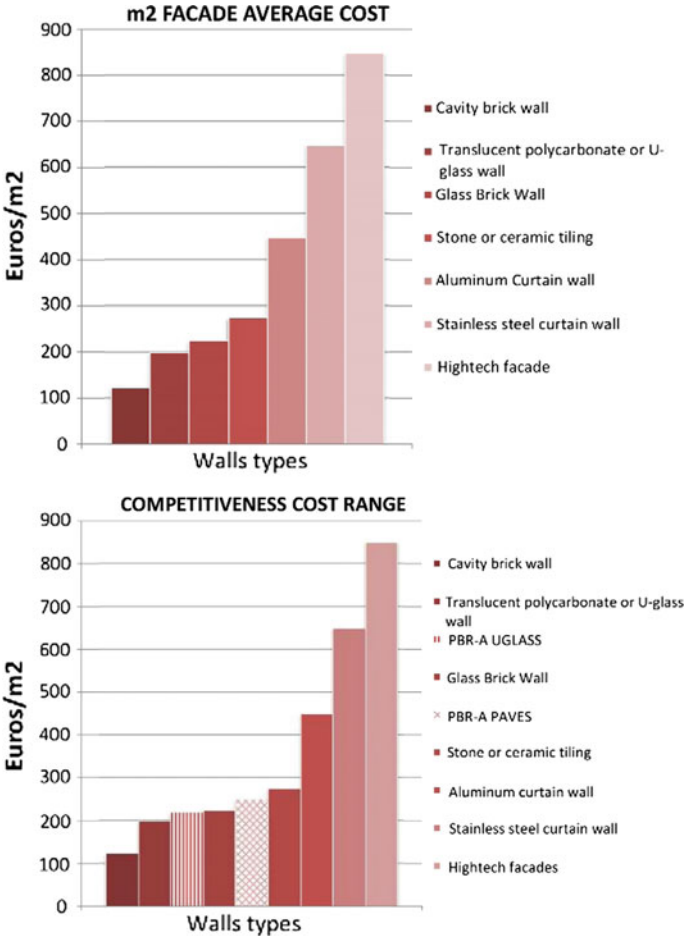

Fig. 17.17 Comparative analysis of cost of PBRs integrated in the architecture and typical architectural façades

According to our estimations, the costs of operating and maintaining some of the proposed PBRs may have, today, a return of between 9 and 13 years payback, according to the PBR type and according to the final product. In the event that the final product is the biofertilizer, the repayment period is significantly lower not exceeding seven years. In any case, the time factor and scale factor performance will improve as the industry reaches its maturity and its use is spreading.

17.5.2 Benefits of the PBRs Integrated in the Façades Due to the Thermal Regulation Factor

The inclusion of water with microorganisms in the construction elements of façades increases its capacity of energy saving due to the following reasons:

- Temperature reduction of the architecture through the absorption of solar radiation due to the algae photosynthesis process (with self-regulation of temperature) and parasol effect, with solar protection and façades shading according to designs.
- Increase of the acoustic and thermal insulation of the architecture by the effect of the water of the cultivation in PBRs attached to façades or by the inclusion of the cultivation water in the façade.

In the designed prototypes of our research, we have proceeded to the calculation of the insulation performance as follow:

Thermal transmittance, also known as U-value, is the rate of transfer of heat (in watts) through one square meter of a structure divided by the difference in temperature in Kelvin across the structure. It is expressed in watts per squared meters kelvin, or W/m^2 K. Well-insulated parts of a building have a low thermal transmittance, whereas poorly insulated parts of a building have a high thermal transmittance.

The formula for the calculation is the following:

$$U = \frac{1}{R_t} = \frac{1}{Rs_i + R_2 + \ldots + R_n + Rs_e}$$

Being:

R_t Total thermal resistance (m^2 K W^{-1})
Rs_i Internal surface thermal resistance (m^2 K W^{-1})
Rj Thermal resistance of each layer that form the element (m^2 K W^{-1})
Rs_e External surface thermal resistance (m^2 K W^{-1})

In which the thermal resistance of each layer is:

$$R_j = \frac{e_j}{\lambda_j}$$

Being:

e_j The thickness of the layer j (m)

λ_j The thermal conductivity of the layer material j, W/(Kim)

The list below shows a theoretical comparative analysis of different basic façades on which different solutions of PBRs are added. The basic walls considered are presented in the following chart:

1. Basic wall 1: thermoclay + filled with cement
2. Basic wall 2: concrete block + filled + thermal insulation + air chamber + polystyrene cladding

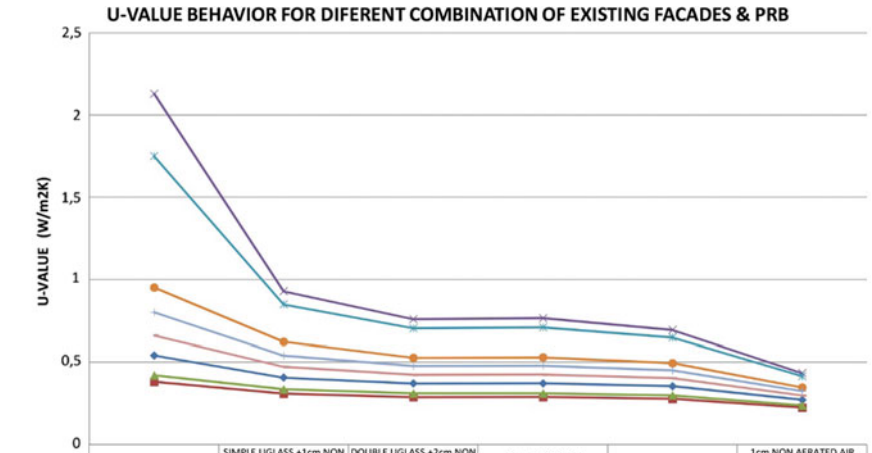

	EXISTING FACADE	SIMPLE UGLASS +1cm NON AERATED 1cm AIR CHAMBER + 3mm PP+ 7 cm MICROALGAE WATER+3mm PP+ 1cm NON AERATED 1cm AIR CHAMBER	DOUBLE UGLASS +2cm NON AERATEDAIR CHAMBER + 3mm PP+ 10 cm MICROALGAE WATER+3mm PP+ 2cm NON AERATED AIR CHAMBER	35mm TERMOGAL CELLULAR POLYCARBONATE + FREELY MOVEMENT GREEN MICROALGAE WATER	4 LAYER ETFE CUSHIONS WITH FREELY MOVEMENT GREEN MICROALGAE WATER	1cm NON AERATED AIR CHAMBER + 7 cm MICROALGAE WATER+1cm NON AERATED AIR CHAMBER + DOUBLE LOW E GLASS 4-20-66, 1A
WALL TYPE 1	0,54	0,4065	0,3701	0,3715	0,354	0,2709
WALL TYPE 2	0,38	0,3086	0,2872	0,288	0,2774	0,2236
WALL TYPE 3	0,42	0,3346	0,3095	0,3105	0,2981	0,2369
WALL TYPE 4	2,13	0,928	0,7579	0,7636	0,6931	0,4329
WALL TYPE 5	1,75	0,8478	0,7035	0,7085	0,6474	0,4146
WALL TYPE 6	0,95	0,622	0,5256	0,5284	0,4936	0,3457
WALL TYPE 7	0,8	0,5382	0,4762	0,4785	0,4498	0,3236
WALL TYPE 8	0,66	0,4709	0,4228	0,4246	0,4019	0,298

Fig. 17.18 Transmittance improvement due to the PBRs integrated in the architecture considering different solutions

3. Basic wall 3: double hollow brick placed in vertical (11.2 cm) + thermal isolation + air chamber + double hollow brick placed in horizontal (24 cm) + air chamber + lined with isolation
4. Basic wall 4: 3-cm lime-based plaster + limestone + gypsum plaster
5. Basic wall 5: 2-cm lime-based plaster + 30-cm solid brick + 1 cm gypsum plaster
6. Basic wall 6: 2-cm external cement plaster + 14-cm perforated brick + 8-cm air chamber + 4-cm hollow brick wall + 1.5 cm gypsum plaster

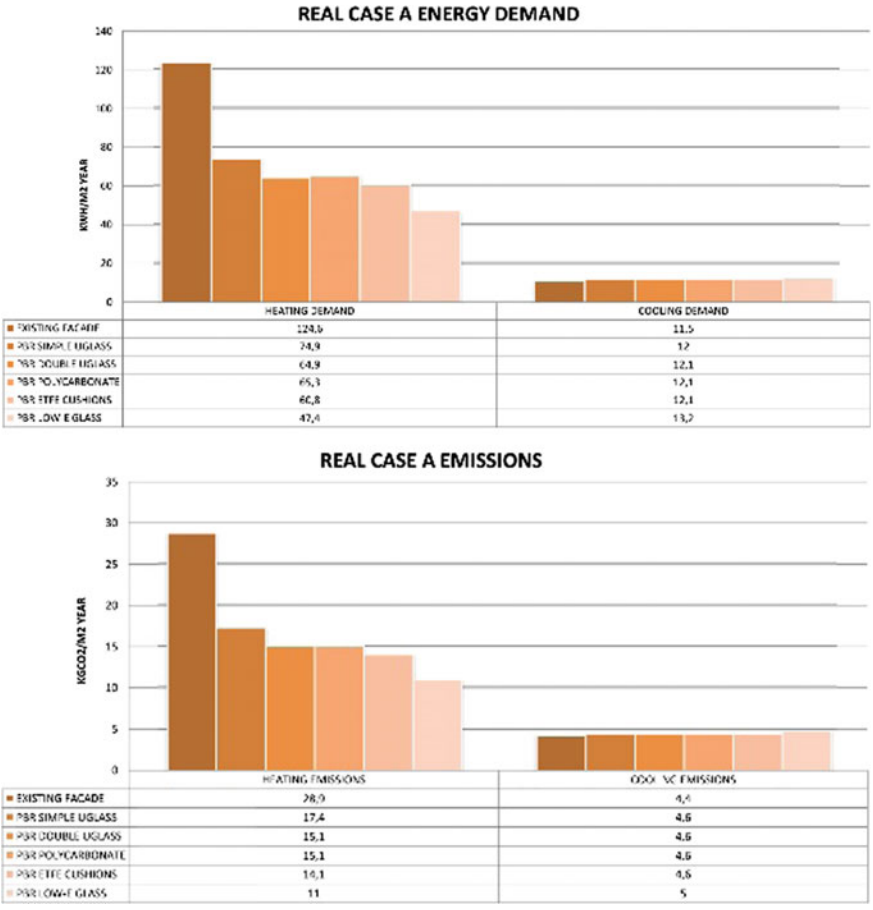

Fig. 17.19 Comparative analysis of the energy demand and emissions in case A and energy saving due to insulation increase produced by the PBRs integrated in the architecture

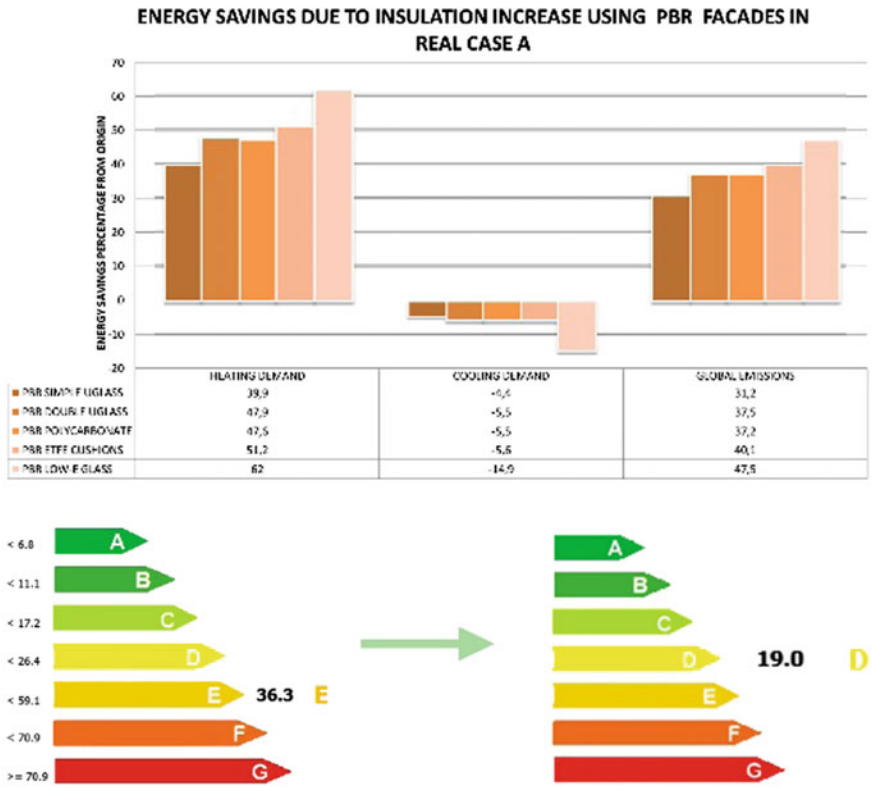

Fig. 17.19 (continued)

7. Basic wall 7: 2 cm external cement plaster + 14-cm perforated brick + 8-cm air chamber + 4-cm hollow brick wall + 1.5 cm gypsum plaster
8. Basic wall 8: 14-cm decorative brick + 10-cm air chamber + 7-cm perforated brick + 1 cm gypsum plaster

The graph shows how in all studied cases the transmittance lows to levels that bring an important energetic saving in terms of comfort demand (Fig. 17.18).

To make sure that estimated values represent the reality, data from 3 different buildings in different locations in the Madrid Community and with different characteristics have been collected. The tool used is the C3X software, approved by the Spanish Government . The software C3X is used as a means of improving energy efficiency in buildings. The addition of external layers effectively contributes to this improvement. The graphs below explain the demands and the emissions of CO_2 in the 3 cases of this study. The following graphs show the saving as percentage against the original study of the buildings without PBRs integrated: (Figs. 17.19, 17.20, and 17.21).

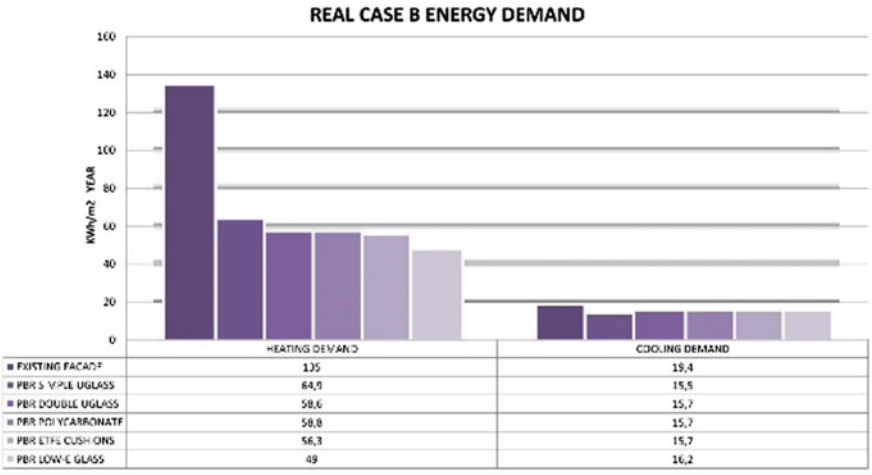

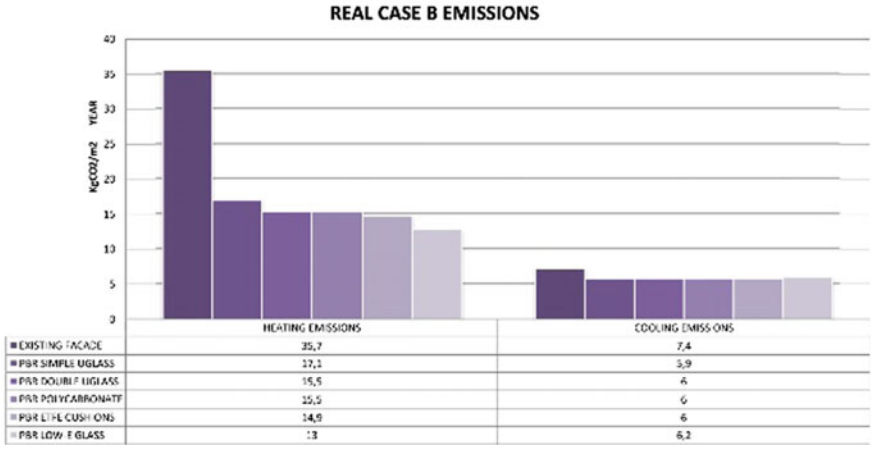

Fig. 17.20 Comparative analysis of the energy demand and emissions in case B and energy saving due to insulation increase produced by the PBRs integrated in the architecture

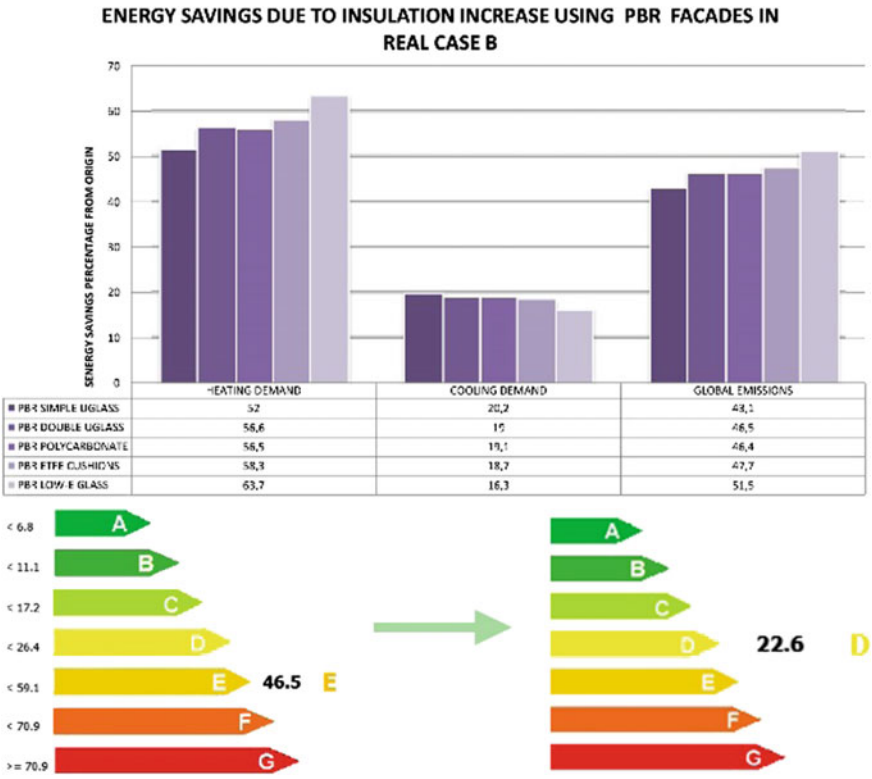

Fig. 17.20 (continued)

In all cases, an energetic saving is produced due to the insulation with the corresponding saving of emissions.

The amortization of investment according to current official prices reaches between 6 and 10 years. If to these benefits expressed in terms of isolation is added the concept of productive farm, then the system is converted in a complex and complete system whose exhaustive analysis calls for a superior detail than that obtained from any firm till now. The PBRs integrated in the architecture and in urban space will be with no doubt an element that any designer will take into account in the future.

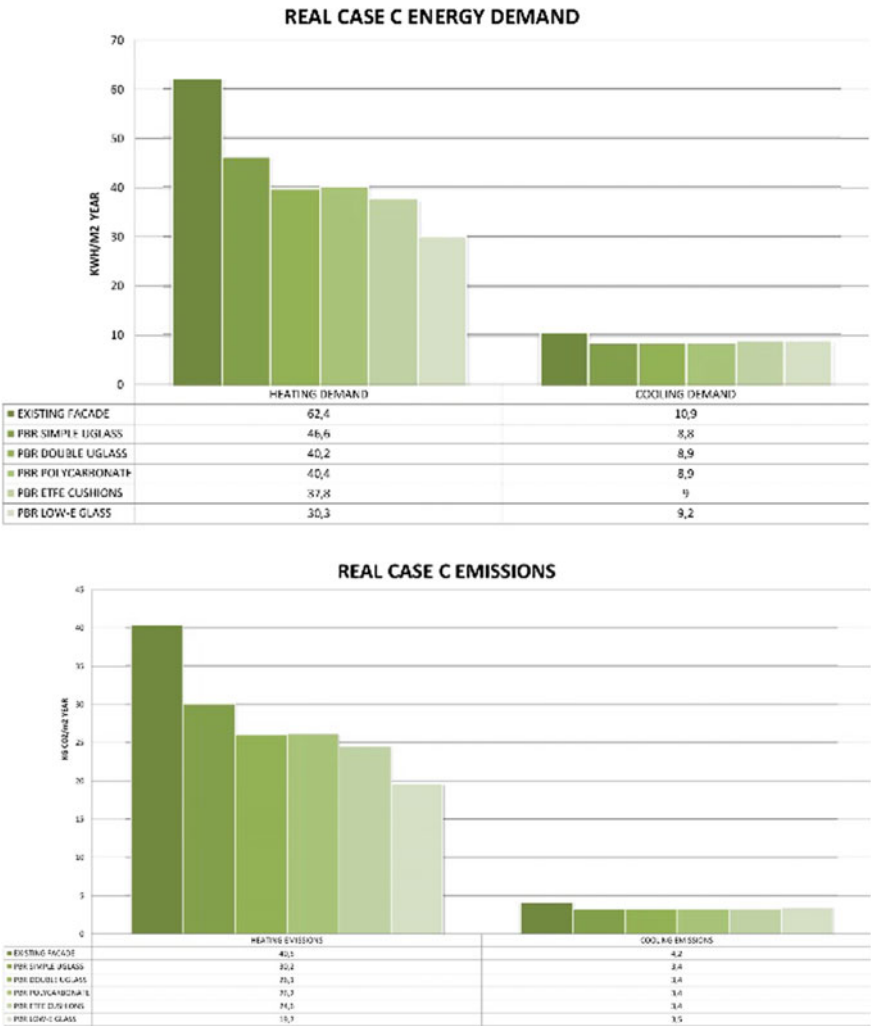

Fig. 17.21 Comparative analysis of the energy demand and emissions in case C and energy saving due to insulation increase produced by the PBRs integrated in the architecture

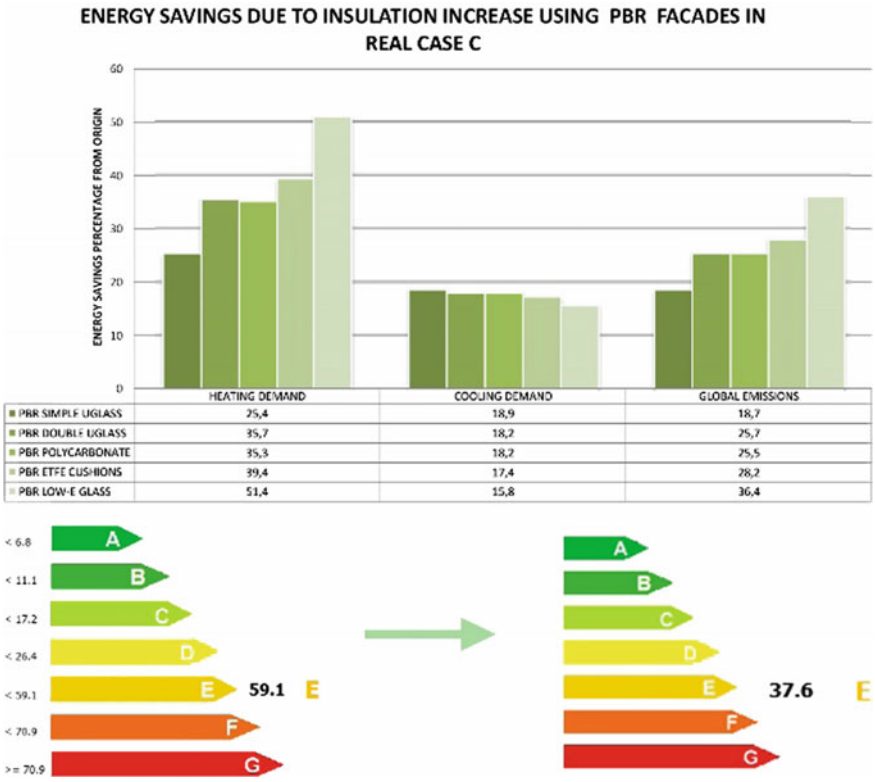

Fig. 17.21 (continued)

17.6 Conclusions

The work performed addresses a highly innovative subject such as the transformation of traditional façades of buildings in architectural photobioreactors cultivating microalgae. The examples built in the world up to now are very few and still are at an experimental level; however; it can be seen as the combination of algae and architecture as an alternative for the production of biomass and CO_2 absorption. The research that we show here goes one step further considering solutions that may cover the entire spectrum of usual building construction. So are proposed models type of photobioreactors of easy and economic installation that can be well adapted to existing buildings for an efficient energetic rehabilitation; either integrated in the façade itself as curtain walls or converted in parasol façades shields and finally designed as façades with high iconic value. In the accomplished study in order to walk toward applicable solutions consistent with a moderate economic cost and with an appropriate energetic balance, it has deepened in the contribution of the PBRs in façades to the thermal regulation of buildings.

After the comparative study of some of the cases presented, a surprising result was obtained: Only considering the benefit due to the increase of isolation, the investment would be amortized in a period of 6–10 years. On the other hand, the impact of the installations needed to transform a PBR façade has a value practically irrelevant from a certain surface. These competitive results are completed with the environmental, energetic, and esthetic values that make the conversion of the enveloping architectural in a productive farm to have a successful future.

Acknowledgments We acknowledge the financial support by competitive pre-industrial research program given by CDTI (Centro para el Desarrollo Tecnológico Industrial) and the Government of Spain, Economic and Competitiveness Ministry. It has also been funded by Cervera and Pioz Architects S.L.P. We also acknowledge the cooperation of Professor Antonio Ruiz Elvira (University of Alcala, Professor Javier Sánchez Alejo (Madrid Polytechnic University) and Fernando Ochoa (Instituto Europeo de Design).

References

Acién FG, Fernández JM, Sánchez JA, Molina E, Chisti Y (2001) Airlift driven external loop tubular photobioreactors for outdoor production of microalgae: assessment of design and performance. Chem Eng Sci 56(8):2721–2732

Colt International GmbH (2013) Solarleaf bioreactor façade. http://www.coltinfo.co.uk/system/html/luftblasen-algen-in-bioreaktorfassade

Gemeente Amsterdam Dienst Ruimtelijke Ordening (2008) Amsterdam Teleport—Nieuwe ronde, nieuwe kansen. Plan Amsterdam 5

Growenergy (2013) One technology, unlimited possibilities. Retrieved April 6 2013, from https://www.growenergy.org/research/28|Page

Mirón SA, Gomez CA, Camacho GF, Grima ME, Chisti Y (1999) Comparative evaluation of compact photobioreactors for large scale monoculture of microalgae. J Biotechnol 70:249–270

Pruvost J et al. Symbiotic integration of photobioreactors in a factory building façade for mutual benefit between buildings and microalgae needs. http://www.researchgate.net/profile/Jeremy_Pruvost/publications

Qui F (2013) Algae architecture, Thesis, Delft University http://repository.tudelft.nl/view/ir/uuid:b0b6e05d-49d8-4cc0-9e28-f510b0a8b215/

Shannon BA (2013) Quantifying the fertilizer value of algal meal: an evaluation of an integrated Dairy-Anaerobic Digester-Algae Production Facility, Master thesis in Soil Science, https://ir.library.oregonstate.edu/xmlui/bitstream/handle/1957/40443/AndrewsShannonB2013.pdf?sequence=1

Wurm J (2012) Photobioreactors as adaptive shading devices. Retrieved 12 May 2013, from http://smartgeometry.org/index.php?option=com_content&view=article&id=154:photobioreactors-as-adaptive-shading-devices&catid=45:sgarticles&Itemid=160